Loughborough University

This item is held in Loughborough University's Institutional Repository (https://dspace.lboro.ac.uk/) and was harvested from the British Library's EThOS service (http://www.ethos.bl.uk/). It is made available under the following Creative Commons Licence conditions.

creative commons

COMMONS DEED

Attribution-NonCommercial-NoDerivs 2.5

You are free:

- to copy, distribute, display, and perform the work

Under the following conditions:

Attribution. You must attribute the work in the manner specified by the author or licensor.

Noncommercial. You may not use this work for commercial purposes.

No Derivative Works. You may not alter, transform, or build upon this work.

- For any reuse or distribution, you must make clear to others the license terms of this work.
- Any of these conditions can be waived if you get permission from the copyright holder.

Your fair use and other rights are in no way affected by the above.

This is a human-readable summary of the Legal Code (the full license).

Disclaimer

For the full text of this licence, please go to:
http://creativecommons.org/licenses/by-nc-nd/2.5/

A STUDY OF CYCLIC VARIATION IN GAS VELOCITY

AND THE TURBULENCE STRUCTURE IN SPARK IGNITION ENGINES

by

N.S.M. SALAMA

A Doctoral Thesis

Submitted in Partial Fulfilment of the Requirements

for the Award of

Doctor of Philosophy of Loughborough University of Technology

November 1974

Supervisor: J.C. Dent, Ph.D., C.Eng.

c by Nabil Salama Mohamed Salama

SUMMARY

The thesis is concerned with the study of the characteristics of the turbulent flow field inside the combustion chambers of spark ignition engines.

A comprehensive literature survey has been undertaken of the problem of cyclic variation in spark ignition engines, and the role of turbulence on flame propagation.

The experimental methods used involve a detailed application of hot wire anemometry, signal processing and computer techniques to the statistical analysis of the problem of cyclic variation in gas velocity and turbulence structure (intensity, scale, power spectrum and eddy diffusivity), at the spark plug location of motored spark ignition engines.

Two engines have been used in the investigation, a Rolls-Royce V-8L and a Ford 2 litre V4. Extensive test programs were carried out on both engines at a range of engine speeds and throttle settings, and a range of turbulence promoting devices have been investigated with regard to their suitability for promoting small scale turbulence during the ignition period.

The variation of flow field characteristics with depth inside a wedge combustion chamber of the Rolls-Royce engine has been investigated. Cylinder-to-Cylinder variation in turbulence characteristics has also been investigated for the Rolls-Royce engine.

The spectral composition of turbulent eddies inside a wedge and a heron combustion chamber was investigated over a wide range of engine speeds. It was found that increasing engine speed resulted in increases of both the fluctuating velocity components and the high frequency content of the eddies. Both effects are believed to be responsible for increases in turbulent flame speed in engines with increases in engine speed.

Comparisons between the results obtained in the present work and the reported data of other investigations on turbulence measurements in spark ignition engines and closed vessels, show close agreement.

A direct correlation has been established between the characteristics of the turbulence field in engines and other isotropic flow fields. In particular, a correlation is found to exist between the eddy diffusivity as obtained from the anemometer measurements in an engine and the eddy diffusivity data for highly turbulent pipe flow obtained by other workers. These findings establish a relatively straightforward method for obtaining quantitative information on turbulence characteristics from mean velocity measurements on an engine, which require simple equipment.

A theoretical model of combustion variation has been developed, based on the assumption that cyclic variation originates during the growth period of the initial flame kernel. This process was related to variations in eddy diffusivities of the small scale turbulence for different

cycles. The model equations are checked by making use of the established correlation between eddy diffusivity and gas mean velocity and using the reported experimental data of other workers, which shows very good agreement between the predictions of the model and the measured values.

A C K N O W L E D G E M E N T S

The author wishes to express his thanks to:

Dr. J.C. Dent for his guidance throughout the project.

Mr. P. Clayton for manufacturing hardware.

Messrs. K. Topley and G. Smith for photographic work.

Mrs. J. Smith for typing the completed thesis.

A great debt is also due to my wife for her encouragement during the period of study.

Finally I would like to express my appreciation to Rolls-Royce Motors Limited for scholarship support during the course of this research.

NOTATION

A	Cross Sectional Area of a Hot Wire	(m^2)
	A Constant in the Heat Transfer Equation (3-2)	(-)
A*	Isotropic Area of Inlet Port	(m^2)
a	Overheating Ratio of a Hot Wire	(-)
B	A Constant in the Heat Transfer Equations (3-1) and (3-2)	(-)
C	Correction Factor for the Effect of Finite Wire Length on Turbulence Measurements	(-)
C_w	Heat Capacity of a Hot Wire	(J/°K)
c_f	Skin Friction Coefficient	
c_p	Specific Heat at Constant Pressure	(J/Kg°K)
c_v	Specific Heat at Constant Volume	(J/Kg°K)
D	Cylinder Diameter	(m)
d	Hot Wire Diameter	(m)
E	Instantaneous Value of Bridge Voltage	(volts)
$\bar{E}$	Mean Value of Bridge Voltage	(volts)
e	Fluctuating Voltage Component	(volts)
$F(\eta)$	Power Spectral Density Function	(sec)
$F(K)$	Power Spectral Density Function	(m^{-1})
$F(X)$	Fourier Transform of a Random Variable X	
$F^{-1}(x)$	Inverse Fourier Transform of a Random Variable X	
f	Friction Factor	(-)
g_{tr}	Transconductance of Hot Wire Circuit	(ohms)
h	Heat Transfer Coefficient	(W/m^2 °C)

R_g	Resistance of a Hot Wire at Gas Temperature	(ohms)
R_o	Resistance of a Hot Wire at a Reference Temperature	(ohms)
R_W	Resistance of a Hot Wire at its Operating Temperature	(ohms)
Re_D	Reynolds Number ($U.D/\nu$)	(-)
Re_L	Turbulence Reynolds Number ($u' L_x/\nu$)	(-)
Re_λ	Turbulence Reynolds Number ($u' \lambda_y/\nu$)	(-)
$R_t(\tau)$	Auto-correlation Function	(m^2/sec^2)
$R'_t(\tau)$	Auto-correlation Coefficient	(-)
$R'_L(\tau)$	Lagrangian Correlation Coefficient	(-)
$R'_x(x)$	Longitudinal Correlation Coefficient	(-)
$R'_y(y)$	Lateral Correlation Coefficient	(-)
r	Separation Distance Between two points in a Fluid Field	(mm)
S_l	Laminar Flame Speed	(m/sec)
S_t	Turbulent Flame Speed	(m/sec)
S(x)	Standard Deviation of the Variable x.	
T_g	Gas Temperature	(^oK)
T_W	Operating Temperature of a Hot Wire	(^oK)
t	Time	(sec)
U	Instantaneous Value of the Turbulent Gas Velocity	(m/sec)
$\bar{U}$	Average Value of Gas Velocity	(m/sec)
u	Fluctuating Velocity Component in Flow Direction	(m/sec)
v	Fluctuating Velocity Component in Y Axis Direction	(m/sec)
W	Rate of Energy Dissipation	($Kg/m\ sec^3$)
w	Fluctuating Velocity Component in Z axis Direction	(m/sec)

I	Instantaneous Value of the Bridge Current	(A)
$\bar{I}$	Mean Value of the Bridge Current	(A)
Int	Turbulent Intensity	(-)
i	Fluctuating Component of Bridge Current	(A)
K	Slope of Hot Wire Calibration Curve $(K = \frac{dE}{dU})$	(volts/m/sec)
K_g	Thermal Conductivity of Gas	$(W/m^2\ {}^oC/m)$
K_S	Thermal Conductivity of Wire Material at Gas Temperature	$(w/m^2\ {}^oC/m)$
K_T	Thermal Conductivity of Wire Material at its Operating Temperature	$(w/m^2\ {}^oC/m)$
L_t	Time Macro-Scale of Turbulence	(sec)
L_x	Longitudinal Space Scale of Turbulence (Macro-scale)	(mm)
L_y	Lateral Space Scale of Turbulence (Macro-scale)	(mm)
L_m, ℓ_m	Prandtl Mixing Length	(mm)
ℓ	Wire Length	(m)
l^*	Von-Karman Characteristic Length	(mm)
$\mathcal{L}_t$	Lagrangian Time Scale of Turbulence	(sec)
$\mathcal{L}_L$	Lagrangian Space Scale of Turbulence	(mm)
Nu	Nusselt Number	(-)
n	Polytropic Index	(-)
	Frequency of Eddy Rotation	(Hz)
P	Pressure	(N/m^2)
Pr	Prandtl Number	(-)
Q_c	Heat Loss by Conduction along the Hot Wire	(J)
Q_e	Heat Supplied to a Hot Wire	(J)
Q_h	Convective Heat Transfer from the Hot Wire to the Surrounding Fluid	(J)
R_c	Cold Resistance of a Hot Wire	(ohms)

X	Coordinate Axis in the Flow Direction	(mm)
Y	Coordinate Axis Perpendicular to the Flow Direction	(mm)
Z	Coordinate Axis Perpendicular to the Flow Direction	(mm)
α	Temperature Coefficient of Resistance	($/^{o}C$)
β	Electrical Resistivity of Wire Material	
γ	Ratio of Specific Heats	(-)
τ	Delay Time between the Signal at Two Different Instants of Time	(sec)
	Shear Stress	(N/m^2)
λ_t	Time Micro-Scale of Turbulence	(sec)
λ_x	Longitudinal Micro-Scale of Turbulence	(mm)
λ_y	Lateral Micro-Scale of Turbulence	(mm)
ρ	Gas Density	(Kg/m^3)
δ_ℓ	Width of Laminar Flame Front	(mm)
δ_t	Width of Turbulent Flame Front	(m)
μ	Gas Dynamic Viscosity	(Kg/m sec)
ν	Gas Kinematic Viscosity	(m^2/sec)
ε_m	Coefficient of Eddy Diffusivity	(m^2/sec)
θ	Crank Angle	(degrees)
Γ	Kovasznay Criterion ($\Gamma = \frac{\delta_\ell}{S_\ell} \cdot \frac{u}{\lambda_x}$)	(-)

Subscripts

g	Gas Conditions
ℓ	Laminar
Lin	Linearized
meas	Measured
micro	Small-scale Turbulence Eddies (micro-scale)
macro	Large-Scale Turbulence Eddies (macro-scale)
t	Turbulence,Time
w	Wire Operating Conditions, conditions at the walls

Abbreviations

ADC	Analog-to-Digital Converter
ATDC	After Top Dead Centre
BTDC	Before Top Dead Centre
TDC	Top Dead Centre
Ir	Iridium
MBT	Maximum Brake Torque
Pt	Platinum

INDEX OF CONTENTS

	Page Nos.
SUMMARY	(i) - (iii)
ACKNOWLEDGEMENTS	(iv)
NOTATION	(v) - (ix)
1.0 INTRODUCTION	1 - 8
1.1 General	1 - 6
1.2 Object of the Investigation	7 - 8
2.0 LITERATURE SURVEY	9 - 130
2.1 Relation between Cyclic Variation and Engine Performance	9 - 10
2.2 Choice of Characteristic Parameters as a Measure of Cyclic Variation	10 - 19
2.3 The Effect of Engine Operating Variables on the Extent of Cyclic Variation	19 - 55
2.3.1 Ignition	25 - 31
2.3.2 Mixture Preparation	32 - 34
2.3.3 Exhaust Gas Dilution of the Charge	34 - 37
2.3.4 Compression Ratio	37 - 39
2.3.5 Throttling	39 - 42
2.3.6 Cylinder Water Jacket Temperature and Oil Contamination of the Charge	42
2.3.7 Air/Fuel Ratio	42 -- 50
2.3.8 Type of Fuel	50 - 52
2.3.9 General Characteristics of Cyclic Variation	52 - 55
2.4 Effect of Gas Velocities and Turbulence on the Combustion Process in S.I. Engines	55 - 102
2.5 Effect of Mixture Motion on Flame Speed	103 - 123
2.6 Possible Cause of Cyclic Variations	123 - 130

	Page Nos.
3.0 HOT WIRE ANEMOMETER AND ITS CHARACTERISTICS FOR TURBULENCE MEASUREMENTS	131 - 196
3.1 The Constant Temperature Hot Wire Anemometer	132 - 133
3.2 Calibration of the Hot Wire Anemometer	133 - 144
3.2.1 Physical Properties of Hot Wire Probes	140 - 142
3.2.2 Anemometer Drift	143 - 144
3.3 The Response of Constant Temperature Hot Wire Anemometer To Turbulence	144 - 152
3.4 Statistical Analysis of Turbulence	152 - 170
3.4.1 Definitions of Correlations and Scales of Turbulence	152 - 161
3.4.2 The Spectrum of Isotropic Turbulence	161 - 167
3.4.3 The Relationship between the Micro-Scale and the Macro-Scale for Isotropic Turbulence	167 - 170
3.5 Effect of Large Turbulence Fluctuations on the Response of a Hot Wire	170 - 175
3.6 The Effect of Wire Length on Turbulence Measurements	175 - 181
3.7 Turbulence Diffusion, Lagrángian Analysis	181 - 185
FIGURES (3-1) - (3-16)	186 - 196
4.0 DATA ACQUISITION AND PROCESSING SYSTEM	197 - 279
4.1 Data Collection	202 - 214
4.1.1 DISA 55M onstant Temperature Anemometer System	203 - 206
4.1.2 Timing Mark	206
4.1.3 Measurements of Cylinder Gas Temperature and Pressure	207 - 208
4.1.4 Signal Recording System	208 - 212
4.1.5 Probes and Traverse Mechanisms	213 - 214

Page Nos.

4.2 Data Preparation 214 - 224

4.2.1 Digitization of Mean Velocity and Pressure Traces 214 - 216

4.2.2 Calibration of the Digitized Data 216

4.2.3 Calibration of Recorded Signals 217 - 218

4.2.4 Preparation of Turbulence Signals 218 - 224

a) Preparation for Multiple Records

b) Data Preparation for Individual Records

4.3 Data Qualification (Basic Assumptions about the Structure of the Turbulent Field) 224 - 235

4.3.1 Stationarity and Ergodicity of the Data 226 - 228

4.3.2 Test for Stationarity 228 - 232

4.3.3 Isotropy and Homogeneity of Turbulence 233 - 235

4.4 Data Analysis 235 - 247

4.4.1 Analysis of Gas Mean Velocities 235 - 237

4.4.2 Analysis of the Fluctuating Velocity Components 237 - 247

1) Analysis of Multiple Data Records

2) Analysis of Individual Data Records

4.5 Programming of the Data Analysis Procedures 247 - 254

FIGURES (4-3a) - (4-29) 255 - 279

5.0 MOTORED ENGINE CONFIGURATION AND EXPERIMENTAL TEST PROGRAM 280 - 307

5.1 Experimental Test Programmes and their Objectives 284 - 297

5.1.1 Details of the Experimental Test Programme carried out on the Rolls-Royce Engine 287 - 293

Page Nos.

5.1.2 Details of the Experimental Test Program Carried out on the Ford Engine 294 - 297

FIGURES (5-1) - (5-15) 298 - 307

6.0 DISCUSSION OF RESULTS 308 - 460

6.1 General Characteristics of Gas Velocities inside the Combustion Chambers of Spark Ignition Engines 308 - 324

6.1.1 Effect of Hot Wire Direction on the Measured Gas Velocities 310 - 311

6.1.2 Variation of Gas Velocities with Depth inside the Combustion Chamber of a Rolls-Royce Engine 312 - 315

6.1.3 Investigation of the Flow Pattern inside a Wedge Combustion Chamber 315 - 318

6.1.4 Variation of Gas Velocity Characteristics with Engine Speed 318 - 323

6.1.5 Investigation of Gas Velocity Characteristics inside the Intake Manifold 323 - 324

6.2 Variation of Flow Field Characteristics with Different Modifications of Intake System 325 - 330

6.3 Investigation of Turbulence Characteristics inside the Combustion Chambers of Spark Ignition Engines 330 - 355

6.3.1 General Characteristics of Turbulence Field in Engines 331 - 335

6.3.2 Variation of Turbulence Characteristics with Engine Speed 336 - 340

6.3.3. Variation of Turbulence Characteristics with throttling 340 - 342

6.3.4 Investigation of the Extent of Cyclic Variation in Turbulence Characteristics 343 - 345

6.3.5 Effect of Different Intake Modifications and Local Turbulence Promoter at Spark Plug on the Characteristics of the Turbulence Field 345 - 355

Page Nos.

6.4 Investigation of Cylinder-to-Cylinder Variations in Flow Field Characteristics 356 - 357

6.5 Effect of Combustion Chamber Configuration on Turbulence Characteristics 358 - 361

FIGURES (6-1) - (6-51) 362 - 460

7.0 CORRELATION BETWEEN THE CHARACTERISTICS OF TURBULENCE FIELD INSIDE THE COMBUSTION CHAMBERS OF SPARK IGNITION AND OTHER FLOW FIELDS 461 - 494

7.1 Approximate Design Procedure for Predicting Turbulence Characteristics in Spark Ignition Engines 479 - 482

FIGURES (7-1) - (7-14) 483 - 494

8.0 MODEL OF CYCLIC VARIATION 495 - 516

8.1 Experimental Verification of Cyclic Combustion Variation Model 510 - 514

FIGURES (8-1) - (8-3) 515 - 516

9.0 CONCLUSIONS AND RECOMMENDATIONS FOR FURTHER WORK 517 - 528

9.1 Conclusions 517 - 525

9.2 Recommendations for Further Work 526 - 528

10.0 REFERENCES AND APPENDICES 529 - 565

REFERENCES 529 - 544

APPENDICES 545 - 565

PART I: A1 New Analysis of Other Investigations. 545 - 553

A2 Statistical Definitions 554 - 558

A3 Physical Properties of Air 559 - 564

A4 A Guide for the Sources of Different Equations Presented in Chapter 3. 565

PART II: PROGRAMMING OF THE DATA PROCESSING SYSTEM

NOTE ON FIGURE ARRANGEMENTS

The illustrations within this thesis are grouped at the end of the corresponding chapters, with the exception of the first two chapters.

1.0 INTRODUCTION

1.1 General

The process of combustion in the cylinder of a spark ignition engine is initiated by a single intensely high temperature spark which gives rise to a nucleus of flame, and after the lapse of a certain time interval representing the delay period, this nucleus produces a stable advancing flame front, blue at first, but closely followed by the main heat releasing front, which generally has an orange colour.

Examination of the combustion pressure diagrams of-any gasoline engine, operating under normal conditions, show that there is a large cycle to cycle variation in the rate at which the flame propagates across the combustion chamber in successive cylinder firing. This results in a variation in the rate of pressure rise (due to combustion), in the peak cylinder pressure, and in the work done by the gas on the piston. For maximum efficiency, reliability and acceptance of engines, it is necessary that their pressure development should be repeatable from one cycle to another.

In spite of the fact that this combustion problem was noted in some of the earliest research on spark ignition engines (1), a firm understanding of its origin and means for its reduction have never been realised.

Patterson (2) showed that fast burning mixtures produce less cyclic variations, Fig. (1-1) and consequently will produce less torque variation and will supply power to an automobile more smoothly. This could be accomplished by: enrichening the mixture to

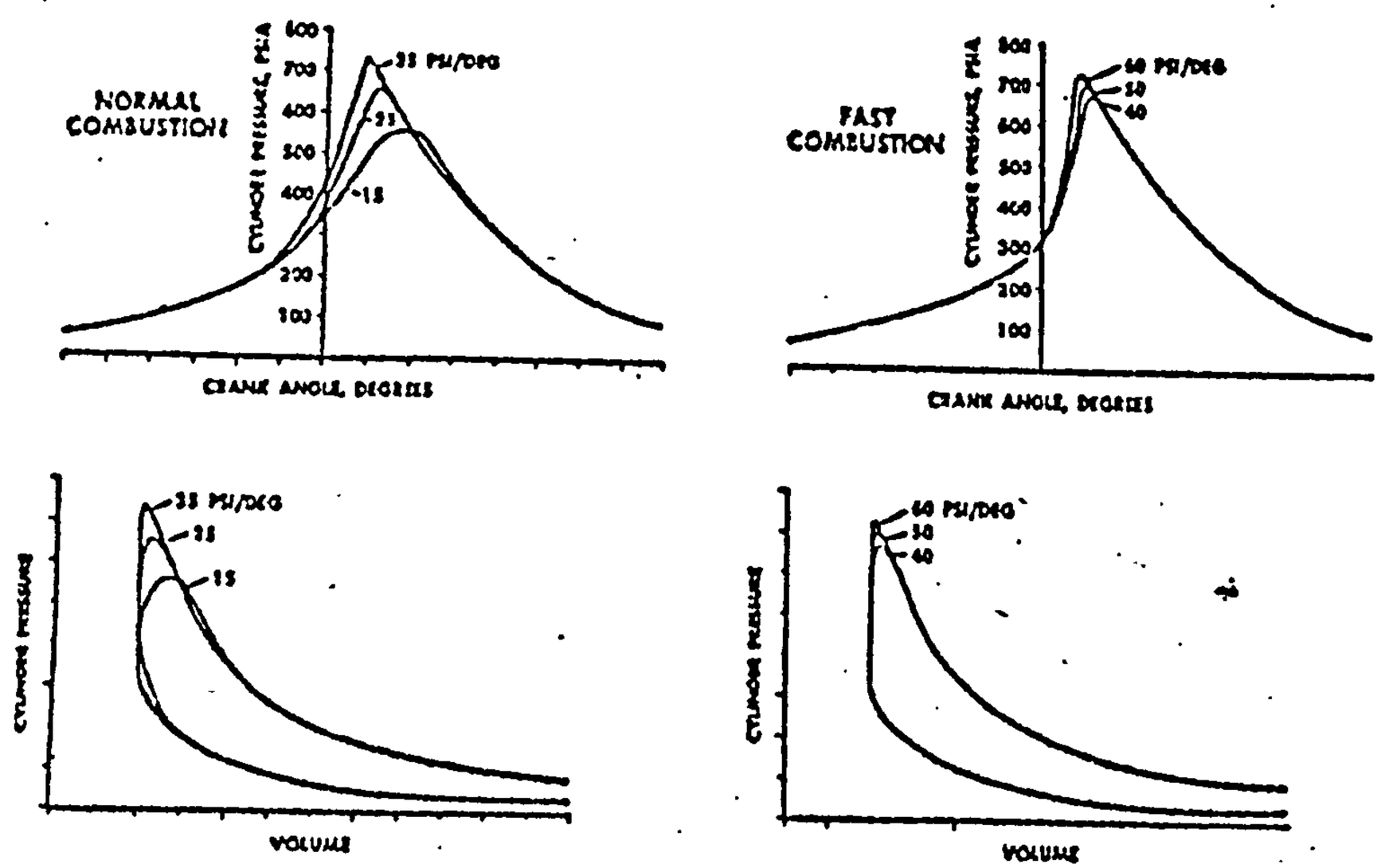

Fig (1-1). Pressure-time and pressure-volume diagrams for one engine with normal rate of combustion and one with fast rate - showing the effect of fast combustion on reducing cyclic power variations (2).

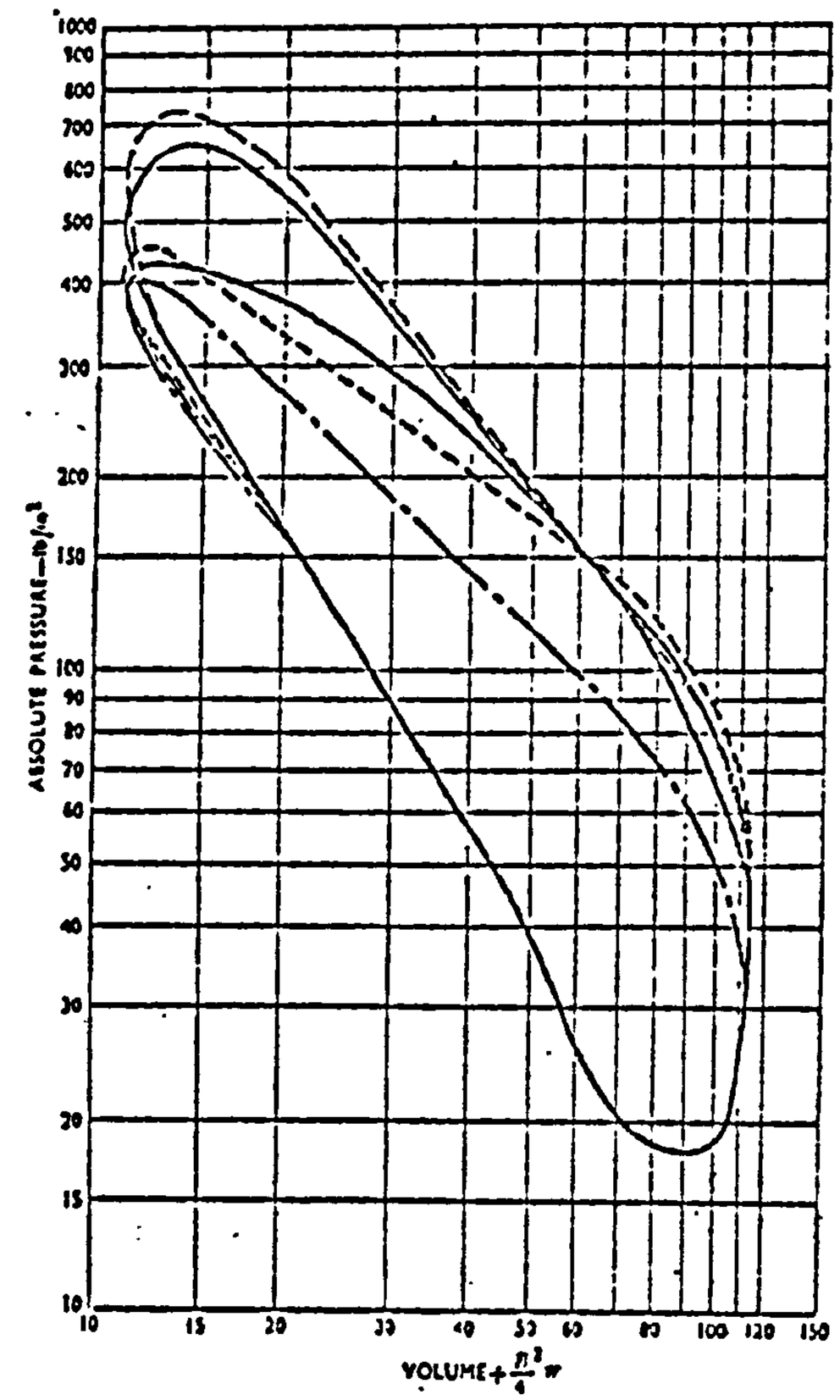

Fig. (1-2). Log P-Log V diagrams for five consecutive cycles with lean mixtures (4).
(2000 r.p.m., 10:1 compression ratio, 20:1 air/fuel ratio and fully opened throttle).
Coefficient of variation in i.m.e.p. = 22.39%.
Coefficient of variation in peak pressure = 19.55%.

best power mixture ratios (4, 30, 16), reducing exhaust residuals (4, 13), installing shrouded valves (2) (to increase the charge turbulence), and multiple ignition of the charge (4). However, as a result of the present interest in the use of lean mixtures to reduce exhaust emissions, the method of reducing cyclic combustion variation by richening the mixture, as employed by most manufacturers will no longer be viable. At lean fuel air ratios, the effect of cyclic variation becomes severe (2, 3, 4, 30), and one lean misfire will negate any emission reduction.

If it were possible to run an engine at weak mixtures and obtain each cycle equivalent to the best observed during normal weak mixture operation, then, according to Patterson (2), Soltau (4), Clarke (5) and Vichnievsky (6), gains of 10-20% in power and fuel economy might be possible, Fig. (1-2), as well as important reductions in exhaust emissions. It will further reduce the octane number requirements and would permit a higher compression ratio, but without requiring higher octane fuel (7, 8), Fig. (1-3).

Previous investigations have attempted to explain qualitatively cycle to cycle variation by a number of factors. Among the more important factors influencing this variation are:-

i) Variations in the overall air/fuel ratio of the cylinder with successive cycles.

ii) Non -homogeneous distribution of air and fuel through the cylinder, particularly in the vicinity of the spark plug.

iii) Variations in the spark-timing, the type of spark, or the spark energy.

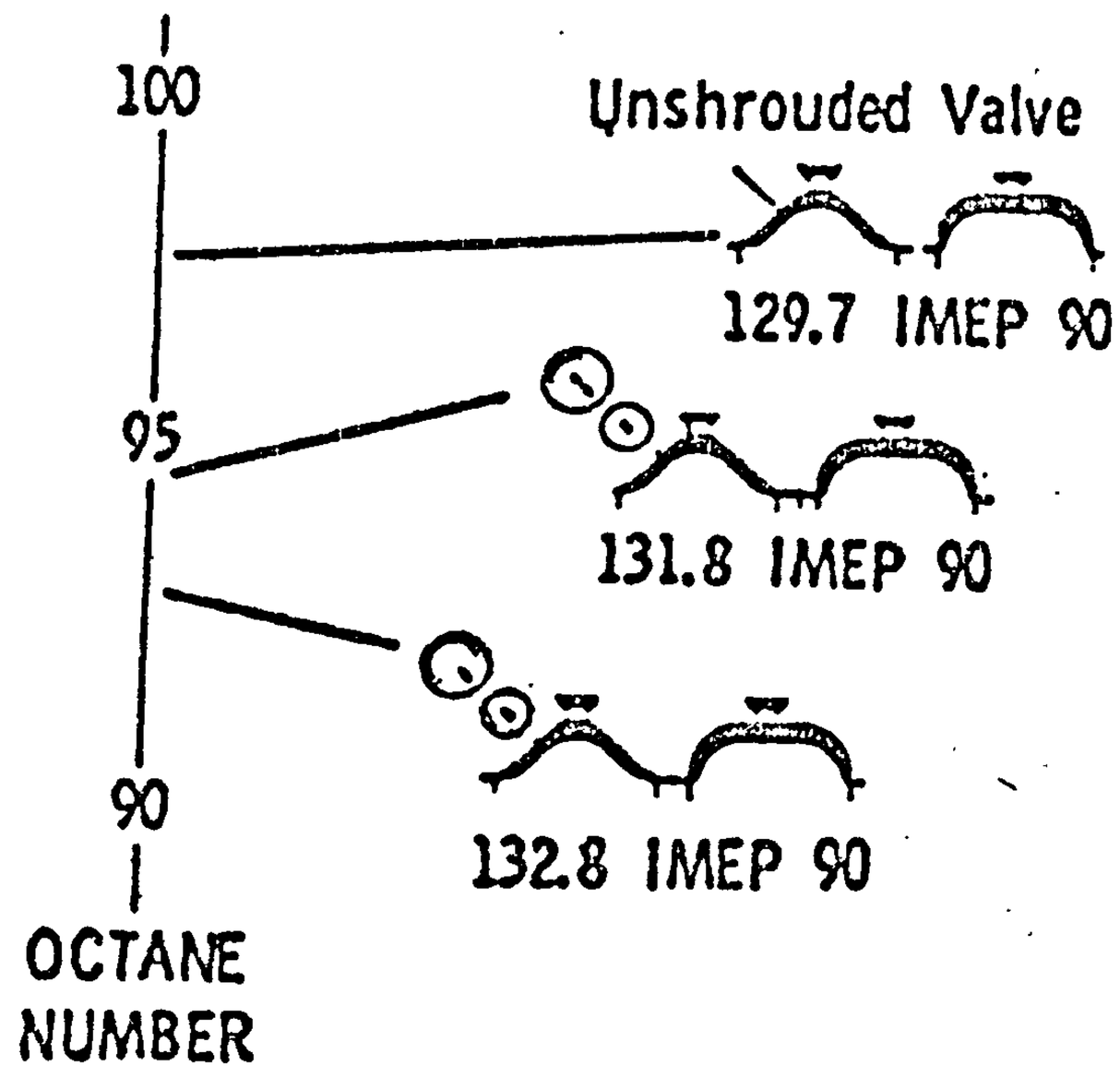

Fig. (1-3). Effect of intake valve shrouding on 99% power octane requirements (8). (1000 r.p.m. 9:1 compression ratio).

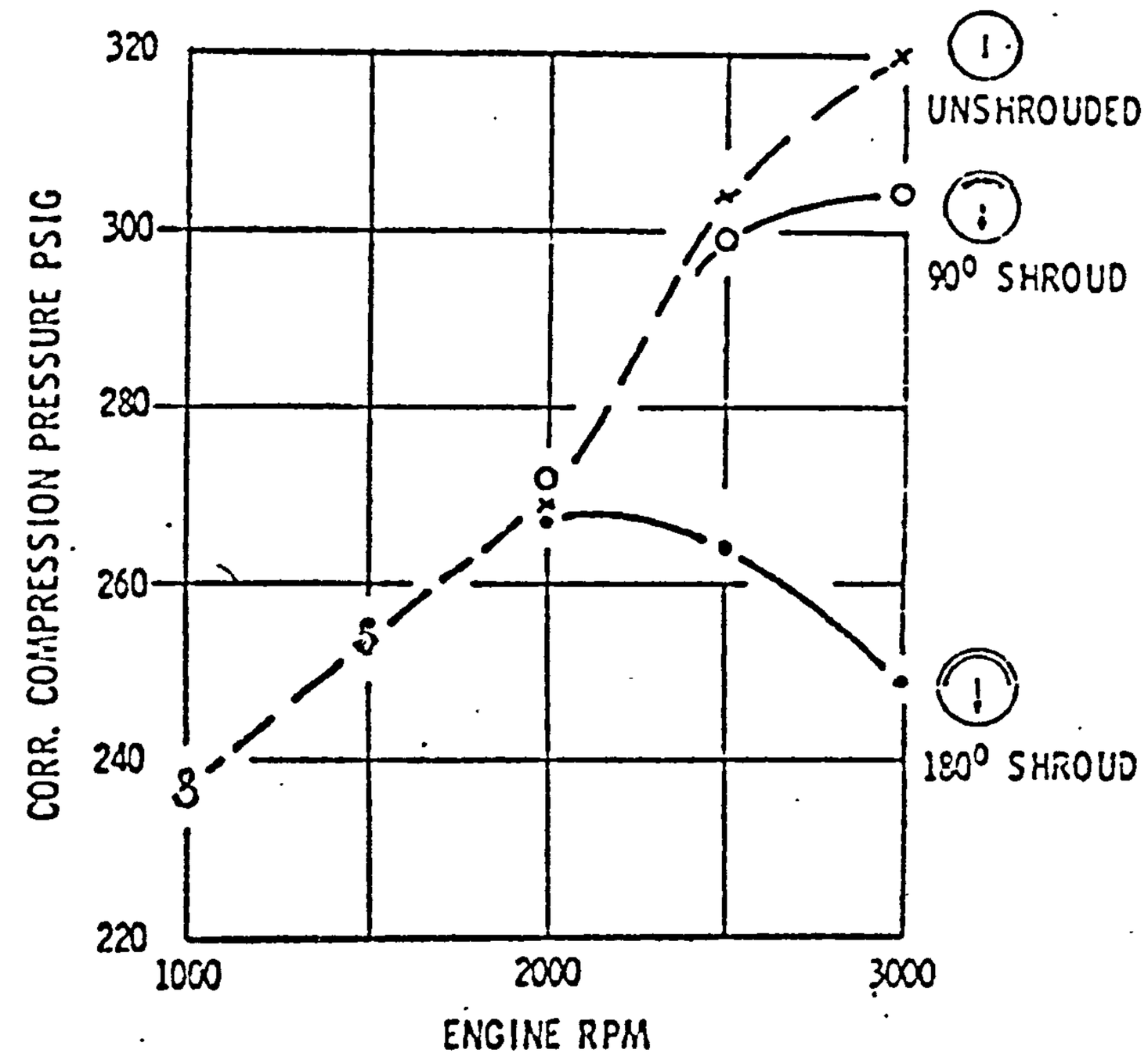

Fig. (1-4). Effect of intake shrouding on compression pressures (8).
(9:1 compression ratio).

iv) The temporal variation in the velocity gradients and turbulent mixture motion, again, particularly in the vicinity of the spark plug.

All these factors may cause cyclic variation, but the effect of each is not the same. The last factor appears to be receiving the most interest, and is regarded as the major cause of combustion variation (2, 9-13, 15, 17, 23).

There is a general agreement that cyclic variation originates in the early development of the initial flame kernel. During this period, the size of the flame kernel is very comparable with the small scale turbulence eddies. Consequently, the growth of such a kernel is greatly affected by the random nature of the turbulent field. When the size of flame front approaches that of the large scale eddies, the flame propagates at a more or less constant speed and the effect of eddies will be averaged across the front. A detailed analysis of this concept of cyclic variation will be discussed in detail in chapter 8.

Several investigations tend to support this explanation due to the observed amelioration of dispersion in tests where turbulence intensity was increased either by: shrouding the inlet valve (2, 15, 16, 17, 20), modification of the inlet port (16, 18), or reducing the inlet valve lift (19). However, the actual flow mechanism of these modifications have never been studied quantitavely.

Although the effect of turbulence on increasing the flame propagation and reducing the flame travel time and consequently cyclic variation is well known, the constant impetus for better

breathing to provide increased full load output has resulted in engines with relatively large inlet ports and unshrouded valves. Fig. (1-4) shows a comparison between the compression pressures for three types of inlet valves; a plain valve, a valve with a 90 degree shroud and a valve with a 180 degree shroud. The effect of the shrouds on restricting the engine breathing at higher speeds is clearly evident. On the other hand, large inlet valves and inlet valve ports with good aerodynamic design cause small pressure drop in the cylinder and consequently low velocities and turbulence intensities at the low loads and speeds required for automotive applications. These usually result in longer flame travel times and probably high cyclic dispersion (9).

Elucidation of the effect of turbulence on the cyclic variation necessitates, therefore, a detailed study of the turbulence intensities, scales and spectrum. So far as is known, few attempts (21, 22, 24) have been made to measure directly the intensities of turbulence in a cylinder of a spark-ignition engine using hot wire anemometers. Moreover, no measurements of the scales of turbulence or the eddy diffusivity in engines have been reported. This provides the impetus to study such explicit factors in an attempt to determine the parameters which affect the flame propagation and consequently the cylinder pressure development (resulting from combustion) in a spark ignition engine, and which it would be desirable to control to reduce cyclic combustion variation.

1.2 Object of the Investigation

It has been concluded, by many investigators, that even with engine operating variables under control, cyclic combustion variation still exist due to cyclic variation in mixture motion and the random nature of the turbulent flow field inside the combustion chamber.

The available knowledge about the characteristics of the turbulent gas motion inside the combustion chamber of S.I. engines are limited and most of the published investigations in this field are concerned with measurements of mean gas velocities. However, part of the problem could be attributed to the complexity of the flow field after inlet valve closure and the difficulties of using hot wire anemometry in such a flow which undergoes very rapid changes of its characteristics.

Therefore, the main objective of the present investigation could be summarized in the following points:-

i) Development of a suitable technique for studying the characteristics of turbulent flow inside the combustion chamber of S.I. engines in terms of intensities, scales and spectrum functions.

ii) Obtaining a detailed and reliable measurement of gas velocities inside the combustion chamber of actual commercial S.I. engines under variable operating conditions.

iii) A study of the cyclic variations in gas velocities and turbulence as a possible cause for cyclic combustion variations.

iv) An attempt to achieve better understanding of the flow mechanism and the associated turbulence characteristics of some devices which have been employed by other investigators and resulted in some improvement of cyclic combustion variation and to investigate the flow characteristics developed by some new ones.

v) An attempt to establish some correlation between the turbulence characteristics inside the combustion chamber of S.I. engines and those predicted from pipe flow experimental data. Such an object, which if achieved, could reduce the amount of experimental work and make such a complex problem somewhat predictable.

vi) The establishment of a model for cyclic combustion variation relating such phenomenon to the structure of the turbulent field inside the combustion chamber of S.I. engines.

2.0 LITERATURE SURVEY

2.1 Relation between cyclic variation and engine performance

Recently, most interest has been shown in lean mixture combustion as a means for reduced exhaust emissions, because of its low concentration of oxides of nitrogen as well as carbon monoxide in the exhaust gas (the lowest HC (exhaust hydrocarbons) contents are reached at fuel/air ratios 20-30% weak (60)). Moreover, most modern spark-ignition engines attain their lowest fuel consumption at approximately 5-15% excess air. Generally, however, when the mixture is weakened to a considerable extent beyond the stoichiometric, problems are encountered due to poor combustion and occasional misfire which results in increased specific fuel consumption, rough engine operation and increased hydrocarbon emissions.

Therefore, reduced cyclic variation results in a number of improvements in both engine performance and reduced exhaust emissions.

In fact a correlation between the irregularities of combustion process and the exhaust emissions has been always assumed (59, 61). Tests on the effect of reducing cyclic variation by modifying ignition system design or increasing the charge turbulence tend to support the previous assumption (20, 27, 60), where it has been observed that factors which reduced cyclic combustion variation resulted in a corresponding reduction of exhaust emission level. Among these modifications of ignition system; are extended gap location, wider gap size, longer spark

duration, higher spark energy and smaller centre electrode diameter, Figs. (2-1 - 2-3). On the other hand, controlled turbulence in the combustion chamber represents another means of reducing combustion variation and consequently exhaust emissions. This could be accomplished by fitting swirl generators in the inlet port (60), inserting guide vanes on the valve seat (20) or using shrouded valves (2, 15). Fig. (2-4) shows the extension of the lean limit, (defined as the largest air/fuel ratio for operation without misfire), by using an inlet valve fitted with six guide vanes inclined at 60 degrees to the mixture flow direction. Fig. (2-5) shows the resultant effect on engine performance when this valve was used in conjunction with an improved ignition system and higher inlet air temperature. Also, increasing the small scale turbulence, which is generally observed to reduce cyclic combustion variation, could result in a reduction of unburnt hydrocarbons, especially where the turbulence is generated within a general mixture motion tangential to the chamber wall (28). Fig. (2-6) shows the effect of small scale turbulence on the unburnt hydrocarbons in a constant volume bomb where turbulence was generated by rapid opening and closing of a magnetic valve connecting the bomb to a variable volume chamber filled with the same mixture at higher pressure.

2.2 Choice of Characteristic Parameters as a Measure of Cyclic Variation

Investigators have employed various characteristic parameters for measuring the extent of cyclic variation in the cylinder pressure

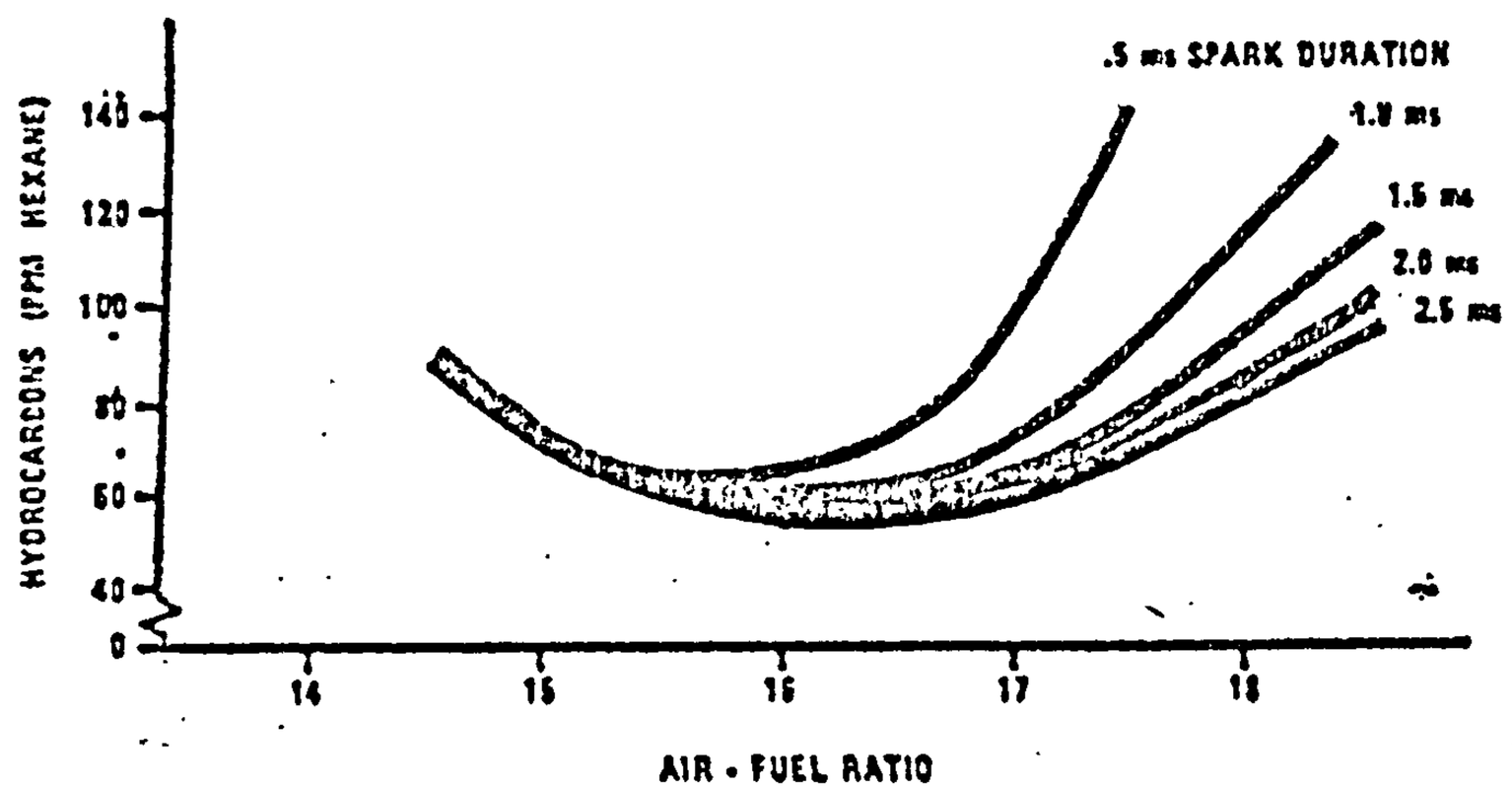

Fig (2-1). Spark duration effects on unburned hydrocarbons (27). (2000 r.p.m., 41 deg. spark advance, 0.89 mm spark plug gap and 4.37 mm gap projection).

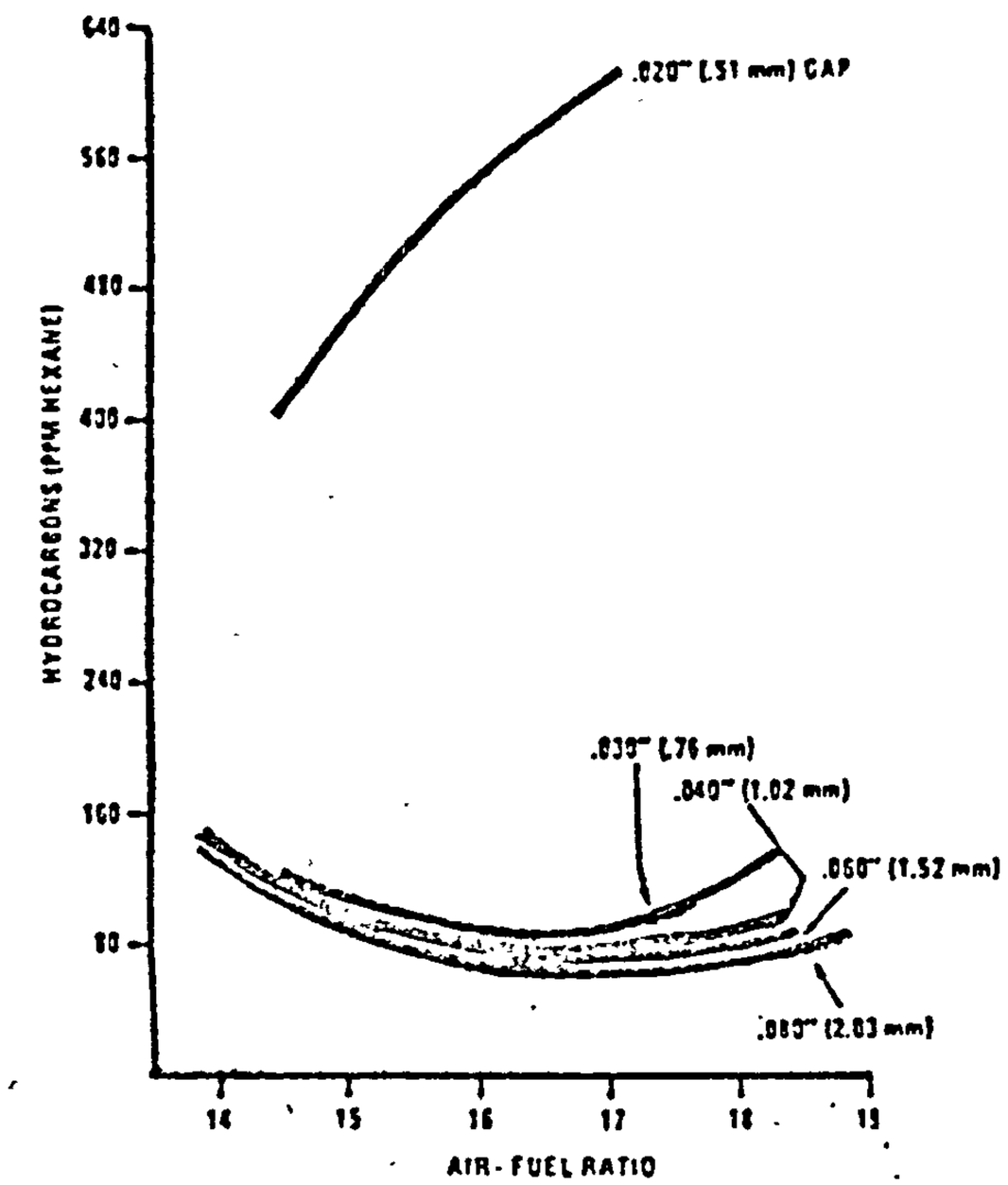

Fig. (2-2). Effect of gap size on unburned hydrocarbons (27). (2000 r.p.m., 41 deg. spark advance, 1.0 m sec spark duration and 4.37 mm spark plug gap projection).

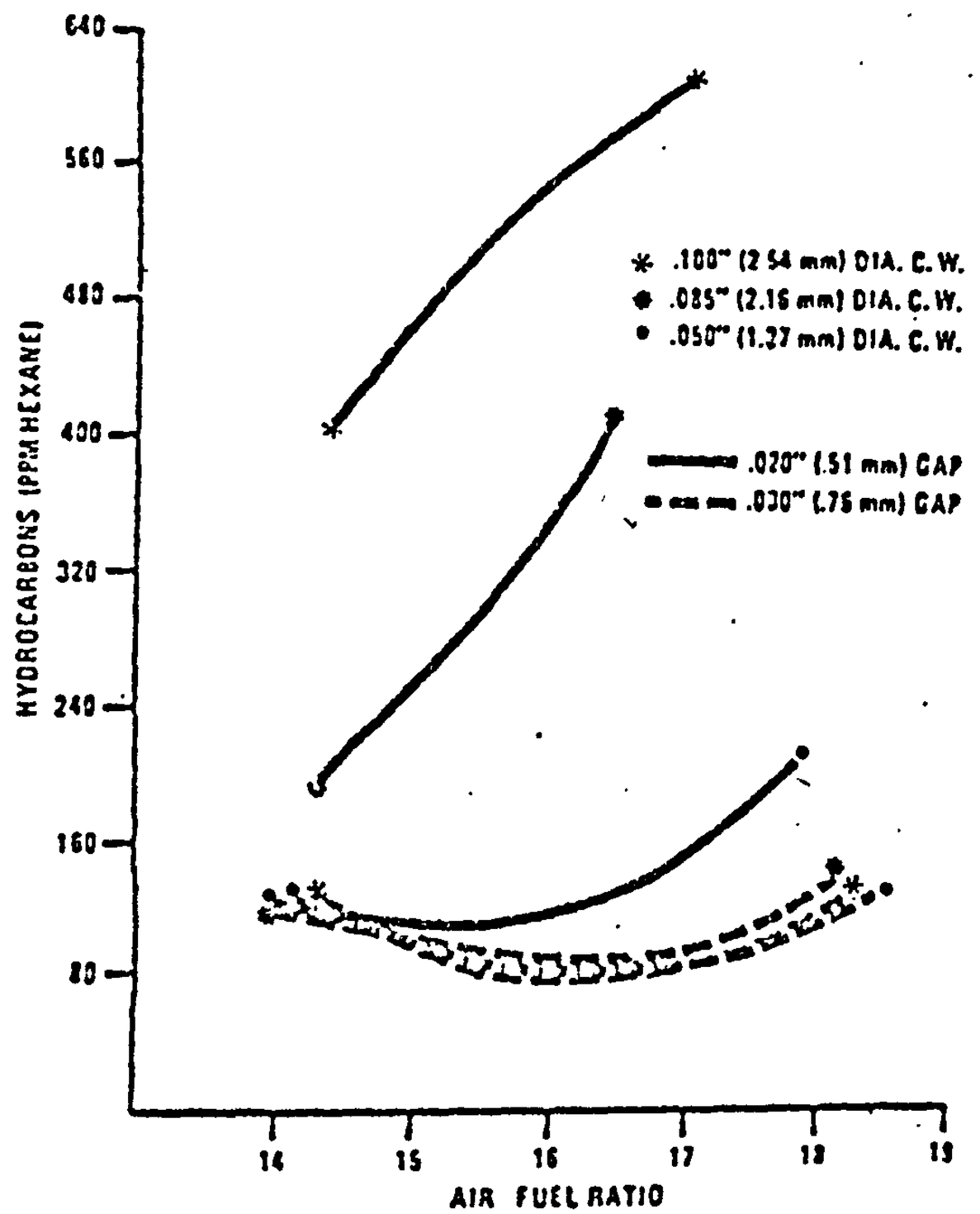

Fig (2-3). Effect of centre electrode size on unburned hydrocarbons (27).
(2000 r.p.m., 41 deg. spark advance, 1.0 m sec spark duration and 4.37 mm spark plug gap projection).

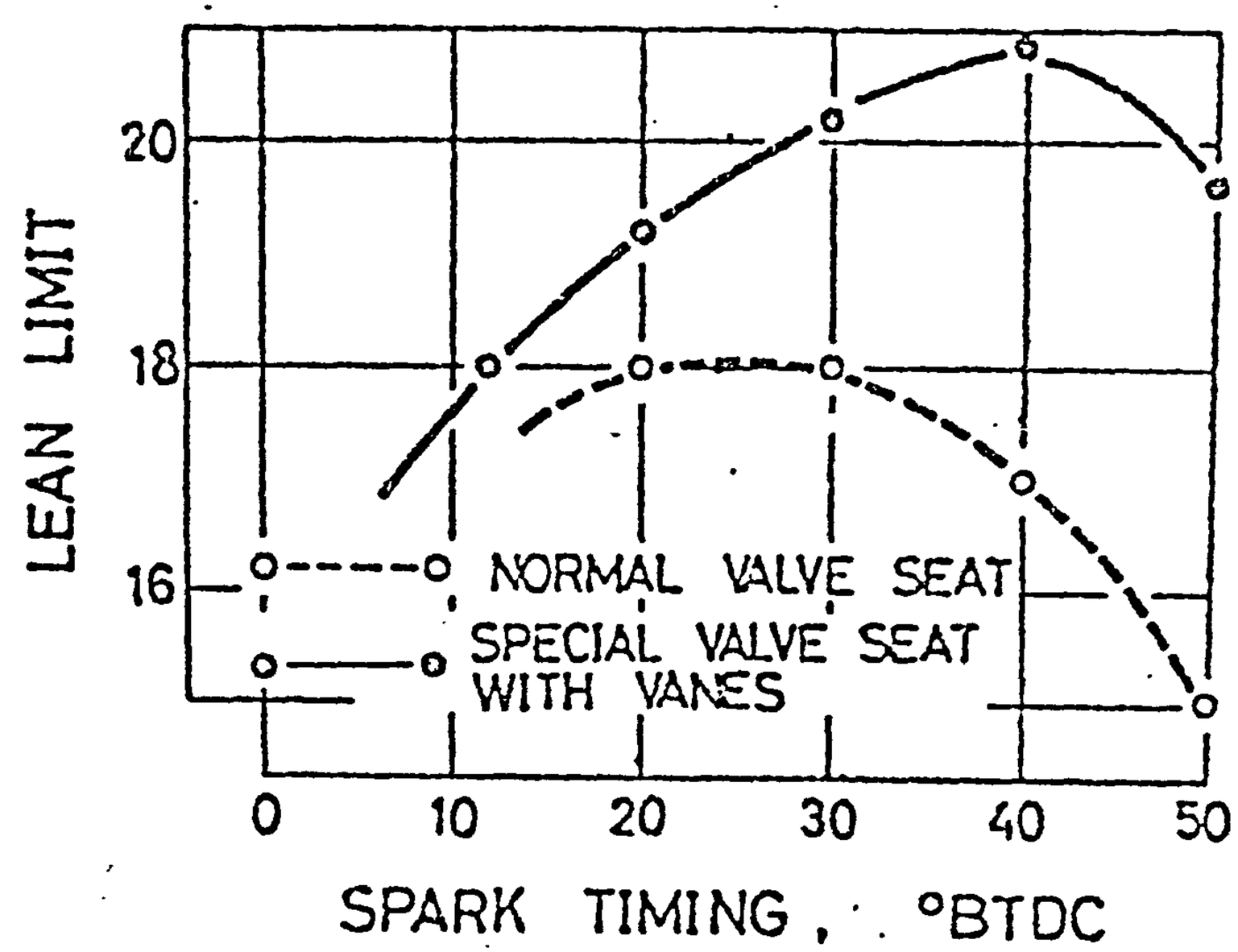

- Effect of mixture turbulence on lean limit

Fig. (2-4). Effect of mixture turbulence on lean limit (20).

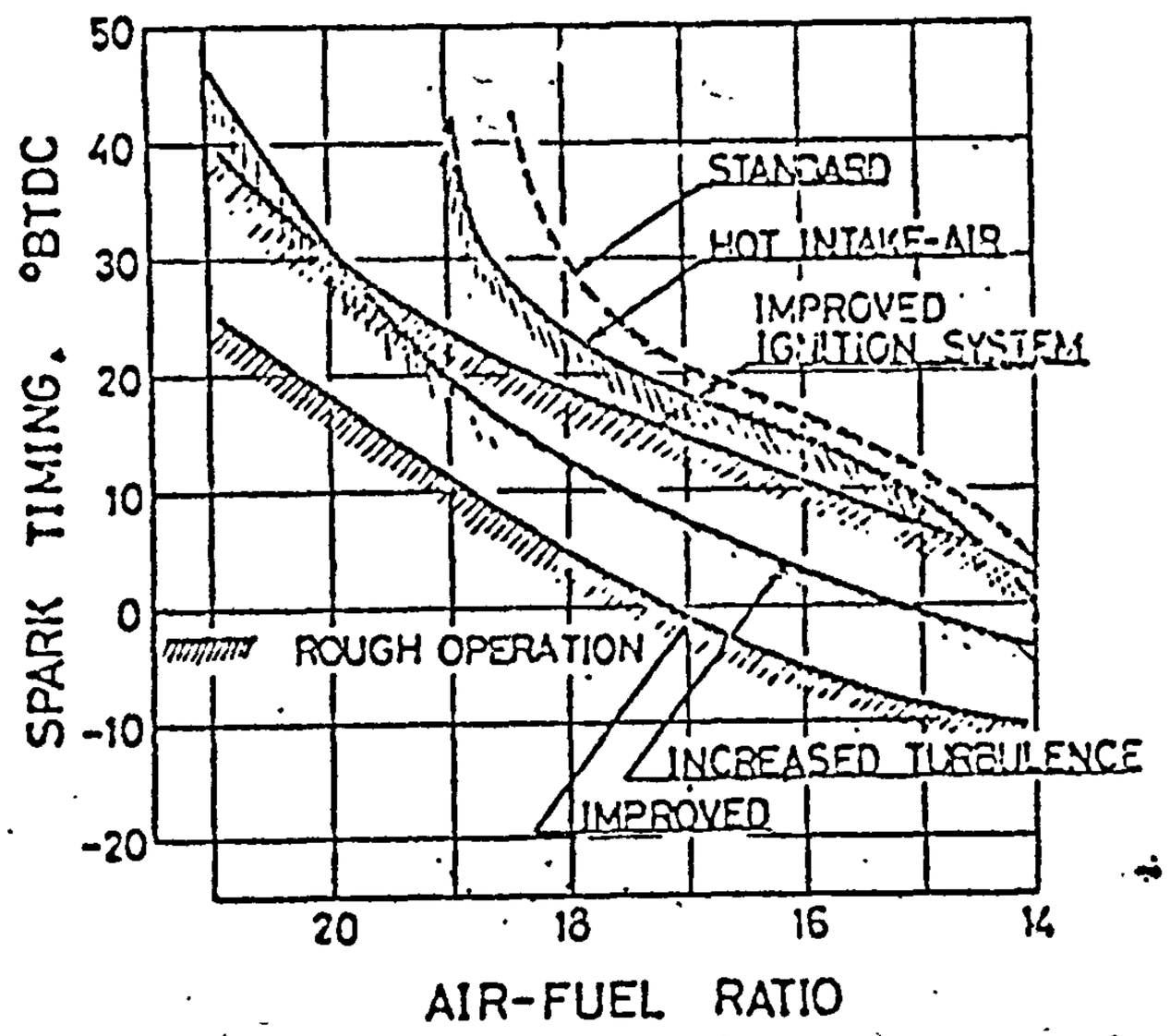

Fig. (2-5). Widening of the zone (air/fuel ratio and spark timing) of smooth operation by different engine modifications (20).

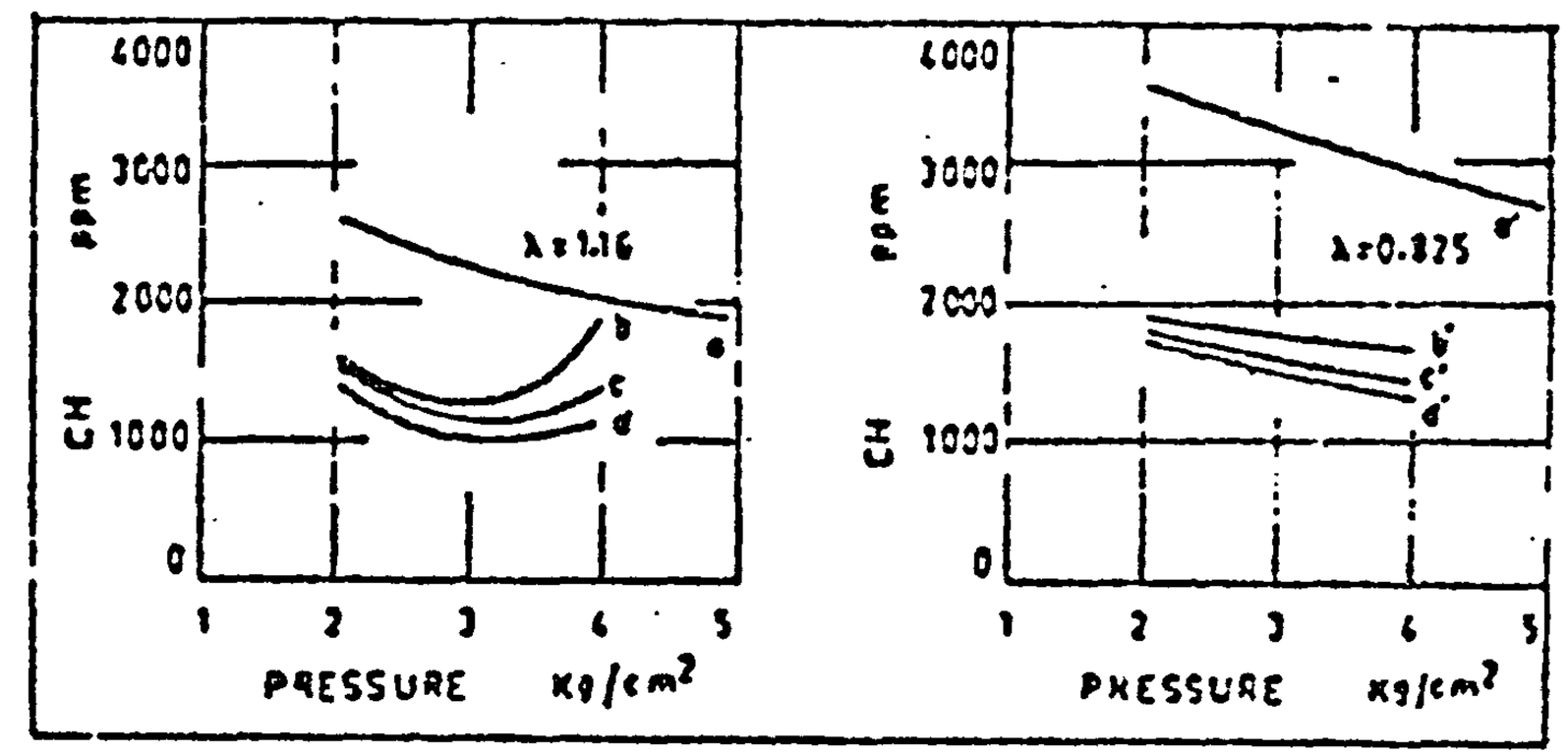

Fig. 2(2-6). Effect of small scale turbulence on unburned CH_4 concentration (ppm of dry exhaust products) at different initial pressure. Curves a and a' for ignition under quiescent conditions, b, c, d, b', c' created with pressure difference 1 Kg/cm^2, chamber volume for b and b', 250 cm^3, c and c', 120 cm^3, and d and d', 30 cm^3, time of ignition 30 msec after closing the magnetic valve (28).

development of spark ignition engines. One can summarize the most important ones as follows:-

i) Maximum cylinder pressure, (P_{max}).

ii) Maximum rate of pressure rise, ($\dot{P}_{max}$).

iii) Crank angle of occurrence of $\dot{P}_{max}$ or P_{max} relative to TDC , ($\theta_{\dot{P}_{max}}$) and $\theta_{P_{max}}$ respectively.

iv) The time for the flame front to travel across the combustion chamber or across any specified path or the apparent flame propagation velocity as given by the distance of flame travel divided by flame travel time.

v) The time of pressure rise to a certain arbitrary value of the compression pressure measured from the time of ignition.

vi) The indicated work per cycle (i.m.e.p).

vii) The mass burning rate.

The maximum cylinder pressure (P_{max}) and the maximum rate of pressure change ($\dot{P}_{max}$) are very sensitive to cyclic variation and were employed as characteristic parameters in most of the studies on the cyclic combustion variations (2, 10, 12, 13, 32), because of the easiness in their measurements, Figs. (1-1), (2-7). Moreover, Barton et al (10) have shown that there is a one to one correlation between P_{max} and $\dot{P}_{max}$ Fig. (2-8), hence one or the other need be considered. The disadvantage of using only P_{max} or $\dot{P}_{max}$ is that it depends on the entire combustion process and does not provide specific information about the combustion process variation.

Soltau (4) and Burgett (27) have studied the problem in terms of the indicated mean effective pressure of each cycle, Fig. (2-9). This reflects directly the effect of cyclic variation on engine brake torque variations.

Peters and Borman (33) have used the mass burning rates (which could be estimated from the curves of mass burned fractions versus crank angles), as a parameter characterising the cyclic variation, since it is closely related to the rate of pressure change. Low peak pressure cycles have a much smaller burning rate initially after the spark than high pressure cycles Figs. (2-10(a) and 2-10(b)). Peters and Borman also noticed that the low peak pressure cycle continued to be lower than the high pressure cycle even after the combustion was well under way.

Many investigators have concentrated on variation of flame front speed because of its close relationship to the possible causes of cyclic variation. Measurements of flame travel times between ionisation probes located in the combustion chamber or the reciprocals of these travel times as a representation of the flame speeds, were studied statistically (29-31), (34), (35), Fig. (2-11). However, as the flame front in an engine travels at a varying rate, it was difficult to elucidate the phenomenon systematically when the effects of operating conditions are taken into account. Harrow and Orman (30) have derived the flame arrival frequency by expressing the number of flames reaching ionisation gaps, (located at 15.6mm and 65 mm from the spark plug gap), as a percentage of the number of cycles. Two criteria were

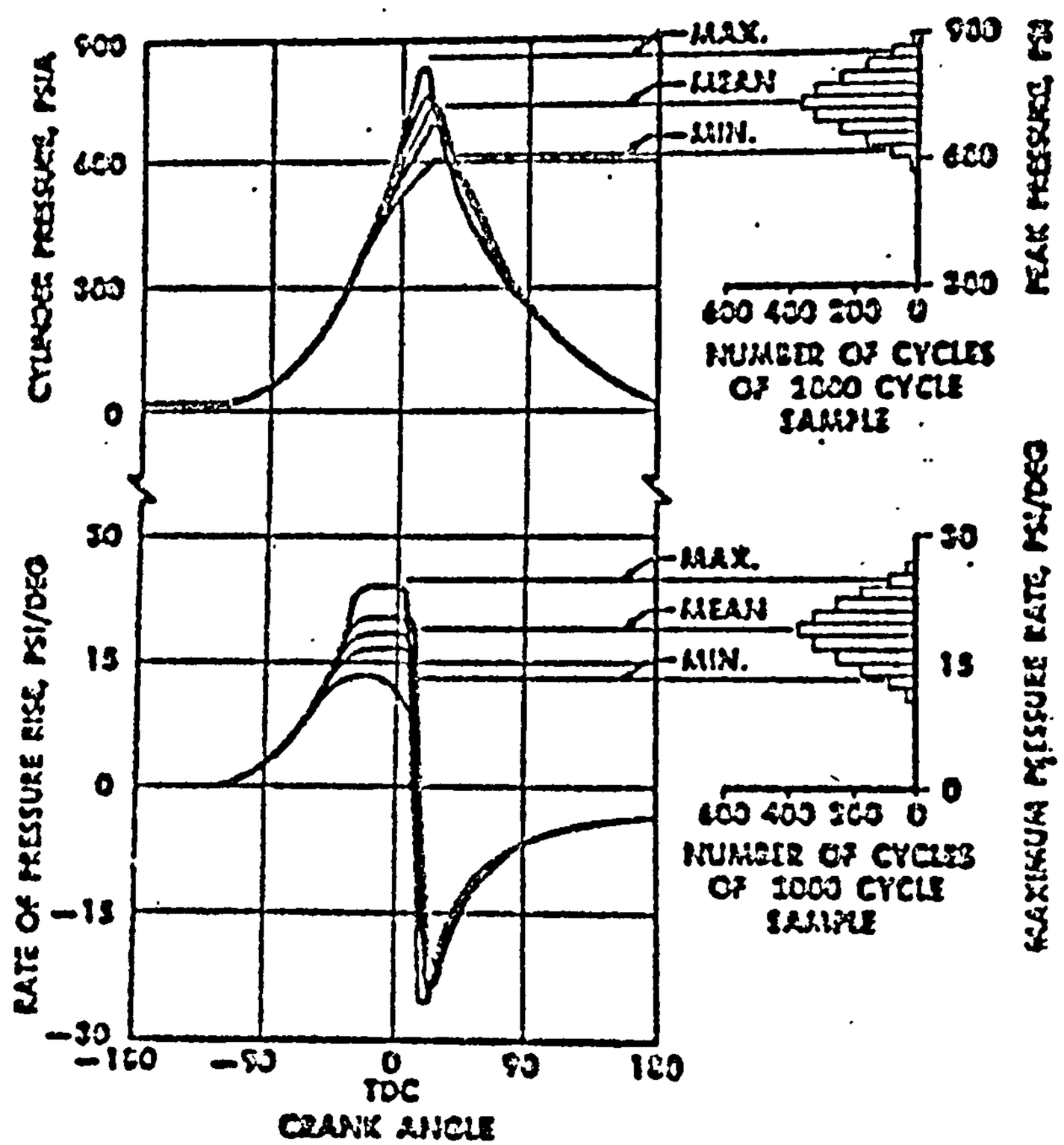

Fig (2-7). Pressure-time and rate of pressure rise records for 2000 cycles showing cyclic variations.

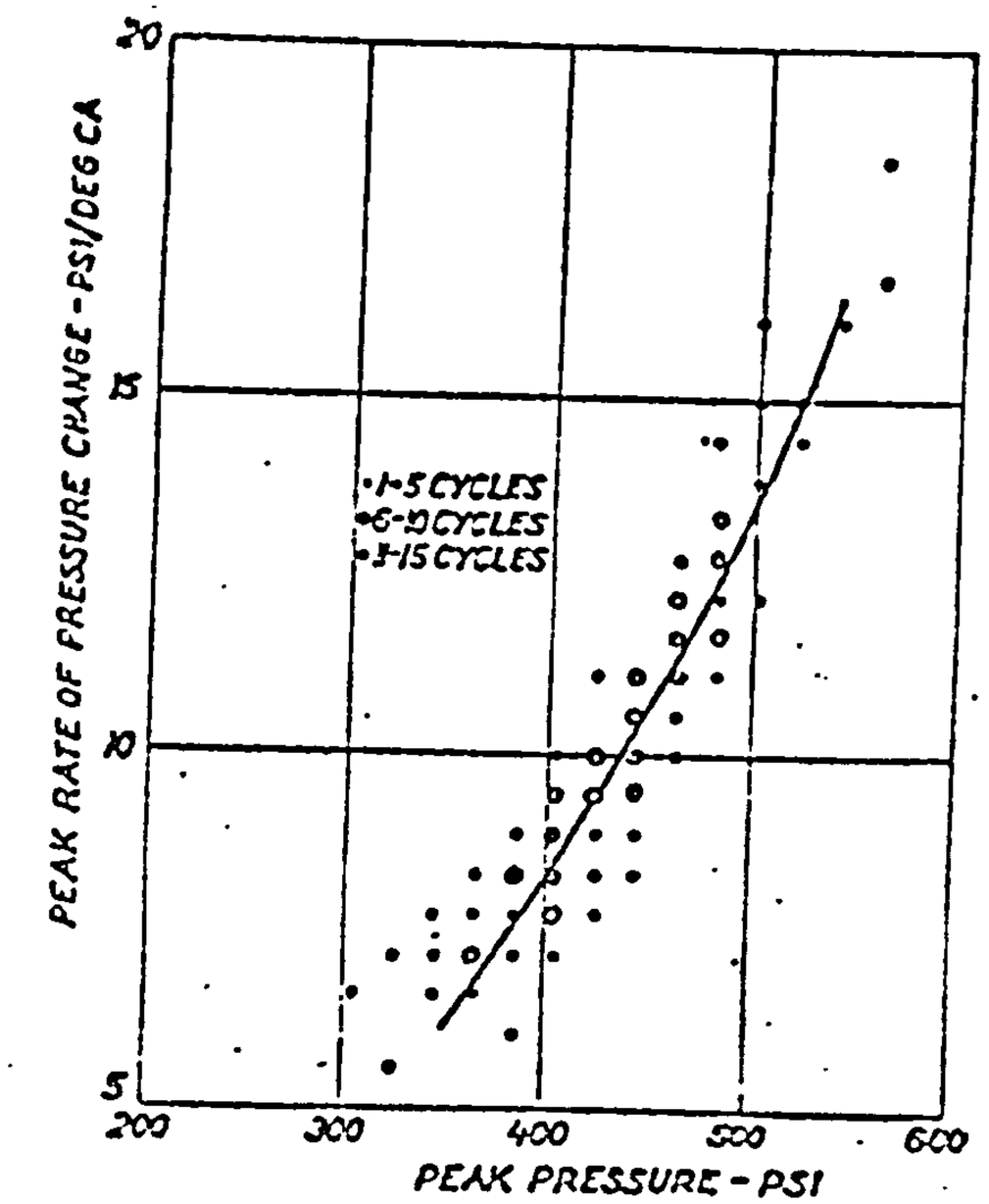

Fig (2-8). Correlation between peak pressure and peak rate pressure change (10).
(1200 r.p.m. and 15.2 air/fuel ratio).

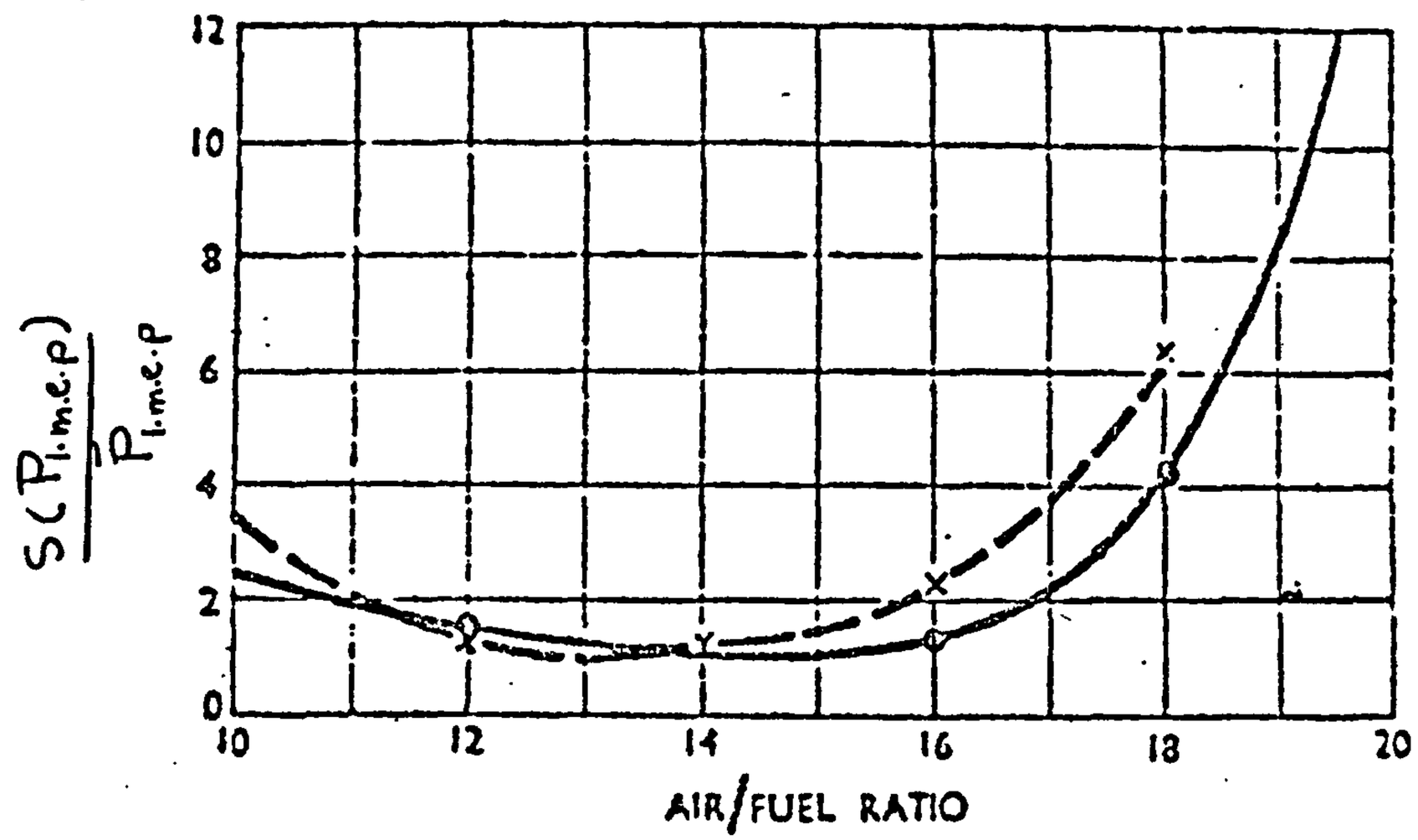

Fig (2-9). Variation of the coefficient of variation with air/fuel ratio at different compression ratios (4). Compression ratio - 10:1 ------- 9:1.

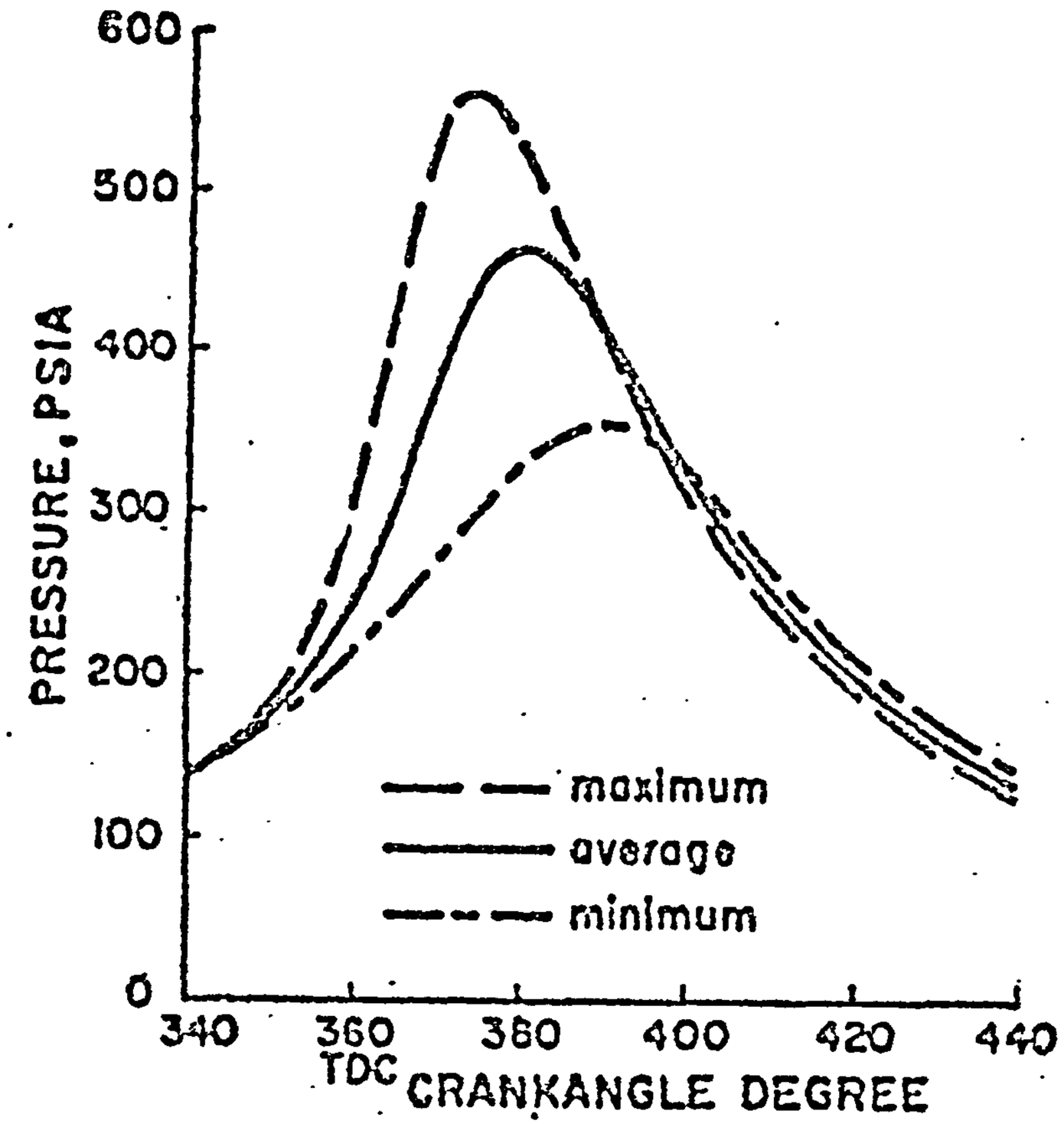

Fig. (2-10a) Data for 300 individual cycles indicating that there is a substantial spread between the maximum and minimum pressure traces (33).

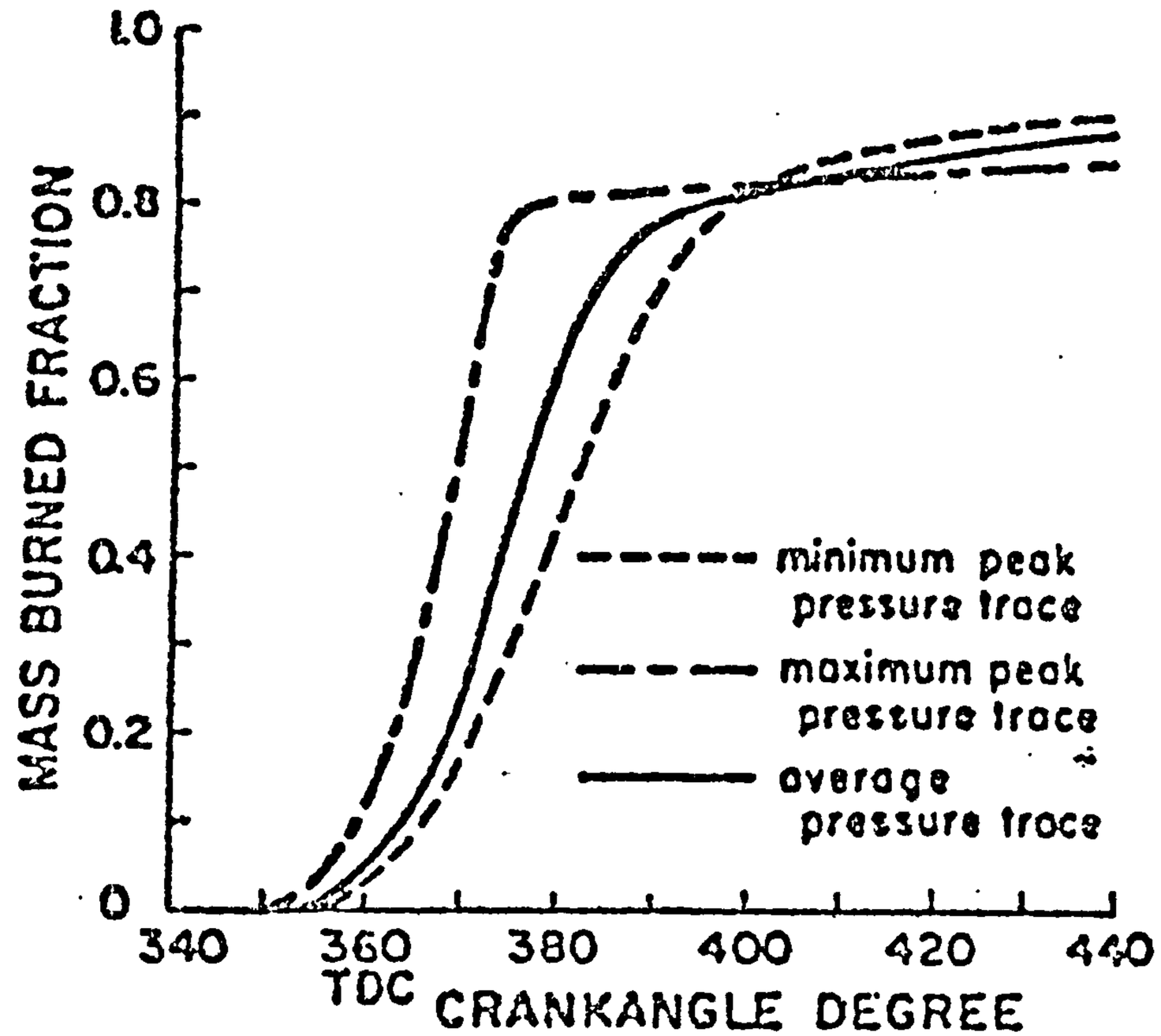

Fig. (2-10b). Mass burned fraction versus crank angle for three cycles showing that low peak pressure cycle corresponds to small burning rate.

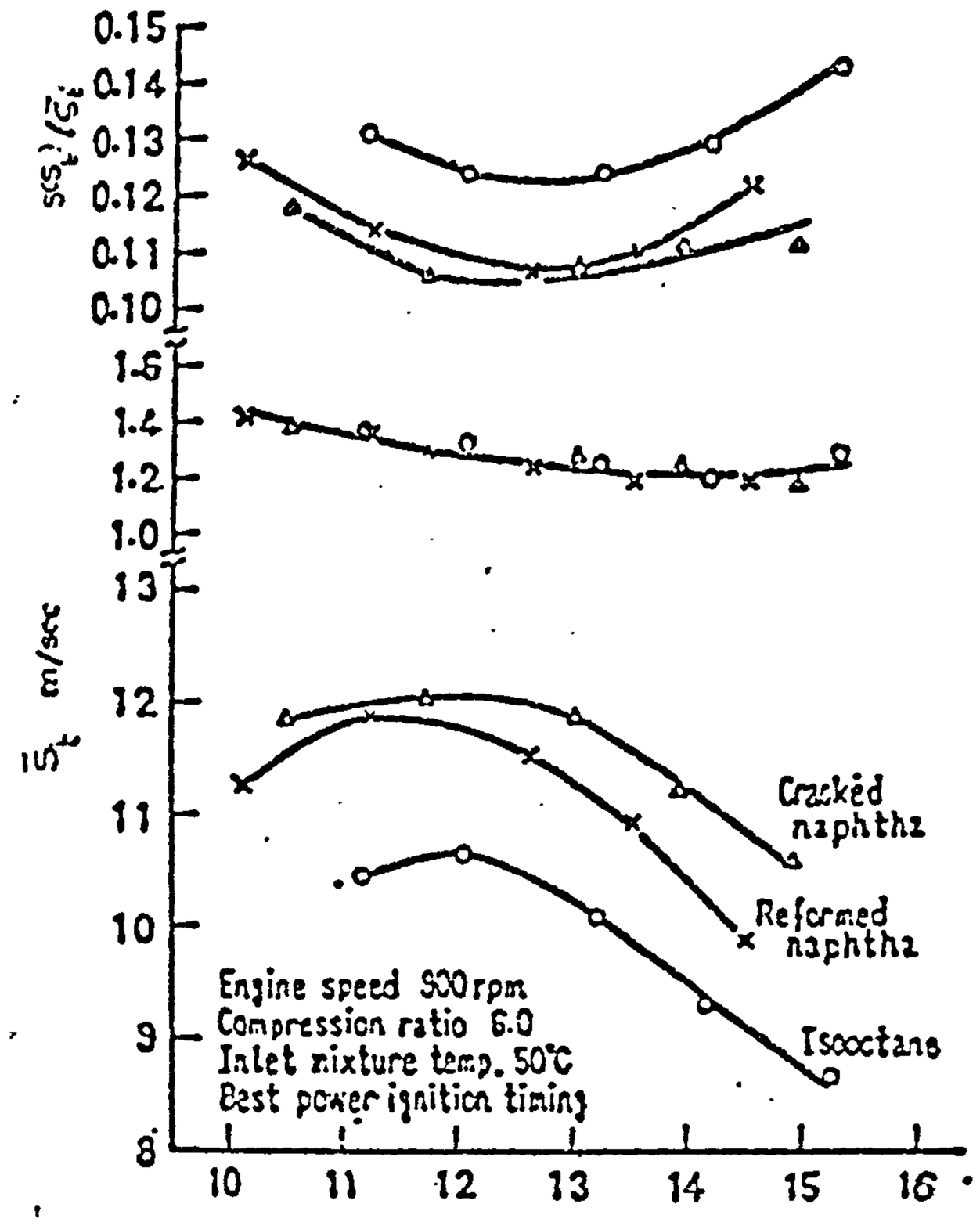

Fig. (2-11). Changes of mean apparent flame propagation velocity, standard deviation and coefficient of variation with air/fuel ratio (30).

employed on the distribution curve to represent combustion characteristics. Firstly, the time interval between the instant of spark and the point at which 50% of the flames have arrived was taken to describe the mean flame travel time (t_b) and secondly, the time interval between the 10% and 90% point on the flame arrival curves was taken as describing the extent of cyclic dispersion, Figs. (2-12) and (2-13).

Other characteristic times were employed by different investigators. Barton et al (10) have used the time between ignition and the instant of maximum pressure or maximum rate of pressure rise ($\theta_{P_{max}}$ and $\theta_{\dot{P}_{max}}$), while Annand et al (9) have used the time between ignition and the attainment of three times the compression pressure as characteristic time Fig. (2-14). Winsor (23) used the time between ignition and the cessation of combustion as a characteristic burn time, where the cessation of combustion was selected to be the time at which curves for the rate of pressure change with and without ignition intersects Fig. (2-15).

2.3 The Effect of Engine Operating Variables on the Extent of Cyclic Variation.

The engine cycle pressure variation is a direct consequence of variations in the progress of the combustion process and the rate of energy releasedby combustion. The various operating characteristics which were discussed in the literature as affecting cycle to cycle variation in combustion rate and pressure are:-

i) Ignition.

(Number of sources, timing, energy and duration).

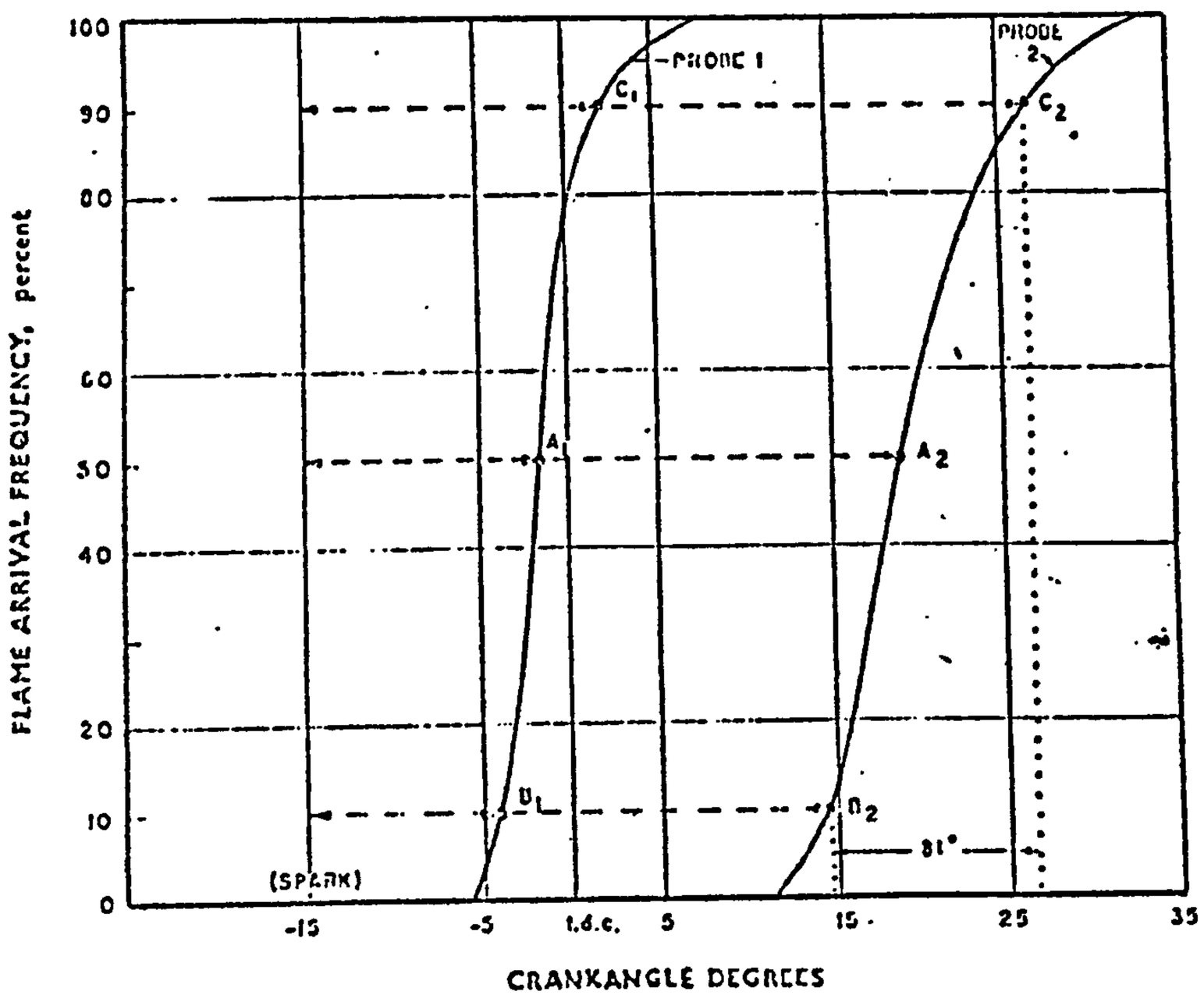

g (2-12). Typical flame arrival curves for two ionisation probes, located at 15.6 mm and 65 mm from the spark plug gap (30).
(1000 r.p.m., 10:1 air/fuel ratio and 15 deg. B.T.D.C. spark timing).

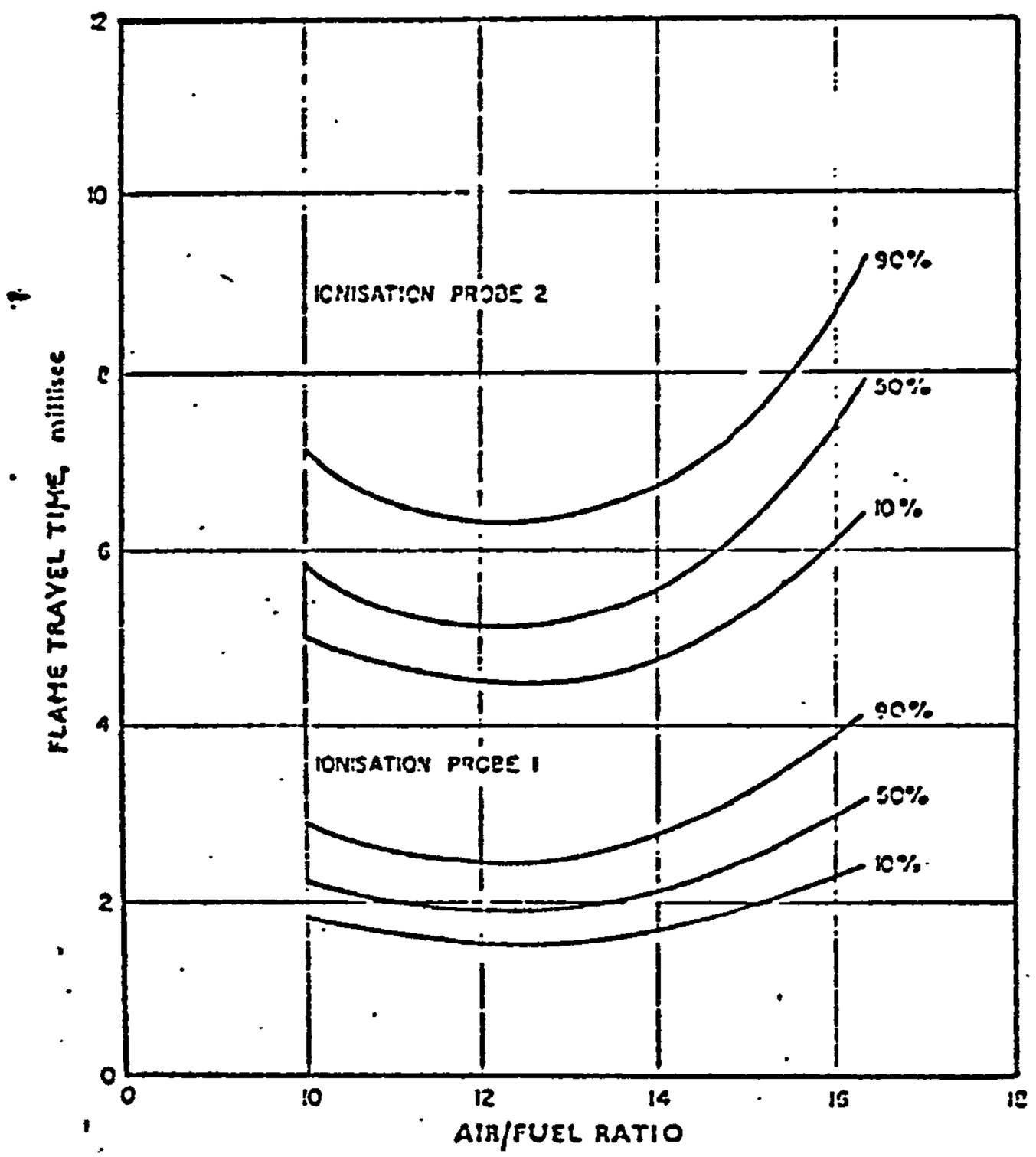

Fig (2-13). Variation of flame travel time with mixture strength (30).
(Iso-octane fuel, 1000 r.p.m. and 15 deg. B.T.D.C. spark timing).

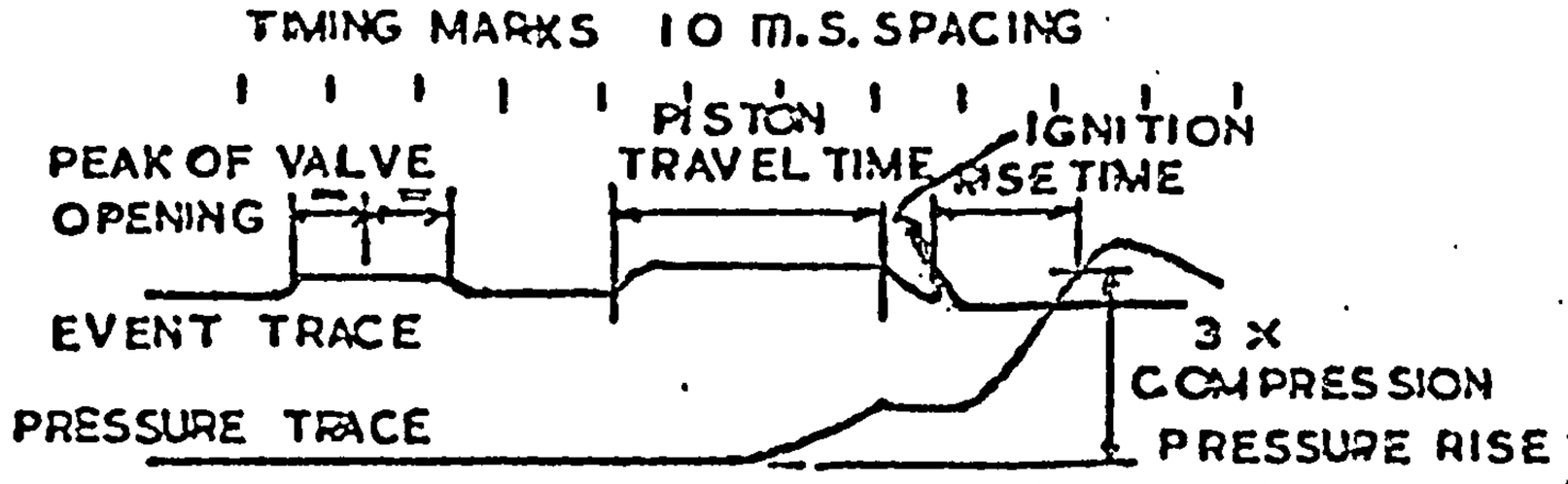

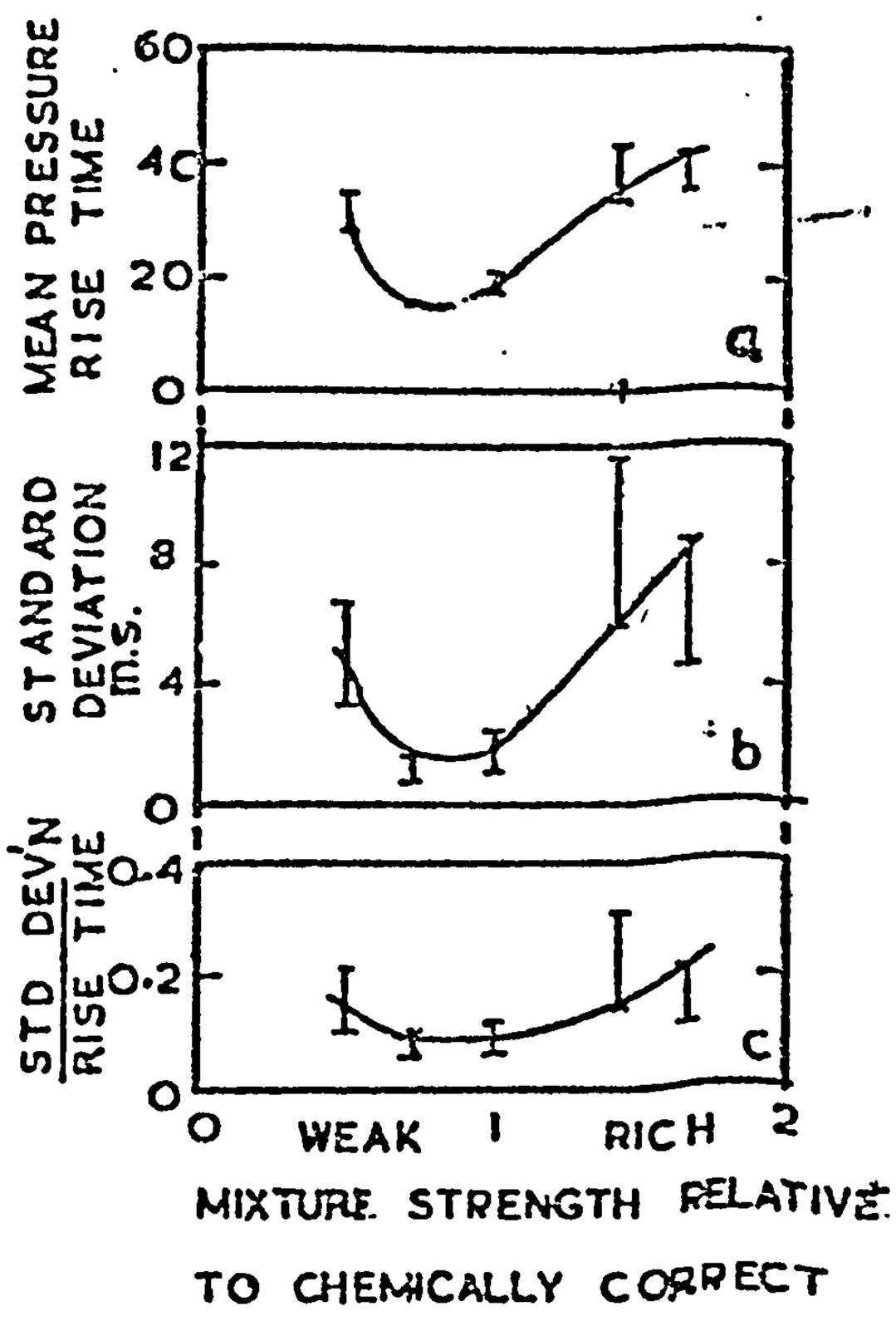

Fig (2-14). Effect of mixture strength on pressure rise time and its standard deviation (9).

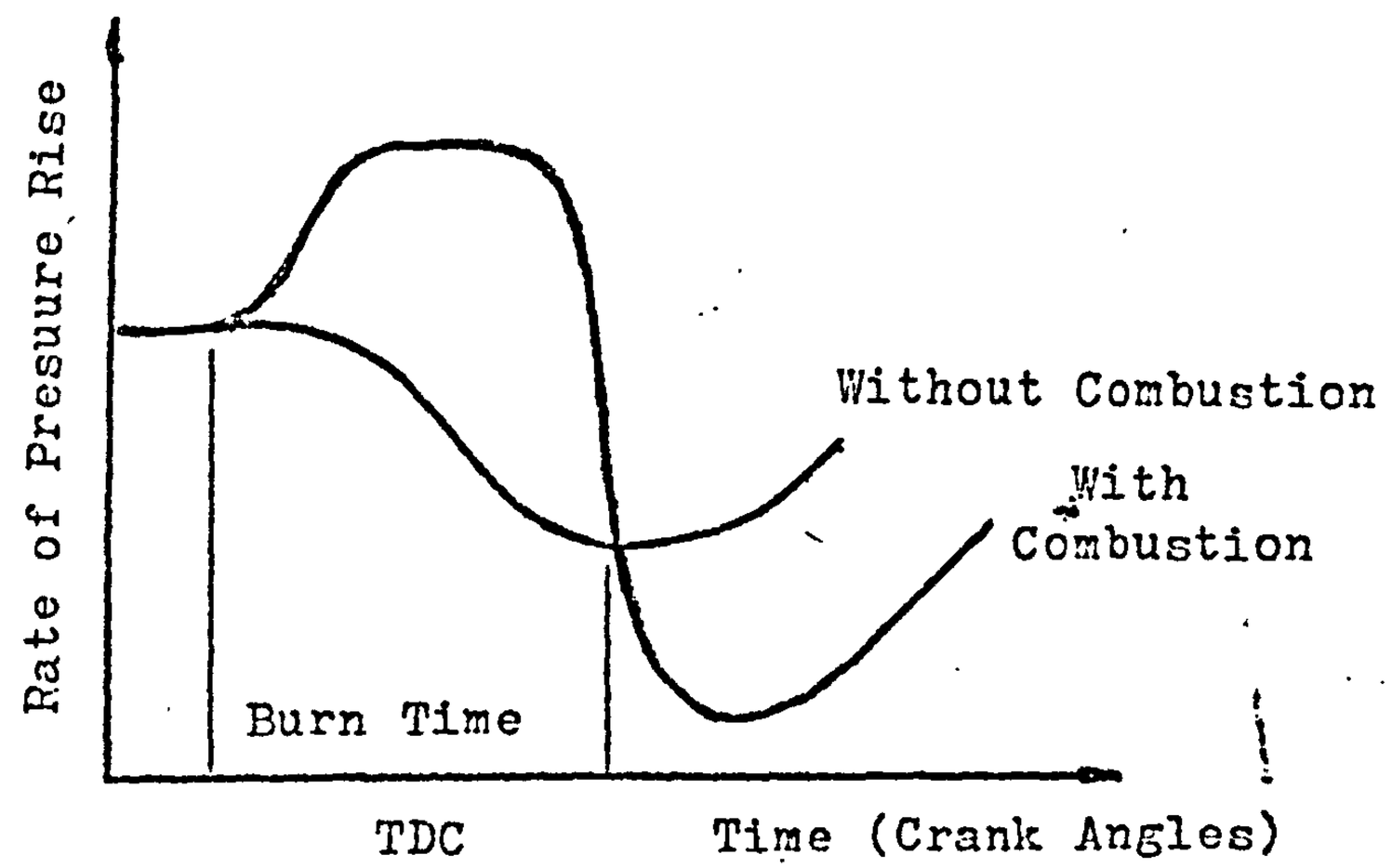

Fig (2-15) Definition of burn time (23).

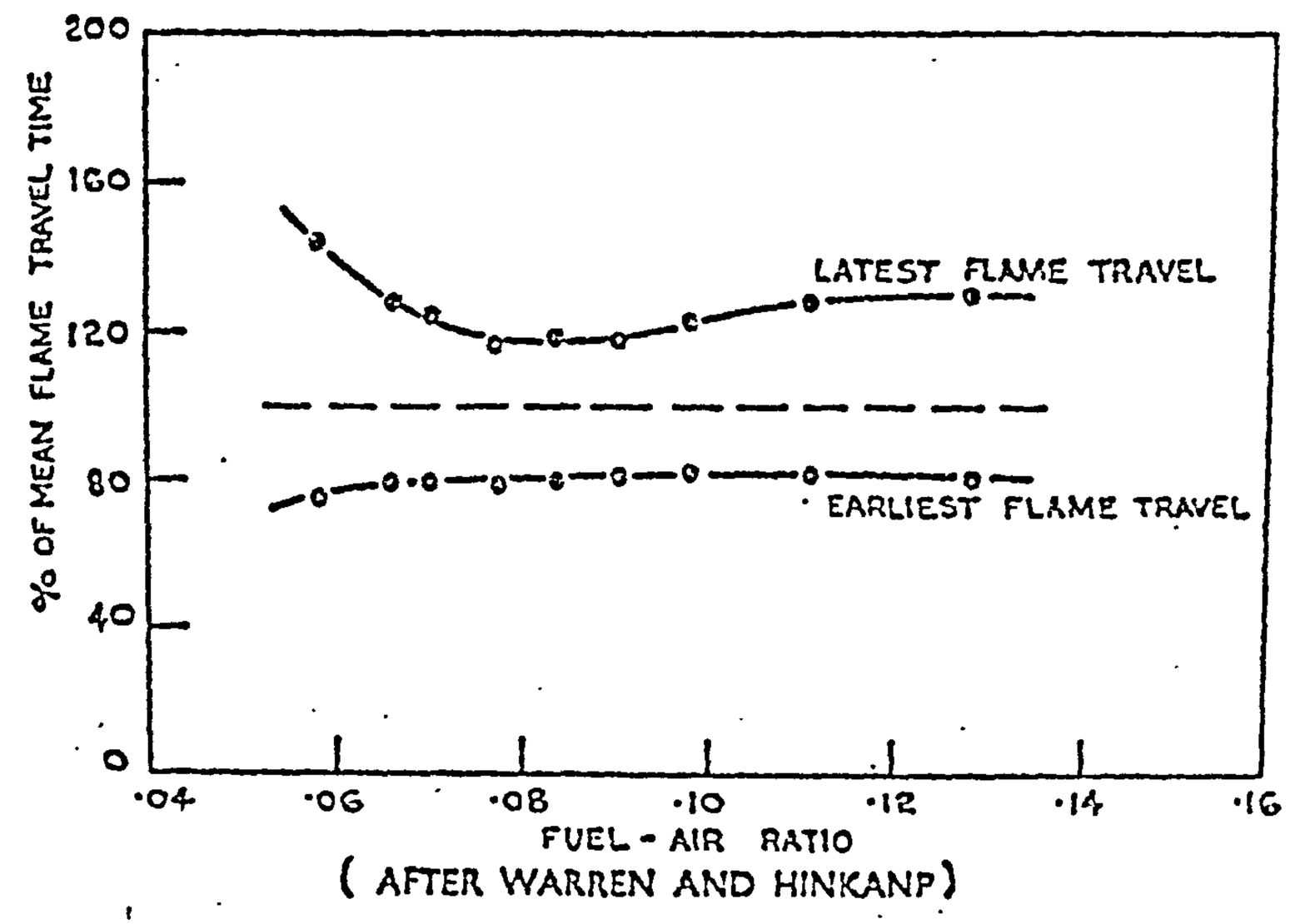

Fig (2-16). The extreme boundaries of flame travel timo versus fuel/air ratio, measured by ionisation gaps (56).

ii) Mixture preparation.

iii) Exhaust gas dilution of the charge.

iv) Compression ratio.

v) Throttling.

vi) Temperature.

(Initial charge and engine coolant).

vii) Oil contamination of the charge.

viii) Air/fuel ratio.

ix) Fuel composition.

x) Mass of the charge per cycle.

xi) Turbulence and mixture motion as a function of: engine speed, intake charge motion, and combustion chamber design.

In almost all investigations, the engine variables affect significantly the extent of cyclic variation. This is not unexpected, as changes in air/fuel ratio, compression ratio, speed and inlet configuration should alter the combustion process specifically, flame speed and the effect of turbulence on flame speed. The average flame speed and the variation of flame speed are considered to be the most important causes of combustion variation. Any operating condition which is not repeated from one cycle to another influences the progress of the combustion process and causes cyclic variation. This will increase the longer the time taken for the flame to traverse the chamber and hence the slower the flame propagation, the greater is the cyclic dispersion (56), Fig. (2-17).

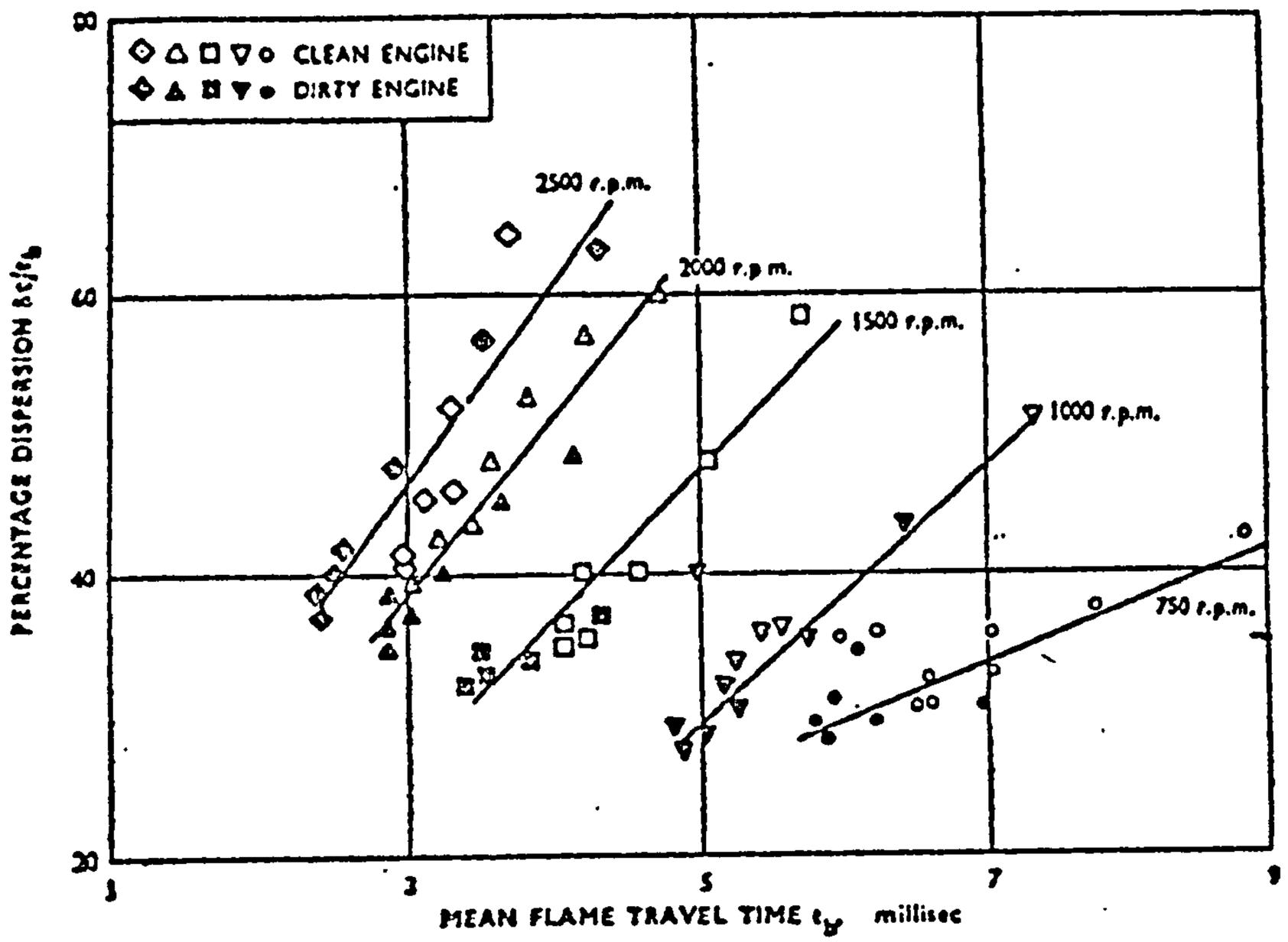

Fig (2-17). Relation between the percentage dispersion (δ_t/t_b) for iso-octane at various engine speeds (30).

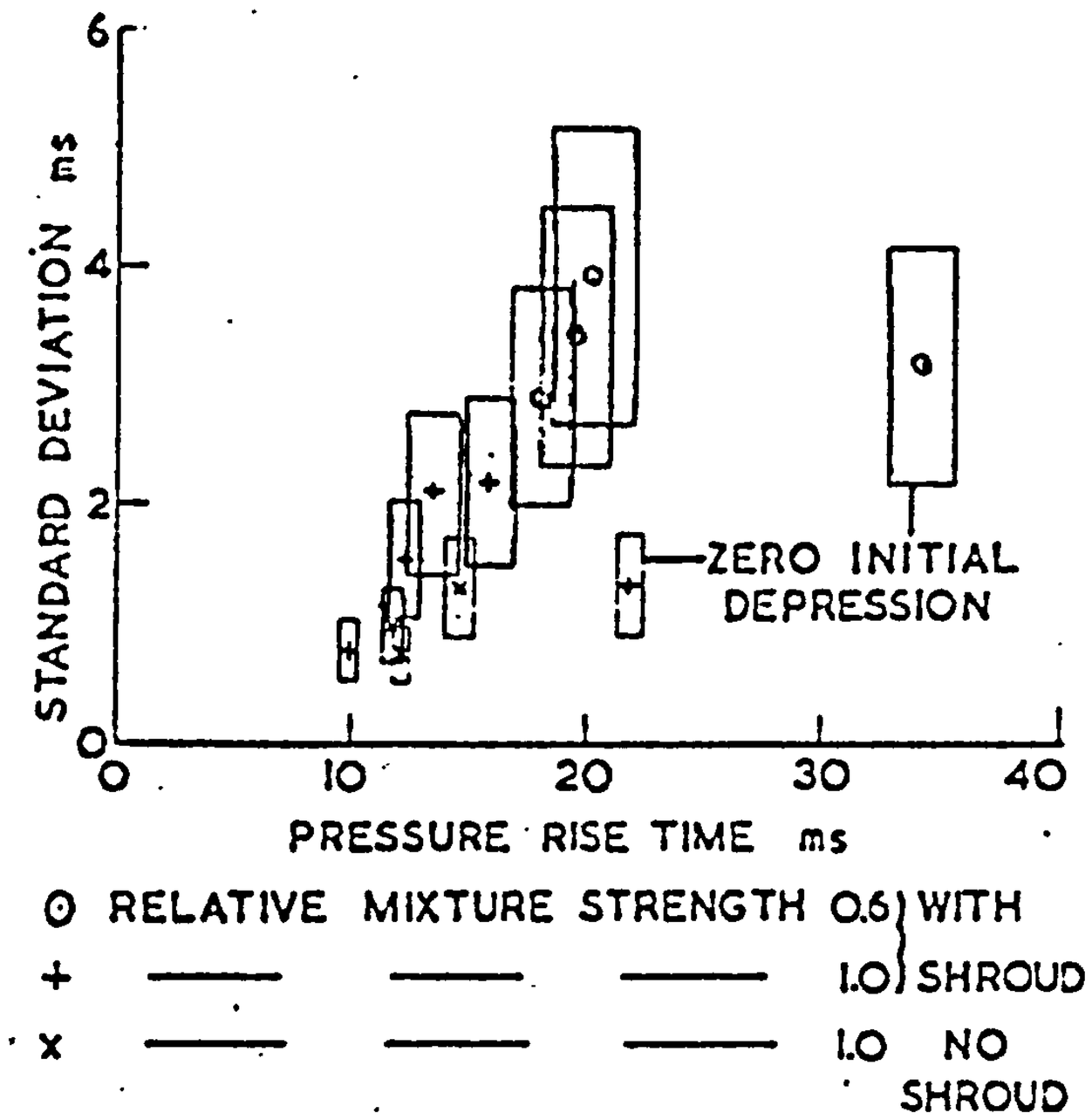

Fig (2-18). Standard deviation as a function of mean pressure rise time (9).

Harrow et al (29, 30) have shown that the relative dispersion in the flame travel time is almost proportional to the propagation time, Fig. (2-17). Similar results are reported by Winsor (23). This is also supported by the observation of Annand et al (9) that the standard deviation of the pressure rise time, (as defined earlier), which was taken as an indication of the rate of combustion, decreases as the rise time itself decreases, Fig. (2-18).

2.3.1 Ignition

There are several factors in the ignition system which could alter the ensuing combustion process in the cylinder head. These are:-

i) The timing of the spark in relation to the piston motion.

ii) The type of the spark.

iii) The energy content of the spark.

iv) The igniter position.

v) The number of ignition sources.

vi) The spark plug gap projection.

vii) The spark plug gap size.

viii) The physical configurations of the sparking plug electrodes.

ix) The size of the spark electrode.

Most earlier investigations (2, 4, 32) of the cyclic pressure variation problem have concluded that its extent under normal operating conditions appears to be independent of the characteristics of the spark ignition system and improves when more than one sparking plug is used Figs. (2-19) and (2-20).

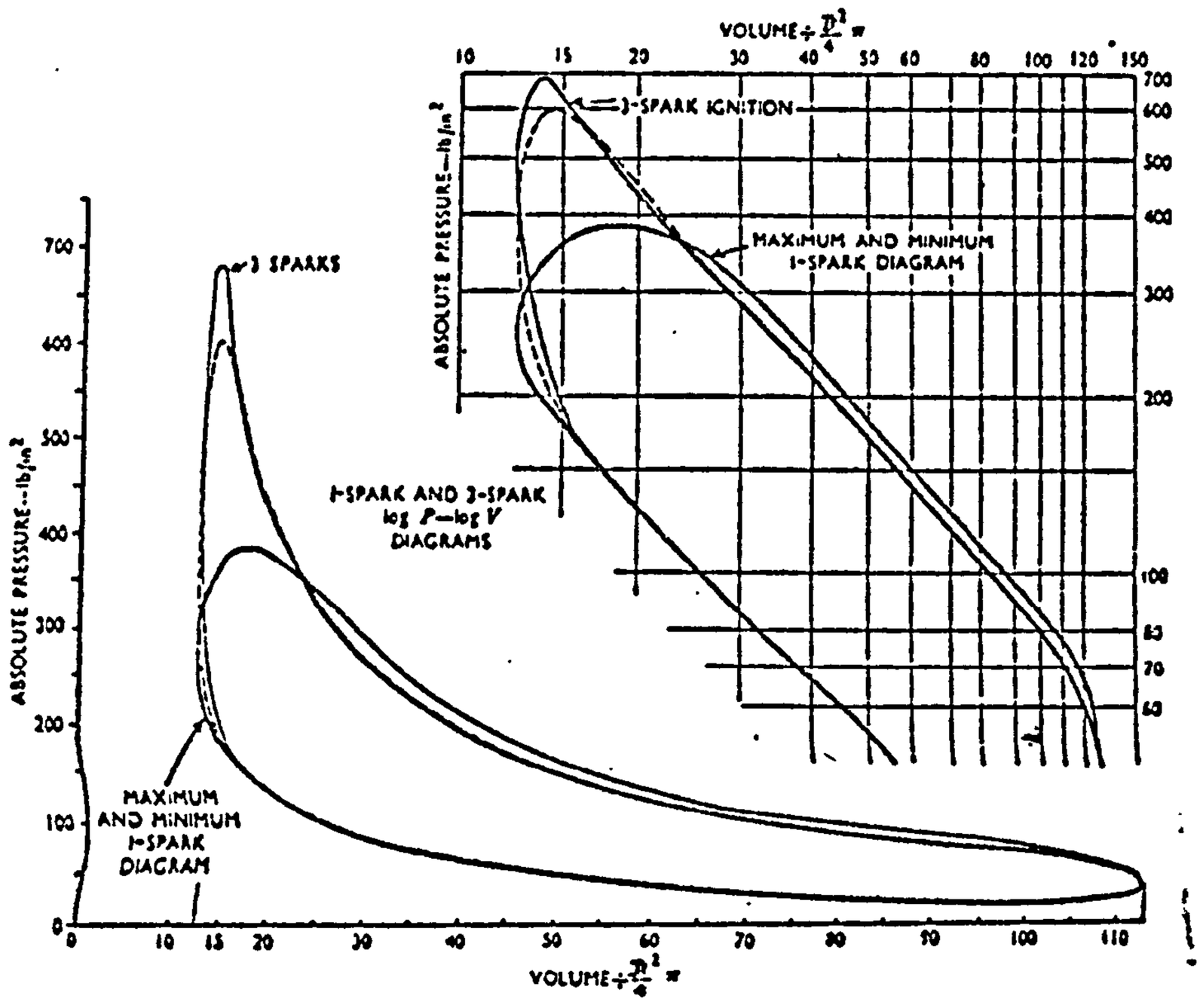

Fig (2-19). One and three spark P-V diagrams. Ignition timing giving identical torque (4).

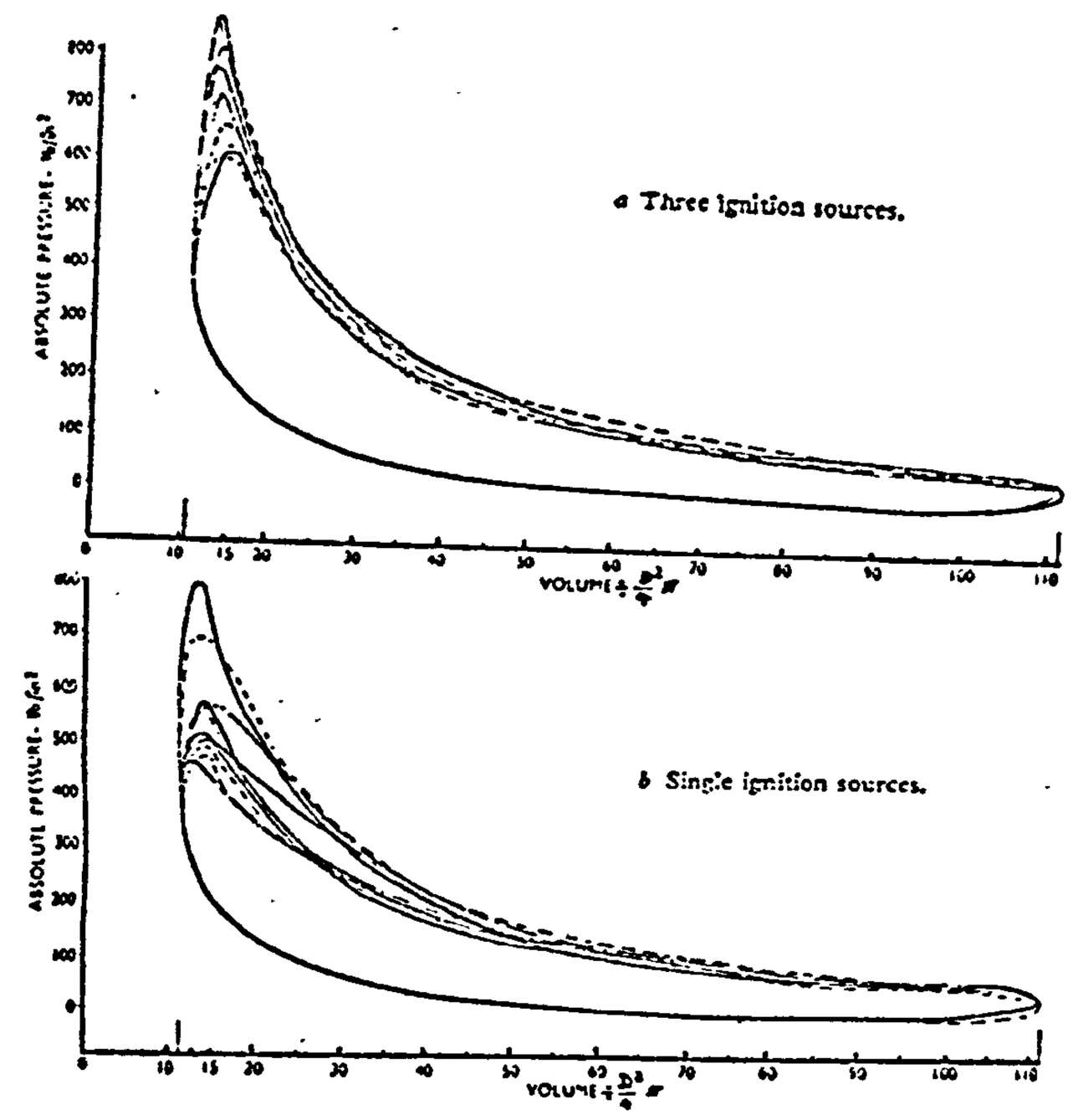

Fig (2-20). Ten consecutive cycles with weak mixtures with one and three ignition sources (4).

However, some recent research studies (20, 27) have shown that some improvement in the cyclic combustion variation could be obtained, especially with lean mixtures, by proper design of the spark plug and ignition systems, Figs. (2-21 - 2-27). These modifications could be summarized in the following points:-

i) Increasing the gap penetration into the combustion chamber reduces cyclic variation due to the increased heat release from the flame kernel before contact with the cylinder walls, thereby reducing wall quenching Fig. (2-28). Moreover, this introduces favourable conditions for the flame kernel growth due to the increased temperature of the electrodes and consequently the reduction of their quenching effect on the kernel.

ii) Increased gap size and spark duration increases the probability of igniting lean non-homogeneous mixture by exposing a larger volume of the mixture to the ignition source.

iii) Increased spark energy, may overcome the quenching effect of spark plug electrodes particularly for narrow gap widths or when the spark timing is so advanced that the mixture pressure and temperature are low.

It is also required when the mixture velocity and turbulence levels are high Fig. (2-29). For the former case, the heated volume is increased due to the mass motion during the spark discharge, thus the energy is distributed over a larger mixture volume. For the latter case, the rate of heat dissipation is increased by the higher turbulence intensities and the corresponding increase in the eddies diffusivity.

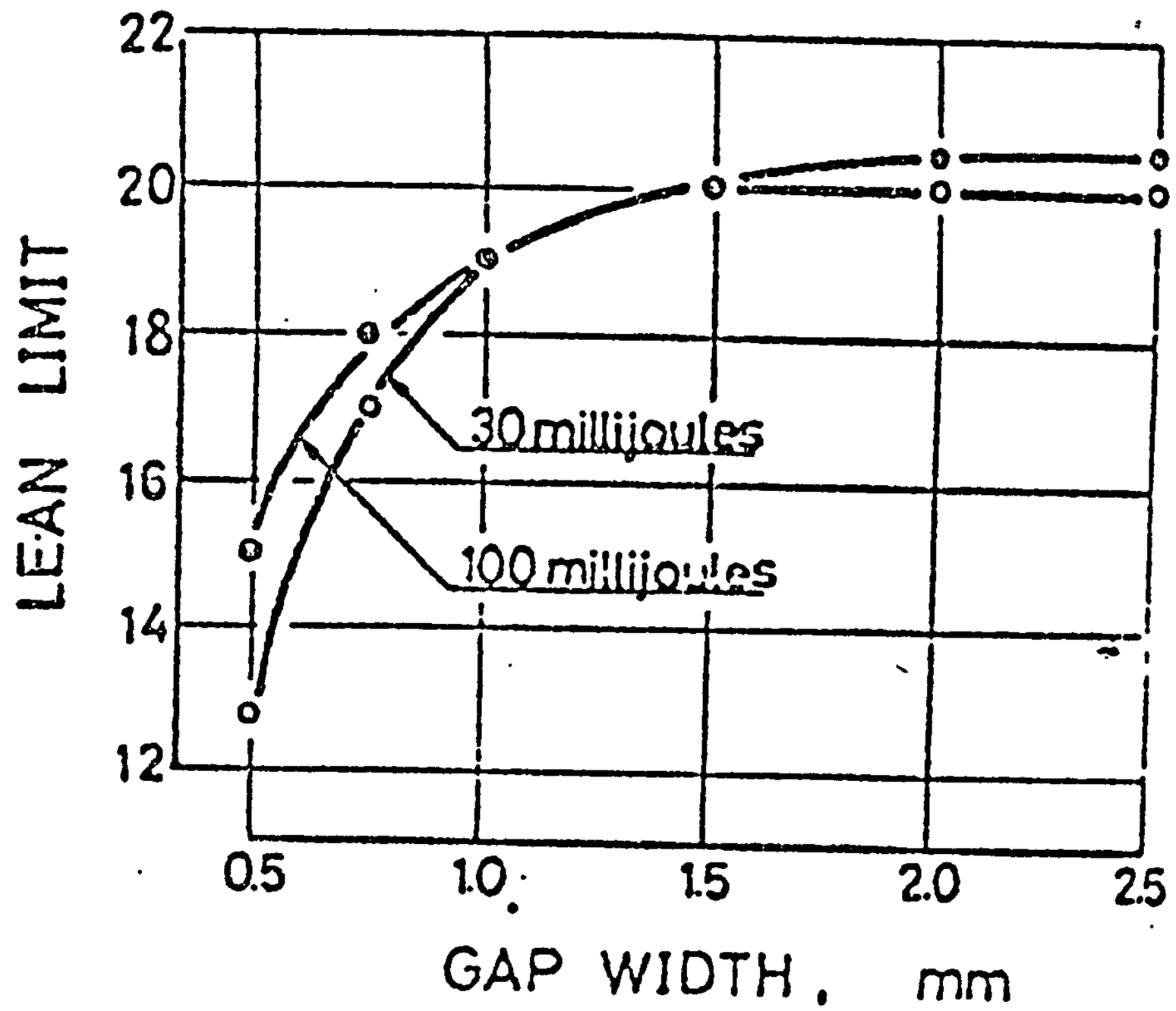

Fig (2-21). Effect of spark energy on the lean limit (20). (40 deg. B.T.D.C. spark timing, 2.5 mm centre electrode diameter and 3.5 mm gap projection).

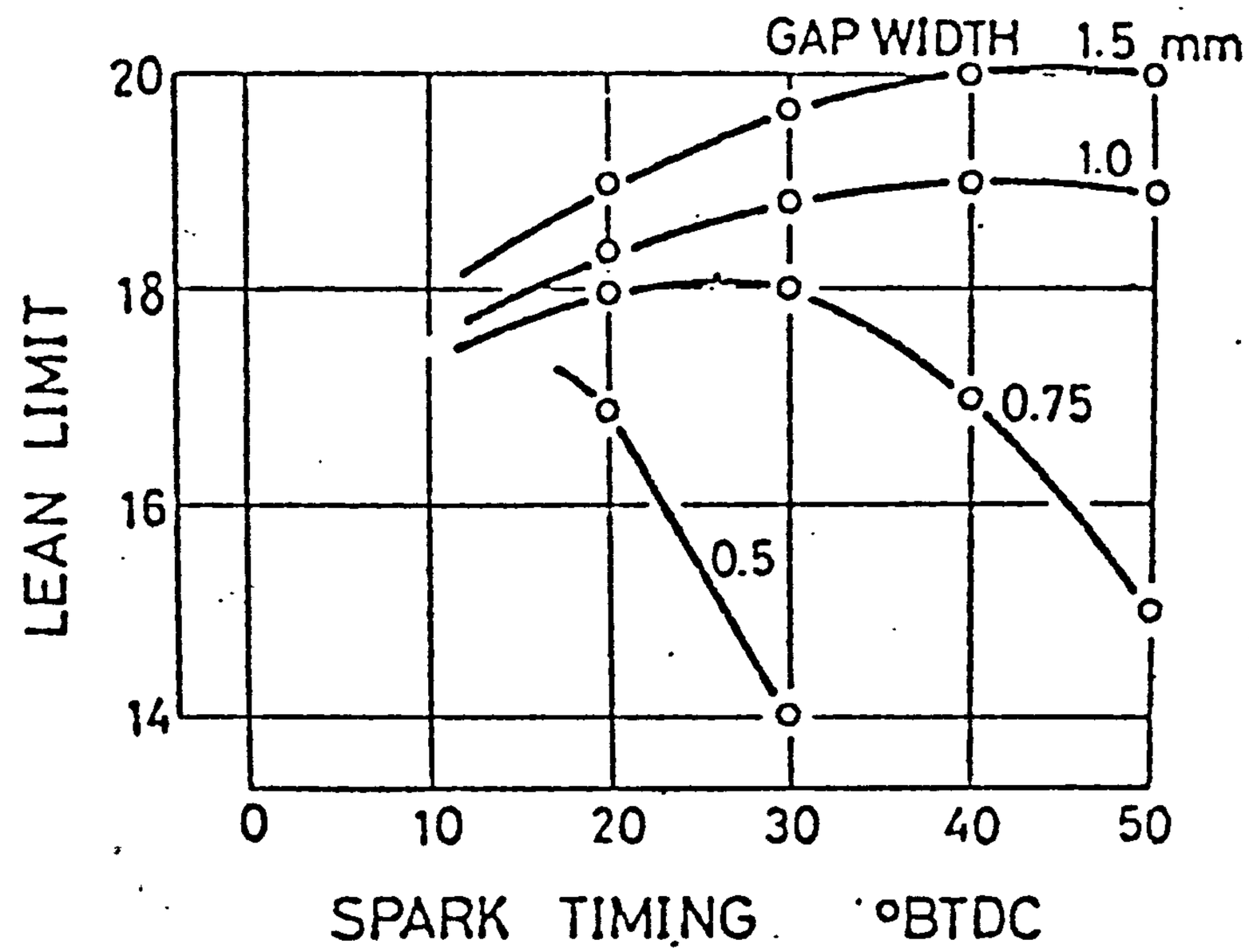

Fig (2-22). Effect of gap width and spark timing on the lean limit (20).
(2.5 mm centre electrode diameter, 3.5 mm spark gap projection and 30 mj spark energy.

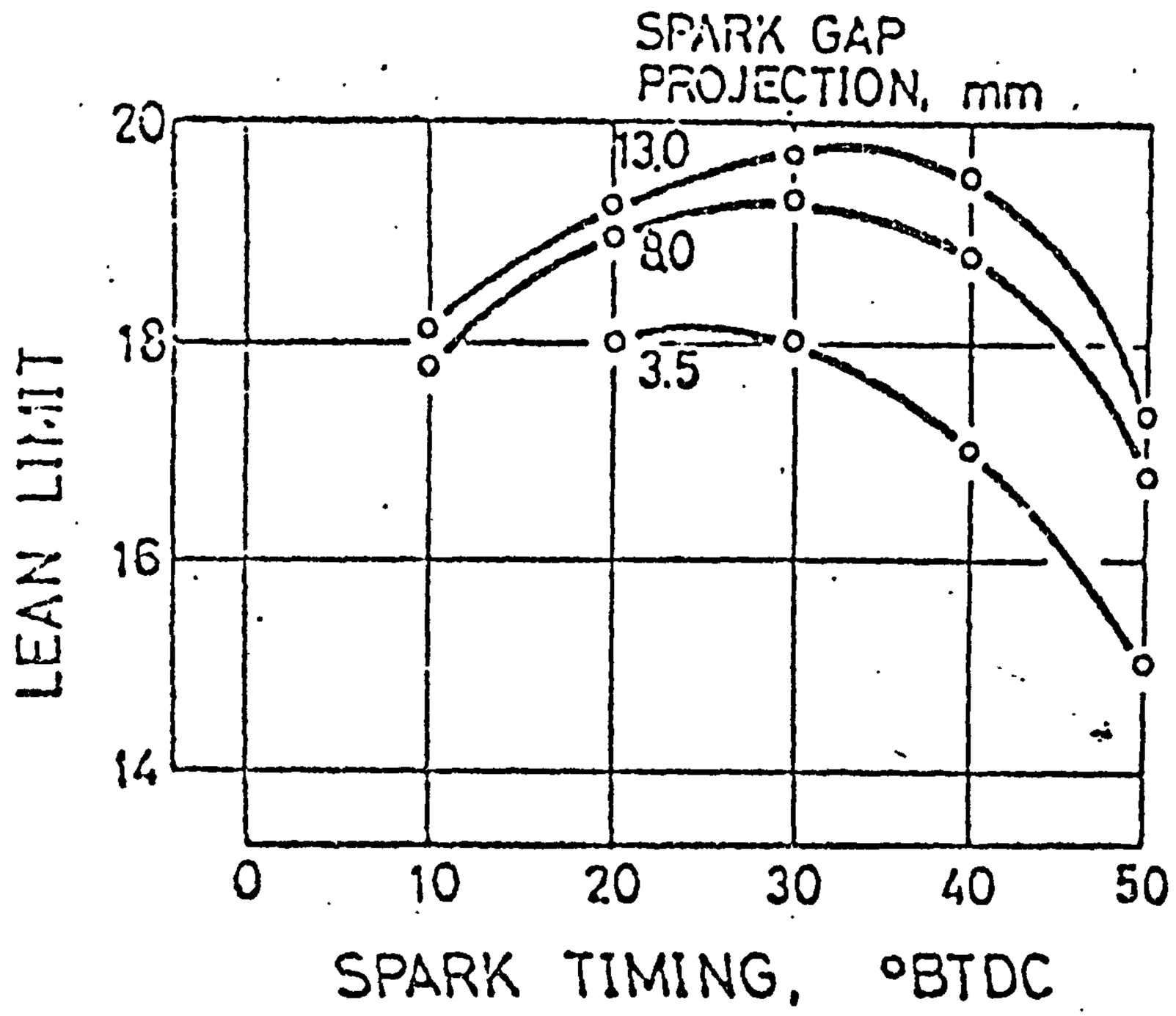

Fig (2-23). Effect of spark gap projection on lean limit (20). (0.75 mm gap width, 2.5 mm centre electrode diameter and 30 mj spark energy).

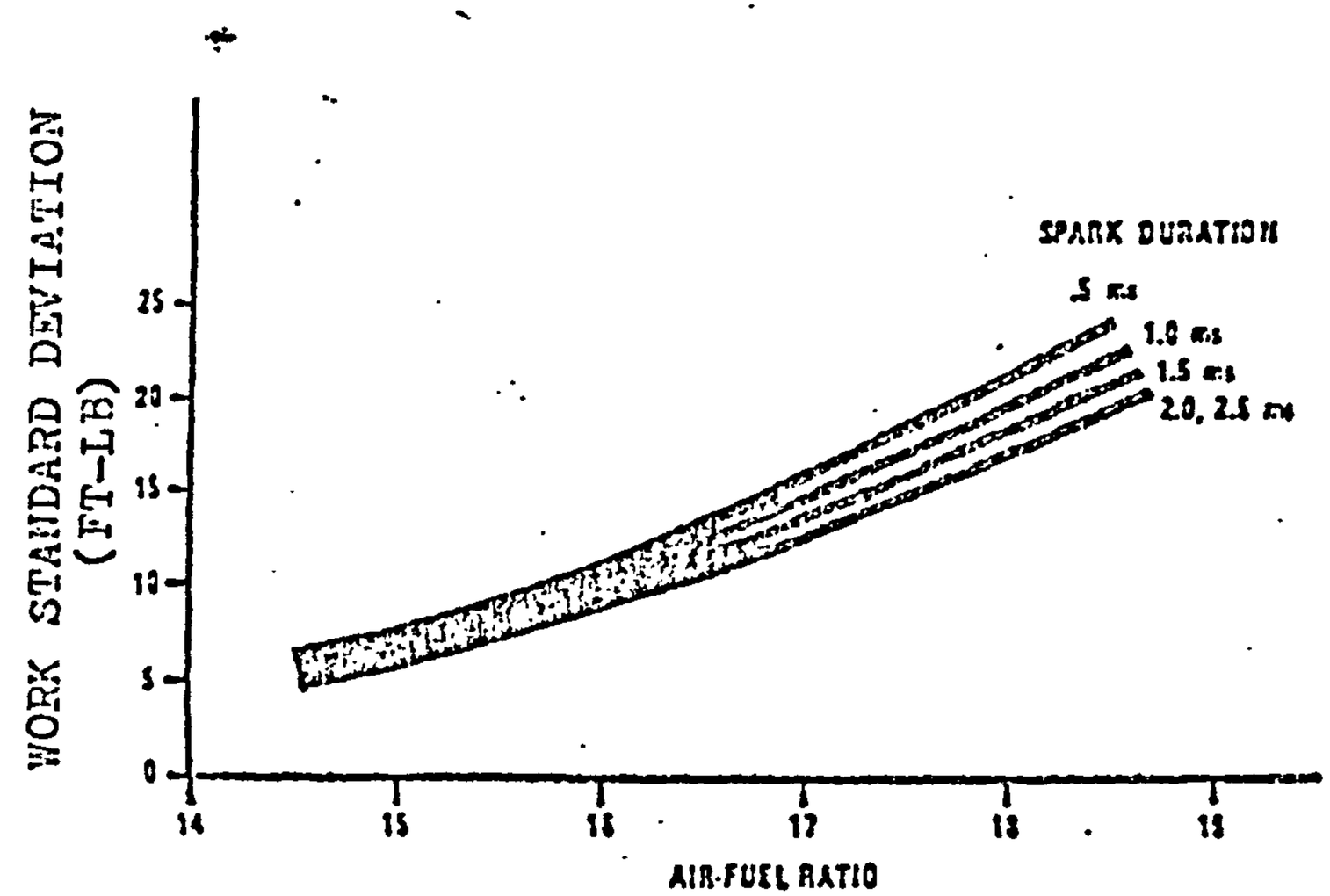

Fig (2-24). Effect of spark duration on combustion variation (27).
(2000 r.p.m., 41 deg. spark advance, 0.89 spark plug gap width and 4.37 gap projection).

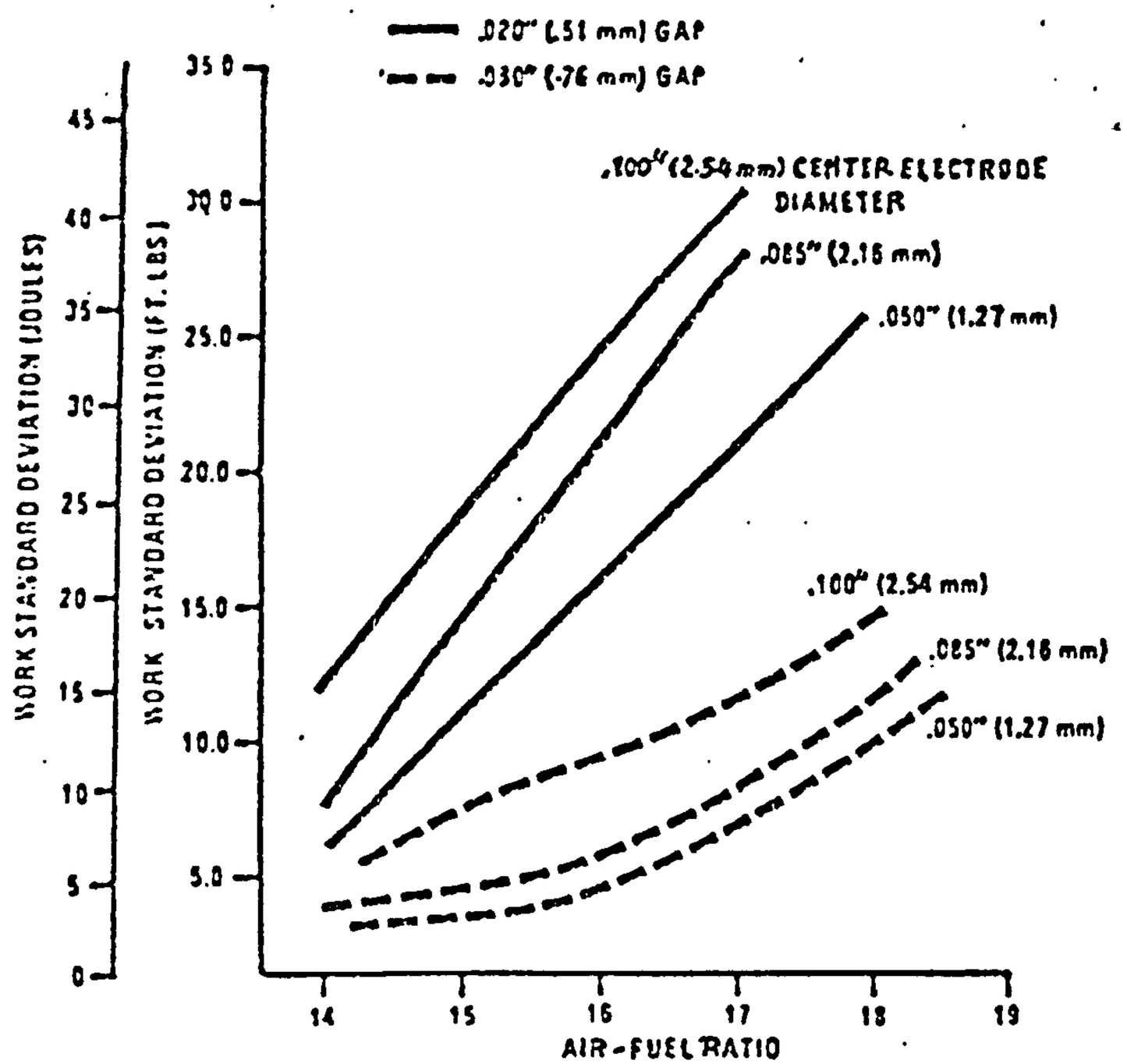

Fig (2-25). Effect of centre electrode size on combustion variation (27).
(2000 r.p.m., 41 deg. spark advance, 1.0 m sec spark duration and 4.37 mm spark plug gap projection).

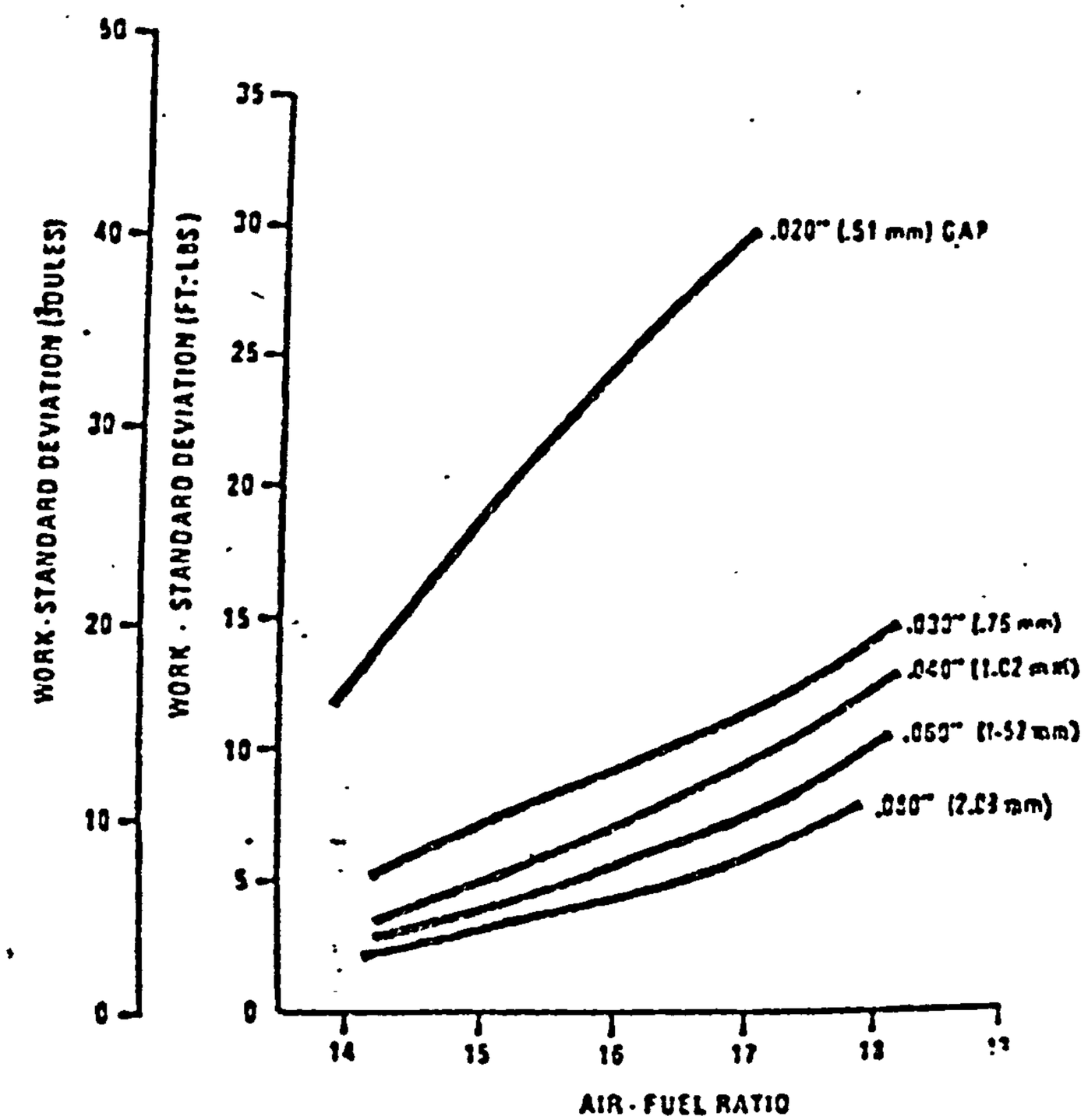

Fig (2-26). Effect of gap width on combustion variation (27).
(2000 r.p.m., 41 deg. spark advance, 1.0 m sec spark duration and 4.37 mm spark plug gap projection).

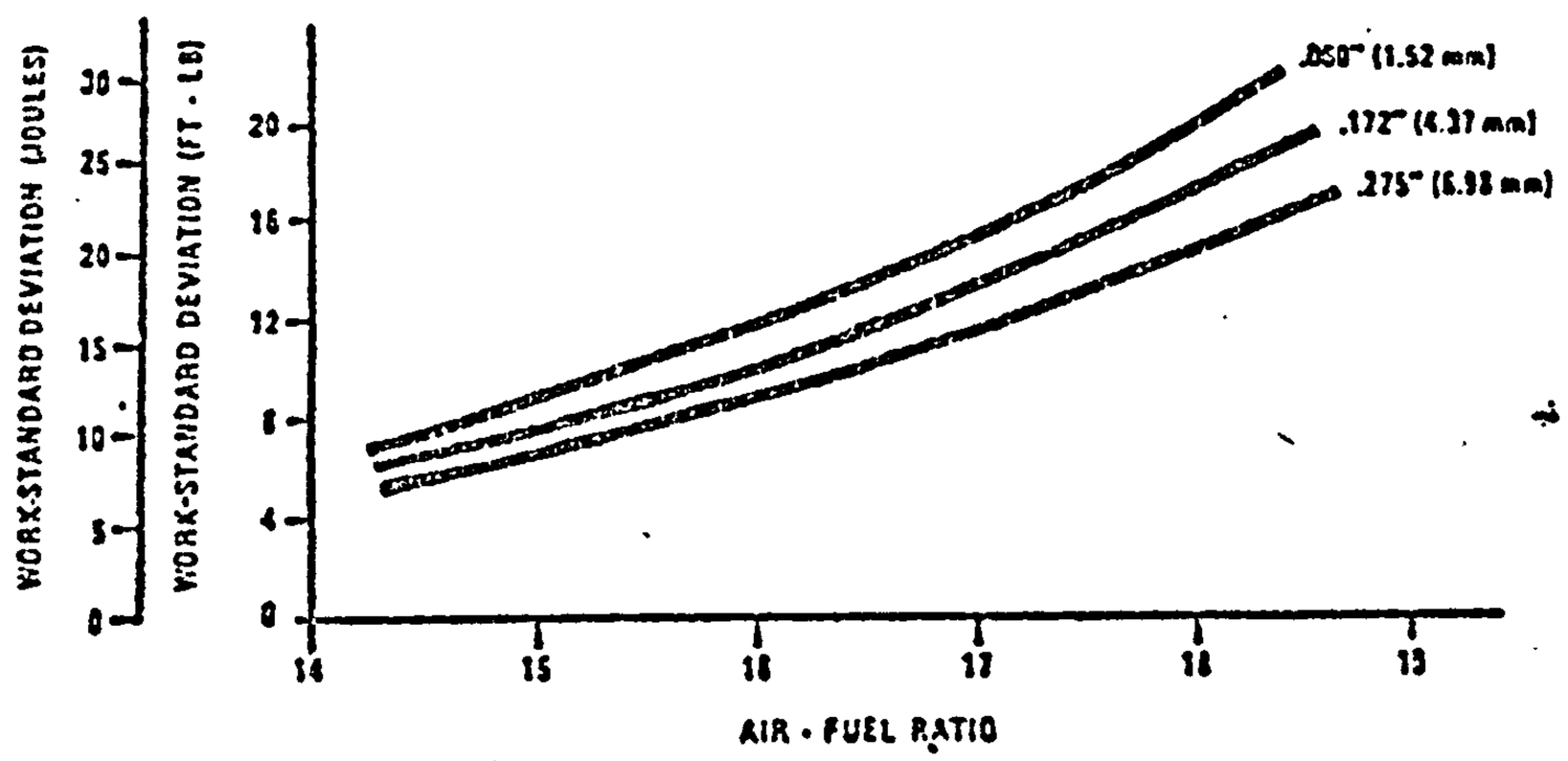

Fig (2-27). Effect of spark plug gap projection on combustion variation.
(2000 r.p.m., 41 deg. spark advance, 0.89 mm spark plug gap and 1.0 m sec spark duration).

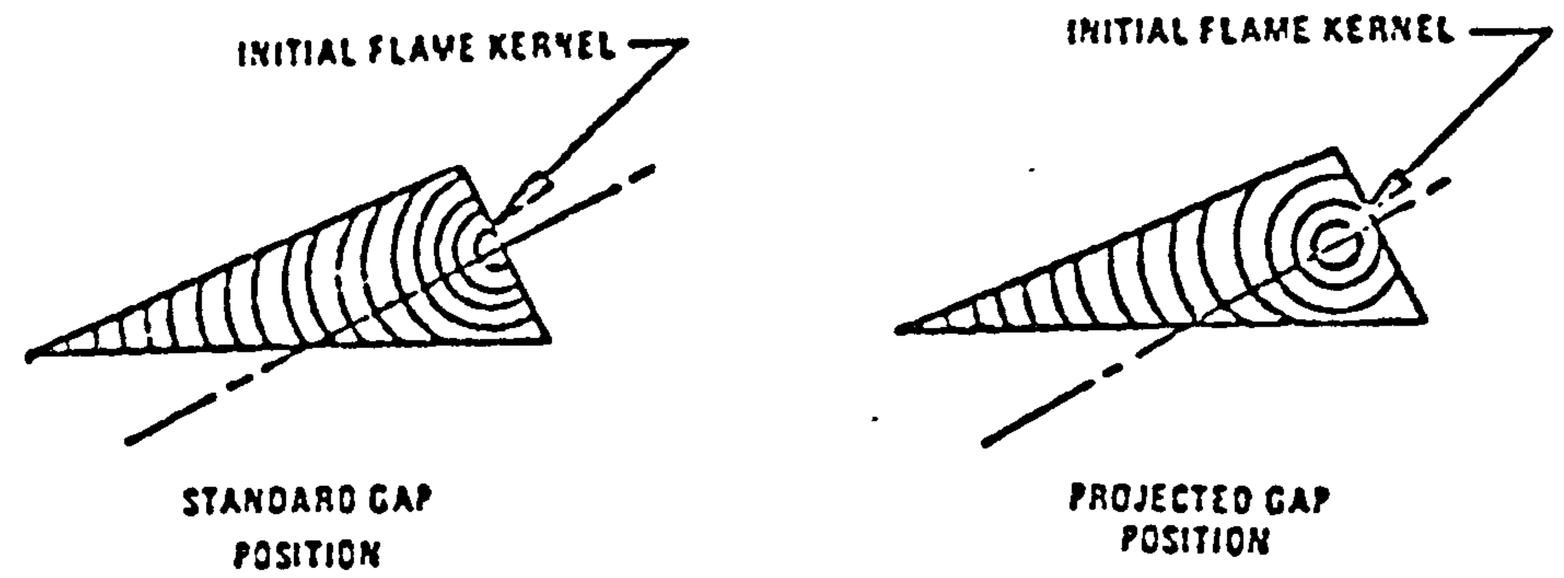

Fig (2-28). Effect of gap projection on flame propagation.

2.3.2 Mixture Preparation

Satisfactory combustion in a S.I. engine requires a proper mixing of fuel and air. Therefore, variations in the uniformity of the mixture could lead to corresponding combustion variation.

Soltau (4) noted that a premixed charge obtained with a gaseous fuel such as butane or methane does not show less peak pressure fluctuations than a liquid fuel mixture which is either carburetted or sprayed in the manifold; but if the fuel is injected directly into the combustion chamber the stability of the cycle worsens. However, the latter situation could be improved by placing the injector near to the inlet valve (60). In fact, the fuel and air mixing process depends more on air turbulence than on the actual time interval during the cycle, and at high speed, although the available time is reduced, the increased turbulence gives much improved mixing.

Hansel (13) has reported a reduction in cyclic variation when propane was used rather than gasoline under the same test conditions and attributed such effect to the perfect mixing of propane and air. The values of $(\Delta P/\bar{P})_{max}$ was reduced from 0.34 to 0.23 for the two cases respectively. The effect of fuel composition on this experiment is also included in this reduction.

Patterson (2) has found that improved mixing decreases cyclic variation slightly. It also increases the average burning rate with lean mixtures, Fig. (2-30). He noticed that cylinder-to-cylinder pressure rate differences are strongly related to fuel distribution. However, the large rate differences remaining when

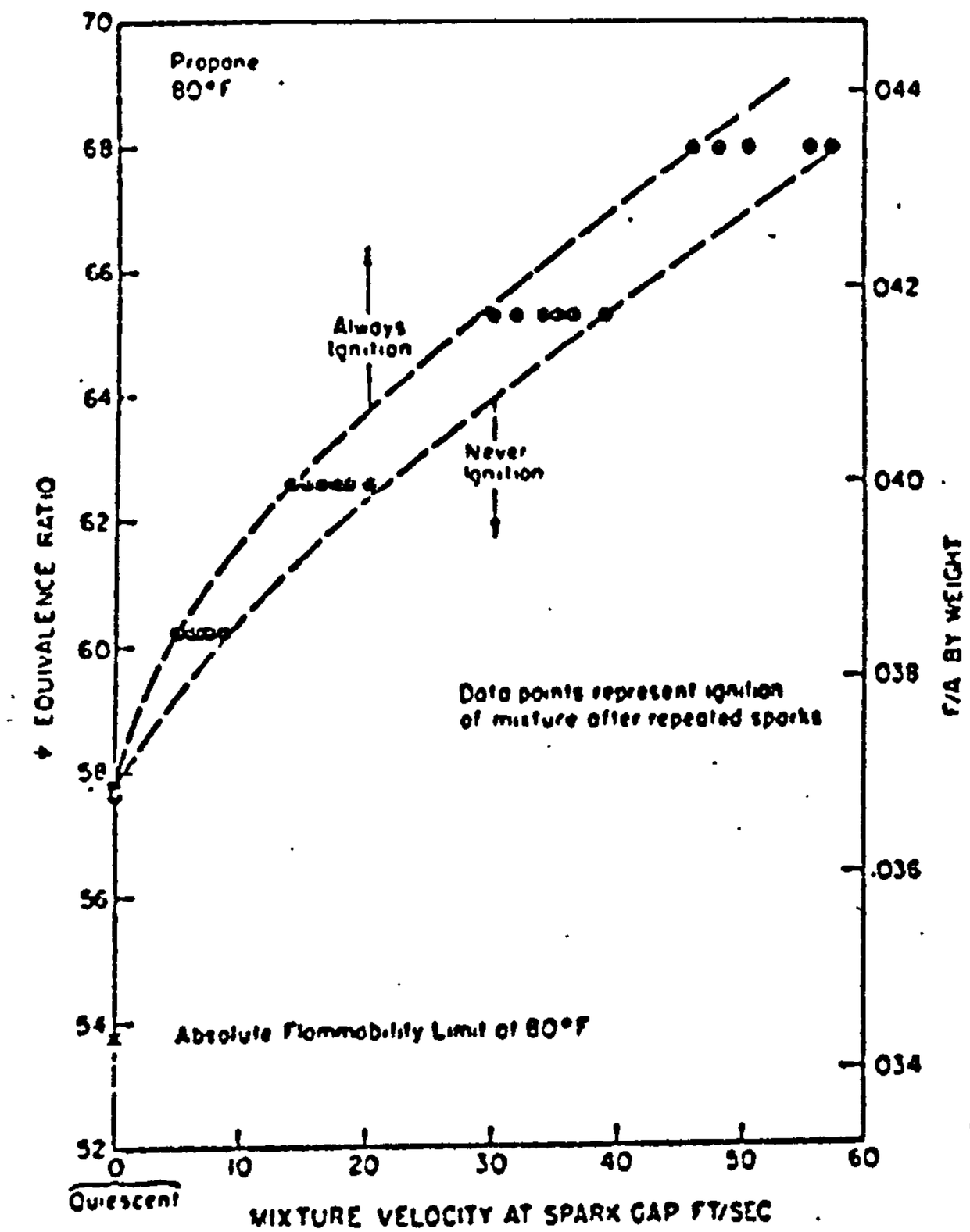

Fig (2-29). Variation in spark ignition lean limit with mixture velocity (3).

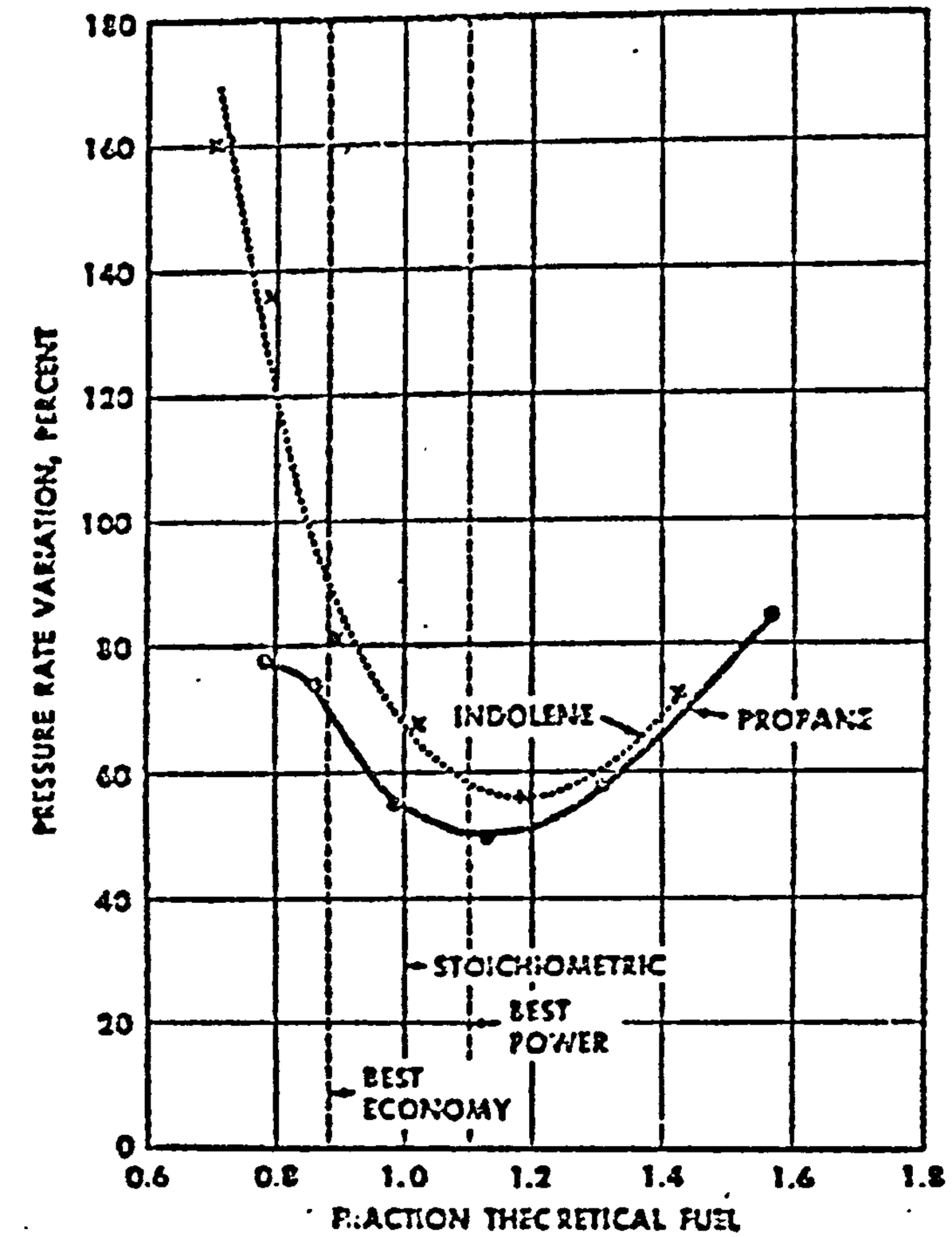

Fig (2-30). Effect of mixing on cyclic variation. Well-mixed propane mixture is advantageous on percentage basis at lean mixtures (2).

fuel distribution and preparation are carefully controlled, led him to conclude that the other factors such as differences in mixture motion between the cylinders are equally important, Fig. (2-31). Barton et al (10) have noticed that any improvement in air/fuel mixture uniformity obtained by using a mixing tank instead of a direct induction method was completely masked by a very large change in flame speed variation, and, although the average flame speed increased, the flame speed variations also increased by almost 3:1. This contradicts the notion that increases in average flame speed reduces the variations in flame speed. They attributed such contradiction to large differences in the intake process between the two systems. These differences must affect substantially the variations in mixture motion which is thought to be the primary cause of combustion variation.

2.3.3 Exhaust Gas Dilution of the Charge

The effect of exhaust gas dilution on cyclic dispersion was studied by purging the cylinder of residuals between firing cycles. Firing the engine every second or every fourth cycle, the cycles in between scavenge the exhaust residuals. As the exhaust gas dilution decreases as the square of the number of cycles which do not fire, three idle cycles are sufficient to obtain a nearly perfect fresh gas charge.

Tests carried out by Soltau (4) and Patterson (2) have indicated that when the engine is fully scavenged, combustion is much more rapid, but still not similar from cycle to cycle, Figs. (2-32), (2-33). Also, no effect was found when the engine back pressure was raised to increase the exhaust gas residual.

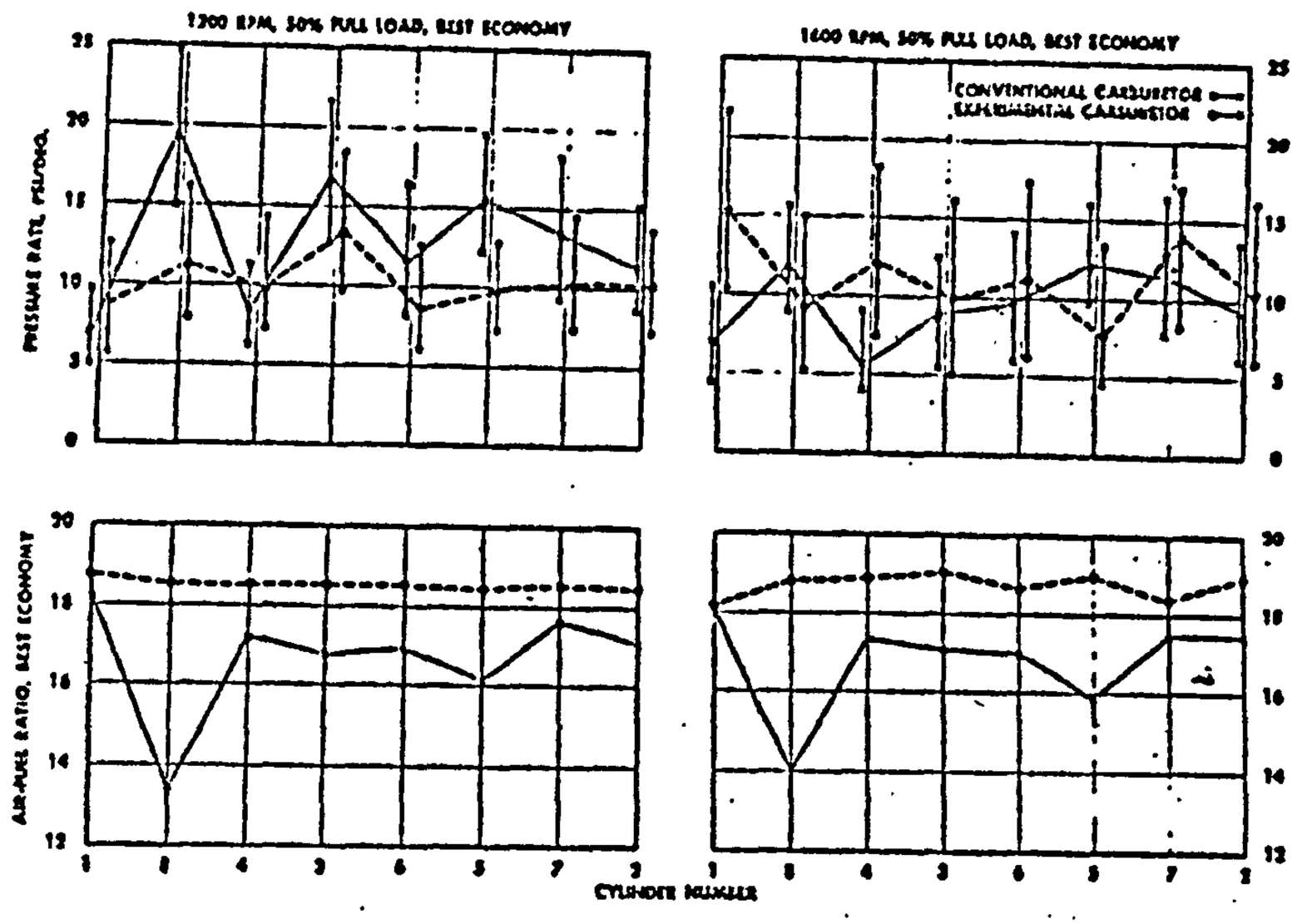

Fig (2-31). Effect of improved fuel distribution on cylinder fuel distribution (2).
(389 cu in V-8 engine, 10:1 compression ratio).

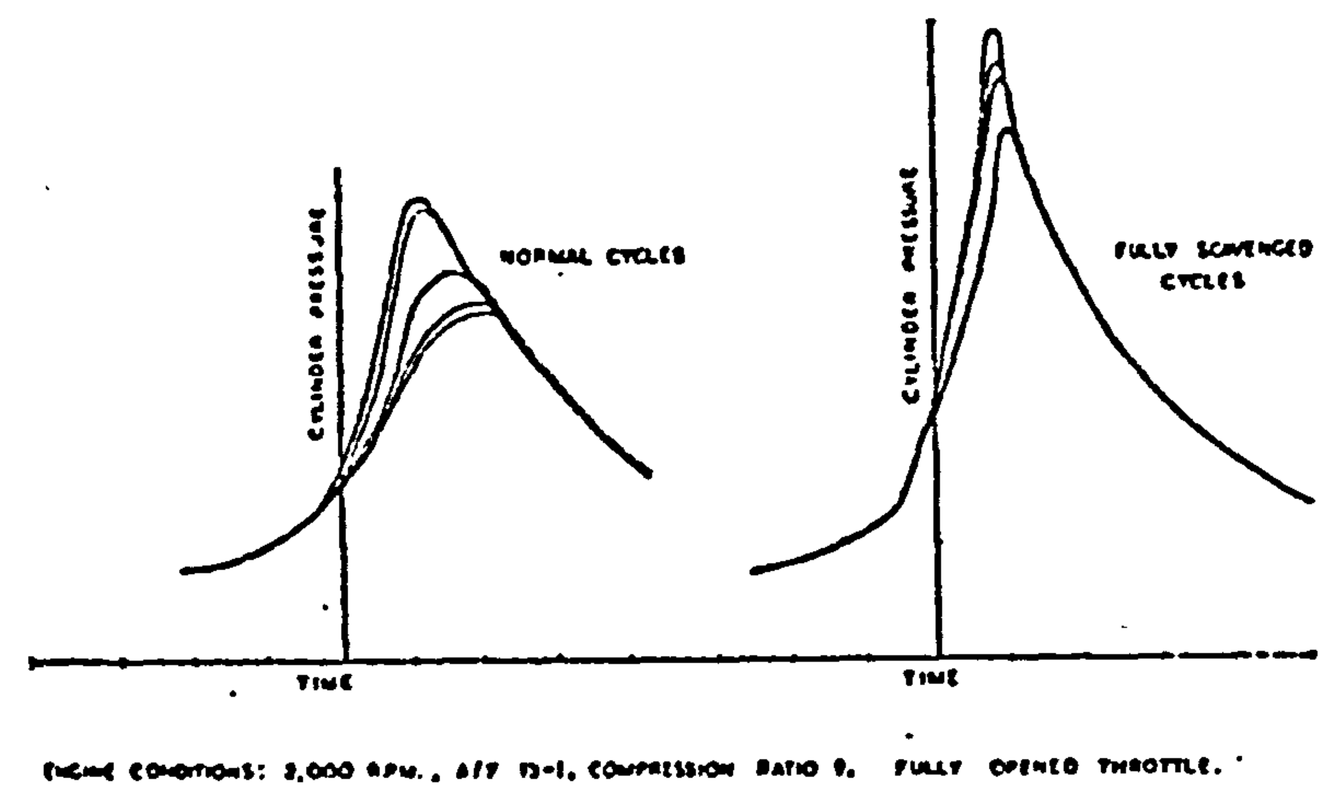

Fig (2-32). Effect of exhaust gas residuals on cyclic variations. Five consecutive cycles (4).
(2000 r.p.m., 13:1 air/fuel ratio, 9:1 compression ratio and fully opened throttle).

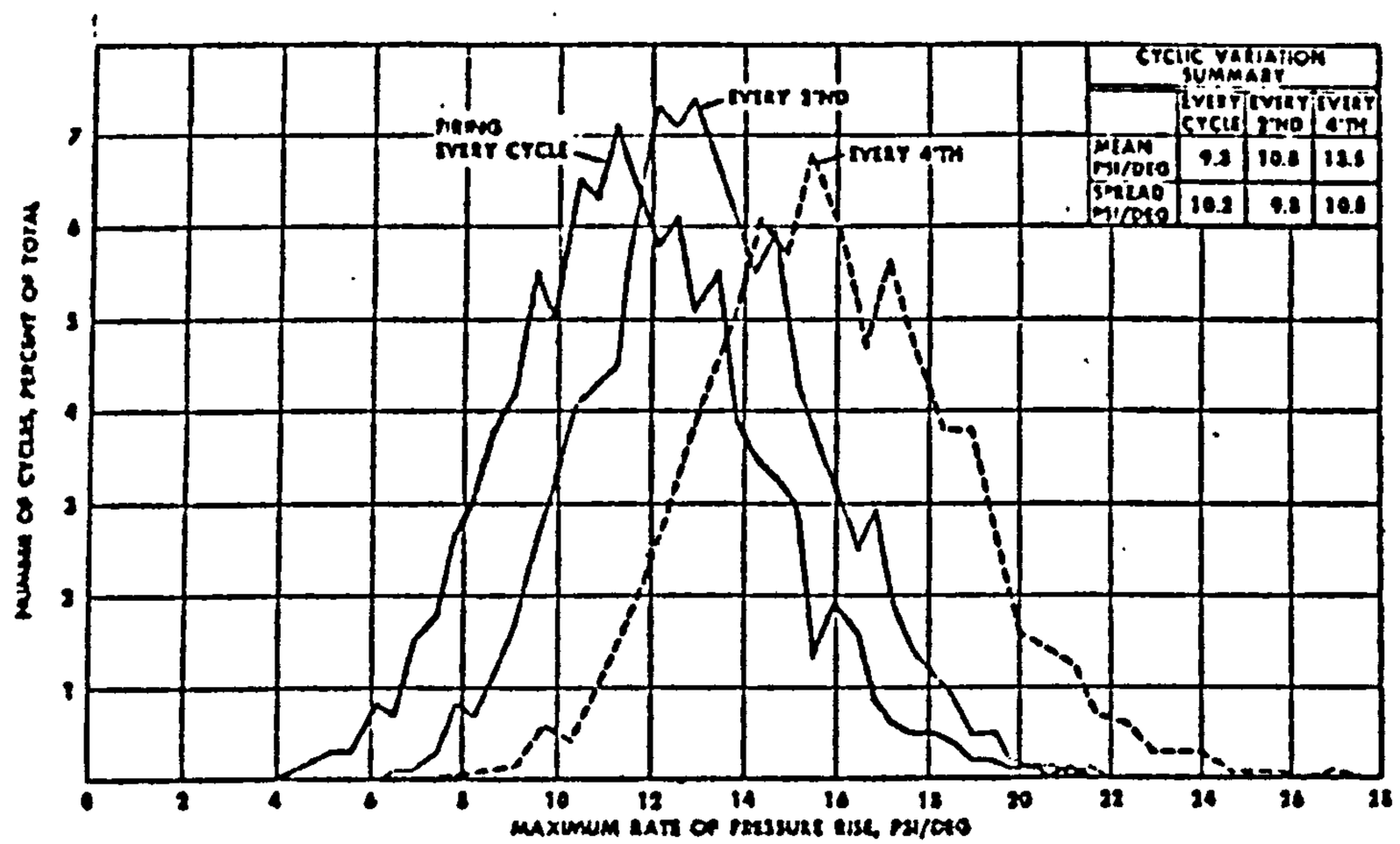

Fig (2-33). Effect of exhaust gas residuals on rate of pressure rise and cyclic variations (2).

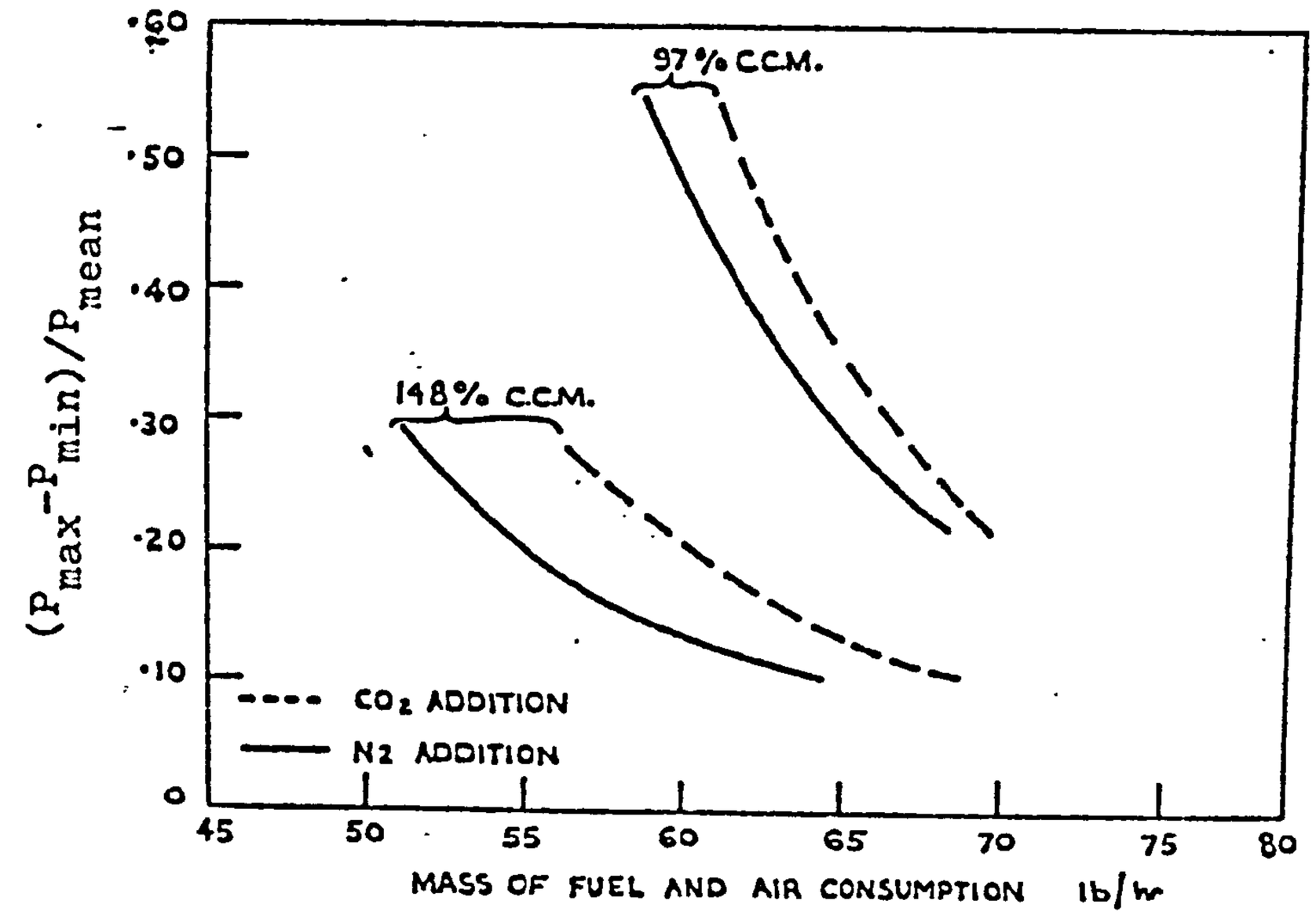

Fig (2-34). Relative range of variation versus the net mass of charge induced into the cylinder for overall mixtur strengths when CO_2 and N2 are added to intake charg (32).
(2000 r.p.m., 9.5:1 C.R., Full throttle with iso-octane fuel).

On the other hand, Karim (32) had carried out some tests where addition of CO_2 or N_2 to the engine air supply was made over a wide range of operating conditions. He found that increasing the concentration of the dilutents in the charge increases the maximum pressure variations and that CO_2 is relatively more effective in that respect than N_2. These changes can be seen from Fig. (2-34) and are relatively small. Karim (32) also concluded that the probable kinetic role of some active species in the residuals, depending on their nature and concentrations, can, however, play an important role in 'seeding' the charge and influencing the combustion process.

Hansel (13) carried out some experiments with propane as fuel (to eliminate any effect of non-uniform mixing between the fuel and air). The engine cylinder was purged of residual gas by interrupting the spark for 200 engine revolutions. The data was compared with another test at higher engine speed which has the same value of initial peak pressure under normal running. He reported a reduction in the cyclic variation measured by $(P_{max} - P_{min})/P_{mean}$ from 0.23 under normal conditions to 0.1 for the purged case.

2.3.4 Compression Ratio

The average flame speed increases by increasing the compression ratio and consequently the differences in peak pressure diminish, but the trend is very small and increases slightly as the air/fuel ratio changes from maximum power setting to weaker mixtures (4), (10). The steadier influence of the high compression ratio is thought to be due to the improved scavenging (and hence the

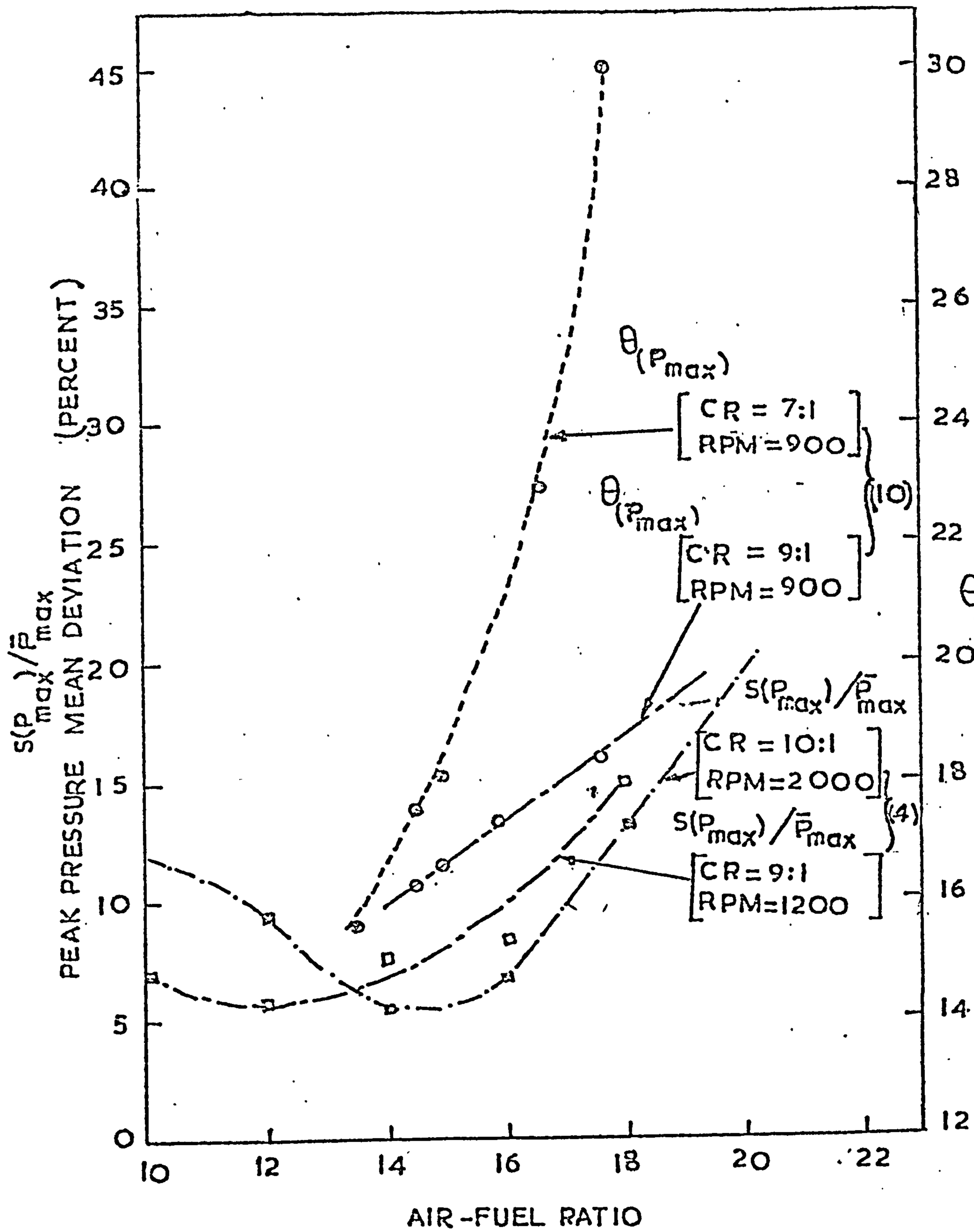

Fig (2-35). Effect of compression ratio on cyclic variations.

smaller exhaust gas dilution) and to the higher gas temperature which promotes a more rapid flame propagation rate, Fig. (2-35).

Barton et al (10) showed that at 7:1 compression ratio decreasing the air fuel ratio (17.73 - 14.5) decreased the variation in the maximum pressure, while at 9:1 the variations increase slightly and at 10.5:1 the variations in maximum pressure were greatly increased. The overall effect is that increasing compression ratio increases the combustion variations. The reasons for this were attributed to the combustion phasing and also the fact that flame speed variations are increased when the flame speed increases. The latter effect could be attributed to density and temperature changes produced by increasing the compression ratio which in turn augment the effect of phenomenon like 'flame generated turbulence'.

Tests carried out by Curry (37) at maximum power air/fuel ratio, constant engine speed and spark timing corresponding to maximum brake torque (MBT), indicated a slight improvement in the cyclic variations for increases in the compression ratio from 8 to 10:1 and results in a more repeatable initial phase of combustion Fig. (2-36) while slight adverse effects could be shown from Fig. (2-37) when increasing the compression ratio from 16 to 20.

2.3.5 Throttling

Throttling the charge will affect both the extent of pressure variations and the maximum pressure value, and hence will increase the variations Fig. (2-38). This is to be expected as the effect of increased dilutents and the reduced burning rate

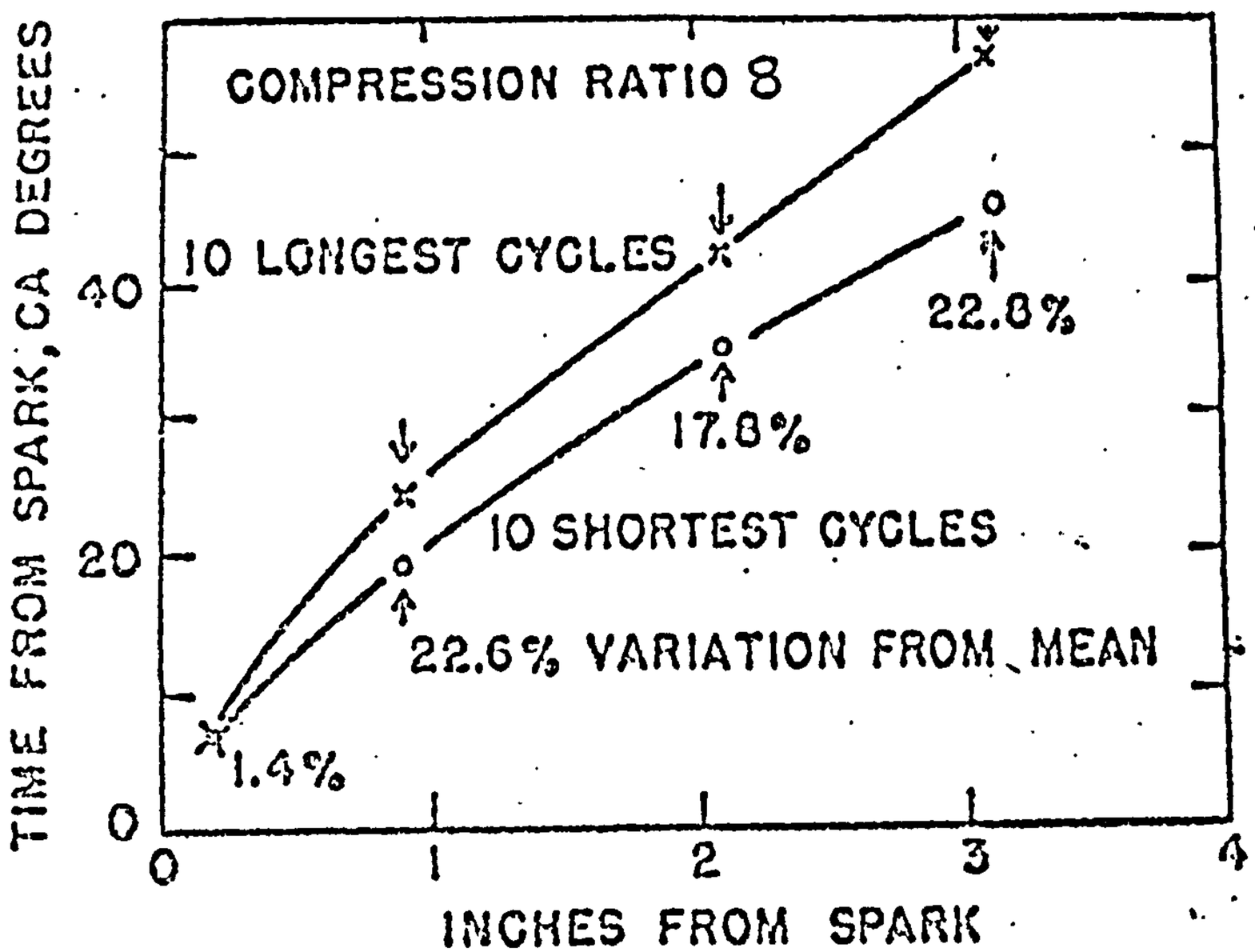

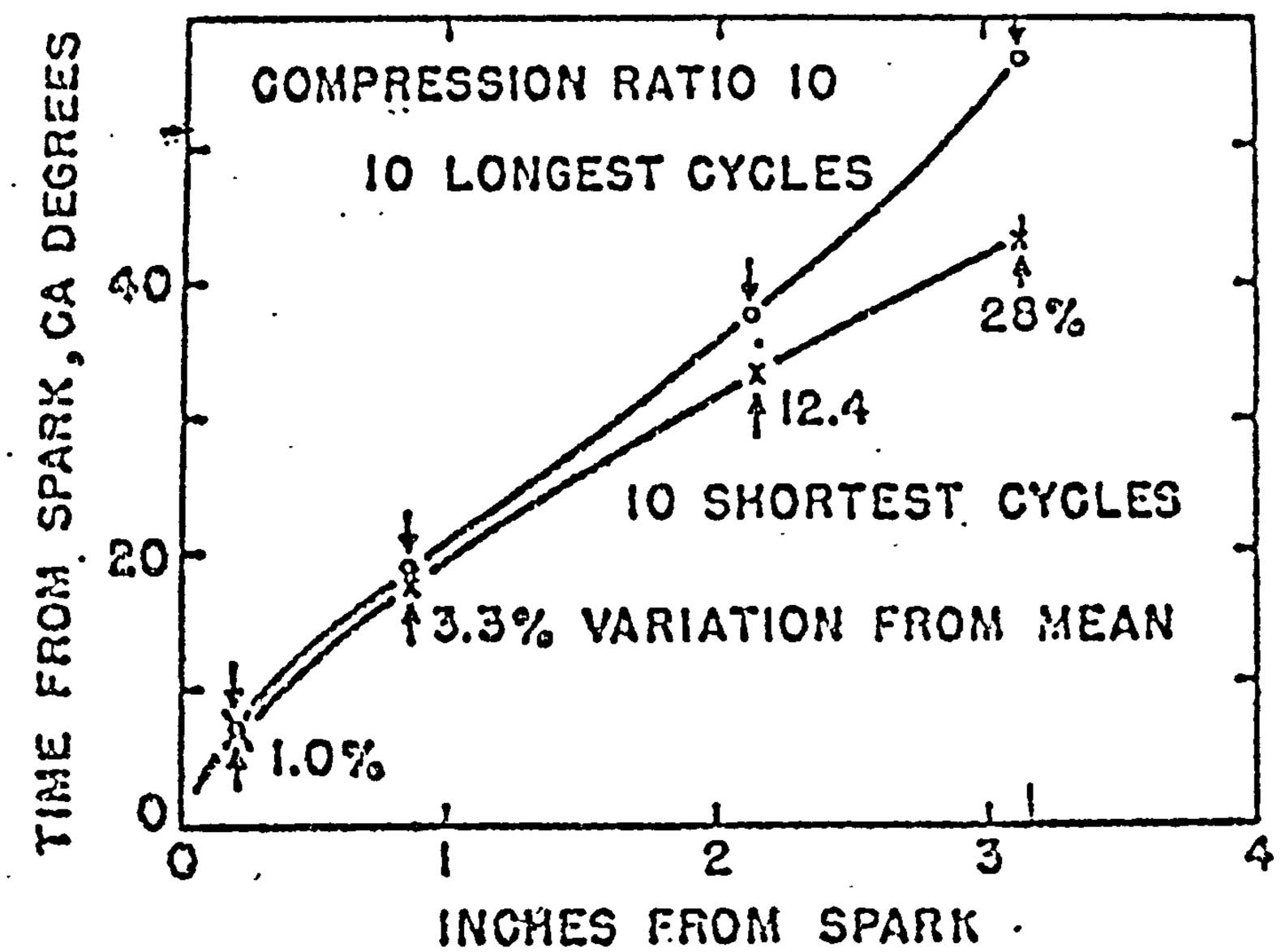

Fig. (2-36). Cycle-to-cycle variations in early part of cycle were minimised by increasing compression ratio. Fuel - isooctane + 3 ml TEL/gal; speed - 1000 r.p.m.; spark advance - 15 deg. btc; F/A ratio - 0.073; mixture temperature - 150F; MAP - 30 in. Hg; coolant temperature - 212F. (37)

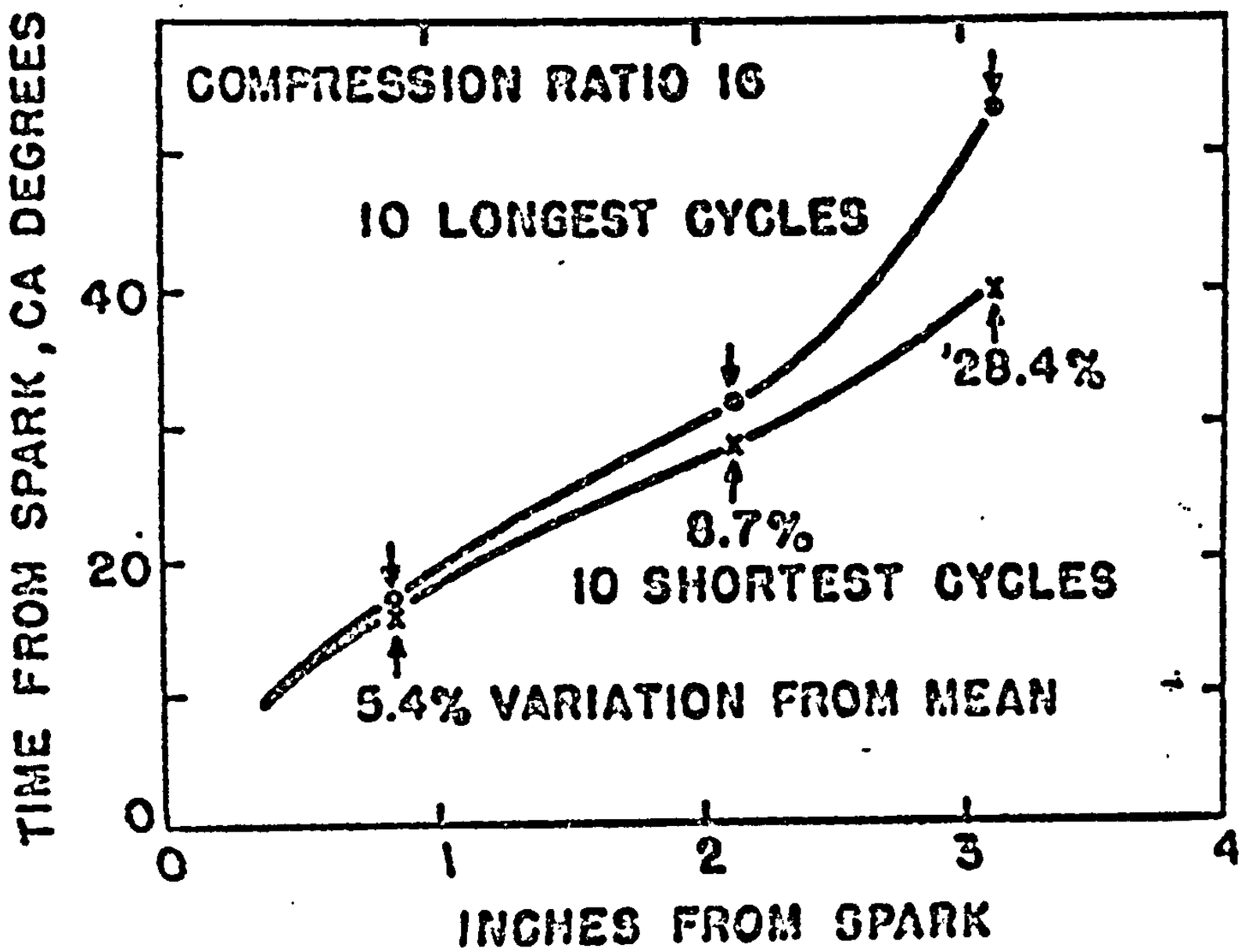

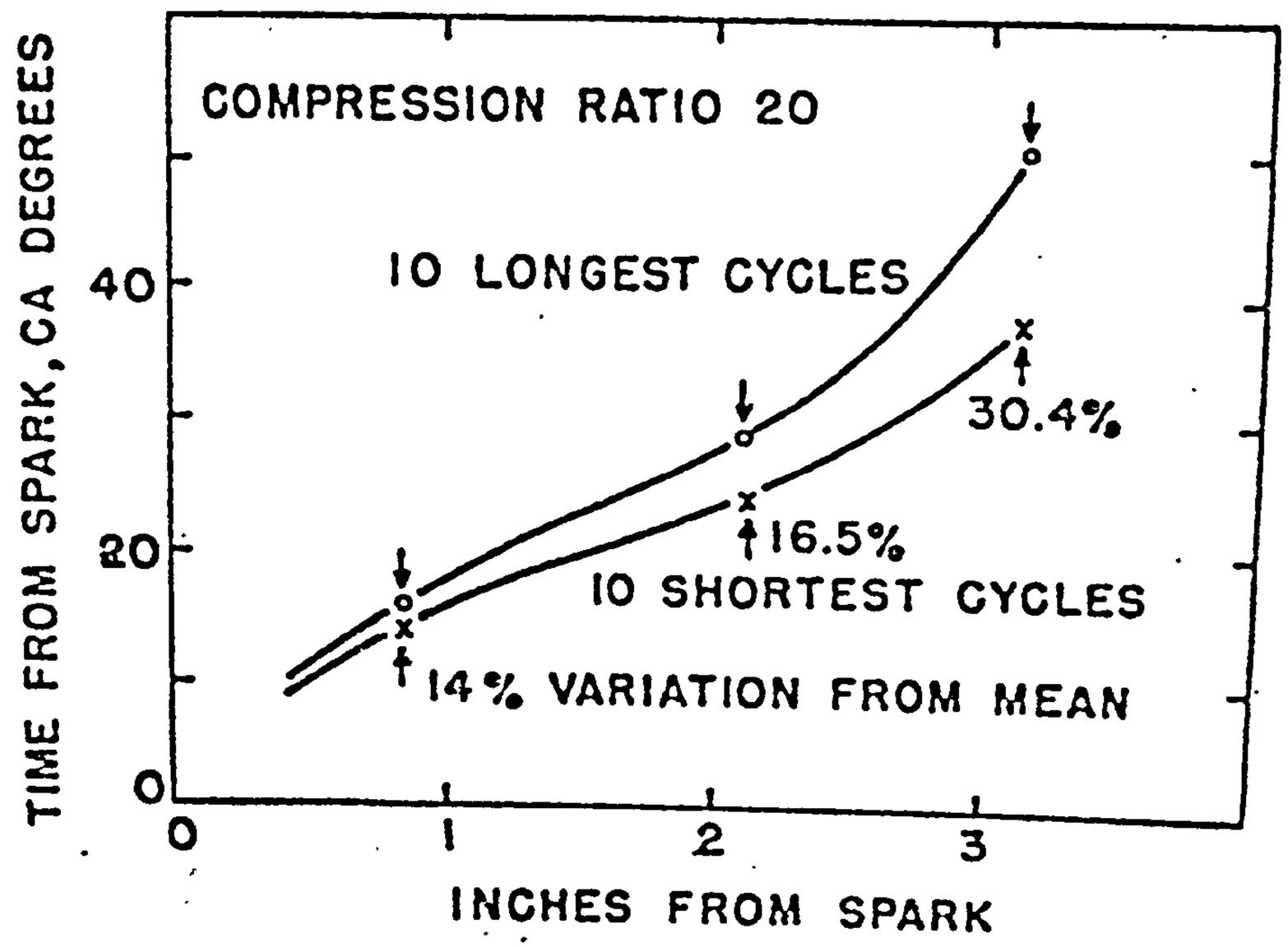

Fig. (2-37). At very high compression ratios, total cycle-to-cycle variability was not greatly different, however, variations were most pronounced in latter portion of cycle. Fuel - isooctane + 6 ml TEL/gal; engine speed - 1200 r.p.m.; spark advance - 15 deg btc at 20:1 and 16 deg btc at 16:1; F/A ratio - 0.073; mixture temperature - 100F; MAP - 20 in Hg; coolant temperature - 212F. (37)

will be the dominant factors, while a faster flame speed and reduced effects of dilutents contribute to the marked improvement in the cyclic variation observed with an increase in throttle opening.

Peters and Borman (33) have shown that low load cycles have burning rates that were slower than the full load cycles Fig. (2-39) and consequently greater cyclic variations. They have attributed this to the presence of increased residual fraction left from the previous cycle and to reduced mixture motion in the combustion chamber because of the lower flow rates at low loads.

2.3.6 Cylinder Water Jacket Temperature and Oil Contamination of the Charge

Soltau (4) has concluded that the lubricating oil in the combustion chamber and the heat effect of the cylinder head walls do not contribute too much to the problem. However, Karim (32) has reported some reduction in the extent of cyclic dispersion when the cylinder water jacket temperature was increased.

2.3.7 Air/Fuel Ratio

Soltau (4) reported a very great influence of the air/fuel ratio on the cycle-to-cycle variations. The most stable combustion occurs with air/fuel ratio in the region of 13:1, which in fact corresponded to the region of maximum flame speed as reported by Taylor's work at M.I.T. It is lower than this value for low compression ratios and higher for higher ratios (taking a mean value of around 9:1). As the air/fuel ratio range is traversed and

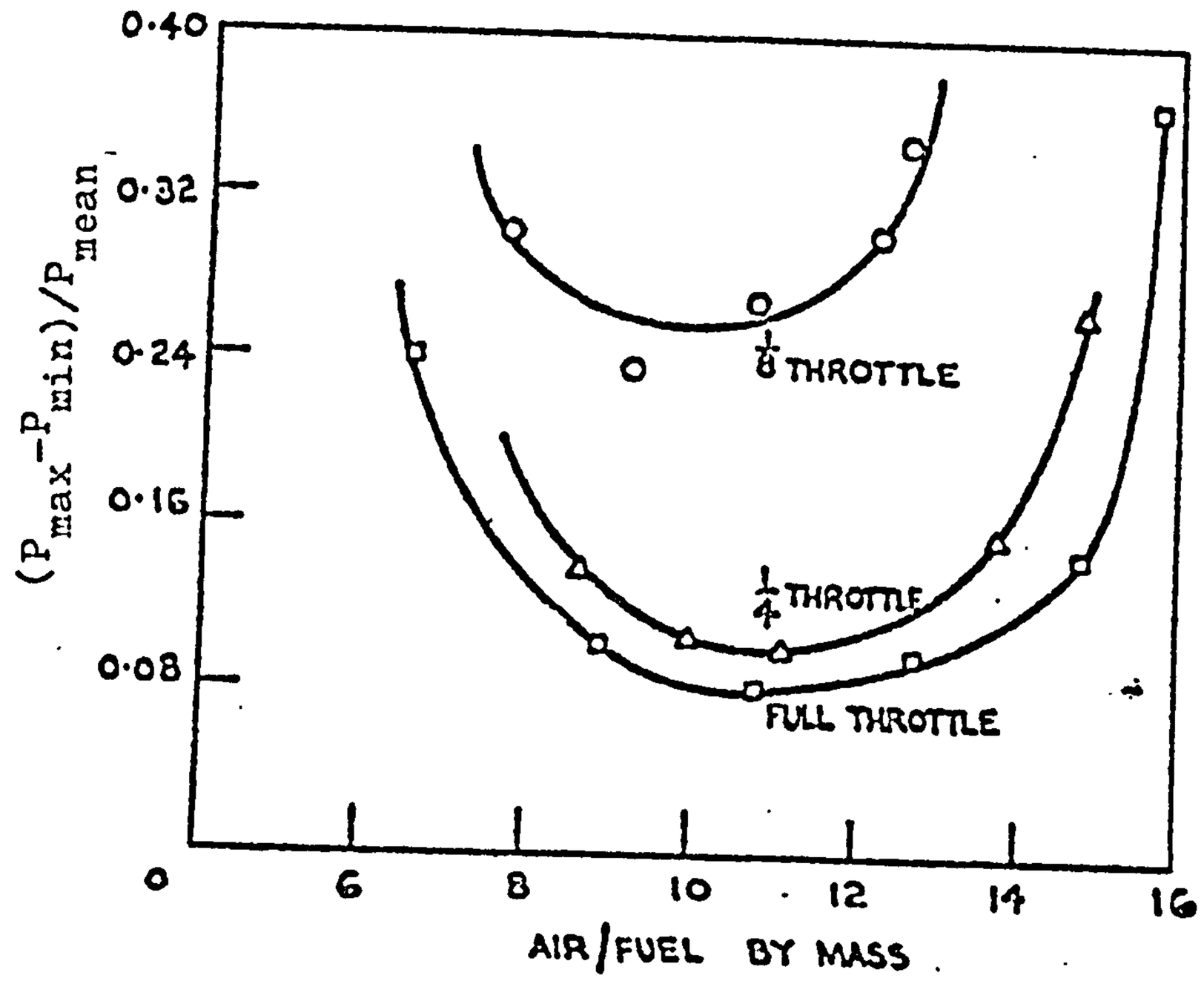

Fig (2-38). The relative range of variation in peak cylinder pressure versus mixture strength for different throttle setting (32).

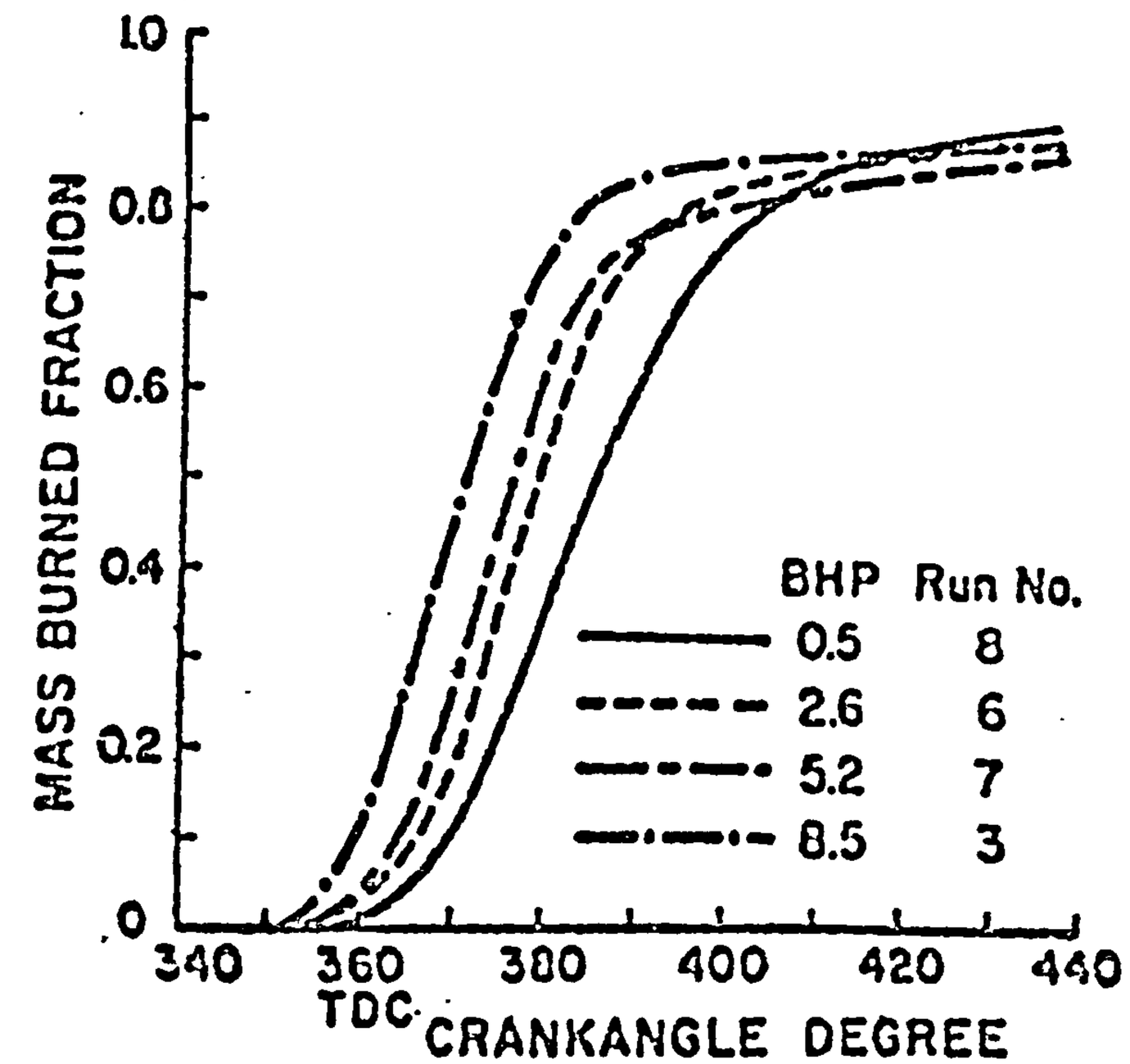

Fig (2-39). Mass burned fraction versus crank angle for different engine loads, (33).

as the mixture becomes either richer or weaker, the deviation of peak pressure and i.m.e.p. from the mean increases, Fig. (2-9). It is mainly this phenomenon which prohibits the use of very weak mixtures. Near the limit of burnability, there is no sharp dividing line where it could be said that the mixture on one side burned and on the other did not burn. There is a very wide band where decreasingly efficient combustion can be maintained, as every cycle has a different burnable limit.

Peters and Borman (33) have reported small effects of the air/fuel ratio in the range of between 19.2 and 14.1 with isobutylene as fuel on the mass burning rates with the stoichiometric mixture having higher burning rates rather than rich or lean mixtures, Fig. (2-40).

The data of Miller, Uyehara and Mayers (38) using iso-octane as fuel show the same trends as the data of Peters and Borman Fig. (2-40), i.e. combustion with stoichiometric mixtures burn faster than rich or lean mixtures. However, they show a large influence of air/fuel ratio on mass burning rates Fig. (2-41). This discrepancy was attributed to the variation of fuel type between the two tests.

Harrow et al (29) have found that at any given engine speed the mean flame travel time reached a shallow minimum at approximately 12:1 air/fuel ratio. On the rich side of the minimum, the mean time increases slowly to that corresponding to the richest mixture examined (about 9:1 air/fuel ratio), while on the weak side of the minimum the flame travel time increased quite rapidly, until at the weak mixture limit some of the flames failed to reach the ionisation gap. Fig. (2-42) shows the mean flame travel time for benzene, iso-

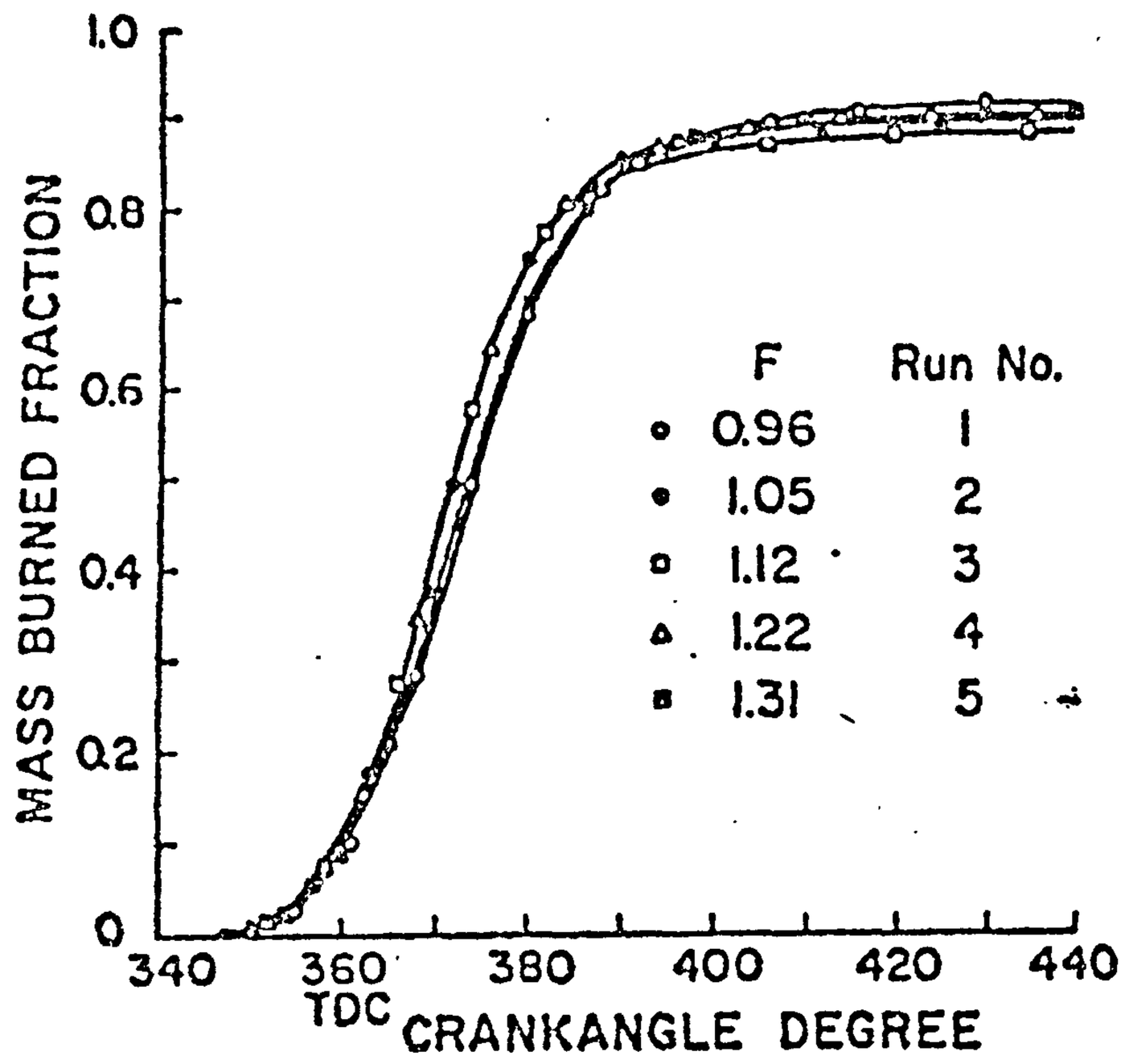

Fig (2-40). Mass burned fraction versus crank angle for different fuel/air ratios using average pressure-time diagrams (33).

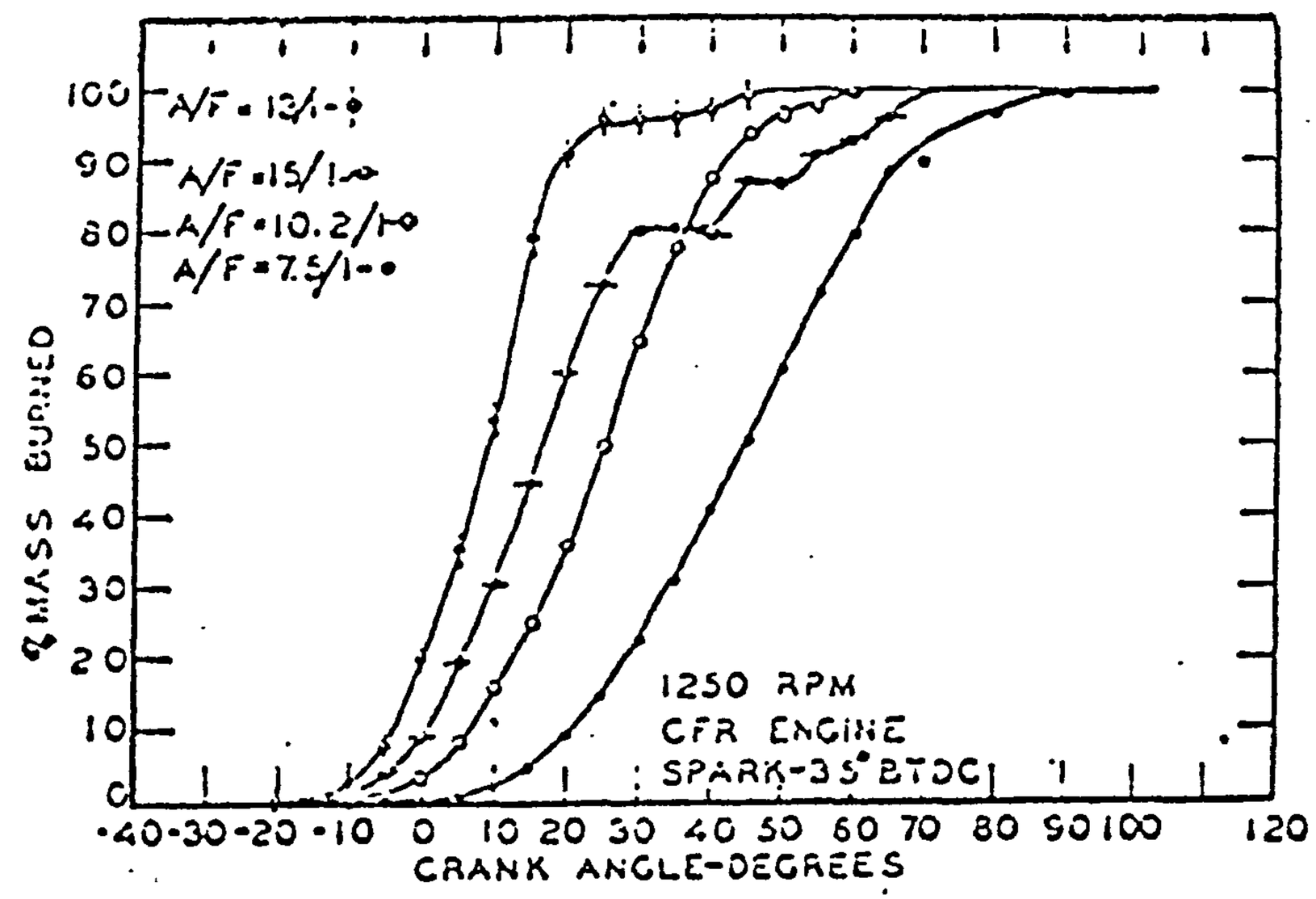

Fig (2-41). Percentage mass burned as a function of air/fuel ratio (38).

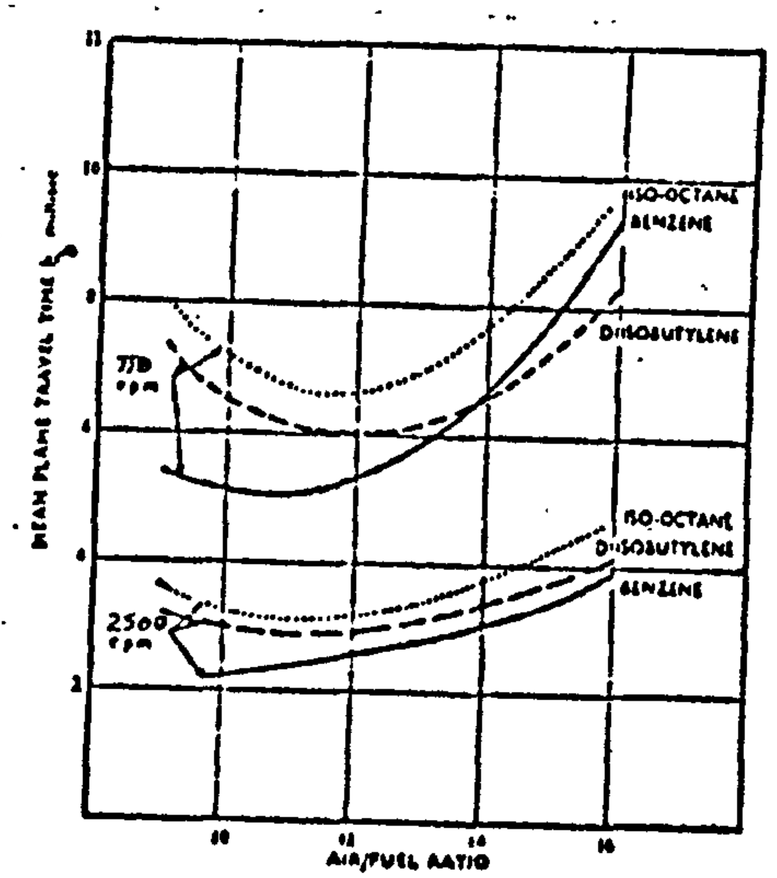

Fig (2-42). Mean flame travel times of iso-octane, di-isobutylene and benzene, (29).
(750 and 2500 r.p.m., 15 deg. B.T.D.C. spark timing and fully opened throttle).

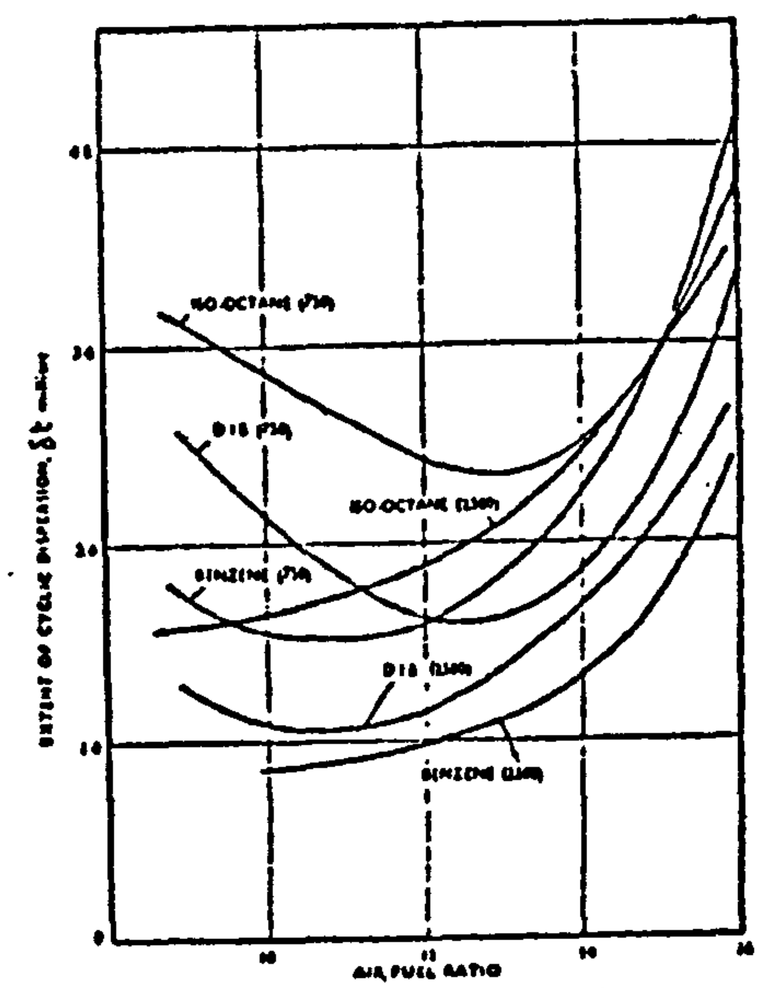

Fig (2-43). Variation in the extent of cyclic dispersion with mixture strength of iso-octane, di-isobutylene and benzene, (29).
(750 and 2500 r.p.m., 15 deg. B.T.D.C. spark timing and throttle fully opened).

octane and di-isobutylene at various air fuel ratios and for engine speeds of 750 and 2500 r.p.m. The corresponding extents of cyclic variations for the same range of experimental results are shown in Fig. (2-43). The same trends were shown by Mori and Yamazaki (34) for the mean flame velocity and its standard deviation for iso-octane, reformed naphta and cracked naphta as fuels at 900 r.p.m. and 6:1 compression ratio Fig.(2-11).

Barton et al (10) have conducted their tests with air/fuel ratios in the range of 17.73 to 13.5:1 which are not rich enough to cause the flame speed to pass through its maximum value. Therefore, they have reported an increase in the flame speed as the air/fuel ratio was decreased which agreed with the previously mentioned data reported by Harrow et al, Fig.(2-35). The maximum pressure variation also decreased with decreased air fuel ratio in this investigation and the deviation of flame speed, (as measured by the angle of occurrence of maximum pressure θp_{max}) also decreased as the average flame speed increased. Thus increasing flame speed in their tests by decreasing the air/fuel ratio did not increase the deviations in flame speed but rather lowered these deviations. Again these results are in agreement with Harrow's (29) and Patterson's(2) tests where faster burning fuels were used to increase the flame speed and reduce cyclic variation.

Hansel (13) attempted to explain the general trend of cyclic variation to increase on both sides of the stoichiometric mixture Fig. (2-44) by developing a semi-quantitative turbulent model based on the assumption of proportionality between variations

in mass burning rate (or peak pressures) and turbulent flame speed and consequently the effect of turbulence on flame speed. Assuming the effect of turbulence as an additional term to the laminar flame speed the following relation was obtained:

$$\frac{\Delta P}{\bar{P}} \sim \frac{u'}{S_l + u'_{min}} \qquad (2\text{-}1)$$

Further assumptions that maximum variations in the turbulence intensity is invariant over the speed range of his tests (1180 - 2150 r.p.m.) and that $u'_{min} < S_l$ led to the following relations:

$$\frac{\Delta P}{\bar{P}} \sim \frac{1}{S_l} \qquad (2\text{-}2)$$

or

$$\frac{\Delta P}{\bar{P}} \sim A/F \text{ (for lean mixtures)} \qquad (2\text{-}3)$$

and

$$\frac{\Delta P}{\bar{P}} \sim 1/(A/F) \text{ (for rich mixtures)} \qquad (2\text{-}4)$$

However, such a model predicted only 40% of the observed variations in $(\Delta P/\bar{P})_{max}$ for lean mixtures and over-estimated such variations for rich mixtures (by about 150% in the reported example).

In fact these discrepancies between the predictions of the model and experimental results are not unexpected in view of the severe assumptions used in developing the model. For example,

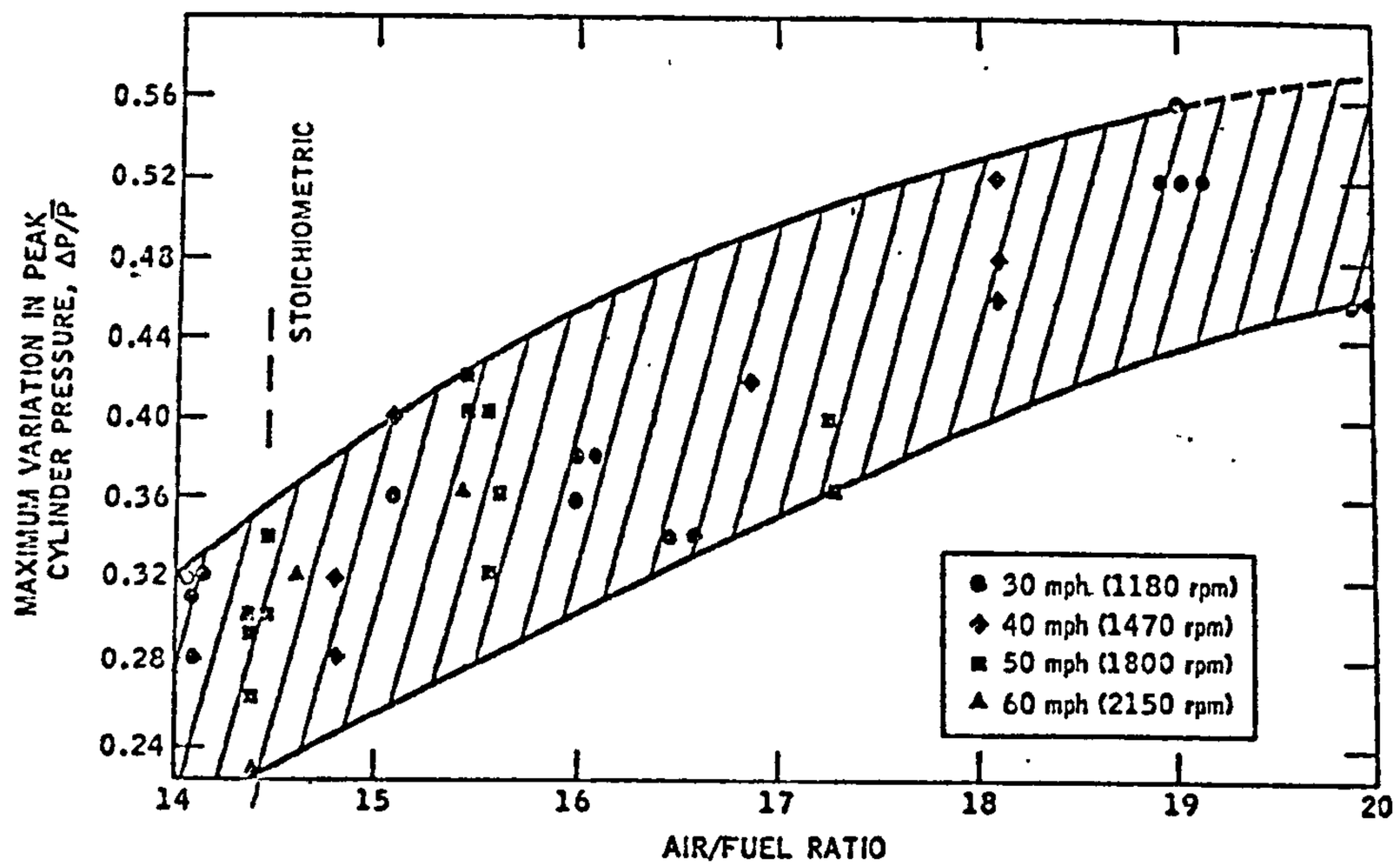

Fig (2-44). The influence of air/fuel ratio on the variation in peak cylinder pressure (13).

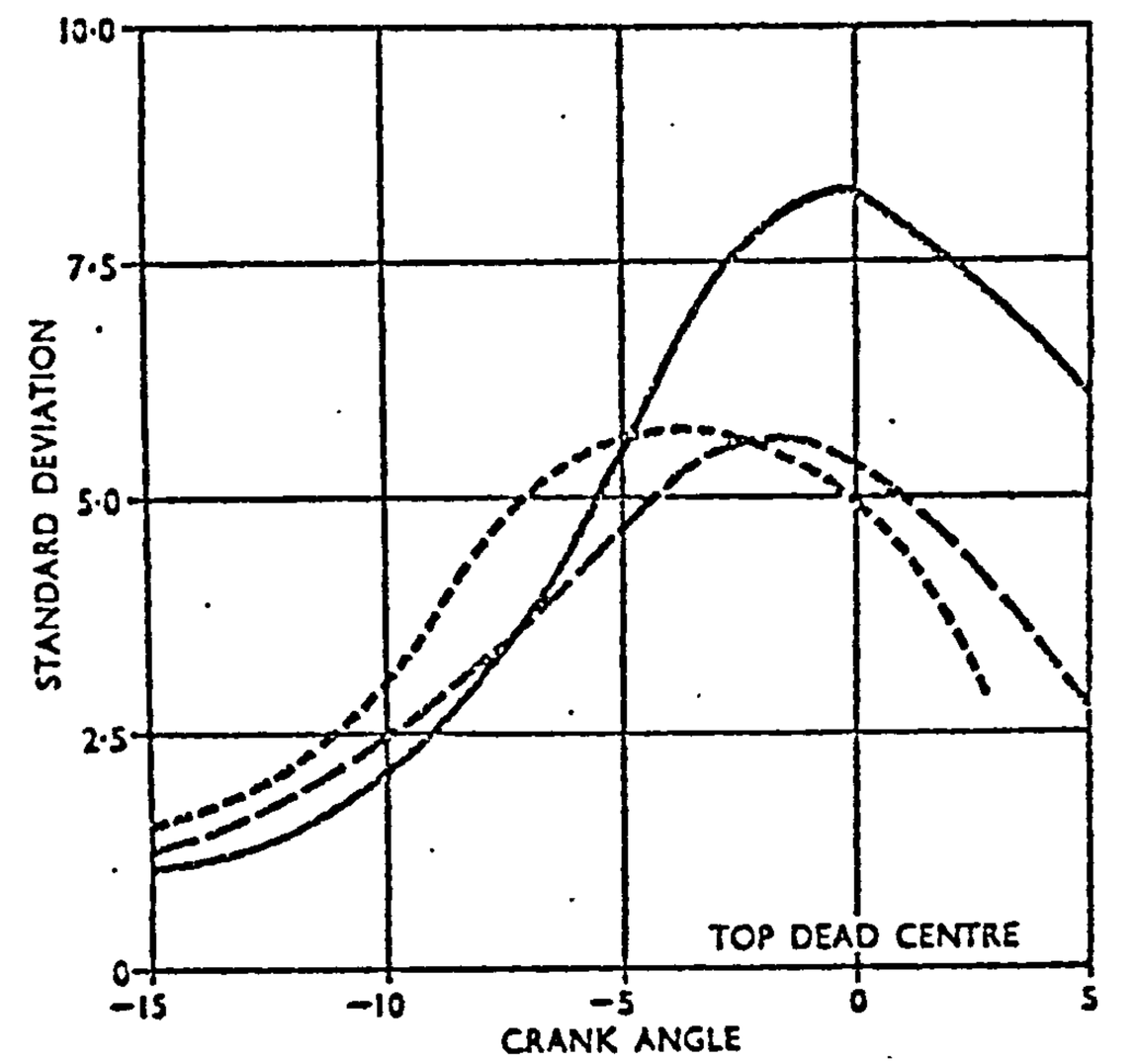

Fig (2-45). Pressure standard deviation during the combustion phase (6).
(CFR engine, 4.38:1 compression ratio, mixture 4% rich 900 r.p.m. and 31 deg. B.T.D.C. spark advance - iso-octane, ------ benzene, ------ petrol).

the assumption of a fixed variation in turbulence intensities irrespective of engine speed is not true, as will be seen from the discussion of the anemometer results of Matsuoka et al (15) section (2-4), as well as the results of the present investigation. Moreover, expressing the turbulent flame speed as the sum of the fluctuating velocity component and the laminar flame speed is only justified for the conditions of very weak turbulence, as will be discussed in section (2-5). Obviously such conditions never exist inside the combustion chamber of a S.I. engine, especially during the latter part of the compression stroke.

2.3.8 Type of Fuel

There is some connection between the type of fuel and cyclic variations in peak pressure and indicated mean effective pressure. The fuels with more rapid average combustion speed are less prone to produce cyclic variation. This is because less time is spent in burning phase and more on expansion phase. All hydrocarbon fuels exhibit the same kind of fluctuations, although their severity changes slightly with the chemical composition. Fuels which are rich in hydrogen exhibit very little variation as both their diffusion and flame speed are extremely rapid. Table (2-1) gives a comparison between flame speeds of some hydrocarbon flames.

Harrow et al (29) have examined the effect of the type of fuel on cyclic dispersion in terms of the flame travel times for a fixed path across the combustion chamber. Using three types of fuels of different flame speeds, namely: iso-octane, di-isobutylene

and benzene, they have found that at each mixture strength iso-octane burned appreciably more slowly than the others. The extent of cyclic variations in flame travel times were larger for iso-octane than for either di-isobutylene or benzene, Fig. (2-43). The extent of dispersion depended markedly on mixture strength. Minimum dispersion was reached at about 12:1 air/fuel ratio with all three fuels. The greatest dispersion occurred at weak mixtures. Advancing the spark timing reduced the extent of cyclic dispersion and reduced the differences between fuels.

Tests carried out by Vichnivesky (6) on a CFR engine is in agreement with the previous conclusions, Fig. (2-45).

Karim (32) carried out some experiments using a range of commercial petrols, which indicated that differences in the extent of cyclic dispersion from one fuel to another were very small and being within the experimental error in determining the values of maximum pressure deviation.

Thus among the commercial petrols available, there is nothing to choose between one and the other, and the choice will remain purely economic.

Table (2-1) Burning Velocities of some Hydrocarbon Flames (70)

Compound	Formula	Burning Velocity (cm/sec)
Methane	(CH_4)	33.8
Ethane	(C_2H_6)	40.1
Propane	(C_3H_8)	39.0
Butane	(C_4H_{10})	37.9
Ethylene	(C_2H_4)	68.3
Benzene	(C_6H_6)	40.7
Acetylene	(C_2H_2)	131.0
Heptane	(C_7H_{16})	38.6
Hexane	(C_6H_{14})	38.5
2-Methylpentane	(C_8H_{18})	36.8
3-Methylpentane	(C_8H_{18})	36.7
2, 3-Dimethylpentane	(C_8H_{18})	36.5
2, 4-Dimethylpentane	(C_8H_{18})	35.7
1-Pentene	(C_5H_{12})	42.6

2.3.9 General Characteristics of Cyclic Variation

Summing up the conclusions of previous investigators, one could outline the general characteristics of cyclic variation as follows:

i) Cyclic variations do not depend on events of any other cycle, but mainly on the intake, compression and combustion of each individual cycle. However, it can be seen from typical cylic pressure records taken when large

cyclic variations are exhibited that a cycle with a very low maximum pressure will be generally followed by a few cycles with relatively low maximum pressure before the apparently true randomness of the records is restored.

ii) The dispersion is not due to variations in the spark timing or the type of spark. It improves slightly by using more than one spark plug, or modifying the ignition system so as to decrease the quenching of the flame kernel or increasing the energy given to the mixture when spark timing is advanced.

iii) Cyclic dispersion in combustion process occurs even with gaseous fuels and still persists when the quantity of fuel/air mixture delivered to the engine cylinder is the same on each cycle.

iv) The extent of cyclic dispersion is less for fast burning fuel such as benzene than for a slow burning fuel such as iso-octane. Factors which tend to increase the rate of flame travel in an engine, e.g. enriching the mixture to best power mixture ratios, reducing exhaust residual, installing shroud valves, and multiple ignition of the charge, tend also to reduce the extent of dispersion. Factors which slow down the flame in the engine tend to increase the dispersion.

v) The variations of peak pressure, burning time and rates of pressure rise from cycle to cycle becomes greater as the mixture is made leaner, since mixture velocity has a great effect on the ignition and combustion characteristics of lean mixtures.

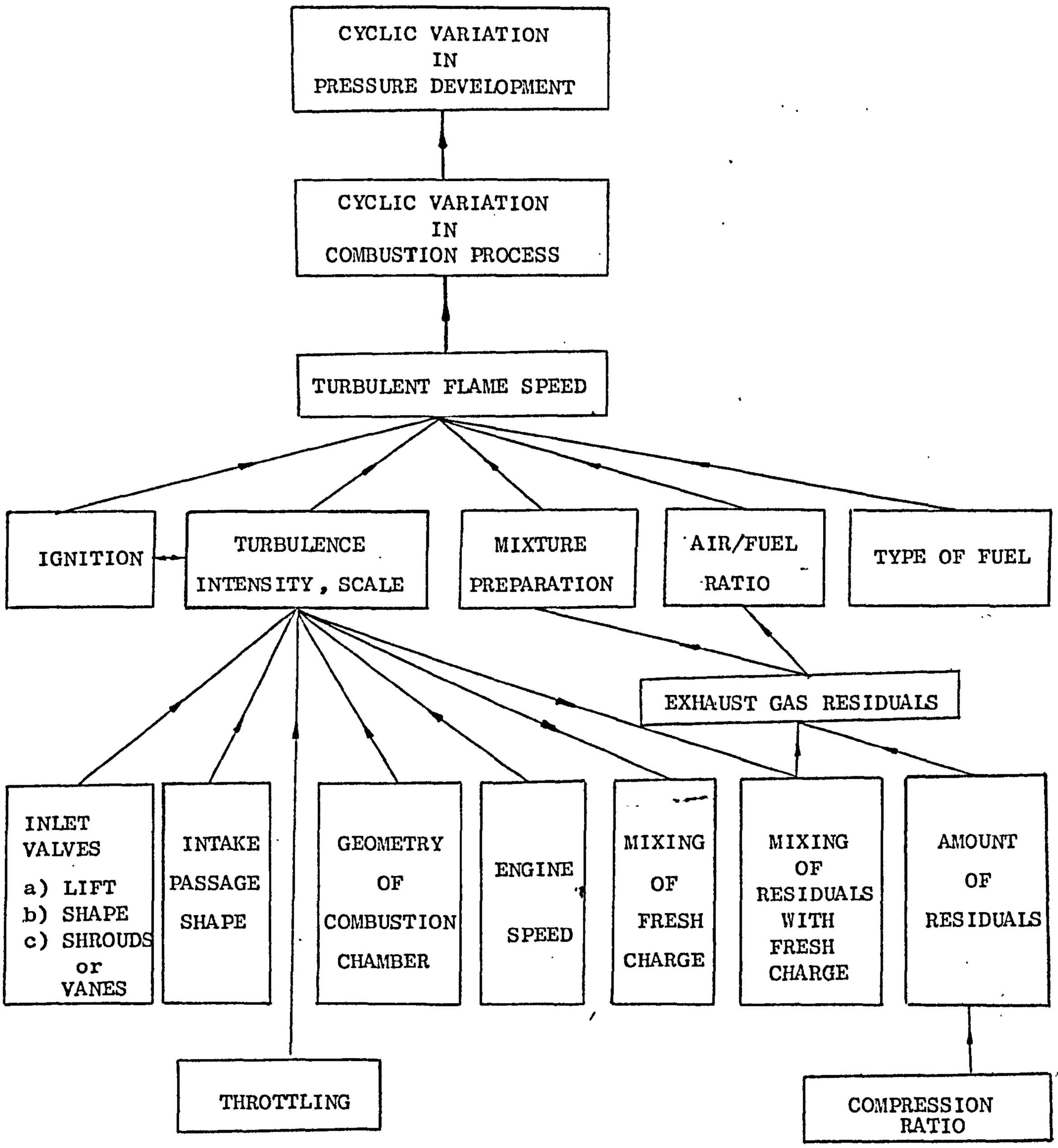

FIGURE (2-46) Relationship between engine operating variables which affect the mechanism of cyclic combustion variation in spark ignition engines.

vi) For rapid combustion and minimum heat loss, it is desired to have a high swirl velocity, especially at very lean mixture ratios.

vii) For minimum variations in rates of pressure rise, peak pressures and burning times, it is desired to minimise the variation in gas velocity or, if this cannot be done, to use the highest nominal swirl velocity and avoid very lean mixtures, since variation in gas velocity and turbulence in the vicinity of the spark plug at the time of ignition appears to be the main cause of combustion variation.

Fig. (2-46) shows the relationship between engine operating variables which affect the mechanism of cyclic combustion variation in S.I. engines.

2.4 Effect of Gas Velocities and Turbulence on the Combustion Process in S.I. Engines

Investigations of the flow field inside the combustion chambers of S.I. engines are very limited in the literature and most of them have concentrated on mean gas velocity measurements. The study of the structure of the turbulent flow field, in terms of intensities and scales, has received little attention, in spite of the fact that such knowledge is very fundamental for combustion studies in engines. This may be attributed to the difficulties in applying the conventional techniques used in the field of aerodynamics to the transient processes occurring during engine cycles.

A review of the most important studies in this field will be discussed in this section.

Lee (18) has studied the air movements in an experimental engine, which was basically a 5 by 7 inch single cylinder engine with a glass cylinder and cylinder head to permit photography, Fig. (2-47 a) . Different types of air flow were produced in motored tests by using shrouded intake valves and by altering the shape of the intake port in the cylinder head. The air motion was studied by use of high speed photography of feathers introduced into the main air stream which showed the following:

i) For a plain intake valve air movements created in the engine cylinder during the intake stroke continued throughout the compression stroke at a slowly reducing velocity. By the time the piston had descended far enough on the expansion stroke most of the turbulence died out. During the last two strokes of the cycle, the air movements were mostly due to expansion and expulsion of the air by the piston.

ii) The velocities of induced air currents were approximately proportional to the engine speed and about inversely proportional to the flow area at the intake valve. They were about the same whether the air flow was orderly or turbulent.

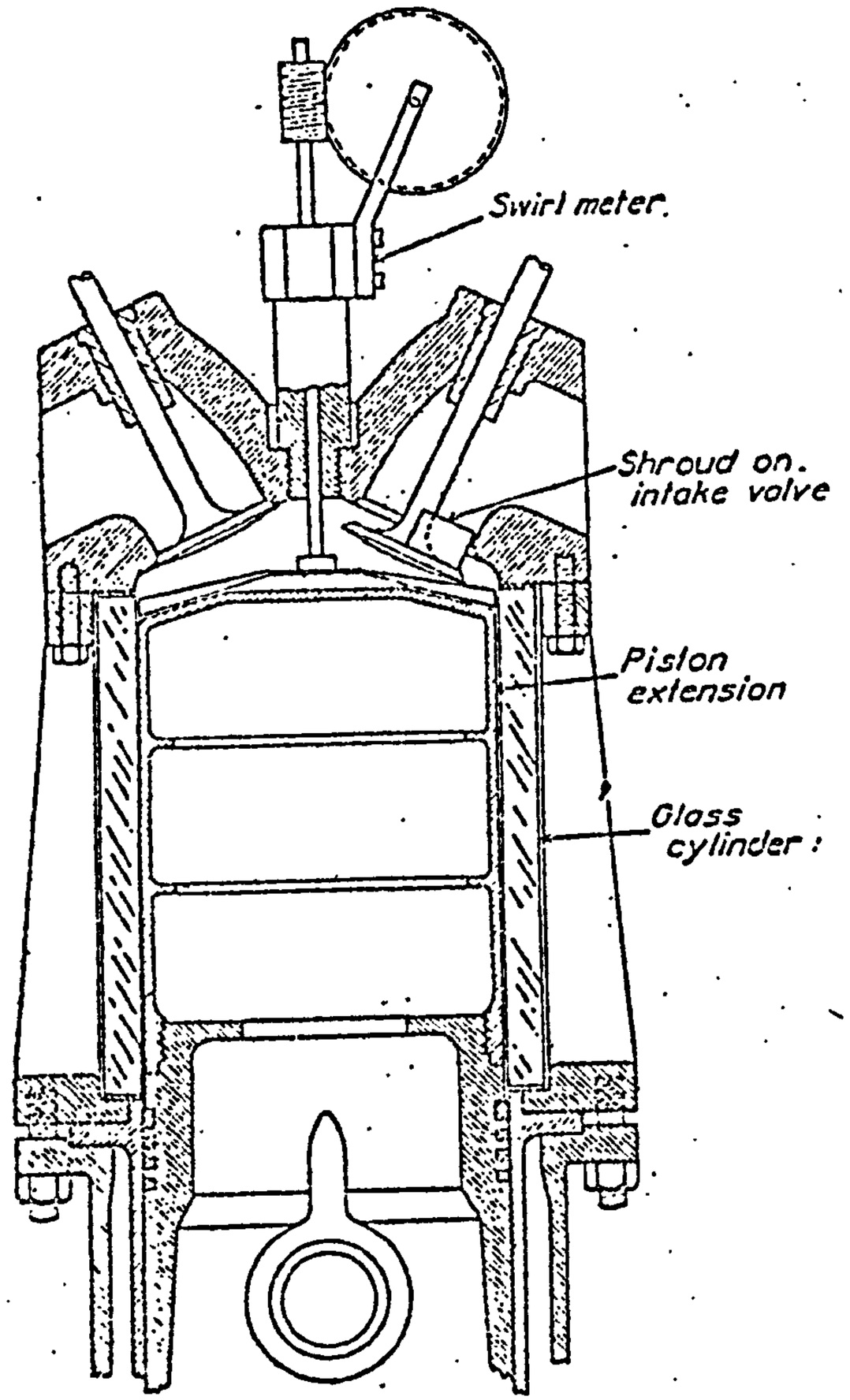

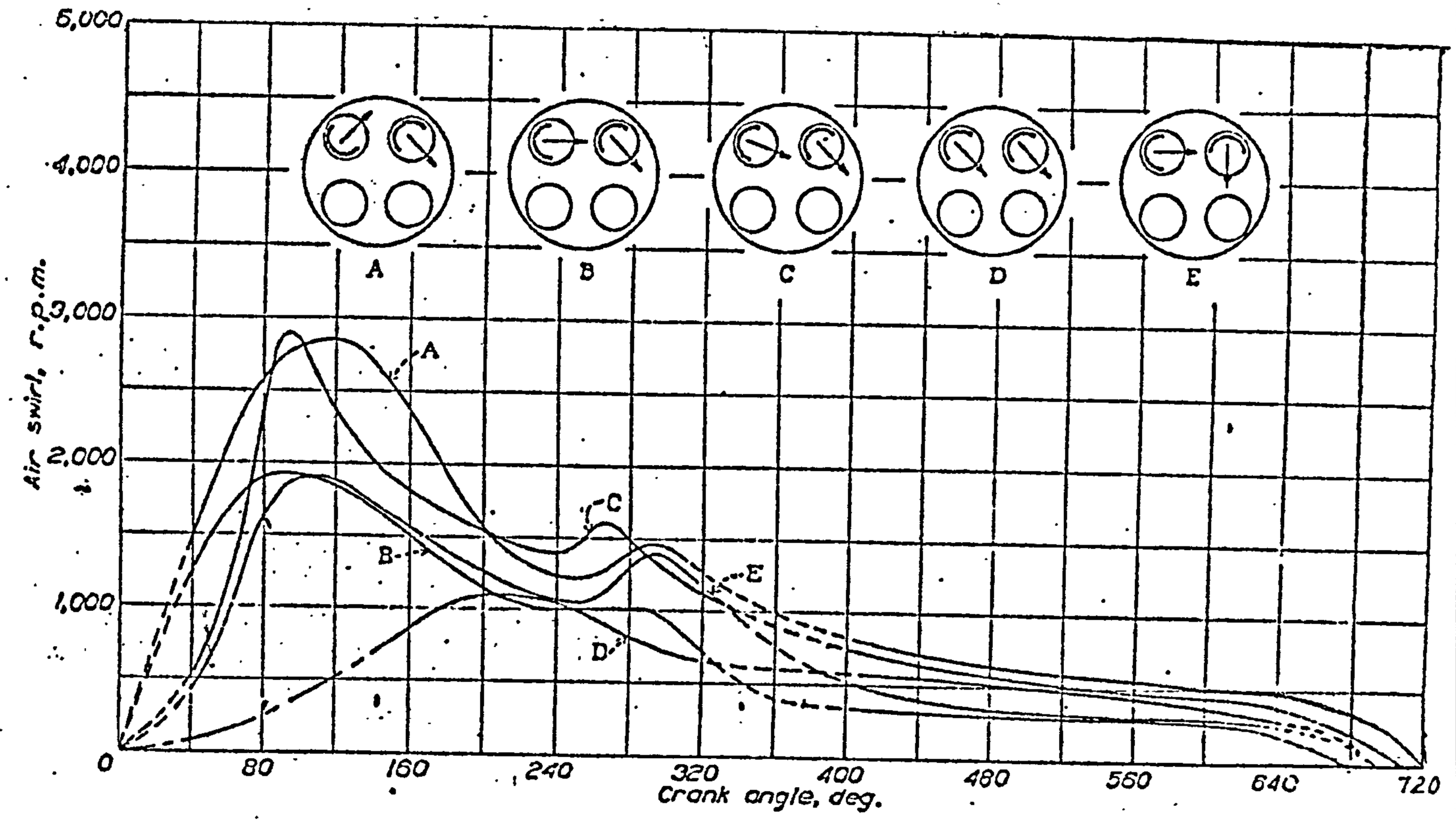

Fig (2-47a) Sketch showing the glass cylinder and cylinder head used for Lee's investigation (18).

Fig (2-47b) Effect of shrouded intake-valve arrangement on rate of air swirl (18).
(Engine speed 500 r.p.m.)

iii) The use of shrouded intake valves set to direct the incoming air tangentially caused the air to rotate rapidly about the cylinder axis. The maximum rate of rotation was reached at about 110° crank angle after the beginning of the intake stroke and the rotation continued until the end of the exhaust stroke, Fig. (2-47b).

iv) The use of a single plain intake valve with its manifold shaped to direct the incoming air tangentially resulted in a rotation of air accompanied by considerable turbulence and some vertical movements.

In fact, apart from the inaccurate qualitative description of turbulence, particularly during the expansion stroke, (as will be discussed later), most of the conclusions of this very early investigation (1939) regarding the general flow pattern inside the engine have been confirmed by the recent anemometer measurements of Winsor (23), James (24), as well as the present study.

Rothrock and Spencer (16) have studied the combustion process and its cyclic variation using the same engine and valve arrangements of Lee. The engine was fired only once by injecting and igniting a single charge of fuel. Table (2-2) lists the test conditions of these experiments. The burning times were determined from the high speed photographs of the combustion process while the cyclic reproducibility were examined from the pressure diagrams. Table (2-3) gives a comparison between the burning times for different valve arrangements. The main conclusions of this study could be summarized in the following:

i) Excellent cyclic reproducibility was obtained by directing the air so that the swirl moved past the spark plug and was in a plane normal to the axis of the cylinder.

ii) Doubling of the engine speed without increasing the linear velocity of the inlet-air caused an increase in the rate of combustion of the same magnitude as that caused by doubling the inlet-air velocity without increasing the engine speed, Table (2-4).

iii) When the valves were shrouded so that the inlet-air velocity was doubled and were set to cause a directed air swirl, the rate of burning was increased.

iv) When the valves were shrouded so that the inlet-air velocity was doubled but were set so that there was no directed swirl, the rate of burning was not necessarily increased.

Examination of these conclusions reveals the importance of mixture motion and turbulence, especially the small scale eddies, in increasing the flame speed. The increased burning rate accompanying an increase in engine speed is caused equally by increased turbulence intensities (higher intake velocities) and by decreased time intervals. The latter factor reduces the effect of turbulence damping by viscous action and results in higher turbulence intensities at the time of ignition. Moreover, the persistance of a directed mixture motion inside the cylinder for longer periods (in terms of crank angle degrees) on the compression stroke enhances the process of generating small eddies by friction forces on the cylinder head walls, together with the increased

Table (2-2) Test Conditions for the Investigation of Rothrock and Spencer (16)

Compression ratio	7
Engine coolant temperature	250°F
Fuel	C.F.R. S-1 reference fuel - octane number (100) without the addition of tetraethyl lead - 90/100 iso-octane.
Air/fuel ratio	14:1
Spark advance	300 BTDC (± 1°)
Fuel injection start	200 ATDC on intake stroke

Table (2-3) Comparison between Burning Times for Different Valve Arrangements and Altered Inlet Passage

Case	Burning Time (Crank Angle deg)	Burning Time (sec)
Plain valve	35	0.0117
H	32	0.01067
I	31.5	0.0105
E	29.5	0.00983
D	29	0.00967
G	27.5	0.00917
A	27.5	0.00917
F	28.5	0.0095
Altered Inlet Passage	28.0	0.0095

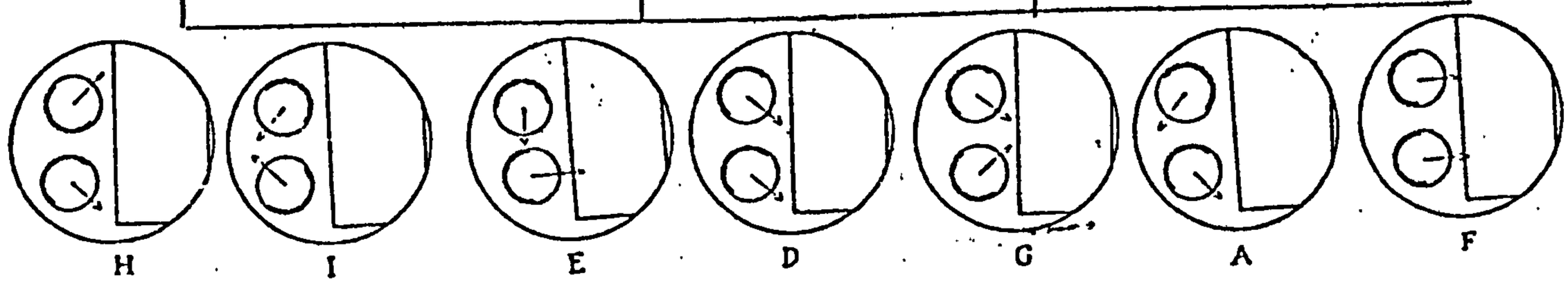

Table (2-4) Variation of Burning Times with Inlet-Air Velocity and Engine Speed

Engine Speed	Number of Valves	Burning Time (Crank Angle deg)	Burning Time (sec)
500	2	35	0.0117
500	1	25	0.0083
1000	2	35	0.0058
1000	1	25	0.0042

homogeneity of the mixture. This explanation is supported by the results of the present study, (as will be discussed later in detail) where comparison of the power spectral density curves for turbulence at any particular crank angle during the compression stroke shows an increase in the percentage of kinetic energy of small scale turbulent eddies at higher engine speeds. Similar arguments could be applied to the case of increased inlet-air velocities by shrouding the inlet valves or proper directing of inlet ports.

Wenger (1939) (21) has conducted the first attempt of investigating gas motion inside the combustion chamber of a motored single cylinder engine, using hot wire anemometry. Fig. (2-48) shows the shape of combustion chamber and piston head used and the location of the measuring probe. A constant current anemometer system was used. The hot wire was made of tungsten material with 15 μ in diameter and a length between 19 and 21 mm. Measurements were carried out at different points in the cylinder. Their distance from the cylinder wall was 20, 40, 60, 80, 100 and 120 mm. Engine speed was varied between 500 and 1800 r.p.m. at compression ratios of 4.8 and 5.2:1 and different throttle openings. The main conclusions of this study could be summarised as follows:

i) Gas velocities attain their maximum value during induction period and decay on the compression stroke. Further peaks occur during expansion and exhaust strokes.

ii) Measurements at different points have shown practically the same range of scatter so that it was impossible to detect any functional relation between the behaviour of gas velocities and the distance from the wall, Fig. (2-49).

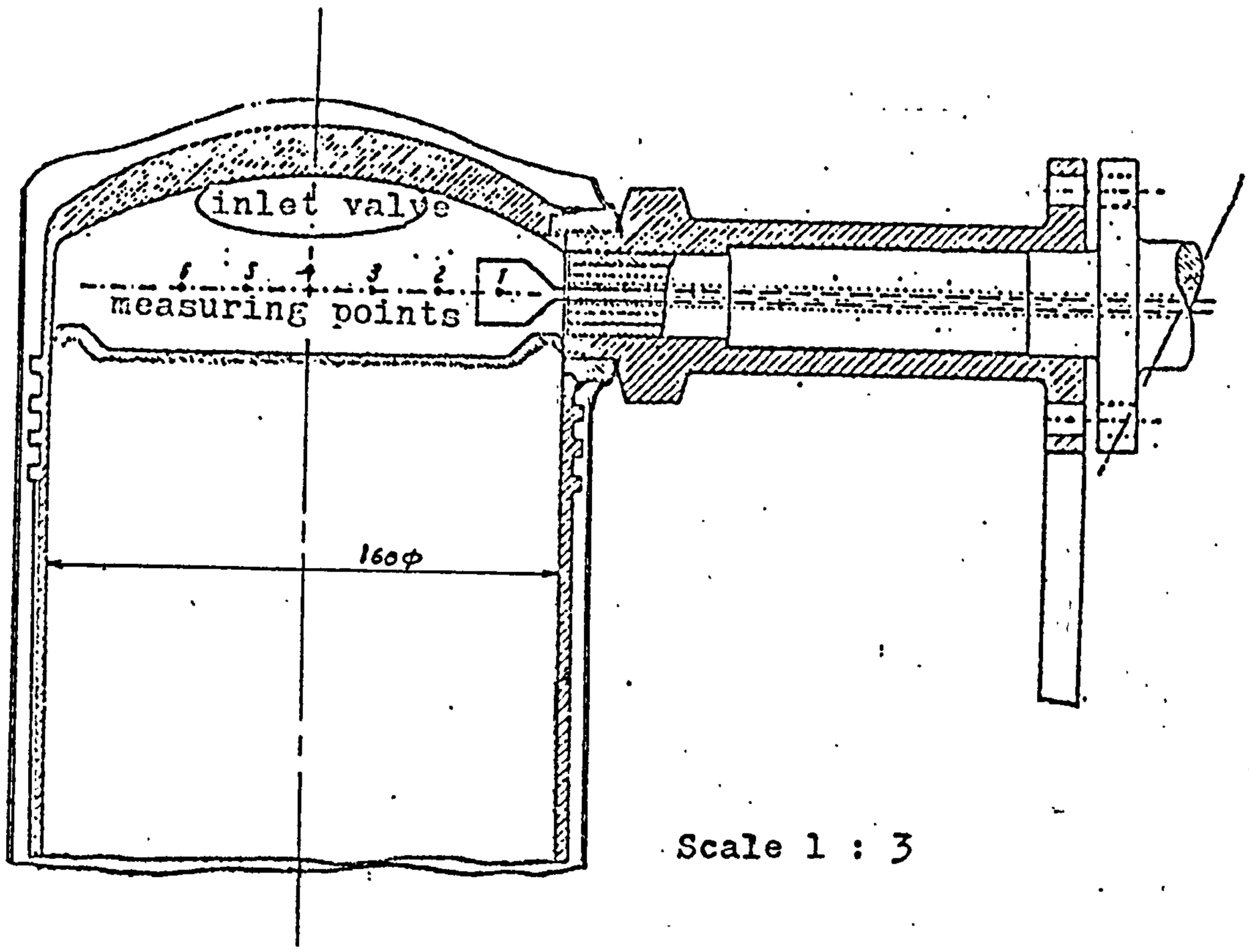

Fig (2-48) Installation of measuring probe in the combustion chamber (21)

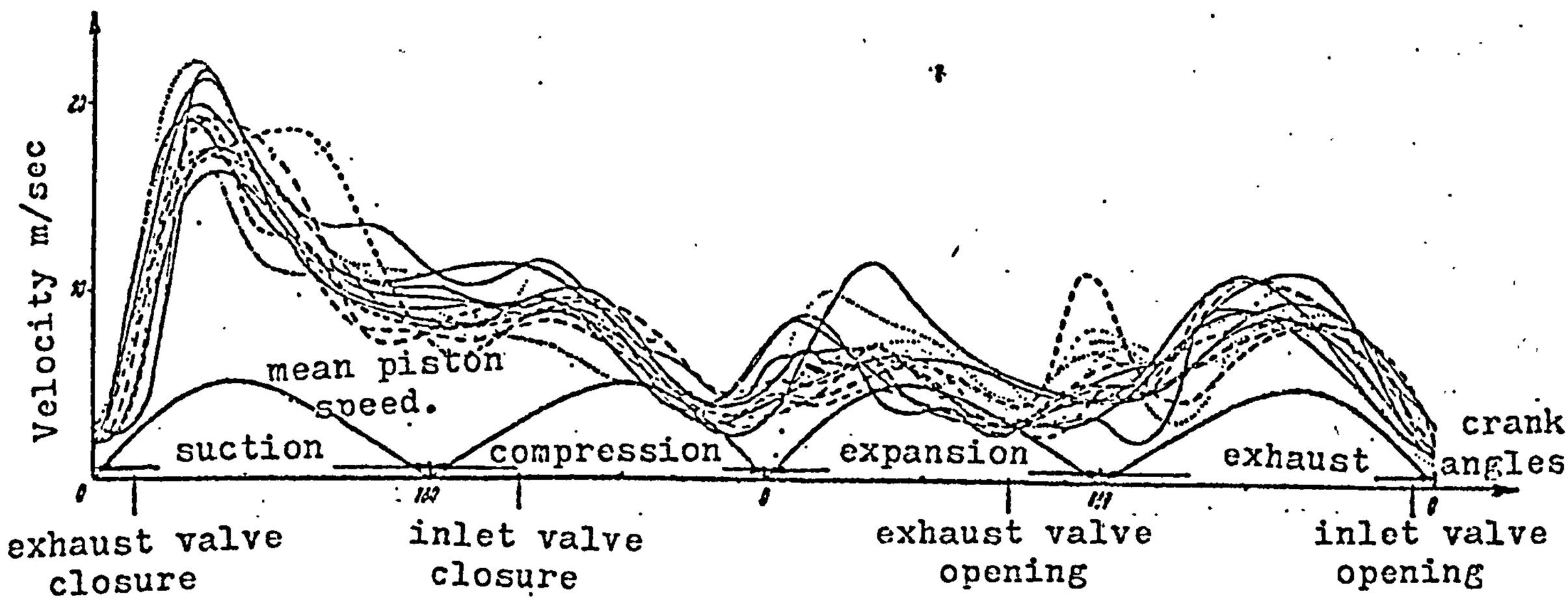

Fig (2-49) Air velocities versus crank angles for the six measuring points in Wenger's investigation (21).(500 RPM,CR = 4.8:1)
—— Point 4 ,.....Point 2 ,---- Points 1,3,5,6.

iii) Air velocities averaged over the whole chamber length increase with an increase in engine speed. However, this increase always remains below the increase in mean piston velocity. Gas velocities increase also with opening the throttle. The same trends were observed for gas velocities averaged over the whole cycle.

With the exception of the general trends of variations in gas velocities during different strokes of the cycle with engine speed and throttle opening, the characteristics of the turbulent field inside the combustion chamber have not been investigated at all in this work. Moreover, the conclusion of random variation of gas velocities at different points in the combustion chamber has been proved by Semenov (22) and Molchanov (62) to be incorrect. In the latter two investigations, large velocity gradients have been observed between neighbouring points in the combustion chamber and are believed to be the main source of turbulence generation during the induction period.

Nevertheless, this earlier work (1939), has ascertained (at that time) the suitability of hot wire anemometry for investigating the characteristics of flow fields inside engine cylinders where rapid variations of pressure and temperature take place.

Molchanov (1953) (62) measured gas velocities and turbulent fluctuations in a cylindrical combustion chamber with a flat piston head, using a hot wire anemometer. The measuring sensor was a tungsten wire of 19 μ in diameter and 4.5 mm in length. The anemometer bridge used had a frequency response up to 2000 cycle/sec. Measurements

were carried out at different locations in the combustion chamber as well as different orientations of the hot wire probe, which was introduced radially across a displacer ring at the top of the combustion chamber, Fig. (2-50). The compression ratio was varied during these measurements in a wide range (6 - 12:1) at a constant engine speed of 900 r.p.m. and full throttle opening.

The results of this investigation could be summarized as follows:

i) The gas velocities increase rapidly at inlet valve opening and is followed by a continuous decay until inlet valve closure when it becomes approximately equal to piston speed at that moment, Fig. (2-51). Periodic oscillations were noticed during the decay period at all the points of measurement which have been explained later by Sokolik (48) as caused by oscillations in the inlet pipe. The measurements showed that the flow field during induction does not have a continuous distribution of velocities throughout the cylinder.

ii) During the compression stroke, a conceptional flow pattern was proposed which consisted of local vorticities resulting from the disruption of the orderly motion created during induction stroke. This was drawn from the observations of insignificant changes in the hot wire output when rotated through 360° about its axis, Fig. (2-52). Moreover, a regularly repeated transition of local gas velocities from maximum to minimum for two adjacent positions of the

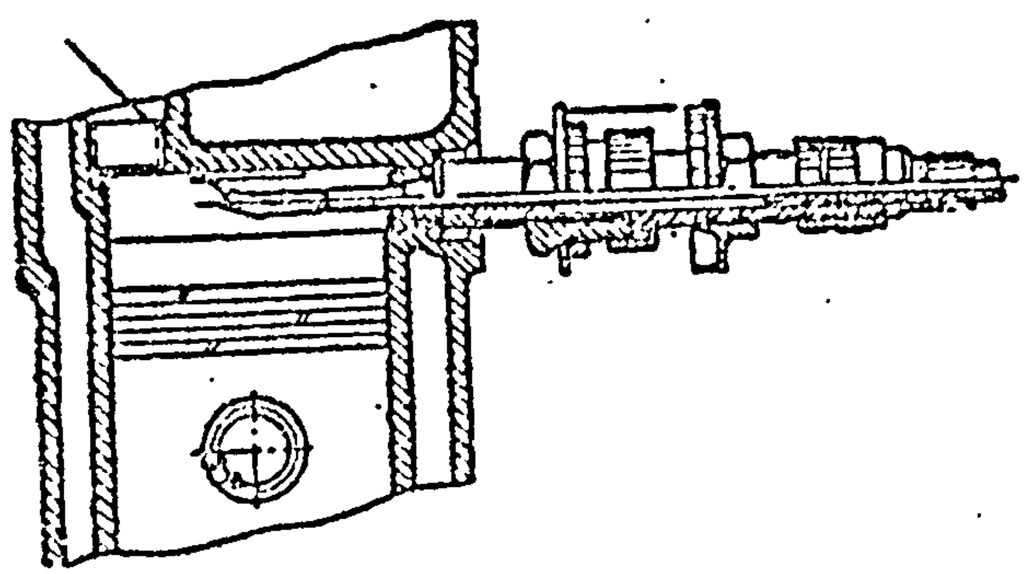

Fig (2-50). Schematic diagram of insertion of anemometer probe into combustion chamber (62).

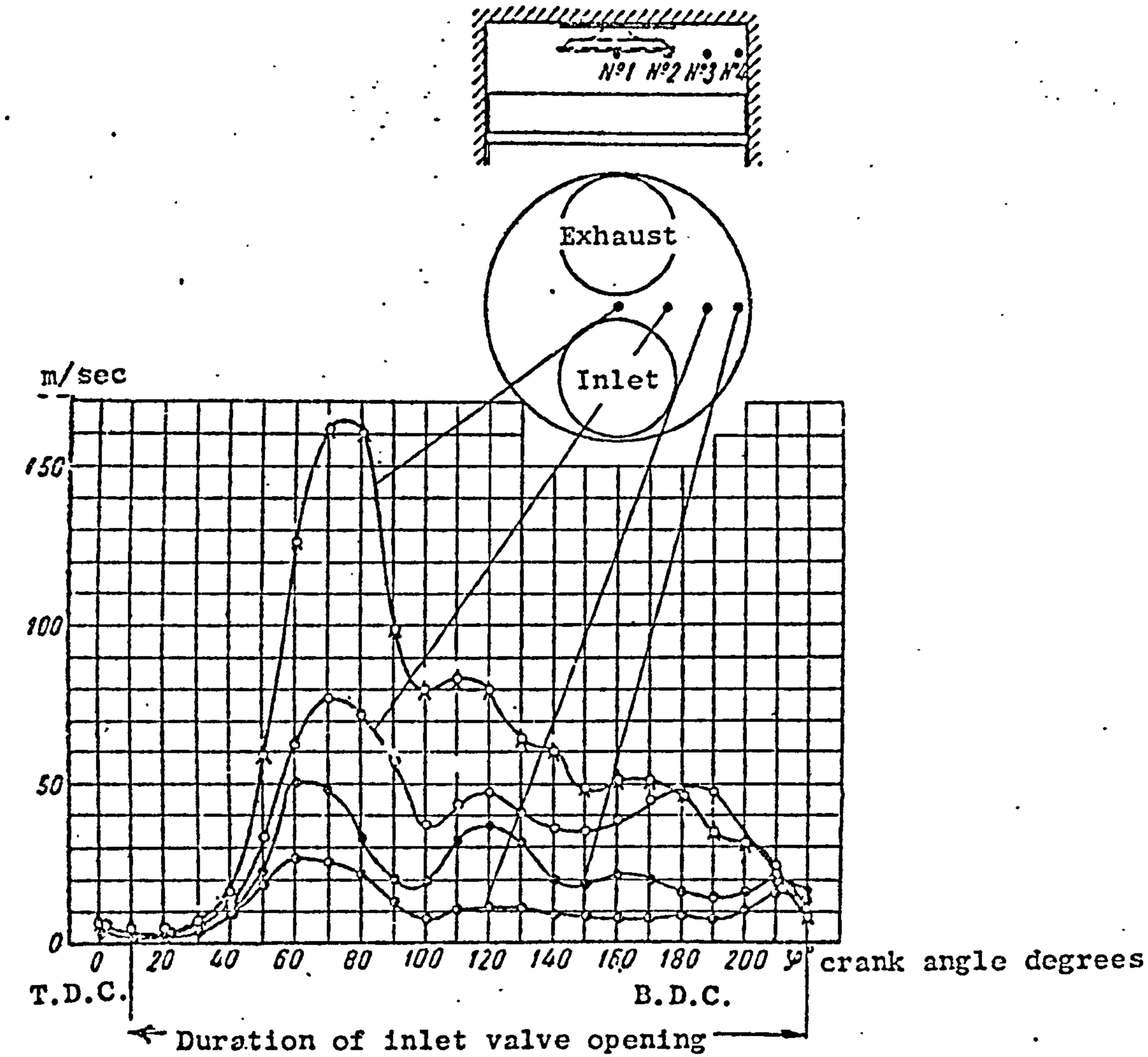

Fig (2-51). Variation of gas flow velocities at various points during the induction period (62).

wire was observed and interpreted by the presence of locally directed streams of different magnitudes at neighbouring points in the combustion chamber.

iii) The flow velocities vary in different ways as a function of compression ratio (between 6 - 12:1), up to about 20 degrees before top dead centre. After this period, it appeared that they decreased slightly as the compression ratio increased. This led Molchanov to state that 'variations of compression ratio within wide limits has practically no effect on the velocities of ordered gas streams in the combustion chamber', Fig. (2-53).

iv) Velocity traces without filtering the high frequency fluctuations showed an increase in the intensity of turbulent fluctuations towards the end of the compression stroke and towards the beginning of expansion, Fig. (2-54). The turbulent fluctuations are reported to be greater than the mean velocity in some cases. Once again, varying the compression ratio from 6 to 12 does not cause any sharp variations in turbulent motion of the gas. However, varying combustion chamber shape by inserting annular displacers resulted in a considerable increase in turbulence intensities.

Although the response of the anemometer bridge used in this work covers the range of frequencies of turbulent eddies in an engine, as will be seen later, the very long wire used reduces its sensitivity to turbulent fluctuations and results in an under-estimation of actual intensities. This effect is very significant because of the very small size of eddies in S.I. engines as will be

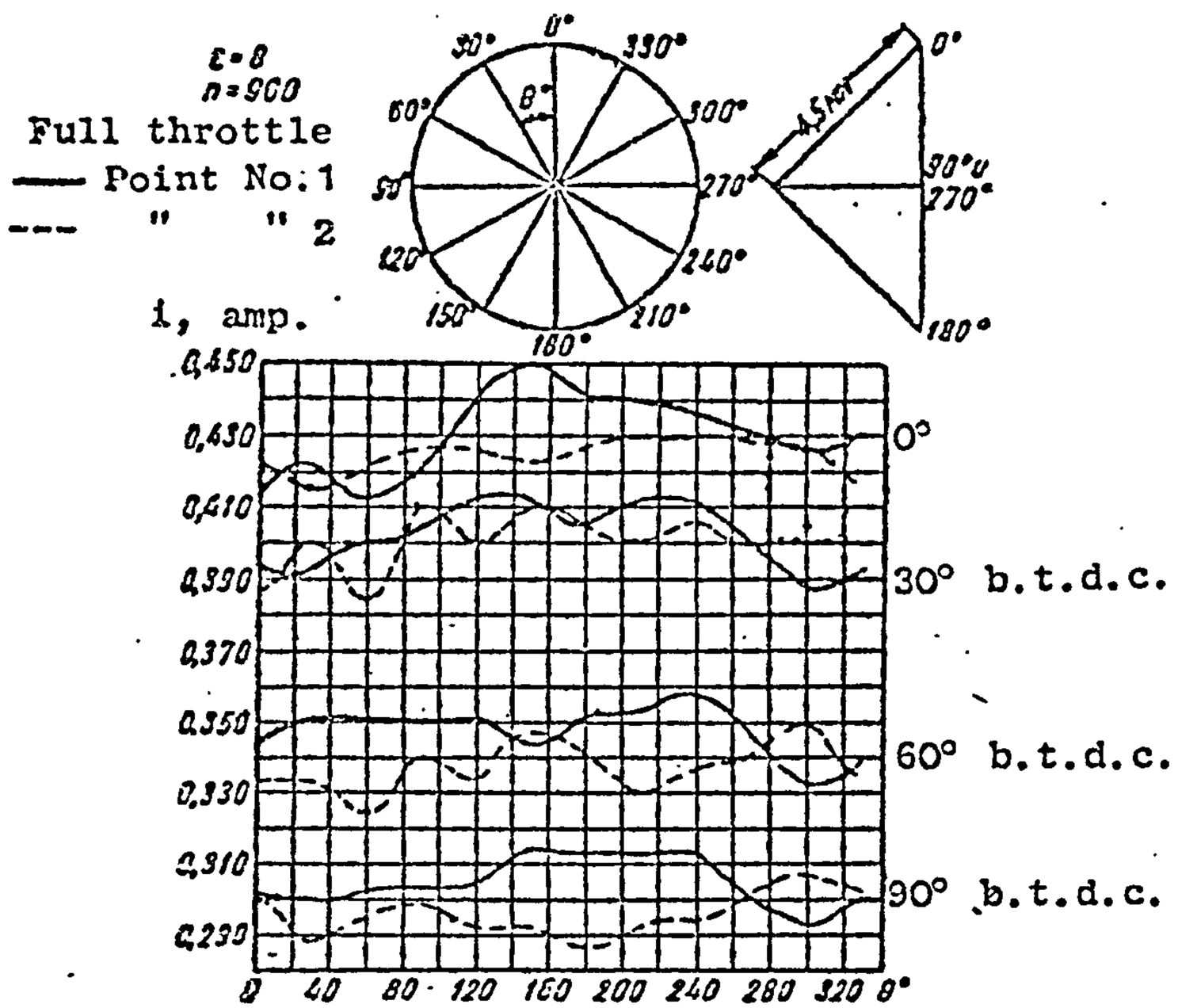

Fig (2-52). Dependance on anemometer current (i) on wire orientation in combustion chamber (62).

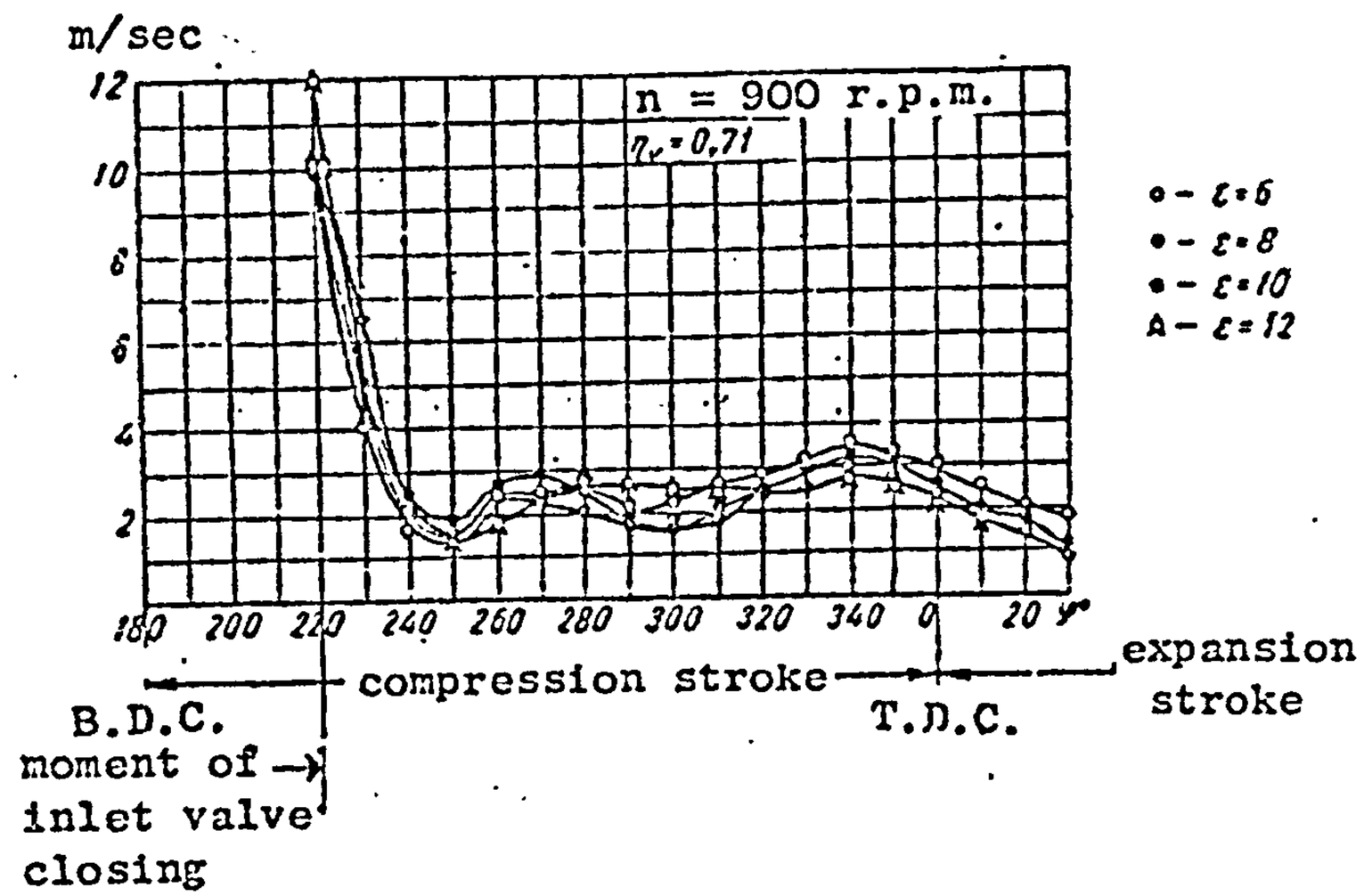

Fig (2-53). Air velocities in combustion chamber at various compression ratios (62).

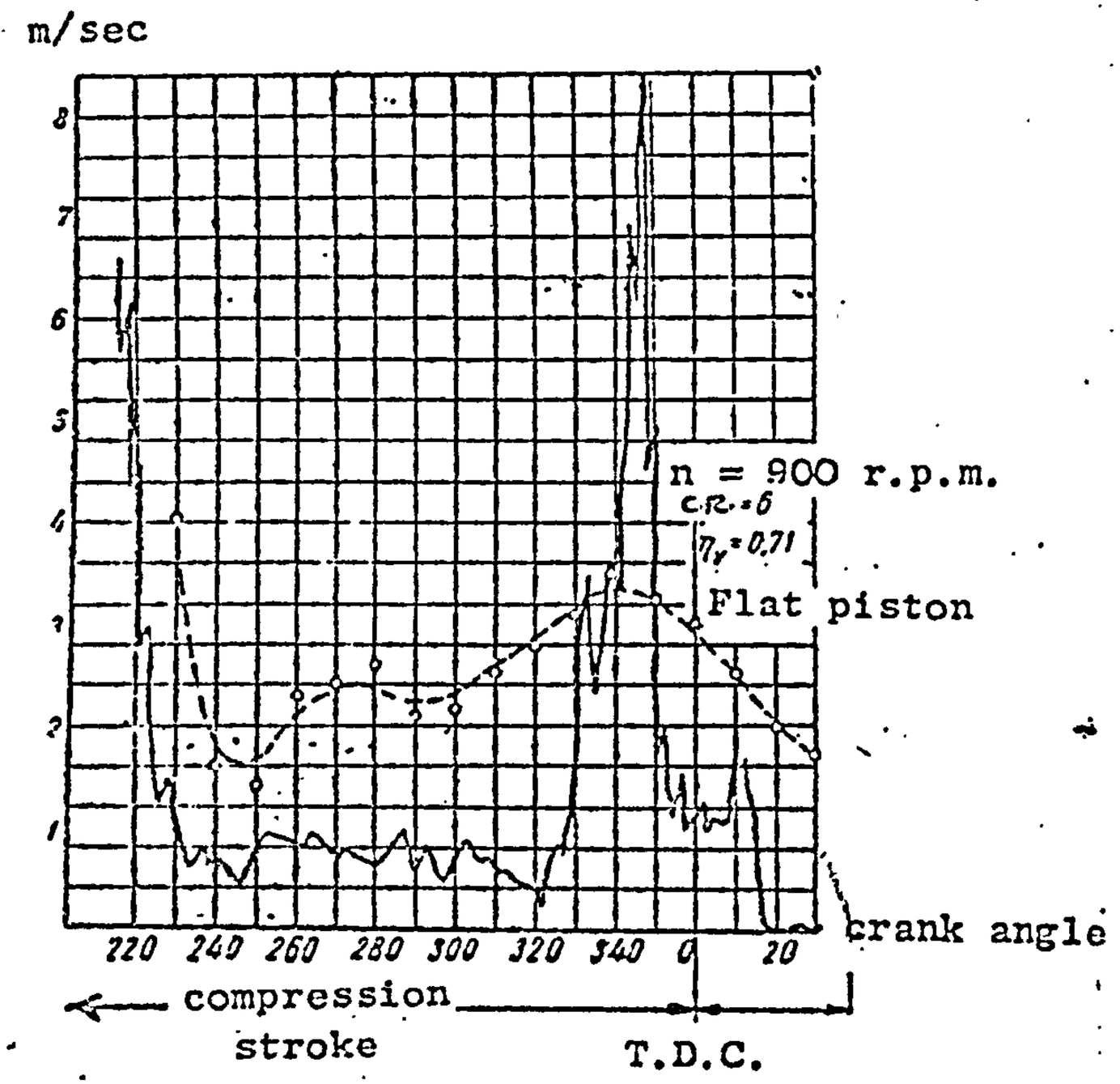

Fig (2-54). Variation in the projection of air flow velocity fluctuations in the combustion chamber during compression stroke (62).

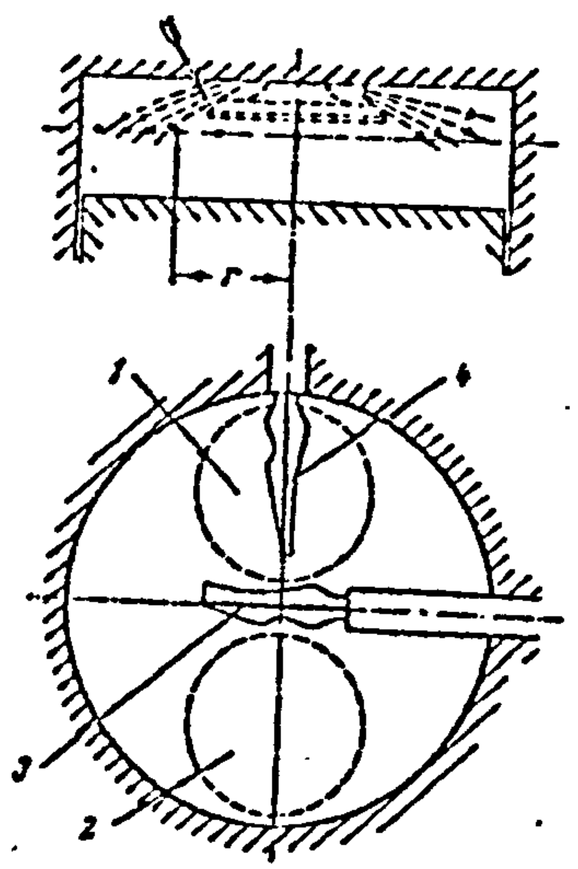

Fig (2-55). Positions of hot wire anemometer and correction resistance thermometer in the combustion chamber used by Semenov (22).

discussed in a re-analysis of Semenov's work (22), (using the same anemometer system and combustion chamber shape under similar engine operating conditions). Moreover, the use of tungsten wire material was unsuitable for the previous investigation, especially at higher compression ratios (e.g. 12:1) since this material is known to oxidise at about 350°C. This results in an increase in wire resistance and consequently reduces the output current of the anemometer which could lead to an under-estimation of gas velocities if the ambient calibration of the wires before test is used.

The reported observation about magnitudes of fluctuating velocity components greater than the mean gas velocity could be only explained by an increase in the energy content of eddies in the high frequency range. Unfortunately the bandwidth of the filters used have not been reported to enable a definite explanation of this observation, particularly in view of the measurements of the spectral distribution of turbulence in S.I. engines which have shown that most of the turbulent energy is concentrated in the low frequency range (below 700 Hz) (22, 24).

It is generally recognised that the pioneer work of Semenov (1958) (22) represents the most complete research on mixture motion in a S.I. engine. These experiments were carried out using a single cylinder CFR engine with a variable compression ratio. The combustion chamber was flat and cylindrical as shown in Fig. (2-55).

Semenov used a compensation hot wire anemometer system (developed by Chebyshev (66)). Its main principle is based upon reducing the hot wire current (i) under engine operating conditions

of pressure and temperature (P,T) to a corresponding value (i_o) at some initial conditions (P_o, T_o) as given by the following relationship:

$$i_o = K(P,T).\ i \qquad (2\text{-}5)$$

where the coefficient of reduction K(P,T) could be obtained experimentally and introduced into the electronic compensation circuit used.

The measuring sensors of the anemometer system used in this work consisted of the following:

a) a two wire sensor, in which a resistance thermometer wire 12 mm in length regulates the overheating current in the anemometer wire itself, which was 2.5 mm long. (However a value of 4 mm is reported by Sokolik (48) in a discussion of this work). Both wires were 11 microns in diameter and of tungsten material.

b) An additional resistance thermometer which reduces the recorded current to the initial temperature conditions.

The product of the voltage across the second resistance thermometer, corresponding to the instantaneous gas temperature times the signal from the hot wire anemometer circuit, gives the bridge voltage referred to the initial state of the charge, a quantity which determines directly the gas flow velocity. By chopping the continuous signal from the hot wire anemometer into pulses of 24 crank angle degrees in duration, (which was an arbitrary chosen period), the average gas velocities were measured and averaged over 20 to 40 successive cycles. Pulses of the fluctuating velocity component were separated from the continuous

velocity signals using band pass filters which consisted of 5 filters covering the following frequency ranges 850-1300, 1300-1950, 1950-2900, 2500-4250 and 4250-6200 cycles per second. This assembly was used also to obtain the spectral composition of the turbulent fluctuations. The root mean square values of the fluctuations were obtained over the same number of cycles, using a vacuum tube voltmeter. Further details about this measuring and recording system are given in reference (65).

The main conclusions of Semenov's work could be summarized as follows:

i) The gas velocity during induction periods varies considerably at various points across the combustion chamber which reflects the jet nature of the gas motion during this period and flatly contradicts Wenger's conclusions (21), according to which the gas flows into the cylinder with the same velocity over the whole cross section. This jet nature of the filling process leads to formation of velocity gradients in the cylinder which is believed to be the main source of generation of turbulence in the engine cylinder.

ii) The average gas velocity during the induction increases almost linearly with engine speeds and decreases with throttling and increased distance from the centre of the combustion chamber.

iii) The average gas velocity and the fluctuating velocity component decrease rapidly to a minimum during the first third of the compression stroke, after which they remain

almost constant for the remaining period of the compression stroke and finally drop smoothly near TDC, Fig. (2-56). However, a part of this observation could be attributed to the shape of the combustion chamber used (open cylindrical chamber) where no secondary flows are created during compression as will be the case for squish combustion chambers.

iv) The average gas velocity at TDC compression, drops by about 20% with an increase in compression ratio from 4 to 9.5, increases with engine speed according to the approximate relation $\bar{U} \sim r.p.m.^{2.1}$ and increases by about 4% with an increase in throttle opening from 0.2 to 0.8 of its maximum value. The velocity gradients between various points in the combustion chamber are, markedly, reduced from the values attained during induction, (e.g. 20 sec^{-1} compared with 6000 sec^{-1} for the two cases respectively).

v) The spectrum distributions of the turbulent fluctuations showed that most of the energy during the compression stroke lies in the frequency region below 500 Hz.

The most serious concern with regard to Semenov's work are the adequacy of his calibration procedure and the suitability of the wire material used which is known to oxidise above 350°C, (the operating wire temperatures are not reported in any of the published literature about this work). The latter problem results in inaccuracies due to the changes of wire cold resistance and consequently the basic calibration used as reference conditions.

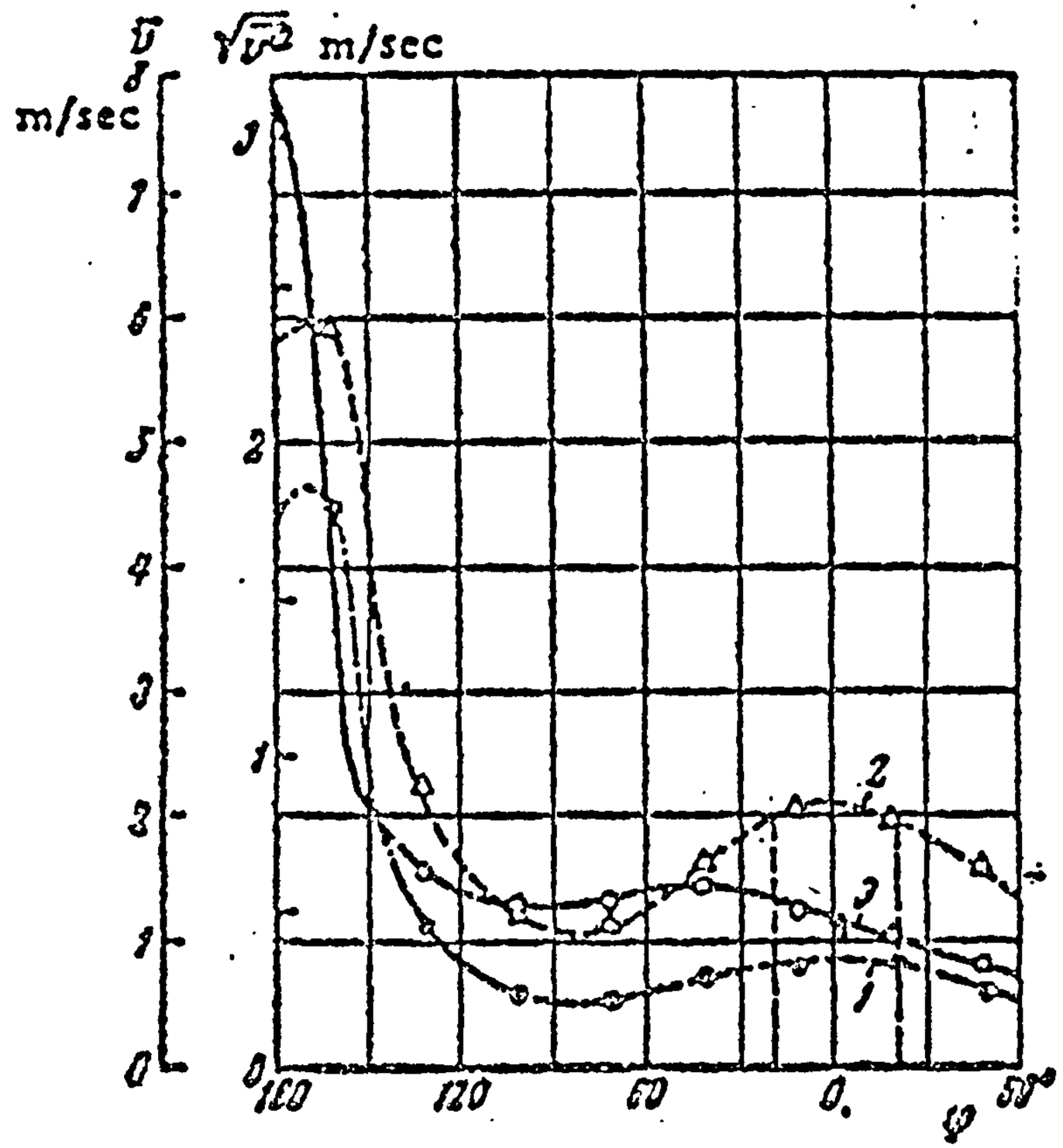

Fig (2-56) Average and fluctuating velocities during intake; (22)

1) $\sqrt{\overline{v'^2}}$; 2) $\Sigma_1 \sqrt{\overline{v'^2}}$; 3) $\bar{v}$

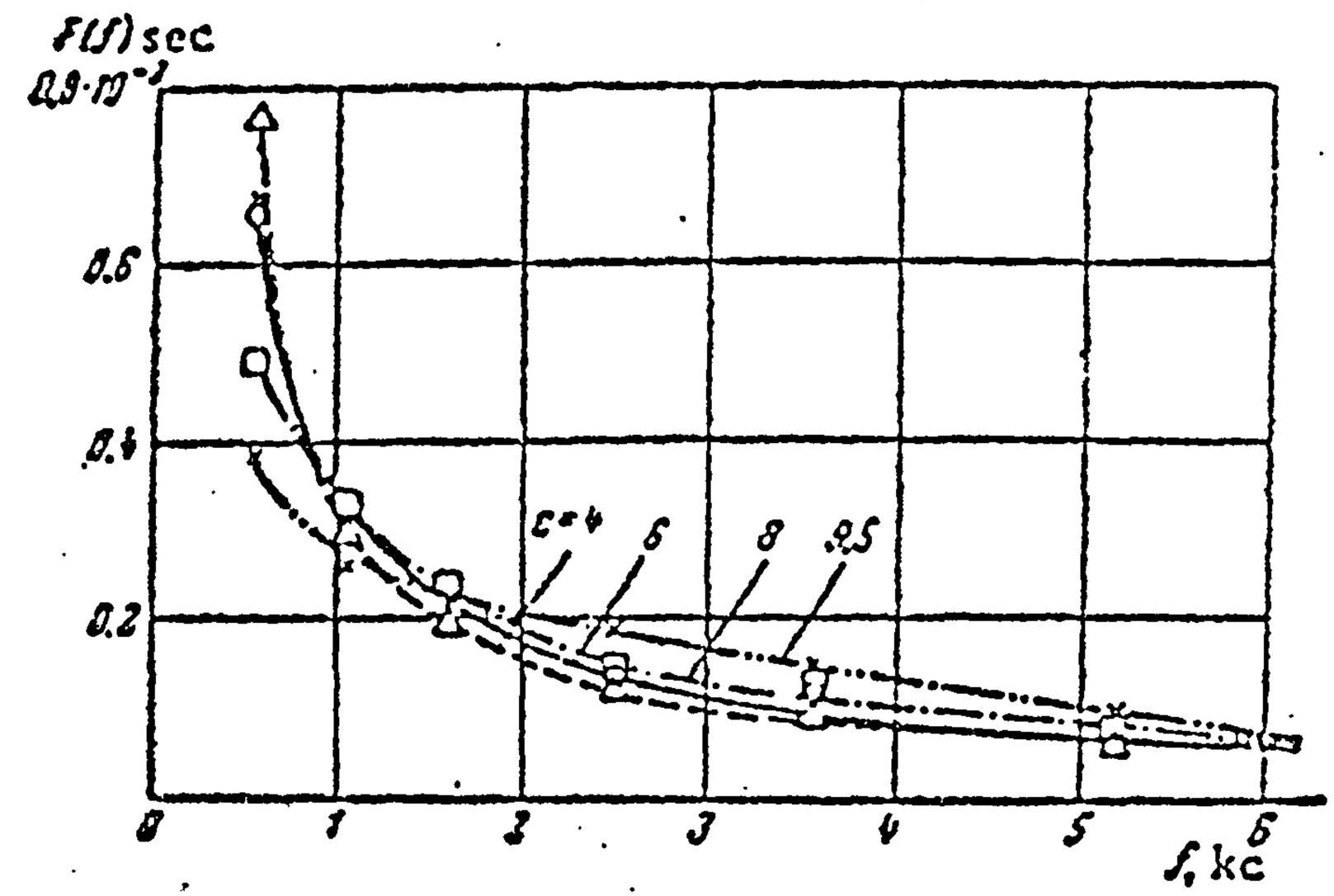

Fig (2-57) Curves of $F(f)$ at TDC during compression, for various c; (22).

r=23 mm; η_v=0.71; n=900 r.p.m.

Moreover, even when operating these wires at their maximum safe temperature results in a small temperature difference between the hot wire and the surrounding gas in the later period of the compression stroke, especially at the higher compression ratio used 9.5:1. This decreases the accuracy of measurements during such a period.

The macro-scale of turbulent eddies during induction were estimated to be of the order of 1.8 - 2.2 mm, but no estimation was given for the compression period. Also, the micro-scales of turbulent eddies have not been estimated in the original work, but a re-analysis of the reported power spectrum curves, Figs. (2-57 and 2-58) resulted in values of micro-scales between 0.3 and 0.7 mm as shown in Table (2-5).

The conclusions of Semenov's work should be taken with some reservation because of the limited range of engine speeds investigated (600 - 1200 r.p.m.), and that only one shape of combustion chamber was used.

Table (2-5) Estimation of the Micro-Scale of Turbulence from the Spectrum Curves of Semenov

Compression Ratio	$\int F(n)n^2 d_n$	$\bar{U}$(m /sec)	λ_x (mm)
4	$.672 \times 10^7$	1.439	0.6765
6	$.636 \times 10^7$	1.31	0.52
8	$.717 \times 10^7$	1.181	0.4425
9.5	$.835 \times 10^7$	1.084	0.376

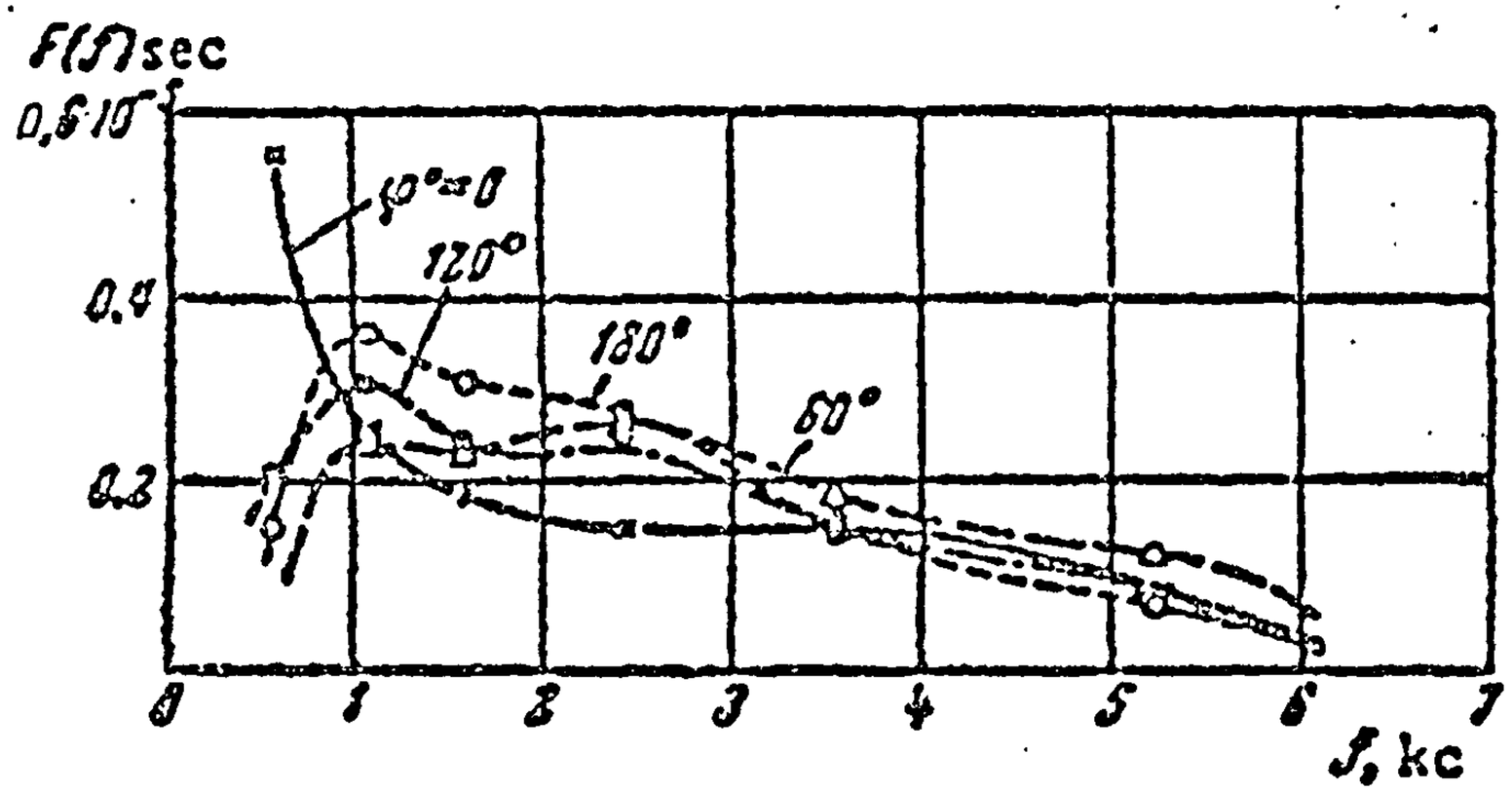

Fig (2-58) Energy-distribution functions $F(f)$, plotted against frequency; (22).

$\varphi=0$ curve is at TDC during compression; $\varphi=60$, 120, and 180° curves are after BDC during intake; $s=6$, $r=10$ mm, and $n=900$ r.p.m.

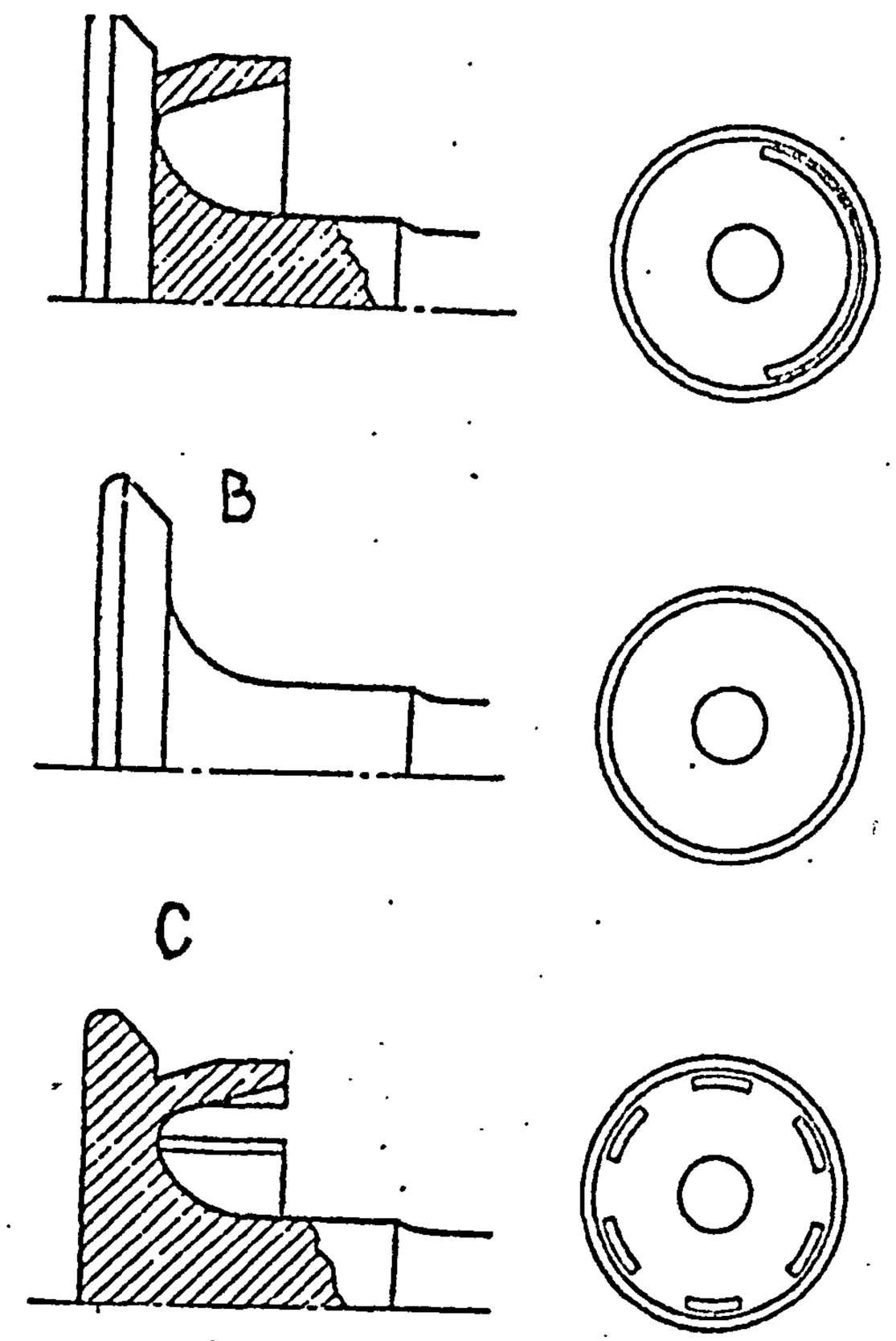

Fig (2-59). Three types of inlet valves (15).

Matsuoka et al (15) have used a hot wire anemometer at the spark plug gap location, for measuring gas velocities in a motored CFR engine with flat and cylindrical combustion chamber. Three types of inlet valves were used, namely: a plain valve, a shrouded valve and a notched valve as shown in Fig. (2-59). The compression ratio was varied from 4 to 7 while the engine speed was varied from 500 to 1200 r.p.m. Measurements were made only at top dead centre under the assumption that this would adequately represent gas velocities during combustion. The same engine was fired every cycle and every third cycle to investigate the effect of exhaust residuals on the combustion cyclic variation. The combustion process was studied in terms of maximum combustion pressure, the time from ignition to the attainment of maximum pressure, the maximum rate of change of pressure and flame arrival times to two ionisation probes located at 6mm and 76mm from the spark plug gap. The conclusions of the air motion and combustion studies could be summarised in the following:

i) The flow direction at top dead centre on compression stroke is two dimensional and parallel to the top of the piston.

ii) The flow velocity in the cylinder during the compression stroke reached a maximum slightly before top dead centre and then declined due to damping of the vortex motion.

iii) For a shrouded inlet valve the average flow velocity was higher than the other inlet valves at all crank angles and the rate of decrease was smaller during the intake and compression stroke.

iv) The swirl flow created by the shrouded valve was not damped as much during the compression stroke as that created by the notched valve, which was especially designed to create turbulence.

v) In the case of the shrouded inlet valve the value of the flow velocity $\bar{U}$ and its standard deviation $S(\bar{U})$ were twice or more as large as in the case of the other two valves, but the coefficient of variation $S(U)/\bar{U}$ of the shrouded valve was less than half the value of the other two valves, Fig. (2-60).

vi) Increasing engine speed increases the standard deviation in flow velocity but does not greatly change the coefficient of variation.

vii) Increasing compression ratio increases gas velocity and its standard deviation for the case of the shrouded valve and has a negligible effect for the other two valves.

viii) The flame arrival time to the first ionisation probe (located at 6 mm from the spark plug gap) was reduced with increased compression ratio and engine speed, but was not affected by changing the valve type, Fig. (2-61). The latter result was explained by the fact that this measured value represents the ignition delay, acceleration and flame arrival period and that flow velocity affects only the last term and could be masked by the experimental error. This explanation may be true with regard to the comparative order of magnitude of this small arrival time and the experimental error, because of the well known effect of turbulence on the growth of the initial flame

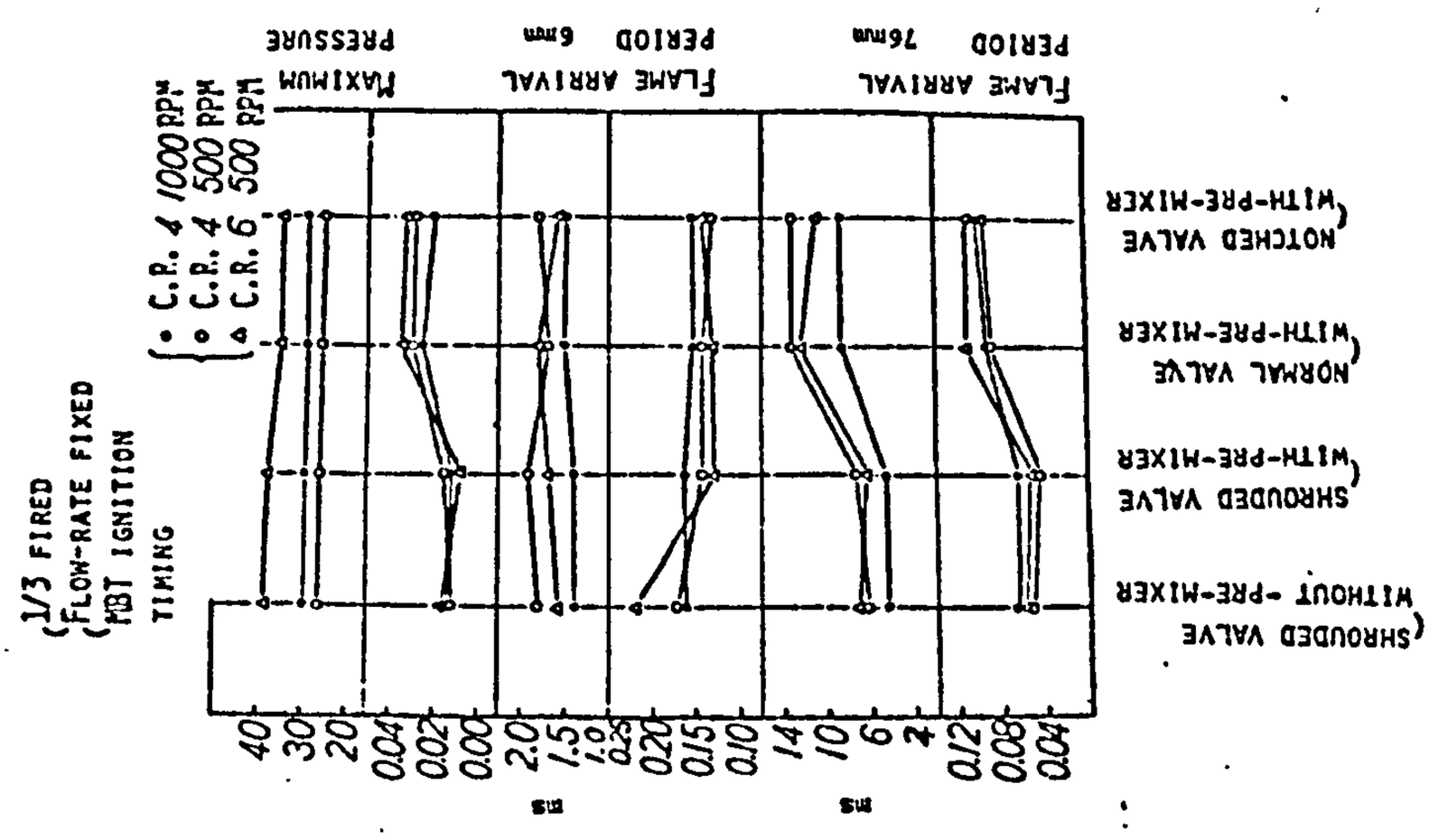

Fig (2-61). Variation diagram of flame arrival period and peak pressure, (15).

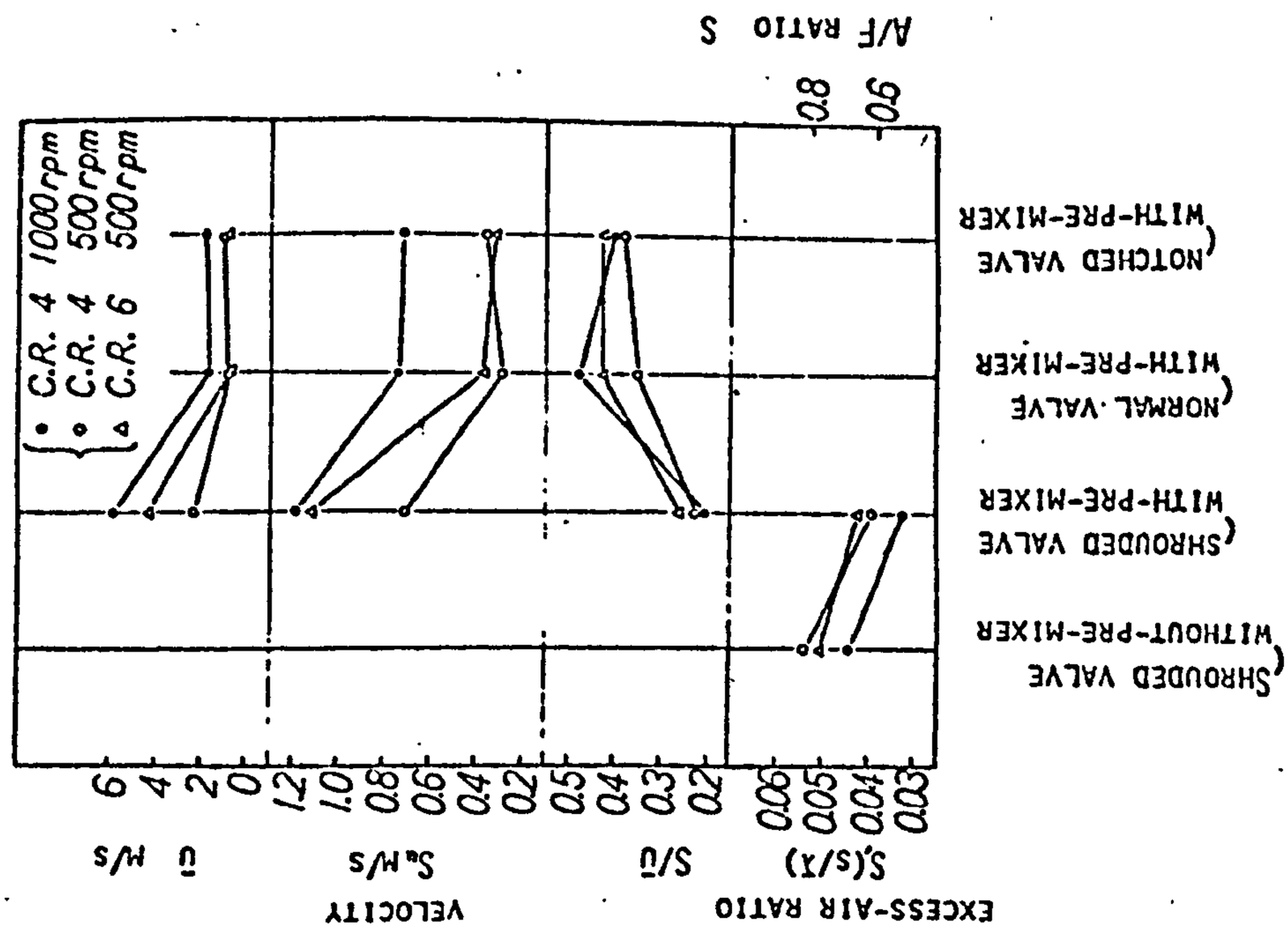

Fig (2-60). Variation diagram of gas velocity inside the cylinder of CFR engine (15).

CYCLIC MIXTURE VARIATION NON EXIST

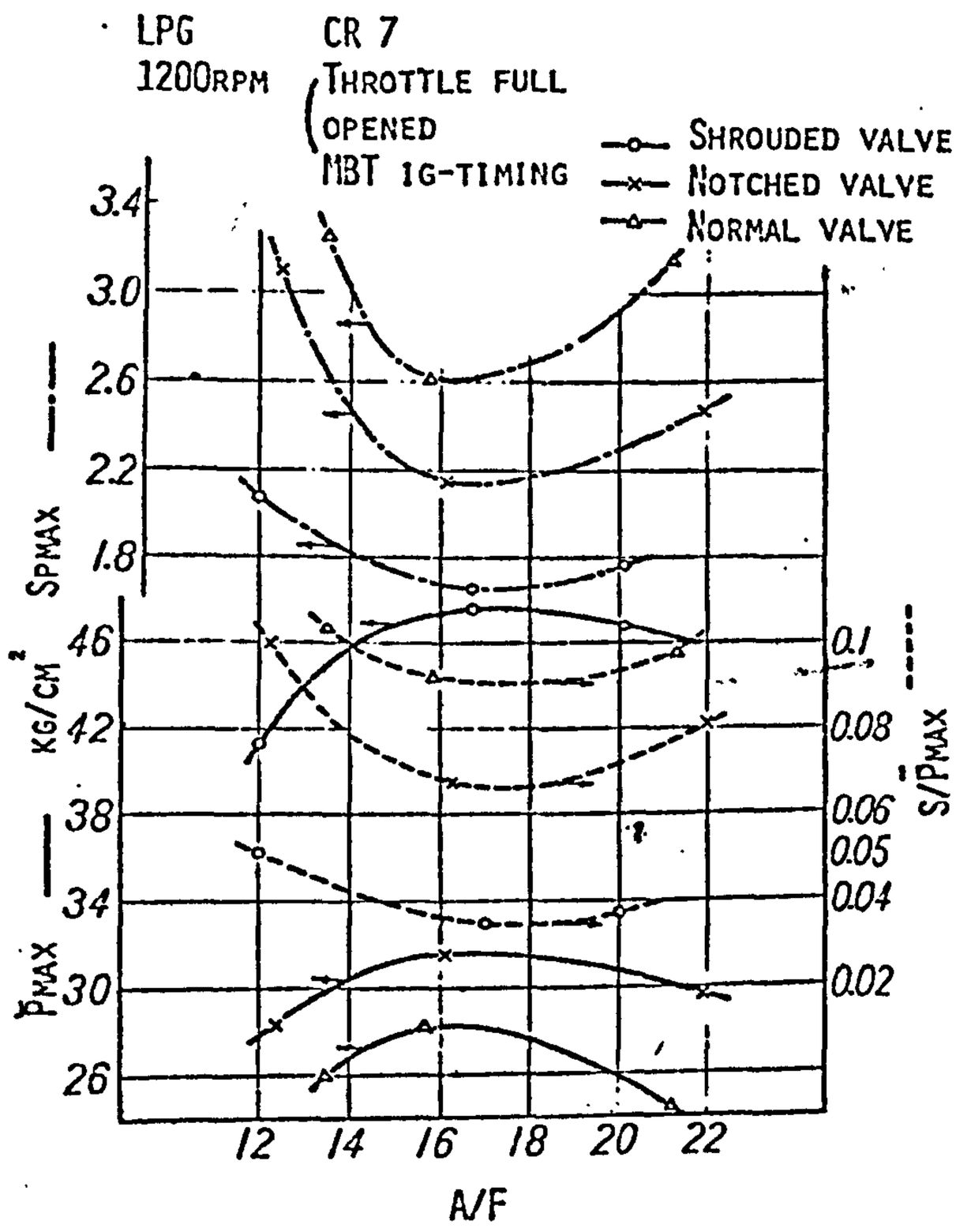

Fig (2-62) Variation diagram of maximum cylinder pressure (P_{max}) with air-fuel ratio for three types of inlet valves,(15).

kernel (acceleration period). Nevertheless, the effect of valve type and its associated flow velocities were clearly reflected on the flame arrival times to the second ionisation probe (located at 76 mm from the spark plug gap), where a good inverse correlation exists between gas velocities and flame arrival times. This discrepancy between the trends of flame arrival times at the two ionisation probes is also reported by Harrow et al (30), where no correlation could be established between flame arrival times at two ionisation probes located at 16.5 mm and 65 mm from the spark plug gap, of a Ricardo E6 engine. However, in this work both ionisation probes showed similar trends of cyclic dispersion in flame arrival times at different fuel/air ratios.

ix) The effects of valve type become very noticeable when the engine was fired every cycle. In this case the peak pressure and the maximum rate of change of pressure were exceptionally large for tests with a shrouded valve as compared with the other two types of valves. The standard deviation and coefficient of variation of these two parameters have followed inverse trends, Fig. (2-62). These results are in agreement with Patterson's studies Figs. (2-63 a) and(2-63 b).

In fact, the very low frequency response of the anemometer system used in this study (250 Hz), means that the collected bridge voltage signals, as measured from oscilloscope traces, represent

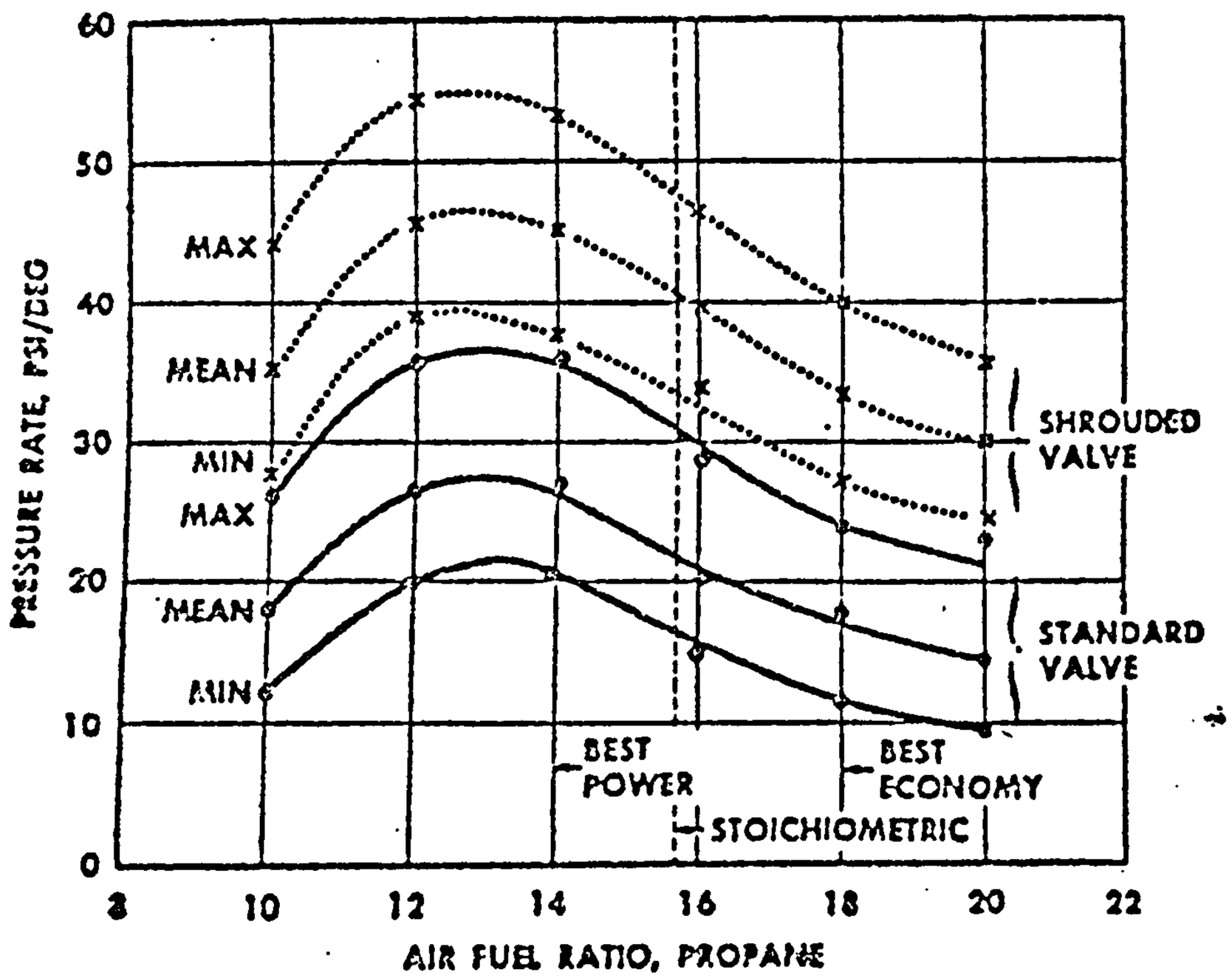

Fig (2-63a). Effect of intake valve induced swirl on cyclic variation. Primary effect of increased swirl into increase rate of combustion. Cyclic variation remained essentially constant (2). (1600 r.p.m. and fully opened throttle).

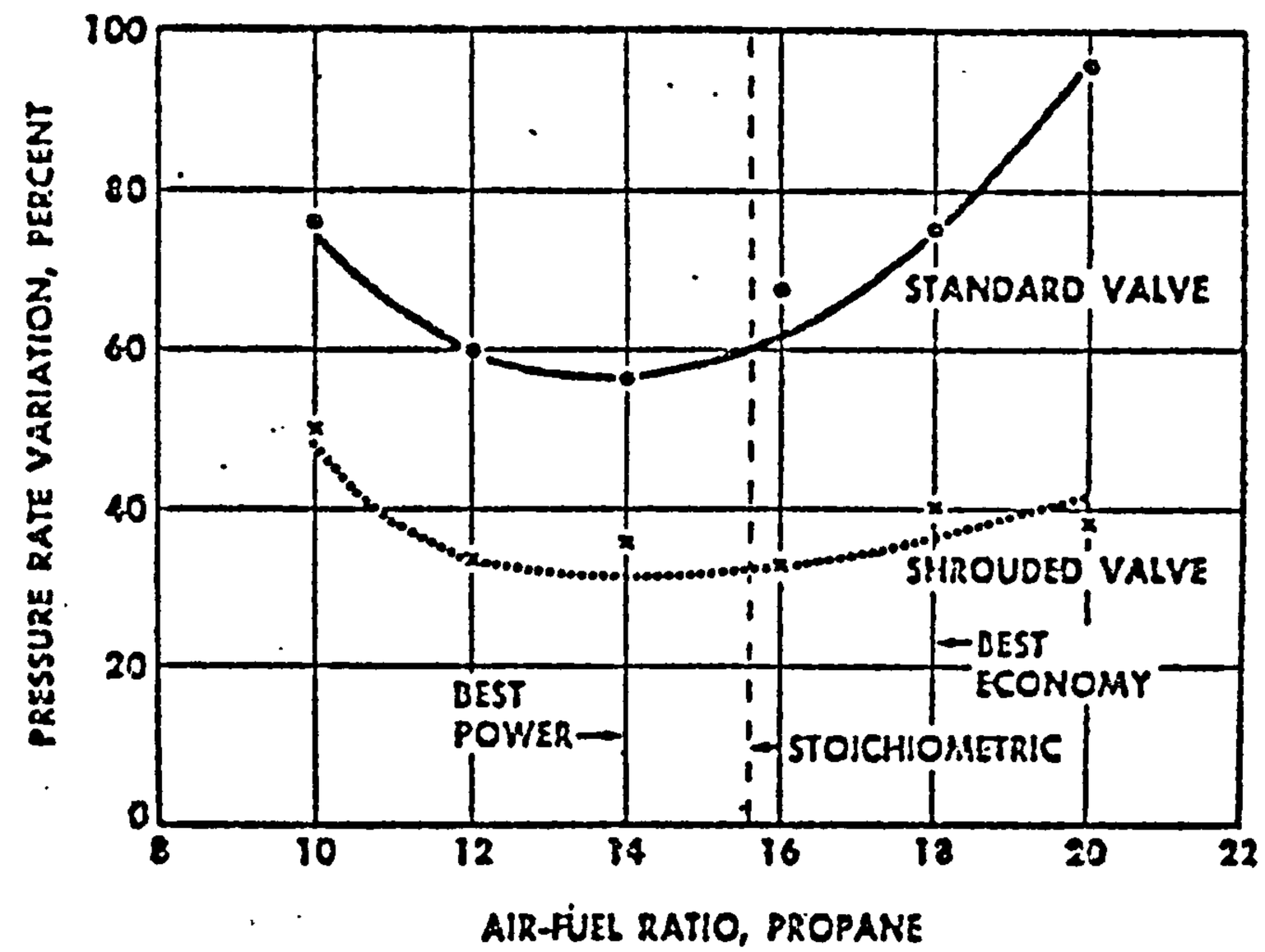

Fig (2-63b). Effect of shrouded valve on percentage variation showing that higher combustion rates are associated with minimum percentage variation (2).

only the mean gas velocity variation during the cycle, rather than any turbulent fluctuations. Nevertheless, these general trends of mean gas velocity variation, especially the performance of the shrouded valve, are in agreement with the observations of Lee (18), as well as the anemometer measurements of the present investigation (as will be discussed later).

The distinguished effect of the shrouded valve and its associated higher flow velocities and turbulence intensities on increasing the burning rate of the charge and reducing the cyclic combustion variation, could be explained by the same argument put in the earlier discussion of the work of Rothrock and Spencer (16). On the other hand the unexpected performance of the notched valve could be explained by its restriction to the inlet flow without any gain in directing the flow inside the combustion chamber. With this type of valve, one would expect some increase in inlet velocities, as well as the shedding of trailing vorticities from the edges of the notches, but these will be damped later on the compression stroke, probably at the same rate as in the case of a plain valve or even at higher rates. Similar observations have been reported by Patterson (2), where an abrupt right angle change in flow direction near the intake port has increased the cyclic dispersion. Also a more pronounced increase in cyclic dispersion resulted when a shrouded intake valve was used that disrupted the flow to the combustion chamber.

Barton et al (10, 11) have investigated the air motion in a hemispherical combustion chamber of a CFR engine using a hot film anemometer. The sensor was located halfway between the piston crown and cylinder head wall with piston at TDC, Fig. (2-64).

The angular position was such that the velocity through the intake valve opening was normal to the sensor length. Only mean gas velocities were measured in this investigation and their standard deviation calculated. A typical velocity trace is shown in Fig. (2-65), which indicates the general trend of decay after inlet valve closure, and the cyclic variation in gas velocity. The values of gas velocities at the time of ignition at engine speeds varying between 600 and 1800 r.p.m. are reported to lie between 8.74 and 16.1 ft/sec, with standard deviations ranging between 43% and 48% of the mean value. Cyclic variations in gas velocities during induction and compression stroke could not be correlated. However, the velocity magnitudes at the time of ignition were found to persist for approximately 10 to 15 crank angle degrees later.

The authors assumed a statistical pattern of velocity regions with different levels inside the combustion chamber. Regions of higher velocities at the spark plug gap at the time of ignition accelerate the growth of the initial flame kernel and consequently reduce the time required for its development into a stable flame front. This period was termed "the initial burn time" and was assumed to represent the time required to burn a fixed amount of the fuel between 2-5% of the total charge. Moreover, the variations in this initial burn time were assumed to be responsible for the subsequent cyclic variation in the cylinder pressure development during the cycle.

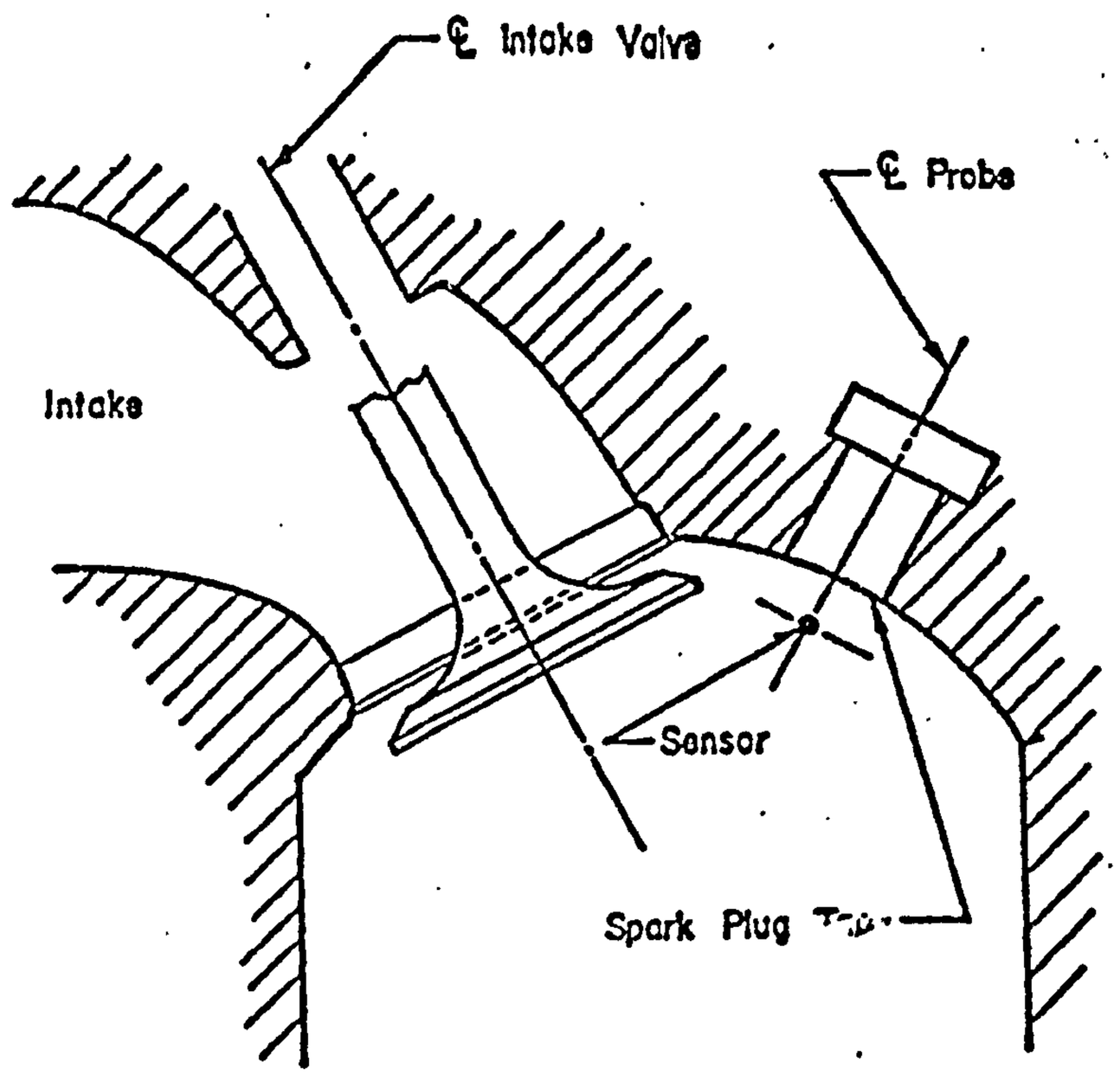

Fig (2-64). Sensor location in combustion chamber (10).

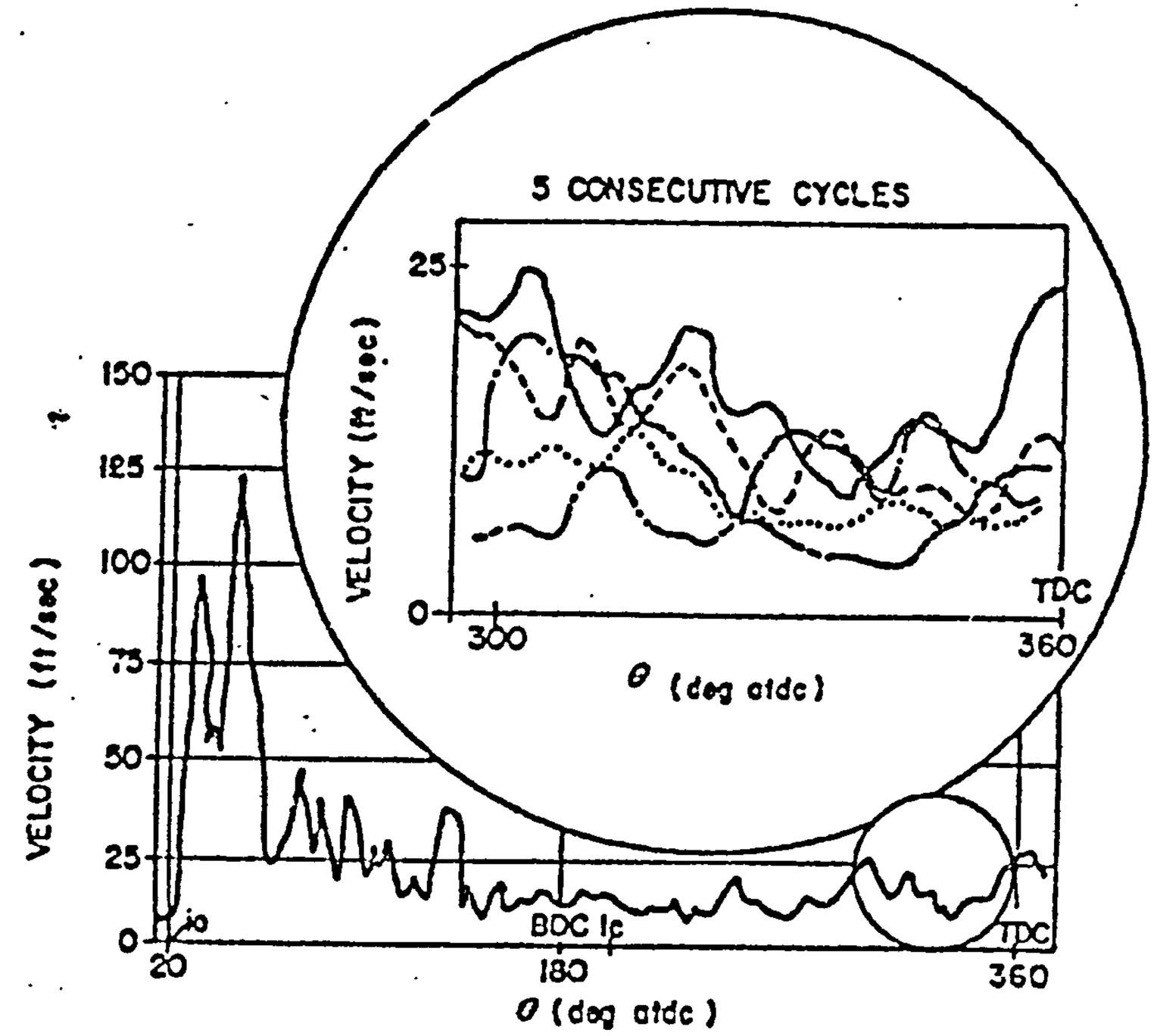

Fig (2-65). Intake and compression velocity record with offset of velocity records for five consecutive cycles at crank angles corresponding to ignition (10).
(7:1 compression ratio and 900 r.p.m.).

These assumptions were expressed in mathematical form as follows:

$$dV_r = 0 \quad , \quad (V_r = \frac{V_b}{V_i}) \qquad (2\text{-}8)$$

and

$$\frac{dt_b}{dU} = \frac{S(t_b)}{S(U)} \qquad (2\text{-}9)$$

where V_r is the ratio between the burned volume during the initial period V_b and the cylinder volume V_i.

t_b is the initial burn time, defined as the time required to burn the initial fixed percentage of fuel which governs cyclic variation.

U is the gas velocity at the time of ignition.

and $S(t_b)$, $S(U)$ are the standard deviations in the initial burn time and the gas velocity respectively.

Using an expression for the rate of change of the burned volume as used in constant volume bomb tests, and assuming a hemispherical burning flame front of radius r_b gives the following expression:

$$\frac{dV_b}{dt} = A_b.S_l.E.f(U) \qquad (2\text{-}10)$$

or

$$\frac{dr_b}{dt} = S_l.E.f(U) \qquad (2\text{-}11)$$

where A_b is the flame front area.

S_l is the laminar flame speed, which was approximated from the experimental data of Dugger (67) and Garner (68).

E is the expansion ratio $= \frac{T_b \ M_u}{T_u \ . M_b}$ (2-12)

which could be expressed in terms of mixture temperature at the time of ignition and air fuel ratio.

T is the mixture temperature.

M is the molecular weight of the mixture.

f(U) is the increase in the laminar flame speed as a function of gas velocity.

Substituting for S_l, E into equation (2-11) and making use of the conditions given by equations (2-8) and (2-9) led to the final expression of the proposed model for cyclic variation as given by:-

$$F(o.v) \quad \frac{S(t_b)}{S(U)} = c.g(U) \qquad (2\text{-}13)$$

where F(o.v) is a function of operating variables (e.g. gas temperature and pressure at the time of ignition and mixture air/fuel ratio), and g(U) is some unknown function of gas velocity which could be obtained by fitting experimental data.

Using the measured variation in the crank angle for maximum pressure to represent the variations of initial burn time, a least square fit of the data gives the form of the function g(U) as:-

$$g(U) = \left[\frac{1}{U} \right]^{1.3} \qquad (2\text{-}14)$$

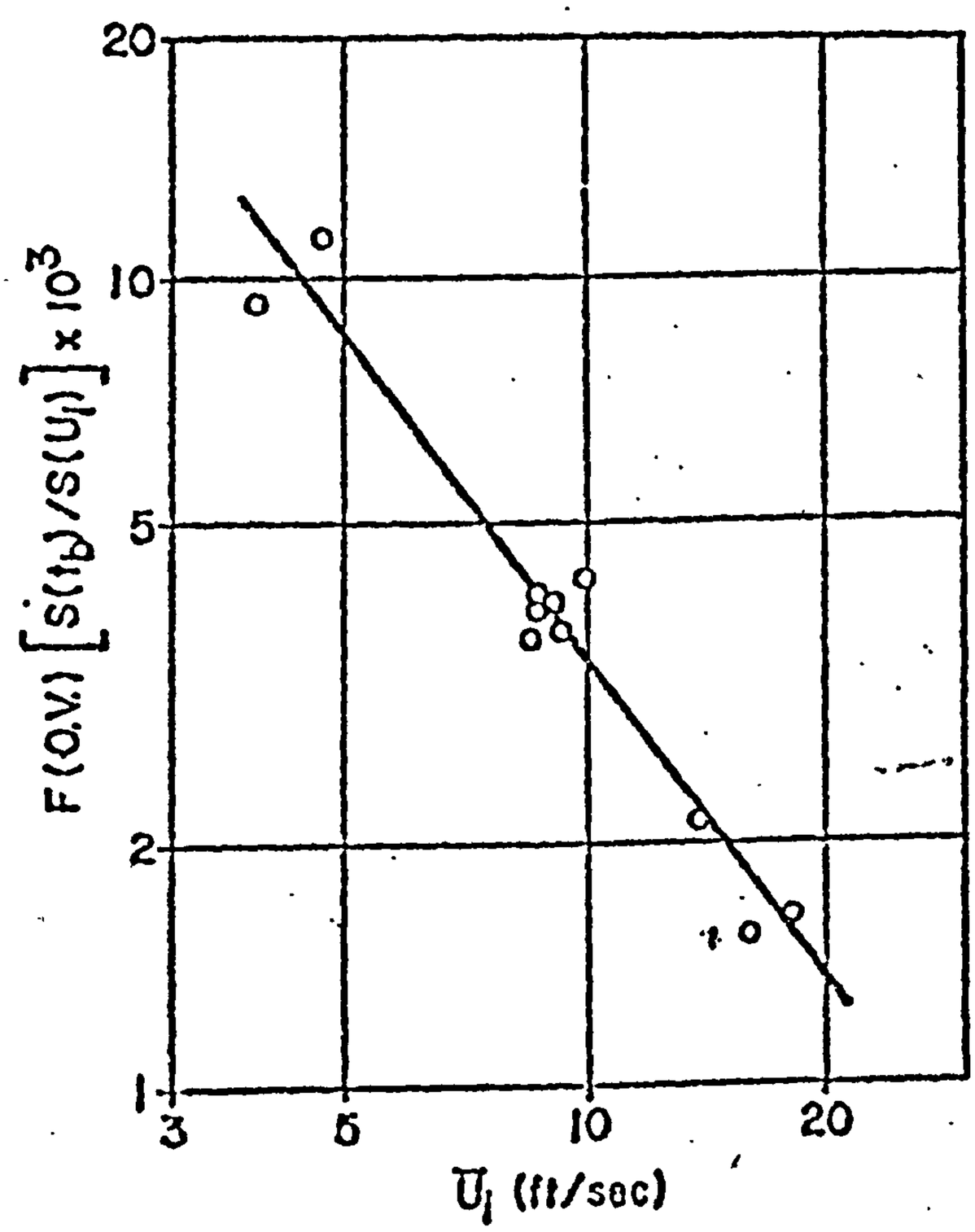

Fig (2-66). Correlation of initial burn duration and velocity variations (10).

This form of g(U) has resulted in a correlation of 0.975 between the variables log $F(o.v)\ S(t_b)/S(U)$ and log (U), Fig. (2-66).

Winsor (23) measured air velocities in a motored CFR engine with flat piston and head surfaces as shown in Fig. (2-67). The hot wire was oriented vertically, radially and tangentially at a location near the spark plug. Platinum and Iridium wires of 0.0002 inch diameter were used. The wire length varied between 0.05 and 0.096 inches.

The vertical wire tended to measure higher velocities during the early part of the compression stroke. Such observation was previously reported by Matsuoka et al (15) and is interpreted as the existence of rotary motion in the horizontal plane. The measured velocities show a definite trend of decay during the compression stroke. Moreover, similar velocities were measured by the three wire orientations from 40 degrees BTDC to TDC, Fig. (2-68). This similarity was interpreted as isotropy of turbulence during such a period. No significant effect of wire depth was observed on velocity measurements and this was interpreted as an indication of homogeneity in the turbulent field. Such conclusions may be justified if one regards the 'turbulent fluctuations' as a result of shear stresses on the walls of the combustion chamber and the breakdown of eddies of different sizes in the process of turbulence decay. A linear increase in mean velocity at TDC with engine speed was observed, which contradicts with the almost quadratic relation reported by Semenov (22).

Neither the fluctuating velocity component, nor the scales of turbulence were measured in this investigation. However the standard deviations in gas mean velocity were presented as a measure of the turbulence in the engine which included, the cyclic variation of mean gas velocity and the actual turbulent fluctuations as measured from the oscilloscope traces. This leads to more confusion for attempts to investigate the effect of engine operating conditions (e.g. speed or throttle opening) on the turbulence characteristics in the engine. Comparison between the measured values of mean velocities by different wire lengths was used to give a crude measure of the eddy size and was believed to be of the order of 0.1 inch.

The author proposed a model of cyclic combustion variation based on the concept that "the average flame speed is sensitive to local turbulent velocities only when the flame radius lies in a certain incremental range, dc, which is located at a finite but unknown distance from the spark electrodes, Fig. (2-69). All cyclic combustion variation is assumed to occur during this critical period". This is not strictly true as shown by Curry (37) and Harrow et al (30) where measurements of flame arrival times at different distances from the spark plug showed that their cyclic variations continue to increase along the path of the flame front, Figs. (2-13) and (2-36). Other than that assumption, the basic concept of the model is the same as Barton's model where cyclic variations in gas velocity are considered as the sole cause of cyclic combustion variation. The only exception in this case is that the turbulent flame speed was expressed as a linear function

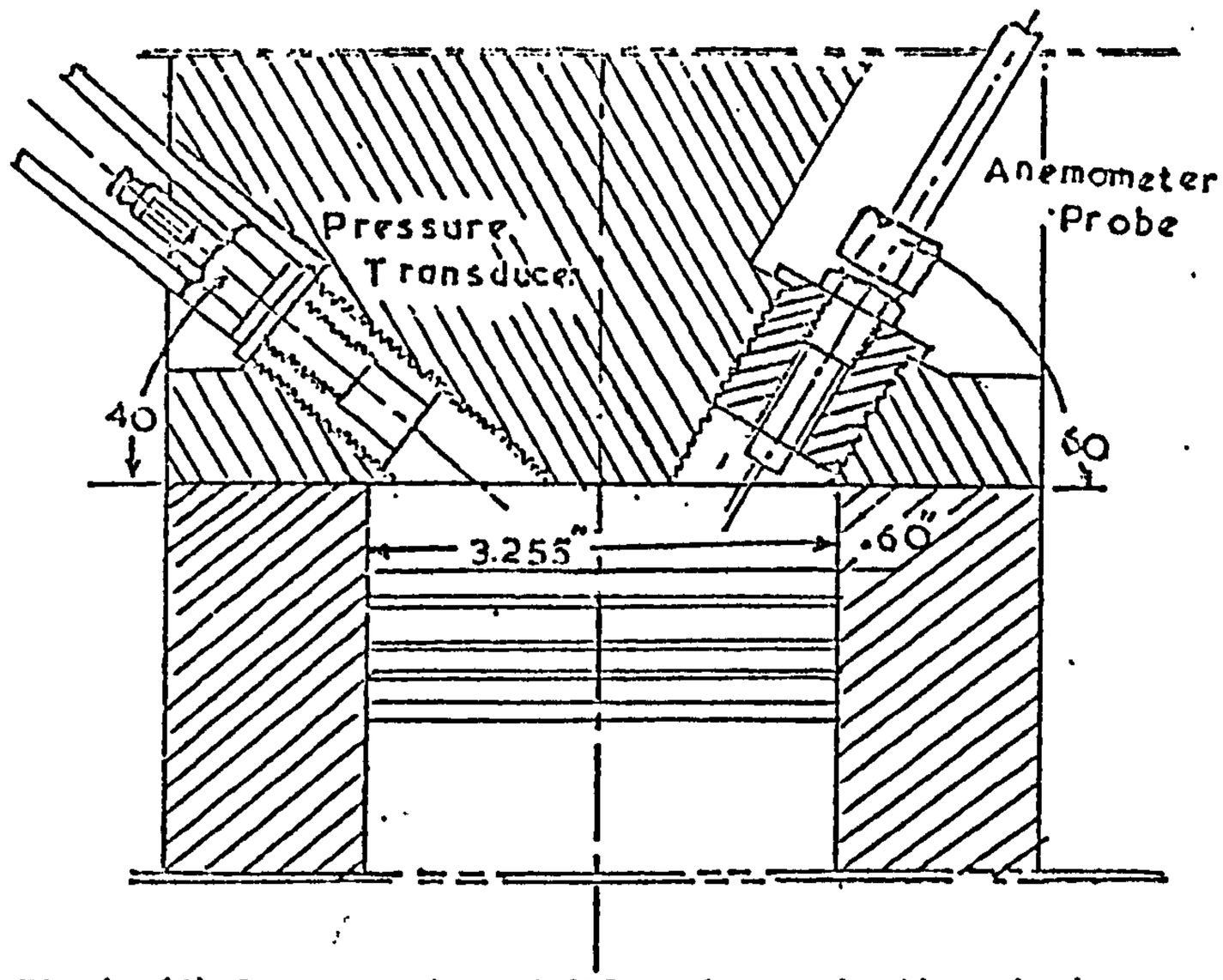

Fig (2-67) Cross-section of CFR engine combustion chamber and cylinder head at TDC (23).

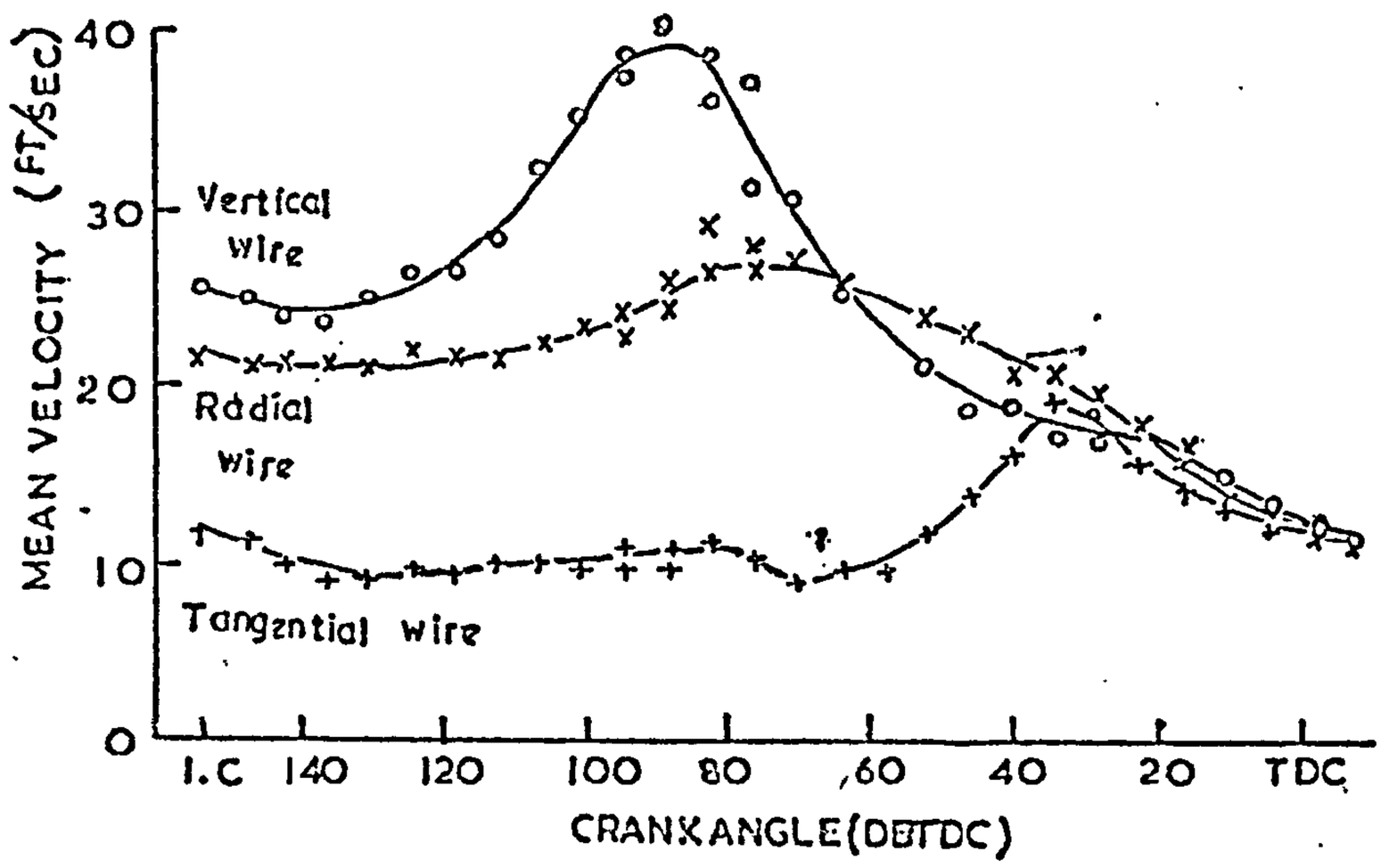

Fig (2-68) Gas mean velocity in CFR engine during compression stroke. (1000 RPM and fully opened throttle),(23).

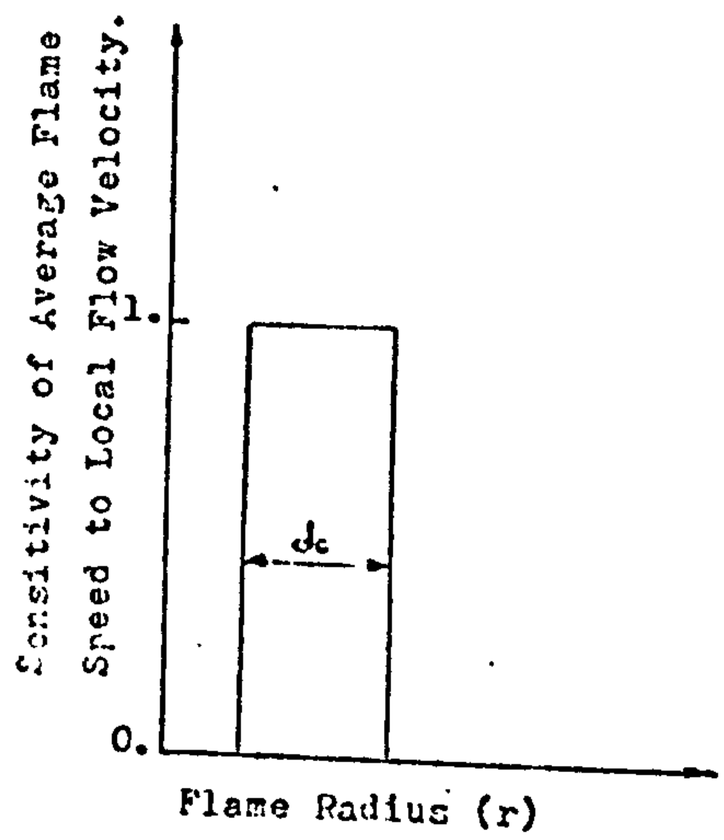

Fig (2-69) Basic assumption of the model of cyclic variation developed by Winsor (23).

of gas velocity as given by

$$S_t = K\,U \qquad (2\text{-}15)$$

where S_t is the turbulent flame speed

K is a constant dependent on mixture conditions

U is the gas velocity

Assuming that the critical distance is constant and using the condition of perfect correlation between the time period during which combustion variation occurs and gas velocity led to the following expression

$$S(t_c) = S(t_b) = \frac{dc.K.S(U)}{S^2_t} \qquad (2\text{-}16)$$

where $S(t_c)$, $S(t_b)$ and $S(U)$ are the standard deviations in the critical period, the total burn time, and the gas velocity respectively. Using the relation between the mean and standard deviation of the flame speed and making use of equation (2-15) led to the expression for the proposed model as given by

$$S(t_b) = \frac{dc}{\bar{S}_t} \quad \frac{S(U)/\bar{U}}{1 + (S(U)/\bar{U})^2} \qquad (2\text{-}17)$$

Substituting for $S(U)/\bar{U}$ from experimental results by a value of 0.41 and for S_t by $\bar{t}_b/D$, where D is the cylinder diameter and using also a linear relation between t_b and $S(t_b)$ gives a value for the critical distance of 0.42 inch.

Tindal et al (25) measured gas velocities during the induction stroke in a Matchless twin cylinder engine with in phase cranks.

One of the pistons was used to provide a reciprocating drive operating a linkage for a hot wire anemometer probe in the test cylinder. Fig. (2-70) shows the engine and traverse mechanism of the probe. Measurements with stationary probes were employed at positions a, b and c as shown in Fig. (2-71). The hot wire was located $\frac{1}{8}$ inch away from the combustion chamber wall. At position a, one of the wires was parallel to a line through the valve centres indicated by (O-O) and the other was in the same horizontal plane but turned 90 degrees (O1O). The two measurements were made separately by one probe which was rotated about its axis, as required.

Fig. (2-72a) shows the results obtained with a stationary probe at position a, in the combustion chamber during induction, using a plane valve. The turbulent nature of the flow is well demonstrated, although the presence of a well defined jet is also evident in the region of the probe. The authors reported that the anemometer did not detect any inlet flow until about 25 degrees ATDC on induction stroke. They explained this as the anemometer wire not being in the immediate jet formed at the valve opening. Fig. (2-72b) shows the velocity variation during the induction stroke and the resultant of the signals from the two perpendicular probes. The decay of gas velocity after reaching the maximum, at about 105 degrees after inlet valve opening, is clear and continues up to inlet valve closure. Fig. (2-73) illustrates examples of traces obtained when a masked inlet valve was fitted, the hot wire being kept in position a with orientation (O-O). In this case the flow over the whole cycle is portrayed.

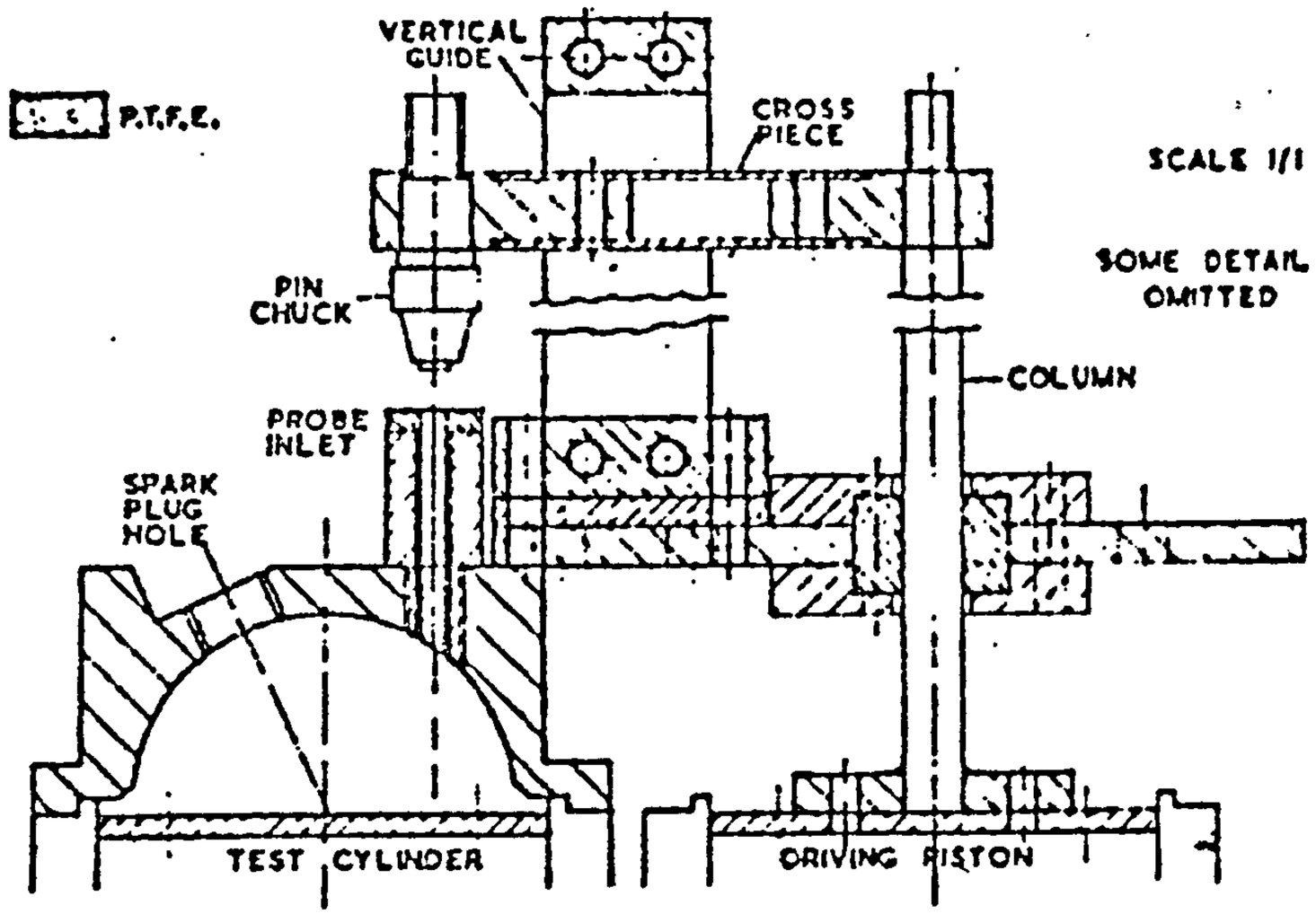

Fig (2-70). General arrangement of cylinder head showing details of traversing mechanism, (25).

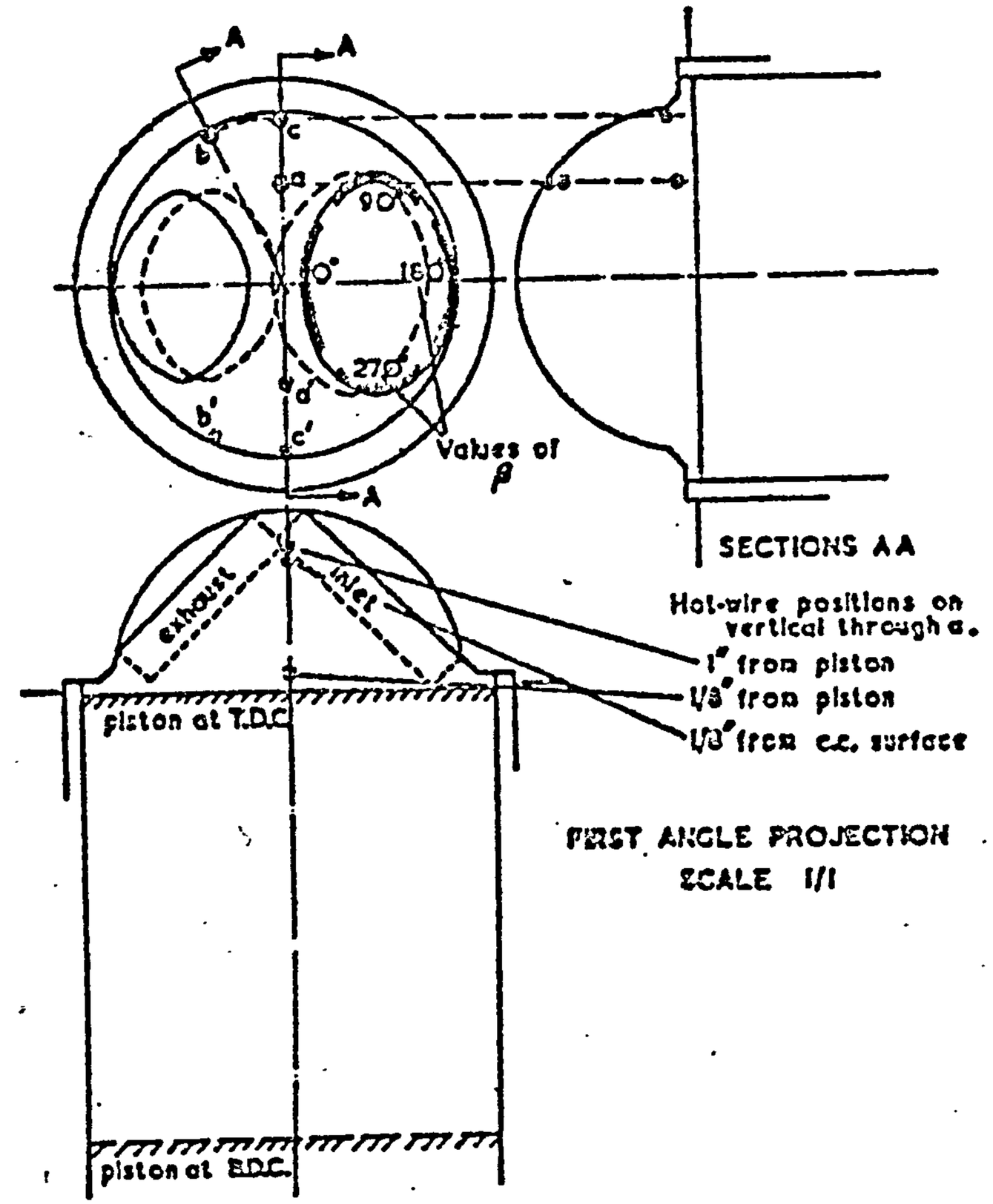

Fig. (2-71). General arrangement of test cylinder, showing the anemometer measuring positions and the angular positions of the mask, (25).

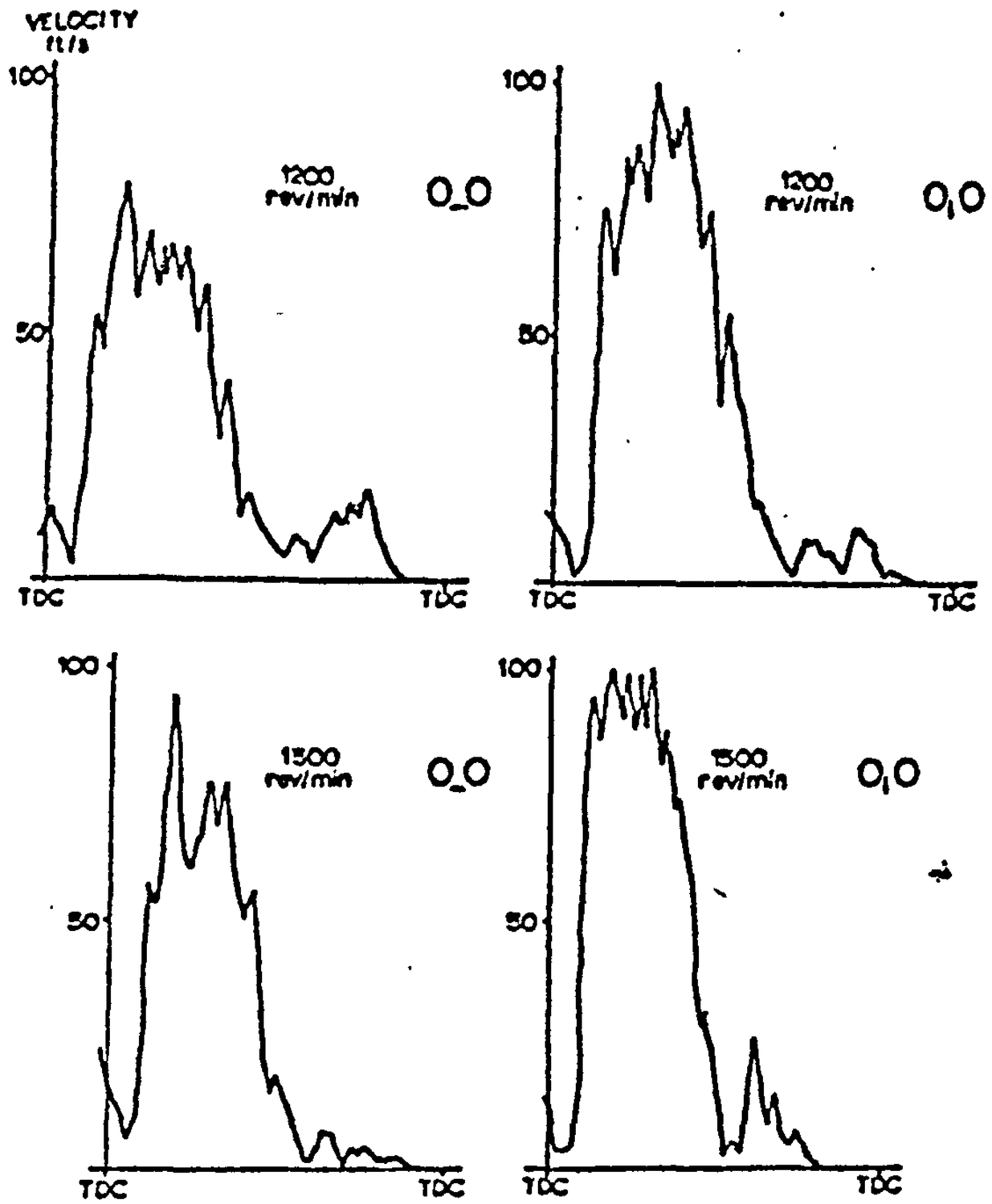

Fig (2-72a). Velocity traces obtained from combustion chamber with plain valve, (25). (1200 and 1500 r.p.m.).

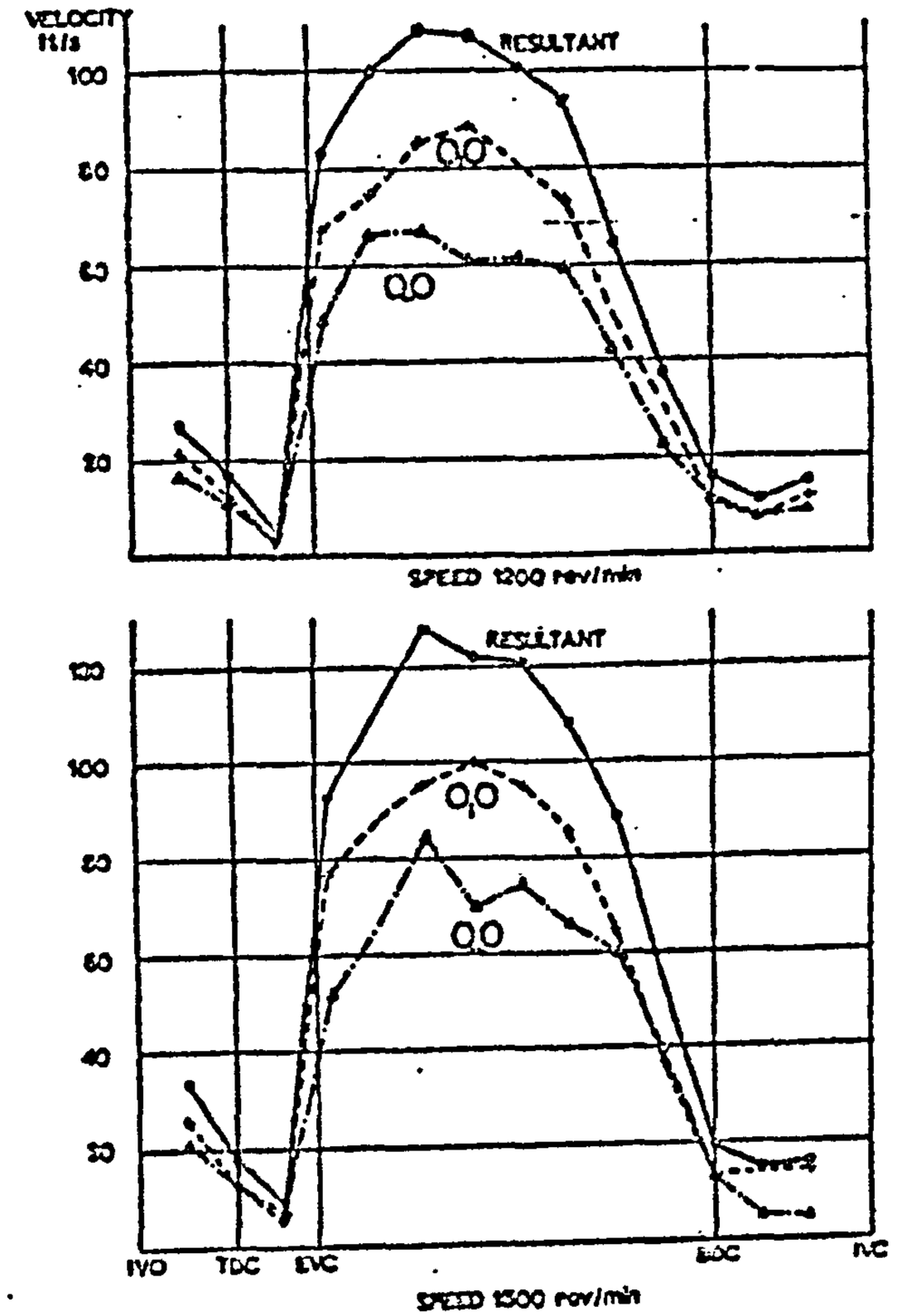

Fig (2-72b). Graphical representation of traces similar to Fig (2-72a) but averaged over four consecutive cycles, (25).

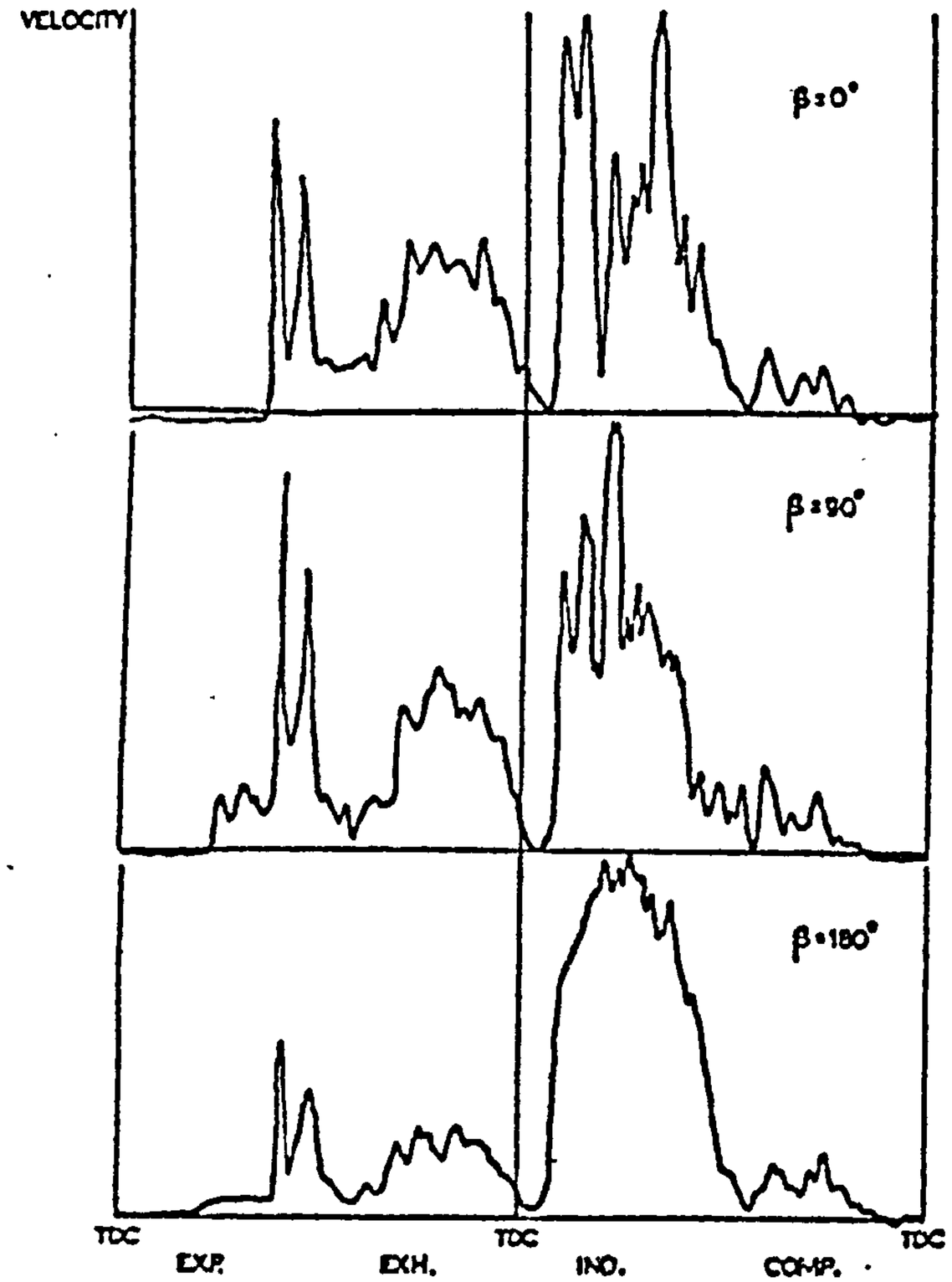

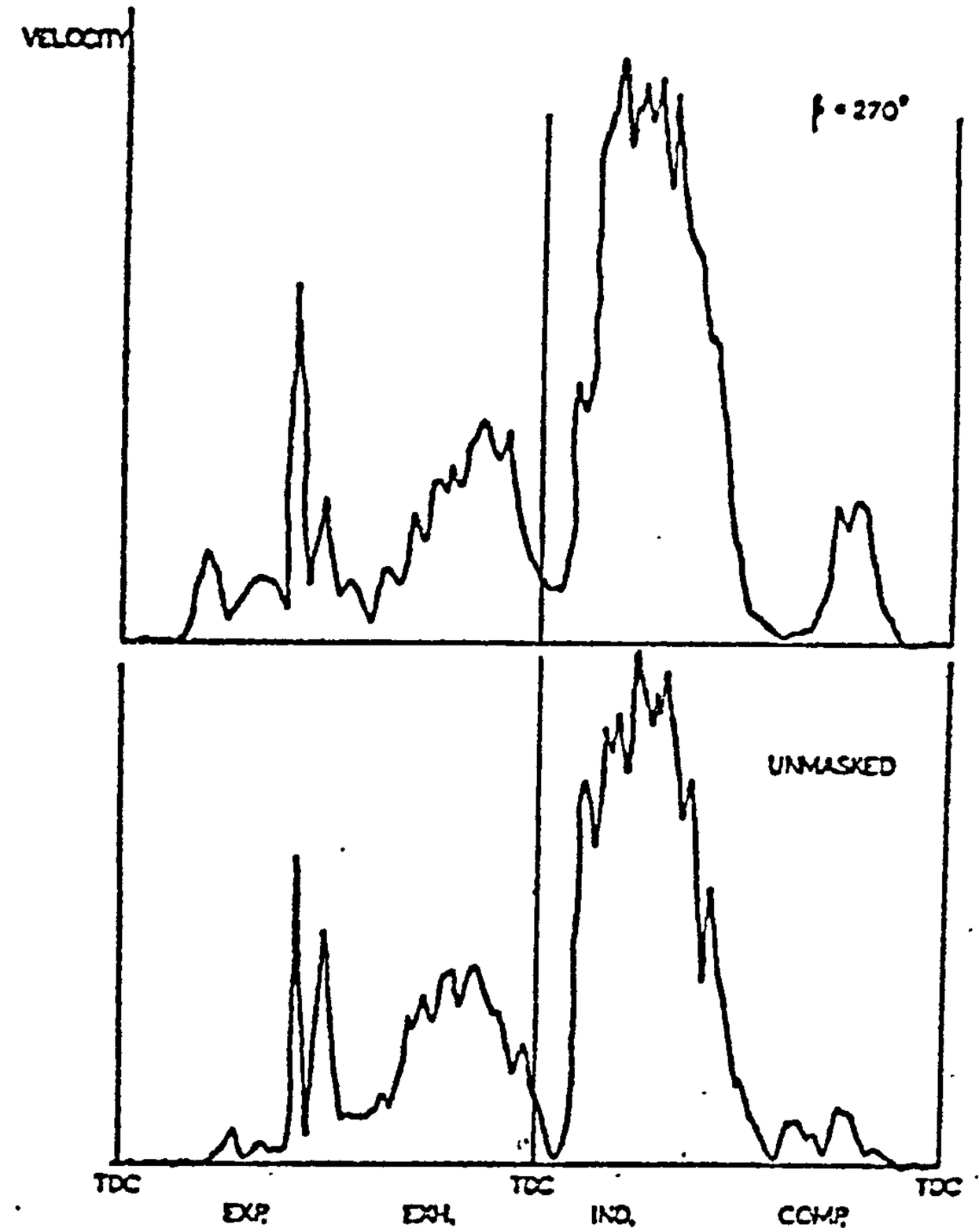

Fig (2-73). Velocity traces obtained from combustion chamber showing effect of altering mask position, (25). (Probe position a, angular position (0-0).

It can be seen on these traces how the signals are attenuated during compression. The negative signals on some traces are probably due to the very low operating temperature of the tungsten wire used (200°C) for the hot wire elements.

Tindal et al reported, also, that the readings from the traversed anemometer were in general less regular than those obtained in the combustion chamber with the stationary probes, and the repeatability of the records was not quite as good. They explained this by the less orderly air motion lower down in the cylinder. The masked valve increased the air velocities by about 30%.

As mentioned earlier, in the discussion of Semenov's and Molchanov's work, the use of tungsten material is unsuitable for investigating gas flow during the compression period and this was the reason for limiting the reported results of Tindal et al to the induction period where successful calibration could be assured.

James (1972) (24) measured mean gas velocities and fluctuating velocity components in different band pass widths of frequencies using a hot wire anemometer. Two combustion chamber shapes were investigated, namely: a squish and a cylindrical as shown in Fig. (2-74). Different compression ratios were obtained by inserting spacers between the cylinder head and the cylinder block. The anemometer output signal below 200 Hz was used to represent the mean flow velocities by averaging over 22 cycles the instantaneous values recorded on UV paper at 10 degree

intervals. The turbulence fluctuations at different band widths were obtained by subtracting instantaneous values of gas velocities from the mean value equation (2-18) and averaged over 12 cycles to give a mean value of u'.

$$u' = U - \bar{U} \qquad (2\text{-}18)$$

The band widths for these filters were: 90-180, 180-360, 360-700, 700-1500, 1500-2800 and 2800-5800 cycles per second. The same technique was used by Semenov (22) with the exception that the later averaged turbulence fluctuations over a sample width of 24 degrees. Due to the difficulties in the recording procedure of James, no attempt was made to measure absolute intensities over the band pass ranges. Also, the scales of turbulence were not investigated. The analysis was concentrated during the period between inlet valve closure and 40 degrees after TDC. A general tendency of decay in the mean velocity throughout the compression stroke was observed and was more pronounced at higher compression ratios and higher engine speeds. This was explained as a transfer of energy from the low frequency band width into the higher band pass ranges, where it is essentially dissipated into heat by the action of viscous friction. A linear increase of mean velocity with engine speed was observed in the latter period of compression stroke while a non-linear increase was observed in the earlier part after inlet valve closure.

A very marked increase in mean velocity at 30-40° ATDC on expansion was observed and were more pronounced at higher compression ratios, Fig. (2-75). No indication of squish velocities were measured at lower compression ratios (3.9 - 5.29) due to the larger width of

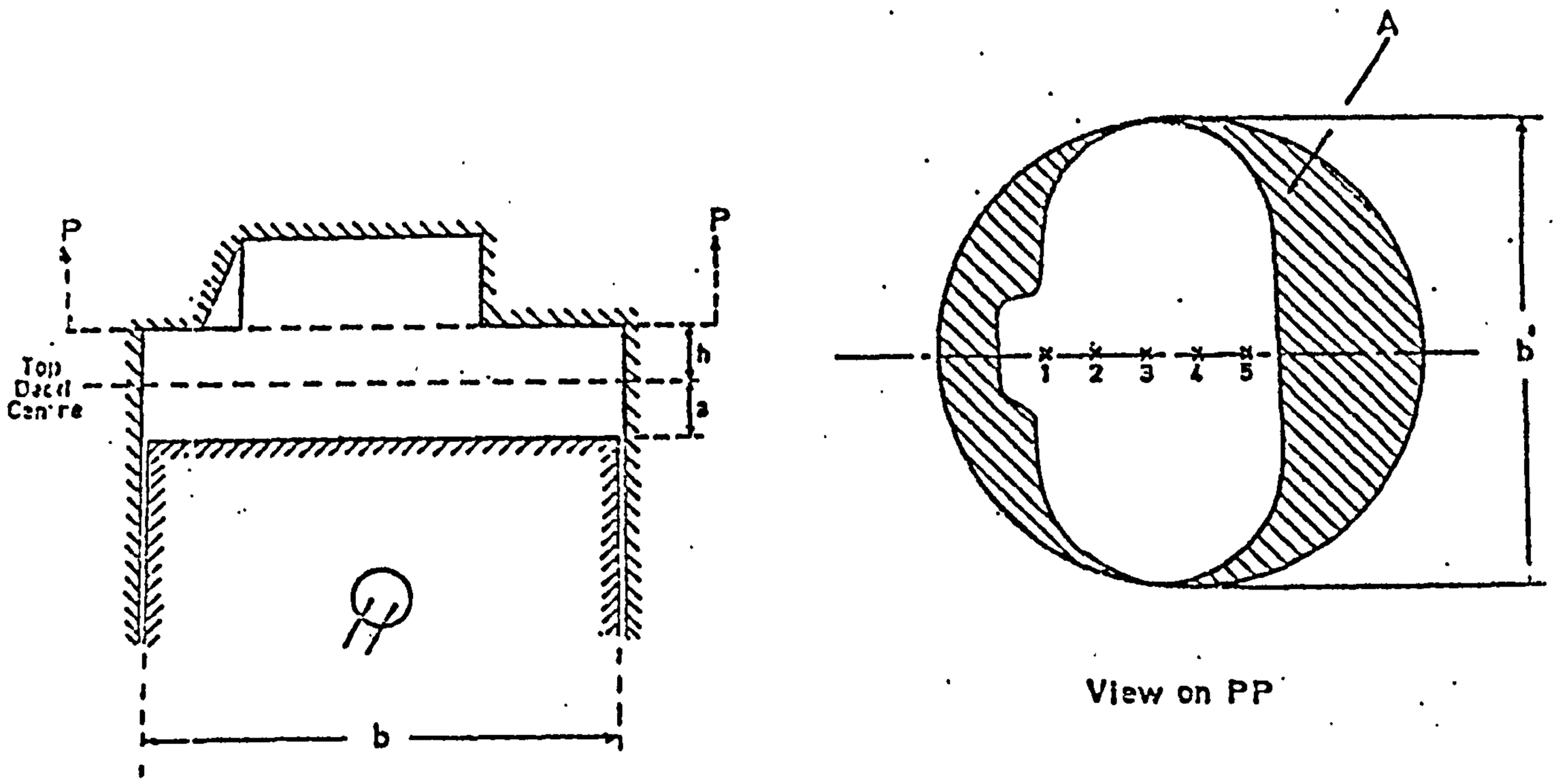

Fig(2-74) Cross-section of the squish combustion chamber used in James's investigation,(24).

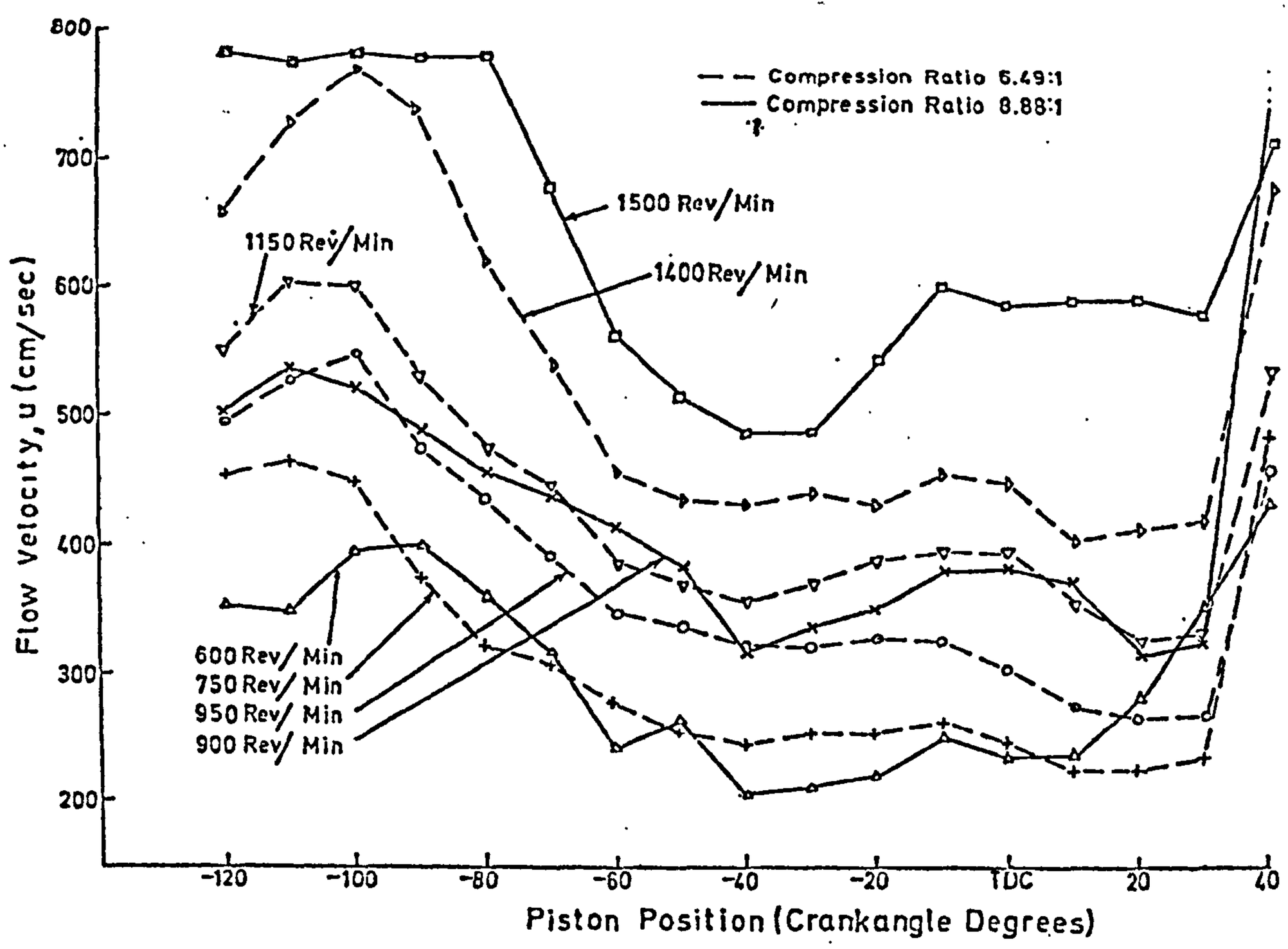

Fig(2-75) Variation of gas velocities with crank angles for a squish combustion chamber,(23).

spacers used (1.89 - 0.6 cm). However such squish appears at a higher compression ratio of 8.88:1 when the spacer was removed and the squish height was that of the gasket width 0.15 cm. Regardless of the scatter in the data, the general trend of decay in the fluctuating velocity component during compression stroke was observed and most of the energy is contained below 700 Hz. However, no definite conclusion was obtained about the predominant frequency band pass range at any speed. Moreover, around TDC the distribution of energy in the most important region between 90 Hz and 700 Hz is not clear.

James attempted to use his measured values of fluctuating velocity component to predict the turbulent flame speed using the expressions developed by Shchelkin and Karlovitz. The first expression was tried with the maximum values of u' in different bands of frequencies and even with a correction factor of 2.5 (as proposed by Semenov in his data), but no agreement was reached. Application of the second expression with its modification for the effect of turbulence amplification by combustion improves the situation, but still a trial and error program was required to try the best fit for each frequency band and finally an arbitrary multiplication factor was employed in conjunction with only the highest cycle value of u' over the 12 cycles analysed. Such peak values were of the order of twice the average values given in Table (2-6).

Further analysis of James' data was carried out using the same procedures of the present investigation, as will be discussed in Chapter 4. The reported values of the fluctuating velocity component at different band pass widths were introduced with a program to a Hewlett Packard Fourier Analyser to yield the energy

content of the fluctuating component and the mean value of u' for all the frequencies at different crank angles over the engine cycles (see Appendix A1). The results of such analysis are shown in Table (2-6) for the values of u' and the turbulence intensities $u'/\bar{U}$ using the corresponding mean velocities at the same operating conditions. The very high values of measured intensities (50 - 80%) of the mean values reflect very clearly the cyclic variation in the mean velocity that was superimposed on the actual fluctuating component in the lower frequency range. Such a cyclic variation in the mean velocity was reported by the author to be of the order of 50%.

Table (2-6) Re-analysis of the Turbulence Measurements of James (24)

1. At TDC

CR	r.p.m.	u'(m/sec)	$\bar{U}$(m/sec)	u'/$\bar{U}$ 100	$\lambda_t \times 10^{-4}$ (sec)	λ_x(mm)
3.9	600	0.758	1.72	45.	1.695	0.282
3.9	950	1.293	2.24	57.75	1.535	0.3482
3.9	1200	1.88	2.76	68.0	1.272	0.352
3.9	1450	2.43	3.16	77.0	1.28	0.405
5.29	700	1.13	2.02	56.0	1.6	0.323
	950	1.529	2.6	58.75	1.319	0.343
	1200	1.985	3.12	63.7	1.2	0.38485
	1450	2.885	3.66	81.5	1.13	0.4035
8.88	900	2.63	3.79	69.4	1.75	0.66
	1500	4.74	5.83	81.4	1.594	0.93

2. Measurements at C.R. = 5.29

	r.p.m.	u'	$\bar{U}$	(u'/$\bar{U}$)100	$\lambda_t \times 10^{-4}$ (sec)	λ_x(mm)
TDC		1.53	2.63	58.2	1.315	0.346
20BTD	950	1.588	2.754	57.7	-	-
40BTD		1.735	3.04	57.0	1.332	0.405

2.5 Effect of Mixture Motion on Flame Speed

It is well known that flame speed increases almost linearly with engine speed. This increase in flame speed is usually attributed to the increased turbulence of the charge caused by the higher inlet air velocities accompanying the higher engine speeds and the increased Reynolds numbers.

Furthermore as the engine speed increases the compression period becomes shorter and the natural decay in turbulence will be less advanced at the time of combustion. The small scale turbulence is also increased at higher engine speeds, as will be discussed later, with a resultant effect of accelerating the propagation of the flame front. Such conclusions were first reported by Bochard, Taylor and Taylor (41) based on the inspection of flame photographs, Fig. (2-76). It is also confirmed by the measurements of Iinuma (36), where both high speed flame photographs and ionisation gap measurements have shown the same trend of linear relationship between flame speed and engine speed, Fig. (2-77). Harrow and Orman (30) and Hodgetts (42) reported similar results for a Ricardo E6 engine and a Ford engine respectively, Figs. (2-78) and (2-79).

The effect of turbulence on increasing the propagation speed could be ascertained also by combining the observations of Clarke's (5) (1912) and Semenov's (22) (1956) experiments on an engine cycle with closed inlet valves. In the former case ignition after two or three previous cycles during which the intake valve had remained closed resulted in a sharply retarded combustion, Fig. (2-80) which was still proceeding some 200° after ignition. In the latter

experiment, Semenov (22) showed that the turbulent fluctuations almost disappear near TDC for a cycle with closed inlet valve and that the fluid energy ($\frac{1}{2}$ ($\bar{U}^2 + \bar{u}'^2$)) consists, in this case, only 10% of the energy of a normal cycle, Fig. (2-81). This illustrates the significant effect of turbulence on accelerating the combustion process in an engine, in spite of the fact that Semenov's experiment was carried out with flat and cylindrical combustion chambers where no secondary flow is created during compression.

Similar conclusions could be drawn from an experiment carried out by Bolt et al (3) in a constant volume bomb, where a complex flow pattern of mean swirl, small scale and large scale turbulence was created by a stirring fan. In this case an increase in the pressure rise due to combustion by about 15 - 20% have been obtained by increasing the mixture velocity as shown in Fig. (2-82). A corresponding increase in the rate of pressure rise has also been observed due to the increased mixture motion, Fig. (2-83).

Unfortunately the relationship between turbulence and flame speed is still disputed and most of the theories developed to explain such type of combustion have fundamental defects and are contradictory in many cases. Such contradictions arise because of the lack of reliable methods for measuring the intensity, scale and spectrum of turbulence in combustion wave, in spite of the intensive efforts of many investigators. This leads to attempts of comparing and interpreting experimental data which may have been obtained under radically different flow conditions.

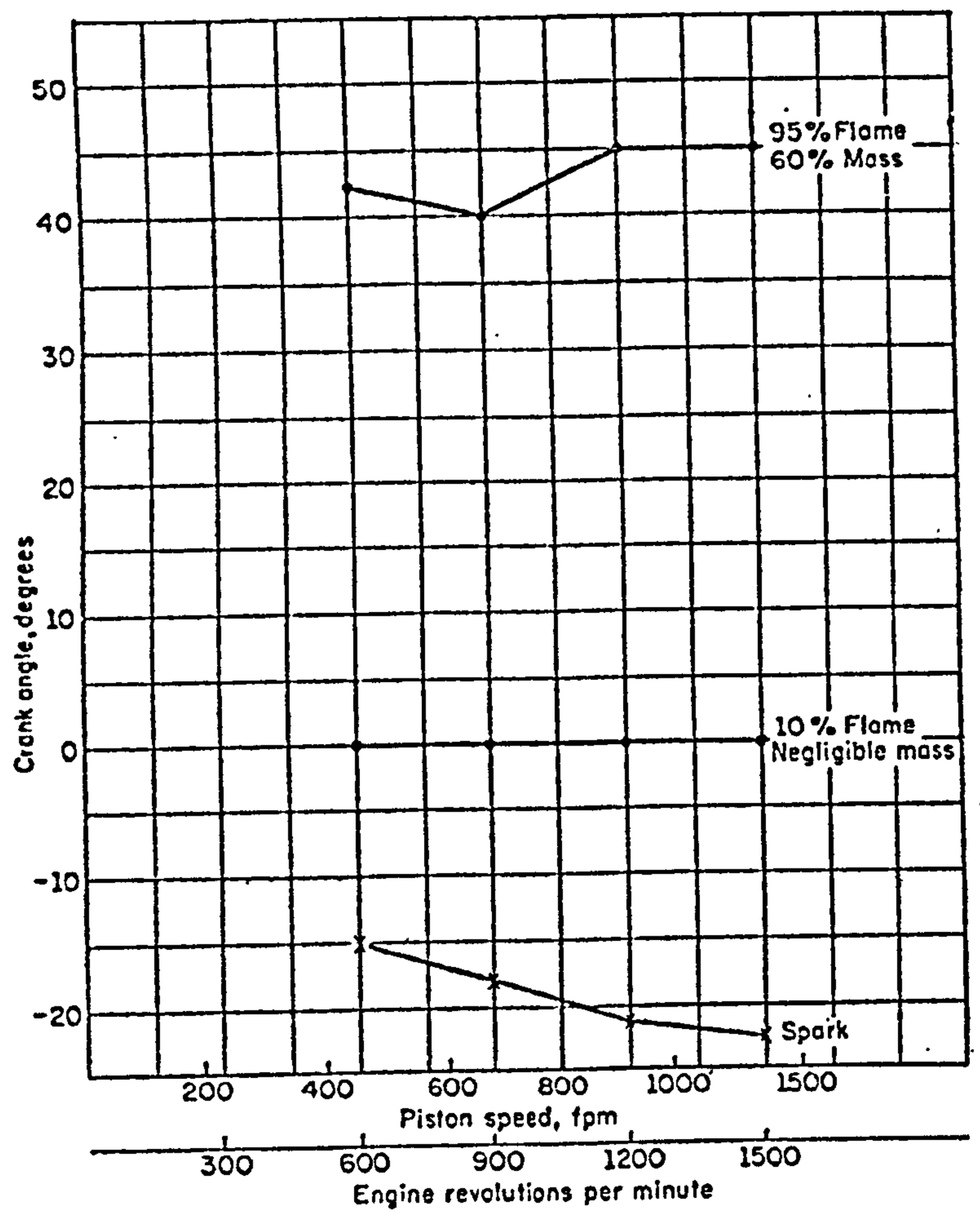

Fig (2-76) Effect of speed on flame travel; CFR engine, $p_i = 14.0$, $T_i = 510°R$, point of 10 per cent travel taken as zero. (Bouchard et al., (41)

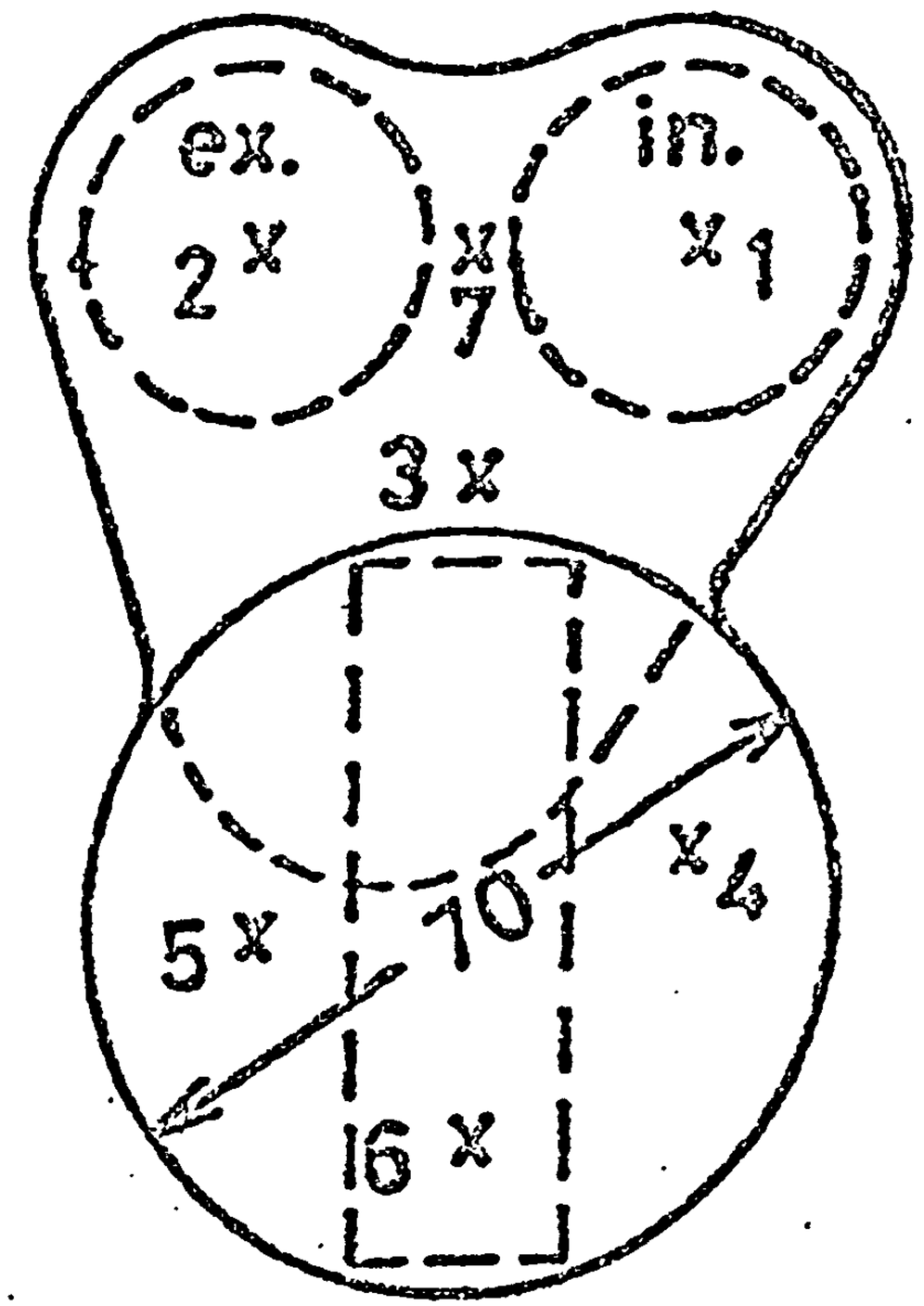

Fig (2-77a). Configuration of combustion chamber and positions of ionisation gaps in Iinuma investigations (36).

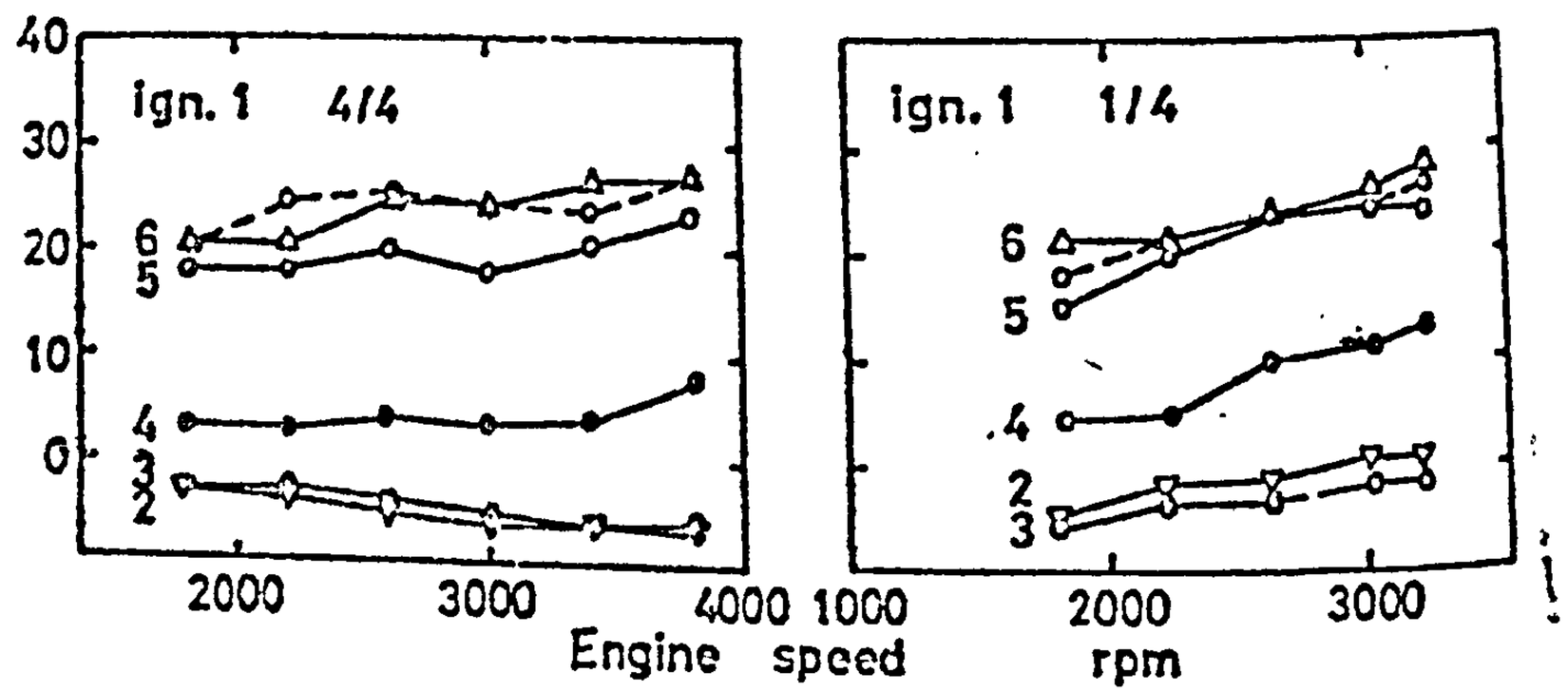

Fig (2-77b). Crank angle of flame arrival and maximum pressure for different engine speeds (36). (Measurements by ionisation probes).

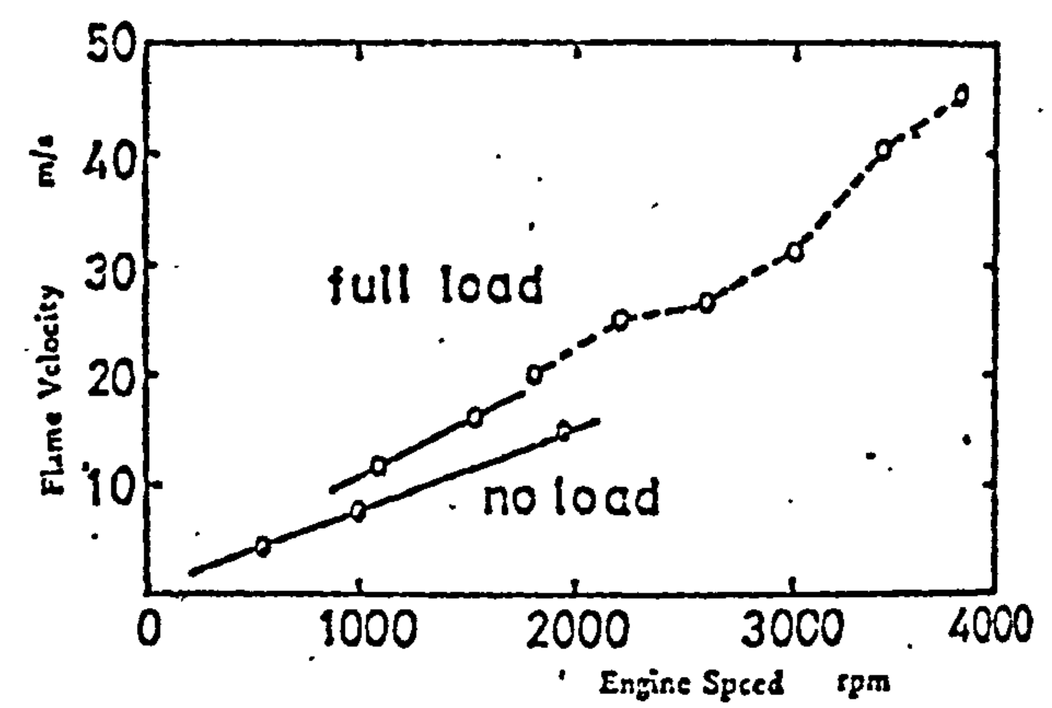

Fig (2-77c). Average flame velocity versus engine speed (36). (Measurements from flame photographs, spark at position 1).

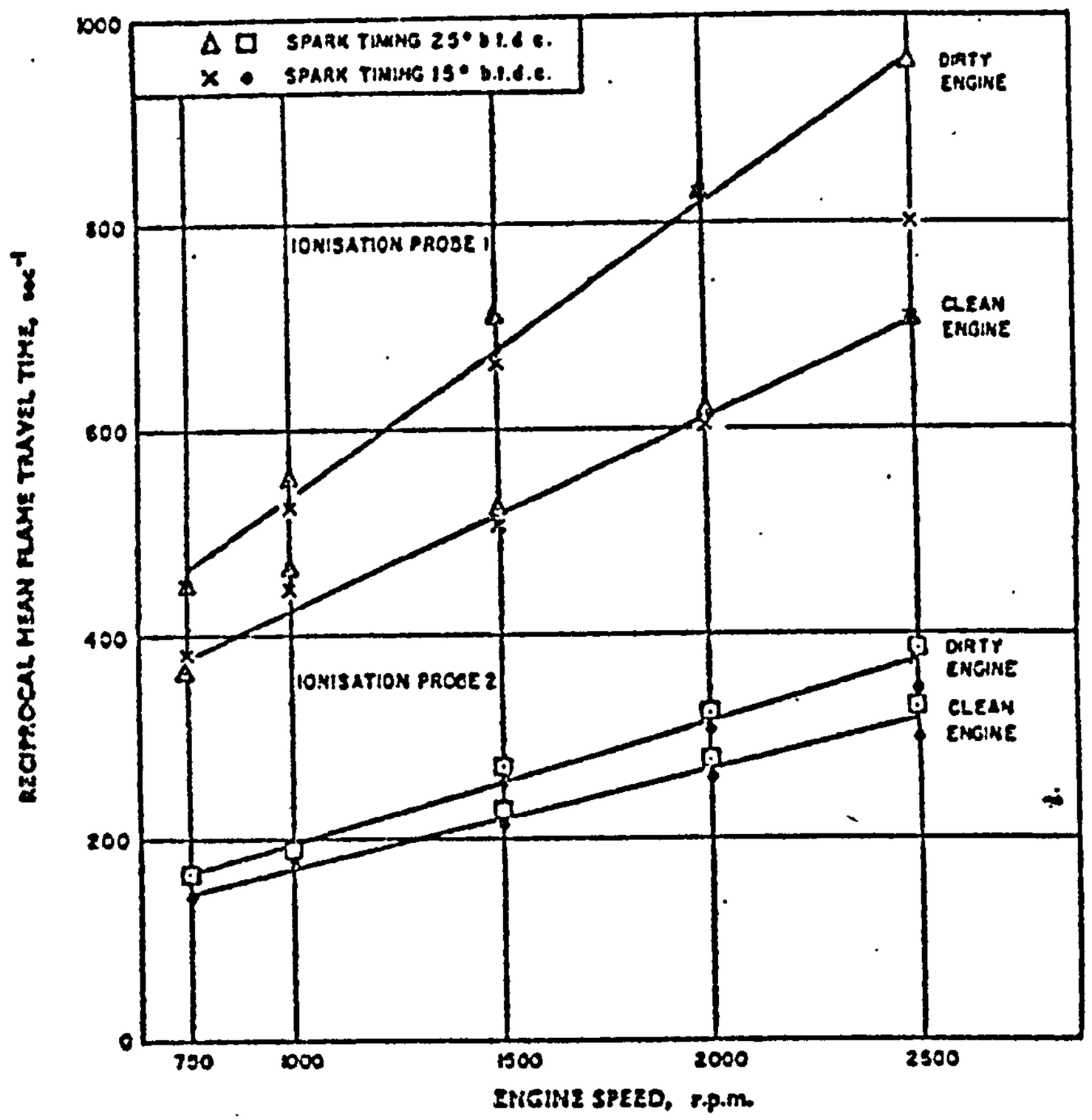

Fig (2-78). Relation between the reciprocal mean flame travel time (flame speed) and engine speed for E-6 engine with iso-octane fuel (30).

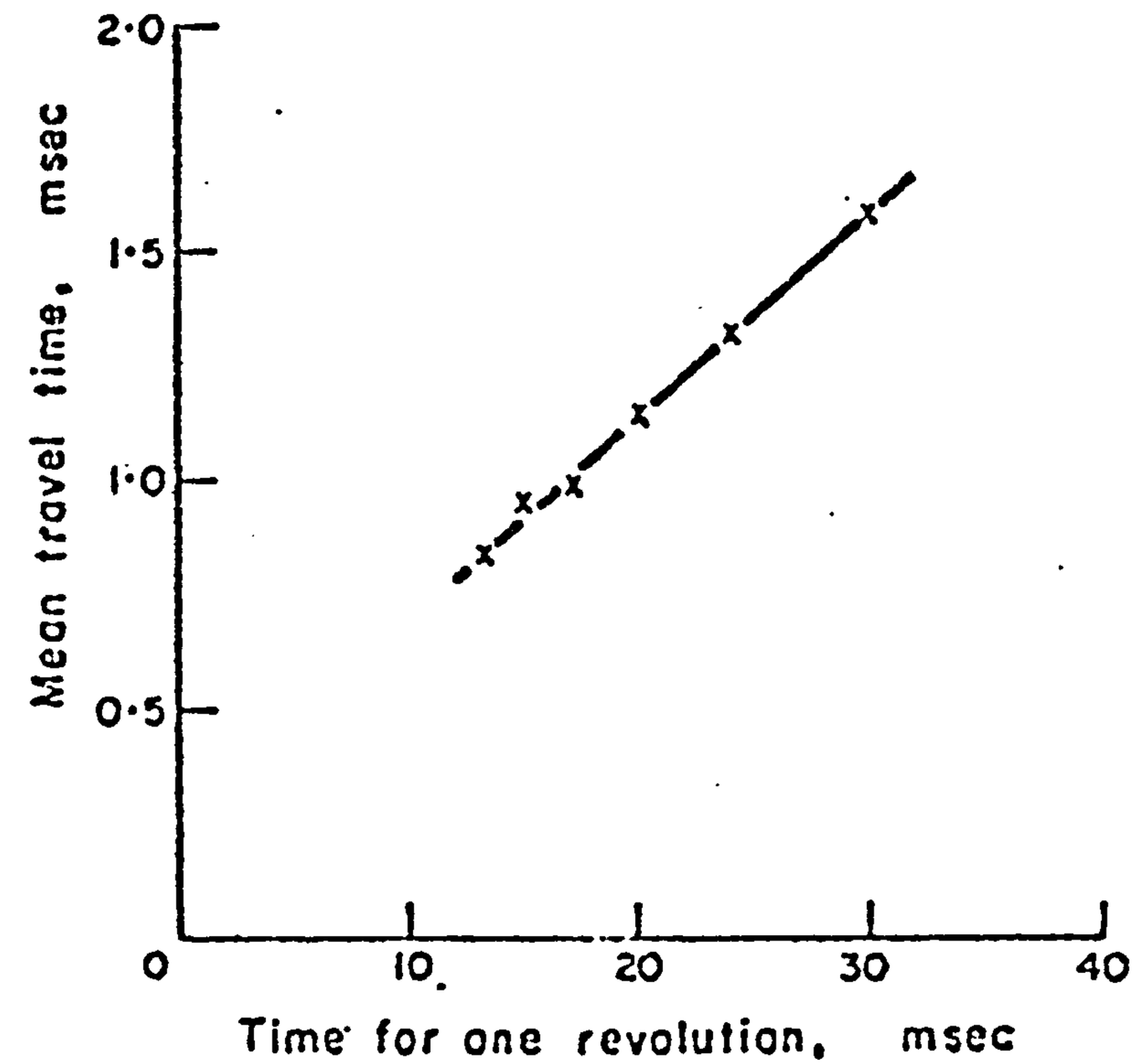

Fig (2-79). Variation of mean travel time for one engine revolution (42).
Ford 2550 cc six cylinder engine and iso-octane fuel.

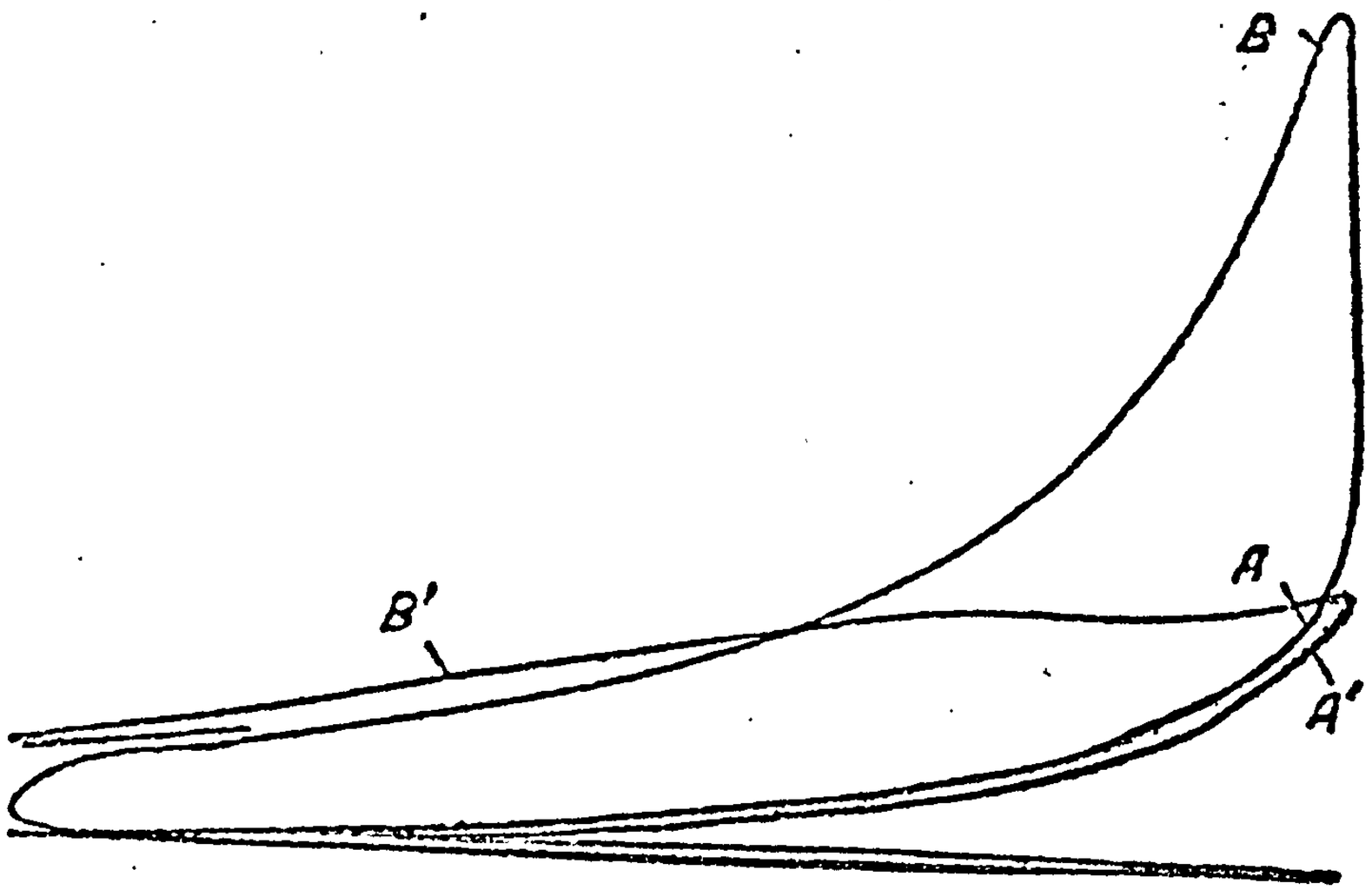

Fig (2-80). Indicator diagram for a normal cycle (AB) and for a cycle without an intake stroke (A'B') (5).

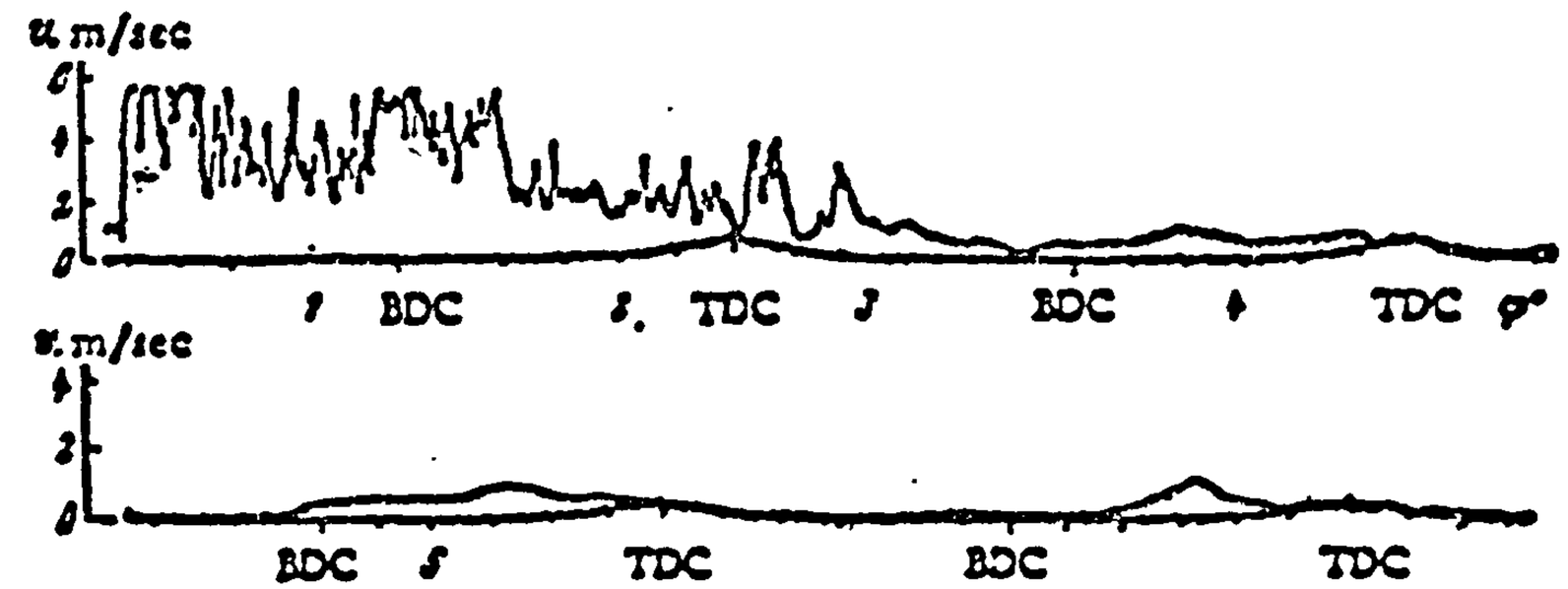

Fig (2-81). Oscillogram of velocity variation during transition from a normal cycle to a cycle in which intake and exhaust are absent, (22).
1) intake, (2) compression, (3) expansion, (4) second compression, (5) third compression.

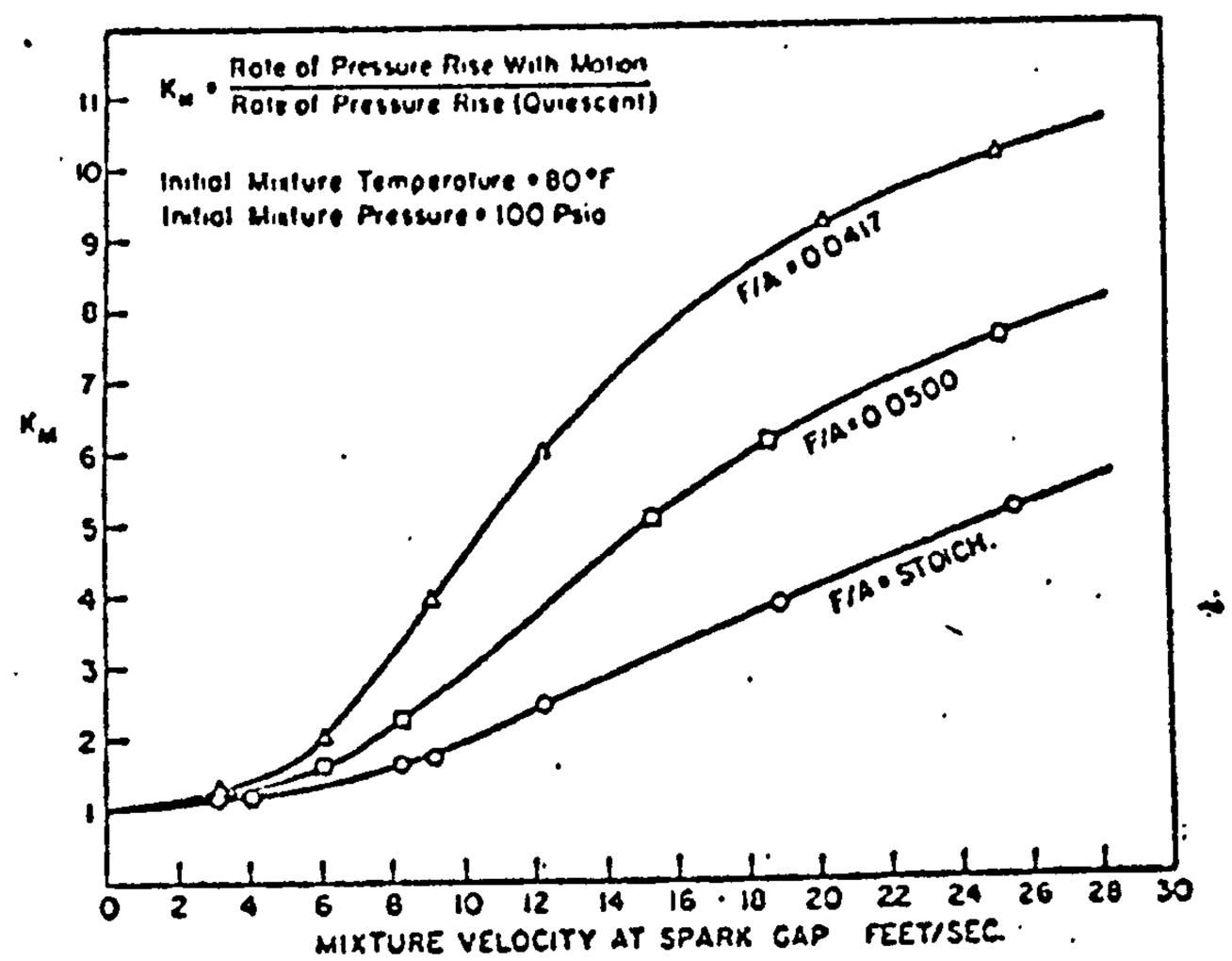

Fig (2-83). Effect of mixture velocity on rate of pressure rise during combustion (3).

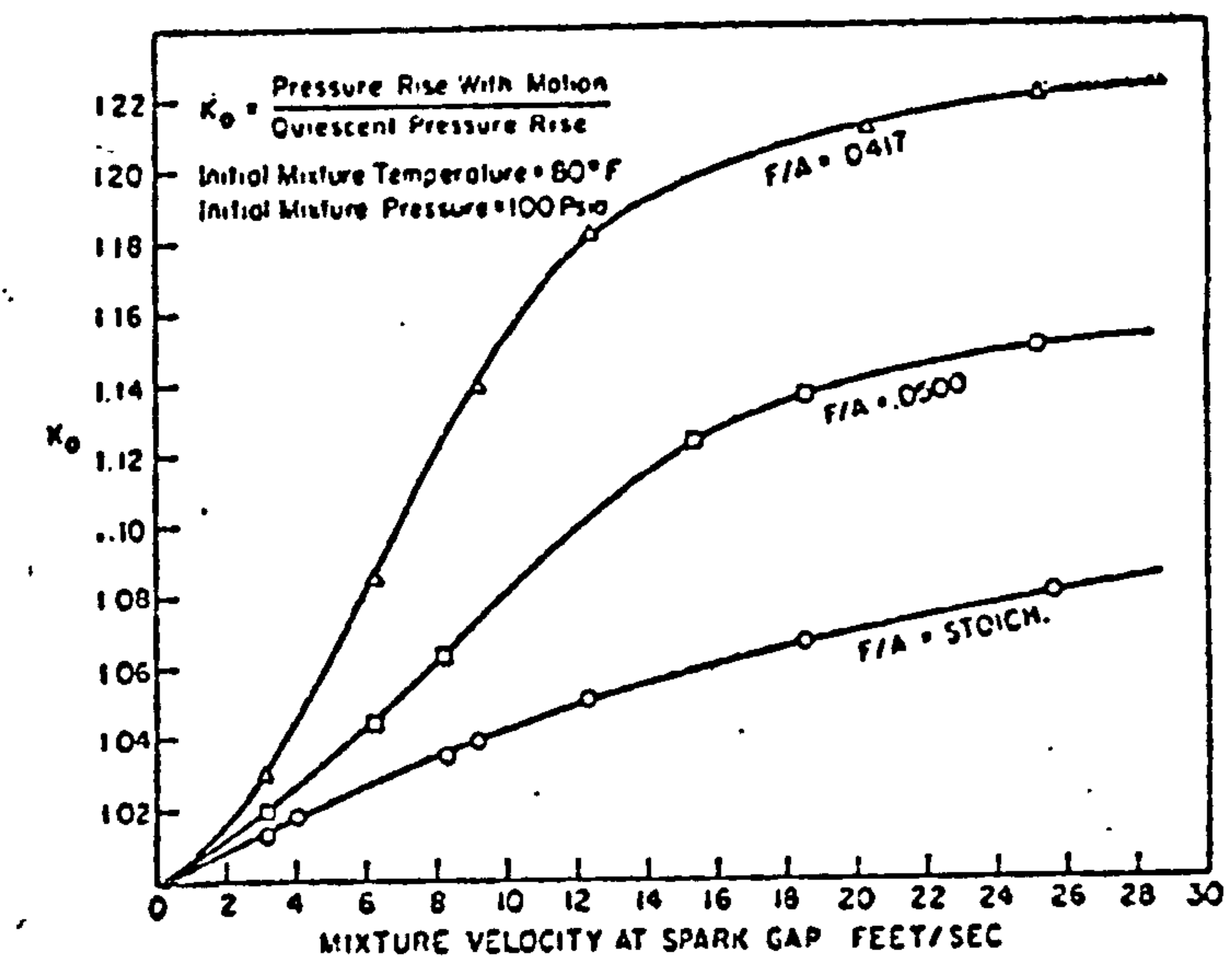

Fig (2-82). Effect of mixture velocity on pressure rise during combustion (3).

Turbulence fields are known to consist of a wide spectrum of eddies of differing sizes. However it is common to distinguish between small scale eddies in which the ratio of eddy size to flame thickness is small and large scale eddies in which this ratio is great. Such distinction is obviously an artificial one for the reference length can only be the flame thickness and the more intense the turbulence the thicker this is. The first class of eddies (small scale) are usually considered of less importance in accelerating the flame speed from its laminar value*, and their role is to cause slight increase by virtue of increasing the diffusivity of gas from its molecular value to some value which is proportional to the scale of turbulence and its intensity. In other words, the flame surface remains even, but the intensity of the transfer process increases. Such effect was formulated by Damkohler (43) as follows;

$$\frac{S_t}{S_l} = \sqrt{\frac{\mathcal{E}}{\nu}} \qquad \text{(for small scale turbulence)} \qquad (2\text{-}19)$$

where S_t and S_l are the turbulent and laminar flame speeds respectively, $\mathcal{E}$ is the eddy diffusivity and ν is the kinematic viscosity.

Using the general principle of combustion theory, Schchelkin (52) also obtained the following relationship for the turbulent flame propagation velocity in the presence of small scale turbulence:

* However, the effect of small scale turbulence on the initiation of the flame kernel in engines is very important and greatly controls the entire combustion process.

$$\frac{S_t}{S_\ell} = \sqrt{1 + \frac{\alpha_t}{\alpha_m}} \quad \text{(for small scale turbulence)} \qquad (2\text{-}19a)$$

where α_t, α_ℓ are the turbulent and laminar thermal diffusivity respectively. In this case the ratio $\frac{S_t}{S_\ell}$ does not go to zero for $\alpha_t = 0$, as follows from the previous relation of Damkohler. It follows that a continuous and smooth transition must exist from turbulent to laminar flame propagation.

Zel'dovich and Frank-Kamentskii (53) also discussed the problem of turbulent combustion and proposed the following relationship for the case of small scale turbulence

$$S_t = \beta\sqrt{\alpha_t} \qquad (2\text{-}20)$$

where β is a constant depending on the rate of chemical reaction.

On the other hand the effect of large scale turbulence has been the subject of many theories and is usually considered to be of much more importance than the microscale. These theories could be put into two main groups according to the model of flame turbulence interaction on which they are based. The first group accepts a surface model and the second, a three dimensional model of combustion. A brief summary of the basis of each theory, and the corresponding proposed expression for the turbulent flame speed, will be discussed in the following.

a) <u>Surface Model (wrinkled and fragmented flame front models)</u>

Such a model assumes that turbulence chiefly affects flame speed by wrinkling the flame front, thereby increasing its area, at each part of the front. Nevertheless it propagates at its laminar

velocity. The turbulent burning velocity can, in this case, be defined in terms of the relative increase in the combustion surface.

$$\frac{S_t}{S_l} = \frac{A_t}{A_l} \qquad (2\text{-}21)$$

Such a model was first proposed by Damkohler who considered the calculation of this area increase impossible in the case of complete fragmentation, while for slight wrinkling the surface may be represented by series of adjacent laminar cones with vertexes oriented differently, Fig. (2-84). The surfaces of these cones are, approximately, proportional to the fluctuating velocity component. Therefore:

$$\frac{A_t}{A_l} \sim u' \qquad (2\text{-}22)$$

and

$$\frac{S_t}{S_l} \sim u'$$

or

$$S_t \sim u' \qquad (2\text{-}23)$$

expressing the fluctuating velocity components in terms of the eddy diffusivity and considering the Lagrangian scale of turbulence ($\mathcal{L}_L$) as constant for the particular test conditions considered, we can write the following relation:

$$u' = \frac{\varepsilon_t}{\mathcal{L}_L}$$

and

$$S_t \sim \varepsilon_t \qquad (2\text{-}24)$$

Defining a turbulence Reynolds number $Re_L = \frac{L_L . u'}{\nu}$ and assuming a constant value for ν we get

$$S_t \sim Re_L \tag{2-25}$$

The experimental data of Damkohler for mixtures of propane-butane with oxygen in Bunsen burners were fitted by a linear relation of the form

$$S_t = a + b\, Re_L \tag{2-26}$$

Shchelkin in his development of Damkohler model assumed the height of the elementary cones to be equal to the distance through which an element of the flame front is carried, by a fluctuation out of the common flame front ($h = u' \cdot t$) where (t) denotes the life time of an eddy, $t = L_x/S_l$, where L_x is the scale of turbulence. The base of the cones was also assumed to be represented by the scale of turbulence L_x. The increase in combustion surface could be, therefore, represented by the ratio between the lateral surface area of the cone and the area of its base. This led to the following expression:

$$\frac{S_t}{S_l} = \sqrt{1 + \left(\frac{2\, u'}{S_l}\right)^2} \tag{2-27}$$

which, for strong turbulence $u' \gg S_l$ gives

$$S_t \sim u' \tag{2-28}$$

However, Sokolik (48) has shown that the determination of the cone height by ($h = u' t$) is justified only for very weak turbulence and it is inconsistent therefore to apply conditions for very strong

turbulence to equation (2-27). He discussed also the case of a fragmented turbulent zone where each eddy is assumed to burn up from its surface at the laminar velocity S_l. Each elementary volume with a surface area of L_x^2 is fragmented by fluctuations when it enters the combustion front. Expressing the distance travelled by any elementary volume during the combustion period by

$$L = t_b \quad u' \quad = \quad (L_x/S_l)u' \tag{2-29}$$

and assuming that the time required to burn the volume L_x^3 is considerably greater than the life time of an eddy. The number of sections of elementary volumes passed over the distance L during the period t_b is $L/L_x = u'/S_l$; which is accompanied by the formation of a new flame surface with an area L_x^2 at each section. The effect of large scale turbulence on the flame, in this case as well, is simply an increase in the combustion surface by a factor $\frac{S_t}{S_l} = u'/S_l$ and once again $S_T \sim u'$.

Karlovitz (45) defines the turbulent burning velocity as the mean velocity over the path of diffusive transport of the eddy during the period of its combustion which could be expressed by the following relationship:

$$S_t = S_l + \frac{\sqrt{\overline{x^2}}}{t} \tag{2-30}$$

where $\sqrt{\overline{x^2}}$ is the average displacement of an element of the front under the influence of turbulence fluctuation and t is the average time during which an element of the combustion flow remains associated with an eddy. Taking into account the theory of

turbulent diffusion the following relationship is obtained:

$$\frac{S_t}{S_l} = 1 + \sqrt{2}\left\{ \frac{u'}{S_l} + \exp\left(-\frac{u'}{S_l}\right) - 1 \right\}^{\frac{1}{2}} \qquad (2\text{-}31)$$

For strong turbulence equation (2-31) reduces to

$$\frac{S_t}{S_l} = 1 + \sqrt{2\,\frac{u'}{S_l}} \qquad (u' \gg S_l) \qquad (2\text{-}32)$$

and for weak turbulence equation (2-31) reduces to

$$\frac{S_t}{S_l} = 1 + \frac{u'}{S_l} \qquad (S_l \gg u') \qquad (2\text{-}33)$$

According to Karlovitz, the values of S_t calculated from u' using such an expression as equation (2-31) are five to ten times smaller than the measured values. He explained the difference by a supplementary turbulence created by the fluctuating flame itself (attributable to the expansion of hot gases). Such supplementary turbulence is expressed by the following relation for the case of isotropic turbulence

$$\frac{u'f}{S_l} = \frac{1}{\sqrt{3}} \left(\frac{\rho_u}{\rho_b} - 1 \right) \qquad (2\text{-}34)$$

where ρ_u and ρ_b are the densities of the unburnt and burnt charge respectively.

Another approach to the problem of turbulence amplification by flames is developed by Mizutani (50) where the kinetic energy of the turbulence is assumed to increase because of the rapid acceleration and its effect on increasing the kinetic energy of the gas, Fig. (2-85).

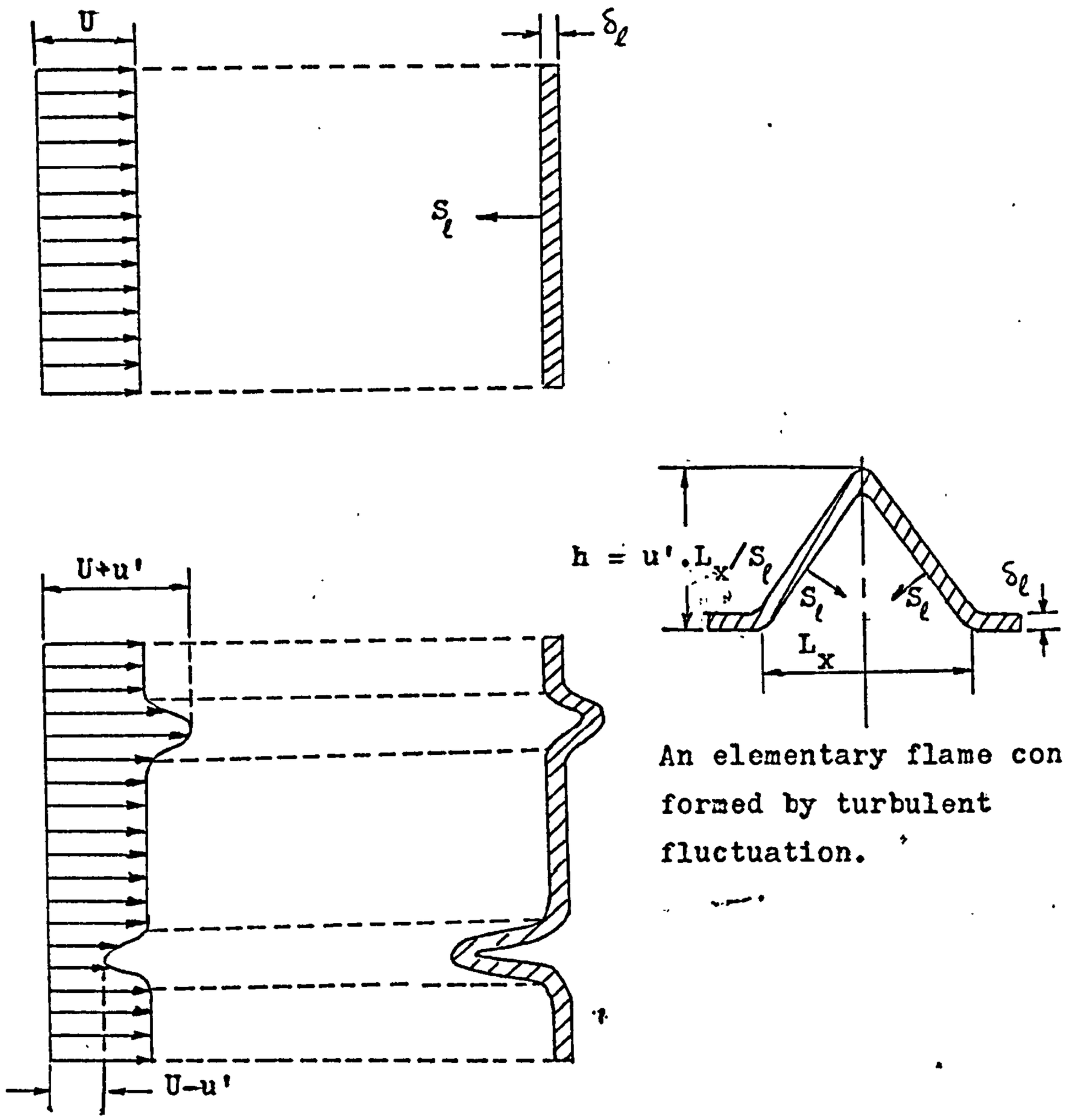

An elementary flame cone, formed by turbulent fluctuation.

Fig (2-84) The effect of large scale turbulence on a flame.

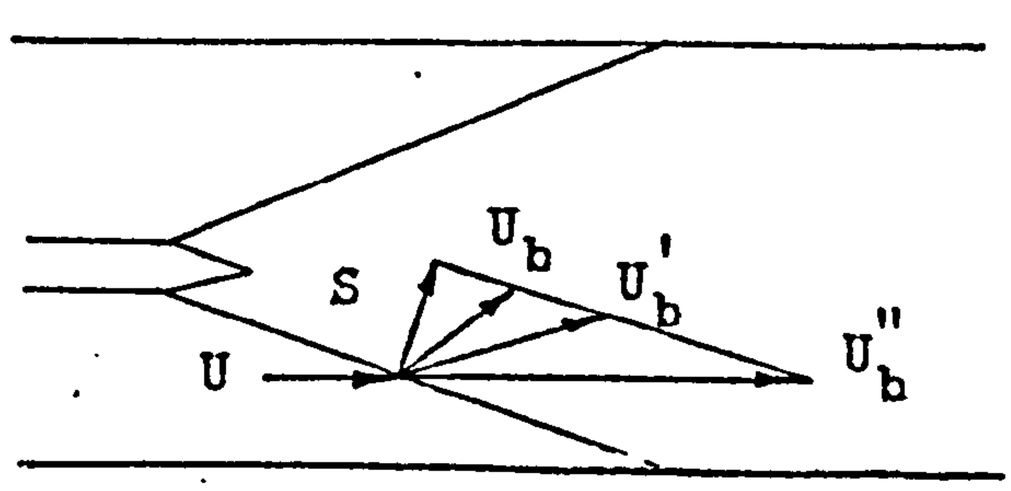

U = Approach gas velocity.
U_b = Actual accelerated gas velocity.
U_b' = Accelerated gas velocity for an infinite plane combustion.
U_b'' = Accelerated gas velocity for a condition of unchangeable flow direction in the combustion wave.

Fig (2-85) Amplification of turbulence level by a flame and turbulent flame speed, (according to Mizutani (50)).

Such increment in the turbulence level is assumed to depend on the turbulence in the approach flow. This condition is expressed by the following relationship:

$$\frac{u'^2_f}{2} = \frac{u'^2_1}{2} + k_1 \left(\frac{u'^2_1}{2}\right)^{\alpha} . (\Delta E)^{\beta}$$

where k_1, α, β are constants, u'_1 is the intensity of turbulence and ΔE is the increase in kinetic energy of the gas.

Using the Karlovitz expression equation (2-31) and substituting for ΔE, the following expression is obtained:

$$\left(\frac{u'_f}{S_l}\right)^2 = \left(\frac{u'_1}{S_l}\right)^2 + K_2 \left(\frac{u'_1}{S_l}\right)^{l} \left(\frac{S_t}{S_l}\right)^{m} U^n \; S_l^{(l+m-2)}$$

$$\times \left[\left(\frac{\rho_u}{\rho_b}\right)^2 - 1\right]^{(m+n)/2} \qquad (2\text{-}36)$$

where K, l, m and n are constants determined from experimental data which gives the following value for the case of confined flames in a combustion chamber:

K_2	l	m	n	
3.6	0.44	2.67	0.75	for 80% reacted portion of the mixture

One of the main contradictions in the Karlovitz model is the determination of the cone height by the diffusion length $(\overline{x^2})^{1/2} = u'.t$ which naturally leads to the conclusion that $S_t \simeq u'$ for very weak turbulence which contradicts the theory predictions for very strong turbulence as mentioned before.

Scurlock and Grover (46) proposed a wrinkled flame surface model where the height of the cones was represented by a diffusion length, defined in terms of both the Eulerian and Lagrangian correlations (R_t and R_x)* as follows:

$$\frac{d\,\overline{x^2}}{d\,t} = 2 \cdot \bar{u}^2 \int_0^\infty R_t \quad R_x \quad dt \tag{2-37}$$

The relative increase in the combustion surface and consequently the burning velocity was expressed in this case in terms of the laminar flame speed (S_ℓ), the Eulerian scale of turbulence L_x and the duration of the effect of turbulent flow (t) on the flame as follows:

$$\frac{S_t}{S_\ell} = \left(1 + C \frac{u'\ t}{L_x \cdot (1+\frac{S_\ell}{2u'})}\right)^{\frac{1}{2}} \tag{2-38}$$

b) Three-Dimensional Models of Combustion

Many objections have been put forward against the surface model of combustion (51, 63, 64) because of the absence of a complete description of the diffusive nature of turbulent flow in such a model. Moreover, experimental data of turbulent flames do not show enough folds of laminar fronts to satisfy the observed large increase in the burning velocity. This led many investigations to reject the idea of wrinkled flame front.

Summerfield (63) has elaborated an expression for the turbulent flame speed by replacing the molecular conductivity in Von Karman's derivation of the laminar flame speed by the corresponding turbulent dimension ($\varepsilon \cdot \rho \cdot C_p$). This led to the

* Definitions of correlations are given in Chapter 3.

following expression:

$$\frac{S_t}{S_\ell} = \frac{\varepsilon}{\nu} \cdot \frac{\delta_\ell}{\delta_t} \qquad (2\text{-}39)$$

where δ_t and δ_ℓ are the turbulent and laminar flame front thicknesses respectively.

Sokolik (48) also considered that the role of turbulence is to augment the diffusion between the unburnt gases and the gases already partially or completely burnt. Dividing the flame front into a number of micro-volumes whose composition, temperature and degree of advancement of the reaction, change under the influence of turbulent diffusion. This led to the derivation of the following expression for the turbulent flame speed:

$$S_t = \frac{u' \cdot \mathcal{L}_t}{t_i} = \frac{\mathcal{L}_L}{t_i} \qquad (2\text{-}40)$$

where t_i is an auto-ignition delay period

$\mathcal{L}_t$ is the Lagrangian time scale

$\mathcal{L}_L$ is the Lagrangian length scale

It is interesting to notice that Sokolik's expression (2-40) for the turbulent flame speed is independent of the laminar burning velocity.

More recently (1972) Van-tiggelen (51), also rejected the model of wrinkled laminar front because of the experimental evidence that only half the apparent volume of the turbulent flame could be statistically filled with wrinkles. He suggested an expression, which was verified by experimental data for an opposed jet burner as follows:

$$\frac{S_t}{S_\ell} = \frac{K \quad u'}{\sqrt{S_\ell}} \qquad (2\text{-}41)$$

Kovasznay (57) developed a criterion to define the conditions which give either a wrinkled laminar flame or a distributed zone. The ratio of velocity gradients in the turbulent approach flow u'/λ to a gradient within the flame δ_L/S_L is equal to Γ, the criterion. The Kovasznay criterion states that a continuous, wrinkled laminar reaction zone is present for small values of Γ, whereas large values of Γ signify the onset of a disrupted or distributed reaction zone which has various degrees of reaction. Povenilli and Fuhs (14) interpreted Kovasznay's criteria in a different way, by considering δ_L/S_L as a characteristic flame time or chemical time. Likewise, λ/u' may be considered a characteristic turbulence time or the time required to distort the flame front. Hence:

$$\Gamma = t\ (\text{chemical})/t\ (\text{turbulence}) \qquad (2\text{-}42)$$

For values of Γ less than unity, the flame consumes the reactants faster than the turbulence can distort the reaction zone, thereby yielding wrinkled flames. When Γ exceeds unity, the consumption of the reactants is not sufficiently fast to prevent the turbulence from disintegrating the flame front.

c) <u>Spectral Theories of Turbulent Combustion</u>

Since states of purely large scale and small scale turbulence do not exist attempts have been made to develop expressions which account for both effects at the same time. Among these is the proposed formulation of Povinelli and Fuhs (14) where both

reaction zone wrinkling and increased transport affect the turbulent propagation velocity. The two effects are accounted for by introducing a "weighting function" based on partitioning the spectrum curve into small and large scale regions as follows:

$$\frac{S_t}{S_\ell} = \frac{A_t}{A_\ell} \int_0^{no} F(n)\, dn + \left(\frac{\varepsilon + \nu}{\nu}\right) \int_{no}^{\infty} F(n)\, dn \qquad (2\text{-}43)$$

where n_o is the frequency of partition which maybe obtained from

$$n_o = S_t/\delta_t$$

The first term $\frac{A_t}{A_\ell}$ is expressed by the effect of large scale turbulence on flame speed as given by Karlovitz's expression (2-33). It is also worth noting that the second term $(\frac{\varepsilon + \nu}{\nu})$ is derived from Summerfield's expression (2-39) with the approximation of $(\delta_t/\delta_\ell) = 1$ and modifying the numerator to be the sum of laminar and turbulent diffusivities, most investigators ((45),(52),(55)) agree on expressions of the form (2-19).

De Soete and Van-tigglen (58) have discussed a similar approach to the problem where the effect of small scale turbulence was expressed by equation (2-18) as follows:

For small scale turbulence (micro-scale eddies)

$$\frac{S_t}{S_\ell} = \sqrt{\frac{\varepsilon + \nu}{\nu}} \qquad (2\text{-}18)$$

The effect of micro-scale eddies could be introduced by defining a micro-eddy diffusivity as follows:

$$\varepsilon_{micro} = v'_{micro} \cdot \mathcal{L}_{micro} \qquad (2\text{-}44)$$

where $\mathcal{L}_{micro}$ is a Lagrangian scale of small scale turbulence and

v'_{micro} is the root mean square value of the turbulent fluctuations contained in the small scale eddies as given by:

$$\overline{v^2}_{micro} = \overline{v^2}_{total} \cdot \int_{n_b}^{\infty} F(n)\, dn \qquad (2\text{-}45)$$

where $\overline{v^2}_{total}$ is the total kinetic energy of the turbulent field.

Also defining the eddy diffusivity of the whole spectrum of eddies in the field by

$$\mathcal{E}_{total} = v'_{total} \cdot \mathcal{L}_{total} \qquad (2\text{-}46)$$

where L_{total} is a representative Lagrangian (diffusion) scale of the whole turbulent field. Thus, we can write:

$$\mathcal{E}_{micro} = \mathcal{E}_{total} \frac{\mathcal{L}_{micro}}{\mathcal{L}_{total}} \sqrt{\int_{n_c}^{\infty} F(n)\, dn} \qquad (2\text{-}47)$$

The effect of macro-scale eddies could be introduced by a corresponding increase in the flame front area as given by:

$$\frac{S_t}{S_{t_{micro}}} = \frac{A_t}{A_\ell} \qquad (2\text{-}48)$$

where S_t is the mean flame speed of the turbulent field, and A_t, A_ℓ are the real wrinkled surface area and the average or apparent surface area respectively.

This increase in the flame front area is mainly caused by the macro-scale eddies and could be expressed from the Karlovitz expression (2-33) as follows:

$$\frac{A_t}{A_1} = 1 + F\left(v'_{total}\sqrt{\int_c^{n_c} f(n)\,dn}\right) = 1 + F(v'_{macro}) \qquad (2\text{-}49)$$

Combining equations (2-48) and (2-18) gives the expression for the mean flame propagation in terms of both effect of small and large scale eddies as follows:

$$\frac{S_t}{S_1} = \left[1 + F\,(v'_{macro})\right]\cdot\left(\sqrt{\frac{\varepsilon_{micro} + \nu}{\nu}}\right) \qquad (2\text{-}50)$$

2.6 Possible Cause of Cyclic Variations

It is now generally accepted that, apart from small improvements resulting from mixture homogeneity and combustion chamber configuration changes, the primary causes for cyclic combustion variations are attributed to fluid motion considerations, particularly with respect to conditions at the spark plug gap and during the early combustion development.

Ricardo (39) has stated "that the observed variations take place for the most part in the initial delay period and are, no doubt, due to variations in the composition of that minute part of the mixture forming the initial nucleus of flame".

Soltau (4) has reported that the principal variable is the delay period between the occurrence of the spark and the formation of a stable reaction front travelling at constant speed. The third stage of combustion which starts behind the premixed blue flame reaction zone and during which most of the heat is released, was also noticed to vary cyclically. Slow reaction resulted always after a long delay period while a rapid initial flame resulted in a better third stage combustion than a much slower one. This led

him to conclude that cyclic variations in combustion processes resulted from variations in the delay period and if this delay period could be made constant, then providing a mixture which burnt at a consistent rate will solve the problem and stabilised pressure traces could be obtained. Also, Peters (33) and Troutman (40) have observed from calculated burning rates that the lower initial burning rate yields lower maximum pressures. The same observations have been reported by Miller, Uyehara and Mayers (38) where two individual consecutive cycles were analysed. The spark was experimentally observed to occur at the same crank angle, the calculated charge weights had indicated no difference in the weight of charged inducted, the rates of heat release were almost identical and the only marked differences were noticed during the early part of the combustion process. After 10% of the mass was consumed little difference existed in the rate at which the fuel/air charge burned, Figs. (2-86) (2-87). This led them to conclude that the propagation of the combustion process just after ignition by the spark appears to be the controlling factor in cyclic variation and that to minimise such variation some means must be found to control the initiation of burning and the rate at which the chemical reaction proceeds during the first 10% of the combustion period.

Curry (37) performed a 3-dimensional study of flame propagation in a Waukesha CFR spark ignition engine. Using ionisation gaps he reported a small variation in the flame travel times at an ignition gap located at 3/16 inch from the centre electrode Fig. (2-36), while a much greater variation was noticed at a second ionisation gap located at less than one inch from the spark plug. Approximately 45% of the total variation in the time required to

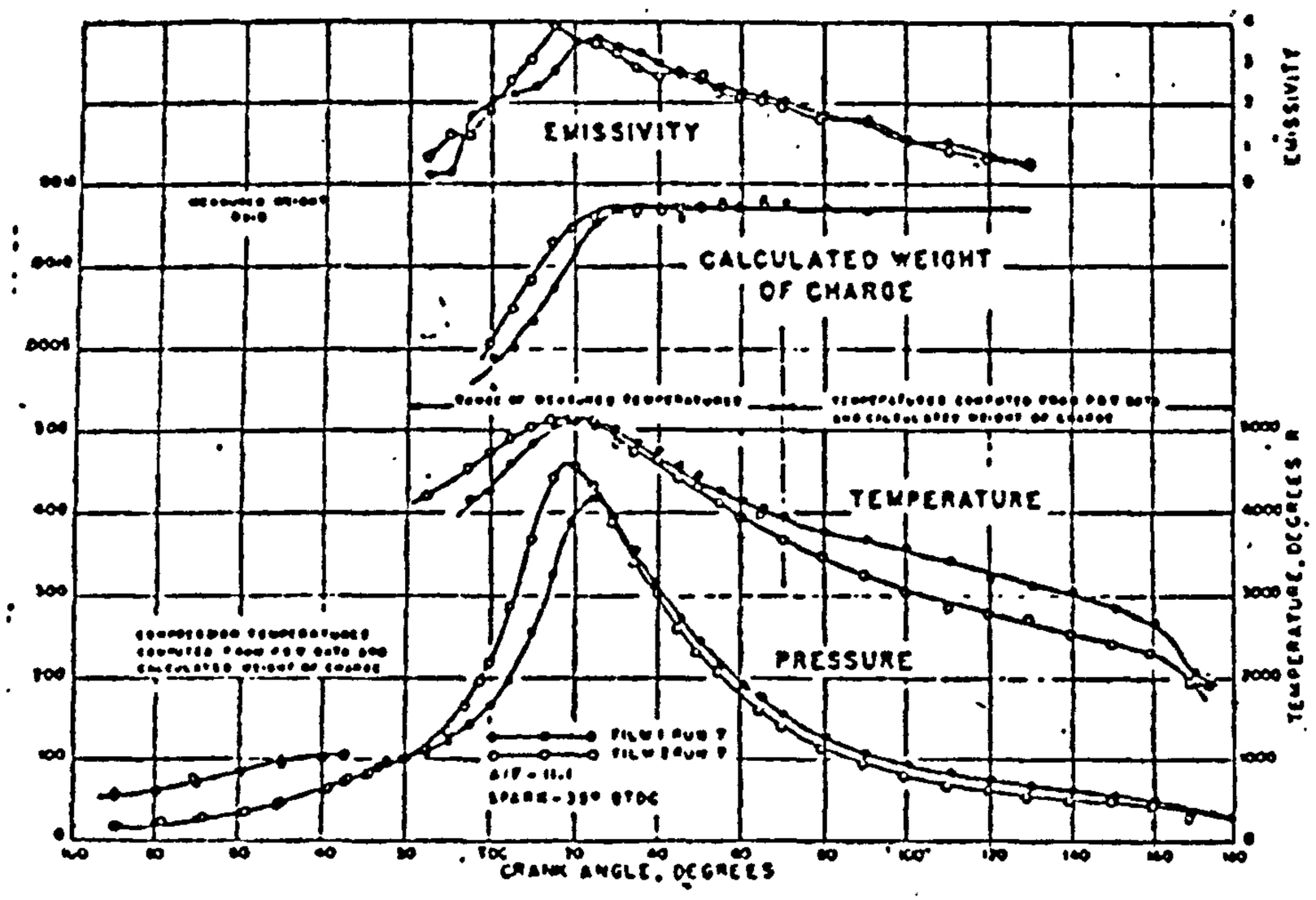

Fig (2-86). Pressure and temperature trace of engine showing cyclic variation - two separate engine cycles under similar operating conditions (38).

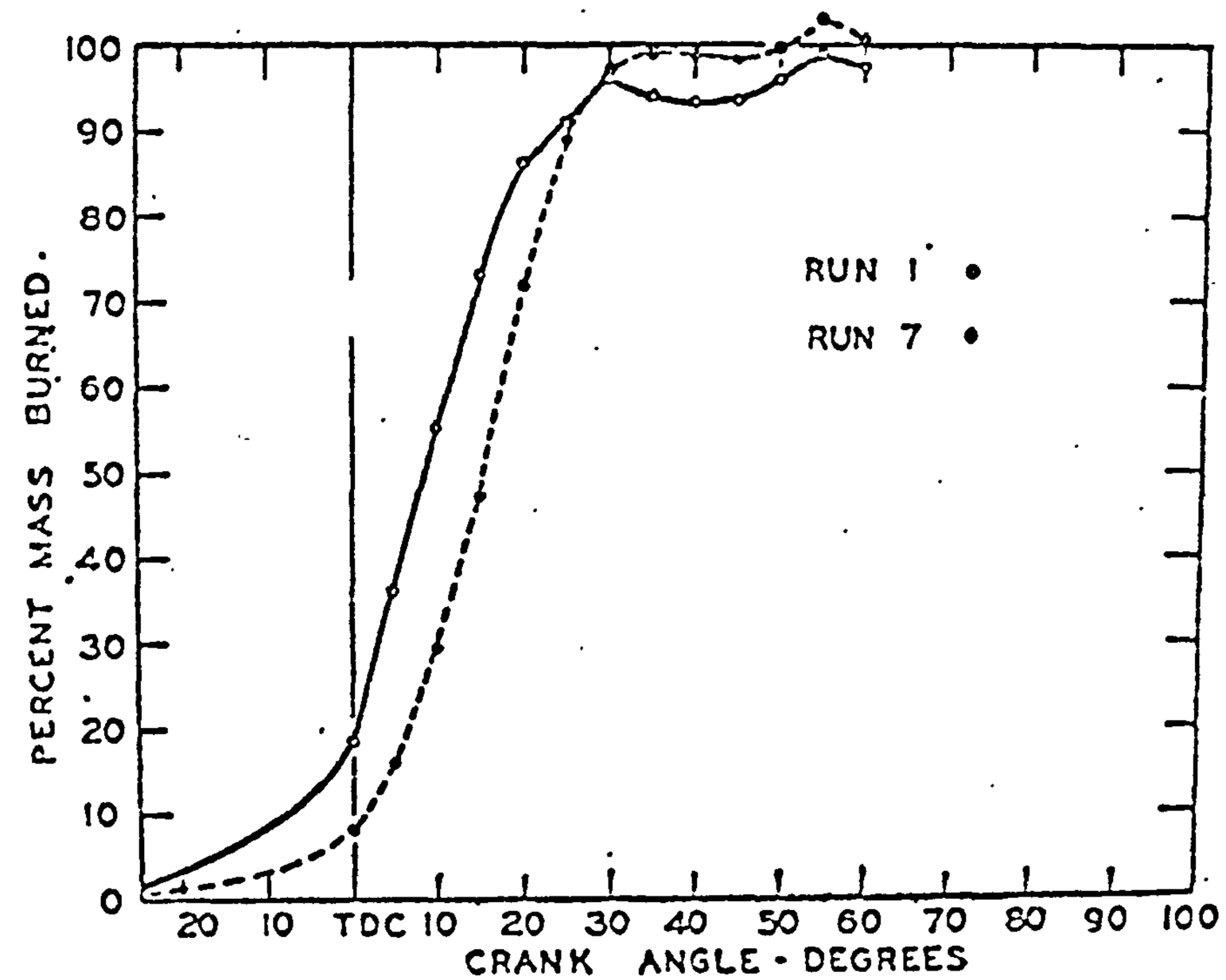

Fig (2-87). Percentage mass burned versus crank angle for two cycles taken under constant operation conditions. (38).

complete combustion had occurred by the time the flame had reached this second point. This led him to conclude that the ignition process and the subsequent initial propagation of the flame kernel was repeatable from cycle to cycle and that the sizeable variations in the time for complete combustion and in the time of maximum pressure signal, which could reach a value of 25% of the average time, occurred beyond the point of ignition in the early development of the flame front. However, one has to notice that this reported data was obtained under relatively ideal conditions of a single cylinder engine at maximum power fuel/air ratio and maximum brake torque (MBT) spark timing.

However, Robinson (37) in his discussion of Curry's work has not excluded the probability that such small variations in flame speed at the spark gap could have a pronounced effect on flame speed later in the cycle. He mentioned that measurements of flame rate at ionisation gaps located ½ in from the spark gap during normal combustion have indicated that slow rates of flame propagation at these gaps resulted in correspondingly slow total combustion time for a particular cycle. Conversely, fast initial combustion time results in fast total combustion time. He concluded that, in general, the primary cause of cyclic combustion variation originated at the spark gap.

Harrow and Orman (30) have noticed a similar general feature of cyclic variations of flame arrival times at two ionization probes located at 16.5 mm and 65 mm from the centre electrode, Fig. (2-12). Furthermore, they noticed no correlations between the deviation of flame arrival times at the two probes. The extent of cyclic variation

was noticed to decrease after the formation of deposits in the combustion chamber. They have shown by a process of elimination that the only cause for such reduction could be an increase in the turbulence intensity. Furthermore, they have noticed that such effects were more marked at the first probe than at the second which one can attribute, in view of the previous discussion, to the effect of small scale turbulence generated by the increased surface roughness due to deposits formed on the early development of the initial flame kernel when its size is comparable with the size of small scale turbulence eddies.

Patterson (2) stated that the combustion rate variations are the result of mixture velocity variations that exist within the cylinder near the spark at ignition. Similar conclusions were reached by Barton et al (10) where correlation was obtained between variations of mean velocity at the spark plug and variation of the initial burn time.

In a basic investigation of the effect of mixture motion on the developing flame kernel, Cole (12) utilised high speed Schlieren photography to observe the combustion process in a constant volume bomb with central ignition. He used a stoichiometric propane/air mixture at one atmosphere pressure and directed in a small jet of mixture into the region of the spark gap. This distorted the development of flame kernel and increased the area of the flame front by an amount dependent on the jet velocity. The increase in flame front area was correlated with the rate of pressure change dP/dt with greater jet velocities, Fig. (2-88). Similar observations are reported when the mixture velocities are increased by means of swirl generators fitted in the inlet ports

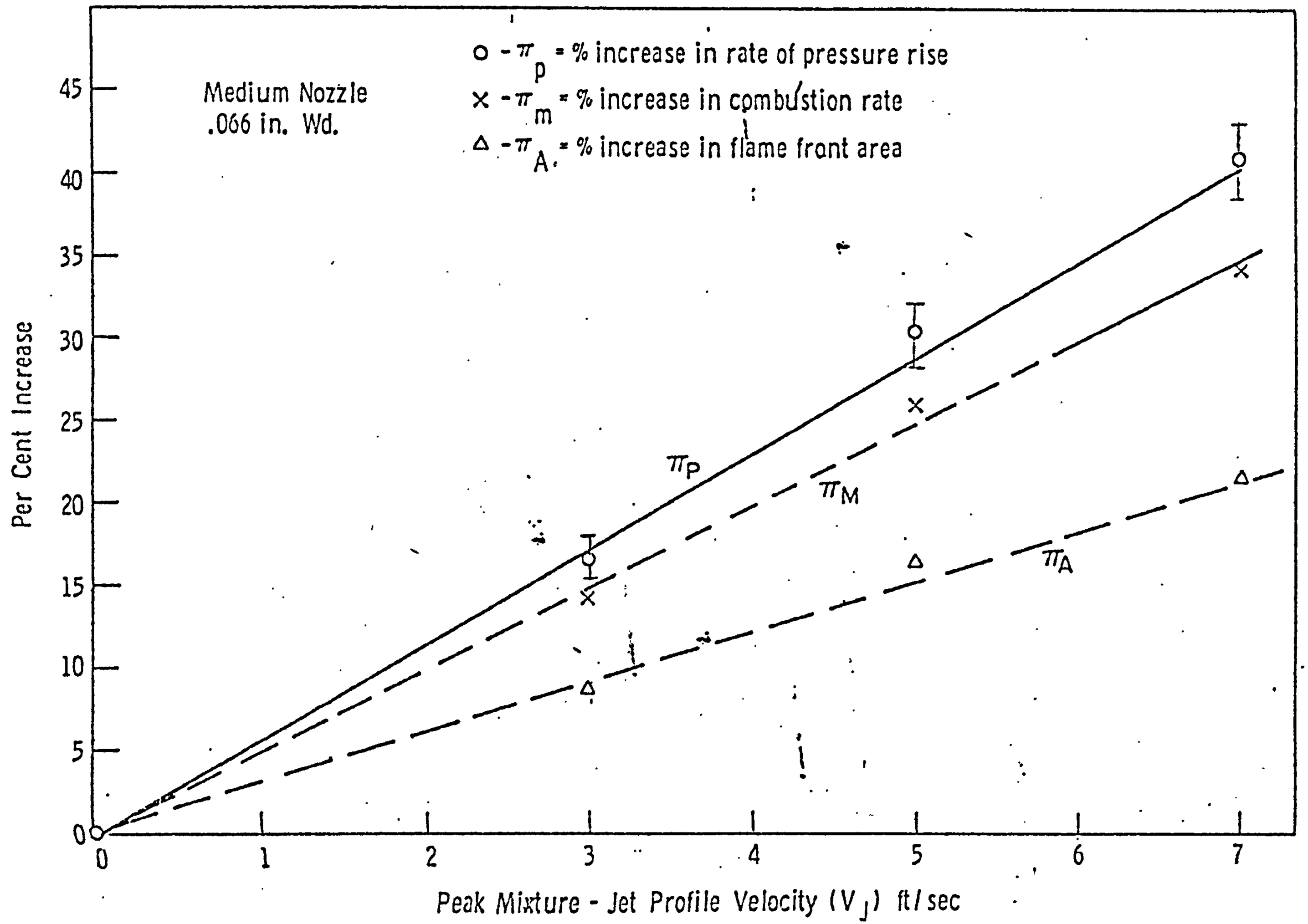

Fig. (2-88). Effect of mixture jet velocity on combustion (12)

(60) or on the valve seat (20), Figs (2-89) and (2-90).

Therefore, it has been concluded, from the foregoing discussion, that the most significant variables affecting cyclic variation are the mixture motion and the effect of small scale eddies on the growth of the initial flame kernel.

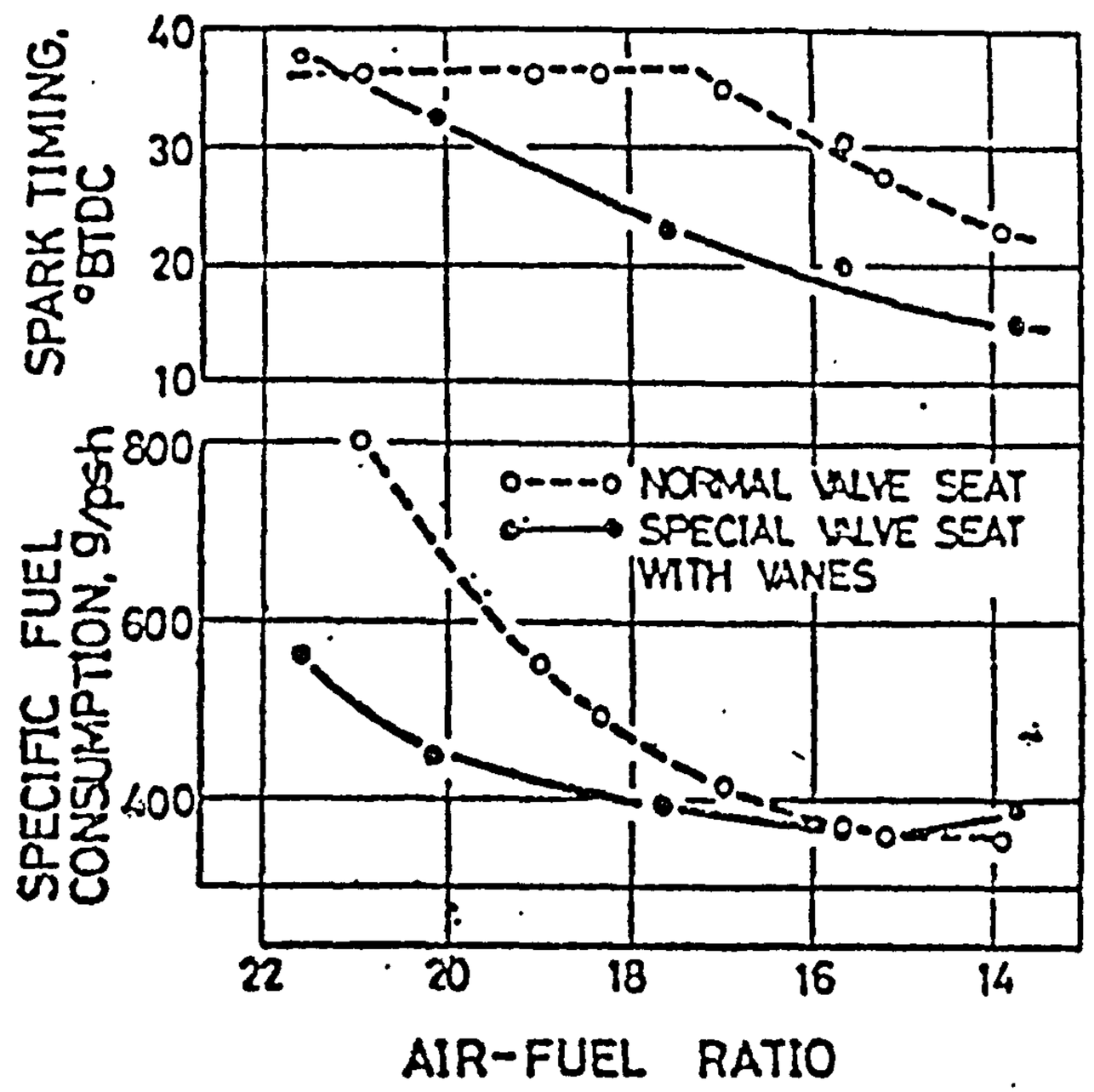

Fig. (2-89). Effect of mixture turbulence on specific fuel consumption and required spark timing; engine speed, 1600 r.p.m.; absolute intake pressure 300 mm Hg. (20)

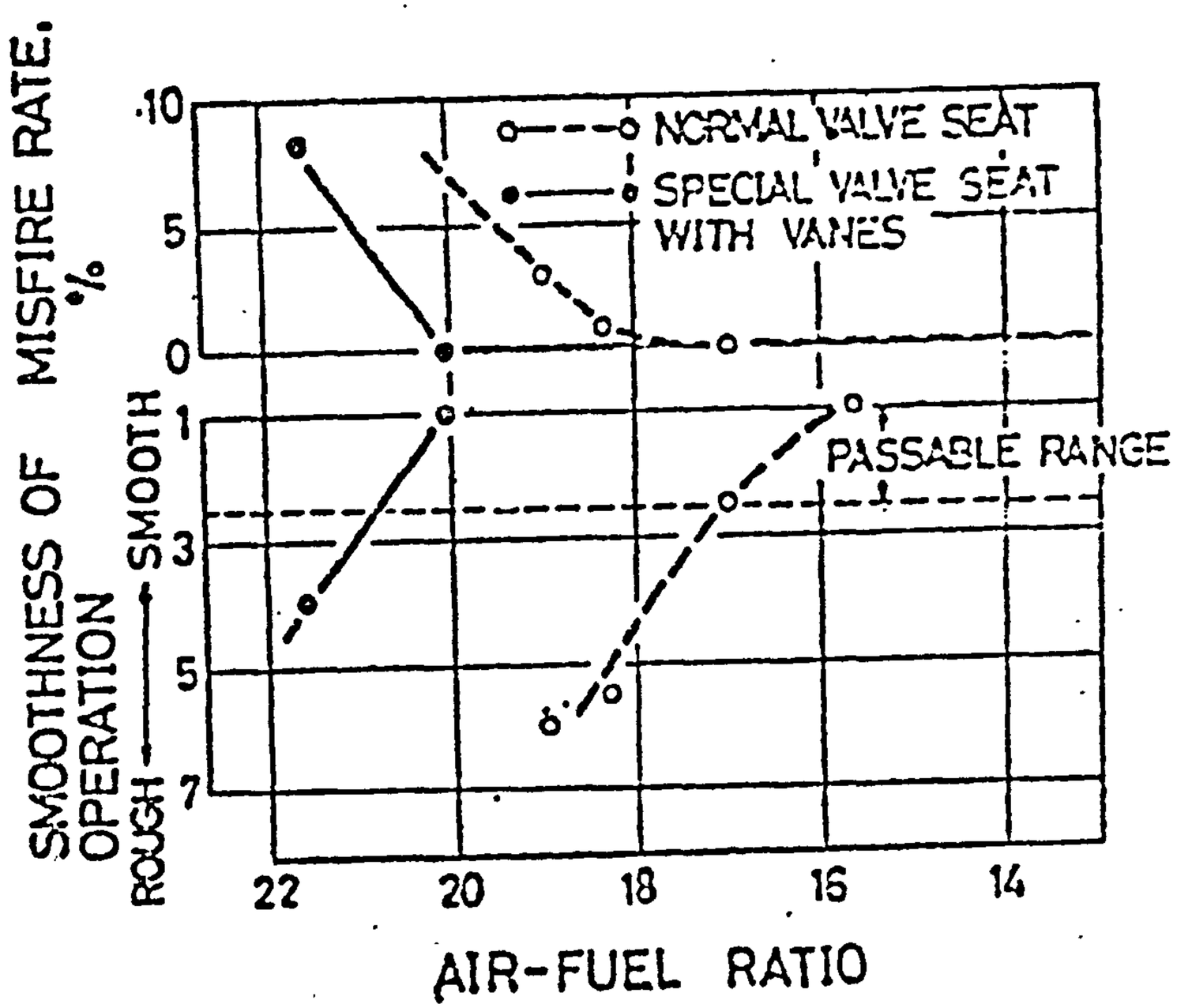

Fig. (2-90). Effect of mixture turbulence on smoothness of operation and misfire percentage. (20)

measure of the flow velocity. The DC component of such unbalance voltage is a measure of the mean flow velocity while the AC component provides a picture of the fluctuations in the flow. Examination of the response of constant current anemometer to turbulence fluctuations (79) shows that its sensitivity is a function of the wire temperature (T_W), the mean flow velocity ($\bar{U}$), and the frequency of the velocity fluctuations (n). It decreases for large values of the frequency and a compensating amplifier must be used to correct the errors due to the thermal inertia of the wire. The time constant of this compensating circuit must be equal to the time constant of the wire. The latter is a function of the mean flow velocity and the compensating network should, therefore, be readjusted when the mean flow velocity changes. Moreover, the constant current anemometer could not be used in a field of high velocity fluctuations because of the risk of burning out the wire at high rates of current flow. Therefore such a technique cannot be used in an engine because of the wide variations in the gas velocities and consequently the heat transfer rate from the wire during the cycle.

3.1 The Constant Temperature Hot Wire Anemometer

This method employs a feedback amplifier to supply current to the hot wire in order to keep the wire resistance, and accordingly its temperature, constant as far as possible. In principle the constant temperature anemometer consists of a Wheatstone bridge and a servo amplifier, Fig. (3-3). The active bridge arm consists of the probe and one of the two top resistances.

The passive bridge arm contains the other top resistance, the comparison resistor and a compensating network to minimise the influences of inductance and capacitance of the probe cable.

When the bridge is in balance, no voltage differences exist between the end points of the horizontal bridge diagonal. Any change in the flow acting on the probe will affect the temperature of the sensor, causing it to grow cooler or hotter as the case may be. The resultant resistance change brings about a voltage difference at the horizontal diagonal which is fed to the input of the servo amplifier. The output voltage of the servo amplifier is applied to the bridge input (bridge top) under such phase relations that the original temperature will be restored by increasing or reducing the bridge operating voltage. The higher the gain of the servo system, the more rapidly the amplifier responds, the lower error voltage will be required at the horizontal bridge diagonal in order to compensate for a temperature change in the sensor. This is of great importance because it is the method employed in attempting to overcome the thermal inertia of the probe.

3.2 Calibration of the Hot Wire Anemometer

Accurate measurement of gas velocities and turbulence in a fluid field depends to a great extent on the accuracy and generality of the expressions used to describe the heat transfer mechanism from the hot wire anemometer used. Such requirement is of paramount importance in engine investigations where the wires are usually operated under conditions of varying pressures and temperatures which are different from the calibration conditions.

The work of many investigators of heat transfer from long cylinders, with flow perpendicular to the axis, was reviewed in 1932 by Ulsamer (72), in 1954 by McAdams (73) and more recently in 1972 by Andrews et al (74). McAdams showed that most of the available data of various investigators are very close to those of Hilpert (75) which cover a very large number of diameters from 0.0079 to 5.9 inches as shown in Fig. (3-4). All these data are correlated by an equation of the form

$$N_u = B\,R_e^{\,n} \qquad (3\text{-}1)$$

where N_u is the Nusselt number and R_e is the Reynolds number. The exponent (n) increases and the factor (B) decreases as the Reynolds number increases.

However a more general expression for the heat transfer from a cylinder to a gas or liquid perpendicular to the cylinder axis, as expressed by many investigators, could be written as

$$N_u = A + B\,R_e^{\,n} \qquad (3\text{-}2)$$

where A, B and n are constants over a specified range of Reynolds number. The constant A in equation (3-2) is intended to represent a combination of the conductive heat loss of the wire supports with buoyancy effects as a component of the total heat loss. This constant has an initial value of the order of 0.3 and is set equal to zero for $R_e > 44$ in Collis and Williams' investigation (76) and for $R_e > 1000$ in McAdam's investigation (73). Davis and Fisher (77) have criticised the existence of such a constant and show that the effect of buoyancy in the analysis of forced convection from heated wires could be ignored, when the wires

are sufficiently small. No other explanation was found for the origin of the constant A and was, therefore, attributed to the error introduced by extrapolating the measurements of electric power over a limited range of velocity to zero velocity.

An error that resulted in an over-estimation of the power loss at zero velocity and could be as high as eight times the true value, as shown in Fig. (3-5).

Different calibration procedures were used in the published investigations on measurements of gas velocity in engines. A review of the important ones will be discussed briefly below.

Semenov (22) overcame the problem of variations in fluid properties during the engine cycle by reducing the current flowing through the anemometer bridge circuit at the temperature and pressure conditions of gas flow in the engine (I) to the bridge current that flows at ambient conditions (I_o). The flow velocity, U, was then evaluated from the calibration curve U = f(I) obtained at ambient conditions as follows

$$I_o = K\,(p,T).I \qquad (3\text{-}3)$$

The coefficient of reduction K (p,T) is determined from the equation of the heat balance of the wire as given by

$$I^2 R_W = h.A\,(T_W - T_g) \qquad (3\text{-}4)$$

where A is the lateral surface area of the wire, h is the heat transfer coefficient, T_W and T_g are the wire and gas temperatures respectively. Using a relationship between Nusselt and Reynolds

numbers in the form

$$N_u = B\,R_e^{m} \tag{3-5}$$

Substitution for the heat transfer coefficient from equation (3-4) the coefficient of reduction K(p,T) was given by

$$K(p,T) = \left(\frac{\rho_o}{\rho_g}\right)^{m/2} \left(\frac{K_o}{K_g}\right)^{\frac{1}{2}} \left(\frac{\mu_g}{\mu_o}\right)^{m/2} \tag{3-6}$$

Making use of the polytropic relation and expressing the gas density in the cylinder in terms of a filling coefficient η_v, the following expression for K(p,T) resulted

$$K(p,T) = \left[\frac{1}{\eta_v}\cdot\left(\frac{T_g}{T_o}\right)^{\frac{1}{n-1}}\right]^{m/2} \left(\frac{K_o}{K_g}\right)^{\frac{1}{2}} \left(\frac{\mu_g}{\mu_o}\right)^{m/2} \tag{3-7}$$

where

ρ is the fluid density

T is the fluid temperature

K is the fluid thermal conductivity

μ is the fluid viscosity

n is the polytropic index of compression

B,m are constants

and the subscripts o and g refer to conditions at ambient and gas conditions respectively.

Barton et al (11) calibrated their sensors using a heat transfer law as in equation (3-2). The values of the constants A, B and n were obtained experimentally. Matsuoka et al (15) used a similar expression for their calibration of gas velocities at TDC. The values of the constants A, B in the latter case were obtained by taking the ratio of gas properties at TDC and at ambient conditions, while the exponent n was taken as 0.5, as proposed by King (78).

Winsor (23) operated his hot wires at two different temperatures and used King's expression for the heat transfer from the wires. He derived a relationship between the pressure-velocity product and the differencein the dissipated power from the wire at the two temperatures as given by:

$$\left(\frac{E_H^2}{R_H} - \frac{E_L^2}{R_L}\right) = C_1 + C_2 \, (P\,U)^{\frac{1}{2}} \qquad (3\text{-}8)$$

where E is the bridge voltage, R is the operating resistance, P is the pressure and U is the gas velocity. The subscripts H and L refer to the high and low operating temperatures respectively. The values of the constants C_1 and C_2 were obtained experimentally.

James (24) used a heat transfer expression developed by Collis and Williams (76) and accounts for end losses from the wires by an expression derived by Davis and Fisher (77). The radiation losses were also considered. However, their effects are almost negligible (77, 79).

A calibration procedure based on analytical methods, which was experimentally checked, was presented by Davis and Fisher (77) in 1961. This procedure has been successfully used by Dent et al (92, 93) in engine investigations and was employed in the present work. In this case, a comprehensive heat balance for the wire leads to an implicit equation in a single unknown variable (K_1) which could be obtained by successive iterations. This equation is given by:

$$\frac{I^2 R_w}{A\,K_T \ell\,(T_w - T_g)}\left[1 - \frac{2}{\ell}\,\frac{K_s}{K_T}\,\frac{R_g}{R_w}\,\frac{\tanh\left(\sqrt{|K_1|}\;\ell/2\right)}{\sqrt{|K_1|}} - \left(\frac{R_w - R_g}{R_w}\right)\right] - |K_1| = 0 \qquad (3\text{-}9)$$

where $K_1 = \frac{I^2 \beta_g \alpha}{K_w \cdot A^2} - \frac{\pi dh}{K_w A}$ (3-10)

d is the wire diameter

ℓ is the wire length

A is the wire cross sectional area.

K_T, K_s are the thermal conductivities of wire material at the operating temperature and supports temperature respectively

T_w, T_g are the wire and gas temperatures respectively

R_w, R_g are the wire resistances at the operating temperature and gas temperature respectively

β_g is the electrical resistivity of the wire at gas temperature

α is the coefficient of temperature for wire material

I is the electric current

and h is the heat transfer coefficient.

Davis and Fisher (77) showed that the heat transfer coefficient could be related to the mass flow past the wire by the following relation

$$h = c_f \cdot \rho \cdot \frac{C_v \; K_w}{\pi \; K_g} \; U \qquad (3\text{-}11)$$

where ρ is the fluid density

C_v is the specific heat at constant volume

K_w, K_g is the thermal conductivities of the gas at the wire operating temperature and gas temperature respectively

U is the fluid velocity

and c_f is the skin friction coefficient which is given by:

$$c_f = 2.6\, R_e^{-2/3} \qquad \left[0 < R_e < 40\right] \qquad (3\text{-}12a)$$

$$c_f = 1.4\, R_e^{-1/2} \qquad \left[40 < R_e < 1000\right]. \qquad (3\text{-}12b)$$

where R_e is the Reynolds number based on flow conditions approaching the wire and the wire diameter. The lower range of Reynolds number ($R_e < 40$) covers most of the practical range of hot wire anemometers. Substituting equation (3-12a) into equation (3-11) gives the following relation

$$\frac{hd}{K_w} = \frac{2.6}{\pi\gamma} \left(\frac{C_p \mu_g}{K_g}\right) \left(\frac{\rho . d . U}{\mu_g}\right)^{1/3} \qquad (3\text{-}13)$$

or

$$N_u = \frac{2.6}{\pi\gamma} \; Pr. \; R_e^{1/3} \qquad (3\text{-}14)$$

where N_u is the Nusselt number, Pr is Prandtl number, μ_g is the dynamic viscosity of the fluid at its temperature, C_p is the specific heat of gas at constant pressure and γ is the ratio between specific heats at constant volume and constant pressure.

The variation of gas properties with temperature is required for such a calibration procedure. This was obtained from a polynomial curve fit of the published data in the literature (95-100), as will be discussed in appendix A3.

3. HOT WIRE ANEMOMETER AND ITS CHARACTERISTICS FOR TURBULENCE MEASUREMENTS

The hot wire anemometer has been the most satisfactory instrument for measuring turbulence and turbulent fluctuations. This is because its small size introduces a very small disturbance of the flow field and its low thermal inertia makes a reasonably high frequency response practical. Fig. (3-1) shows an example for the frequency characteristics of a constant temperature hot wire anemometer as a function of flow velocity.

A hot wire anemometer consists of a fine electrically heated wire stretched across the ends of two prongs. The wire is cooled by the flowing fluid, causing the temperature to drop and consequently the electrical resistance of the wire to diminish. There are two basic methods of operating hot wire anemometers which are the 'constant current' and the 'constant temperature'. In the first method the electrical current is kept constant and the fluid speed is determined from the changes in electrical resistance, while in the second method the wire is maintained at a constant temperature and the fluid speed is determined from the measured value of the electric current. In either method, the hot wire consists of one arm of a Wheatstone bridge circuit.

The constant current anemometer uses a probe powered by a constant current from a power source having high internal resistance so that the current through it will be independent of any resistance change in the bridge. Fig. (3-2) shows a practical set up of a constant current bridge. The probe resistance changes are the result of flow changes acting on the probe. The consequent voltage difference across the horizontal bridge diagonal is a

3.2.1 Physical Properties of Hot Wire Probes

Calibration of hot wire probes requires an accurate knowledge of the physical properties of the hot wires. This includes wire length, wire diameter, electrical resistivity, thermal conductivity of the wire material and the temperature coefficient of resistance of wire material.

The physical properties of wire material can be obtained from the published data or measurements of individual wires. The first method requires that the wire dimensions should be known with sufficient accuracy. The temperature coefficient of resistance for the wire material (α) used in the present work (pt - 20% I_r) was obtained by heating a sample of wire material in an electric oven for a long period of about two hours for annealing before measurements of its resistance is carried out during heating up and cooling down processes. Plotting of (R_H/R_C - 1) against (T_H - T_C) yields the value of (α) as given by:

$$\alpha = \frac{(R_H/R_C) - 1}{T_H - T_C} \qquad (3\text{-}15)$$

where R is the wire resistance and T is the wire temperature. The subscripts H and C refer to the hot and cold conditions of the wire respectively.

A typical example for the graphs obtained for a 10 micron diameter wire of pt - 20% I_r material is shown in Fig. (3-6). The value of α is obtained from a least square fit of the data, appendix B13. The wire length was measured using a travelling microscope and uncertainties of the order of $\pm$0.02 mm is likely

to exist. This could result in an error in calculating the wire cold resistance of about ± 0.07 ohms for a wire having the following nominal values of $R_c = 7$ ohms, and length of 2 mm. If such a wire is operated at a resistance of 10 ohms ($T_w = 520^oC$), the error in the calculated wire operating temperature would be of the order of $\pm 20^oC$ (or $\pm 3.85\%$ of the nominal value of wire operating temperature). Such an error would result in an error in the estimated heat transfer coefficient and a more pronounced effect on the estimated gas velocity because the velocity is proportional to the third power of the heat transfer coefficient. Moreover, because the probes have several junctions of dissimilar material, a temperature difference is developed when a small electric current (about 2 mA) is passed through the wire to measure its cold resistance and hence a small power dissipation will exist in the probe assembly, owing to these temperature gradients. This results in an over-estimation of the measured cold resistance and consequently in the predicted wire temperature.

Davis and Fisher (77) showed that although these small power dissipations will be negligible at current densities sufficient to heat the wire appreciably during its operation, it could lead to an over-estimation of the measured cold resistance at very low levels of dissipation. For example, a wire of 6.5 ohms cold resistance exhibits the following measured resistances:

7.6 ohms at 6.5 μW power dissipation

7.75 " at 2 μW power dissipation

A much better estimation of the probe cold resistance could be achieved by operating the hot wire at a constant air velocity while reducing its operating resistance until no change is observed in the output voltage. This is usually a very small value which could be attributed to an extraneous noise in the system. Repeating the same experiment at another air velocity, which could be the case of zero flow and plotting the difference in the output voltage between any two cases, shows a levelling of the curve after a certain value of operating resistance. Such a value could be used as a better approximation to the exact value of the probe cold resistance and represents the conditions where the heating up of the wire by the flowing current has been just equal to the power dissipation at the various dissimilar material junctions of the probe. Fig. (3-7) shows typical graphs of the difference in the output voltage of the hot wire anemometer between two cases of air velocities and the zero flow conditions. Therefore a reasonable calibration procedure could be achieved if the measured cold resistance is changed slightly to yield an agreement between the experimental and theoretical calibration curve. An iteration program (94) is used for such a purpose and the amount of change in the cold resistance has always been within the tolerance of measurements as stated before.

The correct value of cold resistance should, therefore, ensure coincidence with all curves produced for the same wire at different operating conditions. Figs. (3-8) and (3-9) show a set of experimental calibration curves together with the theoretical prediction of the iterated cold resistance where an excellent agreement could be easily observed.

3.2.2 Anemometer Drift

It has been noticed that some wires change their characteristics during engine tests, especially after long periods of engine running at higher speeds. This is observed as slight changes in the wire cold resistance in most cases which results in a shifting of the calibration curve, while in a few cases the cold resistance remains very close to its original value but shifting of the calibration curve still occurs. These changes could be due to: contamination of wires with oil or dust particles inside the combustion chamber, oxidation of wire, erosion of wire surface or any other unknown factors.

Every care was taken to run the wires below their oxidation temperature, which was about 700°C, together with running the engine with a heavy oil but the trends were unpredictable.

As such changes in the wire characteristics could not be tolerated in the present investigation, a very careful checking procedure on the wire characteristics was employed before and after tests. Wires which did not maintain their characteristics were replaced and their results excluded.

The checking procedure could be summarised as follows. Every new wire was operated for about one hour before starting its original calibration process in the wind tunnel. This anneals the wire and usually its cold resistance drops slightly but remains constant after that. A first calibration is then carried out. The wire was introduced into the engine and run for about

$\frac{1}{2}$ hour and when it cooled down, its resistance was checked and the test was carried out if consistent values of cold resistance was maintained before and after the engine run. A second calibration procedure was always carried out after each test to make sure that the calibration curve was maintained. All the reported data in the present work corresponds to wires which have proven repeatability in their calibrations.

3.3 The Response of Constant Temperature Hot Wire Anemometer to Turbulence

As shown in (3-2) the heat transfer relation between the wire and the surrounding gas could be expressed by equation (3-14)

$$\frac{hd}{K_w} = \frac{2.6}{\pi \gamma} \left(\frac{\rho_g d\ U}{\mu_g}\right)^{1/3} \left(\frac{C_p \mu_g}{K_g}\right) \qquad (3\text{-}14)$$

This relation could be rearranged in the following form

$$\frac{h}{K_w} = \left(\frac{2.6\ P_r}{\pi \gamma\ d^{2/3}}\right) \left(\frac{\rho_g}{\mu_g}\right)^{1/3} U^{1/3}, \qquad (3\text{-}14a)$$

The first group of variables on the right hand side of equation (3-14a) is a constant value for a certain wire diameter and for air as a working fluid. For a given operating wire temperature K_w is constant and equation (3-14a) could be simplified to the following form

$$h = C_1 \left(\frac{\rho_g}{\mu_g}\right)^{1/3} U^{1/3} \qquad (3\text{-}14b)$$

where $$C_1 = \frac{2.6\ P_r\ K_w}{\pi \gamma\ d^{2/3}} \qquad (3\text{-}16)$$

Using the equilibrium relation between the heat generated in the wire (Q_e) and the heat loss by convection, one can write

$$h = \frac{Q_e}{\pi d \ell (T_w - T_g)} = \frac{I^2 R_w \alpha R_o}{\pi d \ell (R_w - R_g)} \qquad (3\text{-}17)$$

where α is the coefficient of temperature for wire material and R_o is the wire resistance at a reference temperature. Substituting for (h) from equation (3-14b) into equation (3-17) we get

$$\frac{I^2 R_w}{(R_w - R_g)} = C_2 \left(\frac{\rho_g}{\mu_g}\right)^{1/3} U^{1/3} \qquad (3\text{-}18)$$

where

$$C_2 = \frac{C_1 \pi d \ell}{\alpha R_o} \qquad (3\text{-}19)$$

Now defining the instantaneous turbulent velocity (U) as the sum of an average value ($\bar{U}$) and a fluctuating component (dU) as given by

$$U = \bar{U} + dU \quad , \quad (dU \equiv u) \qquad (3\text{-}20)$$

Furthermore defining the turbulence intensity (In_t) as the ratio between the fluctuations to the mean value, one can write

$$d\,In_t = \frac{dU}{\bar{U}} = \frac{dU}{dE} \frac{dE}{} \frac{1}{\bar{U}} \qquad (3\text{-}21)$$

or

$$(\overline{In_t}) = \frac{\sqrt{\overline{u^2}}}{\bar{U}} = \frac{\sqrt{\overline{e^2}}}{K\,\bar{U}} \qquad (3\text{-}22)$$

where $\sqrt{\overline{u^2}}$ and $\sqrt{\overline{e^2}}$ are the root mean square values of the fluctuating components in gas velocity and bridge voltage respectively.

K is the slope of the calibration curve. (E vs U) at appropriate gas conditions.

and E is the bridge voltage at gas conditions.

An expression for the slope of the calibration curve (K) could be derived from equation (3-18) after rearrangement of terms as follows:

$$\frac{E^2}{R_w\,(R_w - R_g)} = C_2 \left(\frac{\rho_g}{\mu_g}\right)^{1/3} U^{1/3} \qquad (3\text{-}18a)$$

or

$$E = \left[C_2\, R_w\, (R_w - R_g)\right]^{\frac{1}{2}} \left(\frac{\rho_g}{\mu_g}\right)^{1/6} U^{1/6} \qquad (3\text{-}18b)$$

Differentiating equation (3-18b) we get

$$K = \frac{dE}{dU} = \frac{\left[C_2\, R_w\, (R_w - R_g)\right]^{\frac{1}{2}}}{6} \left(\frac{\rho_g}{\mu_g}\right)^{1/6} \frac{1}{U^{5/6}} \qquad (3\text{-}23)$$

Multiplying both sides of equation (3-23) by U we get

$$KU = \frac{\left[C_2\, R_w\, (R_w - R_g)\right]^{\frac{1}{2}}}{6} \left(\frac{\rho_g}{\mu_g}\right)^{1/6} U^{1/6} \qquad (3\text{-}24)$$

Combining equations (3-18b) and (3-24) gives

$$KU = \frac{E}{6} \qquad (3\text{-}25)$$

Substituting for KU into equation (3-22) gives a simple expression for the turbulence intensity in terms of the root mean square value of the fluctuating voltage component and the mean value of the bridge voltage at the appropriate gas conditions as given by:

$$\overline{In_t} = \frac{\sqrt{\overline{u^2}}}{\bar{U}} = \frac{6\sqrt{\overline{e^2}}}{\bar{E}} \qquad (3\text{-}26)$$

Another approach to the problem could be carried out using the definitions of temporal values of variables as the summation of a mean component and a fluctuating component as given by

$$U = \bar{U} + u' \qquad (3\text{-}27a)$$

$$I = \bar{I} + i' \qquad (3\text{-}27b)$$

$$E = \bar{E} + e' \qquad (3\text{-}27c)$$

where u', i' and e' are the root mean square values of the fluctuating components of gas velocity, current and bridge voltage respectively.

From the thermal equilibrium conditions, the heat transferred per unit time to the surrounding fluid must be equal to the heat generated per unit time by the electric current through the wire. Therefore:

$$I^2 R_w = \pi d \ell h (T_w - T_g) \qquad (3\text{-}28)$$

Now substituting for h from equation (3-14) we get, after some rearranging of terms,

$$I^2 R_w = \frac{d^{1/3} \ell K_w (R_w - R_g)}{\alpha R_o} \left(\frac{2.6 P_r}{\gamma}\right) \left(\frac{\rho_g}{\mu_g}\right)^{1/3} U^{1/3} \qquad (3\text{-}29)$$

or

$$I^2 R_w = C_4 (R_w - R_g) \left(\frac{\rho_g}{\mu_g}\right)^{1/3} U^{1/3} . \qquad (3\text{-}29a)$$

where $C_4 = \dfrac{2.6\ Pr\ K_w\ \ell\ \ d^{1/3}}{\gamma\alpha\ R_o}$ (3-30)

Expanding U in a power series and neglecting second order terms, knowing that the electric resistance of the wire is constant and equal to $\bar{R}_w$, and substituting for I from equation (3-27b), we get

$$\bar{I}^2\ \bar{R}_w + 2\ i'\ \bar{I}\ \bar{R}_w = C_4\ (\bar{R}_w - R_g)\ (\frac{\rho_g}{\mu_g})^{1/3}\bar{U}^{1/3} + C_4\ (\bar{R}_w - R_g)\ (\frac{\rho_g}{\mu_g})^{1/3}\ \bar{U}^{1/3}\ \frac{u'}{3\bar{U}} \quad (3\text{-}31)$$

whence

$$\bar{I}^2\ \bar{R}_w = C_4\ (\bar{R}_w - R_g)\ \ (\frac{\rho_g}{\mu_g})^{1/3}\ \bar{U}^{1/3} \quad (3\text{-}32)$$

and

$$2\ i'\ \bar{I}\ \bar{R}_w = C_4\ (\bar{R}_w - R_g)\ (\frac{\rho_g}{\mu_g})^{1/3}\ \bar{U}^{1/3}\ \ \frac{u'}{3\bar{U}} \quad (3\text{-}33)$$

Equation (3-33) could be written in the form

$$i' = \frac{C_4\ (\bar{R}_w - R_g)}{\bar{I}\ \bar{R}_w}\ \ (\frac{\rho_g}{\mu_g})^{1/3}\ \bar{U}^{1/3}\ \ \frac{u'}{6\bar{U}} \quad (3\text{-}33a)$$

The consequent fluctuating voltage component e' could be given by

$$e' = i'\ \bar{R}_w = \frac{C_4\ (\bar{R}_w - R_g)}{\bar{I}}\ \ (\frac{\rho_g}{\mu_g})^{1/3}\ \ \bar{U}^{1/3}\ \ \frac{u'}{6\bar{U}} \quad (3\text{-}34)$$

or

$$e' = S.\ u' \quad (3\text{-}35)$$

where S is the sensitivity of the constant temperature hot wire anemometer

$$S = \frac{2.6\ Pr\ \ k_w\ \ell\ \ d^{1/3}}{\gamma \pi\ R_o} \frac{(\bar{R}_w - R_g)}{6\ \bar{I}\ \bar{U}^{2/3}} \qquad (3\text{-}36)$$

The turbulence intensity (In_t) could be obtained, therefore, by substituting for $\bar{U}$ from equation (3-32) into equation (3-34) which gives once again

$$In_t = \frac{\sqrt{\overline{u^2}}}{\bar{U}} = \frac{u'}{\bar{U}} = \frac{6\sqrt{\overline{e^2}}}{\bar{E}} = \frac{6\ e'}{\bar{E}} \qquad (3\text{-}22a)$$

where $\bar{E} = \bar{I}\ \bar{R}_w$ is the mean value of the bridge voltage corresponding to the gas velocity $\bar{U}$ at the appropriate gas conditions.

The above analysis has assumed a perfect equilibrium between the heat developed by the electric current and the heat transferred to the flowing gas. This is possible only if the thermal inertia of the wire is infinitely small. Due to the finite thermal inertia of the wire, however, a time delay exists between the rapid fluctuations of gas velocity and the corresponding temperature fluctuations of the wire. Therefore, in order to study the dynamic behaviour of the wire a term representing this thermal inertia of the wire should be introduced into equation (3-29). Moreover the slight variations in wire resistance should be considered. This could be written in a similar form to equation (3-27) as follows:

$$R_w = \bar{R}_w + r'_w \qquad (3\text{-}37)$$

Also equation (3-29) is modified into the following form:

$$I^2 R_w = C_4 (R_w - R_g) \left(\frac{\rho_g}{\mu_g}\right)^{1/3} U^{1/3} + C_w \frac{d T_w}{dt} \qquad (3\text{-}38)$$

where C_w is the heat capacity of the wire

$$C_w = c_w \rho_w \frac{\pi}{4} d^2 \qquad (3\text{-}39)$$

c_w is the specific heat of wire material per unit mass

ρ_w is the density of wire material

Substituting equations (3-27a), (3-27b) and (3-37) into equation (3-38), calculating and neglecting quadratic terms in the small fluctuations i', r'_w and u' we obtain;

$$\bar{I}^2 r'_w + 2 \bar{I} \bar{R}_w i' = \left[C_4 \left(\frac{\rho_g}{\mu_g}\right)^{1/3} U^{1/3} \right] \left[r'_w + \left(\bar{R}_w - R_g \frac{u'}{3\bar{U}}\right) \right] + \frac{C_w dT_w}{dt} \qquad (3\text{-}40)$$

Introducing the relationship between the compensating electronic current i' and the change in wire resistance r'_w as given by

$$i' = -g_{tr} \cdot I r'_w \qquad (3\text{-}41)$$

where g_{tr} is the transconductance of the electronic circuit.

Equation (3-35) could be written in the form:

$$\frac{di'}{dt} + \alpha \frac{R_o}{Cw} \left(C_4 \left(\frac{\rho_g}{\mu_g}\right)^{1/3} \bar{U}^{1/3} - \bar{I}^2 + 2 \bar{I}^2 \bar{R}_w g_{tr}\right) i' \qquad (3\text{-}42)$$

$$- \frac{\alpha C_4 g_{tr} \bar{I} R_o (R_w - R_g)}{C_w} \left(\frac{\rho_g}{\mu_g}\right)^{1/3} \bar{U}^{1/3} \frac{u'}{3\bar{U}} = 0$$

Using equation (3-32) we can write

$$C_4 \left(\frac{\rho_g}{\mu_g}\right)^{1/3} \bar{U}^{1/3} - \bar{I}^2 = \frac{R_g \bar{I}^2}{R_w - R_g} \qquad (3\text{-}43)$$

Substituting equation (3-43) into equation (3-42) gives

$$\frac{di'}{dt} + \alpha \frac{R_o \bar{I}^2}{C_w} \left[\frac{R_g}{R_w - R_g} + 2 \bar{R}_w \cdot g_{t_r} \right] i' - \alpha \frac{R_o g_{t_r} \bar{I}^3}{C_w} \cdot R_w \frac{u'}{3\bar{U}} = 0 \qquad (3\text{-}44)$$

Hence the time constant for the constant temperature hot wire anemometer (τ_{CT}) is given by

$$\tau_{CT} = \frac{C_w}{\alpha R_o \bar{I}^2 \left\{ \left[R_g/(R_w - R_g) \right] + 2 \bar{R}_w g_{t_r} \right\}} \qquad (3\text{-}45)$$

Examination of equation (3-45) shows that the frequency response of the constant temperature anemometer system could be improved by operating the wires at higher operating temperatures and by increasing the transconductance of the electronic circuit. The latter effect could not be easily achieved because of the appearance of high frequency oscillations in the bridge system (due to the feedback technique employed in the circuit). Nevertheless, such a feedback has increased the frequency response of the anemometer system by a factor of several hundred compared with constant current operations. Anderson (115) has performed similar analysis for estimating the performance of the

system and shown that the anemometer's upper frequency limit is increased, due to feedback, by a factor g as given by

$$g = 2\,a\,R_w\,g_{tr} \tag{3-46}$$

where a is the overheating ratio $a = (R_w - R_g)/R_g)$

3.4 Statistical Analysis of Turbulence

3.4.1 Definitions of Correlations and Scales of Turbulence

Taylor (84-86) introduced new notions in the study of turbulence problems which are the correlation functions or the coefficients of correlation between two fluctuating quantities in turbulent flow. These correlations could be either between velocity components at two points in the flow field, or between the values of a velocity component in a given direction at a fixed point in the flow field at two different instants (t) and $(t + \tau)$. The latter type of correlation which is usually called the 'auto-correlation function' was employed in the present investigation because it is easy to measure with a single hot wire anemometer and because it gives most of the required information about the turbulence structure (intensity, scale and power spectrum), if the conditions of isotropy and homogeneity are satisfied, as will be discussed later.

The auto-correlation function is defined by

$$R_t(\tau) = \lim_{T \to \infty} \frac{1}{T} \int_0^T u(t) \cdot u(t+\tau)\, dt \tag{3-47}$$

$$\text{or} \quad R_t(\tau) = \overline{u(t)\;u(t+\tau)} \tag{3-48}$$

Such a function describes, therefore, the general dependence of the values of the data at one time $(t + \tau)$ on the values at another time (t). Fig. (3-10a) gives an illustration of the definition of the auto-correlation function while Fig. (3-10b) shows a typical shape of this function.

We can also define an auto-correlation coefficient by

$$R'_t(\tau) = \frac{R_t(\tau)}{\overline{u^2}} = \frac{\overline{u(t) \cdot u(t+\tau)}}{\overline{u^2}} \qquad (3\text{-}49)$$

where the time average of $\overline{u^2}$ is taken with respect to undelayed signals.

The most important properties of the auto-correlation function could be summarised as follows:

$$R_t(0) = \lim_{T \to \infty} \frac{1}{T} \int_0^T u(t) \; u(t) = \overline{u^2} \qquad (3\text{-}50)$$

and correspondingly

$$R'_t(0) = 1.0 \qquad (3\text{-}51)$$

Therefore, the auto-correlation function reduces to the mean square value at zero time delay (τ).

Also

$$R_t(-\tau) = \lim_{T\to\infty} \frac{1}{T} \int_0^T u(t).\, u(t-\tau)\, dt$$

put $t' = t - \tau$ gives

$$R_t(-\tau) = \lim_{T\to\infty} \frac{1}{T} \int_0^T u(t'+\tau)\; u(t')\; d\,t'$$

so

$$R_t(-\tau) = R_t(\tau) \qquad (3\text{-}52)$$

Thus, the auto-correlation function (and correspondingly the auto-correlation coefficient) is a symmetrical function of τ.

Hinze (79) showed that the shape of the auto-correlation coefficient curve in the neighbourhood of $t = 0$ could be expressed in terms of the velocity derivatives with respect to time as follows:

$$R'_t(t) = 1 + \frac{t^2}{2!}\left[\frac{\partial^2 R'_t}{\partial t^2}\right]_{t=0} + \frac{1}{4!}\, t^4 \left[\frac{\partial^4 R'_t}{\partial t^4}\right]_{t=0} + \ldots \qquad (3\text{-}53)$$

$$R'_t(t) = 1 - \frac{t^2}{2\,u^2}\, \overline{\left[\frac{\partial u}{\partial t}\right]^2_{t=0}} + \frac{t^4}{4!\,u^2}\, \overline{\left[\frac{\partial^2 u}{\partial t^2}\right]^2_{t=0}} - \ldots \qquad (3\text{-}54)$$

Now we can define a time λ_t such that

$$\frac{1}{\lambda_t^2} = \frac{1}{2\,u^2}\,\overline{\left[\frac{\partial u}{\partial t}\right]^2}_{t=0} = -\,1/2\,\left[\frac{\partial^2 R'_t}{\partial t^2}\right]_{t=0} \qquad (3\text{-}55)$$

λ_t is called the micro-time scale and is regarded as a measure of the most rapid changes in the fluctuations of u(t). For small values of t equation (3-54) may be written as

$$R'_t(t) = 1 - \frac{t^2}{\lambda_t^2} \qquad (3\text{-}56)$$

Another integral time scale could be defined as

$$L_t = \int_0^\infty R'(t)\,d\,t \qquad (3\text{-}57)$$

This integral scale (or macro-scale) L_t could be considered as a rough measure of the longest connection in the turbulent behaviour of u(t).

Taylor also defined correlation coefficients between the fluctuating velocity components at two different points in space, Fig. (3-11). The longitudinal correlation coefficient R_x between the values of u at two points A and B separated by a distance x measured in the direction of the X axis is given by:

$$R'_x(x) = \frac{\overline{u_A\ u_B}}{\sqrt{\overline{u_A^2}}\ \sqrt{\overline{u_B^2}}} \qquad (3\text{-}58)$$

Also, the lateral correlation coefficient R'_y between values of u at two points A and B separated by a distance y measured in the Y-direction is given by

$$R'_y(y) = \frac{\overline{u_A . u_B}}{\sqrt{\overline{u_A^2}} . \sqrt{\overline{u_B^2}}} \qquad (3\text{-}59)$$

Similar to the auto-correlation (time-correlation), the longitudinal and lateral correlations are symmetrical functions of x and y respectively. The general shapes of these correlations are shown in Fig. (3-12). Both correlation coefficients decrease from a maximum value of unity to zero as the separation distance varies from zero to infinity. The decrease of either may be a monotonous or an oscillating function.

The shapes of these correlation coefficients in the neighbourhood of zero separation distances could be expressed as follows:

$$R'_y(y) = 1 + \frac{y^2}{2!}\left[\frac{\partial^2 R'_y}{\partial y^2}\right]_{y=0} + \frac{y^4}{4!}\left[\frac{\partial^4 R'_y}{\partial y^4}\right]_{y=0} + \ldots \qquad (3\text{-}60)$$

and

$$R'_x(x) = 1 + \frac{x^2}{2!}\left[\frac{\partial^2 R'_x}{\partial x^2}\right]_{x=0} + \frac{x^4}{4!}\left[\frac{\partial^4 R'_x}{\partial x^4}\right]_{x=0} + \ldots \qquad (3\text{-}61)$$

or

$$R'_x(x) = 1 - \frac{x^2}{2}\,\frac{1}{u^2}\overline{\left[\frac{\partial u}{\partial x}\right]^2_{x=0}} + \frac{x^4}{4}\,\frac{1}{u^2}\overline{\left[\frac{\partial^2 u}{\partial x^2}\right]^2_{x=0}} - \ldots \tag{3-62}$$

and

$$R'_y(y) = 1 - \frac{y^2}{2}\,\frac{1}{u^2}\overline{\left[\frac{\partial u}{\partial y}\right]^2_{y=0}} + \frac{y^4}{4}\,\frac{1}{u^2}\overline{\left[\frac{\partial^2 u}{\partial y^2}\right]^2_{y=0}} - \ldots \tag{3-63}$$

For small distances we can define the length micro-scales as follows

$$R'_x(x) = 1 - \frac{x^2}{\lambda_x^2} \tag{3-64}$$

and

$$R'_y(y) = 1 - \frac{y^2}{\lambda_y^2} \tag{3-65}$$

Therefore:

$$\frac{1}{\lambda_x^2} = -\frac{1}{2}\left[\frac{\partial^2 R'_x}{\partial x^2}\right]_{x=0} = \frac{1}{2u^2}\overline{\left[\frac{\partial u}{\partial x}\right]^2_{x=0}} \tag{3-66}$$

$$\frac{1}{\lambda_y^2} = -\frac{1}{2}\left[\frac{\partial^2 R'_y}{\partial y^2}\right]_{y=0} = \frac{1}{2u^2}\overline{\left[\frac{\partial u}{\partial y}\right]^2_{y=0}} \tag{3-67}$$

These micro-scales are considered as a measure of the average dimensions of the smallest eddies in the flow field which are responsible for the dissipation of energy, or more correctly as the dimensions of eddies which at the same intensity produce the same dissipation as the turbulence considered.

We can also define the macro (or integral) scales of turbulence as follows:

$$L_x = \int_0^{\infty} R'_x \, dx \tag{3-68}$$

and

$$L_y = \int_0^{\infty} R'_u \, dy \tag{3-69}$$

These lengths could be considered as measures of the longest connection or correlation distance between the velocities at two points in the flow field. For isotropic flow a relationship exists between the two types of correlation which has been verified experimentally by Von Karman and Howarth (101). Such a relation is given by

$$R'_x(r) + \frac{r}{2}\frac{\partial R'_x(r)}{\partial r} = R'_y(r) \tag{3-70}$$

Substitution of equation (3-60) and (3-61) into equation (3-70) gives the following relation:

$$\left[\frac{\partial^2 R'_y}{\partial r^2}\right]_{r=0} = 2\left[\frac{2 R'_x}{\partial r^2}\right]_{r=0} \tag{3-71}$$

Using equation (3-71) we obtain the following relationship between the longitudinal and lateral micro-scales (λ_x and λ_y) as given by:

$$\lambda_x = \sqrt{2}\ \lambda_y \tag{3-72}$$

Also integrating equation (3-70) from zero to infinity with the condition, $\lim_{r \to \infty} r\, Ry = 0$ gives

$$L_x = 2\, L_y \tag{3-73}$$

As mentioned earlier, if the turbulent field is homogeneous in its average structure, one can expect some relationship between the time correlation and the space correlations. Also, similar relations could exist between the time scales as given by equations (3-55) and (3-57) and the length scales as given by equations (3-66) and (3-68). The relations could be obtained using Taylor's hypothesis for a turbulent flow with a mean velocity $\bar{U}$ in the x-direction where $\bar{U} \gg u$ which could be expressed as follows:

$$t = \frac{x}{\bar{U}} \quad \text{and} \quad \frac{\partial}{\partial t} = -\bar{U}\frac{\partial}{\partial x} \tag{3-74}$$

Lin (109) showed that, for isotropic turbulence and large Reynolds number, an estimate of the accuracy of Taylor's hypothesis could be made from

$$\frac{(d\,u/dt)^2}{\bar{U}^2\,\overline{(\partial u/\partial x)^2}} = 5\,\frac{u^2}{\bar{U}^2} \qquad (3\text{-}75)$$

In fact, the turbulence intensities inside the combustion chamber of an engine reached much higher values than those observed in pipe flow, in spite of the low values of mean flow velocities for the former case. For example, the magnitudes of turbulence intensities in pipe flow are, usually, less than 20% except in a small region very close to the wall where much higher values are observed, depending on the surface conditions (104 - 108), while engine measurements give intensities as high as 40% (22). However, a check on the validity of Taylor's hypothesis for engine investigations could be made by applying such a condition (3-74) to equation (3-75) and calculating the corresponding values of turbulent intensities. This gives an estimation of intensities of the order of 44.7% which is higher than the measured values in engine investigations in some cases, as will be seen later.

The physical interpretation of equation (3-74) is that if $\bar{U} \gg u$, the fluctuations at a fixed point in the field may be imagined to be caused by the whole turbulent field passing that point with a constant velocity $\bar{U}$. The oscillogram of the velocity

fluctuations at that point will then be nearly identical with the instantaneous distribution of the velocity u along the x-axis through that point.

Therefore:

$$R'_x(x) = R'_t(\tau) \tag{3-76}$$

$$\lambda_x = \bar{U}\,\lambda_t \tag{3-77}$$

and

$$L_x = \bar{U}\,L_t \tag{3-78}$$

This explains clearly the reasons, as mentioned earlier, for the selection of the auto-correlation function and auto-correlation coefficient for studying the characteristics of the turbulent field in the present investigation.

3.4.2 The Spectrum of Isotropic Turbulence

Considering turbulence to be made up of eddies of different size, the total kinetic energy of the turbulent field may be considered to be distributed among the eddies. The spectrum of turbulence gives the distribution of kinetic energy over the various frequencies occurring in the field. At any point in isotropic turbulence the mean energy of the eddies is proportional to $\overline{u'^2}$. Taylor defined the one dimensional spectrum function F(n) to be the fraction ($\overline{u_1^2}$) of the total energy ($\overline{u^2}$) which is due to frequencies between n and (n + dn).

$$\frac{\overline{u_1^2}}{\overline{u^2}} = \int_n^{n+dn} F(n)\, dn \qquad (3\text{-}79)$$

and

$$\int_0^{\infty} F(n)\, dn = 1 \qquad (3\text{-}80)$$

There are direct relations between the power spectrum function and the auto-correlation function and correspondingly between the power spectrum function and both the micro-scales and macro-scales of turbulence. These relations could be explained if we imagine the whole field to have a translation with uniform velocity $\bar{U}$ in the X-direction. Then at a stationary point, the largest eddies will cause fluctuations of low frequencies, whereas the smallest eddies will cause fluctuations of high frequencies. Therefore, if the turbulence contains only large eddies, the spectrum function will exist mainly in the region of low frequencies; if there are only small eddies F(n) will exist mainly in the region of high frequencies. Hence one may expect when the auto-correlation curve decreases rapidly to zero, the spectrum will have high values in the region of high frequencies and vice versa. Generally, the auto-correlation and power spectrum functions are Fourier transforms of each other as given by the following relations:

$$R_t'(t) = \int_0^{\infty} F(n)\, e^{j\,2\pi nt}\, dn \qquad (3\text{-}81a)$$

or (using the condition of symmetry of $R_t'(t)$)

$$R_t'(t) = \int_0^{\infty} F(n) \operatorname{Cos} 2\pi\, n\, t\, dn \qquad (3\text{-}81b)$$

Similarly

$$F(n) = 4 \int_0^\infty R'(t) \; e^{-j\,2\pi nt} \; dt \qquad (3\text{-}82a)$$

and

$$F(n) = 4 \int_0^\infty R'(t) \; \cos 2\pi nt \; dt \qquad (3\text{-}82b)$$

Using equations (3-55), (3-57), (3-66), (3-68), (3-81b) and (3-82b) we can write the following relationship between the longitudinal correlation and power spectrum function on one side and the micro-scales and macro-scales of turbulence on the other side as follows:

$$R'_x(x) = \int_0^\infty F(n) \; \cos \frac{2\pi n x}{\bar{U}} \; dn \qquad (3\text{-}83)$$

$$F(n) = \frac{4}{\bar{U}} \int_0^\infty R'_x(x) \; \frac{\cos 2\pi n x}{\bar{U}} \; dx \qquad (3\text{-}84)$$

$$L_t = \int_0^\infty R'(t) = \frac{1}{4} \lim_{n \to 0} F(n) \qquad (3\text{-}85)$$

$$L_x = \frac{\bar{U}}{4} \lim_{n \to 0} F(n) \qquad (3\text{-}86)$$

$$\frac{1}{\lambda_t^2} = -\frac{1}{2} \left[\frac{\partial^2 R'_t}{\partial t^2} \right]_{t=0} = 2\pi^2 \int_0^\infty F(n)\, n^2 \, dn \qquad (3\text{-}87)$$

and

$$\frac{1}{\lambda_x^2} = -\frac{1}{2}\left[\frac{\partial^2 R_t'}{\partial x^2}\right]_{x=0} = \frac{2\pi^2}{\bar{U}^2}\int_0^\infty F(n)\, n^2\, dn \qquad (3\text{-}88)$$

All the above mentioned relations are concerned with the one-dimensional energy spectrum. Because of the three-dimensional character of turbulence , the energy spectrum must also have a three-dimensional character. What is actually measured by means of a hot wire anemometer is, strictly speaking, a one-dimensional cut of the spatial - spectrum. However, for an isotropic flow field, relationships exist between the one-dimensional spectrum functions in different coordinate directions (79).

Hinze (79) made use of the work of Kolmogroff, Von Karman, Lin, Batchelor and Townsend to analyse the spectrum curve and develop a mechanism of the turbulence structure. The analysis is carried out in tems of the wave number (K) instead of the frequency n and an energy spectrum function F(K) instead of F(n) as given by:

$$K = \frac{2\pi n}{\bar{U}} \qquad (3\text{-}89)$$

$$F(K) = \frac{\bar{U}}{2\pi} F(n) \qquad (3\text{-}90)$$

$$\int_0^\infty F(K) = 1 \qquad (3\text{-}91)$$

It is sufficient here to summarise briefly the main ideas of that mechanism. The spectrum curve is divided into different regions according to the size of the eddies and their role in the dynamic behaviour of the turbulence structure as shown in Fig. (3-13). The larger eddies are assumed to produce smaller and smaller eddies through inertial interaction, thereby transferring energy to smaller eddies. At the same time viscosity effects and with them dissipation, becomes more important for the smaller eddies.

In the fully developed state it is not the largest eddies that will have the maximum kinetic energy, but the eddies in the higher wave number range. The range of the energy spectrum where the eddies make the main contribution to the total kinetic energy of turbulence is called the energy containing eddies. In this range the energy spectrum shows its maximum, which could be associated with a wave number K_e.

On the other hand, dissipation by viscous effects increases as the size of the eddy decreases, up to a maximum for a certain size of the smallest eddies, where another wave number K_d could be defined. The value of K_d corresponds roughly to the maximum in the $(K^2 F(K), K)$ curve (see equation (3-87).

Comparing the relative rate of decay of the total kinetic energy of turbulence $(du'^2/dt)/u'^2$ with the frequencies of various eddies $(u' K)$ on the spectrum curve, three main regions could be distinguished. The region of the largest eddies where the frequency $(u'_K K)$ is very small compared with the rate of decay;

the region of the smallest eddies where the frequency ($u'_K K_d$) is very large compared with the rate of decay and in between a region where the frequencies ($u'_K K$) are of the same order as the relative rate of change of the total turbulence. The latter region consists, obviously, of the energy containing eddies, since these eddies make the main contribution to the total energy of turbulence.

In the higher wave numbers, the decay process may be considered as a relatively slow process compared with motion of the eddies. Such a range may be considered, therefore, as nearly steady and the rates of change of the mean value may be regarded as negligible. The eddies corresponding to these higher wave numbers are excited by the transfer of energy by inertia forces from the larger eddies. It may be assumed that, in contrast with the largest eddies they are independent of the external conditions producing the forces that generate the initial largest eddies. This led Kolmogoroff (89) to make the following hypothesis: "At sufficiently high Reynolds numbers there is a range of high wave numbers where the turbulence is statistical in equilibrium and uniquely determined by the parameters ($W = -\frac{3}{2}\frac{d\,u'^2}{d\,t}$) and ν, where W is the rate of energy dissipation and ν is the kinematic viscosity. This equilibrium range is termed 'universal' because the turbulence in this range is independent of external conditions".

Kolmogoroff characterised this region by a length scale and velocity scale as defined by

For the length scale $\eta = \left(\frac{\nu^3}{W}\right)^{1/4}$ (3-92)

For the velocity scale $v = (\nu W)^{1/4}$ (3-93)

The Reynolds number for this region equals unity and the wave number K_d could be considered of the same order as $1/\eta$. Similarly in the region of the energy containing eddies we can define (K_e) as of the order of $1/L_x$ where L_x is the average size of the energy containing eddies.

Kolmogoroff also defined a sub-range in the region of large Reynolds numbers, but where the dissipation is very far below the region of maximum dissipation so that it could be neglected compared with the flux of energy transferred by inertial effects. In such a sub-range the effect of ν would then vanish and the turbulence could be characterised by (W) only.

3.4.3 The Relationship between the Micro-Scale and the Macro-Scale for Isotropic Turbulence

This relation could be established by equating the rate of decay of the kinetic energy as given by $(-\frac{1}{2}\rho \frac{d\bar{q}}{dt})$ to the rate of dissipation in a flow of viscous fluid as given by:

$$W = \mu \left[2\overline{\left(\frac{\partial u}{\partial x}\right)^2} + 2\overline{\left(\frac{\partial v}{\partial y}\right)^2} + 2\overline{\left(\frac{\partial w}{\partial z}\right)^2} + \overline{\left(\frac{\partial v}{\partial x} + \frac{\partial u}{\partial y}\right)^2} + \overline{\left(\frac{\partial w}{\partial y} + \frac{\partial v}{\partial z}\right)^2} + \overline{\left(\frac{\partial u}{\partial z} + \frac{\partial w}{\partial x}\right)^2} \right] \quad (3\text{-}94)$$

where u, v and w are the fluctuating velocity components in the x, y and z directions respectively and

$$\bar{q} = (\overline{u^2} + \overline{v^2} + \overline{w^2})$$

Introducing the condition of isotropy, Taylor (84) simplified equation (3-94) to the following expression

$$W = 6\,\overline{\left(\frac{\partial u}{\partial x}\right)^2} + 6\,\overline{\left(\frac{\partial u}{\partial y}\right)^2} + 6\,\overline{\left(\frac{\partial v}{\partial x} \cdot \frac{\partial u}{\partial y}\right)}$$

or

$$W = 7.5\,\overline{\left(\frac{\partial u}{\partial y}\right)^2} \qquad (3\text{-}95)$$

Substituting for λ_y from equation (3-67) into (3-95) we get

$$W = -7.5\,\mu\,\overline{u^2}\,\frac{\partial^2 R'_y}{\partial y^2}$$

$$= 15\,\mu\,\overline{u^2}/\lambda_y^2 \qquad (3\text{-}96)$$

In fully developed turbulent flow, the Reynolds stresses are proportional to the square of the turbulence fluctuations. Therefore, the work done against these stresses, which in the absence of external forces must come from the kinetic energy of the system is proportional to $\rho\, u^3/L$, where L is a linear dimension defining the scale of the system which may be taken as L_x. Equating the two expressions for the dissipation we get

$$W = \frac{15\,\mu\,\overline{u^2}}{\lambda_y^2} = \frac{A\,u^3}{L_x} \qquad (3\text{-}97)$$

Where A is a numerical constant of the order of unity. Defining two Reynolds numbers based on λ_y and L_x as given by

$$R_{e\lambda} = \frac{u'\lambda_y}{\nu} \tag{3-98a}$$

and

$$Re_L = \frac{u' L_x}{\nu} \tag{3-98b}$$

Equation (3-97) could be written as

$$\frac{L_x}{\lambda_y} = \frac{A}{15} \quad Re_\lambda \tag{3-99}$$

and

$$Re_L = \frac{A}{15} \cdot Re_\lambda^{\,2} \tag{3-100}$$

Robertson (102) has reported experimental values for the ratio between L_x and λ_y at the centre of a conduit where the condition of isotropy is approached and showed a definite tendency for the scale ratio to increase with Reynolds number (Re_x) and approaches the expression predicted by equation (3-99) at $Re > 80$. Similar results have been reported by Sato and Yamato (103) for turbulence measurements behind a grid. In the latter case a curve fit of the experimental data was given by the following equation:

$$\frac{L_x}{\lambda_y} = 0.0228 \; Re_\lambda^{1.23} + 1.06 \qquad (Re_\lambda > 30) \qquad (3\text{-}101)$$

Fig (3-14) shows a comparison between the experimental data of Robertson (102), the prediction of the isotropic theory and the empirical relation (3-101). The measurements of Laufer (107) in channel flow are also plotted.

3.5 Effect of Large Turbulence Fluctuations on the Response of a Hot Wire

In the previous analysis (3-3) for the response of the hot wire to turbulence fluctuations, the relative intensities were considered to be small (of the order of 10%) so that a linear relation is obtained between the voltage fluctuations and the velocity fluctuations.

As will be seen later, the measured turbulence intensities in the combustion chamber are appreciably higher and one may expect a distortion of the linearised hot wire response. The same problem usually exists in investigations of turbulence in pipe flow very near to the walls and in free jets and have been appreciated by many investigators. Therefore, second and higher order terms in the expansion of $U^{1/3}$ in equation (3-31) cannot be neglected and the same argument is applied for the use of the slope of the calibration curve to get dU/dE.

It is also no longer permissible to consider only the turbulence components in the same direction as the mean velocity, $\bar{U}$, We must take into account the other turbulence components also.

Thus if $\bar{U}$ is defined as the true mean velocity (which is assumed to be perpendicular to the wire), u, v and w as the instantaneous components of the fluctuation velocity and U_{meas} as the effective velocity which causes the cooling of the wire, then

$$\sqrt{U_{meas}} = \sqrt{(U + u)^2 + v^2 + w^2} \quad . \tag{3-102}$$

Corrsin (91) showed that the relationship between the actual mean velocity $\bar{U}$ and the measured value U_{meas} may be obtained by

$$\bar{U}_{meas} = U \sqrt{1 + \frac{2\,u}{U} + (\frac{u}{U})^2 + (\frac{v}{U})^2 + (\frac{w}{U})^2} \tag{3-103}$$

or by letting

$$\overline{v^2} + \overline{w^2} = (\alpha - 1)\,\overline{u^2} \tag{3-104}$$

$$\bar{U}_{meas} = U \sqrt{1 + 2\,\frac{u}{U} + \alpha\,(\frac{u}{U})^2} \tag{3-105}$$

and expanding the radical out to terms in $(\frac{u}{U})^4$

$$\bar{U}_{meas} = U \left\{ 1 + \frac{1}{2}(\alpha - 1)\,\overline{(\frac{u}{U})^2} - \frac{1}{2}(\alpha - 1)\,\overline{(\frac{u}{U})^3} - \frac{1}{8}(\alpha^2 - 5\alpha + 5)\,\overline{(\frac{u}{U})^4} \right\} \tag{3-106}$$

since $\bar{u} = 0$.

This expansion converges only for

$$\left[2 \frac{u}{U} + \alpha \left(\frac{u}{U}\right)^2 \right]^2 \leqslant 1$$

Thus it may be seen that what affects the cooling of the wire is a mixture of the three turbulence components u, v and w. The principal difficulty with such a theoretical correction is that the values of $\overline{\left(\frac{u}{U}\right)^n}$ are unknown for the integer $n > 2$. Therefore, the expansion cannot be computed to any desired accuracy. If all powers of $u/\bar{U}$ higher than the second are omitted and α is assumed equal to 2, then from equation (3-106) we get

$$U = \frac{\bar{U}_{meas}}{1 + 2\left(\frac{u}{\bar{U}}\right)^2} \tag{3-107}$$

Hinze (79) obtained similar relations for the case of a two-dimensional flow as follows:

$$\sqrt{U_{meas}} = \sqrt{\bar{U}} \left(1 + \frac{u}{2\bar{U}} - 8 \frac{u^2}{\bar{U}^2} + \frac{1}{4} \frac{v^2}{\bar{U}^2} + \frac{1}{16} \frac{u^3}{\bar{U}^3} - \frac{3}{8} \frac{u\, v^2}{\bar{U}^3} + \ldots \right. \tag{3-108}$$

which reduces to the following expression after taking the time average

$$\sqrt{U_{meas}} = \sqrt{\bar{U}} \left(1 - \frac{1}{8}\frac{\overline{u^2}}{\bar{U}^2} + \frac{1}{4}\frac{\overline{v^2}}{\bar{U}^2} + \frac{1}{16}\frac{\overline{u^3}}{\bar{U}^3} - \frac{3}{8}\frac{\overline{u\,v^2}}{\bar{U}^3} + \ldots\right)$$

or

$$\bar{U}_{meas} = \bar{U}\left(1 - \frac{1}{4}\frac{\overline{u^2}}{\bar{U}^2} + \frac{1}{2}\frac{\overline{v^2}}{\bar{U}^2} + \frac{1}{8}\frac{\overline{u^3}}{\bar{U}^3} - \frac{3}{4}\frac{\overline{u\,v^2}}{\bar{U}^3}\right.$$

$$\simeq \bar{U}\left(1 - \frac{1}{4}\frac{\overline{u^2}}{\bar{U}^2} + \frac{1}{2}\frac{\overline{v^2}}{\bar{U}^2}\right) \qquad (3\text{-}109)$$

If the departure from isotropy is small, so that $\overline{u^2} \simeq \overline{v^2}$ the correction is negative, that is, the actual velocity is smaller than the measured value. Substituting for the measured velocity from equation (3-108) into the heat transfer equation (3-28) and using King's expression for heat transfer from the wire, Hinze (79) showed after lengthy algebraic calculations the relationship between the actual turbulence intensities and the values calculated on the assumption of the linearized theory as follows:

$$\left(\frac{\overline{u^2}}{\bar{U}^2}\right)_{lin} = \left(\frac{\overline{u^2}}{\bar{U}^2}\right)_{act}\left[1 - \psi(u, v)\right] \qquad (3\text{-}110)$$

where

$$\Psi(u, v) = \phi(u, v) + \frac{\alpha_1 + 2\alpha_1^2}{4} \frac{\overline{u^2}}{\bar{U}^2} - \frac{\alpha_1}{2} \frac{\overline{v^2}}{\bar{U}^2} \tag{3-111}$$

$$\alpha_1 = \beta \frac{\sqrt{\bar{U}}}{I^2} \frac{\bar{R}_{w_{lin}} - R_g}{R_g} \tag{3-112}$$

and

$$\phi(u, v) = \frac{1 + 2\alpha_1}{2} \frac{\overline{u^3}}{\bar{U}\,\overline{u^2}} - \frac{\overline{u\,v^2}}{\bar{U}\,\overline{u^2}} - \frac{5 + 12\alpha_1 + 12\alpha_1^2}{16} \frac{\overline{u^4}}{\bar{U}^2\,\overline{u^2}}$$

$$- \frac{1}{4} \frac{\overline{v^4}}{\bar{U}^2\,\overline{u^2}} + \frac{7 + 6\alpha_1}{4} \frac{\overline{u^2 v^2}}{\bar{U}^2\,\overline{u^2}} + \frac{1 + 8\alpha_1 + 12\alpha_1^2}{16} \frac{\overline{u^2}}{\bar{U}^2}$$

$$+ \frac{1}{4} \frac{(\overline{v^2})^2}{\bar{U}^2\,\overline{u^2}} - \frac{1 + 4\alpha_1}{4} \frac{\overline{v^2}}{\bar{U}^2} \tag{3-113}$$

Equation (3-110) shows that what actually is measured is not the turbulence component u alone, but a mixture of u with the other component v.

In order to estimate the order of magnitude of the error made by applying the linearised theory even if the turbulence intensities are not small, we can calculate the value of $\Psi(u,v)$ according to equation (3-111).

Hinze (79) showed that for an isotropic flow if the fluctuating velocity components u and v have normal Gaussian distributions and are normally correlated, then

$$\overline{u^2} = \overline{v^2} \tag{3-114a}$$

$$\overline{u^4} = \overline{v^4} = 3\,u'^4 \tag{3-114b}$$

$$\overline{u^3} = \overline{v^3} = 0 \qquad (u' = \sqrt{\overline{u^2}}) \tag{3-114c}$$

$$\overline{u^2 v^2} = u'^2\,v'^2 = u'^4 \tag{3-114d}$$

Substituting into equation (3-111) gives

$$\Psi(u, v) = -\frac{19}{8}\frac{u'^2}{\bar{U}^2} \qquad (3\text{-}115)$$

Another approach to the problem of correcting hot wire readings at high levels of turbulence, is to simulate such conditions by vibrating the wire sinusoidally in the flow direction of a relatively low turbulence air stream. The correction factor obtained by applying this procedure is much smaller than expected in a one-dimensional randomly fluctuating motion. Fig. (3-15) shows an experimental example of this approach (91).

Thus for a turbulence intensity as high as 25%, the linearised theory would give higher values with a maximum error of the order of 15%. Such an error is permissible in turbulence measurements and we can conclude that the use of the linearised theory is still within the accuracy of the measurements itself.

3.6 The Effect of Wire Length on Turbulence Measurements

Because of the non-uniform velocity distribution of the turbulent flow, very short wires are required for true 'point' measurements. On the other hand, more uniform temperature distribution along the wire requires high values of length to diameter ratio, and since the minimum wire diameter is usually governed by strength considerations, hot wires of relatively longer

lengths than the scales of turbulence are usually used. This necessitates the establishment of some relationship between the measured turbulence parameters and their actual values, as could be sensed by very short wires.

If the length of the wire is very small in comparison with the scale of turbulence and if the variation of the fluctuating velocity component (u') along the wire could be neglected, the value of the mean square of the voltage across the wire could be written as

$$\overline{e^2} = K^2 . \ell^2 . \overline{u'^2} = K^2 \overline{u'^2} \qquad (3\text{-}116)$$

where K is a constant depending on the wire characteristics and on the operating conditions.

When the length of the wire is not neglected (compared with the scale of turbulence), the variation of u along the wire cannot be ignored. The measured value of the square of the voltage could be expressed by the following relationship

$$\overline{e^2_{meas}} = K^2 \overline{\left(\int_0^\ell u \, d s \right)^2} \qquad (3\text{-}117)$$

Frenkiel (81) and Skramstad (82) have deduced by two different methods, the same expression of the measured mean square value of the voltage with a wire of non-negligible length ℓ, as a function of the true value of $\overline{u^2}$ and of the transverse correlation R'_y as follows:

$$\overline{e^2_{meas}} = 2\,K^2\,\overline{u^2} \int_0^{\ell} (\ell - s)\; R'_y(s)\; d\,s \qquad (3\text{-}118)$$

Defining a correction factor C as follows

$$\overline{e^2} = C\;(\overline{e^2})_{meas} \qquad (3\text{-}119)$$

Then

$$\frac{1}{C} = \frac{2}{\ell^2} \int_0^{\ell} (\ell - s)\; R'_y(s)\; d\,s \qquad (3\text{-}120)$$

When ℓ/L_y is large, equation (3-118) could be written as

$$\overline{e^2_{meas}} = 2\,K^2\;\overline{u^2}\;\left[\,\ell\,.L_y - L_{y(1)}\right] \qquad (3\text{-}121)$$

where $L_{y(1)}$ is the first moment of the transverse correlation curve

$$L_{y(1)} = \int_0^{\infty} s\;R'_y(s)\;d\,s \qquad (3\text{-}122)$$

It appears, therefore, that when (ℓ/L_y) is large, the longitudinal energy of the turbulence measured in the flow is a linear function of the wire length and decreases with increasing ℓ. The correction factor C in this case is given by:

$$\frac{1}{C} = 2\left[\frac{L_y}{\ell} - \frac{L_{y(1)}}{L_y^{\,2}}\left(\frac{L_y}{\ell}\right)^2\right] \qquad (3\text{-}123)$$

where $L_{y(1)}/L_y^2$ depends on the shape of the correlation curve. When ℓ/L_y increases indefinitely, it is found at the limit

$$\lim_{\ell/L_y \to \infty} \left(\frac{1}{C} \right) = 0 \qquad (3\text{-}124)$$

and

$$\lim_{\ell/L_y \to \infty} \left(\frac{\overline{e^2_{meas}}}{K^2 \ell^2} \right) = 0 \qquad (3\text{-}125)$$

The longitudinal turbulent energy measured by a wire whose length is very large in comparison with the traverse scale of turbulence will approach zero even if the real energy is not negligible.

For homogeneous and isotropic turbulence one can make use of the relationship between the longitudinal and transverse correlations to express the correction factor C in terms of either of them as follows:

$$R'_y(r) = R'_x(r) + \frac{1}{2} r \frac{d R'_x(r)}{d r} \qquad (3\text{-}70)$$

Substituting for R_y from equation (3-70) into equation (3-120) we get

$$\frac{1}{C} = \frac{1}{\ell} \int_0^{\ell} R'_x(s) \, d s \qquad (3\text{-}126)$$

Making use of equations (3-73) & (3-126) we can write for large (ℓ/L_y) that

$$\overline{e^2_{meas}} = K^2 \overline{u^2} \ell L_x = 2 K^2 \overline{u^2} \ell L_y \qquad (3\text{-}127)$$

or

$$\frac{1}{C} = \frac{L_x}{\ell} = 2 \frac{L_y}{\ell} \qquad (3\text{-}128)$$

When the length of the wire is of the same order of magnitude as the scale of turbulence (L_y), the correction factor (C) depends on the shape of the correlation curve (81).

For a correlation function of exponential form as given by

$$R_y(y) = e^{-y/L_y} \qquad (3\text{-}129)$$

The correction factor, in this case is given by

$$\frac{1}{C} = 2 \left\{ \frac{L_y}{\ell} - \frac{L_y^2}{\ell^2} \left[1 - \exp \left(- \frac{\ell}{L_y} \right) \right] \right\} \qquad (3\text{-}130)$$

Expanding the exponential function in a Taylor series, equation (3-130) could be reduced to the following expression:

$$C = 1 + \frac{1}{3} \ell/L_y - \ldots\ldots \qquad (3\text{-}131)$$

Also, for the case of a correlation function represented by a Gaussian error function

$$R'_y = \exp\left(-\frac{\pi}{4}\frac{y^2}{L_y^2}\right) \tag{3-132}$$

The correction factor for this case is given as follows:

$$\frac{1}{C} = 2\frac{L_y}{\ell}\,\mathrm{erf}\left(\sqrt{\frac{\pi}{2}}\frac{\ell}{L_y}\right) - \frac{4}{\pi}\left(\frac{L_y}{\ell}\right)^2\left[1 - \exp\left(-\frac{\pi}{4}\frac{\ell^2}{L_y^2}\right)\right] \tag{3-133}$$

where

$$\mathrm{erf}\left(\sqrt{\frac{\pi}{2}}\frac{\ell}{L_y}\right) = \frac{2}{\sqrt{\pi}}\int_0^{\sqrt{\pi/2}(\ell/L_y)} e^{-y}\,dy \tag{3-134}$$

Similar corrections for the measured scales of turbulence could be established as follows:

$$K_x = \frac{L_x}{L_{x_{meas}}} \quad \text{and} \quad K_y = \frac{L_y}{L_{y_{meas}}} \tag{3-135}$$

For a correlation function given by

$$R'_y(y) = \exp(-y/L_y) \tag{3-136}$$

it is found that

$$K_y = 2\left(\frac{L_y}{\ell}\right)^2\left[\frac{\pi}{2}\frac{\ell}{L_y} - 2 + \frac{\ell}{L_y}J\left(\frac{\ell}{L_y}\right)\right] \tag{3-137}$$

where

$$J(a) = \int_0^{\pi/2}\left(1 + \frac{2}{a\,\mathrm{Cosec}\,\beta}\right)\exp(-a\,\mathrm{Cosec}\,\beta)\,d\beta \tag{3-138}$$

While for an isotropic turbulence with a longitudinal correlation function given by

$$R'_x \quad (x) \quad = \quad \exp\left(- \frac{\pi}{4} \quad \frac{x^2}{L_x^{\,2}}\right) \tag{3-139}$$

$$K_x \quad = \quad 1 \quad \text{and} \quad L_{x_{meas}} \quad = L_x \tag{3-140}$$

and

$$K_y \quad = \frac{8}{\pi} \quad \frac{1 - \exp\left(- \frac{\pi}{16} \frac{\ell^2}{L_y^{\,2}}\right)}{\frac{\ell}{L_y} \cdot \operatorname{erf}\left(\sqrt{\frac{\pi}{4}} \quad \frac{\ell}{L_y}\right)} \tag{3-141}$$

Corrections of the order of 30% for the effect of wire length on the turbulence measurements have been carried out in the present investigation assuming that the auto-correlation coefficient could be approximated by an exponential function similar to equation (3-129) as proposed by Dryden et al (82) and Hinze (79).

3.7 Turbulence Diffusion, Lagrangian Analysis

Diffusion of heat and mass is one of the major processes controlling the combustion process in engines. This is greatly itensified by the turbulent nature of the flow inside the combustion chamber.

Taylor (1920) (86) was the first to show that turbulent motion is capable of diffusing properties through the interior of the fluid in much the same way that molecular agitation gives rise to molecular diffusion. The main difference between the two

types is that in molecular diffusion, the medium consists of discrete particles, while in turbulent diffusion the medium is continuous. The essential feature of purely turbulent diffusion is that the fluid particles retain their initial properties throughout the history of the motion, but the spatial distribution of the particles changes. Therefore, it is possible to follow a particle of the fluid while it moves in the turbulent field and to find the degree of correlation between the velocity of this particle at time t and the velocity $v_{(t+\tau)}$ of the same particle at a later time $(t+\tau)$ Fig. (3-16). A Lagrangian coefficient of correlation could be defined, therefore, by the following relationship

$$R'_{L(\tau)} = \frac{\overline{v_{(t)} \quad v\,(t+\tau)}}{\overline{v^2}} \qquad (3\text{-}142)$$

where the averaging process is carried out over a large number of particle motions.

This Lagrangian correlation coefficient has properties similar to those of the previously treated Eulerian correlations, namely: R'_L (o) = 1.0, R_L (t) is symmetrical with respect to τ because of the homogeneity of the field, and will decrease to zero for large values of τ.

The displacement of a particle initially at the origin of the coordinate axes, could be obtained after an interval of time t by the following relationship

$$y = \int_{o}^{t} v\,(t)\;d\,t \qquad (3\text{-}143)$$

Because of the random nature of the motion, we can write

$$\bar{y} = 0 \tag{3-144}$$

and

$$\overline{y^2} = \overline{\left[\int_0^t v(t)\, dt \right]^2} \tag{3-145}$$

making use of the definition of the Lagrangian correlation coefficient, the mean displacement of the fluid particles could be expressed by the following relation of Kampe de Feriet

$$\overline{y^2} = 2\,\overline{v^2} \int_0^t R_L'(\tau)\,(t-\tau)\, d\tau \tag{3-146}$$

For very small values of t, where $R_L'(\tau)=1$, the integration of equation (3-146) reduces to

$$\overline{y^2} = \overline{v^2}\; t^2 \tag{3-147}$$

and the diffusion proceeds proportionally with time. While for long periods of time we can define a Lagrangian time scale $\mathcal{L}_t$ by

$$\mathcal{L}_t = \int_0^\infty R_L'(t)\, dt \tag{3-147}$$

and equation (3-146) becomes

$$\overline{y^2} = 2\,\overline{v^2}\,\mathcal{L}_t\,t - 2\,\overline{v^2}\int_0^\infty t\,R_L'(t)\,d\,t\,. \qquad (3\text{-}148)$$

For a very long interval of time t, the second term on the right hand side of equation (3-148) will become very small with respect to the first term, so it may be neglected. Hence:

$$\overline{y^2} = 2\,\overline{v^2}\,\mathcal{L}_t\,t \qquad (3\text{-}149)$$

Defining coefficient of eddy diffusivity $\mathcal{E}$ by

$$\mathcal{E} = \frac{\overline{y^2}}{2\,t} = \overline{v^2}\,\mathcal{L}_t = v'\,\mathcal{L}_L \qquad (3\text{-}150)$$

where $\mathcal{L}_L$ is a Lagrangian space scale (scale of eddy diffusion) given by

$$\mathcal{L}_L = v'\,\mathcal{L}_t \qquad (3\text{-}151)$$

Many investigators (110-114) have attempted to establish some empirical relationship between the Lagrangian and Eulerian correlations and consequently between the macro-scale of turbulence L_x and the scale of eddy diffusion $\mathcal{L}_L$. Unfortunately such a correlation has not been established yet. In fact, the scatter of the data in each investigation and the contradicting trends, if any exist, between different investigators, make it impossible to obtain a definite conclusion about the form of such a

relationship. However, one can say that both L_x and $\mathcal{L}_L$ are roughly of the same order of magnitude. A detailed discussion of this point will be given in Chapter 7.

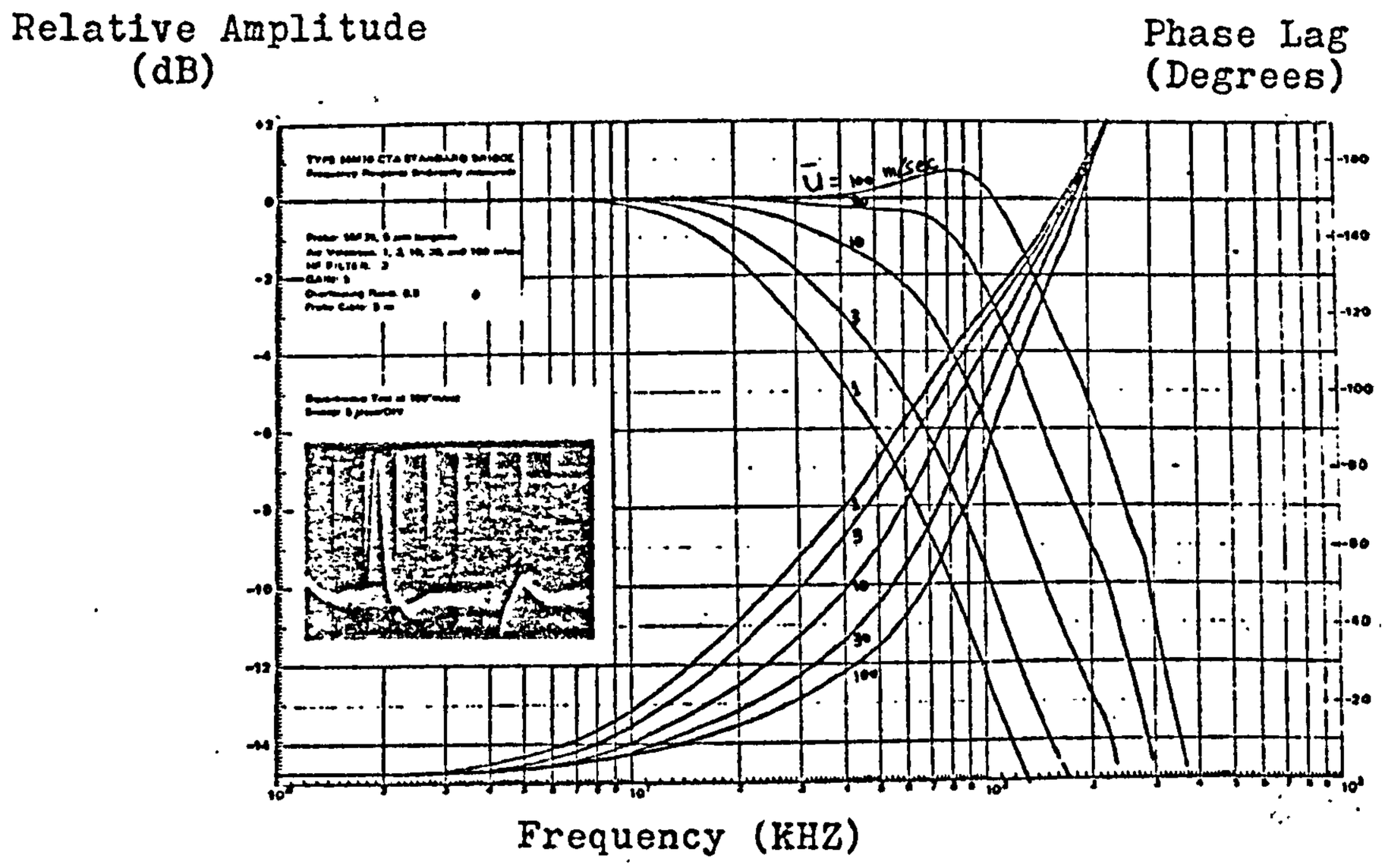

Fig (3-1) Example for the frequency characteristics of a constant temperature hot wire anemometer, (121)

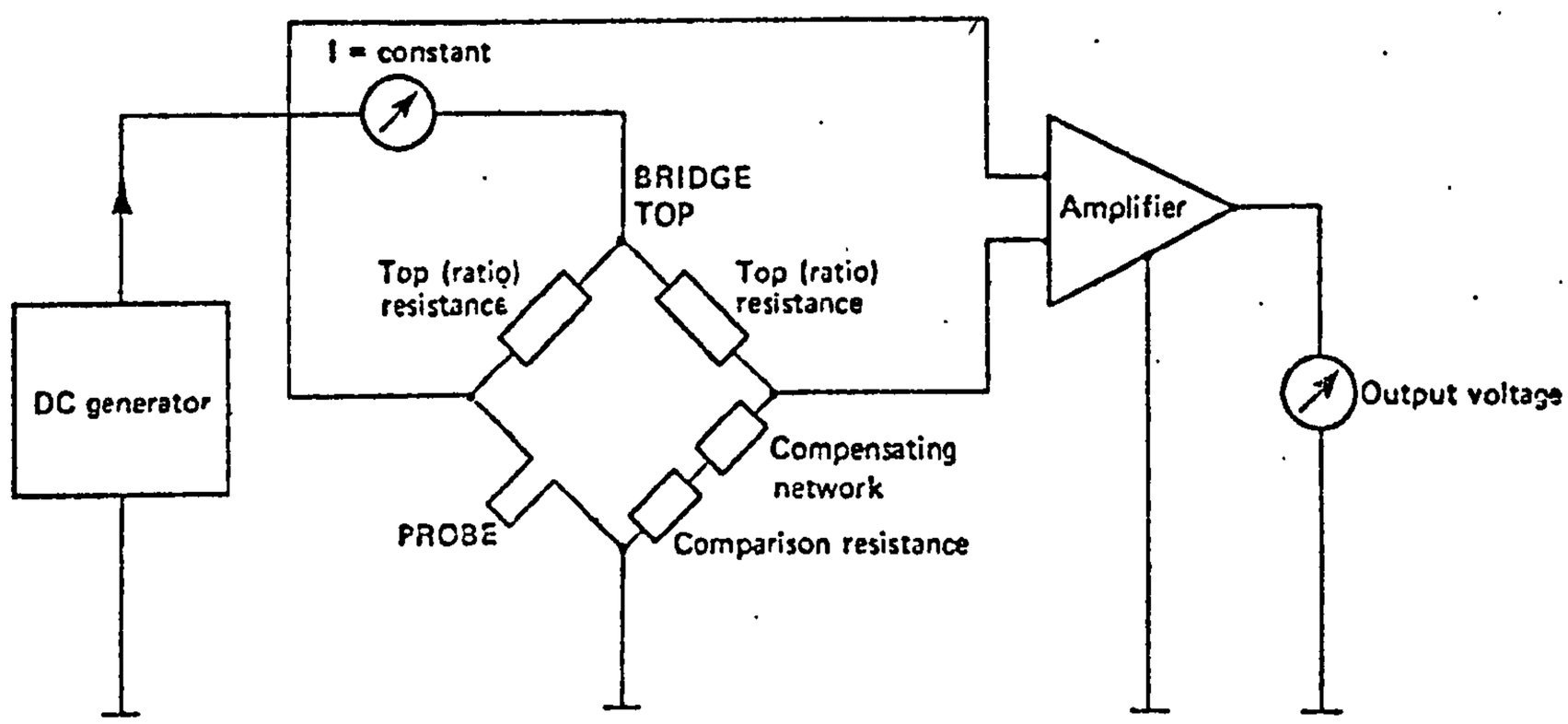

Fig (3-2) Simplified diagram for a constant current anemometer.

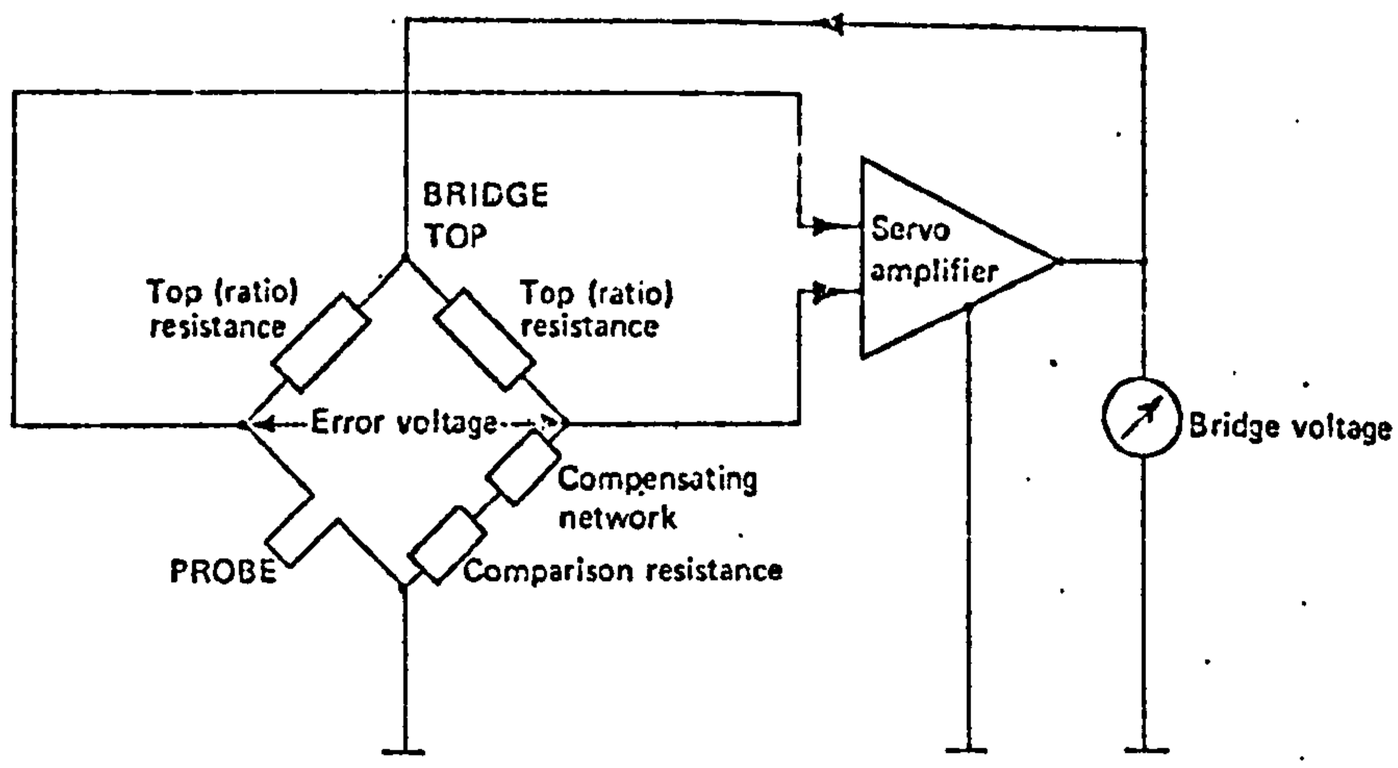

Fig (3-3) Simplified diagram for a constant temperature anemometer.

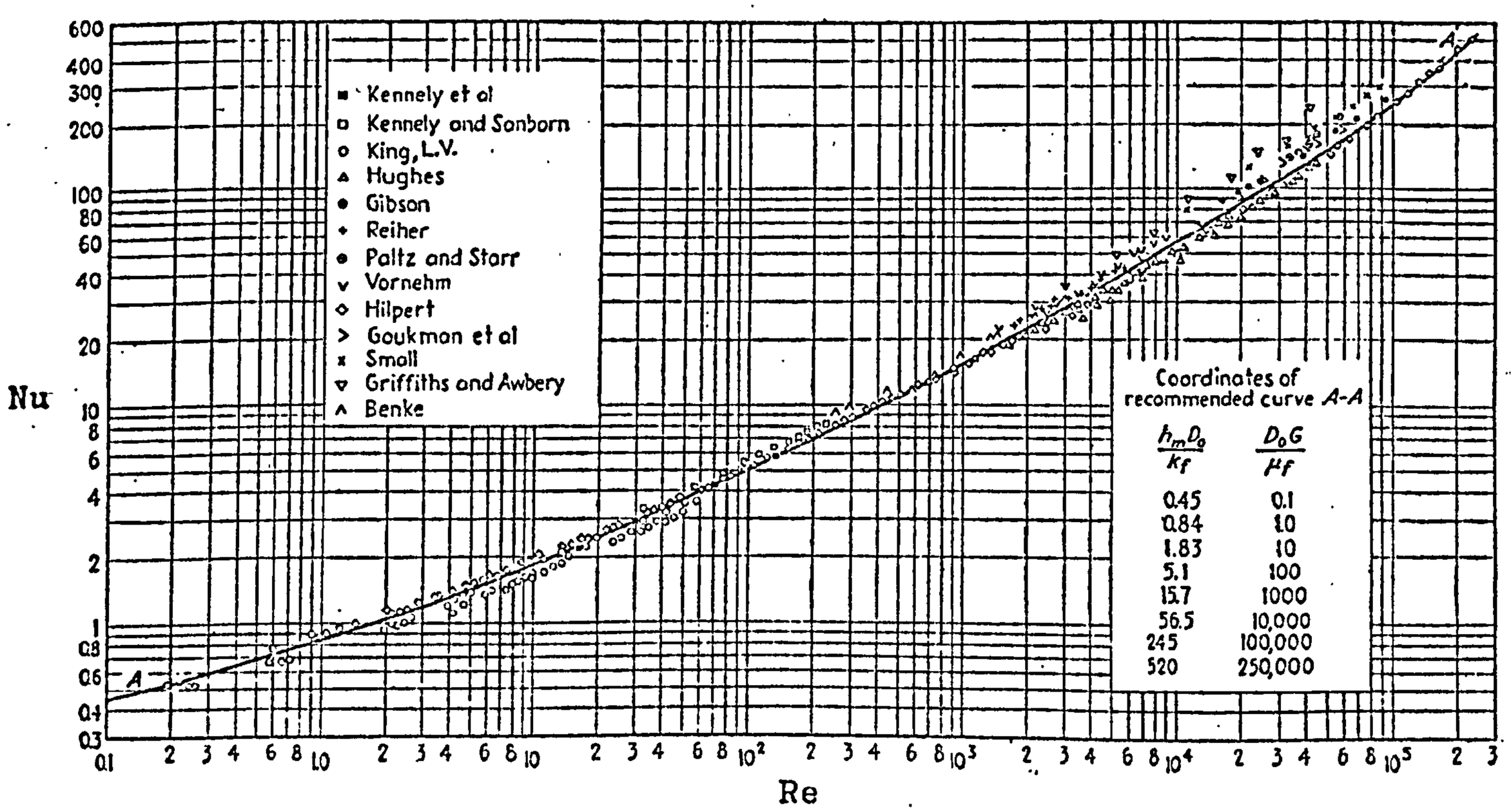

Fig (3-4) Data for heating and cooling air flowing normal to cylinders, corrected for radiation to surroundings, (compiled by McAdams,(73))

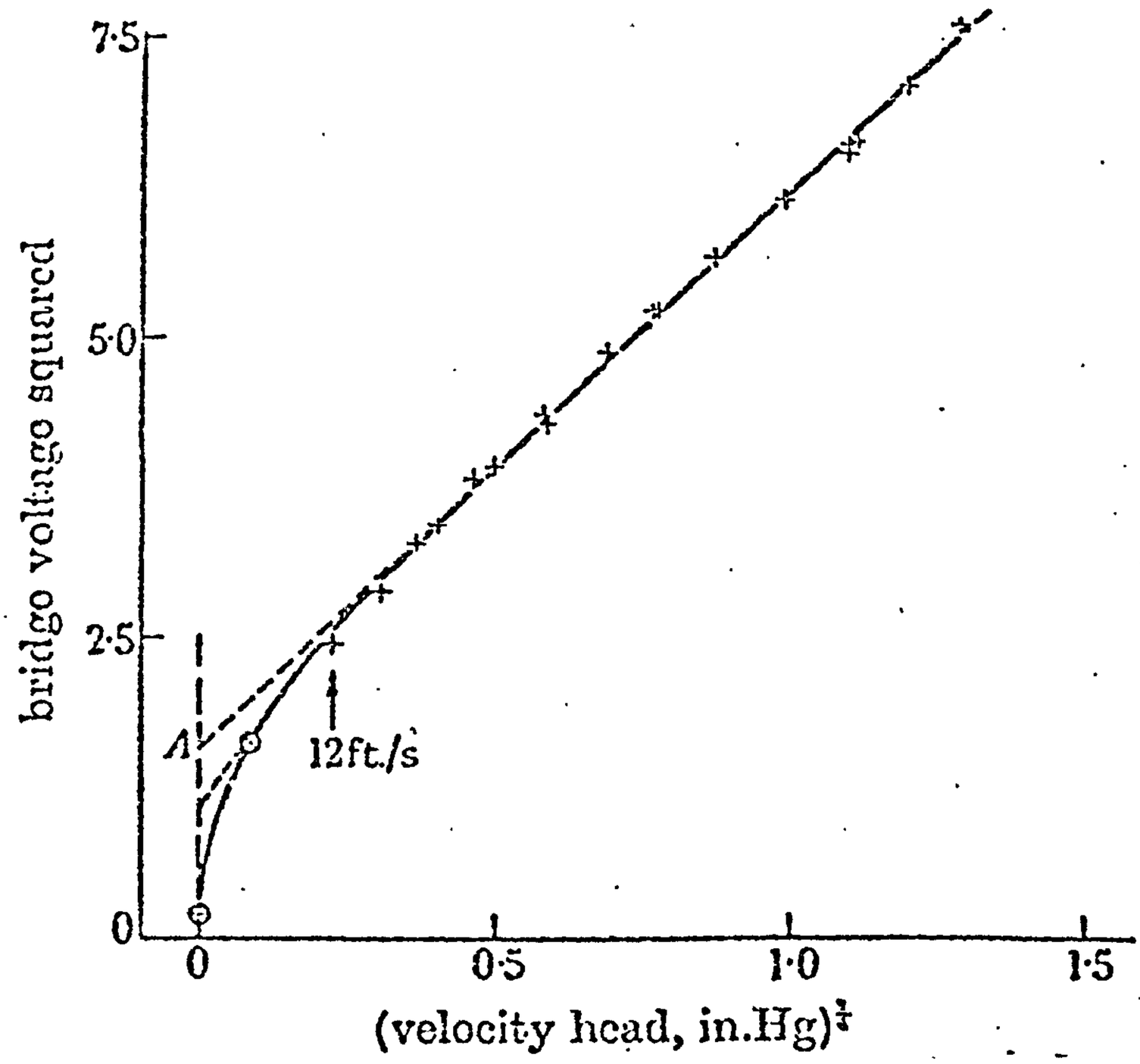

Fig (3-5) Typical hot wire calibration showing the error introduced by extrapolating measurements obtained over a limited range of velocity to estimate the bridge voltage at zero velocity,(77).

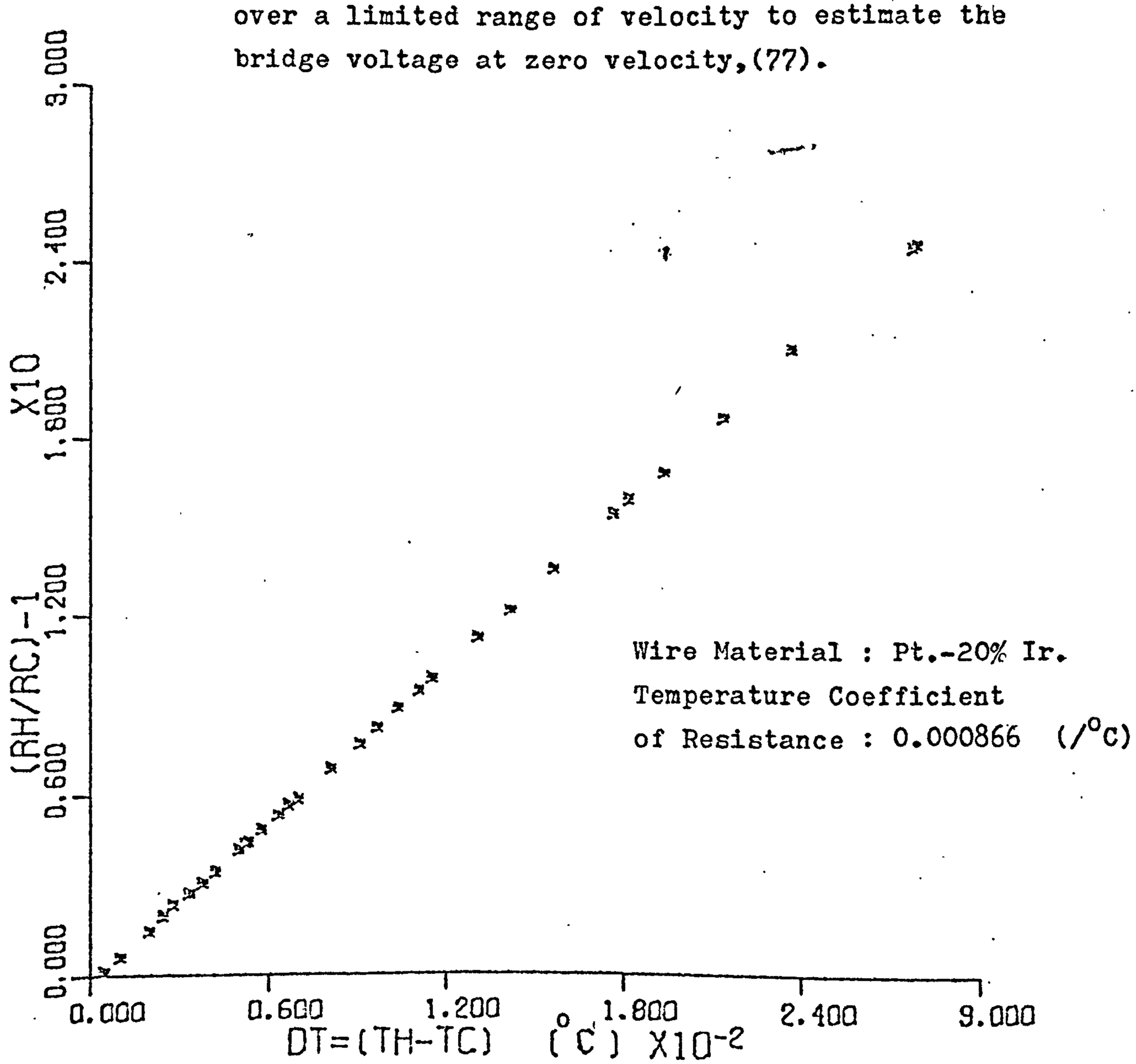

Fig (3-6) Evaluation of the temperature coefficient of resistance.

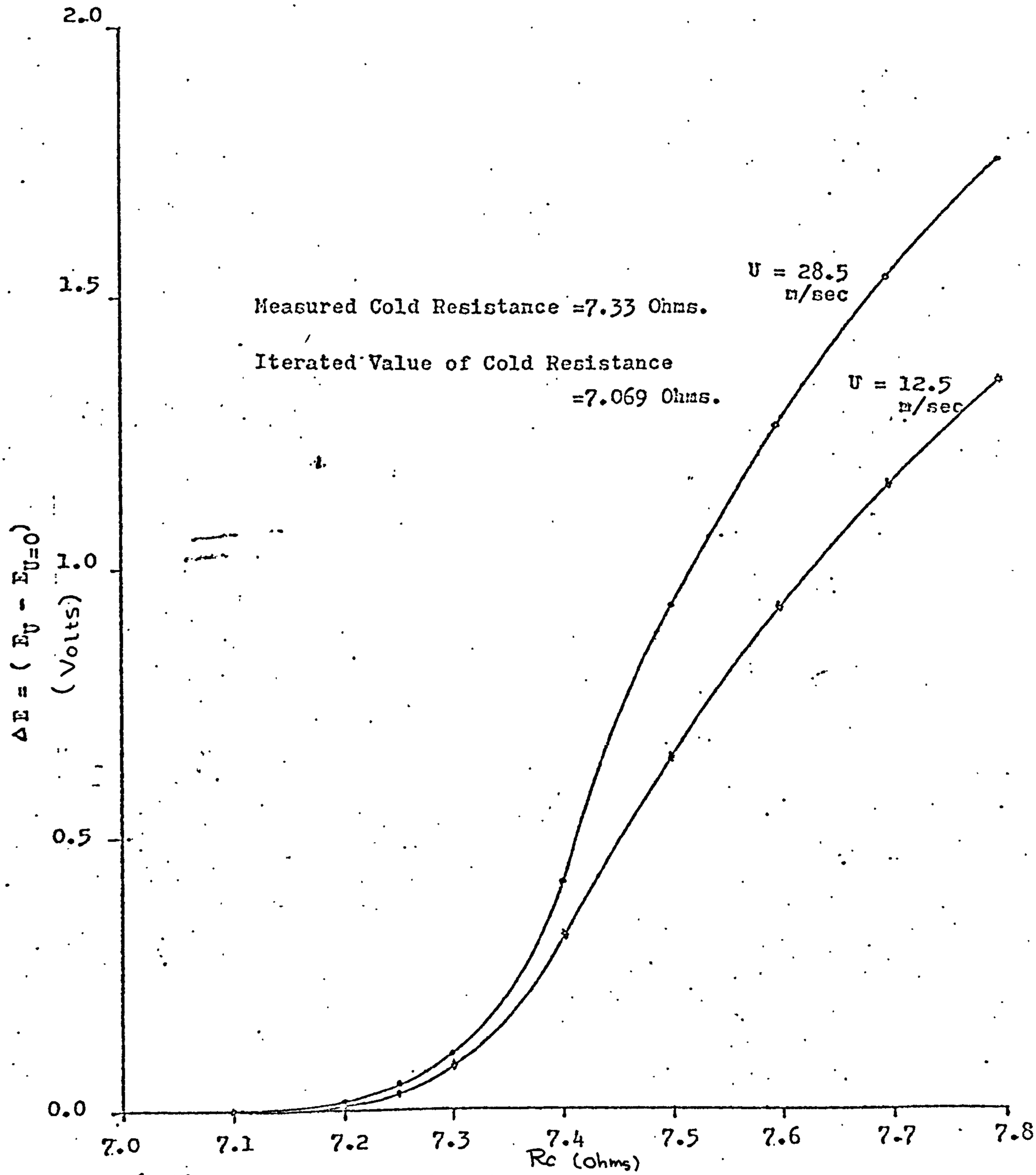

Fig (3-7) Example of operating the hot wire below its measured value of cold resistance, showing the discrepancy between the measured and actual value of cold resistance.

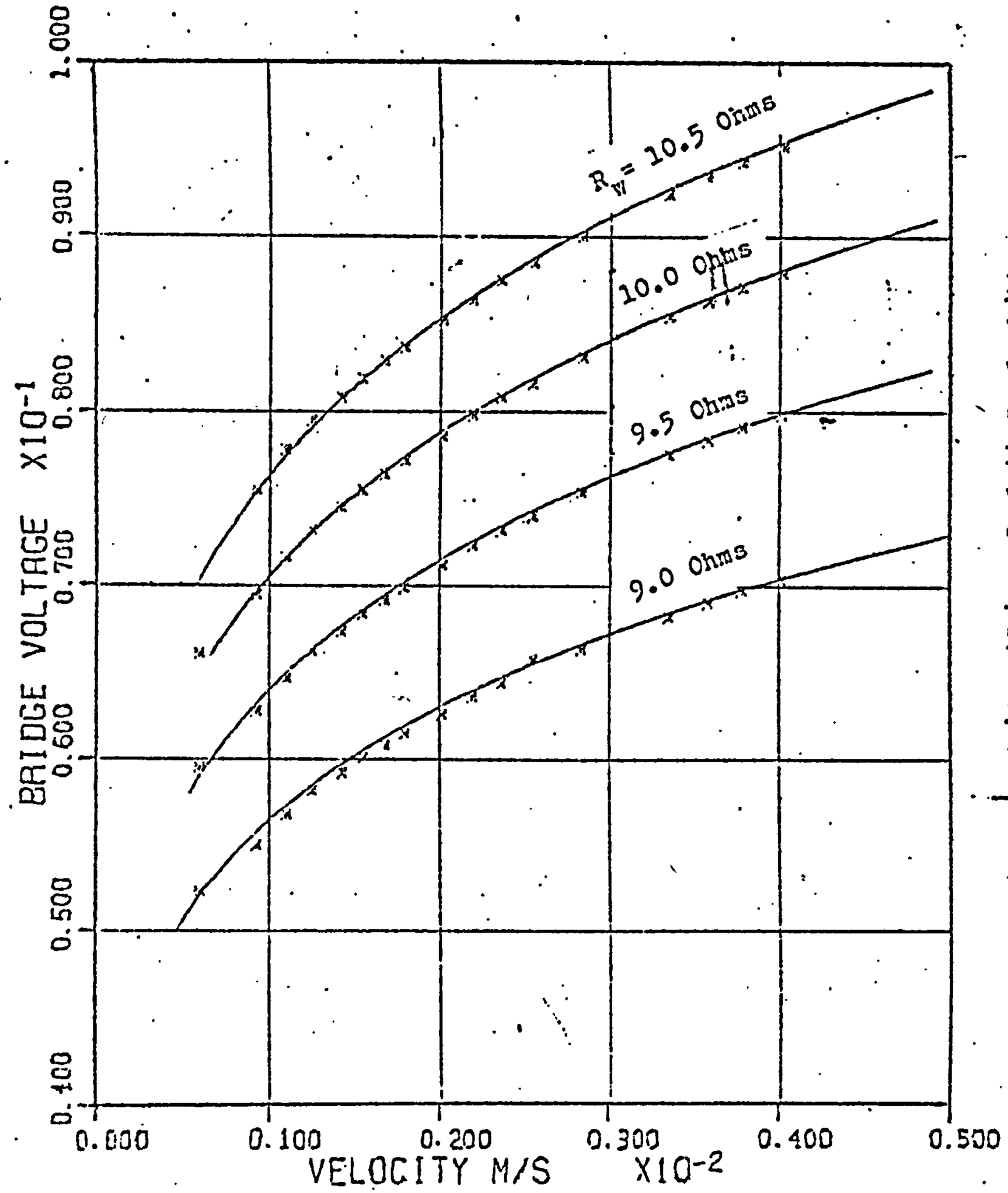

HOT WIRE CHARACTERISTICS :

Wire Length : 1.78 mm
Wire Diameter : 10 μ m
Cold Resistance : 7.069 Ohms
Lead Resistance : 0.825 Ohms
Wire Material : Pt.-20% Ir.
Temp. Coeff. of Resistance for Wire Material: 0.00086 (/°C)

55M10 CTA-DISA Standard Bridge, (50 Ohms Top Resistance).

* Experimental Calibration.
—. Theoretical Calibration.

Fig (3-8) Calibration of a Hot Wire Probe.
(Horizontal Wire)

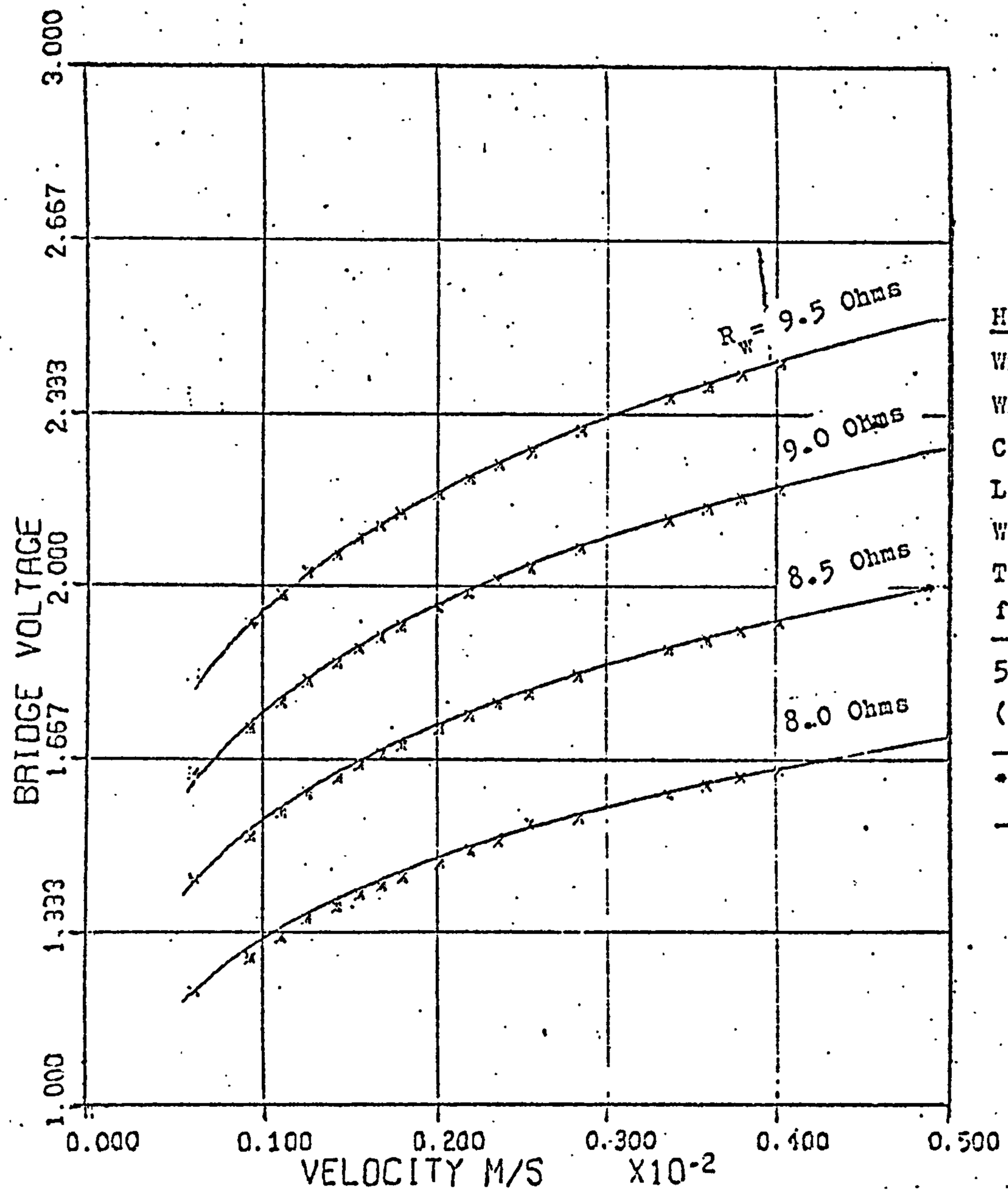

HOT WIRE CHARACTERISTICS :

Wire Length : 1.65 mm
Wire Diameter : 10. μ m
Cold Resistance : 6.157 Ohms
Lead Resistance : 0.55 Ohms
Wire Material : Pt.-20% Ir.
Temp. Coeff. of Resistance for Wire Material: 0.00086 (/°C)

55 M11 CTA-DISA Anemometer Bridge, (5 Ohms Top Resistance).

• Experimental Calibration.
— Theoretical Calibration .

Fig (3-9) Calibration of a Hot Wire Probe. (Vertical Wire)

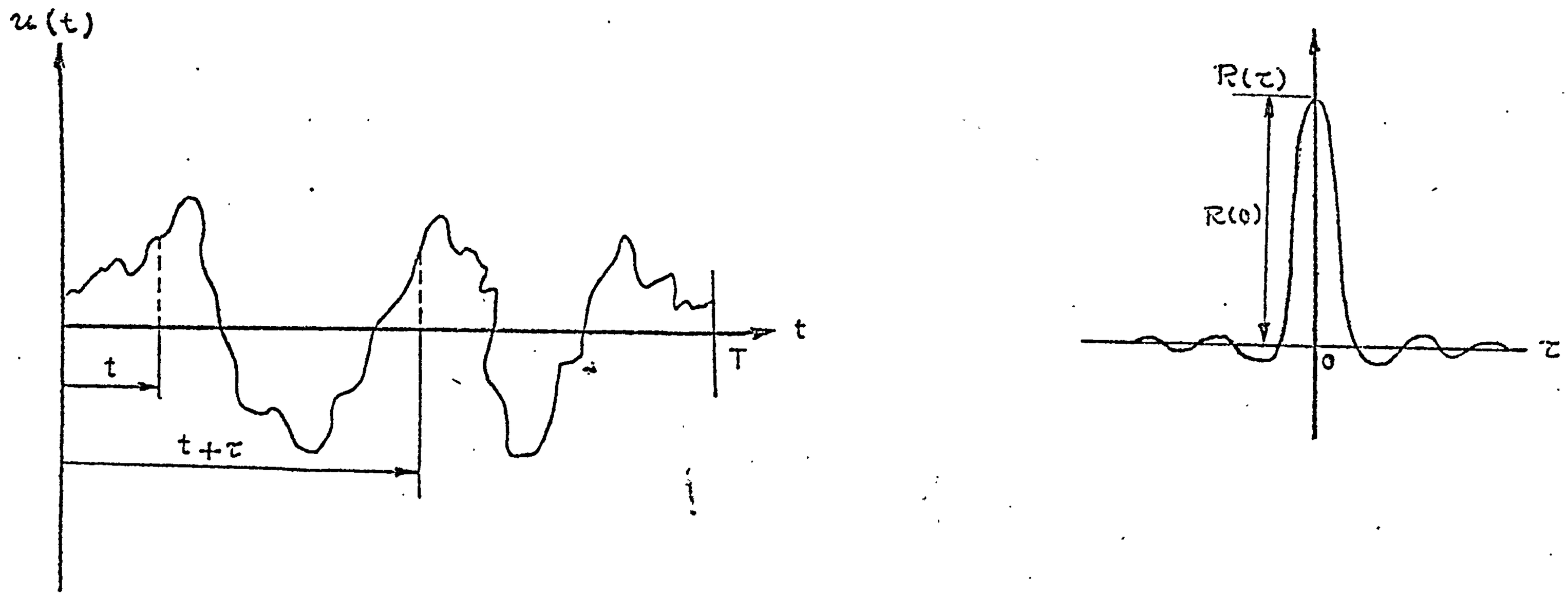

Fig (3-10) Definition of the auto-correlation function.

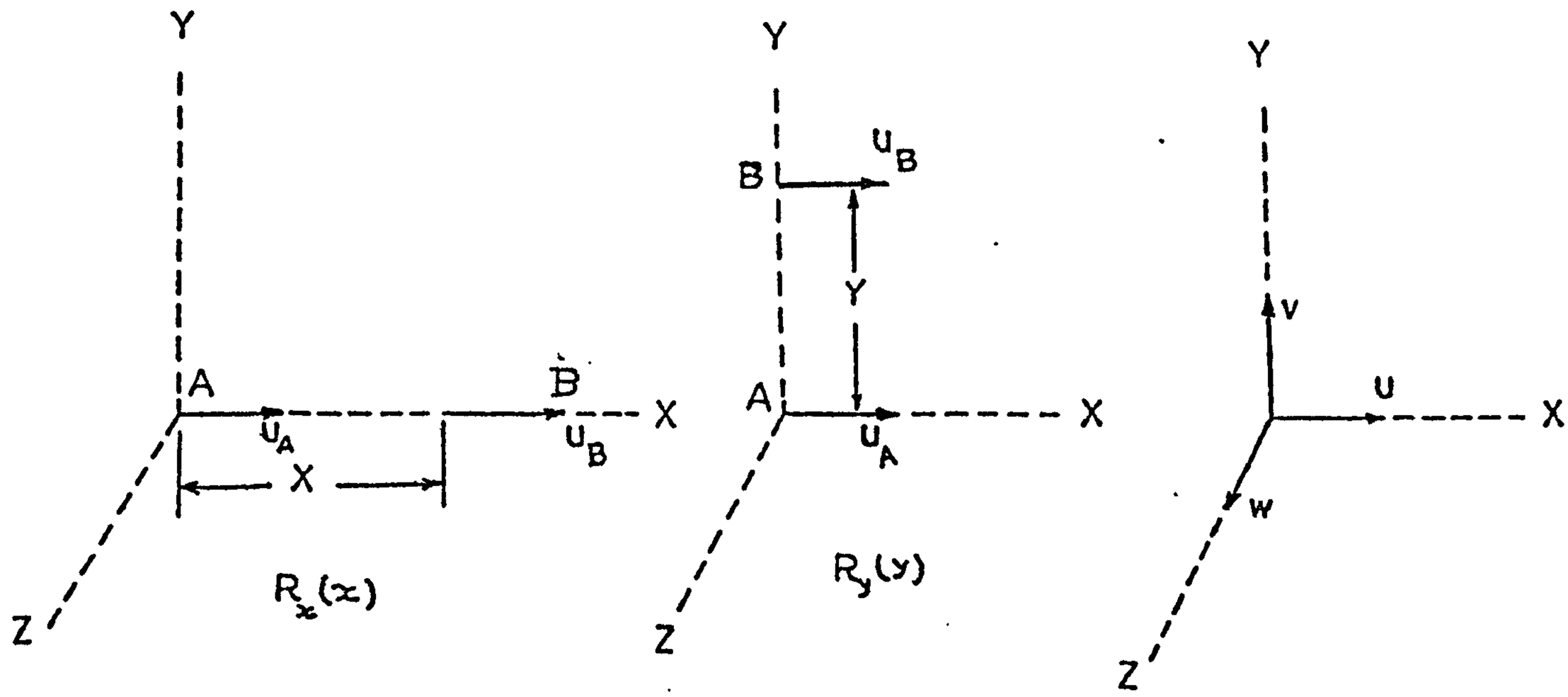

Fig (3-11) Definition of the longitudenal and lateral correlations.

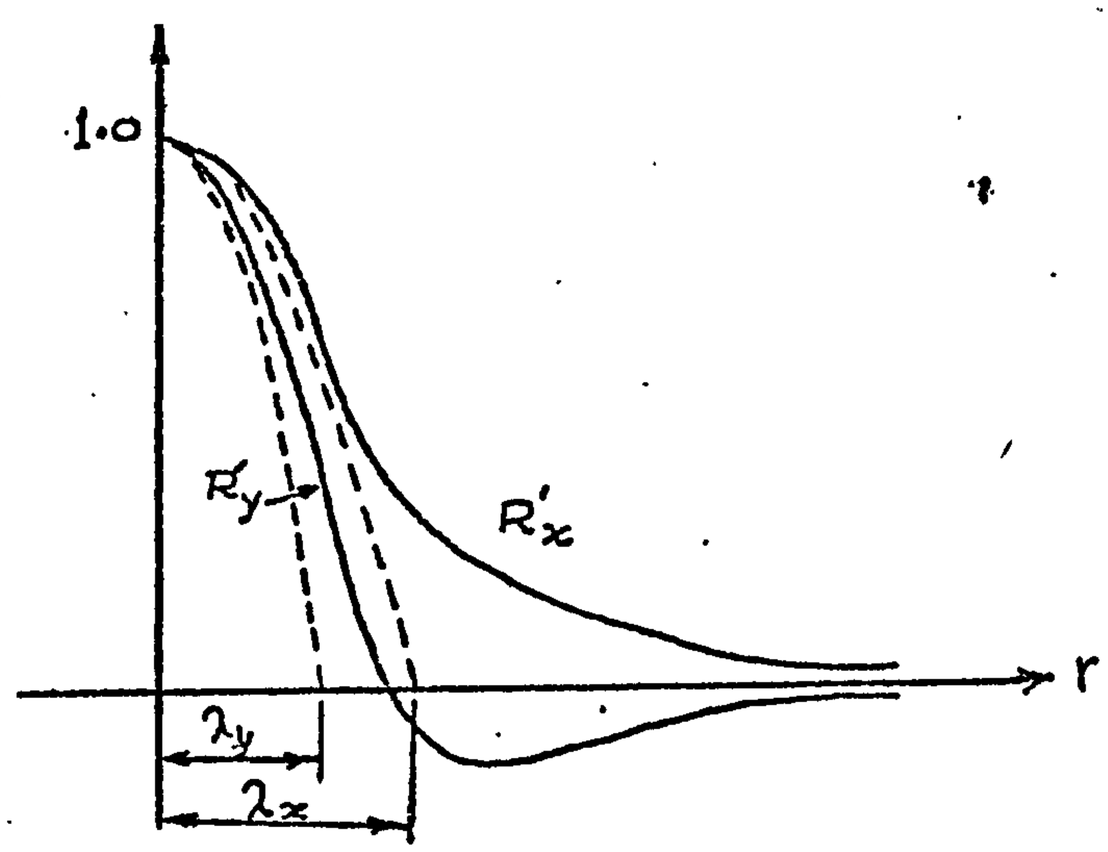

Fig (3-12) General shapes of correlation coefficients.

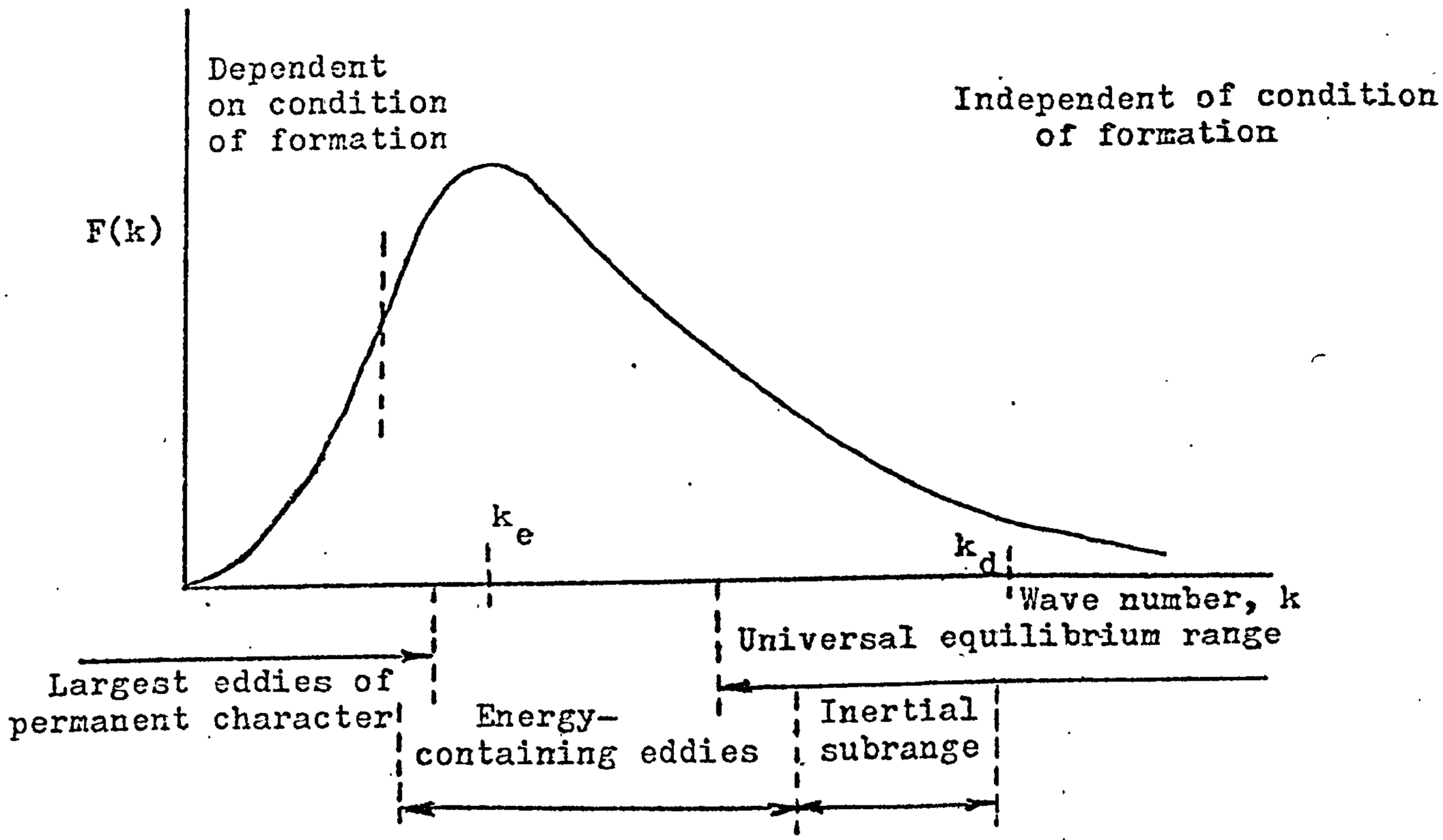

Fig (3-13) Spectrum distribution for isotropic turbulence,(79).

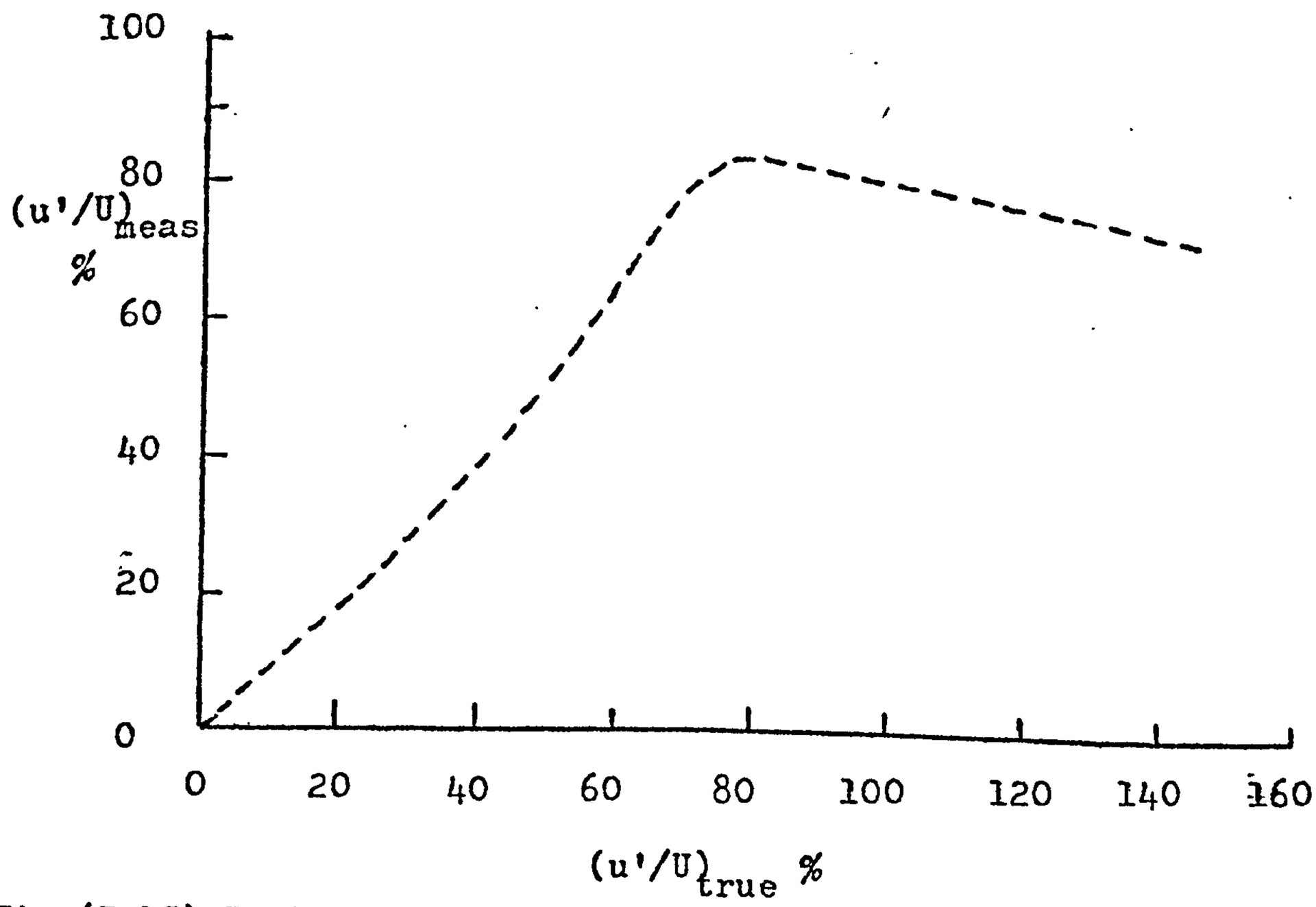

Fig (3-15) Test of hot wire response to high turbulence,(91).

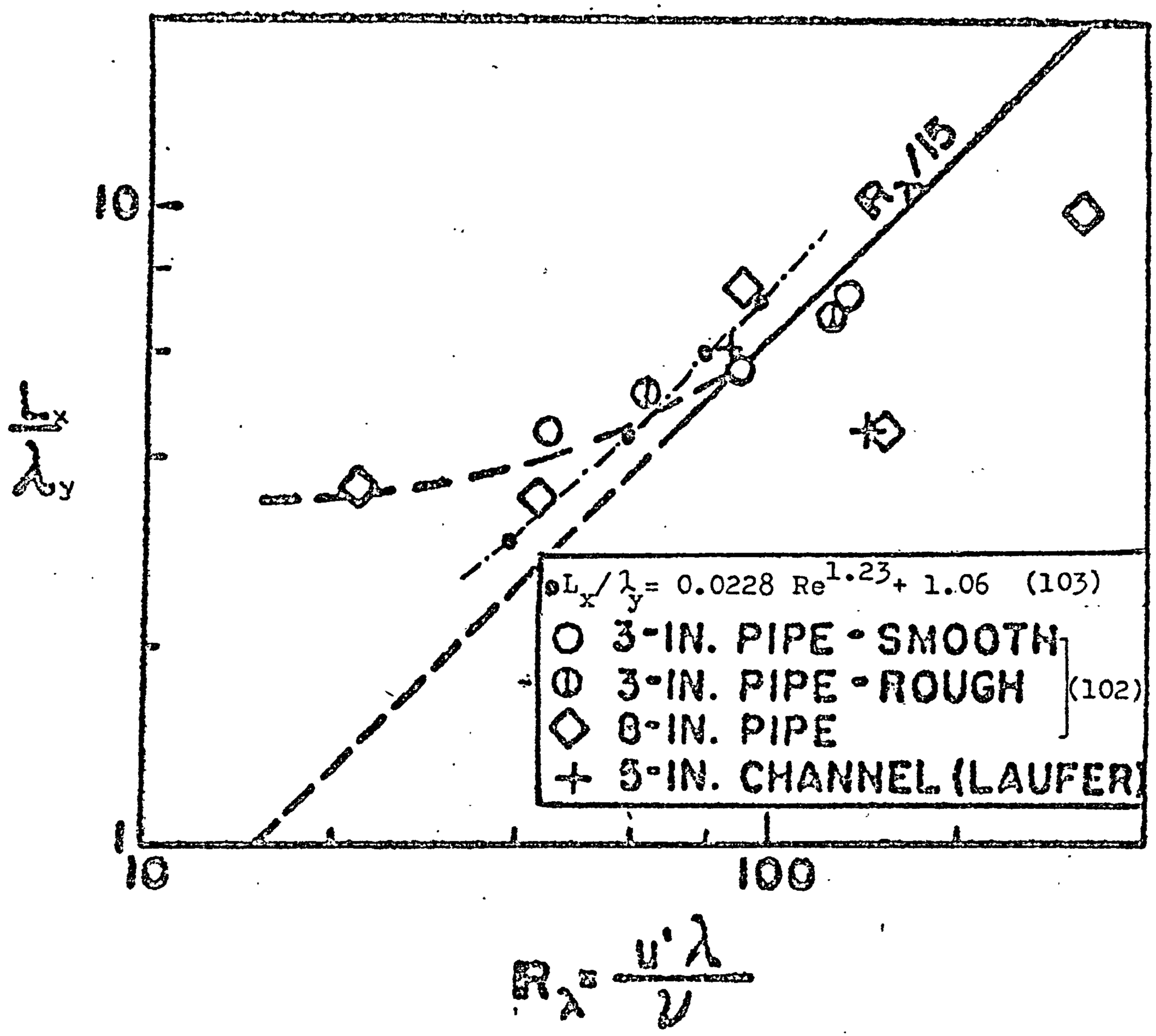

Fig (3-14) Ratio of macro- to microscale of turbulence for isotropic flow.

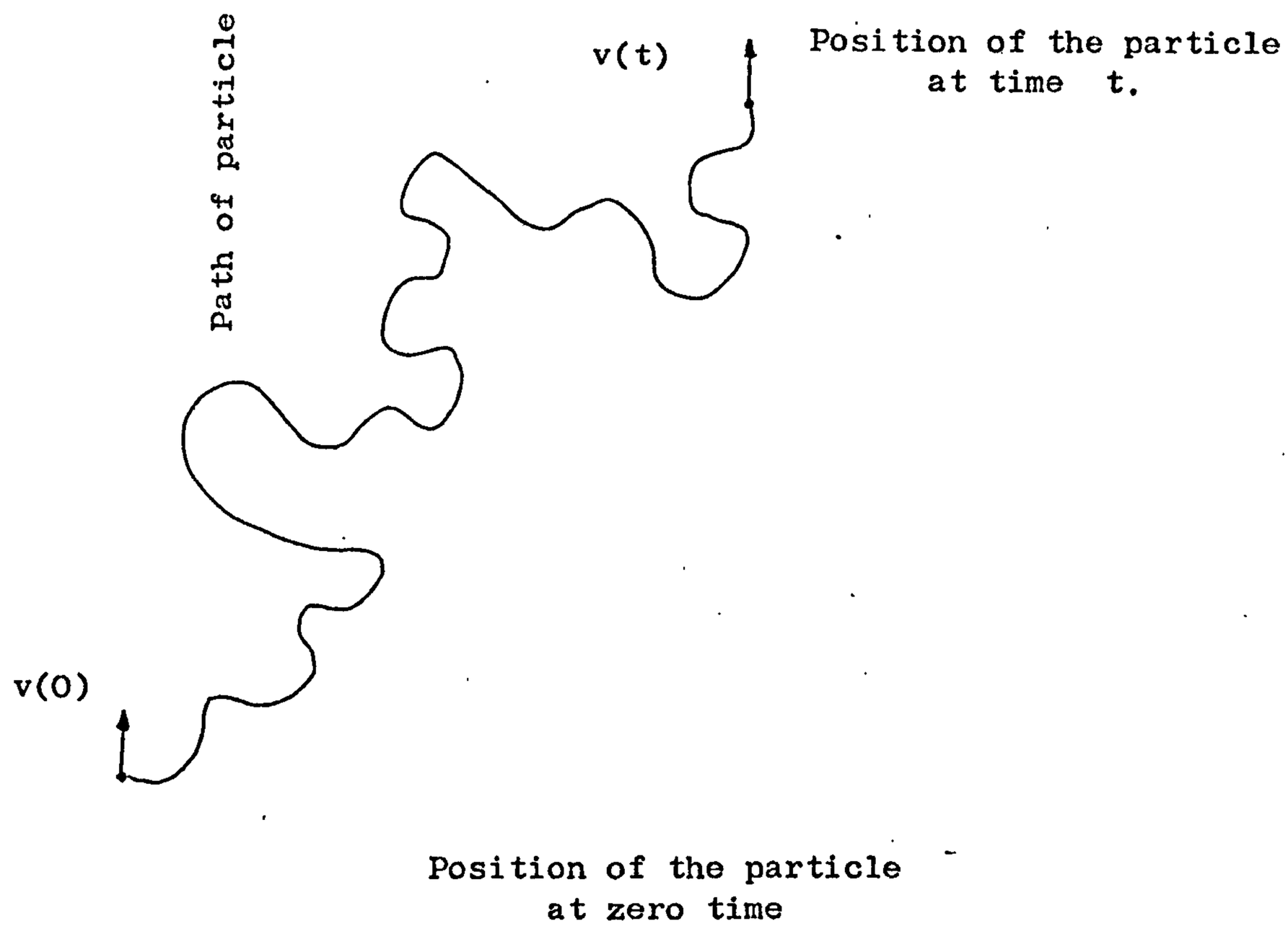

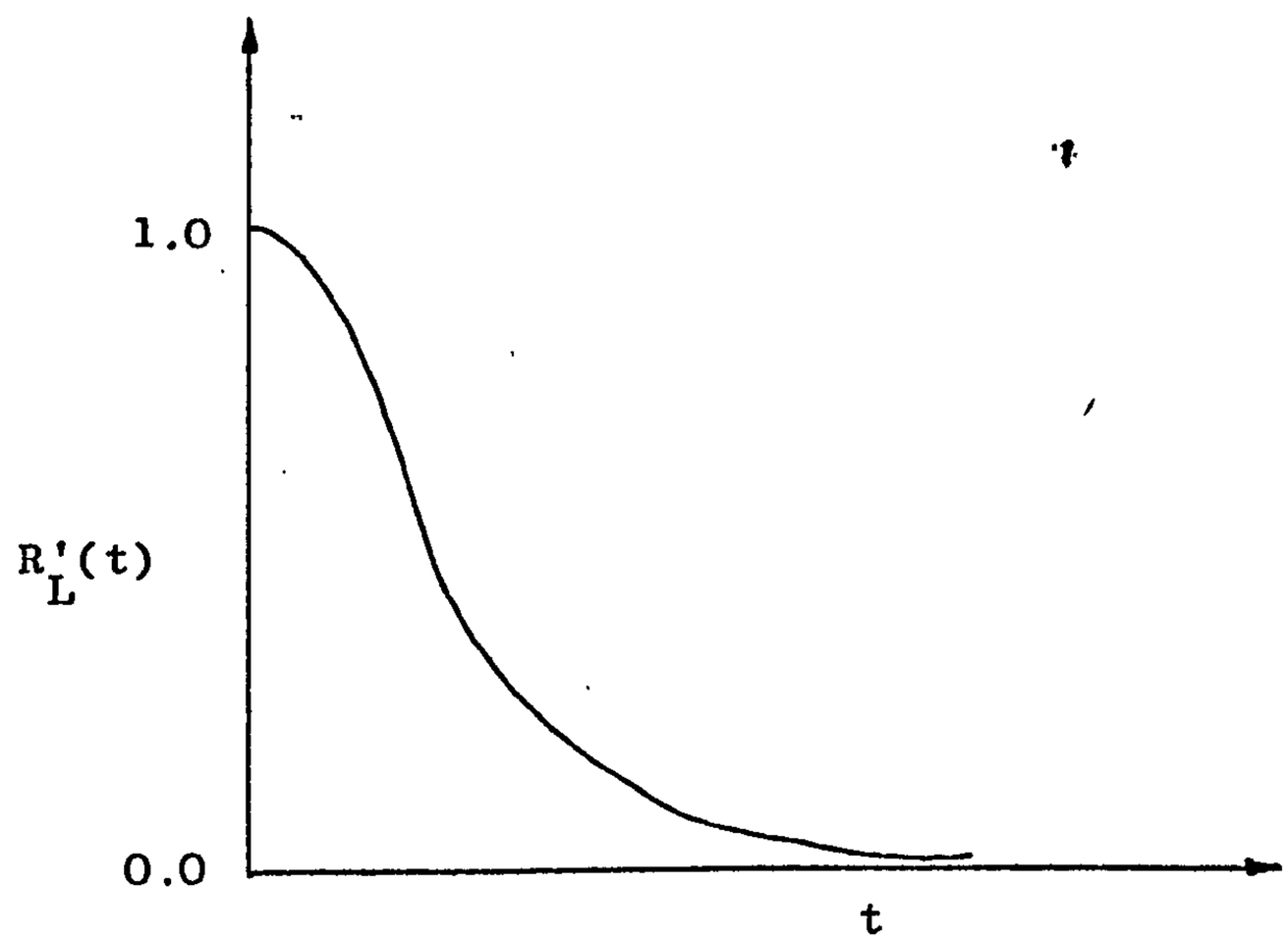

Fig. (3-16). Definitions of particle diffusion and Lagrangian correlation.

4. DATA ACQUISITION AND PROCESSING SYSTEM

The main operations in the Data Acquisition and Processing System used in the present investigation could be summarised as follows:

a) DATA COLLECTION

This includes the timing mark, the output of the hot wire anemometer and the pressure trace.

b) DATA RECORDING

This is carried out using an FM (frequency modulation) tape recorder.

c) DATA PREPARATION

The recorded signals undergo some operations before the final stage of data analysis. This includes: digitization of the recorded signals and storing the output in appropriate format; calibration of the digitized signals and preparation of turbulence signals at some particular crank angle of interest in the engine cycle.

d) DATA QUALIFICATION

This process represents some tests on the validity of the basic assumptions about the characteristics of turbulence signals in the engine.

e) DATA ANALYSIS

This could be divided into two main groups:

1. Analysis of mean gas velocities.

   This includes a statistical analysis of mean gas velocities at different crank angles in the engine cycle. The analysis is carried out over a number of cycles to give an estimation of the extent of cyclic variations in gas velocities in terms of standard deviation, coefficient of variation and range of variation, as will be discussed later.

2. Analysis of fluctuating velocity components.

   This process could be divided into two categories:

   a) Analysis of relatively long data records to estimate the average characteristics of the turbulence field.

   b) Analysis of individual data records for consecutive engine cycles to estimate the extent of cyclic variations in the statistical parameters characterising the turbulent field. These variations will be reflected as combustion variations during engine firing. The statistical parameters of the signals are evaluated in terms of mean values, standard deviations and coefficients of variation.

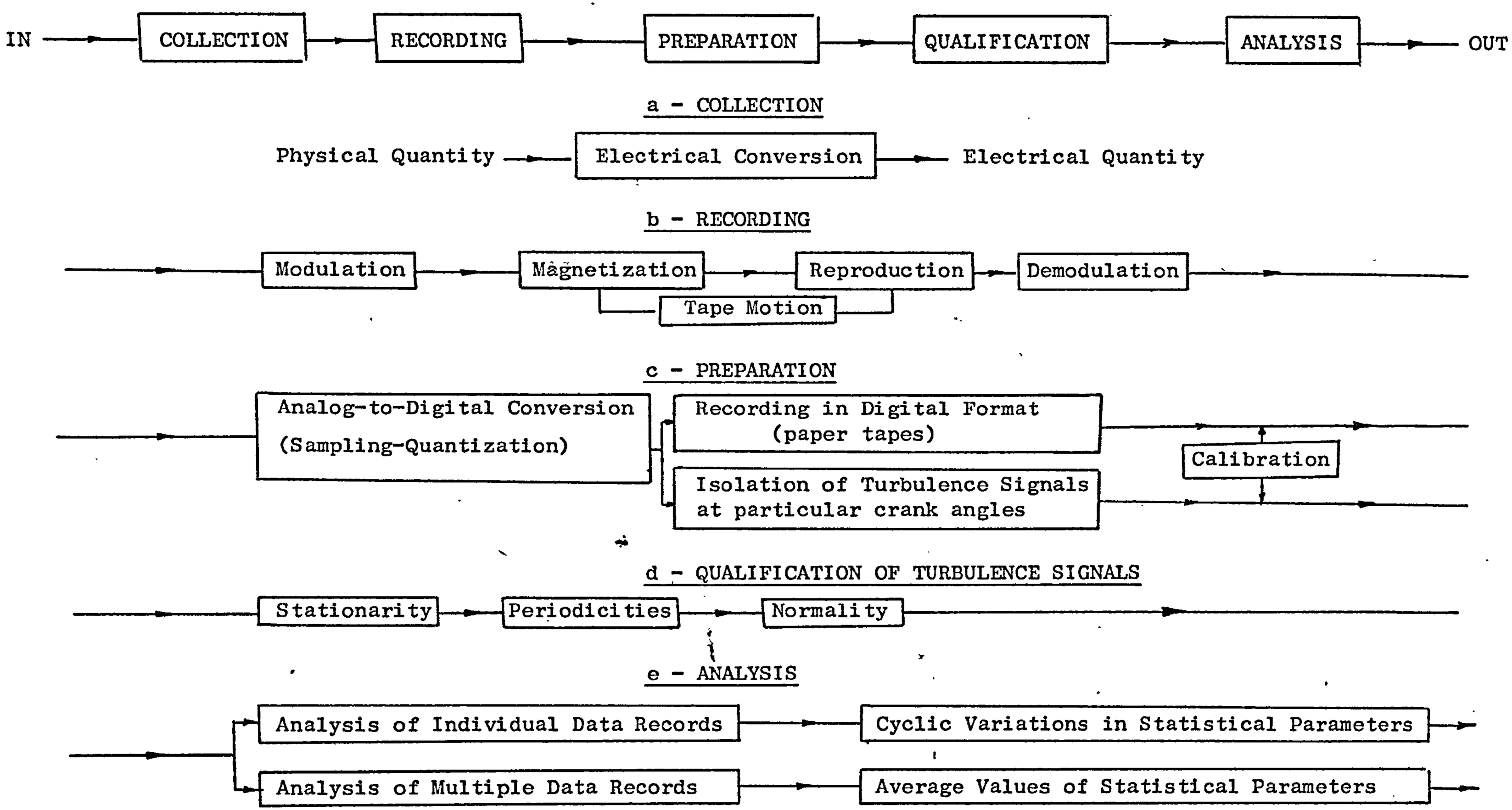

FIG. (4-1) General Procedure for the DATA ACQUISITION AND PROCESSING SYSTEM

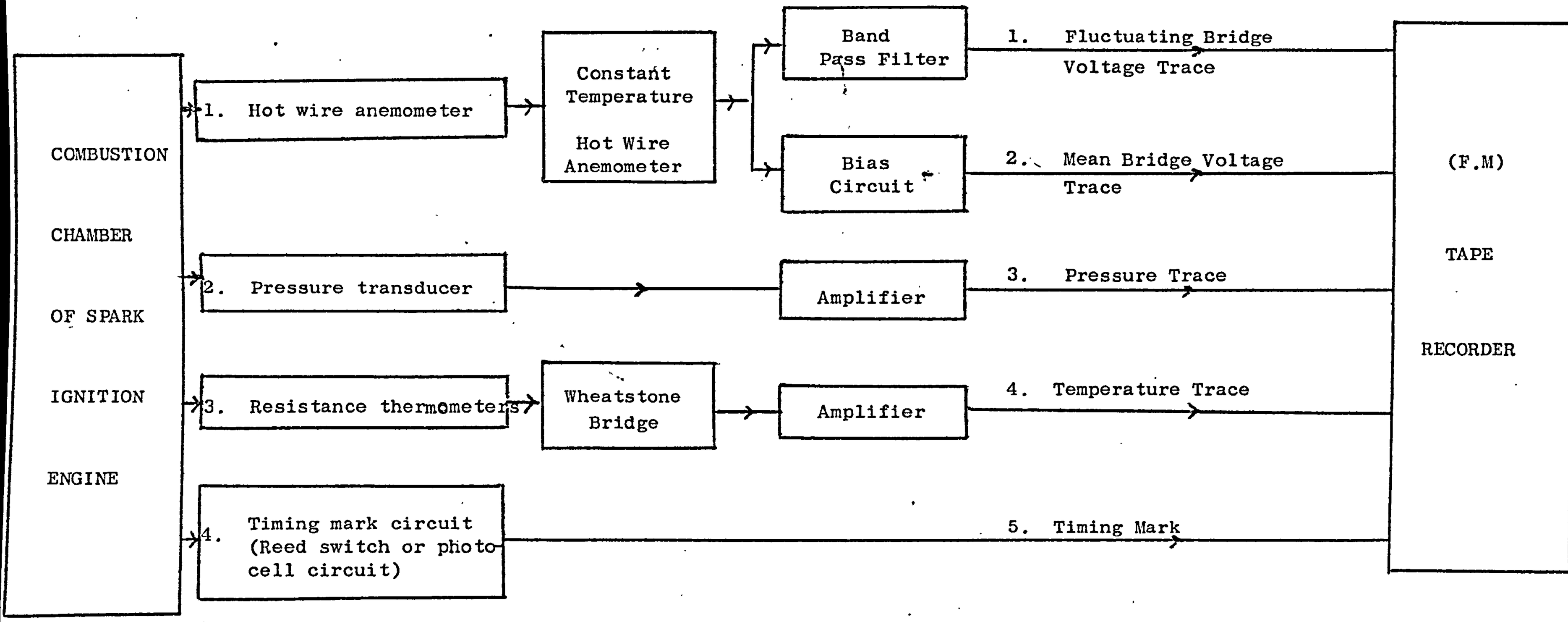

FIG. (4-2a) Collection and Recording of Signals

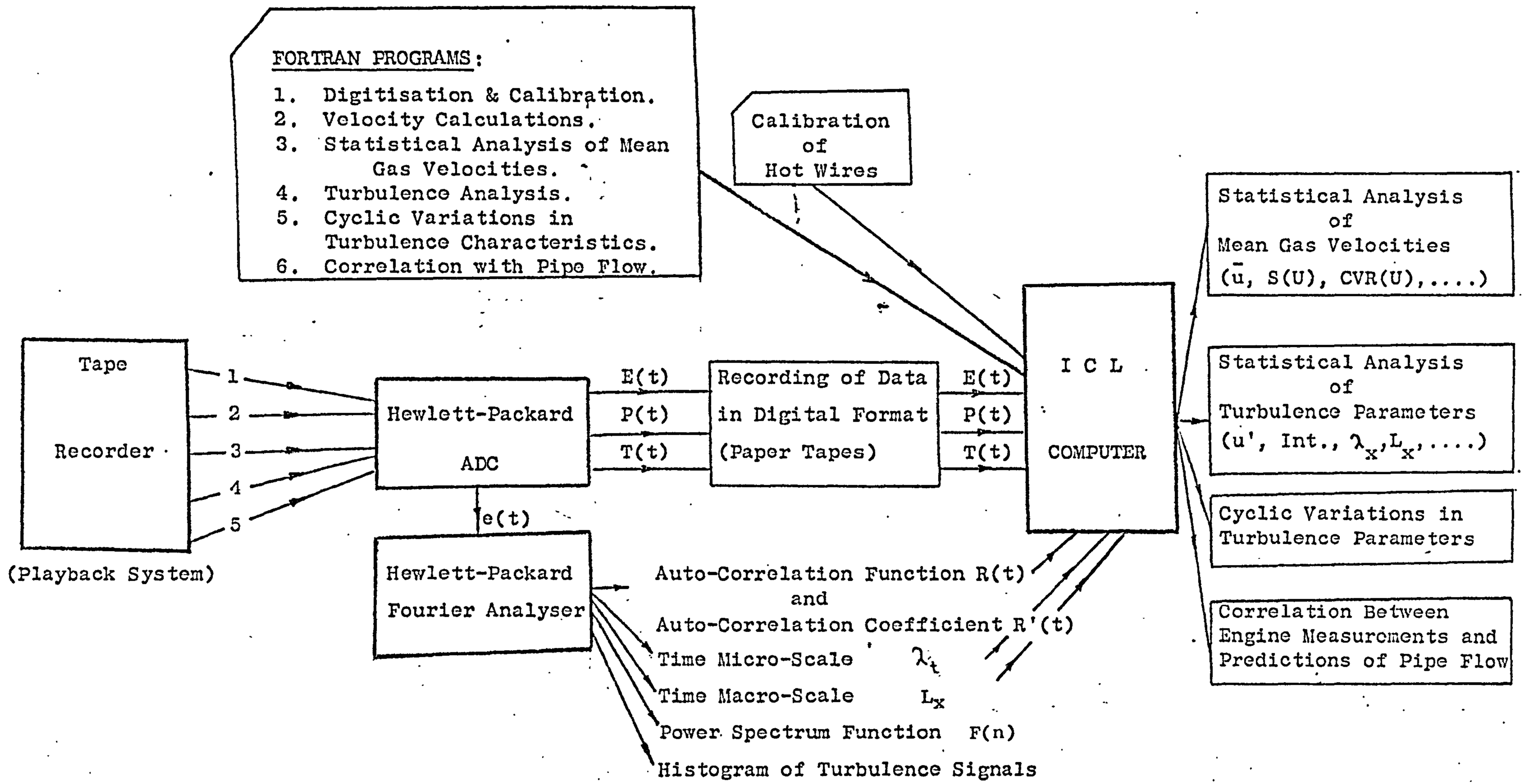

Fig. (4-2b) Statistical Analysis of Mean Velocity and Turbulence Parameters

For both cases (a) and (b) the analysis includes: auto-correlation functions and auto-correlation coefficients; power spectral density functions; micro-scale and macro-scales of turbulence; intensities and eddy diffusivities.

Fig. (4-1) shows a flow chart of the various steps for each operation, while Figs. (4-2a) and (4-2b) show flow charts of the hardware involved in each step and the input/output of each individual operation.

4.1 Data Collection

The required input data for investigating gas velocities and turbulence inside the combustion chamber of an engine could be summarised as follows.

1. Gas mean velocities.
2. Fluctuating velocity components.
3. Instantaneous gas pressures.
4. Instantaneous gas temperatures.
5. A timing mark at a fixed time on the engine cycle.

The first two quantities are obtained from the output of the constant temperature hot wire anemometer bridge with the appropriate filtering conditions, which will be discussed later. The gas pressures and temperatures are obtained by using a pressure transducer and a resistance thermometer respectively, while the timing mark is obtained from a triggering circuit mounted on the crank shaft of the engine. Figs. (4-3), (a), (b),

(c) and (d) show an example of the simultaneously recorded signals for a Ford V4 engine. Detailed descriptions of each instrument are given below.

4.1.1 DISA 55M Constant Temperature Anemometer System

The measurements of gas velocities and turbulence fluctuations are carried out, in the present investigation, using a DISA 55M constant temperature anemometer system. It consists of individual units which could be arranged in any convenient combination to suit each stage of the Data Acquisition system employed. The main units of this system are: the 55 M05 power pack, the 55 M01 main anemometer bridge unit, the 55D26 signal conditioner and the 55D31 digital voltmeter.

The digital voltmeter is used for calibration purposes, either for the hot wire anemometer when exposed to constant flow velocities in the DISA wind tunnel, or for setting known voltages for calibrating the recorded signals on the tape recorder. Its range of measurement varies in three steps from 0.000 to 99.99 volts with a maximum error of 0.1% of full scale range. A built in filter, switchable in seven steps, provides a choice of time constants between 0.1 and 100 seconds.

The power pack unit consists of a complementary part of the main anemometer bridge unit. It contains circuits to rectify and smooth out the AC line voltage, as well as voltage limiting and short circuit protection circuits. The stabiliser circuits are located in the main unit. It also contains a

selector for obtaining either a high output voltage at low current or a lower output voltage at high current.

The 55 M01 main unit contains, except for the power pack, all circuits required for operating the anemometer: amplifier, filter, decade resistance, square wave generator, protection circuits and other auxilliary circuits. Fig. (4-4) shows a simplified block diagram of this unit.

Detailed descriptions of the DISA anemometer bridge circuit and its specification are given in reference (121). The main characteristics of this anemometer system could be summarised as follows:

i) Compensation for lead resistance is provided by a zero ohms potentiometer which is wired in series with the decade resistance.

ii) A probe protection circuit is also provided which serves the purpose of insuring that neither faulty nor broken cables will cause a high current to be fed through the probe that it will burn out or be thermally overloaded.

iii) The square wave generator is used in the measurements of probe cold resistance and in balancing the bridge at high frequencies. The first operation is a simple balance of the bridge arms, where the appropriate value of the decade resistance gives the sensor cold resistance. The second use of the square wave generator in adjusting the bridge balance is based on simulating a sudden change in the velocity of the flow acting on

the probe by feeding a square wave signal into the bridge and monitoring the output. This method is shown by Davis and Fisher (77) to give an under-estimation of the upper frequency limit of the wire as compared with subjecting the wire to a velocity step in a shock tube. However, the errors introduced by employing the former method are not very serious. Exposing the probe to the maximum expected velocity during the measurements and injecting the square wave pulse, the output should show the shortest possible response without superimposed oscillation Fig. (4-5). This condition represents the optimum stability of the bridge and servo-amplifier. If this condition is not satisfied adjustment of the gain and the filter bandwidth is required to obtain damped oscillation, Fig. (4-6). Cable compensation by varying an inductance and capacitance (L and Q) inserted in the bridge circuit results in the fine adjustment of the circuit.

iv) The signal conditioner type 55 D26 was used, in the present work, as a band pass filter for obtaining the turbulence signal from the original anemometer output during engine measurements. The filter circuits of the signal conditioner comprises one low pass filter and one high pass filter both of which are switchable in steps of 1/3 octave. The low pass filter permits alteration of the upper frequency limit between 10 Hz

and 1 MHz; while the lower frequency limit can be varied between 0.1 Hz and 100 KHz by means of the high pass filter.

4.1.2 Timing Mark

A timing mark at a fixed point on the engine cycle is required for triggering the Analog to Digital Converter (ADC) at the beginning of each cycle (TDC induction). This was obtained by generating a square pulse at this particular crank angle. In the early investigation on the Rolls-Royce engine, a triggering pulse was generated by closing a reed switch circuit by a magnet mounted on a rotating disc running at half the crank shaft speed. Later measurements on the Ford engine employed another triggering circuit where a photo-cell was used.

The output of the timing mark circuit was always recorded on one of the tape recorder channels simultaneously with the measured signals. Fine adjustment of the TDC position was carried out by coinciding the generated trigger pulse and the peak of the pressure trace obtained from a cylinder having 360° phase shift in its firing order with respect to the reference cylinder. The use of a Tektronix storage oscilloscope facilitated such a process. This exact setting of the TDC for the reference cylinder was kept constant throughout the experiments for different cylinders and the firing order fed to the computer program to identify the actual beginning of the cycle for each individual cylinder signal.

4.1.3 Measurements of Cylinder Gas Temperature and Pressure

Calculations of gas velocities using the thermal equilibrium equation (3-9) requires evaluation of fluid properties at the appropriate crank angles, determined by the selected sampling rate on the ADC and the engine speed. These fluid properties are generally functions of gas temperature and pressure inside the engine cylinder.

Resistance thermometers are reasonably suitable for engine gas temperature measurements. Hassan (92) discussed the different sources of errors in such a method and concluded that its accuracy lies within 6% of the true values. Semenov (22) has shown that temperature fluctuations may affect the measured turbulence at TDC by only about 2% and could be neglected compared with other sources of errors. Fig. (4-7) shows the output signal from the resistance thermometer in the Ford engine for 17 consecutive cycles at a compression ratio 8.9:1 and an engine speed of 1000 r.p.m. In fact, no severe cyclic variations could be noticed on these results and a typical trace for the mean of a number of cycles could be used in the calculations of gas velocities. In addition, a considerable simplification in the processing of data could be introduced by using the measured gas temperature during induction and applying the polytropic relationship and the pressure trace for evaluating gas temperature at different crank angles during the engine cycle. The latter procedure was used in the present work. Fig. (4-8) shows a comparison

between the measured gas temperature and the computed values from the pressure trace.

Cylinder pressure was measured using a Kistler transducer (Type 750S) with a factory calibrated sensitivity of 16.57 picocoulombs per atmosphere. A Kistler electrostatic charge amplifier (Model 50 01) was used to produce a voltage signal proportional to the pressure. Fig. (4-9a) shows a schematic diagram of the Kistler transducer while Fig. (4-9b) shows a typical pressure trace for the Rolls-Royce engine at 9:1 compression ratio and an engine speed of 1000 r.p.m.

4.1.4 Signal Recording System

Measurements of gas velocities and turbulence in the engine requires simultaneous recording of the following signals: a timing mark occurring at a fixed time on the cycle; the gas pressure; the gas temperature (this is an arbitrary option as discussed in Section 4.1.3) and the output of the hot wire anemometers (mean signal and turbulence).

Magnetic tape recorders represent the most convenient type of data storage systems because of their ability to store large quantities of data and to reproduce them in electrical form. Also, the bandwidth of frequencies for commercial recorders covers the highest frequencies expected in the turbulence signal (up to 10 KHz). In the early period of this investigation a Sangamo (FM) tape recorder Model 3500 was

available. This model has the facilities of 14 recording channels and, therefore, all the required signals were recorded simultaneously. Table (4-1) gives an abstract of the technical specification of this tape recorder. Later on, such recording facilities were not available and were replaced by a Racal Store 4 (FM) tape recorder. The latter recorder has only four recording channels and, therefore, only the raw signal of the anemometer output was recorded during the test. The turbulence signal was obtained by carrying out the filtering procedure at the time of processing and analysing of the data on the Hewlett Packard Fourier Analyser. Table (4-2) gives an abstract of some of the relevant specifications for the Racal Store 4 tape recorder.

The basic principle of the frequency modulation (FM) procedure is to make the frequency of a carrier signal analogous to the amplitude of the input data. With a sinusoidal input, the modulated signal, theoretically, looks like a sine wave which varies in frequency. Actually, the modulated signal looks like a square wave with varying width because FM signals are usually recorded at saturation.

The errors introduced by the tape recording could be summarised as variations in the speed at which the tape passes over the record or reproduction heads. These are called time base errors and may be either static or dynamic in character.

The first type is caused by changes in the dimensions of the tape due to temperature, humidity and tension. For commercial tapes this static time base error is of the order of 0.1 to 0.25%. In addition inter-channel static time base errors are caused by manufacturing tolerances on the angle at which the tape passes the heads and the position of the heads (tolerance from stack to stack as well as from head to head) on a given stack and the azimuth alignment. These errors are generally of the order of 0.001 inch and are therefore a function of tape speed. The dynamic type of time base error is flutter, which is the variation in tape velocity from the nominal. For the Racal type recorder the manufacturer's specification gives a value of 0.35% as the percentage of flutter at the highest tape speed of 60 in/sec.

Therefore, one can conclude from the above mentioned discussion that magnetic tape recording represents the most convenient recording facility for the data acquisition system and that the errors introduced by using such a procedure are quite negligible as compared with other sources of experimental errors.

TABLE (4-1) Abstract of Some Relevant Specifications of the Sangamo 3500 Tape Recorder (119)

Tape Speeds	60, 30, 15, 7.5, 3.75 and $1\frac{7}{8}$ in/sec
Input Sensitivity	0.1 to 2.5 volts r.m.s.
Nominal Input Level	± 1.4 volts peak
Nominal Input Impedance	100 K ohms resistive
Output Level (± 40% deviation)	± 1.4 volts peak, into 1000 ohms with short circuit protection (SCP)
Output Current (± 40% deviation)	± 3 milliamperes peak with SCP.
Output Impedance	Less than 50 ohms, unbalanced to ground with SCP
Bandwidth	DC to 20 KHz at 60 in/sec.
Signal/Noise Ratio	46 dB at 60 in/sec
Harmonic Distortion	< 1.5% total at all speeds

TABLE (4-2) Abstract of Some Relevant Specification of the Racal (Store 4) Tape Recorder (120)

Tape Speeds	60, 30, 15, 7.5 and 11/16 in/sec
Input Sensitivity	Selected by Input Attenuators in the following range: (peaks for full deviation) (± 20 volts, ± 10 volts, ± 5 volts, ± 2 volts, ± 1 volt, ± 0.5 volts, ± 0.2 volts and ± 0.1 volts)
Output Level	Continuously variable from 0 to ± 3 volts for full deviation
Bandwidth	DC to 20 KHz at 60 in/sec
Signal/Noise Ratio	48 dB at 60 in/sec
Harmonic Distortion	< 1% at maximum modulation level

4.1.5 Probes and Traverse Mechanisms

Measurements of gas velocities and turbulence characteristics were carried out in the present investigation at the spark plug location as well as at different locations in the combustion chamber. Fig. (4-10) shows a view of the cylinder head of the Ford engine where measurements were carried out at the spark plug location only, while Figs. (4-11a) and (4-11b) show two views of a cylinder head of the Rolls-Royce engine where measurements were carried out at the spark plug as well as at the different marked positions in Fig. (4-11a). For the latter case, the probes were traversed inside a number of brass tubes (3/16 inch diameter) fixed in the wall of the combustion chamber and sealed at the water jacket of the cylinder head.

The spark plug probe has two perpendicular sensing elements welded on the tips of steel needles, while only a single wire probe could be traversed inside the brass tubes.

For both engines the facilities of probe rotation about its own axis was required to enable detection of any consistent direction of gas flow during the different strokes of the engine cycle. Moreover, a traverse motion of the probe along its axis was required to enable investigations at different depths inside the combustion chamber. These facilities, together with the requirements of adequate sealing and an easy way of insertion and withdrawal without damaging the wires or removing the cylinder heads were satisfied by the construction of the traverse mechanisms shown in Figs.(4-12) and (4-13) for

the spark plug and the different locations inside the combustion chamber respectively. The probes are usually fixed on rigid steel brackets and mounted on the cylinder heads during measurements.

4.2 Data Preparation

4.2.1 Digitization of Mean Velocity and Pressure Traces

The recorded signal is usually reproduced at the same tape recording speed and is introduced to the ADC of a Hewlett Packard Fourier Analyser Model 5451A. Such an ADC has fixed sampling rates varying from 10 μ sec/sample to 2 m sec/sample as shown in Table (4-3). Therefore, a decision on the appropriate sampling rate that will reproduce the original signal accurately was selected on the basis of the required sample width along the engine cycle (crank angle degrees) rather than on an actual time basis which varies with engine speed. This means that a sampling interval in terms of crank angle has to be maintained constant as far as possible for the whole engine speed range under investigation. It has been found that a sample width between 2.5 and 4 degrees is quite sufficient for such purposes. Table (4-3) shows the variation of the number of samples per cycle and the sample size in crank angle degrees corresponding to each sampling rate setting on the ADC for various engine speeds.

TABLE (4-3) Number of Samples and Sample Size at Different Engine Speeds & Different Sampling Rates

SAMPLING RATE μ SEC/SAMPLE	MAX. FREQUENCY	ENGINE SPEED (R.P.M)											
		1000		1500		2000		2500		3000		3500	
		NP*	SS**	NP	SS	NP	SS	NP	SS	NP	SS	NP	SS
1000	500 Hz	120	6	80	9	60	12	48	15	40	18	34	21.1
500	1 KHz	240	3	160	4.5	120	6.0	96	7.5	80	9.0	69	10.42
200	2.5 KHz	600	1.2	400	1.8	300	2.4	240	3.0	200	3.6	172	4.185
100	5 KHz	1200	0.6	800	0.9	600	1.2	480	1.5	400	1.8	340	2.11
50	10 KHz	2400	0.3	1600	0.45	1200	0.6	960	0.75	800	0.9	686	1.048

* NP is the number of samples per engine cycle (the nearest integer number).

** SS is the sample size in crank angle degrees.

The digitized data of recorded signals are usually obtained on paper tapes. Such tapes are produced in incompatible format with the input format to ICL computers. Therefore, an intermediate step is required for such a transfer process and is carried out by a FORTRAN program called DIGITIZATION AND CALIBRATION. A list of such a program together with the input-output formats are given in Appendix B1 . The output of this program could be stored on either magnetic tape or cards for further use by other data analysis programs. Such a program takes into account the scale factors introduced by the ADC and the final stored information represents therefore the actual values of the recorded signals on the tape recorder.

4.2.2. Calibration of the Digitized Data

The term calibration has two distinct meanings when applied to the digitized data. First, of course, is the actual laboratory calibration made of the instrument. This includes calibration of the hot wire and pressure transducer and is discussed in the description of each instrument, Sections (3.2.1) and (4.1.3).

The second use of the term calibration refers to the complete conversion process from digital counts to physical units and is thus an electrical-electronic calibration which accounts for any operation carried out on the signal before recording such as biasing some DC level or attenuating the whole signal level.

4.2.3 Calibration of Recorded Signals

The limitation on the input levels to some tape recorders together with the requirements of keeping the signal to noise ratio of recorded and reproduced signals as high as possible, necessitates some conditioning of the raw signals before recording. This conditioning process includes attenuation processes and in some cases biasing some DC level from the signal.

A calibration process is, therefore, necessary to retain the recorded signals to their actual values at the output of the instruments. This was carried out by introducing a number of known D.C. voltages to the electronic conditioning circuit and the tape recorder at the same points where the actual physical signals are normally introduced in the actual experiment.

A simple conversion relation could be used, therefore, as given by

$$E_{actual} = E_o + K\ (E_{recorded}) \qquad 4\text{-}1$$

where E_o is the biased DC voltage

K is the attenuation factor

E_{actual} is the actual value of the measured signal

$E_{recorded}$ is the recorded signals on the tape.

The biased DC voltage and attenuation factor in equation (4-1) could be obtained from the known values of the calibration signals and the corresponding digitized values from the ADC.

A special case of equation (4-1) when attenuation processes only are carried out, the value of E_o equals zero. In the latter case, where no biasing processes are involved, such as the case of recording a filtered turbulence signal, another calibration procedure could be used when a number of AC signals of accurately known amplitudes could take the place of the DC voltages mentioned earlier. These AC signals are introduced at the same output terminals of the instruments and recorded on the tapes. Attenuation factors could be calculated, therefore, by comparing the actual and digitized (recorded) amplitudes of the calibration signals.

4.2.4 Preparation of Turbulence Signals

Preliminary analysis of turbulence signals for the Rolls-Royce engine, as well as all the published investigations on turbulence measurements in S.I. engines (22), (24) have shown that most of the fluid energy is contained in the frequency range below 6 KHz, especially during the compression stroke. On the other hand, the requirements of obtaining turbulence signals that represent only the fluctuations of flow velocity without any contributions of mean velocity signals, which are known to suffer large cyclic variations, necessitates the

application of a high pass filtering of the raw anemometer signal to get rid of the mean velocity trace Fig. (4-3b). The limits of the minimum filtering frequency will increase at higher engine speeds because of the shortening of the time occupied by the whole engine cycle and correspondingly the increase of the frequency of the mean velocity trace itself.

It is also known from sampling theory (118) that at least two samples per cycle are required to define a frequency component in the original data. Hence, the highest frequency which can be defined by sampling the data at time intervals Δt (seconds/sample) is $1/2\,\Delta t$ cycles per second which is called the cut off frequency or the Nyquist frequency or folding frequency.

$$n_{max} = \frac{1}{2\Delta t} \qquad (4\text{-}2)$$

Frequencies in the original data above n_{max} (CPS) will be folded back into the frequency range from 0 to n_{max} (CPS), and be confused with data in this lower range Fig. (4-14). This problem is called "aliasing" and is inherent in all digital processing which is preceded by an analog to digital conversion. Its spectral effect is to fold back the spectrum about the Nyquist frequency n_{max} as shown in Fig. (4-15). Thus a first requirement for digital analysis is to sample at a high enough rate so that all frequencies of interest are identified properly.

In practice, one will usually wish to maximise (Δt) so that computing time is minimised. Nevertheless, a selection of n_{max} to be $1\frac{1}{2}$ or 2 times the maximum anticipated frequency in the signal is quite sufficient to overcome this problem. Another way for handling the aliasing problem is to low pass filter the analog signal before sampling. The cut off frequency of the filter is usually chosen to be slightly less than the folding frequency.

With these experiments in mind, a sampling rate of 50 μ sec per sample was employed in the digitization of the turbulence signal. This corresponds to a cut off frequency of 10 KHz. Also, to eliminate any contribution of spurious noise picked up at any stage of the data collection, a low pass filter was used and set at a maximum of 10 KHz. The DISA signal conditioner unit Type 55 D26 was used for this purpose.

The tape recorder speed was selected to be 60 in/sec which enables recording of frequencies up to 20 KHz and the signals were reproduced at the same tape speed.

The digitized data was stored in a data block of the Hewlett Packard Fourier Analyser for further spectral analysis. Such data blocks are of variable size with a maximum storage capacity of two blocks of 4096 samples. Other block sizes are multiples of 2^n starting from 2^6 (64).

The triggering of the ADC was actuated from the recorded triggering pulse (timing mark) which occurs at TDC on the induction stroke of the reference cylinder. For cylinders other than the reference one, the firing order was used to account for the shift of the fixed timing mark relative to actual TDC induction of each particular cylinder.

a) Data Preparation for Multiple Records

A sampling procedure is employed in this technique which enables the construction of a continuous data record at a specified crank angle on the engine cycle from isolated samples extracted from consecutive cycles. These samples have a specified width (e.g. 10° of crank angles) and consists, therefore, of a number of digitized samples as governed by the sampling rate of the ADC. We shall call the first one "cycle sample" to differentiate between it and the fixed sample intervals of the ADC. Each extracted cycle sample is joined to the previously assembled ones and the whole record is shifted by a certain time interval equal to the cycle sample to enable the addition of a new cycle sample and so on until the whole data block is filled and then spectrum analysis is carried out. The number of cycles analysed (assembled cycle samples) varies with the specified width of the cycle sample, the size of the data block selected for the Fourier Analyser, and according to the engine speed as shown in Table (4-4).

TABLE (4-4) Variation of Number of Samples and the Maximum Number of Cycles Analysed with the Width of Cycle Sample ($\Delta\theta$).

(Sampling Rate of ADC = 50 μ sec, Data Block Size = 4096 samples)

Engine Speed r.p.m.	Number of Samples per Engine Cycle	Sampling Intervals Crank Angle Degrees	Number of Samples per Cycle Samples			Maximum Number of Cycles Analysed		
	NC		$\Delta\theta = 6^o$	$\Delta\theta = 10^o$	$\Delta\theta = 20^o$	$\Delta\theta = 6^o$	$\Delta\theta = 10^o$	$\Delta\theta = 20^o$
600	4000	0.18	33	56	112	124	73	36
1000	2400	0.3	20	33	66	205	124	62
1200	2000	0.36	17	28	56	246	148	74
1500	1600	0.45	13	22	44	308	184	92
2000	1200	0.6	10	17	34	404	245	123
2500	960	0.75	8	13	36	512	304	152
3000	800	0.9	6	11	22	682	368	184

The width of the cycle sample was chosen, in the present work, to be 10 crank angle degrees, since the auto-correlation function was always found to decay to zero in this period. A similar observation was reported by Barton (11) as well as a re-analysis of Barton's data by Winsor (23). However, a check on the suitability of such a sampling interval was carried out by analysing turbulence signals at some crank angles in the cycle for two different widths of cycle sample namely 10 and 20 degrees. The power spectrum function as well as the auto-correlation coefficients have shown almost identical values Figs. (4-16a) and (4-16b).

A possibility of better utilisation of the computing time could be achieved by simultaneous analysis of the data at more than one crank angle. Typical examples of these programs are given in appendix B2. However, this results in a reduction of the number of cycles analysed at each crank angle (length of data record) at lower engine speeds (e.g. below 1000 r.p.m.) due to the reduction of the data block size. The Fourier Analyser, used in the present investigation, has a maximum storage capacity of two data blocks of 4096 samples. The next step in the size of data blocks is 2048 samples which resulted in storing only half the number of cycles of the first case. Therefore, it is a matter of compromise between the length of the data record required, the specified crank angle width and the expense of computing time.

b) Data Preparation for Individual Records

The study of the problem of cyclic variations in the characteristic parameters of the turbulence field during the compression stroke and especially at the time of ignition necessitate analysing individual engine cycles rather than the averaging procedure employed before. However, for both cases the preparation procedure of the turbulence data remains the same with the exception that after isolating and storing the signal for a large number of cycles at the crank angle of interest a process of analysis is carried out. This continuous record is analysed into its constituent parts and individual cycles are stored separately in an intermediate storage facility (such as numeric magnetic tape or paper tape).

After this stage a process of introducing only one cycle sample at a time to the Fourier Analyser after reducing the data block to an appropriate value prepares individual records for spectral analysis.

4.3 Data Qualification

(Basic assumptions about the structure of the turbulent field).

In the preceding method of analysis of turbulence signals at any particular crank angle (with a record length $\Delta\theta$), some assumptions were made about the characteristics of the signal.

These assumptions are made to permit the application of conventional techniques of analysis used for similar random data or even for turbulence data under steady state conditions. It also helps to reduce the amount of experimental work involved in the investigation. Nevertheless, the validity of these assumptions could be tested by suitable techniques and is discussed below.

The basic assumptions employed in this investigation can be summarised as follows:

i) Data records constructed from individual records of consecutive engine cycles are stationary and ergodic and represent therefore the average characteristics of the turbulence conditions.

ii) The turbulence field, especially during the compression stroke, is isotropic and homogeneous.

iii) The turbulence energy of the flow is distributed over the whole frequency range from the lowest to the highest limits. Therefore, the appearance of peculiar periodic components at any particular frequency represents spurious signals and should be rejected.

4.3.1 Stationarity and Ergodicity of the Data

In the following analysis of turbulence signals at a particular crank angle along the engine cycle, some assumptions have to be made about the characteristics of the signal.

The first assumption implies that the process is 'stationary' which means that the properties of the signal can be described at any instant in time by computing average values over the collection of data records (time histories of the signal observed over a finite time interval) which describes this random process Fig. (4-17). When a single time history record is referred to as being stationary, it is generally meant that the properties computed over short time intervals do not vary significantly from one interval to the next. The word 'significantly' is used here to mean that observed variations are greater than would be expected due to normal statistical sampling variations. For example, if the mean square value or the auto-correlation function of a single sample record $u_K(t)$ obtained from the Kth sample record of a random process $u(t)$ are obtained by time averaging over a short interval T with a starting time t_1, does not vary 'significantly' as the starting time t_1 varies, the sample record is said to be stationary. The same argument is applicable if the averaging processes are carried out over "ensemble" records at time t_1, rather than on single sample records. For the first case we have:

$$\overline{u^2}\,(t_1, K) = \frac{1}{T}\int_{t_1}^{t_1+T} u_K^2(t)\,dt \quad . \qquad (4\text{-}3)$$

and

$$R_t\,(t_1, t_1+\tau, K) = \frac{1}{T}\int_{t_1}^{t_1+T} u_K(t)\;u_K\,(t+\tau)\,dt \qquad (4\text{-}4)$$

While, for the later one we have

$$\bar{u}^2\,(t_1) = \lim_{N\to\infty}\frac{1}{N}\sum_{K=1}^{N}\left[\,u_K^2\,(t_1)\right] \qquad (4\text{-}5)$$

and

$$R_t\,(t_1, t_1+\tau) = \lim_{N\to\infty}\frac{1}{N}\sum_{K=1}^{N}\left[u_K(t_1)\;u_K(t_1+\tau)\right] \qquad (4\text{-}6$$

The second assumption is that the process is 'ergodic' which means that the time average values of the statistical properties of the signals (e.g. mean square value, auto-correlation function..... etc) for any sample record are equal to the corresponding ensemble averaged values. This means that the expressions given in equation (4-3) and (4-5) are equal and similarly equations (4-4) and (4-6).

Examination of the turbulence signal during an engine cycle, Fig. (4-3b) reveals that such a signal is basically a "non-stationary" process because of its transient nature, where the statistical characteristics are, continuously changing with time. A totally adequate methodology does not exist as yet for the analysis of such non-stationary data. However, because our major concern in investigation of physical phenomenon in S.I.

engines is concentrated on the characteristics of such phenomenon at particular times of interest, approximations to stationary processes could be assumed and experimentally checked. For example, a study of cyclic combustion variation concentrates only on the characteristics of the mixture at the time of ignition and during a short period of time after that, compared with engine cycle. This represents the interval of time required for the development of the flame kernel into a steady flame front.

Therefore, a logical approach to the problem is to apply a sampling procedure which extracts the signal under consideration during a small sample width of crank angles from individual cycles and to use these sample records to establish a stationary record of ensemble data. If such a continuous record satisfies the assumptions stated above, (stationarity and ergodicity) analysis by usual methods used for stationary data can be carried out.

4.3.2 Test for Stationarity

It has been shown by Townsend that the probability density distribution of the fluctuating velocity component in an isotropic flow field follows approximately normal distribution. It is better to avoid any assumptions on the specific distribution function of the collected turbulence signal in the engine while running tests on its stationarity and confidence limits. This process could be carried out using what are called "distribution free" or non-parametric procedures.

One of the best known distribution free procedures used for data evaluation techniques is the "run test" (118). To conduct a test on individual sample records to ascertain the stationarity of data, the following assumptions are needed. Firstly, it must be assumed that any given sample record will probably reflect the non-stationarity character of the signal. Secondly, it must be assumed that any given sample record is very long compared to the lowest frequency component in the data. It is also convenient (but not necessary) to further assume that any non-stationarity of interest will be revealed by time trends in the mean square value of the data. The procedure for running this test could be summarised as follows:

1. Individual records from each cycle are extracted from consecutive cycles, in the same way used in Section 4.2.3.

   The mean square value for each cycle sample is determined from the value of auto-correlation ($R_t(0)$) at $\tau = 0$ and these values are aligned in time sequence, with the first cycle sample denoted by (1), the second by (2) and so on..... , until the Nth cycle sample, as follows:

$$\overline{u_1^2}\ ,\ \overline{u_2^2}\ ,\ \overline{u_3^2}\ ,\ \ldots\ldots\ \overline{u_n^2}$$

or

$$R_1\ (0)\ ,\ R_2\ (0)\ ,\ R_3\ (0)\ \ldots\ R_N\ (0)$$

3. The cycle samples mean square values are then classified into one of two mutually exclusive categories which may be identified simply by plus (+) or minus (-). This is carried out by comparing their values with a mean value $\overline{u_m^2}$, calculated over the N cycles, where $\overline{u_1^2} > \overline{u_m^2}$ (+) or $\overline{u_1^2} < \overline{u_m^2}$ (-).

The sequence of plus and minus values might be as follows:

++	-	++	---	+	--	+++	---	++	--	++ -
1	2	3	4	5	6	7	8	9	10	11

A run is defined as a sequence of identical signs that is followed and preceded by a different sign or no sign at all. In the previous example the number of runs is 11 in the sequence of N = 23 cycle samples.

Now, we hypothesised that the sequence of sample mean square values ($\overline{u_1^2}$, $\overline{u_2^2}$.... $\overline{u_N^2}$) are each independent sample values of a random variable with a mean square value of $\overline{u_m^2}$. If the hypothesis is true, the variations in the sequence of sample values will be random and display no trends. Hence the number of runs in the sequence relative to the median value, will be as expected for a sequence of independent random observations of the random variable u(t) as presented in standard tables of the (100α) percentage points for the distribution function of runs, where α is any desired level of significance. If the number of runs is significantly different

from the expected numbers in such tests, the hypothesis of stationarity would be rejected, otherwise, the hypothesis would be accepted.

Applications of such a test on typical sets of data for the Rolls-Royce and the Ford engines have been carried out at different crank angles in the engine cycle. Table (4-5) shows the number of runs observed in the sequence of the root mean square value of the signal relative to the median. While Table (4-6) shows the standard values of the number of runs at various levels of significance (α). A comparison between the experimental data and the standard values indicates that the hypothesis of stationarity is accepted at the different significance levels. For example, at a significance level of 0.975, the number of runs should be between 22 and 39 and the experimental data are always between these two limits. Fig. (4-18) shows a typical graph of the fluctuating velocity component over 60 cycles for a test on the Rolls-Royce engine.

TABLE (4-5) Application of the "Run Test" for Stationarity on Typical Engine Tests over 60 Consecutive Cycles

Engine Type	Engine Speed	Throttle Setting	Intake System	Crank Angle (degrees)	Number of Runs
ROLLS-ROYCE	1000	Fully Opened (Intake Vacuo 0.5 in Hg)	Plain Valve	320 340 360	25 28 26
			Inlet Valve Fitted with 8 Vanes	300 320 330 340 350 360	30 28 27 28 33 27
FORD	1000	Intake Vacuo 4 in Hg	Plain Valve		30
			Inlet Valve Fitted with 4 Vanes	350	33
		Intake Vacuo 11.1 in Hg	Plain Valve	)	34
			Inlet Valve Fitted with 4 Vanes	) 350	27

TABLE (4-6) Percentage Points of Run Distribution (118)

Number of Individual Data Records	Significance Level (α)					
	0.99	0.975	0.95	0.05	0.025	0.01
60	21	22	24	37	39	40

4.3.3 Isotropy and Homogeneity of Turbulence

A great simplification in the study of turbulence is introduced through the assumption of isotropy. This means that the mean value of any function of the fluctuating velocity components and their space derivatives is unaltered by any rotation or reflection of the axis of reference. This may be expressed by

$$\overline{u^2} = \overline{v^2} = \overline{w^2} \tag{4-7}$$

where u, v, w are the instantaneous values of the fluctuating velocity components in the x, y, and z directions respectively.

Isotropy also means that the fluctuations are perfectly random with the result that there is no correlation between components of the fluctuations in different directions, i.e.

$$\overline{uv} = \overline{vw} = \overline{uw} = 0 \tag{4-8}$$

The assumption of isotropy is not far from reality because of the experimental evidence that the fine structure of most actual nonisotropic turbulence flow is nearly istropic (local isotropy). This hypothesis was first introduced by Kolmogoroff (89) in 1901, as discussed in (3.4.2), where the motion of large eddies are assumed to produce smaller eddies, which in turn produces yet smaller eddies. The process continues

to the smallest eddies. From the standpoint of energy dissipation, it is postulated that the larger eddies lose their energy in forming smaller eddies and that in the process very little energy is dissipated as heat. The motion of the smallest eddies is steady and almost all their energy is dissipated as heat because of the molecular viscosity of the fluid. Thus it is seen that the energy dissipated by the turbulent flow is dissipated mostly by smaller eddies. Kolmogoroff also states that, although large eddies of turbulent flow may be nonisotropic, the smaller eddies are isotropic, so most of the energy is thus dissipated in turbulence which is isotropic. Hence, many features of isotropic turbulence may apply to phenomena in actual turbulence that are determined mainly by the fine scale structure, where local isotropy prevails.

This assumption could be tested by analysing the turbulence signals collected from the hot wire anemometer at different orientations and under constant engine operating conditions as shown in Fig. (4-19).

Homogeneity in turbulence means that the statistical characteristics of turbulence are invariant for any translation in the space occupied by the fluid. Batchelor (122) put the following argument for a grid produced turbulence, that "although the random motion dies away with distance from the grid, and to that extent is not statistically homogeneous, but the rate of decay is so small that the assumption of

homogeneity of the turbulence is valid for most purposes." Such a condition is more likely to exist in an engine cylinder, especially during the compression stroke. In fact, a proof of the validity of the isotropic assumption means that the field is homogeneous, otherwise certain directions would be preferred by a lack of homogeneity.

4.4 Data Analysis

The data analysis procedure, employed in the present investigation could be divided into two main groups:

i) Analysis of Gas Mean Velocities.

ii) Analysis of the Fluctuating Velocity Components.

In each case the average characteristic parameters of the signals are evaluated as well as the extent of their cyclic variations.

4.4.1 Analysis of Gas Mean Velocities

The characteristics of the instantaneous turbulent gas velocities were examined statistically in terms of the following parameters:

i) Mean values of gas velocities at different crank angles in the engine cycle, as defined by:

$$\bar{U}_{\theta} = \frac{\sum_{i=1}^{NC} U_{(i,\,\theta)}}{NC} \qquad (4\text{-}9)$$

where the subscripts θ, i refers to the particular crank angle in the cycle (θ) and the cycle number respectively, and NC is the total number of cycles analysed.

ii) The standard deviation of instantaneous gas velocities at different crank angles in the engine cycle, as defined by

$$S(U_\theta) = \left[\frac{\sum_{i=1}^{NC} (U_{(i,\theta)} - \bar{U}_\theta)^2}{NC} \right]^{\frac{1}{2}} \qquad (4\text{-}10)$$

iii) The coefficient of variation, which represents the relative variation as given by

$$CVR = \frac{S(U_\theta)}{\bar{U}_\theta} \qquad (4\text{-}11)$$

iv) The range of variation in gas velocities at any particular crank angle, over the number of cycles analysed as given by

$$\text{Range of Variation} = (U_\theta)_{max} - (U_\theta)_{min} \qquad (4\text{-}12)$$

v) The relative range of variation as defined by

$$RRV = \left[(U_\theta)_{max} - (U_\theta)_{min} \right] / \bar{U}_\theta \qquad (4\text{-}13)$$

Tests on the frequency distribution of the instantaneous gas velocities at any particular crank angle were carried out in terms of the coefficient of 'SKEWNESS' and 'KURTOSIS' as defined in Appendix A2.

4.4.2 Analysis of the Fluctuating Velocity Components

The average characteristics of the turbulence signals (fluctuating velocity components) were evaluated from relatively long data records, constructed by the sampling procedure discussed in Section 4.2.3, while the extent of cyclic variations in the characteristics parameters of the signals were obtained by performing statistical analysis of individual data records for consecutive cycles.

1. Analysis of Multiple Data Records

As mentioned earlier, the original turbulence signal for a complete engine cycle is a non-stationary process. However, the sampling procedure at some particular crank angle and for a relatively short period of time provides a way of approximating the problem to a stationary one, at least during the small time intervals considered. Such approximation enables the application of statistical theory concepts for evaluating the characteristics of the turbulent field. Also, the use of relatively long records synthesised from a large number of cycles results in a good averaging process of the measured statistical parameters.

The procedure for analysing such data records could be summarised in the following steps:

i) Transformation of data to zero mean value.

ii) Calculation of auto-correlation function.

iii) Normalisation of auto-correlation function.

iv) Evaluation of the normalised power spectrum.

v) Evaluation of the time micro-scales and time macro-scales of turbulence.

vi) Running tests on the qualification of data.

vii) Preparing the data for individual records analysis.

i) Transformation of data to zero mean value

Although, the high pass filtering of the anemometer signal removes any DC level in the data in addition to the low frequency signal representing the mean trace, the sampling process itself could produce a fictitious DC level of the signal according to the location of the particular crank angle considered, Fig. (4-20). In addition, some ADCs have an offset DC level which could be detected in a Fourier transform of the data. Therefore, to avoid any bias of the data according to its time sequence (or location in the engine cycle) a transformation of the sampled data to zero mean value is necessary.

This could be carried out in one of two ways, either by obtaining the mean values and shifting the whole trace to a new level of zero mean or by obtaining the Fourier transform of the signal, recognising the DC component (zero frequency) and removing it. Both processes were employed in these analyses. However, the second one is preferred because the Fourier transform represents a step in the analysis for obtaining the 'raw' power spectrum or the auto-correlation function and therefore requires only one additional intermediate step of truncating the DC component. After transferring the data into a zero mean value the auto-correlation calculations follow. Figs. (4-21a) and (4-21b) show a typical engine synthesised turbulence trace (from 228 cycles) before and after the transformation to the zero mean levels, while Figs. (4-22a) and (4-22b) show their corresponding normalised histograms, where the shift (bias) of the probability distributions are quite clear. Figs. (4-23a) and (4-23b) show also the Fourier transform of the signal, in polar coordinates, before and after truncating the DC component.

ii) Auto-Correlation Function

The auto-correlation function could be obtained by two methods. The first method is the standard approach of estimating the correlation function by direct computation of average products among the sample data values, equation (4-14).

The second method is the roundabout approach of first computing a power spectrum by direct Fourier transform procedures and then computing the inverse Fourier transform of the power spectrum.

a) <u>Auto-correlation Estimates via Direct Computation</u>

$$R_r = R_t(r\tau) = \frac{1}{N-r} \sum_{n=1}^{N-r} u_n \, u_{n+r} \qquad (4\text{-}14)$$

$$(r = 0, 1, 2 \ldots m)$$

where

$T_m = T_{max} = m.\tau$ is the maximum time displacement corresponding to m time lags.

and $B_e = \frac{1}{T_m} = \frac{1}{m\tau}$ is the resolution bandwidth for the resulting power spectral density estimate.

b) <u>Auto-correlation Estimates via Fast Fourier Transforms</u>

$$R_t(\tau) = \int_0^{\infty} F(n) \cos 2\pi n \tau \, d n \qquad (4\text{-}81b)$$

Conversely

$$F(n) = 4 \int_{o}^{\infty} R_t (\tau) \cos 2\pi n \tau \, d\tau \qquad (4\text{-}82b)$$

$$= 2 \int_{-\infty}^{\infty} R_t (\tau) \cos 2\pi n \tau \, d\tau \qquad (4\text{-}82c)$$

$$= 2 \int_{-\infty}^{\infty} R_t (\tau) \, e^{-j2\pi n \tau} \, d\tau \qquad (4\text{-}82d)$$

The second method has proved to be from 5 to 100 times faster than the first depending on the maximum delay time (τ_{max}) desired. The available Hewlett Packard Fourier Analyser employs the second method and was, therefore, preferred in view of the time saving and the convenience of obtaining the complete spectral analysis of the data at once.

iii) Auto-Correlation Coefficient

The auto-correlation coefficient is obtained by normalising the auto-correlation function using equation (3-49).

$$R'_t (t) = \frac{\int_{o}^{T} (u_t \cdot u_{t+\tau}) \, d\tau}{\overline{u^2}} = \frac{R_t (\tau)}{\overline{u^2}} \qquad (3\text{-}49)$$

iv) Scales of Turbulence

The time micro-scale of turbulence (λ_t) is obtained by double differentiation of the auto-correlation coefficient applying equation (3-55).

$$\lambda_t^2 = -1/2 \left[\left(\frac{\partial^2 R'_t(\tau)}{\partial t^2} \right) \right]_{t=0} \tag{3-55}$$

On the other hand an integration process of the auto-correlation coefficient curve gives the macro-time scale as given by

$$L_t = \int_0^\infty R'_t(\tau)\, dt \tag{3-57}$$

For the latter case, the correlation curve was arbitrarily interrupted when it intersects the horizontal (time) axis because of its tendency to oscillate about such axis. Another approach to this problem of estimating (L_t) could be carried out by assuming some analytical expression to represent the auto-correlation coefficient curve such as a decaying exponential function (as proposed by Dryden and Skramstad (82)) or a Gaussian error function (as proposed by Frankiel (81) and Hinze (79)). Solving either equation (4-15) or (4-16) will result in the approximate value of the time macro-scale.

$$R'_t(\tau) = e^{-\tau/L_t} \quad \text{(exponential)} \tag{4-15}$$

$$R'_t(\tau) = e^{-\pi t^2/4L_t^2} \quad \text{(Gaussian Error)} \tag{4-16}$$

Neither equation is applicable of course at the points very near to the vortex of the curve or for points after long time delays where the curve starts to oscillate about the time axis. However the latter problem also exists for the integration procedure as mentioned earlier.

v) Normalised Power Spectrum Function

Finally, the normalised power spectrum function is obtained from the Fourier Transform of the auto-correlation coefficient curve as given by equations (3-82)

In fact it is physically impossible to compute the integral of equation (3-82) exactly from real data because only a finite rather than an infinite-length of the sample correlation function is available. For example if the maximum value of τ is T_m, then the power spectrum takes the form

$$F(n) = 4 \int_0^{T_m} R_t'(\tau) \cos 2\pi n \tau \, d\tau$$

$$= 2 \int_{-\infty}^{\infty} U_{T_m}(\tau) \, R_t'(\tau) \cos 2\pi n \tau \, d\tau \qquad (4\text{-}17)$$

where U_{T_m} is a simple "box-car function" shown in Fig. (4-24) and defined by:

$$U_{T_m}(\tau) = 0 \qquad T < -T_m$$

$$= 1 \qquad -T_m \leqslant T \leqslant T_m \qquad (4\text{-}18)$$

$$= 0 \qquad T_m < T$$

The Fourier transform of $U_{T_m}(\tau)$ is

$$U_{T_m}(n) = \int_{-\infty}^{\infty} U_{T_m}(\tau)\, e^{-j\,2\pi n \tau}\, d\tau$$

$$= 2\,T_m \sin \frac{2\pi n \tau}{2\pi n} \qquad (4\text{-}19)$$

$U_{T_m}(n)$ is called a "window function" and is an even function of n as shown in Fig. (4-25). It is also known from the convolution theory that if signals are multiplied together in time, their spectra are convoluted with one another in frequency.

Therefore the raw estimate of a true power spectral density function F(n) is the convolution of F(n) with the window function $U_{T_m}(n)$:

$$F'(n) = \int_{0}^{\infty} F(\alpha)\, U_{T_m}(n-\alpha)\, d\alpha \qquad (4\text{-}20)$$

The net effect of this convolution when computing an estimate $F'(n)$ at frequency n_0 is to move the main peak of the window function to n_0, then to multiply the true F(n) by the translated window function and finally to integrate over all frequencies Fig. (4-26). Hence, the box-car weighting causes "leakage" by spreading the main lobe of the true power spectral density function and by adding an infinite number of smaller side lobes because of the truncation of T_m. Half of these side lobes are negative, a most displeasing result since average power is positive by definition.

A number of ideas have been suggested to alleviate this problem by modifying the box-car function in the time domain (or by an equivalent operation in frequency domain) and by so doing, broaden the principle lobe of the window function in the frequency domain.

In fact, neither of these proposed windows could be employed in the present situation (turbulence analysis) where a wide spectrum of eddies of different frequencies exist, rather than a narrow spectrum centered at any particular frequency. Therefore, the rectangular window is applied, in the present work, on the auto-correlation coefficient curve. The width of such a window was taken equal to the cycle sample width in the time domain.

The auto-correlation coefficient was always found to decrease to zero and starts to oscillate within this period of time delay, as mentioned in (4.2.3). Fig. (4-27a) shows a typical auto-correlation coefficient curve for a maximum time delay (τ) of about 30 times the original sample width, while Fig. (4-27b) shows an expansion of the same curve for a maximum delay period of about 7.5 times the sample width.

Although the auto-correlation function is the inverse of the power spectrum, so that the determination of either one is sufficient, a much more clear description of the frequency composition of the signal could be obtained from the power spectrum function. For example, the percentage of energy content within any frequency bandwidth could be directly

obtained by integrating the area under the F (n) curve between the appropriate limits. Consequently, the same information about the mean square value of the signal could be obtained by integrating the whole area under the power spectrum curve (before normalisation).

The value of the time microscale could be obtained also from the normalised curve using equation (3-87).

Inspection of the power spectrum curve reveals if any periodic signals are picked up during any process of data collection which will appear as a sharp peak centred at some particular frequency in the spectrum curve, Fig. (4-28a).

Corruption of the signal by wide band noise could be detected also as shown in Fig. (4-28b). Typical power spectrum curves for auto-correlation functions represented by exponential curves and exponential cosines are, also shown in Figs. (4-28c) and (4-28d). These last two cases are very similar to the general shapes reported by other investigators for turbulence signals.

Fig. (4-29) shows the schematic flow chart of the different steps in the preparation of the turbulence signals, at a particular crank angle, as well as its spectral analysis.

2. Analysis of Individual Data Records

The main objective of such a type of analysis is to investigate the extent of cyclic variations in the statistical parameters of the turbulence field inside the combustion chamber of the engine.

The same technique for analysing multiple records is applied here with the exception that only one cycle at a time was used in the analysis.

Further statistical analysis of the data in terms of their variance, standard deviation and coefficient of variation are carried out for the various measured parameters (mean square value, micro-scale, turbulence intensity and eddy diffusivity).

Also, the analysis of these individual records enables running the test for the stationarity of multiple data records as discussed before. It provides also another check on the adequacy of the averaging processes involved in the multiple record analysis.

4.5 Programming of the Data Analysis Procedures

The Data Acquisition and Processing System, described in the preceding sections, employs a number of programs at different steps of the investigation procedure. Such programs are written, either in a machine code (for steps carried out on the Hewlett Packard Fourier Analyser) or in FORTRAN language (for steps carried out on the ICL Digital Computer).

A review of the complete procedure will show the different steps where programming is required. This could be summarised systematically as follows:

a) Calibration of the Hot Wire Anemometer.

This step requires the use of a calibration program called (VEL CALB (94)), which is fed from a set of experimental calibration curves at different operating temperatures and performs an iteration procedure to give the correct value of the wire's cold resistance (RC). This accounts for the observed discrepancy between measured and actual values of (RC) due to the Peltier effects resulting from the dissimilar materials used in the hot wire and the support prongs of the probe.

b) Recording of the Data Signals using an FM Recorder.

c) Digitization of the Signals using the ADC of the Hewlett Packard Fourier Analyser.

This step employs a straightforward instruction in machine code for introducing the reproduced signals to the ADC at the selected sampling rates and to produce the digitized output data on punched paper tapes.

d) Preparation of Turbulence Data.

This step consists of the first part of the SPECTRAL ANALYSIS program which is written in machine code. It is carried out in the same procedure for the analysis of either individual data records or multiple data records as discussed earlier. Its function is to isolate the turbulence signal at a particular crank angle during the engine cycle with a fixed sample width ($\Delta\theta$). The isolation procedure is continuously carried out during the replay of the data from the tape recorder and followed by a storing process in a data block of the Fourier Analyser. It ends when the number of extracted samples from consecutive cycles reaches the stated number in the program.

e) Spectral Analysis.

This step is carried out on the extracted data in step (d) for either individual data records or multiple data records. It is mainly concerned with the calculations of turbulence characteristics in terms of auto-correlation function, auto-correlation coefficient, micro-scale of turbulence and macro-scale of turbulence. A machine code program called SPECTRAL ANALYSIS is employed at this step. Different versions of this program are given in Appendix B2 for data analysis at a single and multiple crank angles in the engine cycle.

f) Formating, Scaling and Storing of Data.

The incompatibility between the output format from the ADC and the input format to the ICL computer makes an intermediate step necessary. This employs a FORTRAN program called DIGITIZATION AND CALIBRATION which reads the paper tapes produced in step (c), accounts for the scale factors on the ADC and any conditioning operations carried out on the recorded signals and finally reproduces the calibrated digitized signals on punched cards with a suitable format for the ICL computer manipulation. A listing of this program is given in Appendix B1.

g) Calculations of Mean Gas Velocities.

This step employs a FORTRAN program called VELOCITY PREDICTION which performs the following operations:

i) Calculations of instantaneous gas velocities for a number of consecutive cycles at different crank angles as determined by the sampling rates on the ADC. The mean values of gas velocities, over the number of analysed cycles are also carried out. The output results are obtained on the line printer for any number of cycles.

ii) Plotting of graphs showing the variations of gas velocities at different crank angles for individual engine cycles as well as the mean value over a number of cycles.

iii) Producing of the output results on punched cards for further statistical analysis of gas velocities. This step is made to meet the maximum storage capacity located by the ICL Computer for individual programs.

A listing of this program is given in Appendix B3.

h) Statistical Analysis of Gas Velocities.

This step employs FORTRAN program called STATISTICAL ANALYSIS, which is fed with the output data from step (g). It performs the following operations:

i) Calculations of the various statistical parameters of gas velocities at different crank angles in the engine cycle, e.g. mean value, standard deviation, the coefficient of variation, the range of variation and the relative range of variation. It will also carry out a test on the probability distribution of the samples (gas velocities) in terms of the values of the Skewness and Kurtosis.

ii) Plotting of the different parameters, calculated in step (i), versus crank angle during the cycle. A listing of this program is given in Appendix B4. while a discussion of the definitions of various statistical parameters is given in Appendix A2.

i) Turbulence Analysis.

This step consists of a complementary part of the spectral analysis discussed in step (e). The output data from step (e) is therefore fed into a FORTRAN program called "TURBULENCE ANALYSIS I" together with the calibration of the hot wire anemometer and the digitised data obtained in step (c) to give the following turbulence parameters:

i) Turbulence Intensities (Int).

ii) Fluctuating Velocity Components (u').

iii) Time Micro-scale of Turbulence (λ_t).

iv) Length Micro-scales of Turbulence (λ_x , λ_y).

v) Time Macro-scale of Turbulence (L_t).

vi) Length Macro-scales of Turbulence (L_x , L_y).

The calculated parameters at different crank angles in the engine cycle could also be plotted for any number of tests for comparison purposes.

A second program called "TURBULENCE ANALYSIS II" could also be used for plotting the auto-correlation coefficient, the second derivative curve of the auto-correlation coefficient and the power spectrum function. These data are usually obtained in digital form (on paper tapes) from the Hewlett Packard Fourier Analyser.

Listing of these programs are given in Appendices B5 and B6.

j) Cyclic Variations in Turbulence Parameters.

The analysis of individual data records provides a way of estimating the extent of cyclic variations in turbulence parameters which affects the propagation of the flame front inside the combustion chamber. This step is carried out in the same procedure as for multiple data records, step(h) with the exception of using individual cycle data, instead of the averaging process over the very large numbers of cycles. This also provides a check on the stationarity of the data at different confidence limits and at various crank angles during the engine cycle as discussed in (4.3.2). The corresponding program for this step is called "TURBULENCE CYCLIC VARIATION" and is given in Appendix B7.

k) Correlation Between Turbulence Structure in Engines and in Pipe Flow.

This process is carried out to investigate the possibility of using the semi-empirical theories developed for pipe flow characteristics in engine investigations. Its main function is, therefore, to compare the measured characteristics of the turbulence field inside the combustion chamber with the predictions of pipe flow data for the observed mean velocity at the spark plug. The analytical equations for such a process is discussed in Chapter 7 and the corresponding program (called CORRELATION) is given in Appendix B8. The output data of such a program is usually obtained on the line printer and the graph plotter.

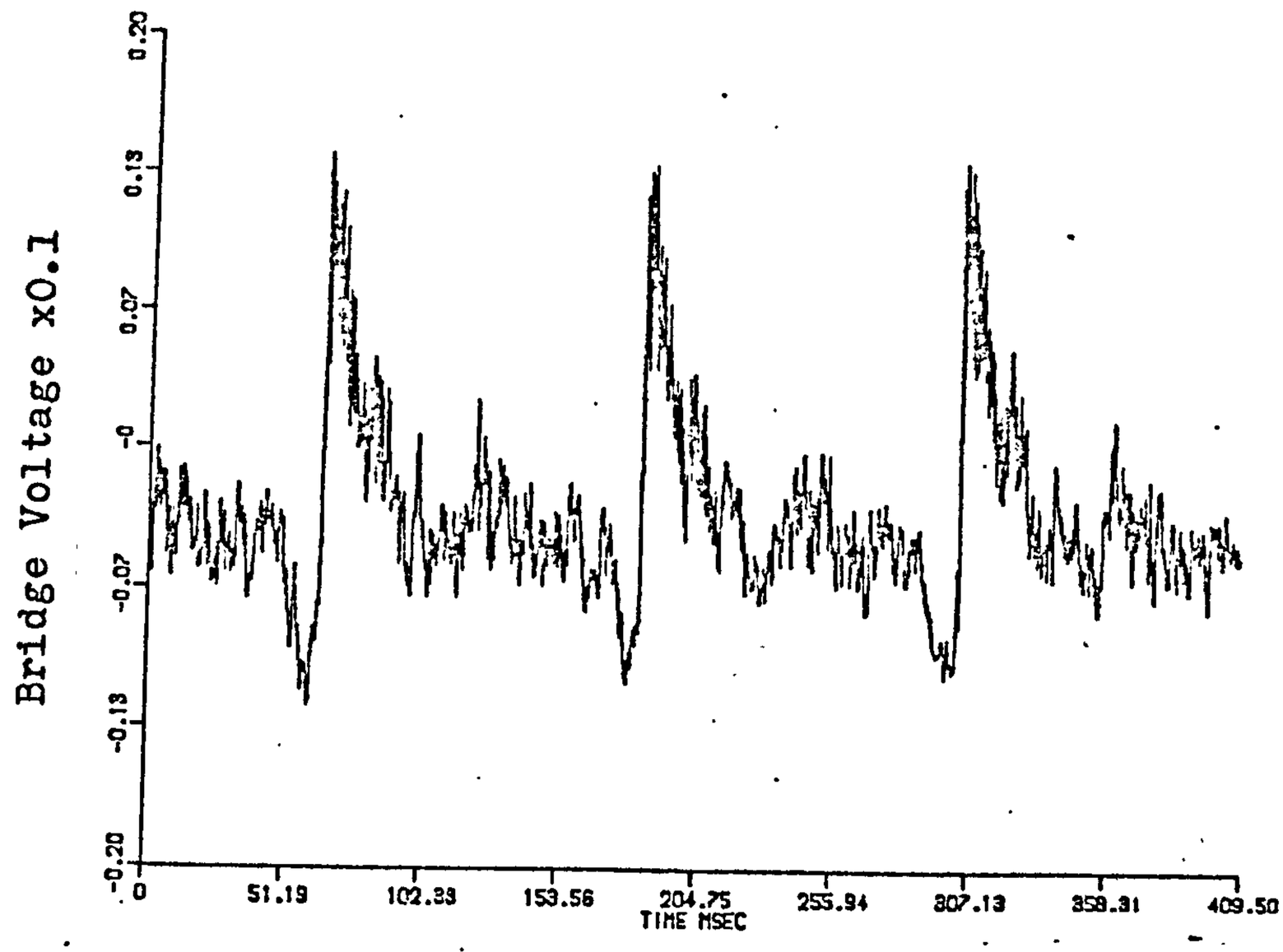

Fig.(4-3a) Instantaneous output signal of a hot wire anemometer in a S.I. engine. Data representing three consecutive cycles for a test on the Ford V4 engine at 1000 RPM.

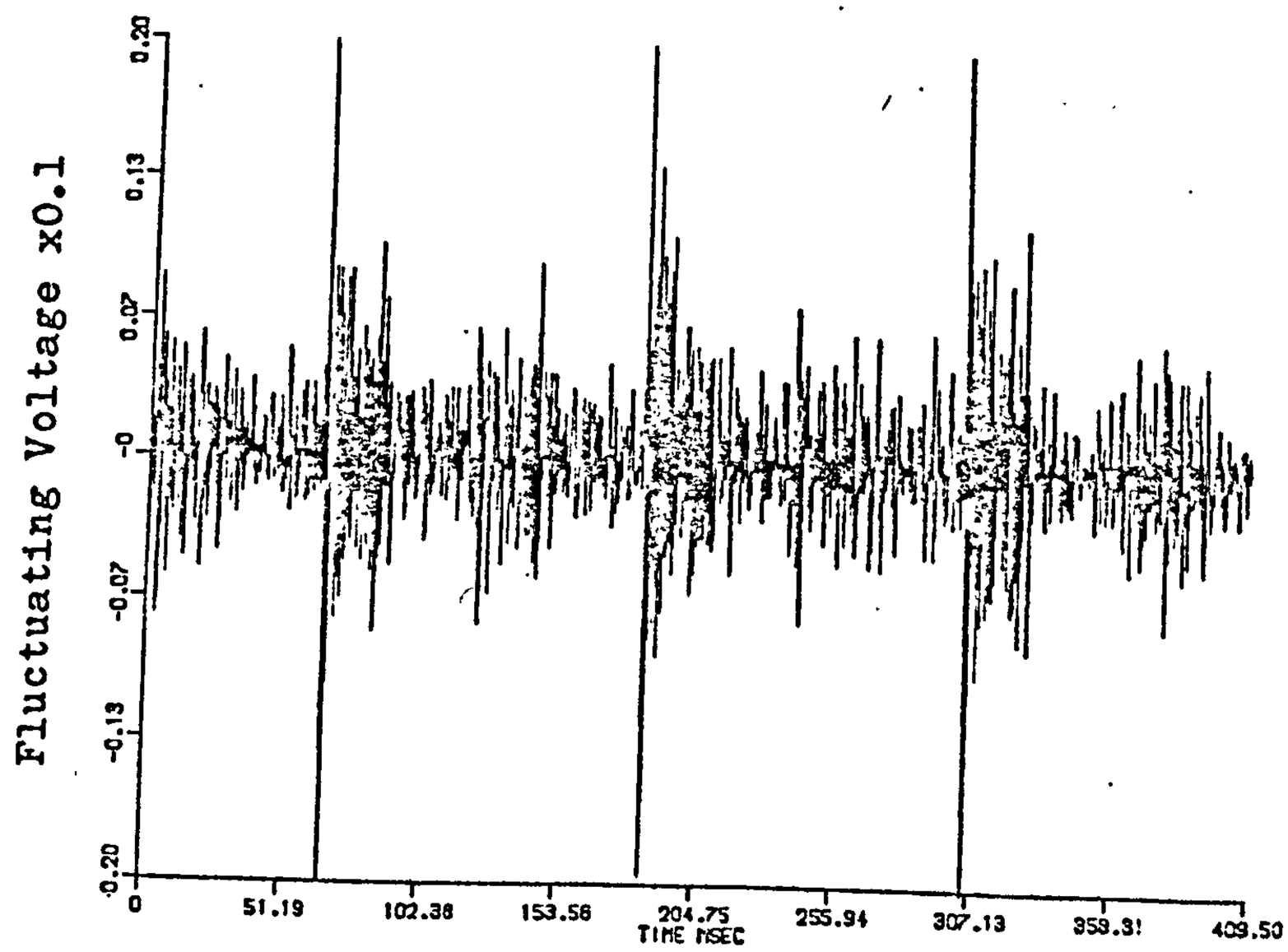

Fig (4-3b) Fluctuating voltage component of a hot wire anemometer in a S.I. engine,(Band pass filter 250HZ-10KHZ). Data correspond to the signal of fig (4-3a).

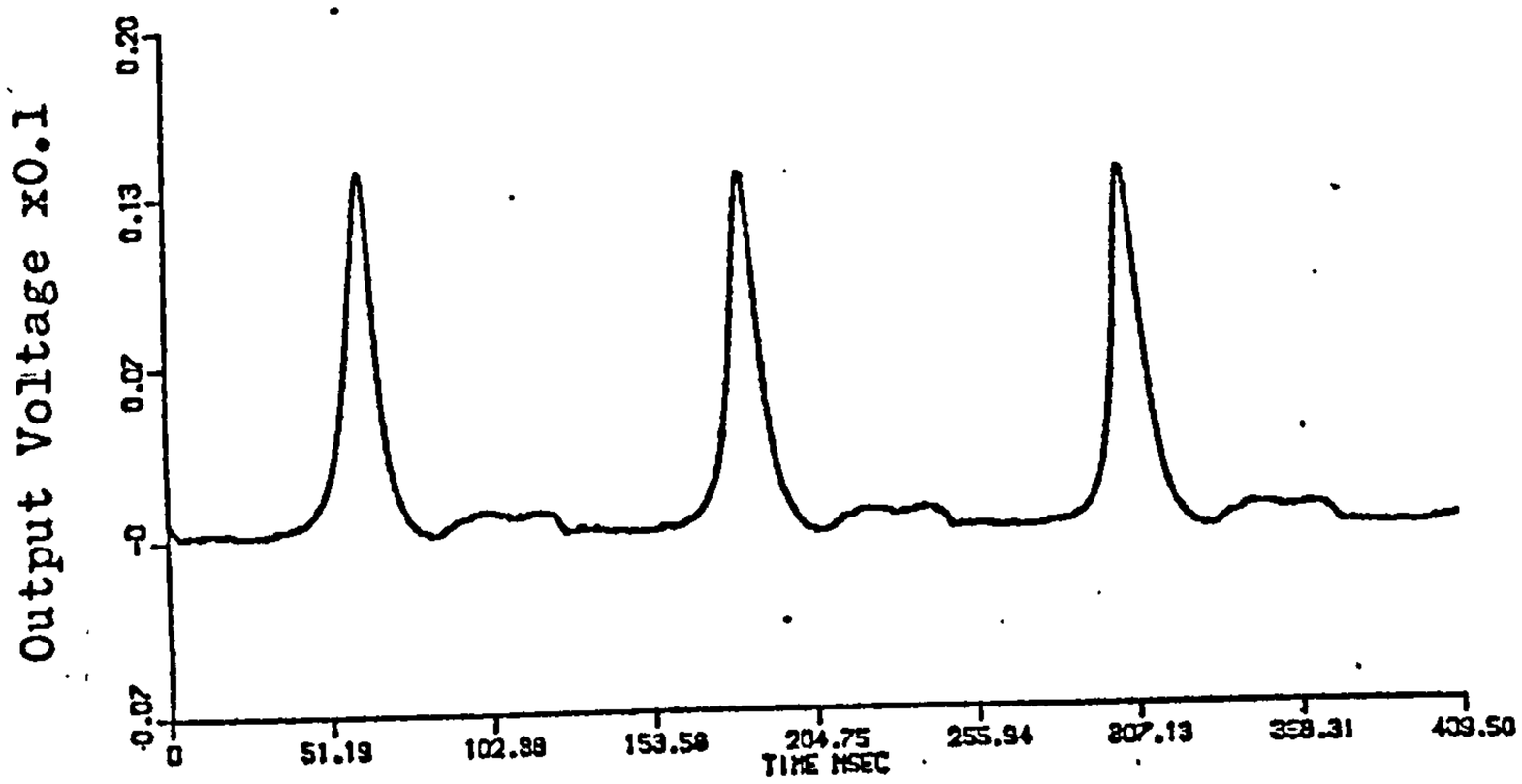

Fig (4-3c) Output signal of a pressure transducer for three consecutive cycles. Data for the same test conditions of fig (4-3a).

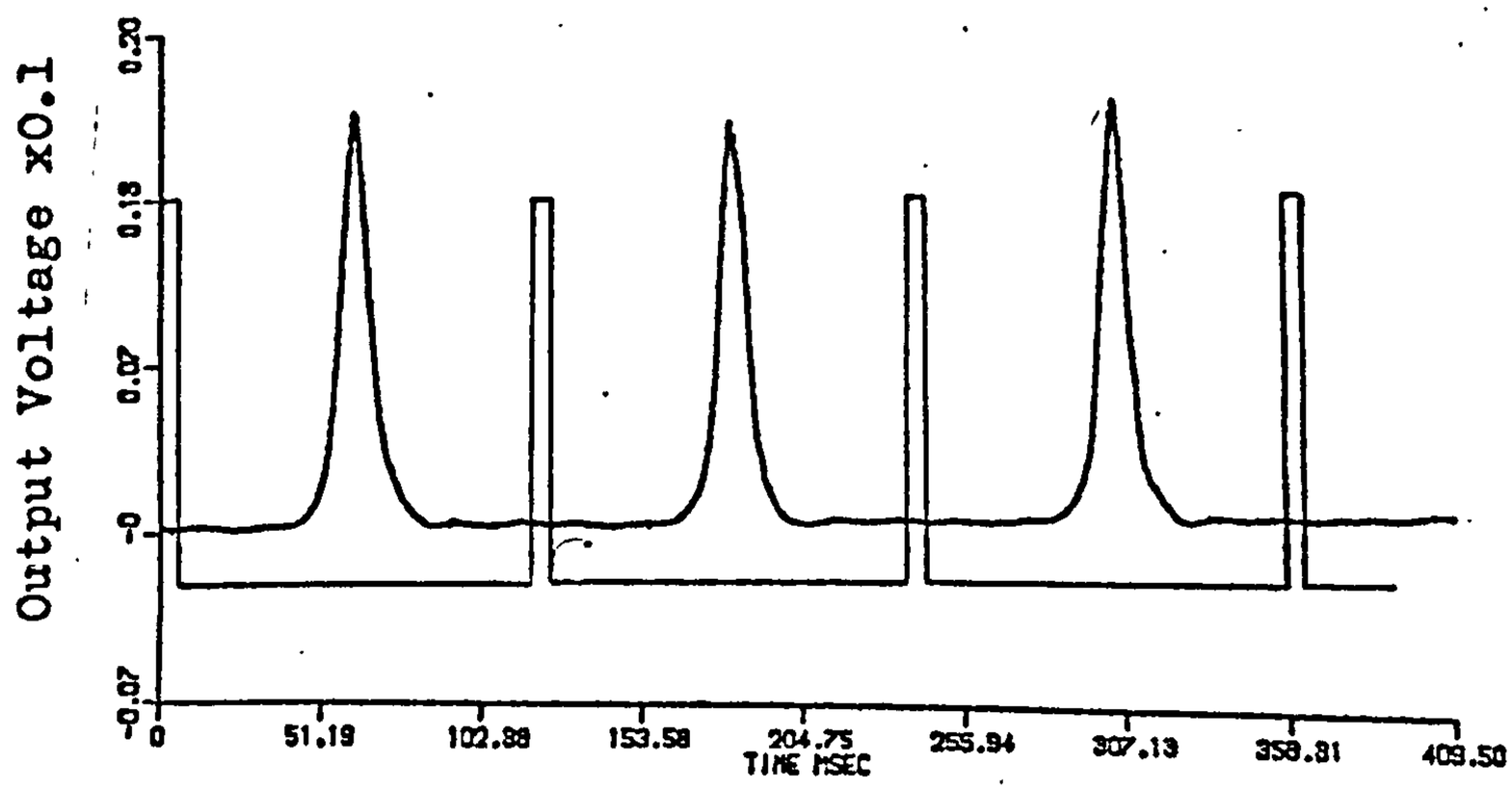

Fig (4-3d) Output signals of the timing mark and a resistance thermometer for three consecutive cycles. Data for the same test conditions of fig (4-3a)

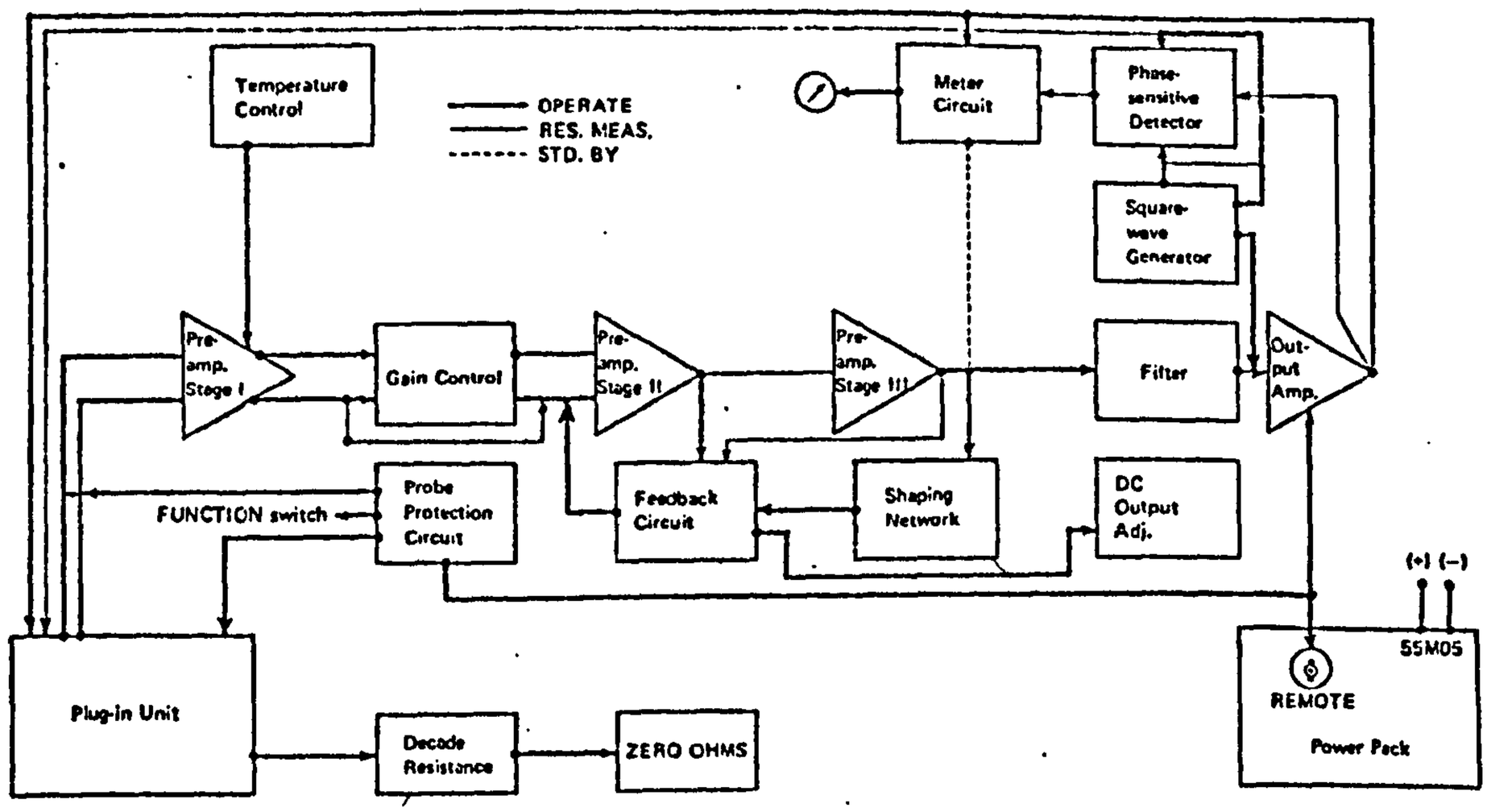

Fig (4-4) Simplified diagram of a constant temperature anemometer.

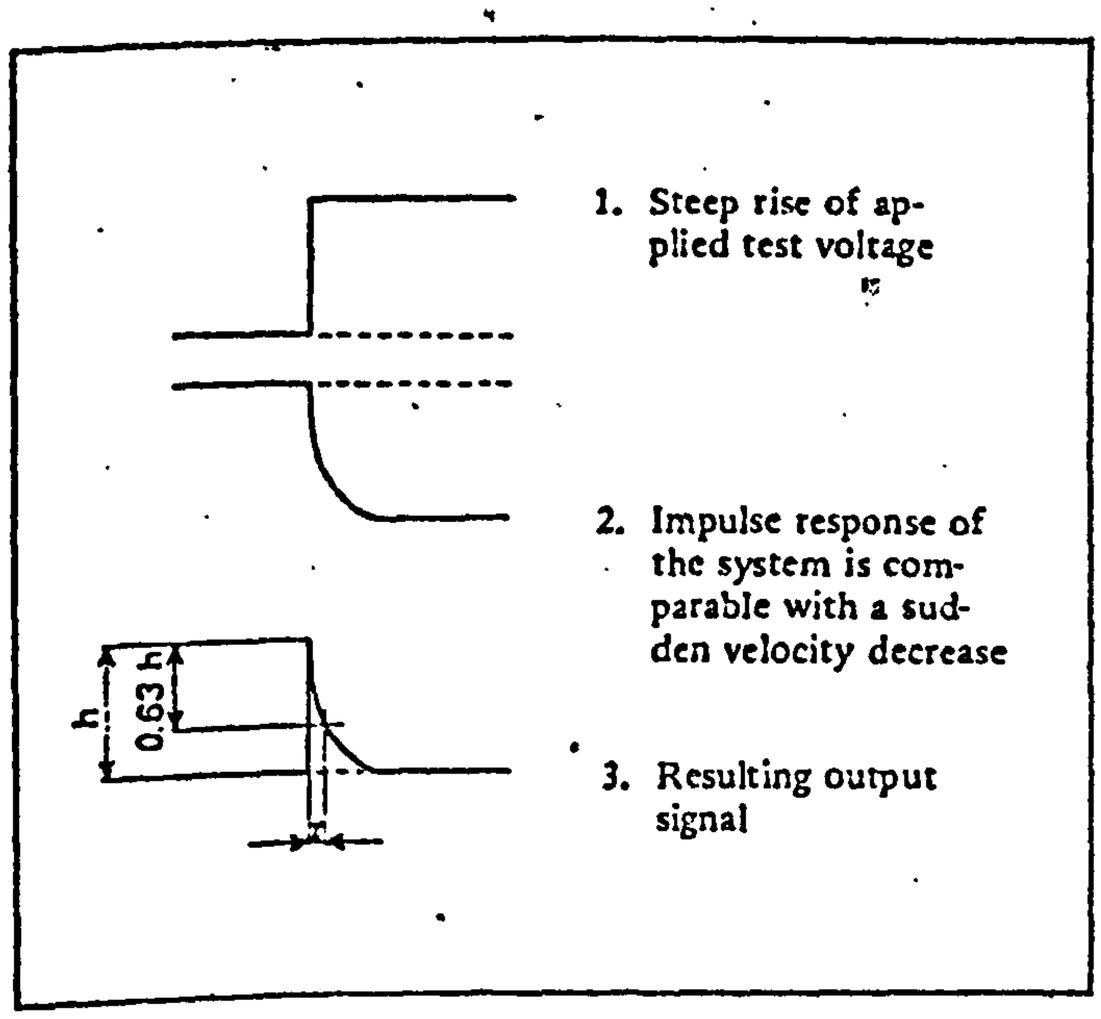

Fig (4-5) Response signal of a constant temperature anemometer to square wave impulse.

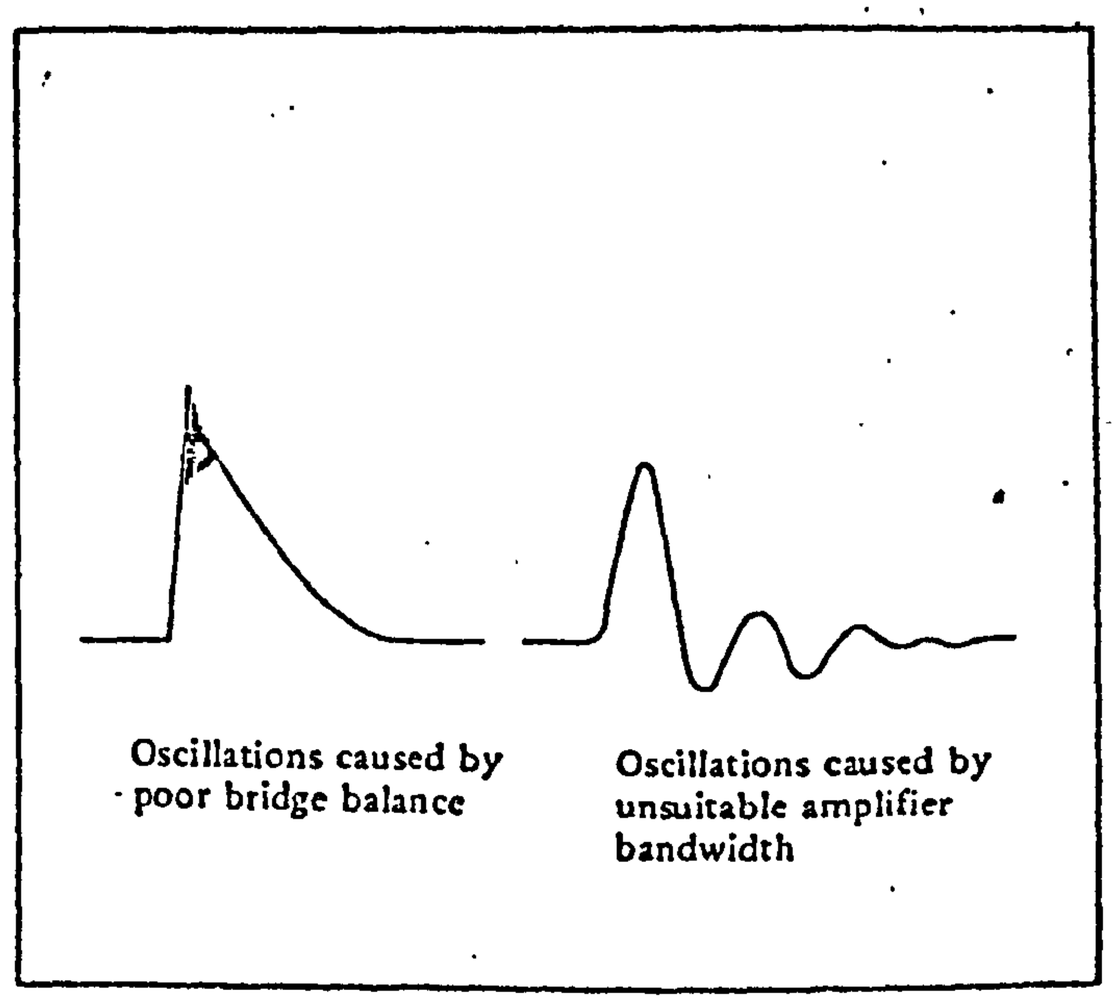

Fig (4-6) Adjustment of the frequency response of a constant temperature anemometer.

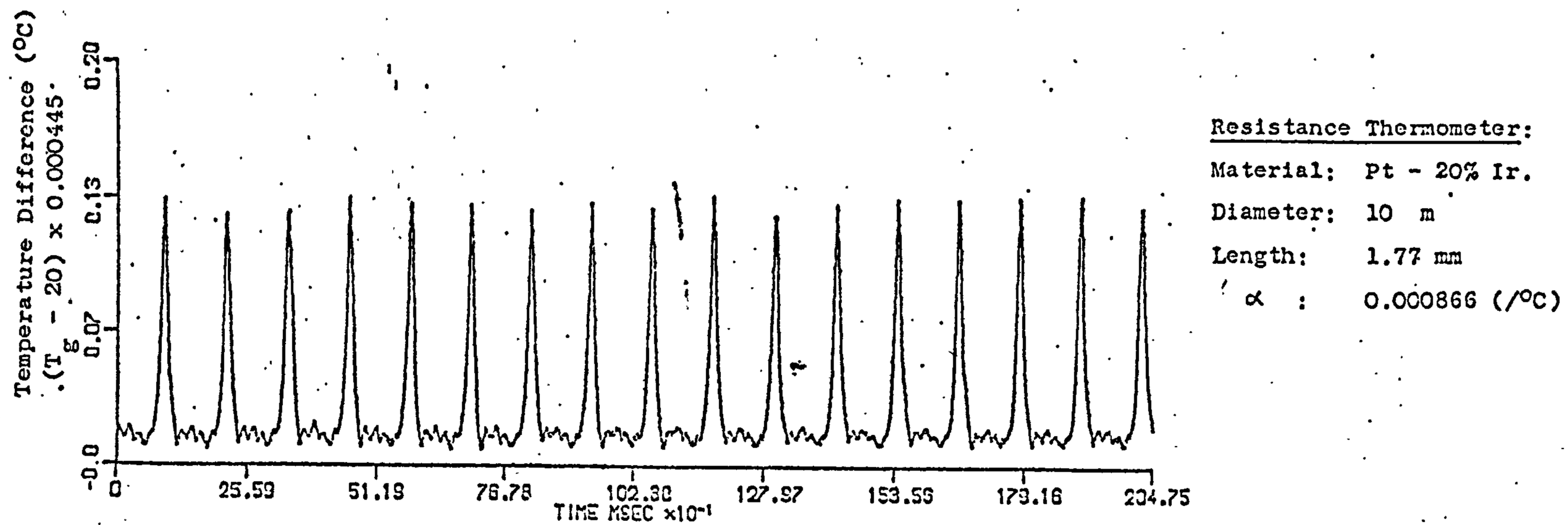

Fig. (4-7) Output Signal of a Resistance Thermometer in a S.I. Engine for 17 Consecutive Cycles showing Repeatable Temperature Traces. (Ford V4 Engine at 1000 RPM and 4 Inches Intake Vacuum).

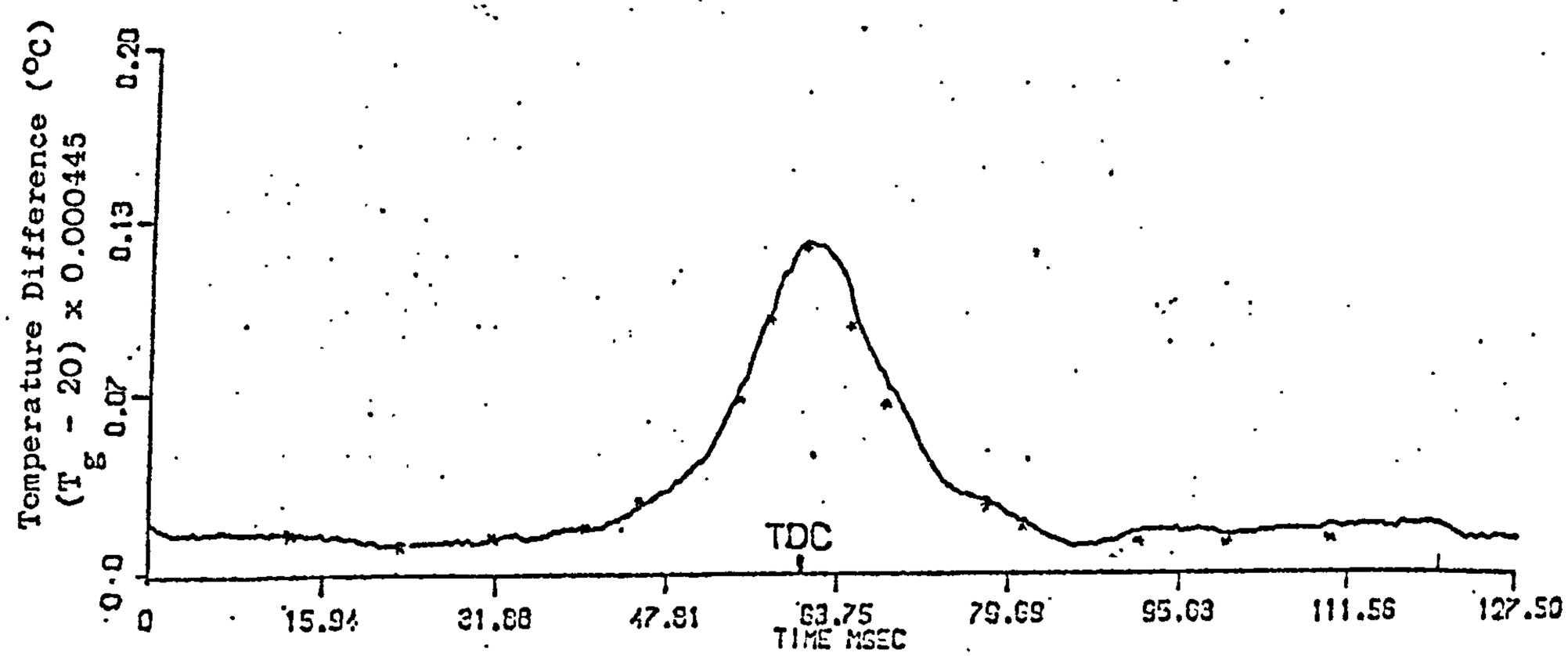

Fig. (4-8) Comparison Between the Output of a Resistance Thermometer and the Computed Gas Temperature using the Polytropic Relation. Data for an Individual Cycle at the Same Test Conditions of Fig. (4-7).
Resistance Thermometer * Calculated from pressure trace.

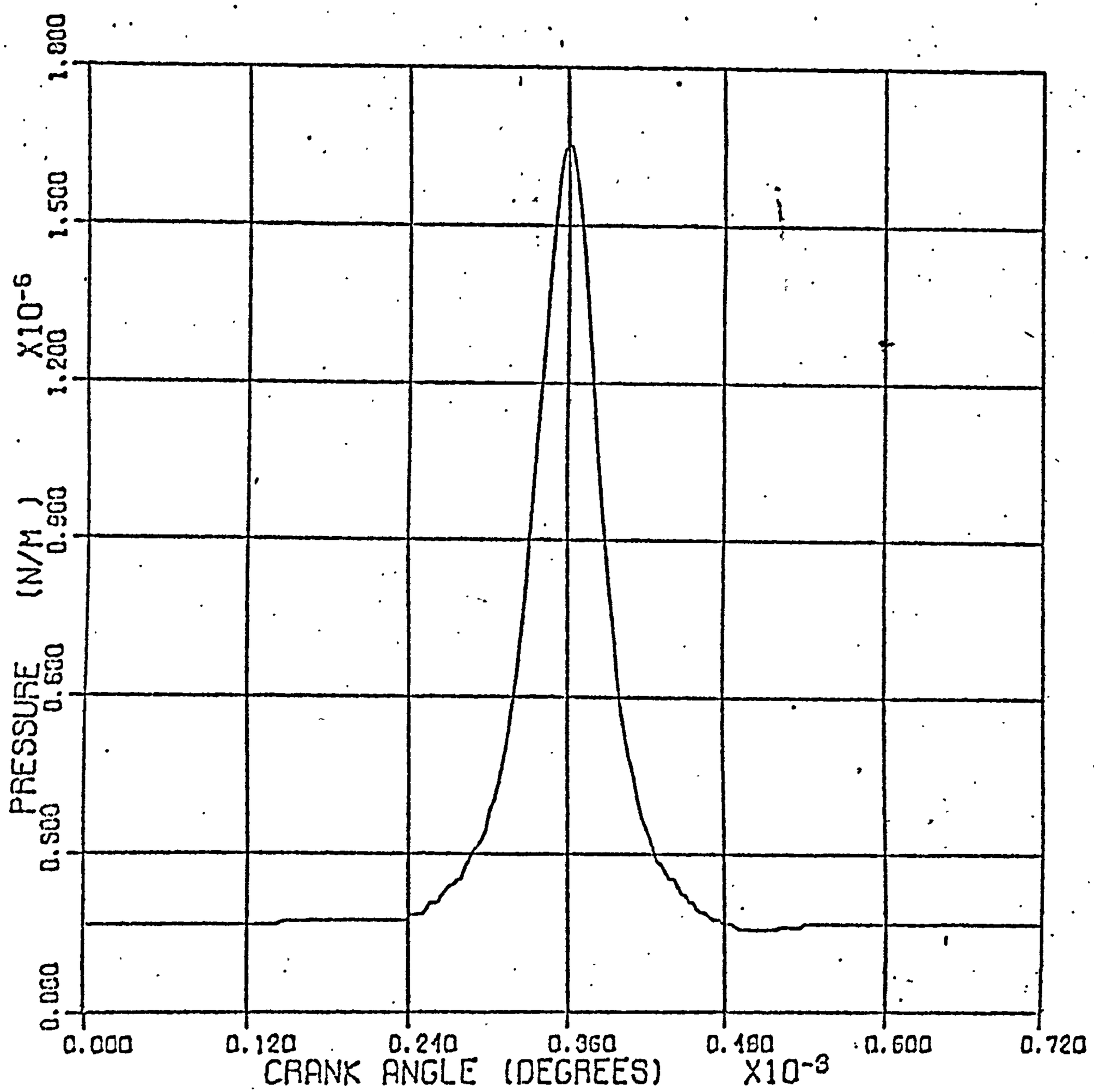

Fig. (4-9b) Typical pressure trace for a test on the Rolls Royce V8 engine at 1000 RPM and fully opened throttle.

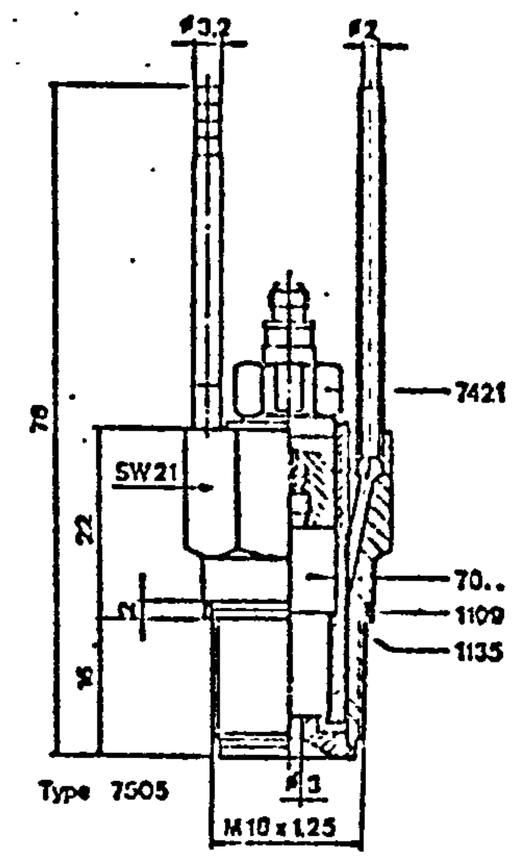

Fig. (4-9a) Schematic diagram of the Kistler pressure transducer.

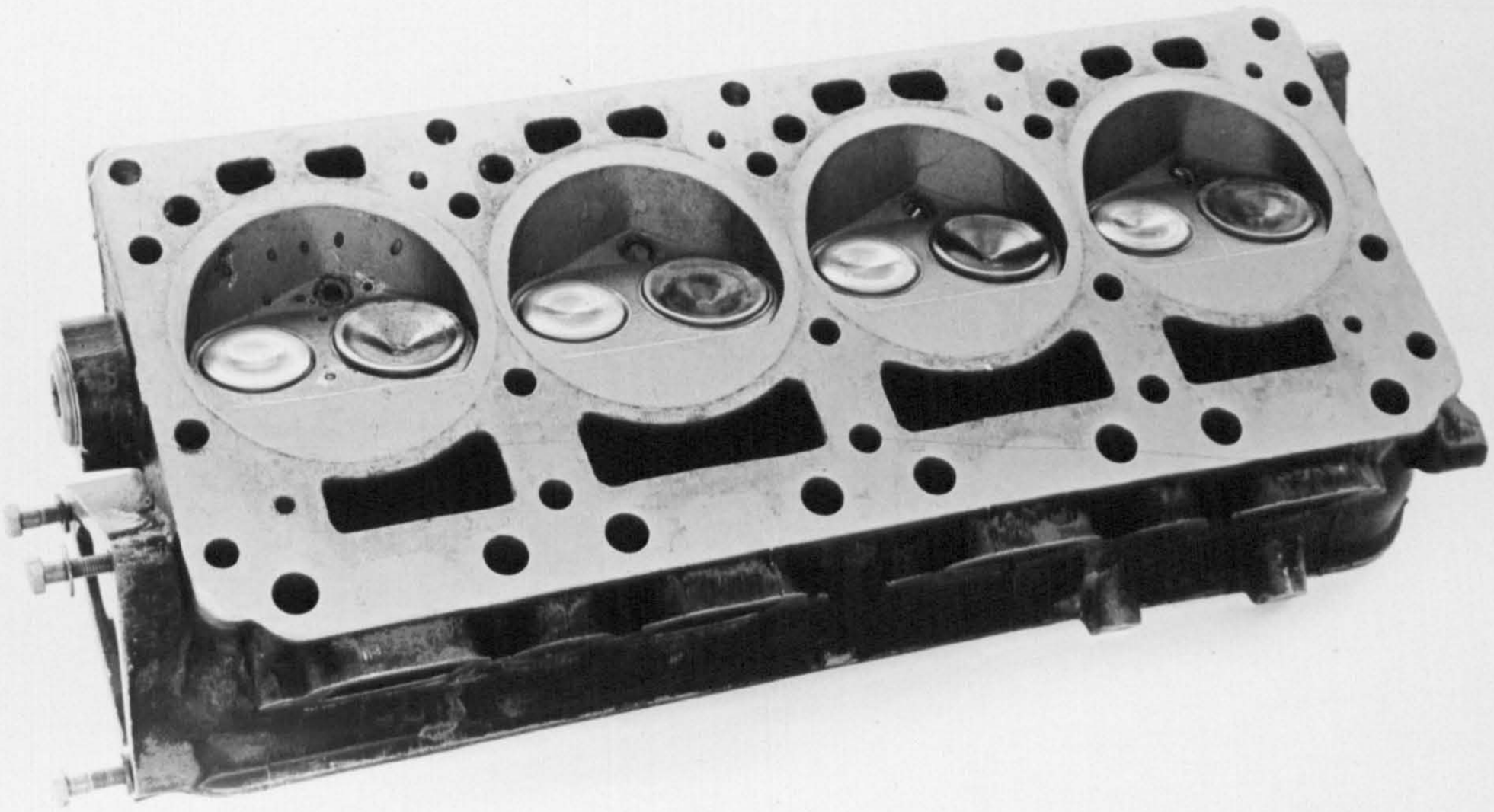

Fig. (4-11a) A view of a Rolls-Royce cylinder head showing the different locations of velocity measurements inside the wedge chamber.

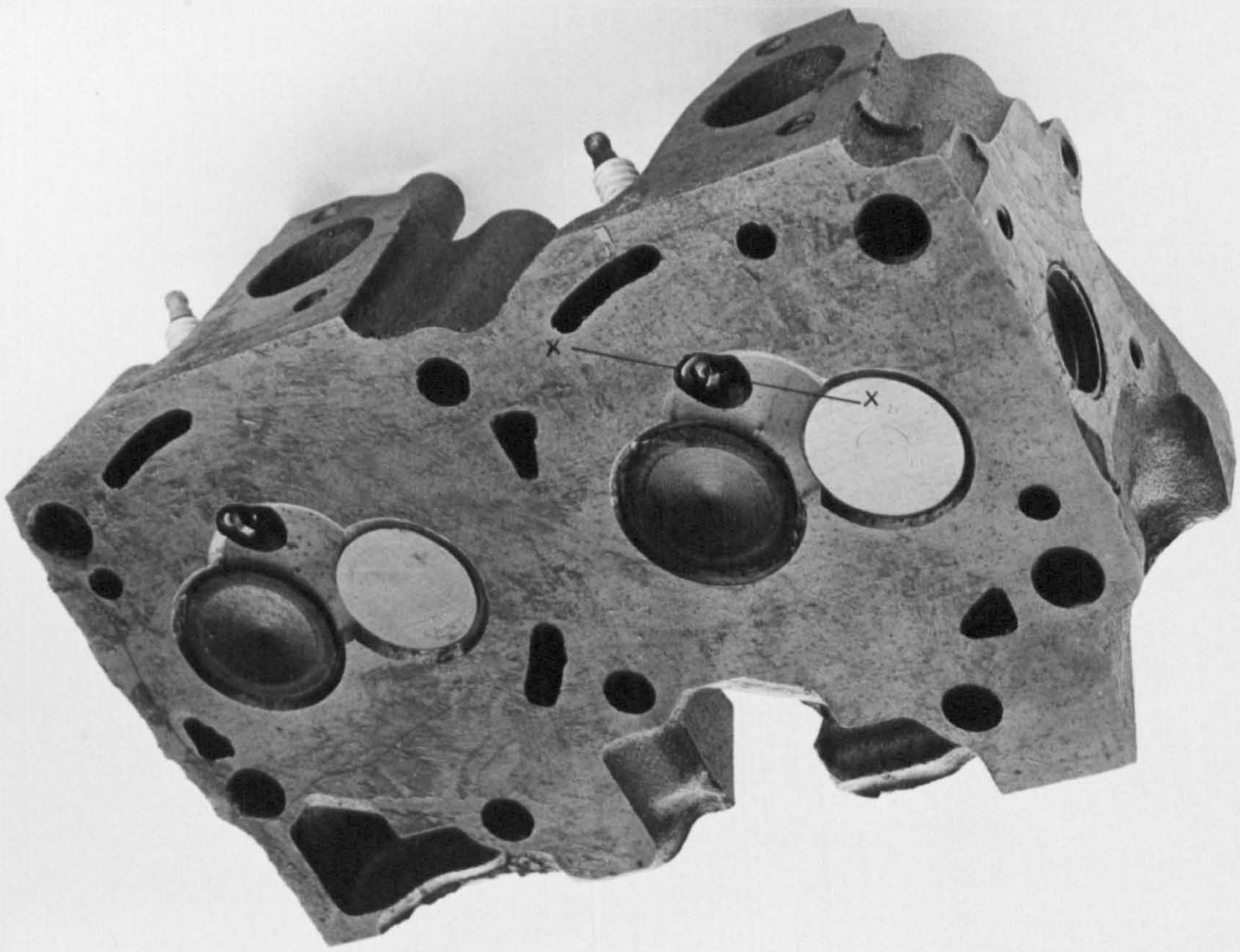

Fig. (4-10) A view of a cylinder head of the Ford engine showing the location of velocity measurements at the spark plug

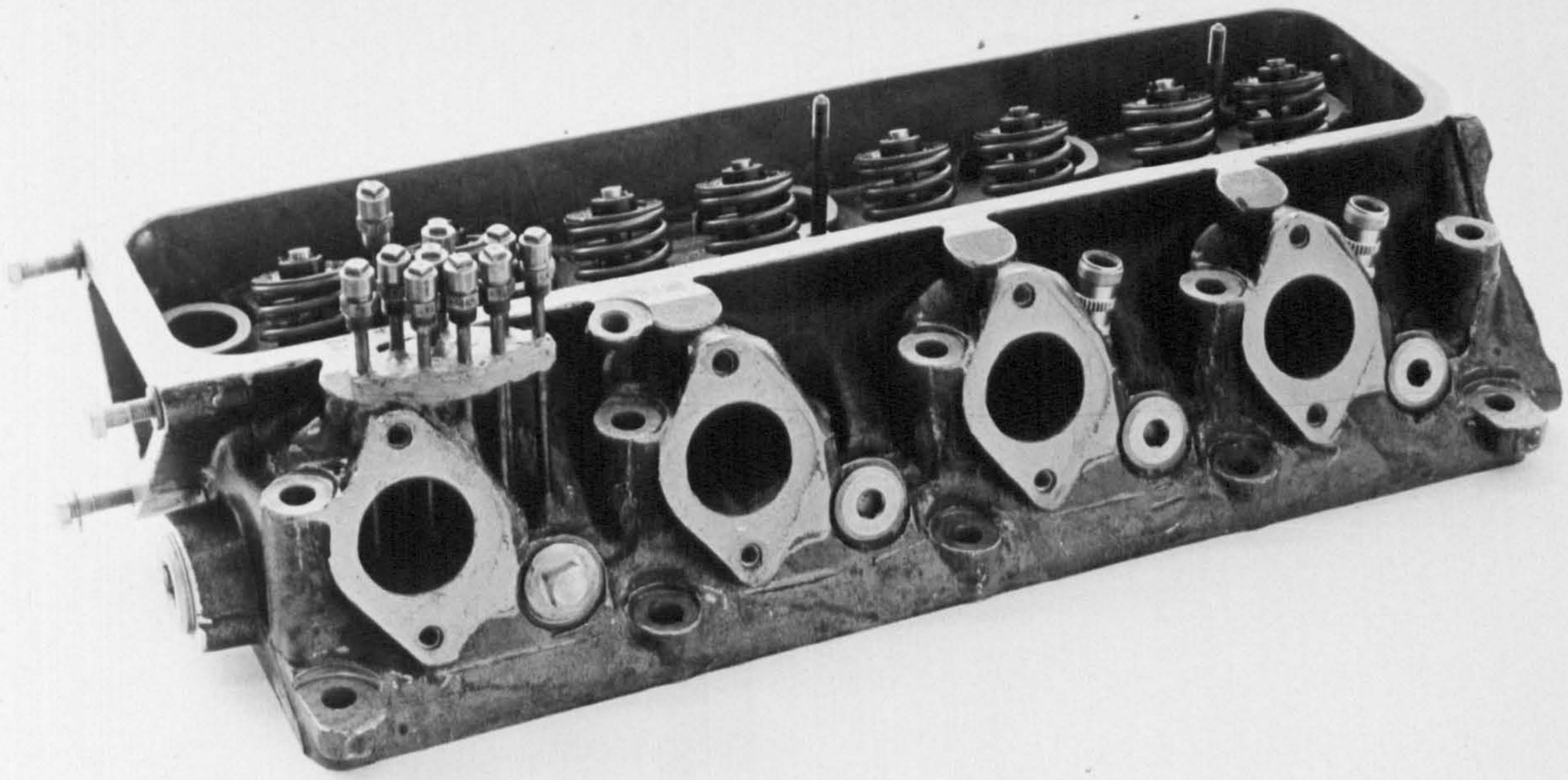

Fig. (4-11b) A view of a Rolls-Royce cylinder head showing the different brass tubes used for probe traversing inside the combustion chamber.

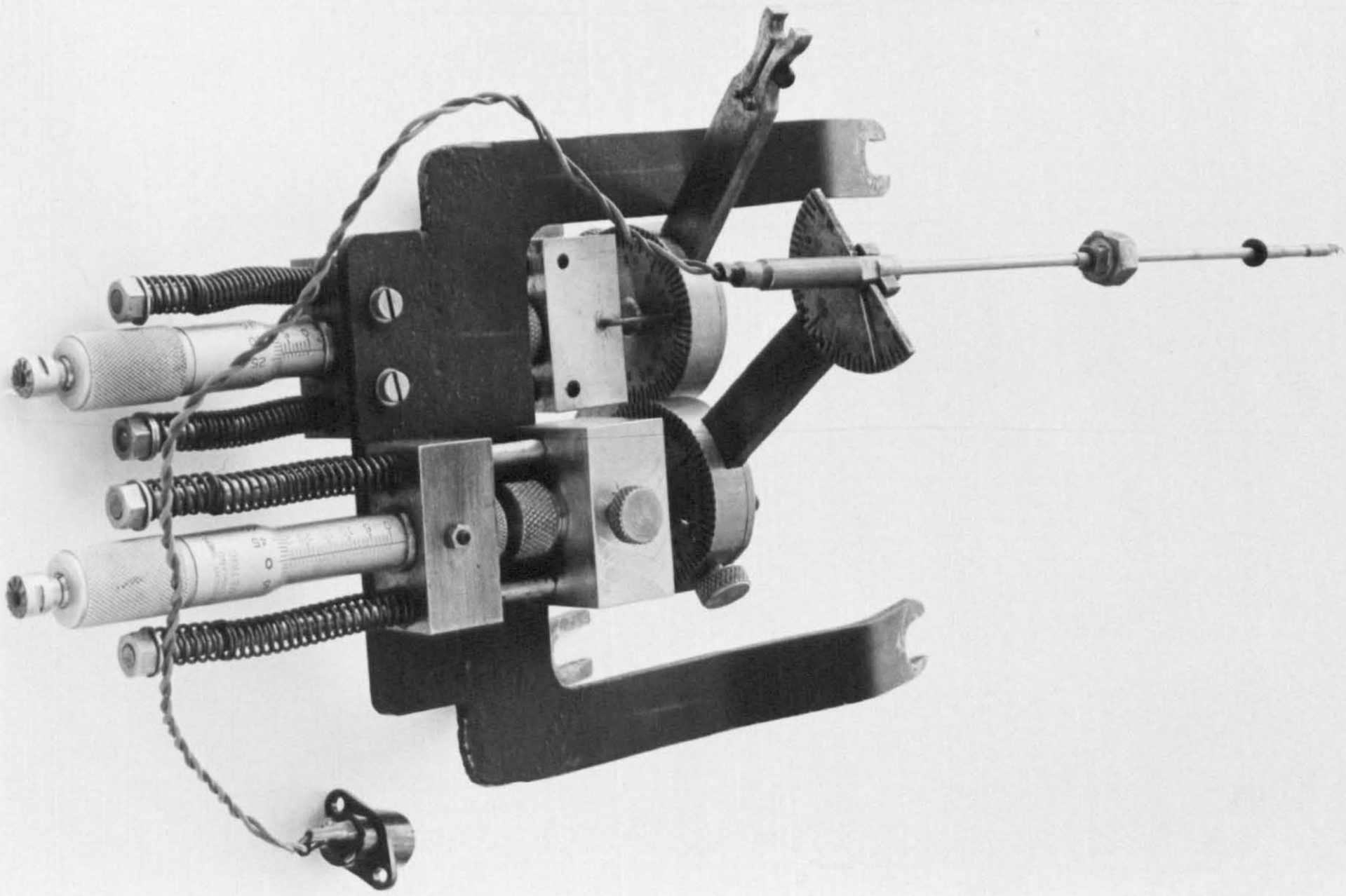

Fig. (4-13) A view showing a single wire probe mounted on the traverse mechanism used for velocity measurements at different locations inside the wedge chamber.

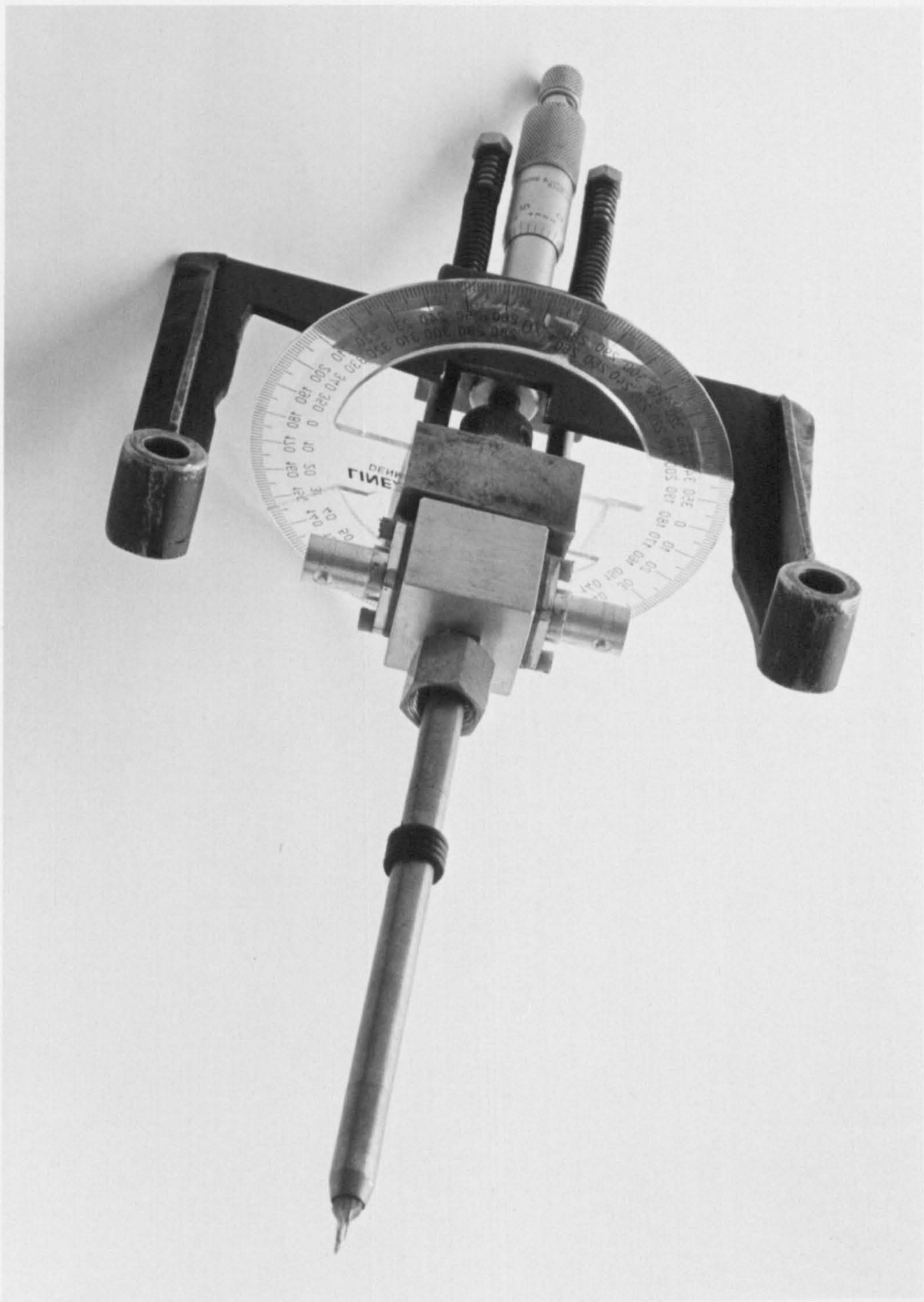

Fig. (4-12) A view of the spark plug double wire probe and its traverse mechanism.

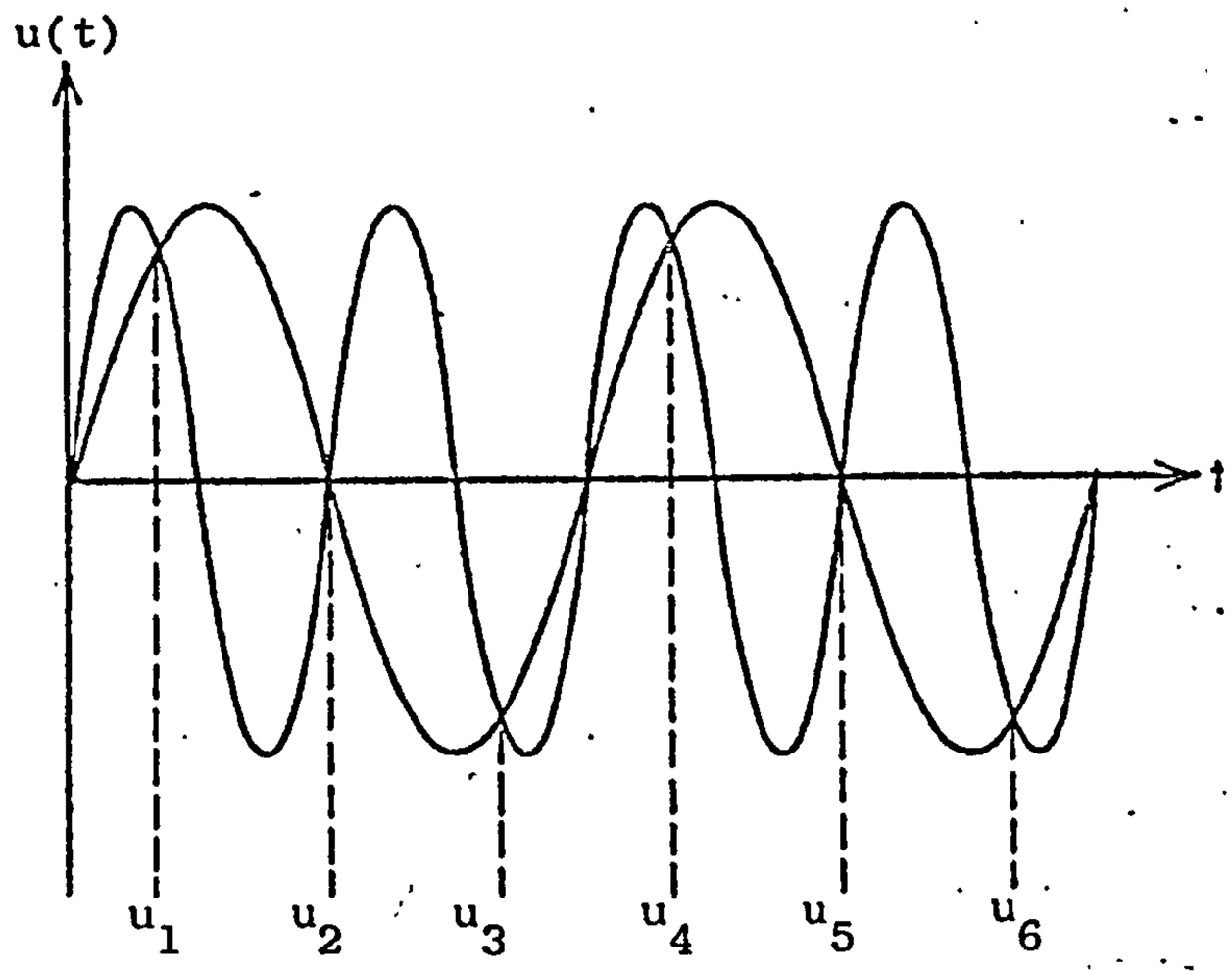

Fig. (4-14). Illustration of aliasing problem.

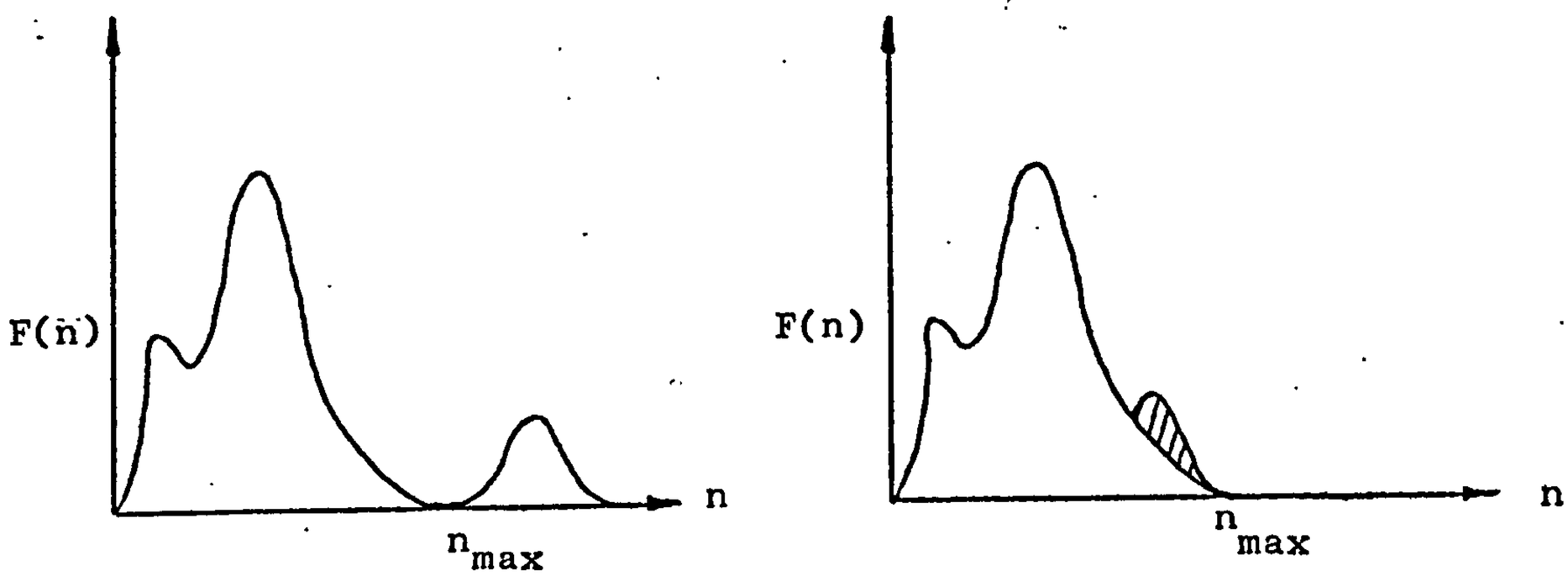

(a) True spectrum (b) Aliased spectrum

Fig. (4-15). Aliased power spectrum due to folding.

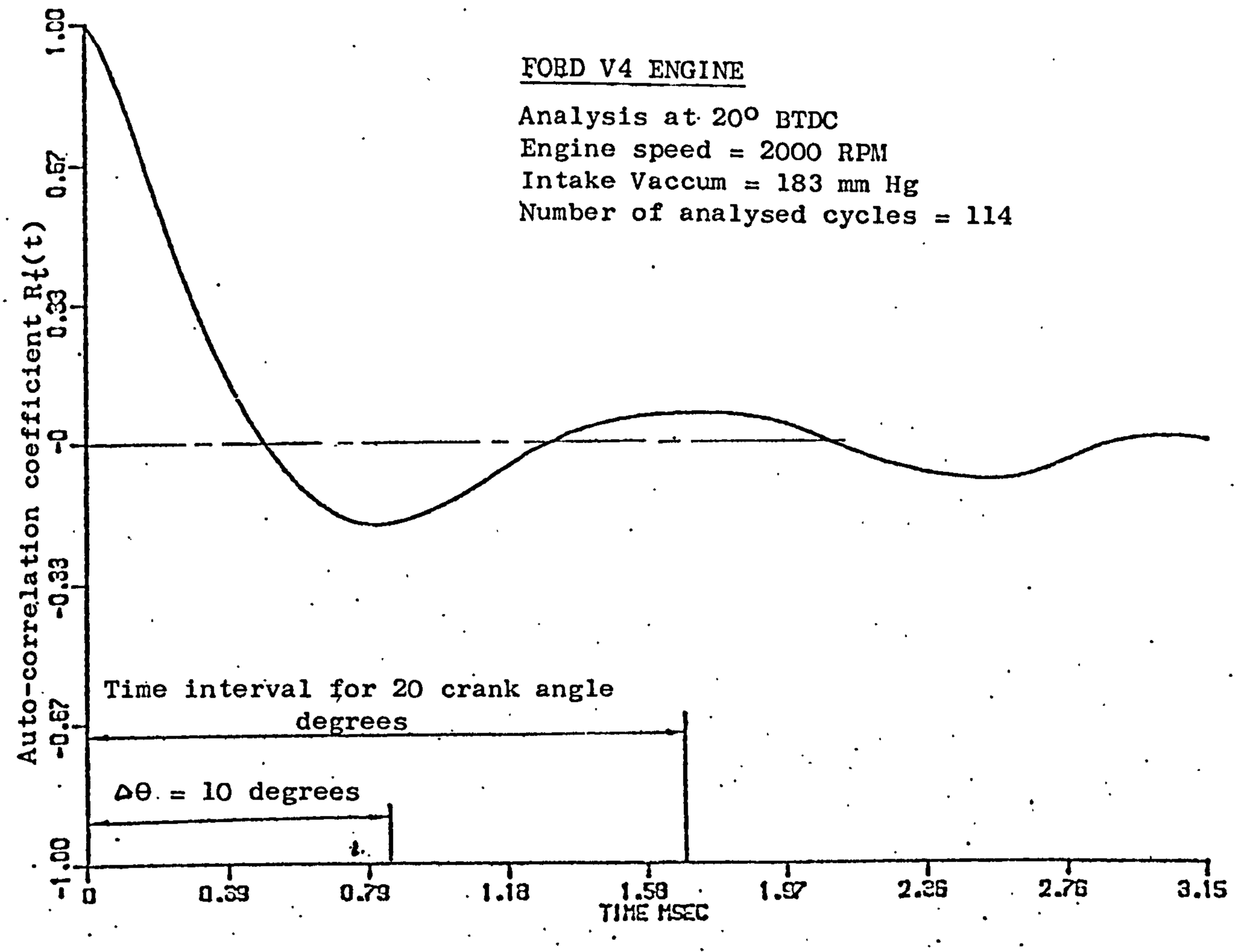

(a) Cycle sample = 20 crank angle degrees

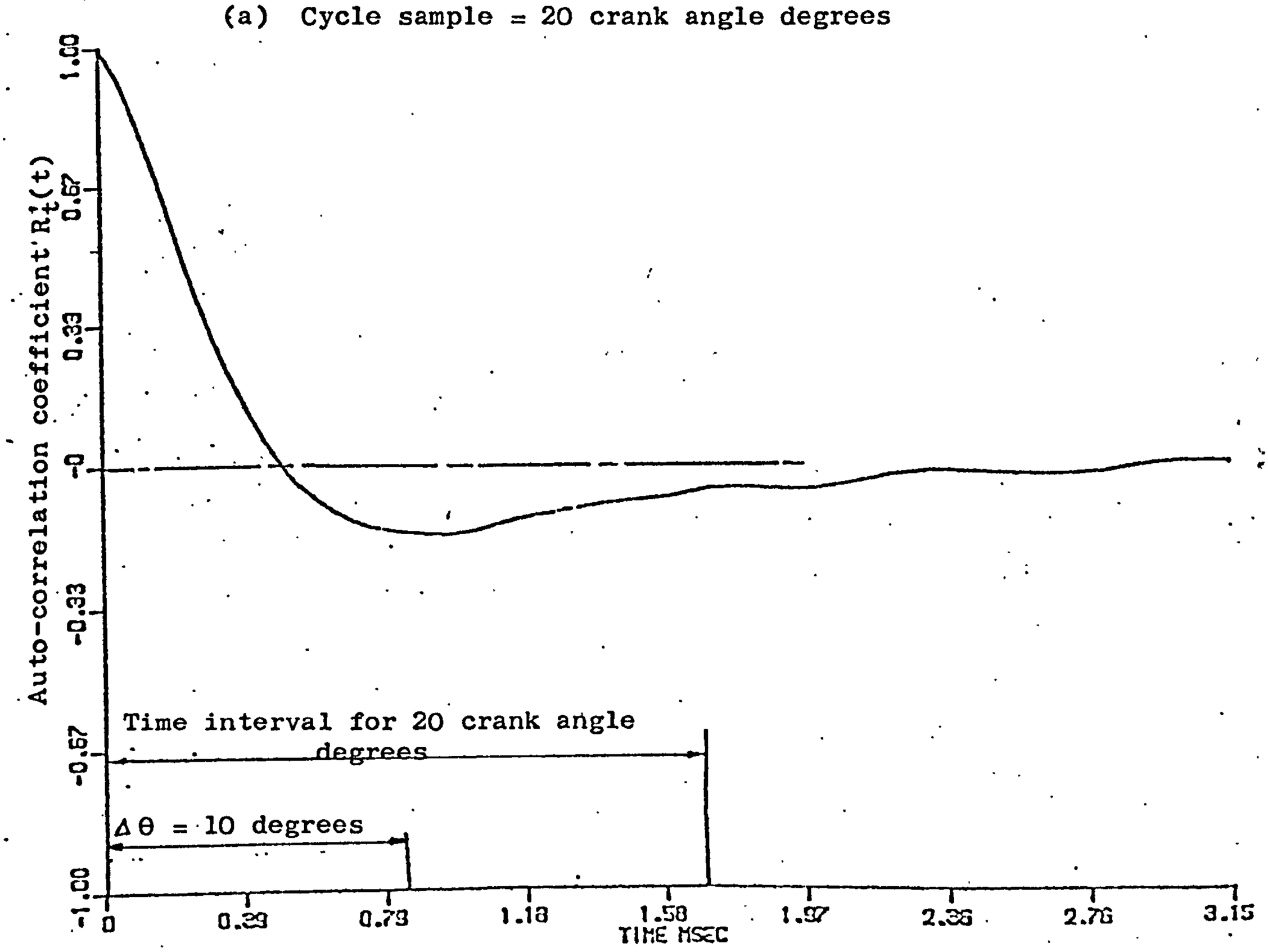

(b) Cycle sample = 10 crank angle degrees

Fig. (4-16a) Comparions between the auto-correlation coefficients for two different widths of cycle sample.

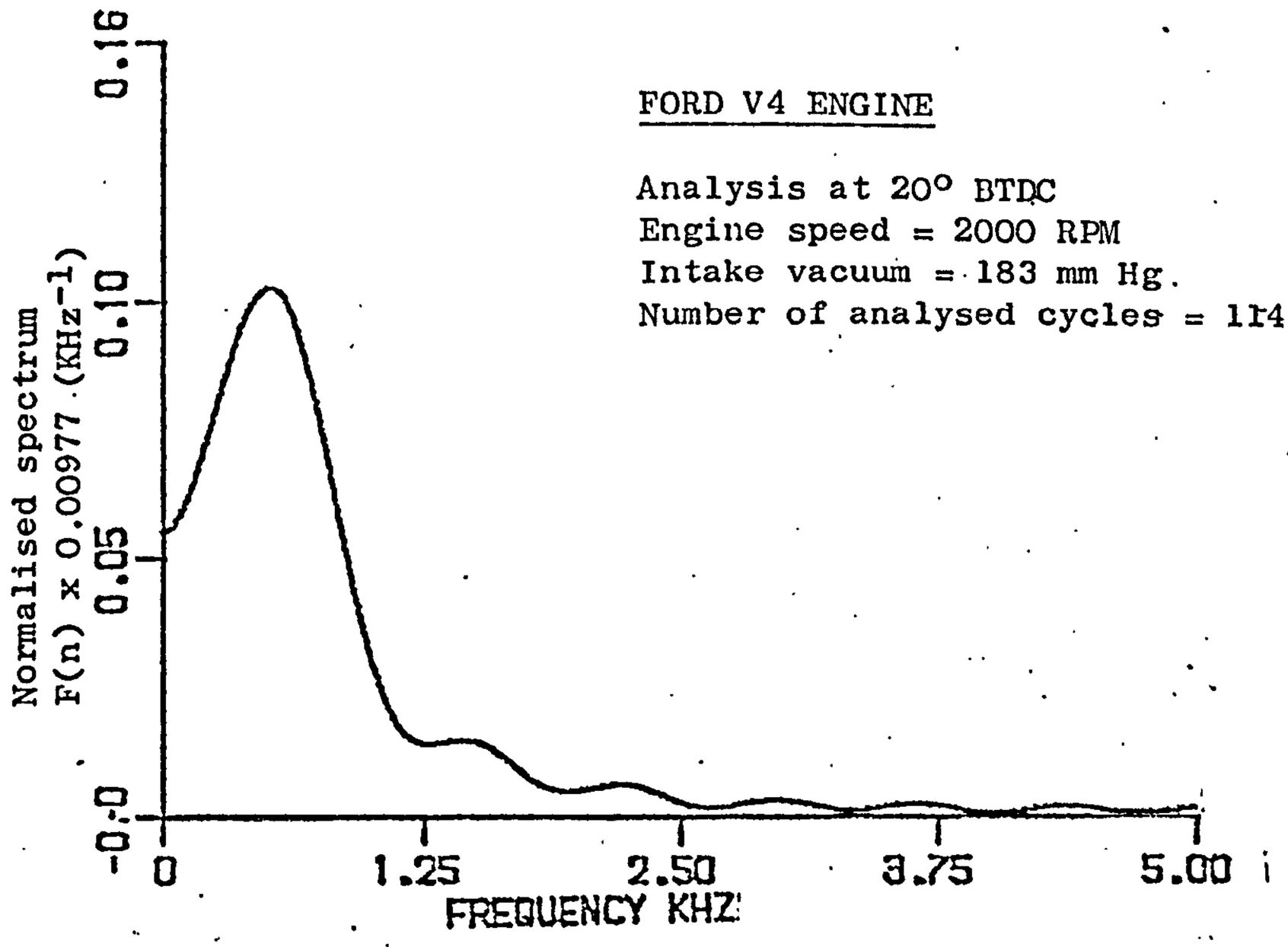

FORD V4 ENGINE

Analysis at 20° BTDC
Engine speed = 2000 RPM
Intake vacuum = 183 mm Hg.
Number of analysed cycles = 114

(a) Cycle sample = 20 crank angle degrees

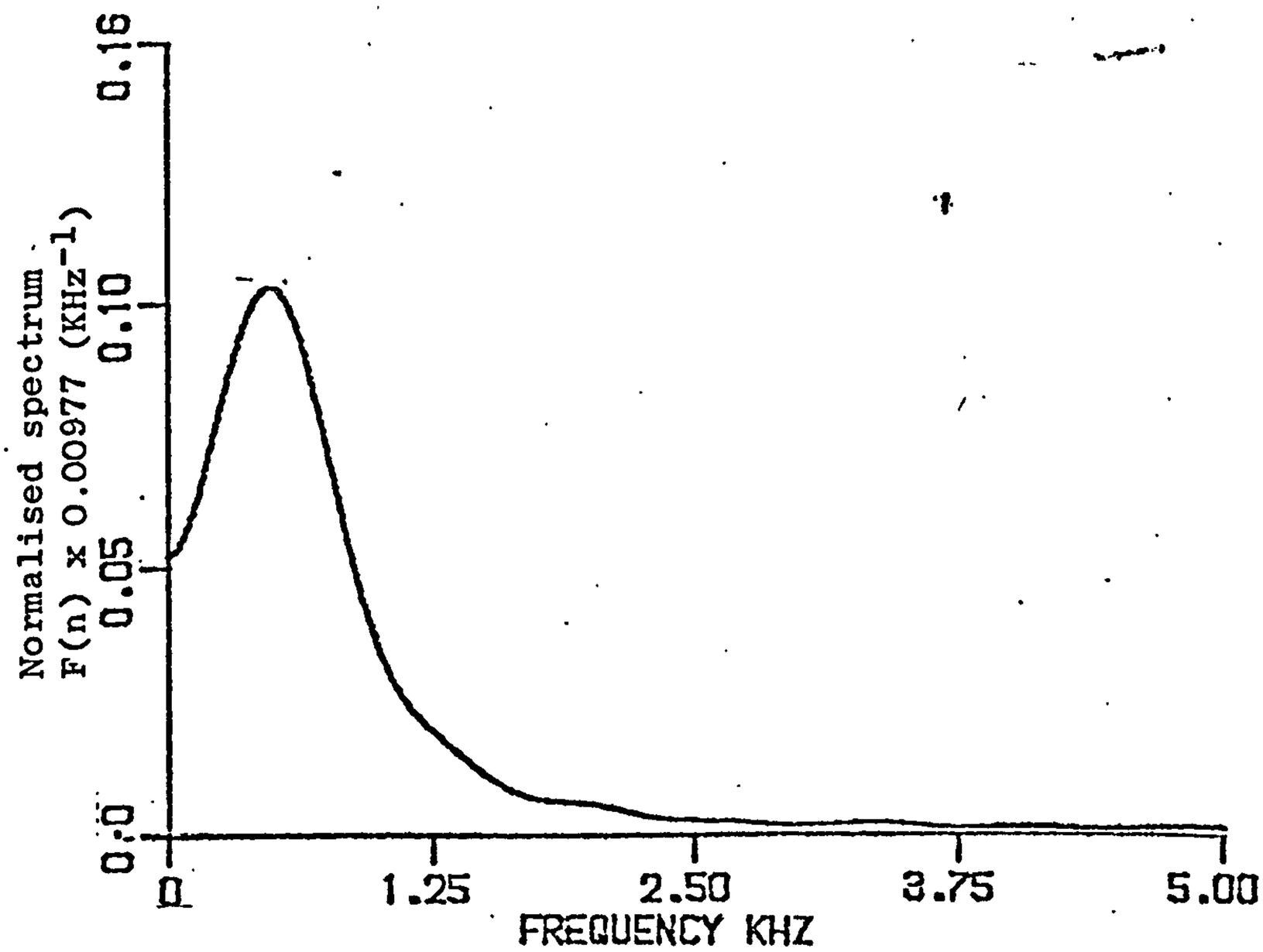

(b) Cycle sample = 10 crank angle degrees

Fig. (4-16b) Comparison between the power spectrum functions for two different widths of cycle sample.

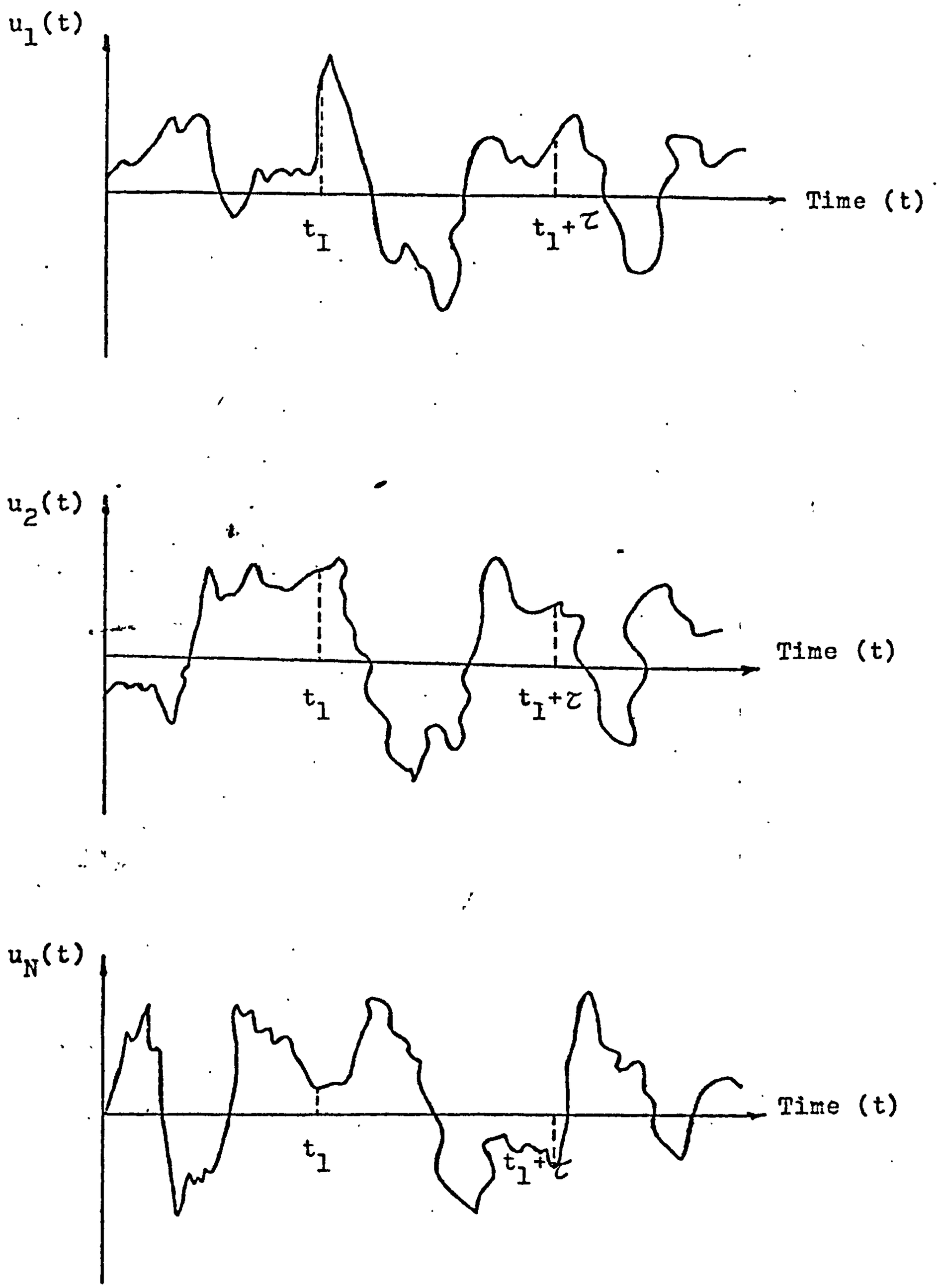

Fig (4-17) Ensemble of sample records forming random process

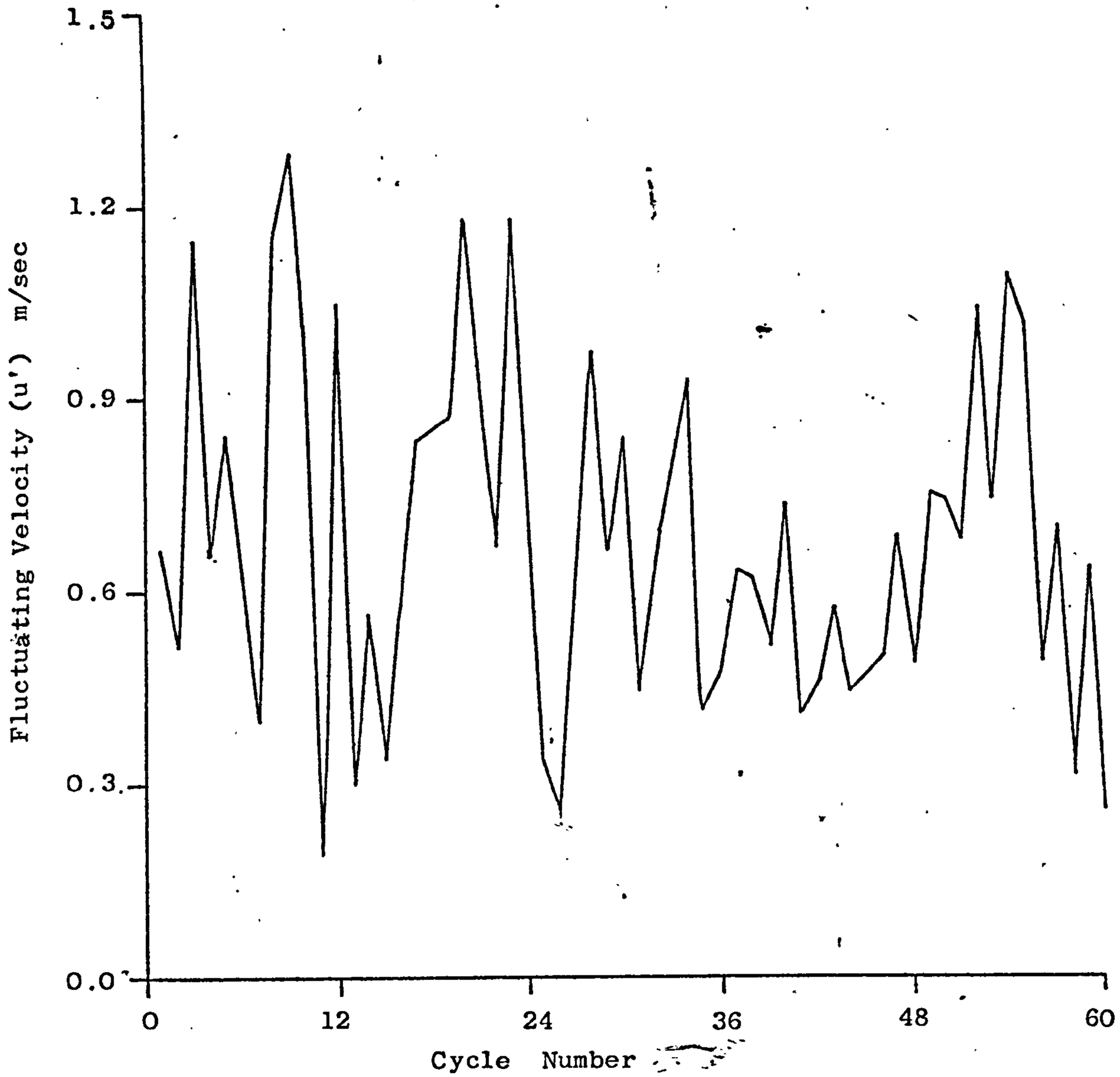

Fig. (4-18). An example of testing the stationarity of turbulence signals. Variation of the fluctuating velocity component (u') for 60 sample records showing 28 'runs'. (Analysis at 40 degrees BTDC, Rolls-Royce engine, 1000 RPM and fully opened throttle).

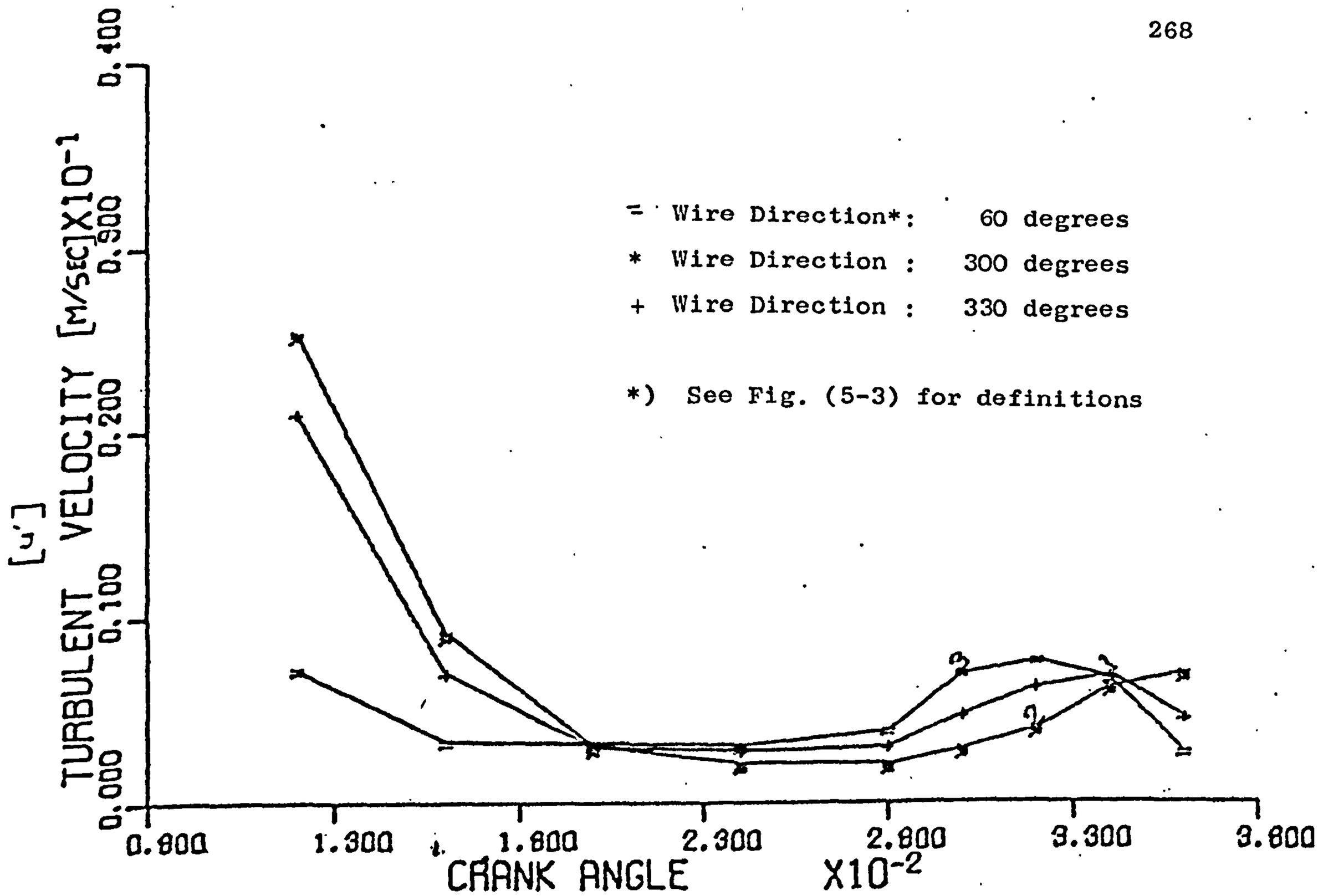

Fig. (4-19a) Variation of the Fluctuating Velocity Component with Crank Angle During the Cycle for Three Different Orientations of a Hot Wire in a Combustion Chamber of a Rolls-Royce Engine. (Compression ratio: 9:1, 1000 RPM and fully opened throttle).

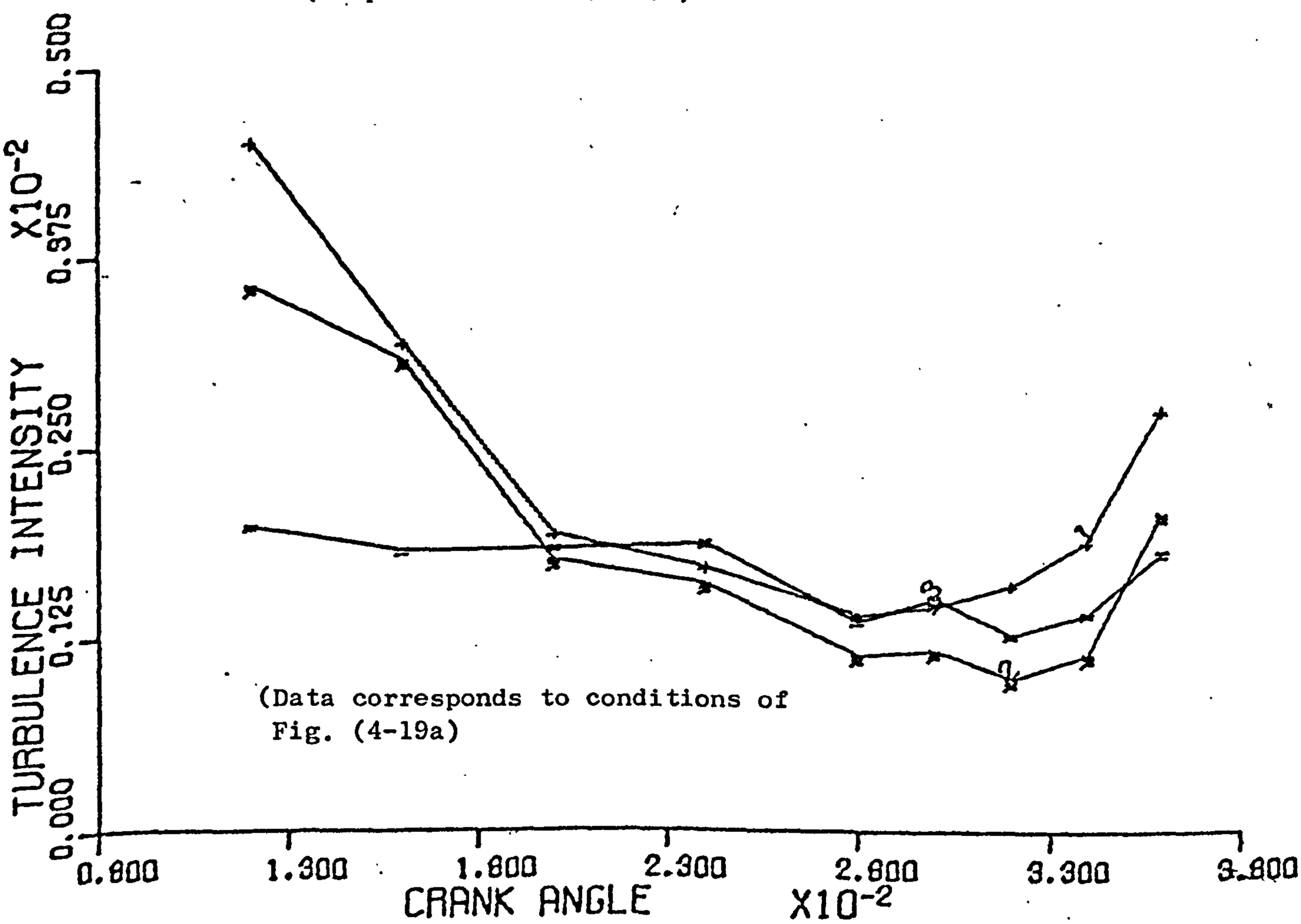

Fig. (4-19b) Variation of Turbulence Intensity (u/U).100 with Crank Angle.

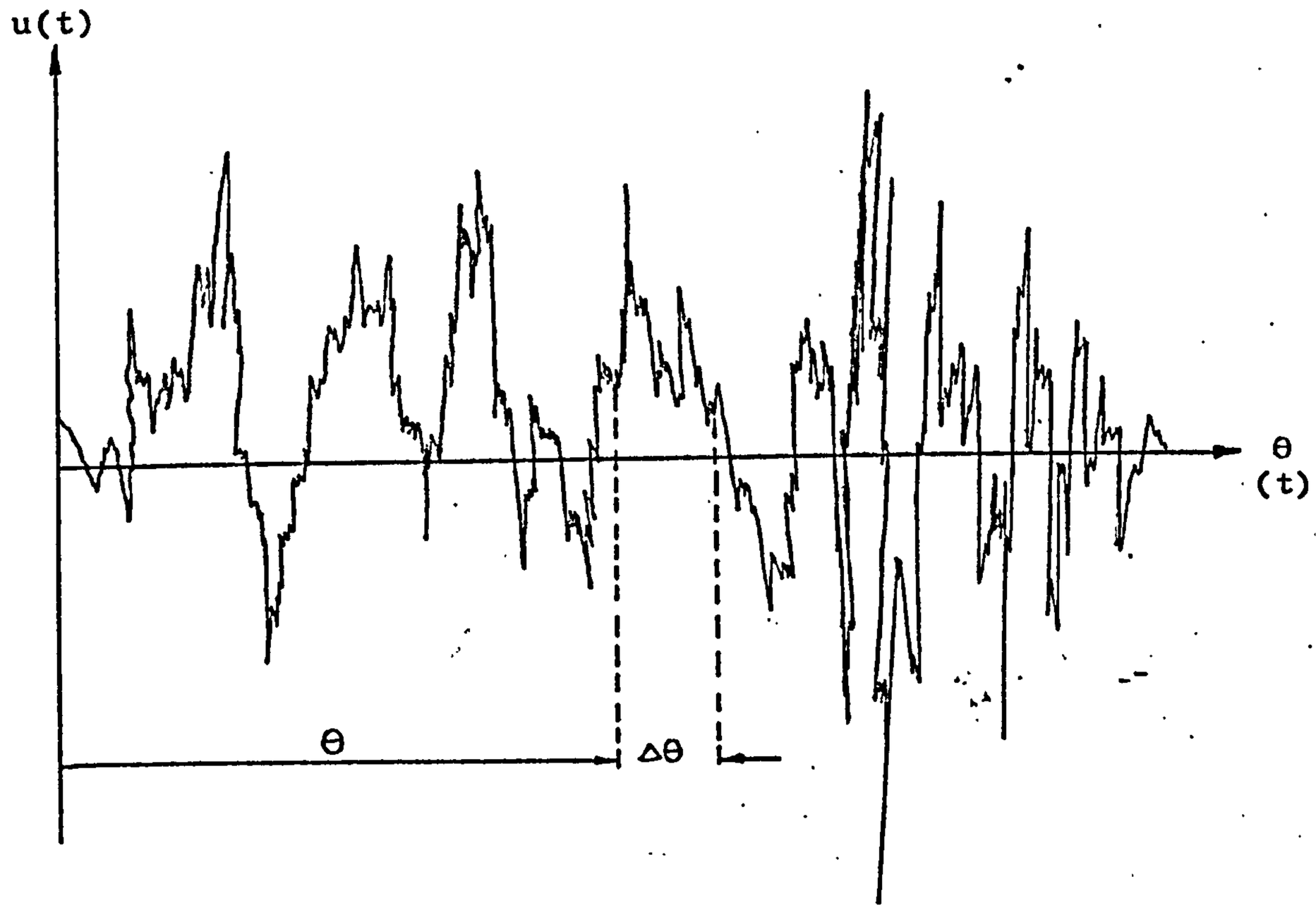

a) Original Turbulence Signal

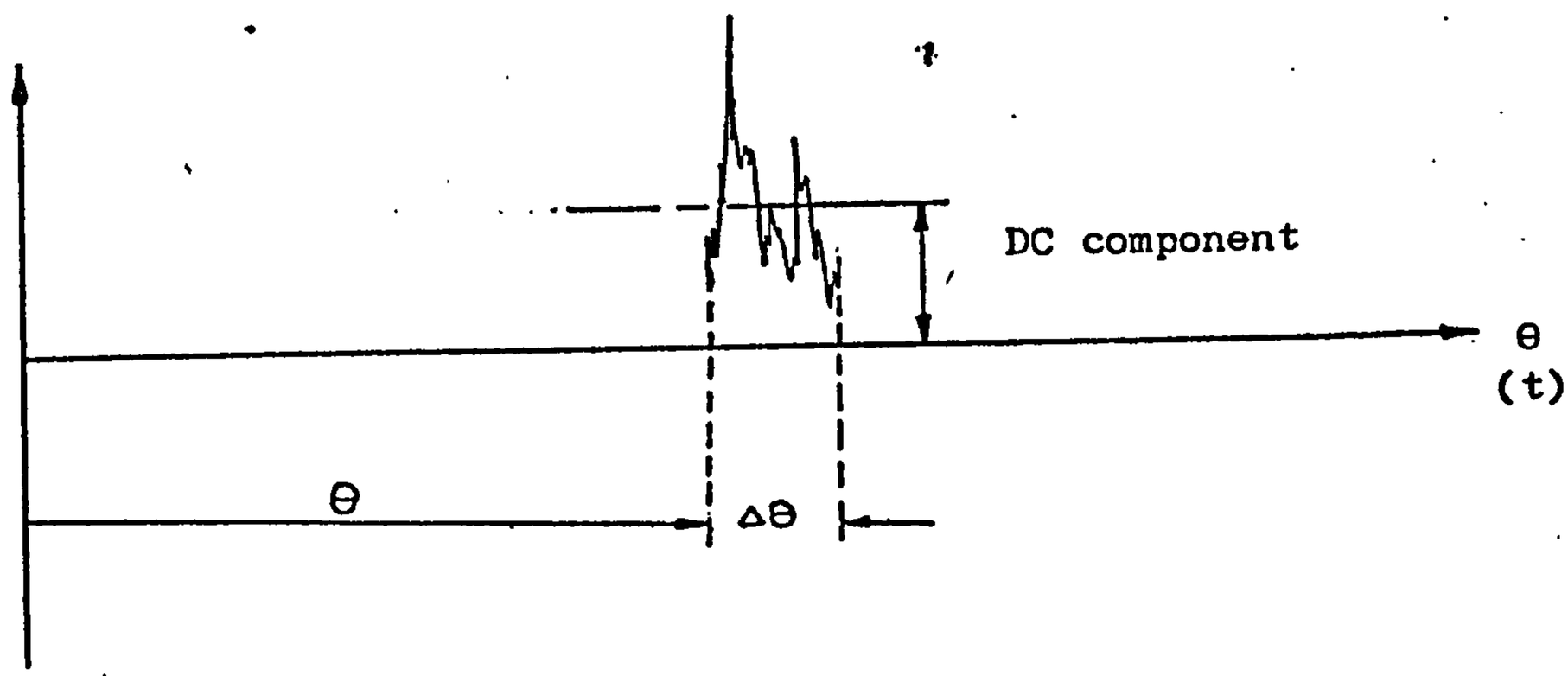

b) Isolated Cycle Sample (θ) at Crank Angle (θ).

Fig. (4-20). Illustration of the introduction of DC component by the sampling process.

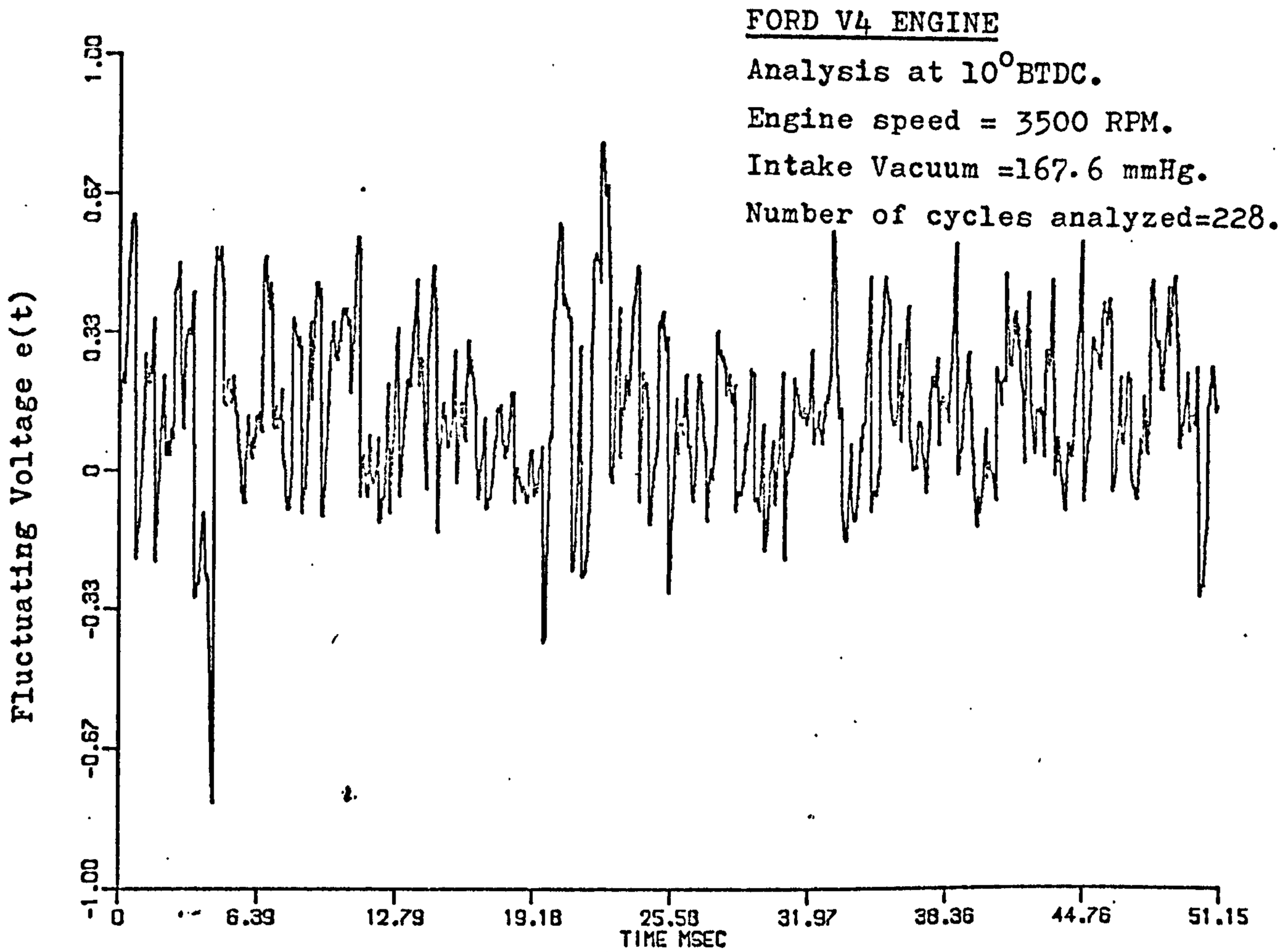

Fig (4-21a) Original synthesised turbulence signal.

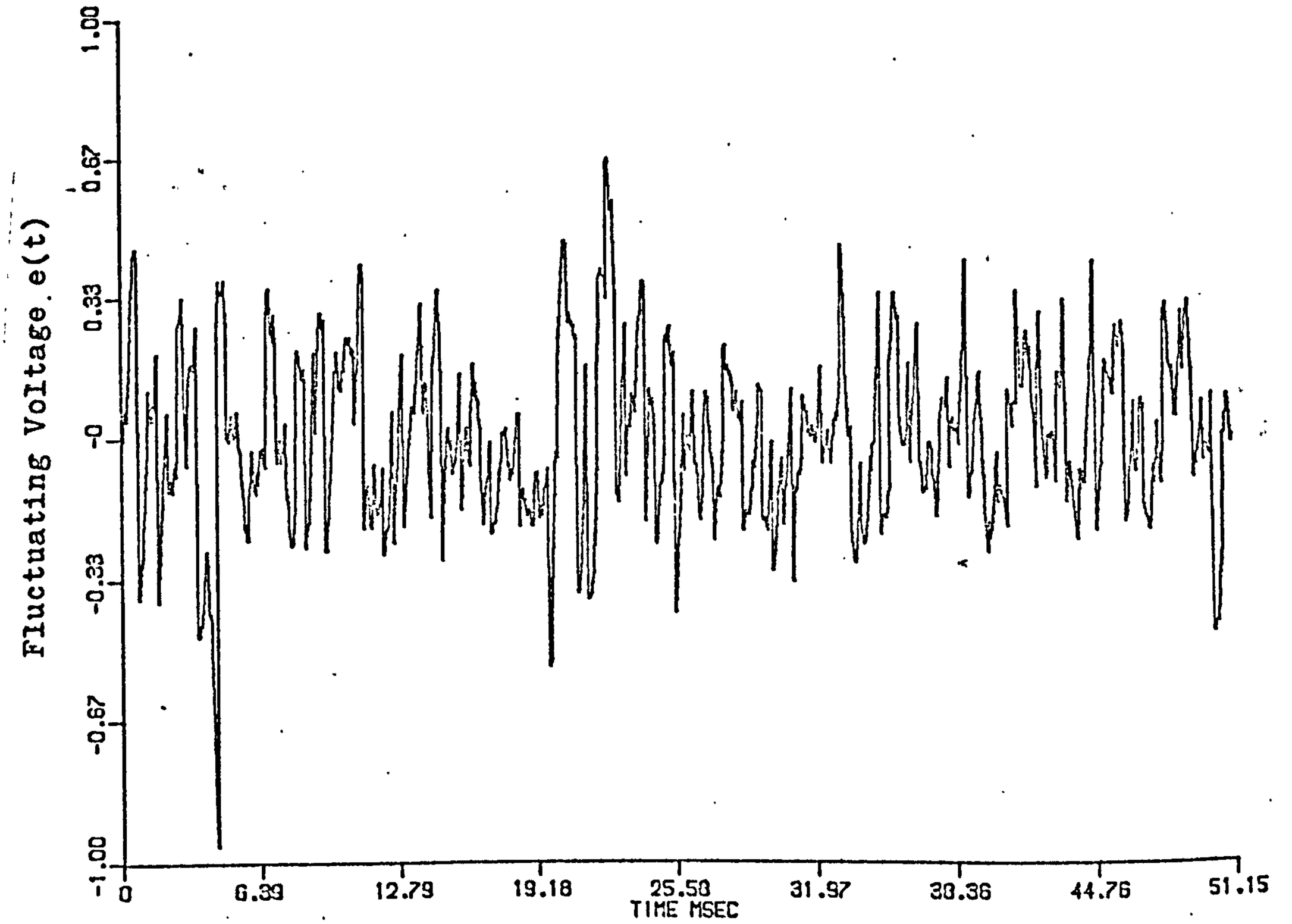

Fig (4-21b) Synthesised turbulence signal after transfering to a zero mean value.

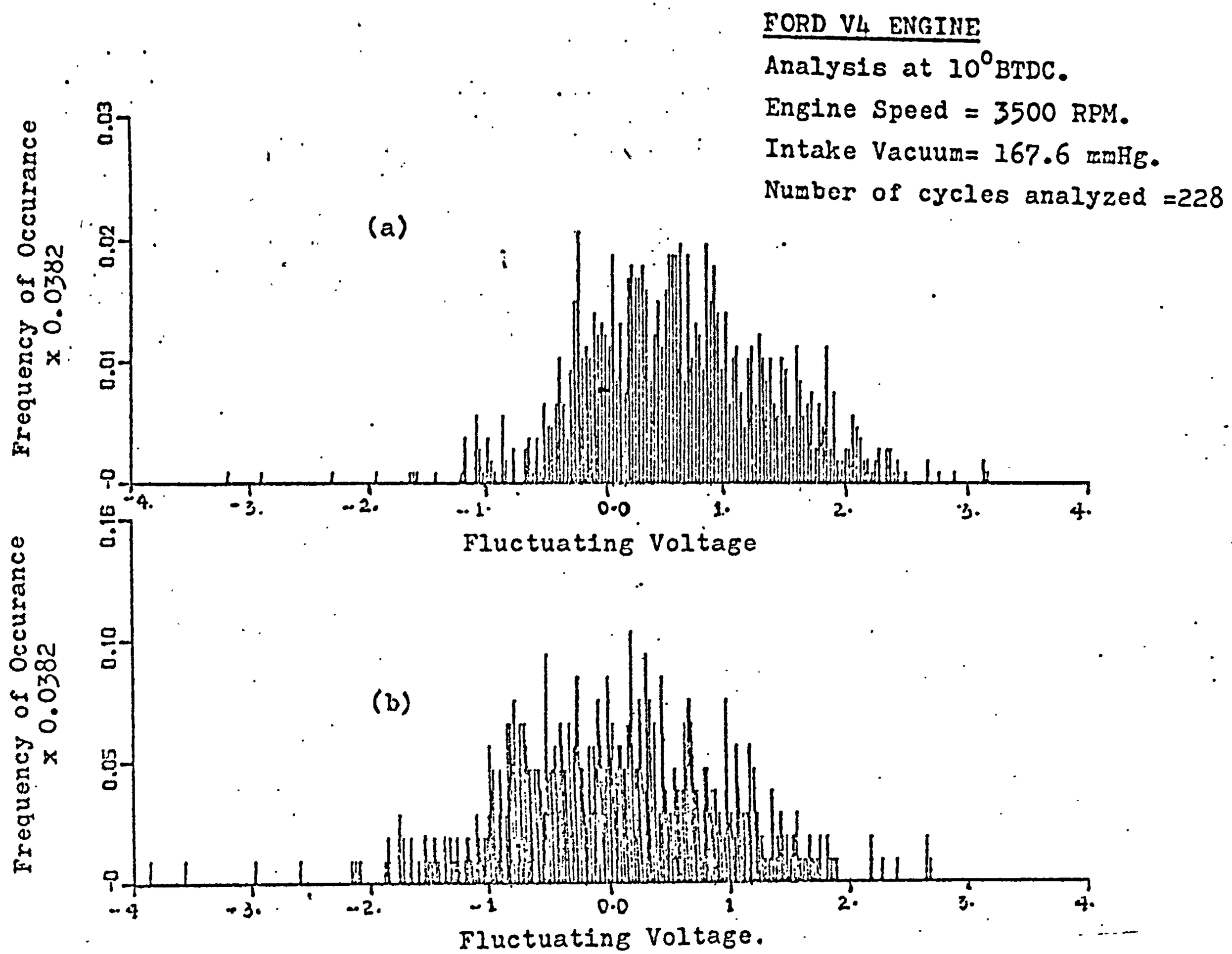

Fig (4-22) Normalized histogram for 228 synthesized' !cycle samples' of turbulence signal in a S.I. engine.

a)- Data before transfering ton a zero mean value.

b)- Data after transfering to a zero mean value.

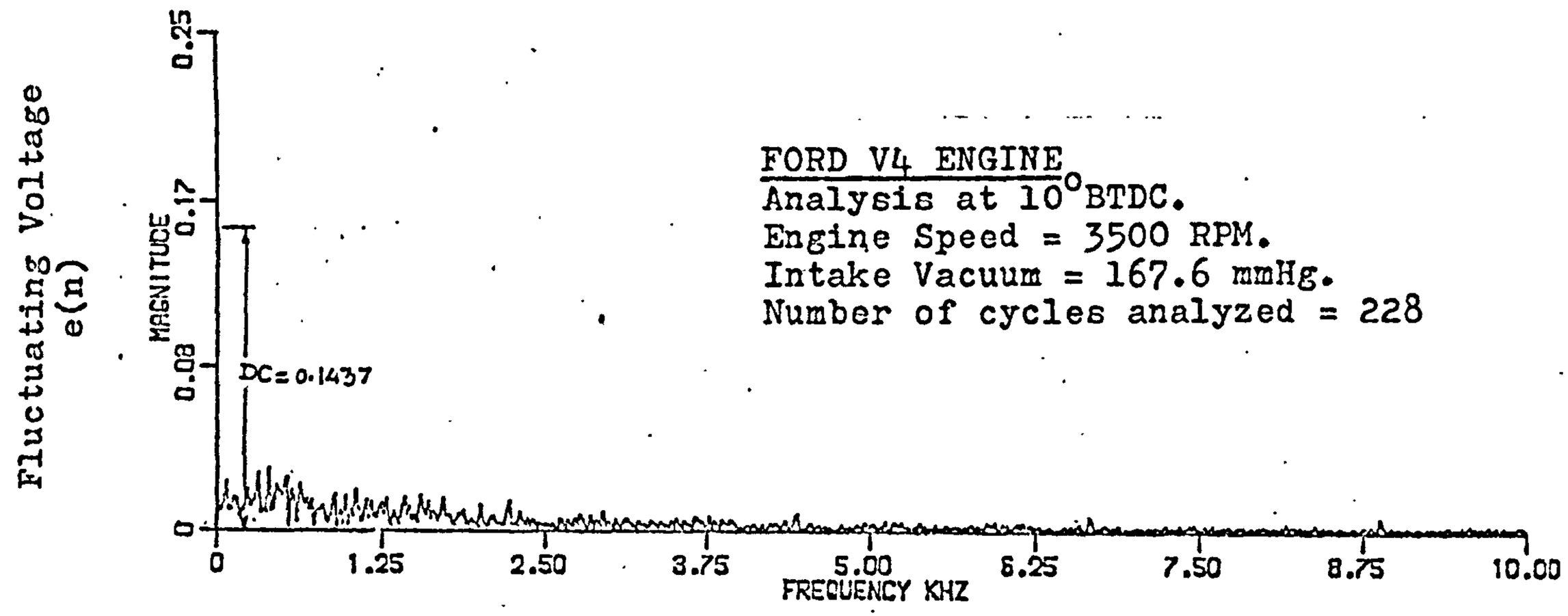

Fig (4-23a) Fourier transform of the original synthesized signal showing the fictious DC component superimposed on the data.

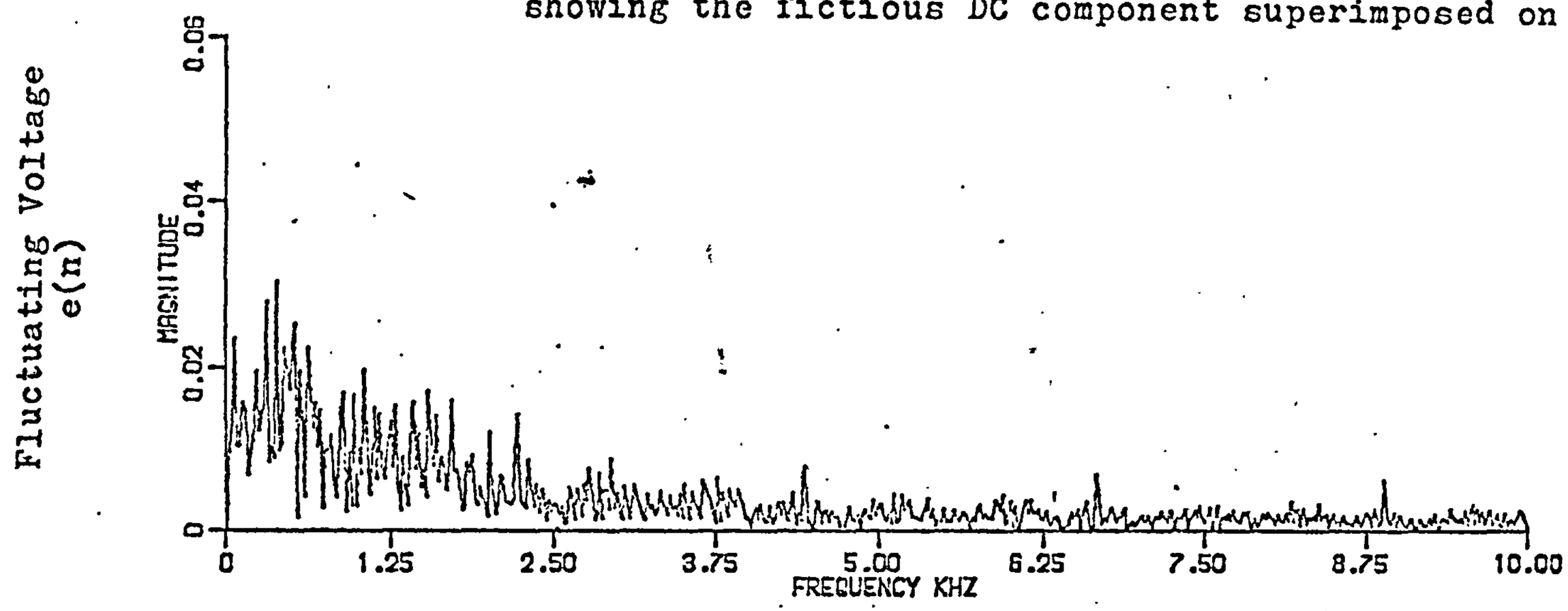

Fig (4-23b) Fourier transform of turbulence signal after removing the DC component.

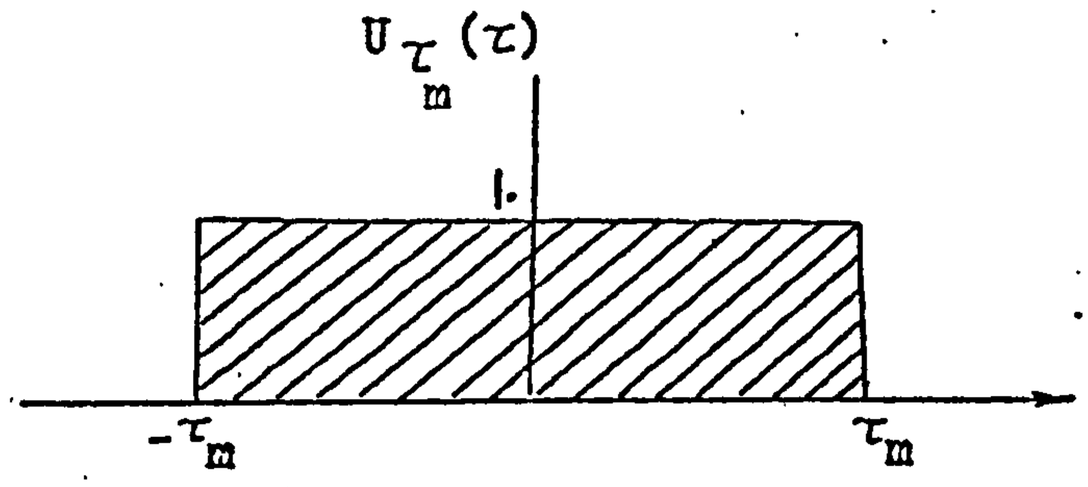

Fig (4-24)Illustration of boxcar function $U_{\tau_m}(\tau)$.

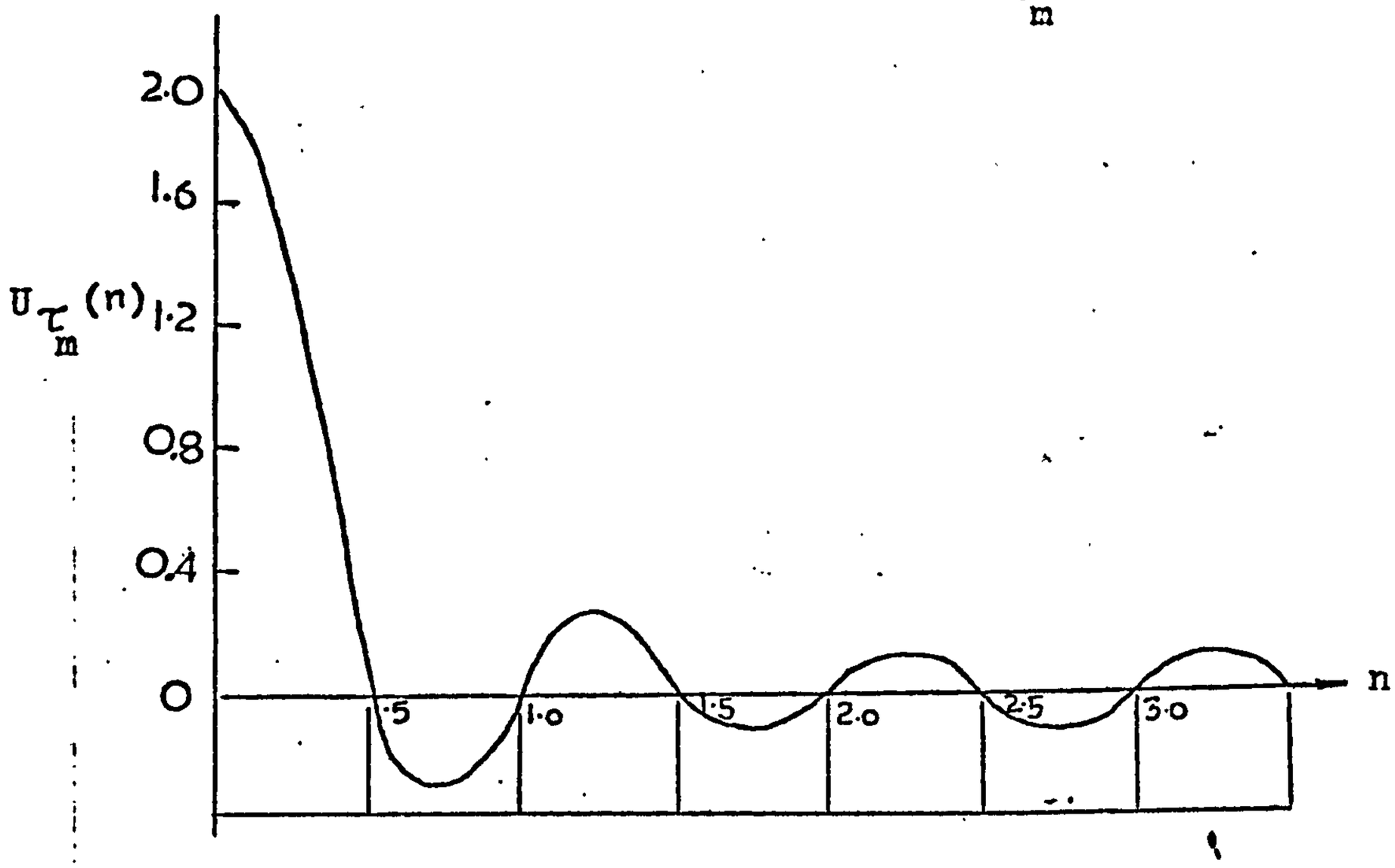

Fig (4-25) Illustration of window function $U_{\tau_m}(n)$.

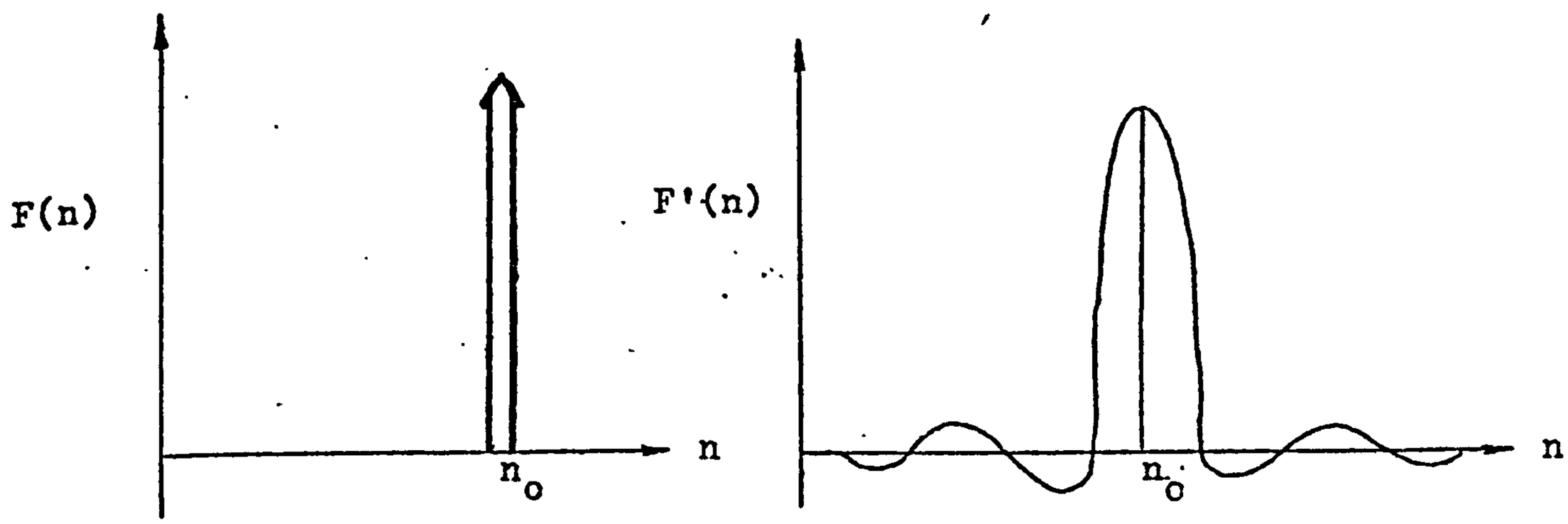

a- Theoretical F(n) b- Resulting F'(n).

Fig (4-26) Power spectrum of a sine wave at frequency n_o.

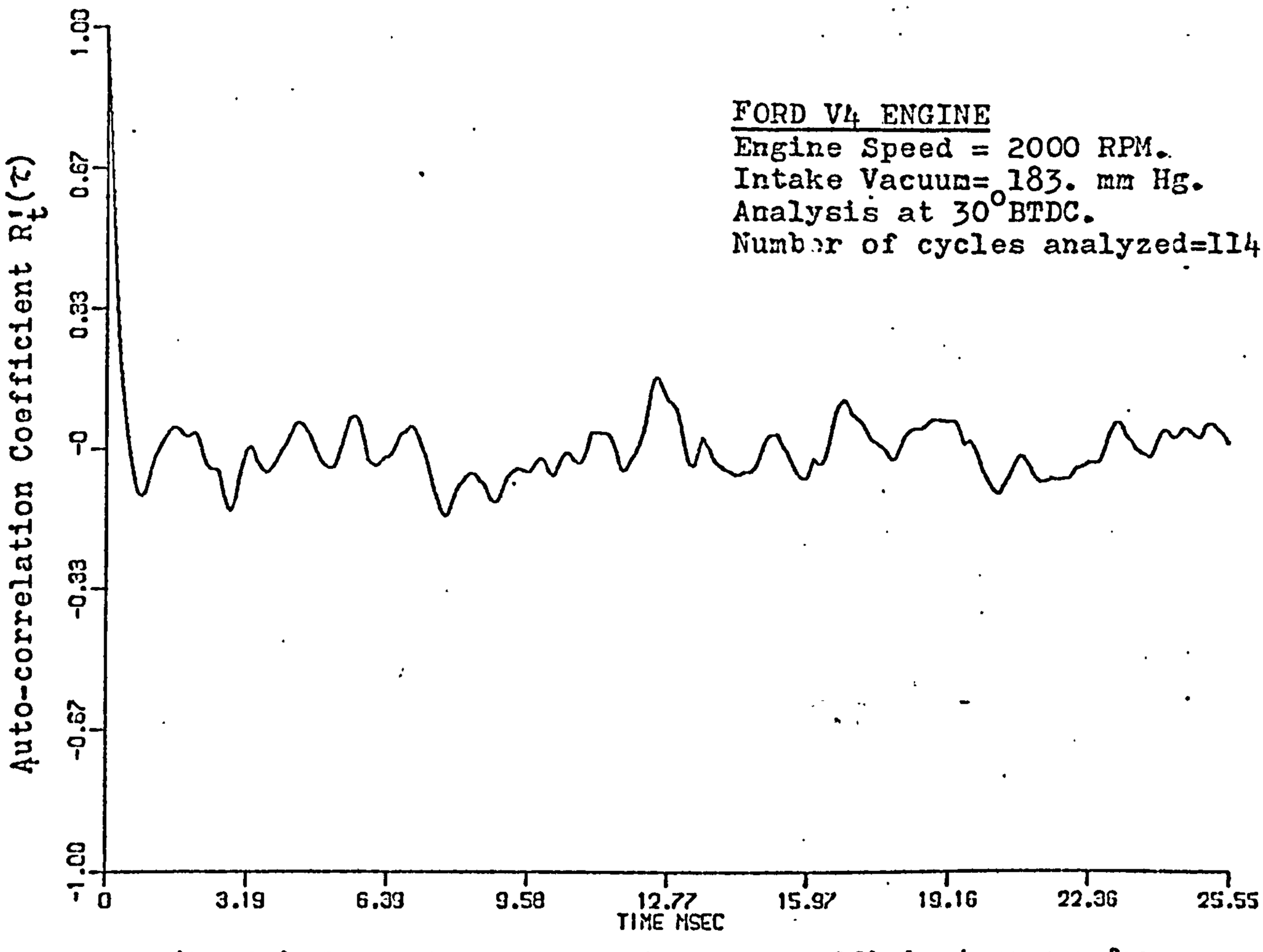

Fig (4-27a) Typical auto-correlation coefficient curve for a relatively long time delay (τ).

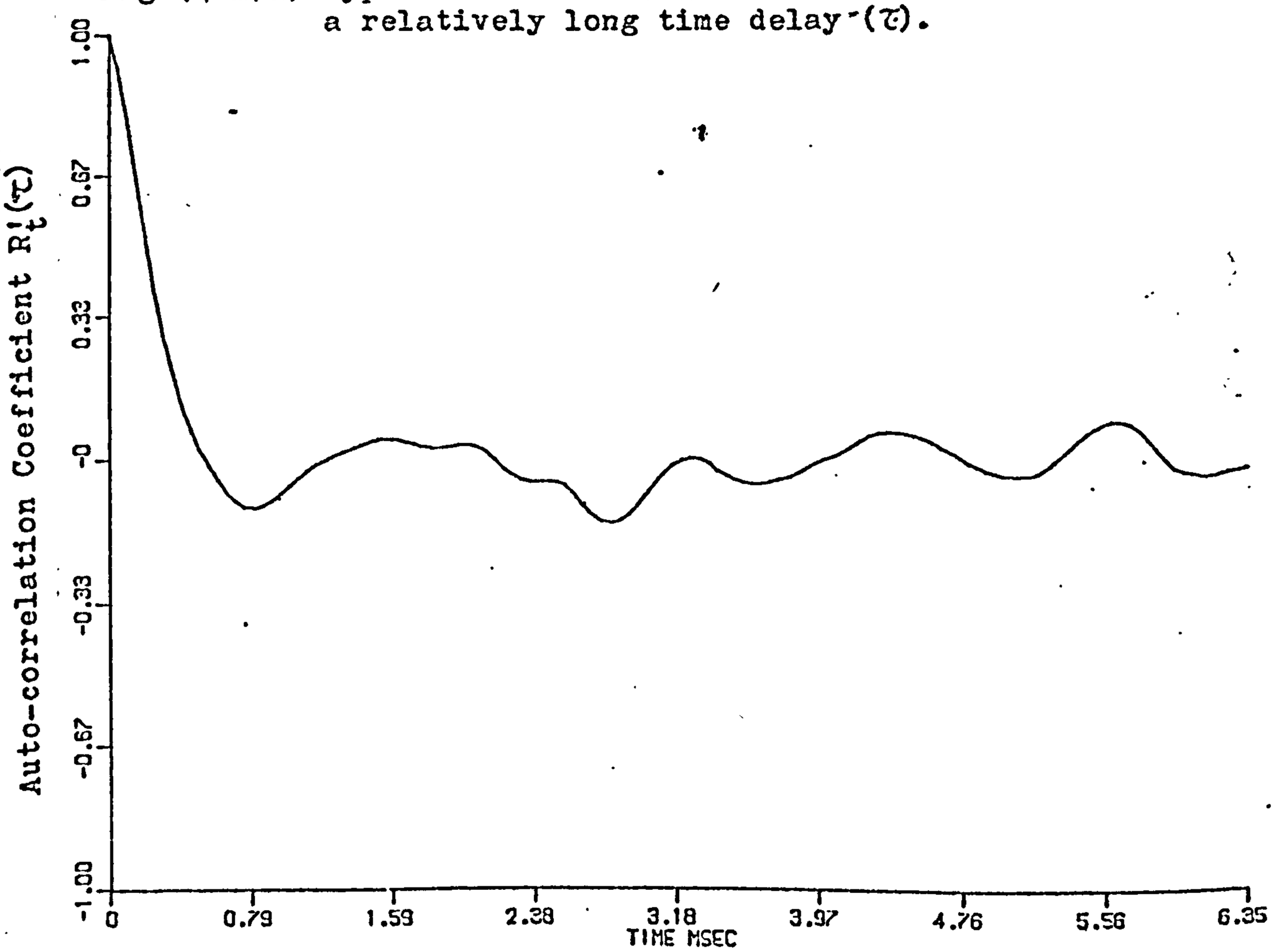

Fig (4-27b) Typical auto-correlation coefficient curve showing the maximum correlation time of turbulence eddies in a S.I. engine.

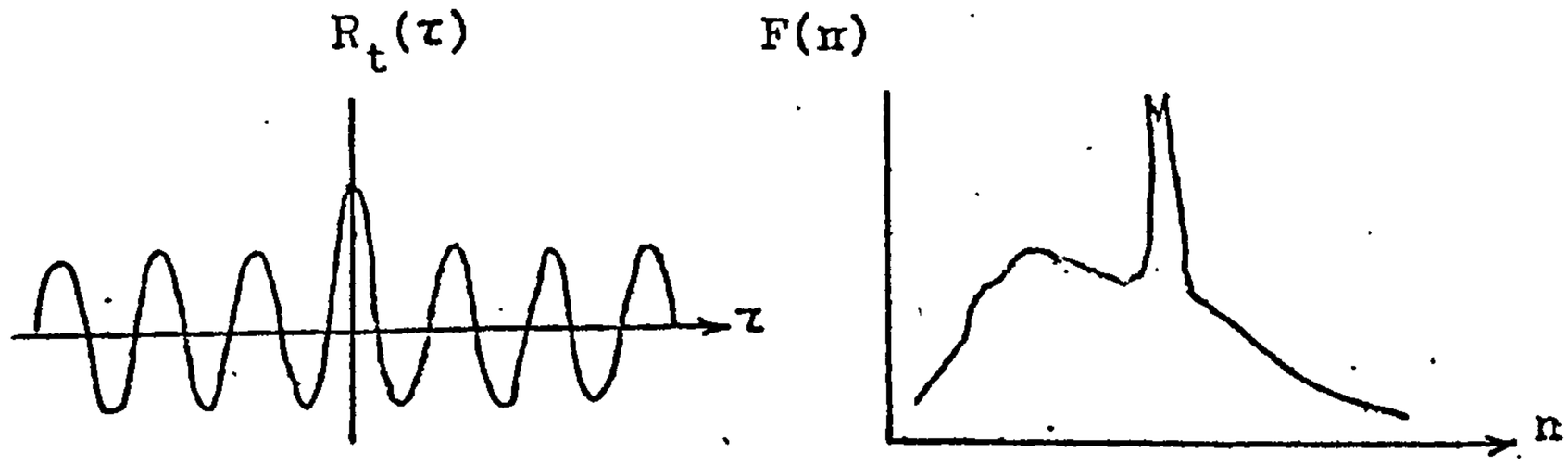

a- Turbulence signal plus sine wave.

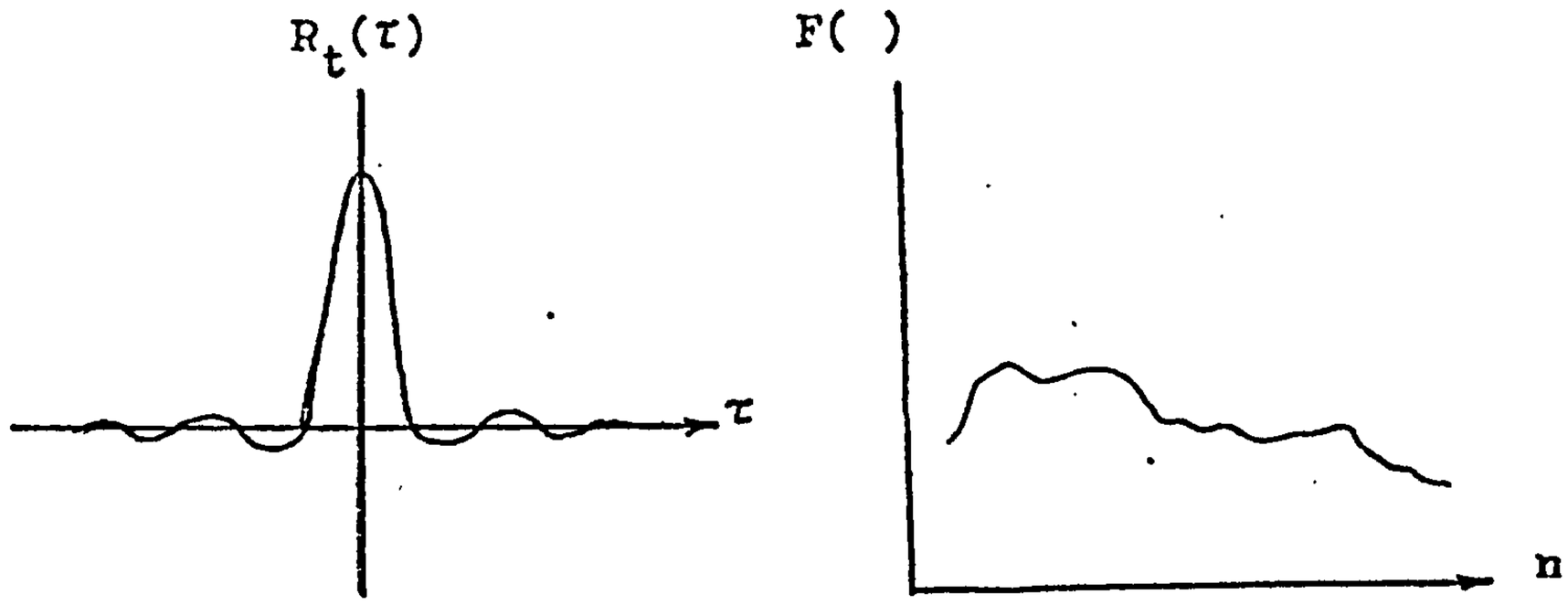

b- Turbulence signal plus white noise

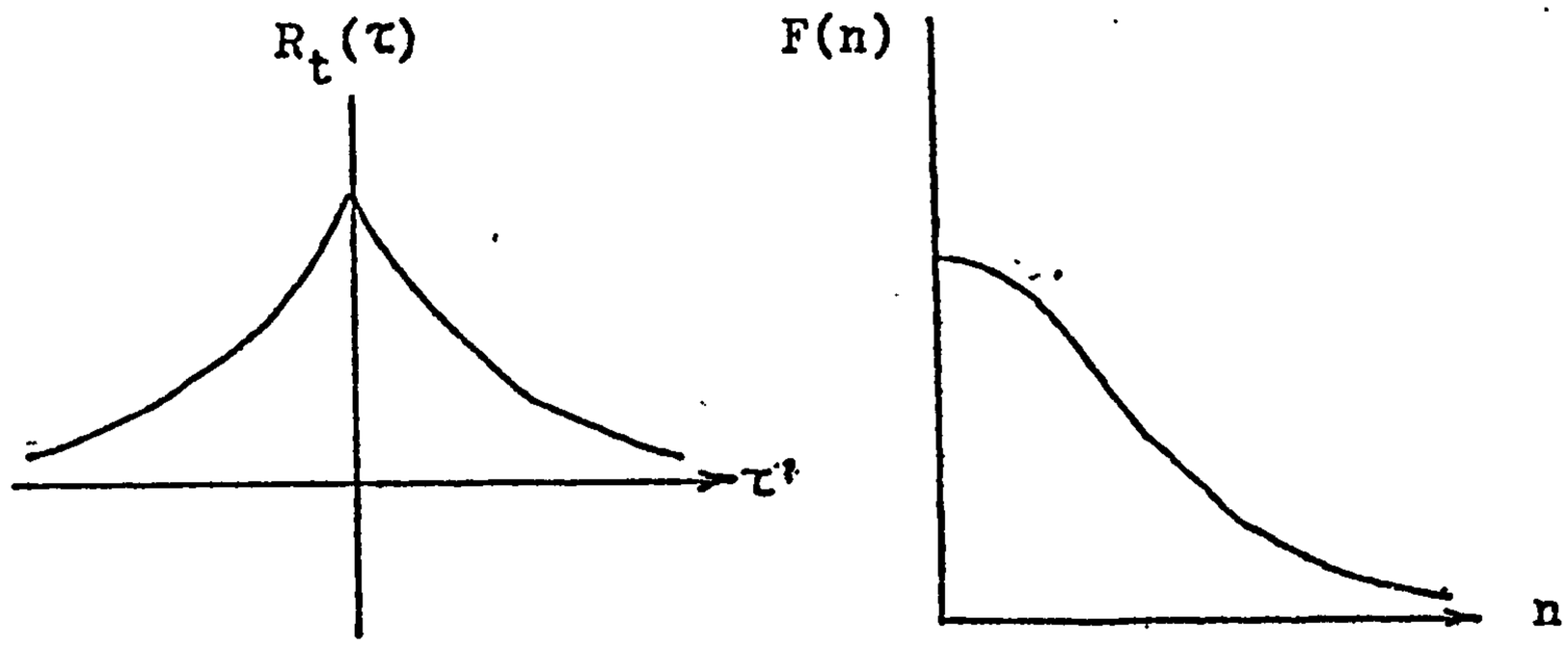

c- Exponential correlation function

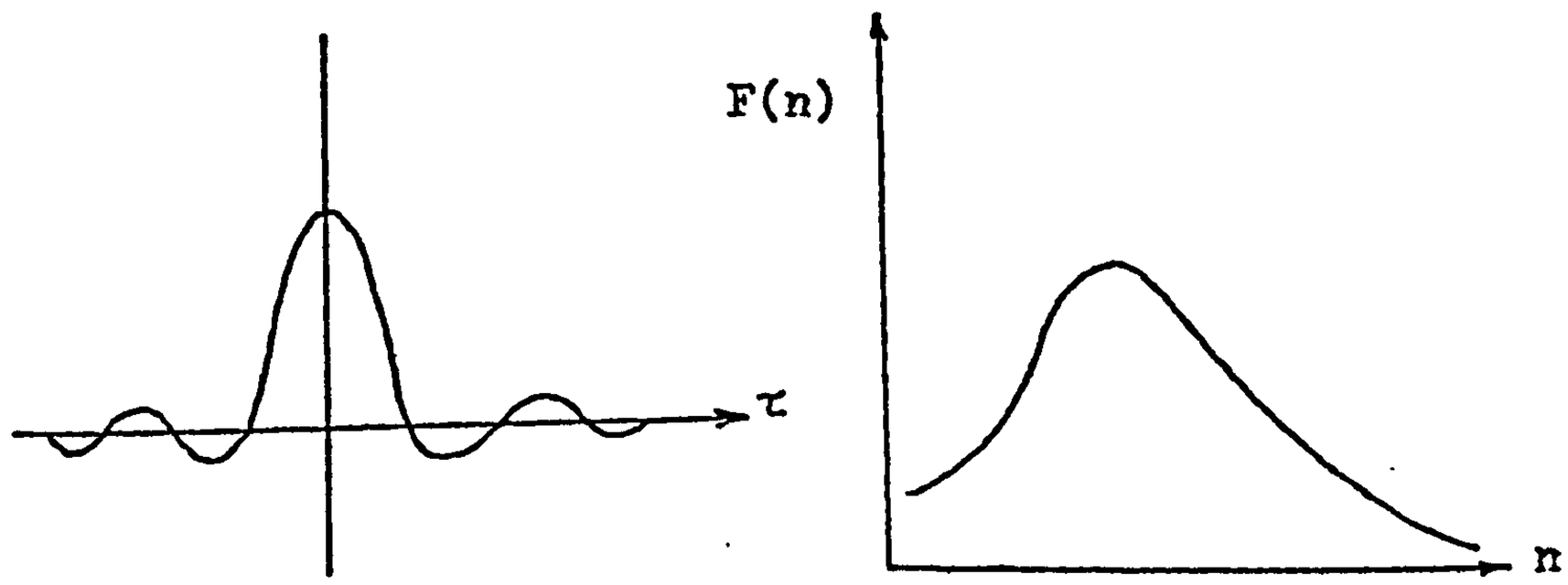

d- Exponential cosine correlation function

Fig (4-28) Typical examples of auto-correlation coefficients and power spectrum functions of turbulence signals when corrupted with a sinusoid signal or white noise as well as the normal signals .

Fig (4-29) A flow chart of the Spectral Analysis program.

1- DATA PREPARATION.

i- Introduce a turbulence signal for an engine cycle.

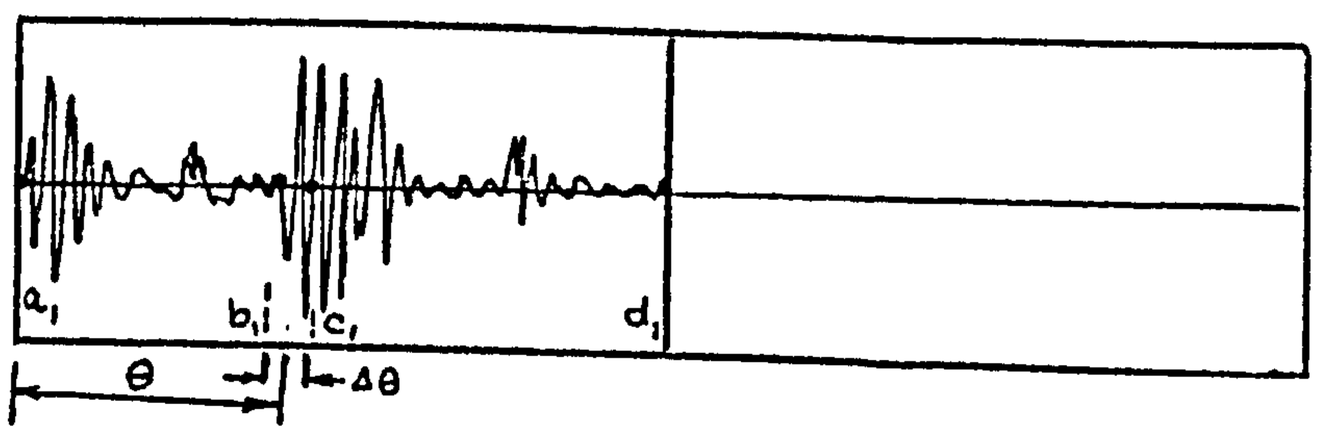

ii- Shift the signal , to the left, by a time interval (θ-Δθ/2)

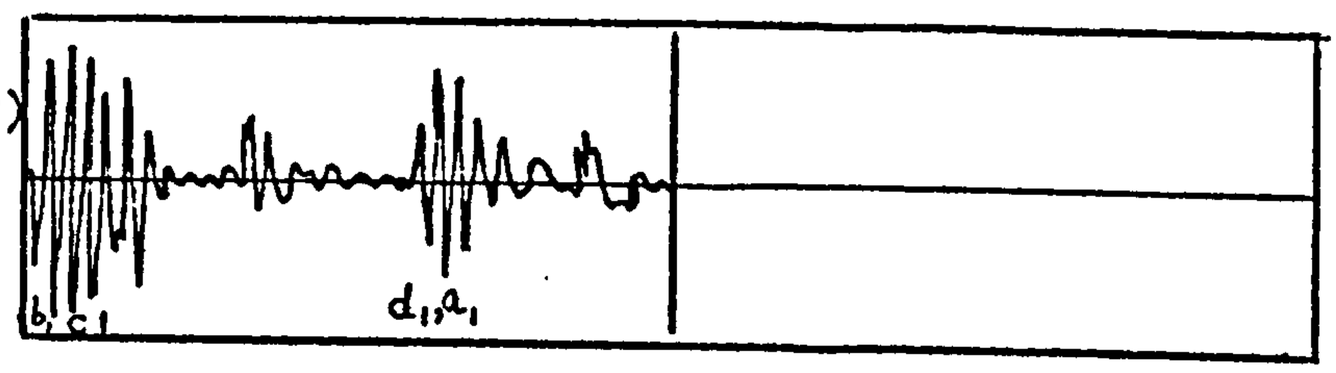

iii-Clear the data block after a signal width of (Δθ).

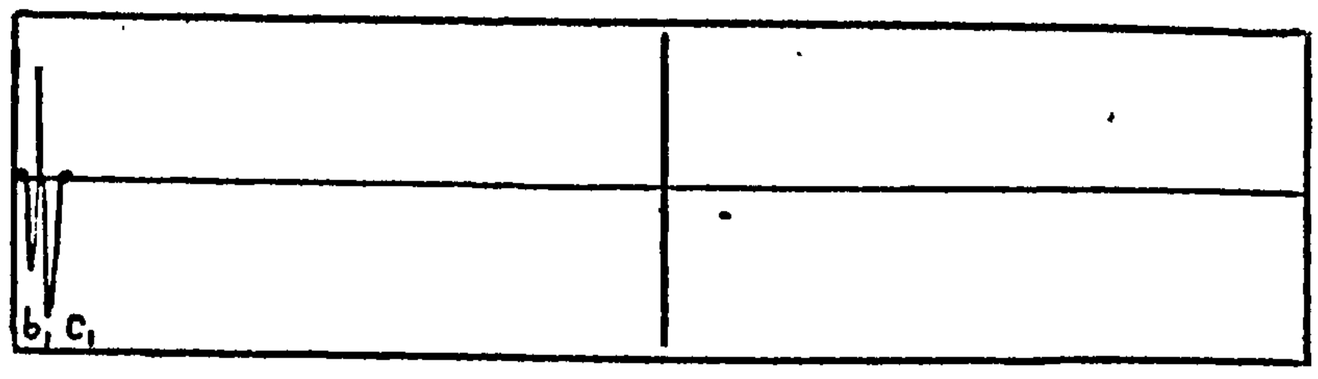

iv-Add the previously isolated and stored signal ,in data block (1), to the isolated signal of data block(0)

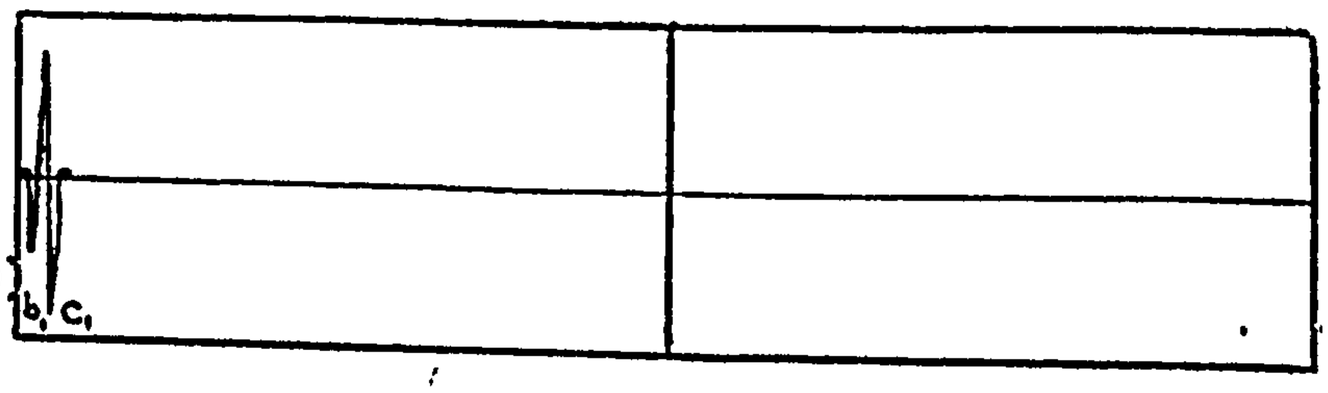

v-Shift the resulting signal in step(iv) by a time interval of(Δθ).

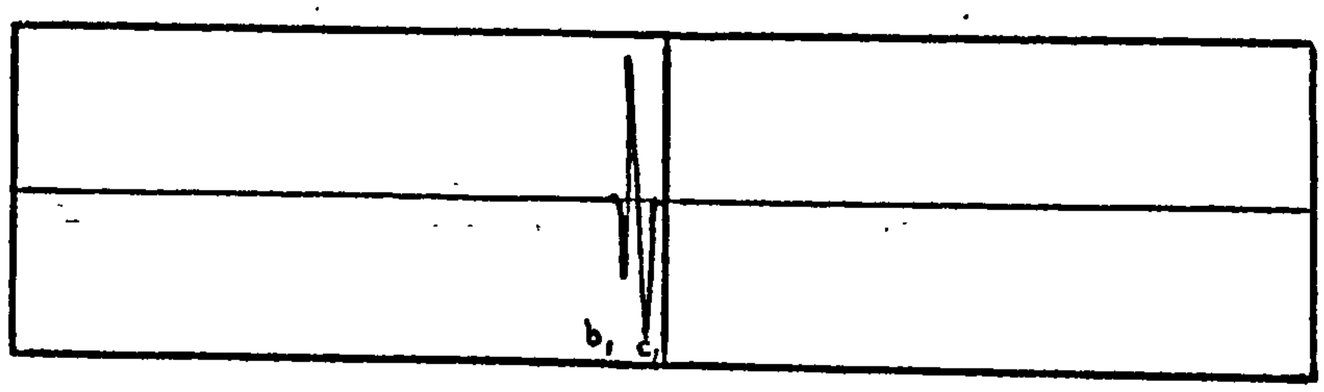

vi-Store the resulting signal in data block (1).

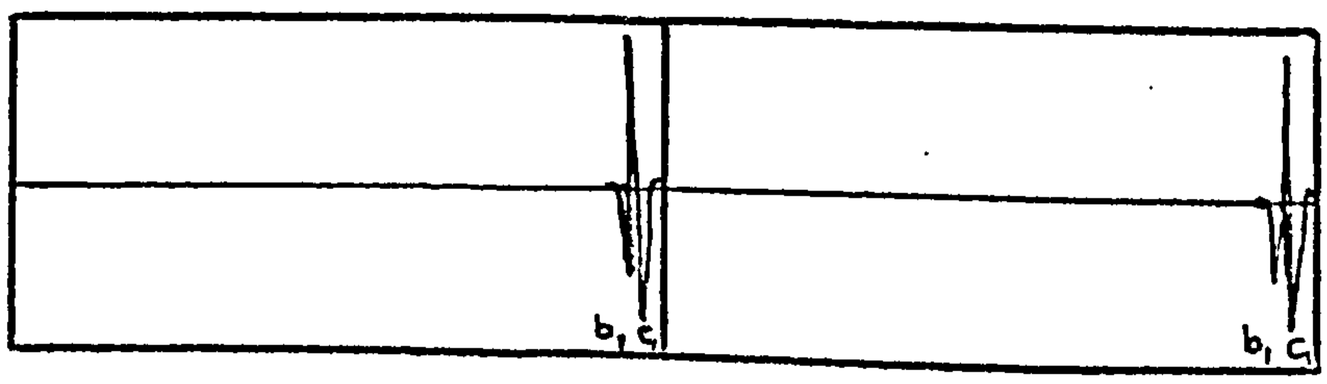

1.1. Isolating the first Cycle Sample ,of a multiple data record, for turbulence analysis at crank angle (θ).

i-

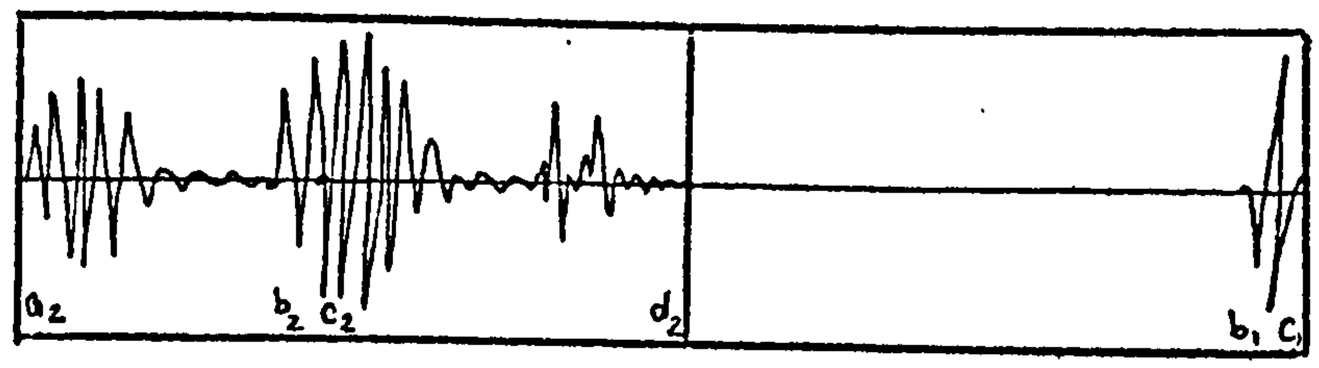

ii-

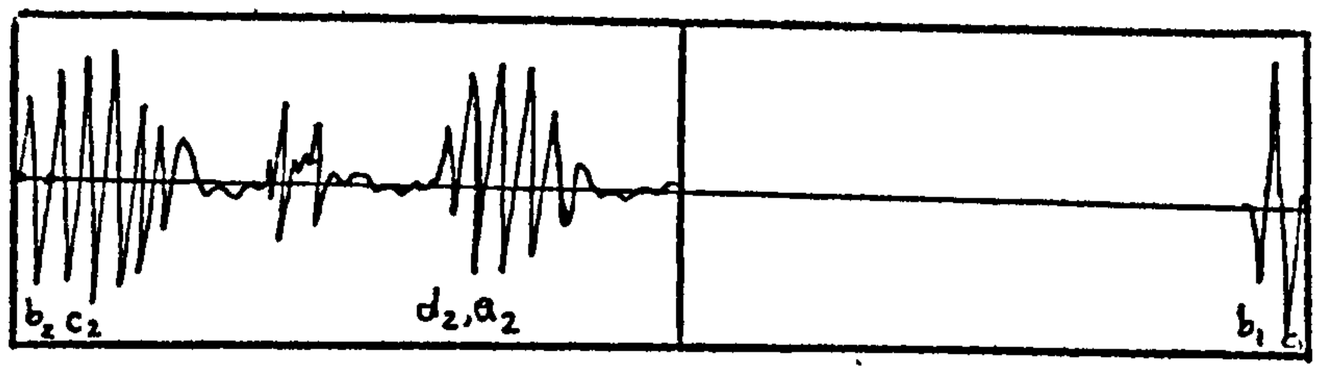

iii-

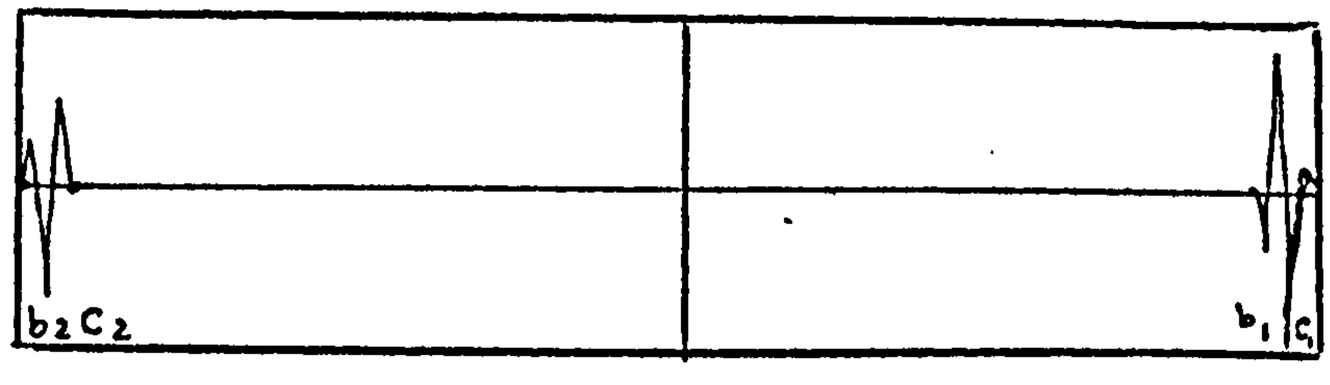

iv-

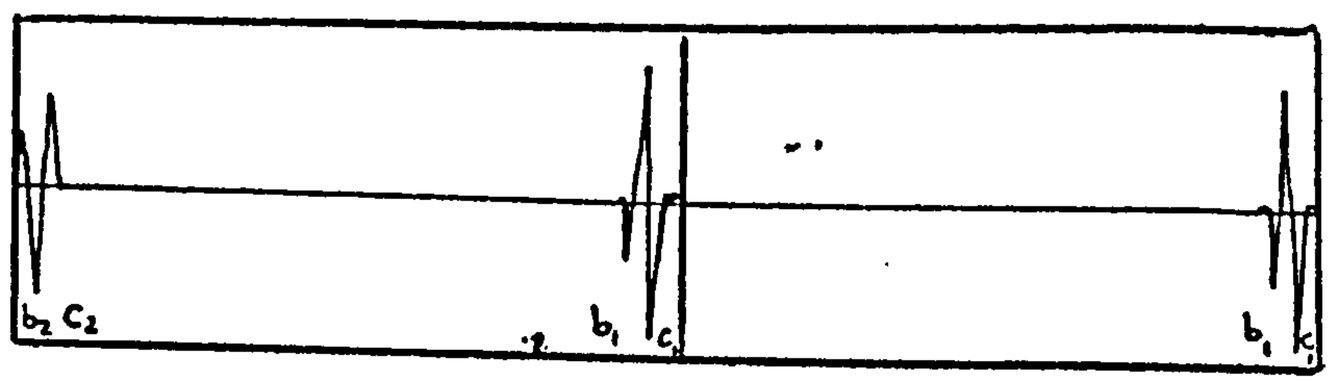

v-

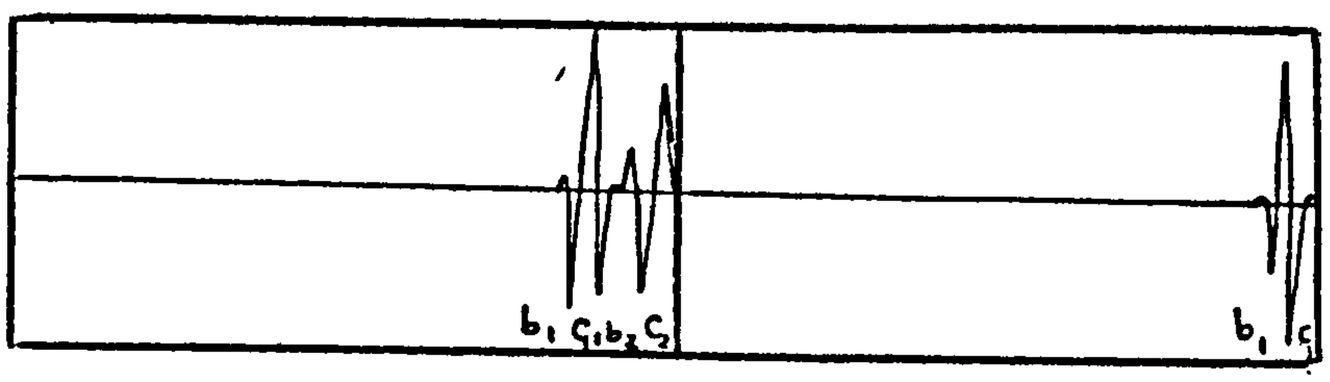

vi-

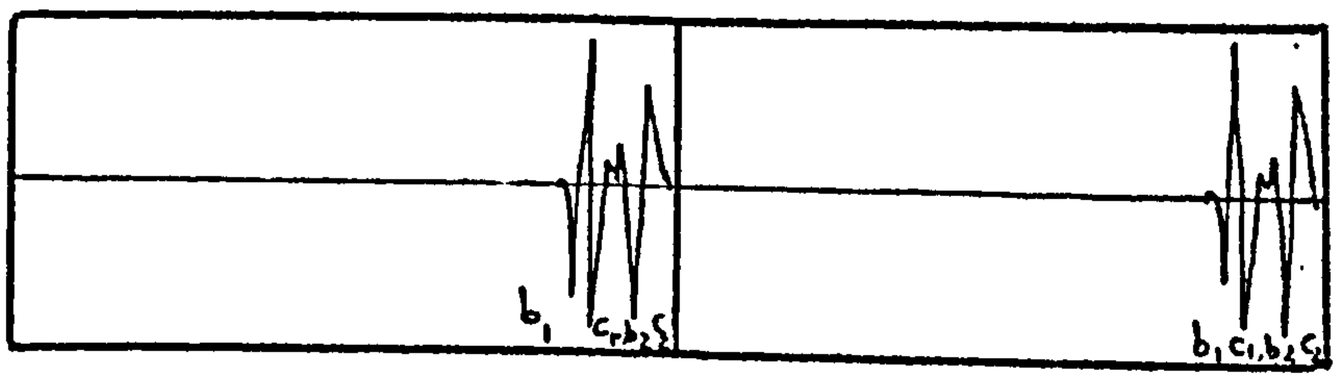

1.2. Isolating, joining and storing the second Cycle sample for turbulence analysis at crank angle (Θ).

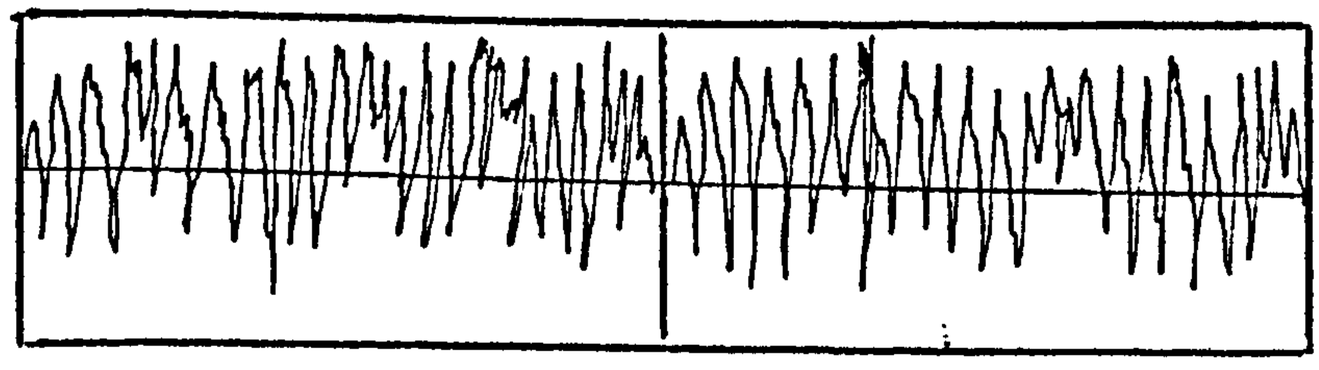

1.N. Final stage of sampling procedure for turbulence signal.

2-Transformation of data to zero mean value.

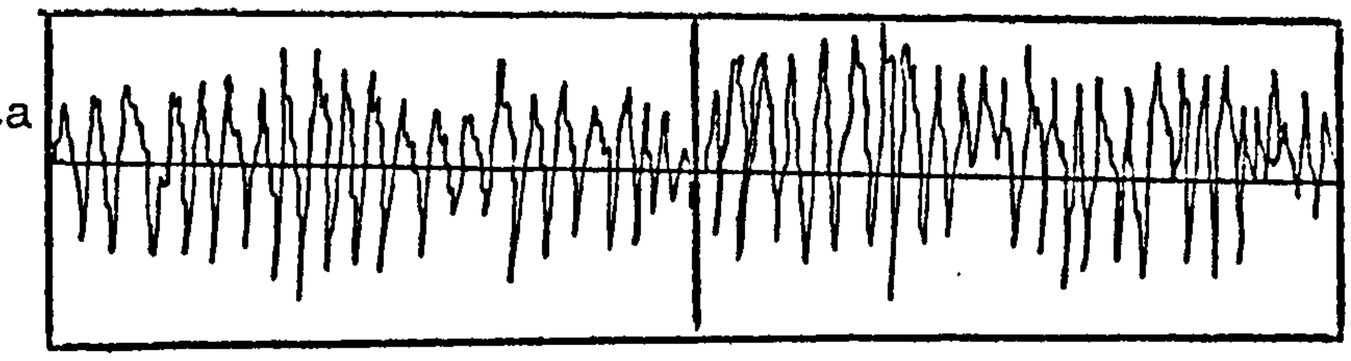

3-Obtaining the original (raw) power spectrum.

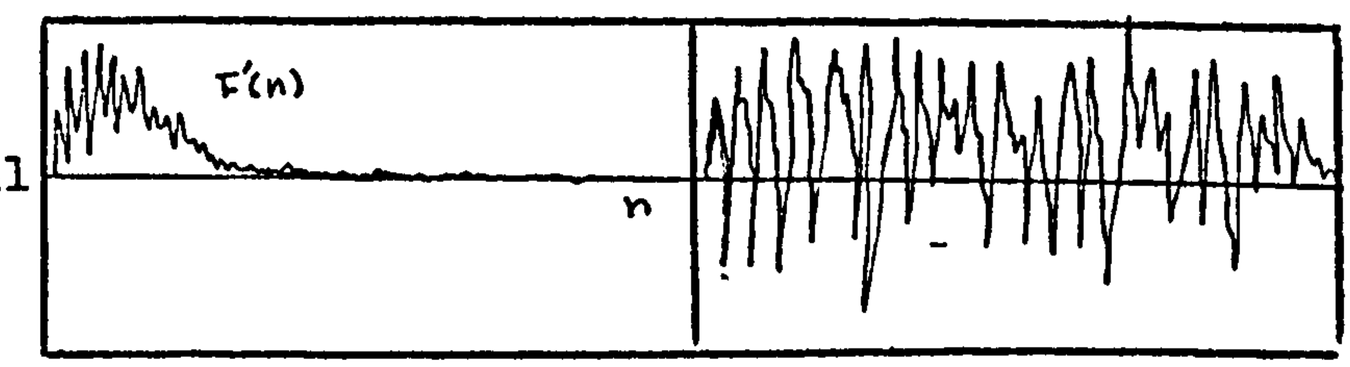

4-Obtaining the auto-correlation function.

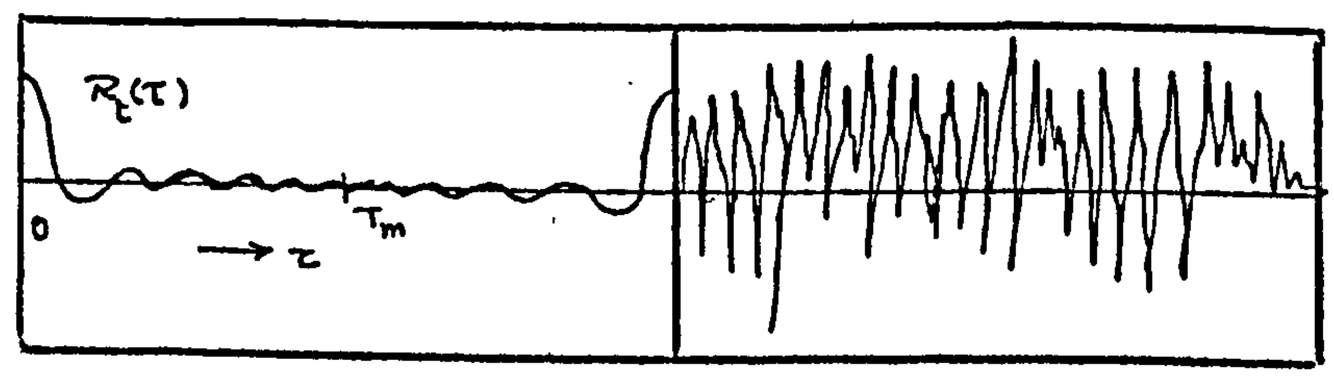

5-Obtaining the auto-correlation coefficient and storing same data in block(1).

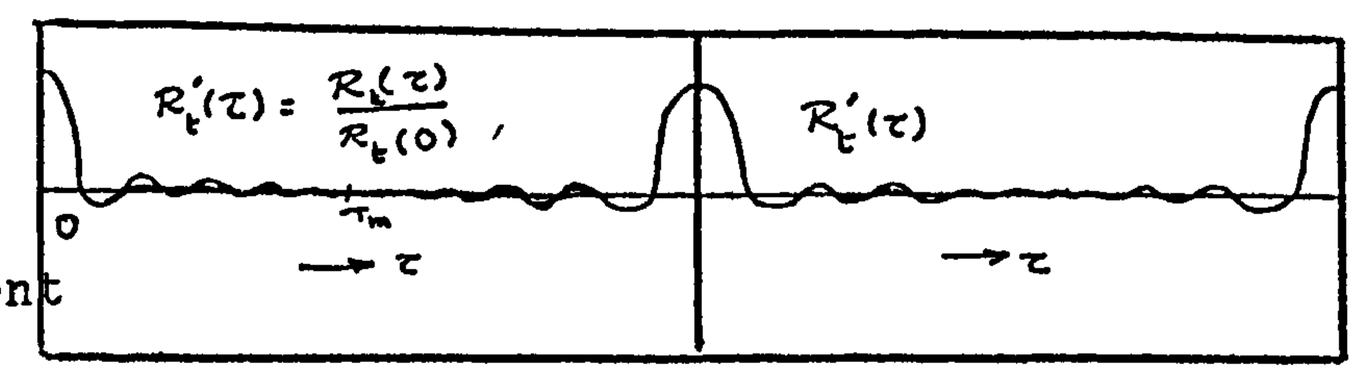

6-Application of a rectangular window on the auto-correlation coefficient.

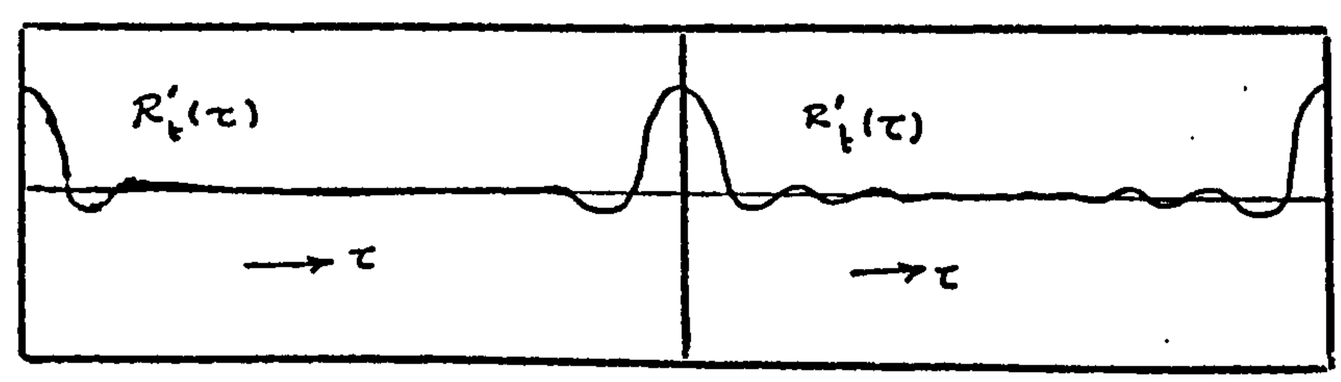

7-Obtaining a smoothed and normalized power spectrum

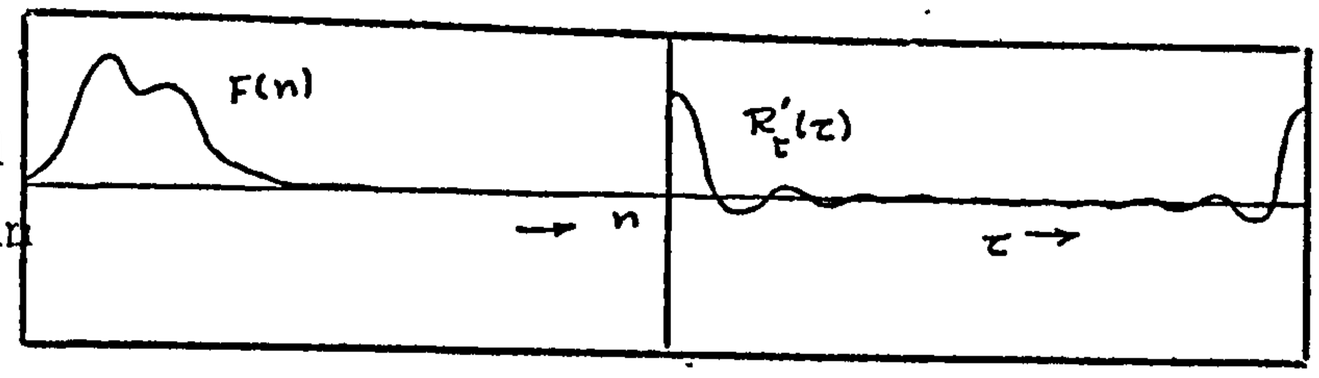

8-Obtaining the percentage of total turbulent energy at different frequencies.

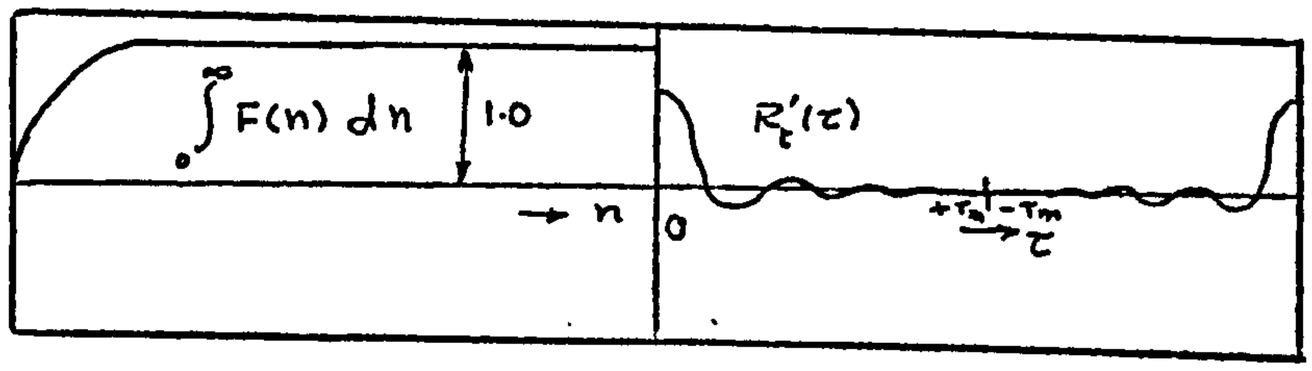

9-Loading $R_t'(\tau)$ into block (0) and shifting the curve to center of data block.

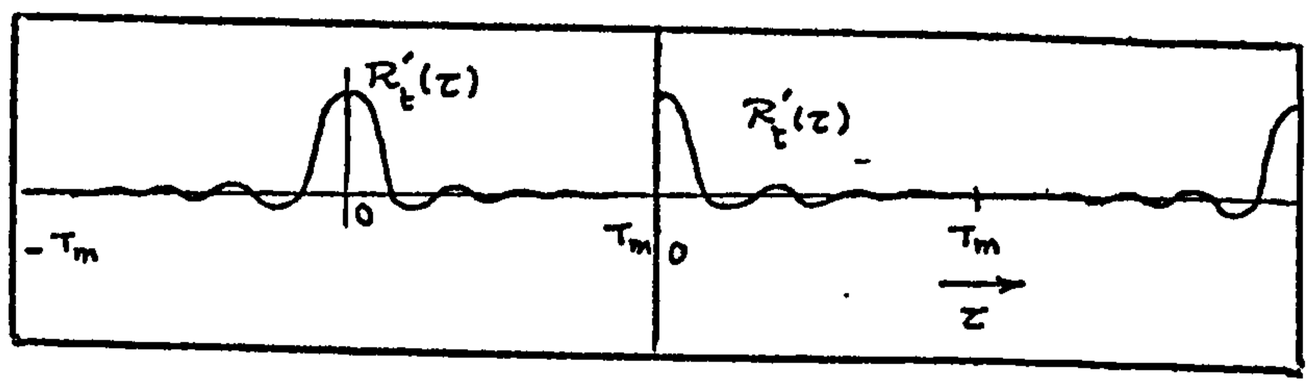

10-Obtaining the 'time micro-scale 'by double differentiation of $R_t'(\tau)$

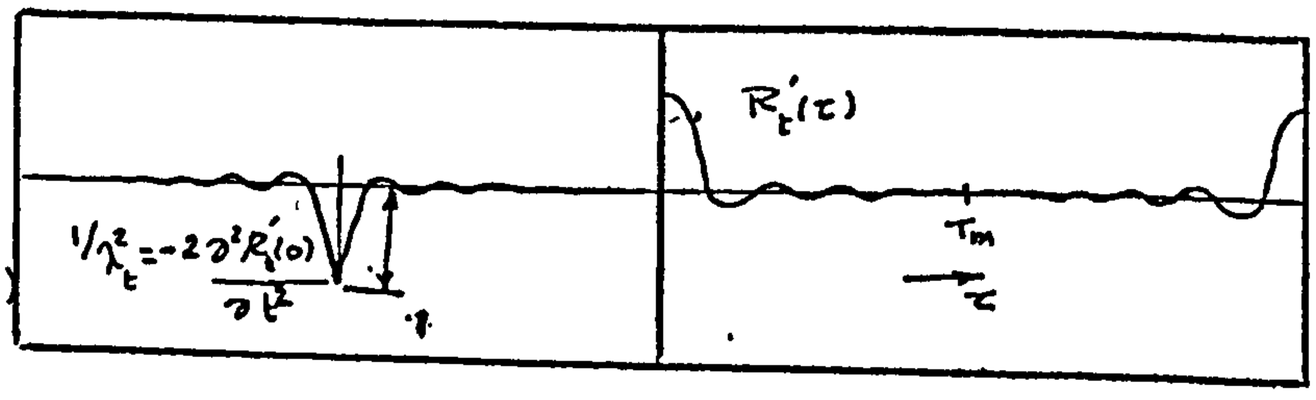

11-Loading $R_t'(\tau)$ into block (0) and isolating its positive part.

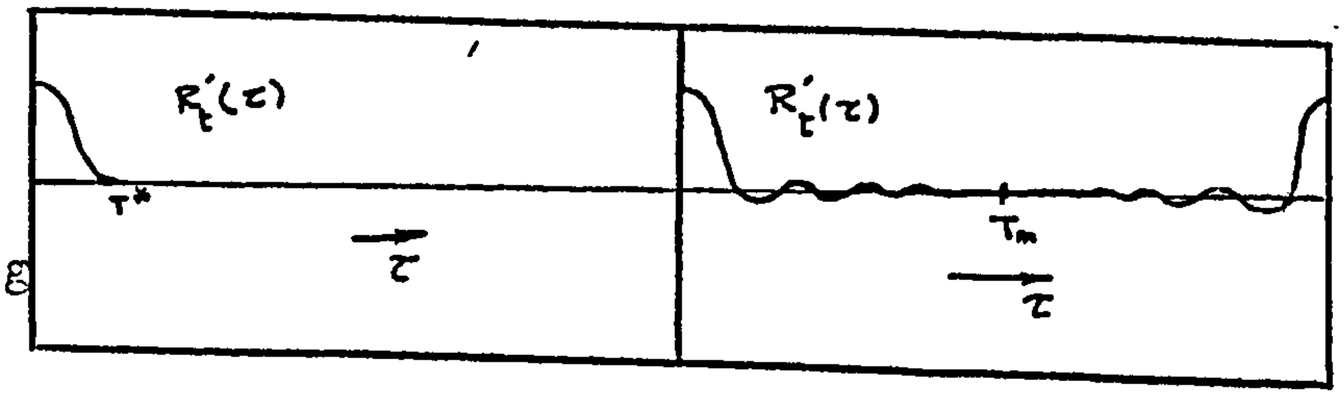

12-Obtaining the 'time macro-scale' by integrating $R_t'(\tau)$.

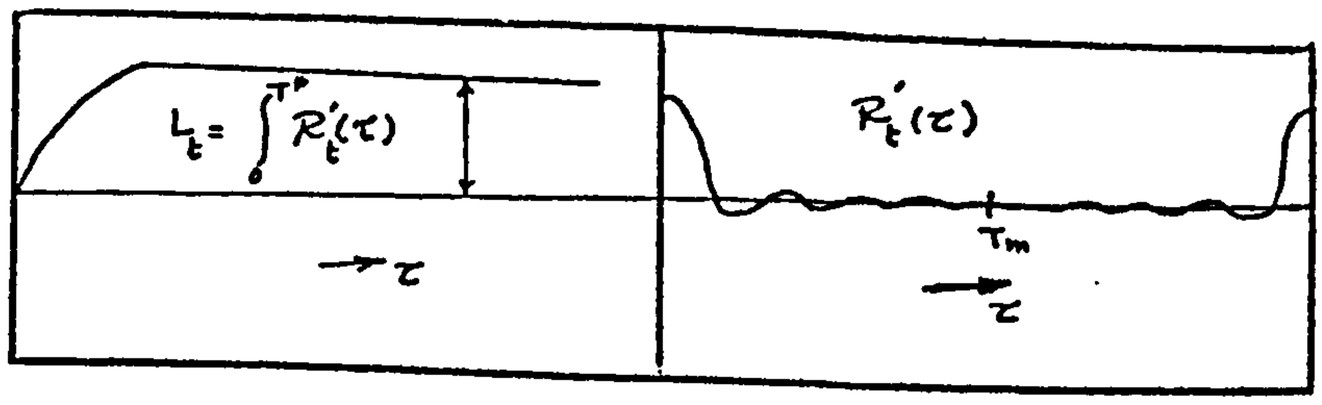

5. MOTORED ENGINE CONFIGURATION AND EXPERIMENTAL TEST PROGRAM

The characteristics of the turbulent flow field inside the combustion chambers of two commercial spark ignition engines were investigated in the present work. These engines are a Rolls-Royce V8 (6 litre) engine and a Ford V4 (2 litre) engine. Tables (5-1) and (5-2) give the technical data of the two engines.

The engines were motored during the tests by a 20 h.p. 3500 r.p.m., AC motor, which was controlled by a double induction regulator. Table (5-3) gives the technical data of the motor and regulator units. Fig. (5-1) shows the motoring configuration for the Ford engine.

Fig. (5-2) shows the combustion chamber of the Rolls-Royce engine which is basically a wedge shape chamber with a shallow bowl in the piston, while Fig. (5-3) shows detailed view and cross sections of wedge chamber. The combustion chamber of the Ford engine is of the Heron type. The dimensions of the bowl in the piston are given in Table (5-1).

The engine tests were carried out using plain inlet valves as well as modified ones fitted with guide vanes. A detailed description of these modifications is given in the following section. Other modifications such as local turbulence promoters at the spark plug location were tested with plain inlet valves.

TABLE (5-1) TECHNICAL DATA FOR THE FORD ENGINE

Engine type 2.0 litre HC-V4 4 stroke engine

Bore	93.67 mm
Stroke	72.42 mm
Connecting Rod Length	143.28 mm
Inlet Valve Diameter	41.0 mm
Exhaust Valve Diameter	37.0 mm
Diameter of Bowl in the Piston at Top	65.786 mm
Diameter of Bowl in the Piston at Bottom	53.34 mm
Maximum Inlet Valve Lift	8.94 mm
Maximum Exhaust Valve Lift	8.865 mm
Cubic Capacity	1996 cc
Compression Ratio	8.9:1
Inlet Valve Opening	27° BTDC
Inlet Valve Closure	65° ABDC
Exhaust Valve Opening	69° BBDC
Exhaust Valve Closure	23° ATDC
Horsepower	82 PS
at	5000 r.p.m.
Torque	14.7 Kg m
at	3000 r.p.m.
Ignition Timing:	(17°-19°) BTDC at 1000 r.p.m.
	(21.7°-23.7°) BTDC at 2000 r.p.m.
	(24.2°-26.2°) BTDC at 2550 and above.

TABLE (5-2) TECHNICAL DATA OF THE ROLLS-ROYCE ENGINE

Engine Type 6 litre - V8 4 stroke engine

Bore	104.14 mm
Stroke	99.06 mm
Connecting Rod Length	165.10 mm
Inlet Valve Diameter	48.26 mm
Exhaust Valve Diameter	39.116 mm
Maximum Inlet Valve Lift	10.668 mm
Inlet Valve Opening	10.5° BTDC
Inlet Valve Closure	75.5° ABDC
Exhaust Valve Opening	52.5° BBDC
Exhaust Valve Closure	33.5° ATDC
Compression Ratio	9:1
Ignition Timing	5.0° BTDC at 800 r.p.m. 13.0° BTDC at 1000 r.p.m.

TABLE (5-3) RELEVANT SPECIFICATIONS OF THE DRIVING MOTOR AND THE REGULATOR

a) Motor

Manufacturer:	Laurence Scott Electromotors Ltd.				
Type:	N.S. Commutator Motor				
BHP:	20/2.85	r.p.m:	3500/500	Cycles:	50
Primary Volts:	400	Amps:	32/29	Phase:	3
Secondary Volts:	129	Amps:	39/42	Phase:	6

b) Regulator:

Manufacturer:	Laurence Scott Electromotors Ltd.				
Type:	Double Induction Regulator				
K.V.A.:	14.1	Galls Oil:	30	Cycles:	50
Primary Volts:	400	Amps:	12/16	Phase:	3
Secondary Volts:	0/112	Amps:	39/42	Phase:	6

5.1 Experimental Test Programmes and Their Objectives

The main objectives of the test programmes carried out on both engines could be outlined under the following items:

i) Measurements of gas velocities in the inlet manifolds of the engines. This enables investigating the extent of cyclic variations in gas velocities inside the intake during the induction period.

ii) Investigation of gas velocity and turbulence characteristics inside the combustion chambers of original engine designs under different operating conditions. This includes the study of the following factors:

   a) Cylinder-to-cylinder variations.

   b) Effect of engine speed.

   c) Effect of throttling.

   The results of this study will enable the determination of the extent of cyclic variations in gas velocities and turbulence characteristics under different operating conditions. Also, the turbulence data obtained during this study will enable the establishment of correlations between the characteristics of the turbulence field inside the engine and other fields such as pipe flow or flow over flat plates.

iii) Investigation of the effect of different turbulence promoting devices on the characteristics of the developed turbulent flow field inside the combustion chamber of spark ignition engines. These devices could be divided into four main groups according to their associated flow mechanisms as follows:

a) Devices which are intended to create strong directed motion during the induction period which could persist during the compression stroke, especially during the time of ignition and the early development of the flame front. A typical example of these devices is the shrouded valve where appropriate setting of the shroud position, could result in a significant increase in intake velocities as well as the creation of a swirl gas motion inside the combustion chamber. Such a swirl motion improves the homogeneity of the mixture and energises the process of generating small scale turbulence by friction forces on the walls of the combustion chamber.

b) Devices which are intended to disrupt the jet nature of the intake flow and create small scale turbulent eddies during theinduction period. Examples of these devices are: the use of a reduced valve lift or insertion of aerodynamic surfaces (such as delta wings) in the flow passage. The effect of reduced valve lift is to increase the pressure drop across the inlet port and increase the ensuing gas velocities which consequently intensifies the mixing process and enhances the process of generating small scale turbulence.
The intended purpose of inserting delta wings in the flow passage is to utilise the known bursting phenomenon of vortex sheets generated by a swept leading edge. A sharp leading edge of a swept back wing set at a particular incidence to the flow direction usually generates a pair of conically-rolled vortex sheets which break down into a turbulent core at some distance from the vortex depending on the angle of sweep back of the leading edge and the incidence of the wing. For large angles of sweep back and low incidences, the burst occurs in the vortex downstream of the wing (151).

Fig. (5-4) shows the flow mechanism of such phenomenon, as interpreted by Lambourne and Bryer (152) from the observations of the behaviour of die filaments in water tunnels using flat plate delta wings. Fig. (5-4c) shows the details of the bursting process.

c) Devices which combine both effects of creating directed gas motion as well as small scale turbulence. These include a group of inlet valves fitted with guide vanes soldered on the valve seat at some angle of incidence to the inlet flow direction.

d) Devices which could disrupt any large scale motion inside the combustion chamber around the spark plug location and generate small scale turbulence eddies without altering the main flow field characteristics inside the combustion chamber.

5.1.1 Details of the Experimental Test Programme Carried Out on the Rolls-Royce Engine

The details of the extensive experimental test programme carried out on the Rolls-Royce engine are described below:

i) Measurements of gas velocities in the inlet manifold at full throttle condition and different engine speeds, e.g. 700, 1000, 1200 and 1500 r.p.m. Fig. (5-5) shows the cross-section of the inlet manifold and the locations of measurements.

ii) Measurements of gas velocities at different locations inside the combustion chamber, as shown in Fig. (5-3) at different probe orientations and different probe traverses. These measurements were carried out at full throttle condition and constant engine speeds of 700 r.p.m.

iii) Measurements of gas velocities and turbulence characteristics at the spark plug location for different engine cylinders at a fixed engine speed of 1000 r.p.m. and full throttle condition.

iv) Measurements of gas velocities for one particular cylinder at the spark plug location for different probe orientations and traverses at different engine speeds (700, 1000, 1200 and 1500 r.p.m.) and full throttle conditions.

v) Measurements of gas velocities and turbulence characteristics for different cylinders where modifications of the intake system were made. The tests were carried out at an engine speed of 1000 r.p.m. and full throttle conditions. These modifications include the following:

a) A shrouded inlet valve with a 180 degree shroud Fig. (5-6). The height of the shroud was 10.66 mm and was set to give the maximum possible swirl.

b) An inlet valve for reduced lift conditions. This valve was manufactured by soldering a steel ring of 5.08 mm heighton the back of a normal valve seat. The angle of inclination of the ring was turned to match the inlet port construction and the volume between the ring and valve stem was filled with epoxy resin and streamlined at the minimum possible radius, Fig. (5-7).

c) An inlet valve fitted with 8 guide vanes soldered on the valve seat at an angle of 60 degrees to the inlet flow direction. The height of these vanes was 10.3 mm, Fig. (5-8).

d) An inlet valve fitted with 6 guide vanes soldered on the valve seat, Fig. (5-9). The configurations of the vanes were similar to those described in item (c).

e) An inlet valve fitted with 4 long guide vanes extending on the valve stem. The vanes were set at an angle of 20 degrees to the axis of the valve stem, while the height of these vanes was 33.86 mm, Fig. (5-10).

f) An inlet manifold fitted with a set of two delta wings having a wedge angle of 20 degrees and a chord length of 55 mm, Fig. (5-11). The delta wings were set at an angle of attack of 14 degrees to the flow direction inside the inlet manifold as shown in Fig. (5-12).

vi) Investigation of the flow field characteristics at the spark plug location where a local turbulence promoter was inserted. This consisted of a serrated plug as shown in Fig. (5-13). The height of the serrations was 2.5 mm and the inner and outer diameters of the serrated ring were 10 and 12 mm respectively. The tests were carried out using plain valves.

Table (5-4) gives a summary of the test conditions for the experimental test programme carried out on the Rolls-Royce engine.

TABLE (5-4) TEST CONDITIONS FOR THE EXPERIMENTAL TEST PROGRAMME CARRIED OUT ON THE ROLLS-ROYCE ENGINE

1. Original Engine Design (plain valves) measurements inside the combustion chamber

A.1 Probe Located at the Spark Plug.

Cylinder Designation*	Probe Vertical Location (mm)**	Wire Direction (Degrees) ***	Engine Speed	Throttle Setting
3A	17.8 12.7 7.6 0.0	))(0.0,90,300))(60, 300,330))	 700 1000 	)) Full) Half)Quarter
2A	17.8	300	1000 1200 1500	)) Full)
4A 2B 3B 4B	17.8 17.8 17.8 17.8	)))) 300	))1000))	)))) Full

A.2 Probes Located at Different Positions in the Combustion Chamber (see Fig. (5-3) for positions and wires orientation)

Cylinder Designation	Probe Vertical Location (mm)	Engine Speed	Throttle Setting
1B	20 15 0.0	)) 700)	Full

TABLE (5-4) continued

2. Measurements in the Intake Manifold (see Fig. (5-5)

Cylinder Designation	Probe Vertical Location (mm)	Engine speed	Throttle Setting
1B	10, 20, 30	1000	)
	20	1200	) Full
	20	1500	)

* See Fig. (5-14)

** Traverses are measured from piston surface at TDC, i.e. at Z = 0.0 mm.

The probe is at its furthest traverse as shown in Fig. (5-3)

*** See Fig. (5-3)

3. Modified Intake System

Engine Speed = 1000 r.p.m. and Fully Opened Throttle

Probe Direction at the 300 degrees position and spark plug location.

Cylinder Designation	Type of Modification
2A	180 degrees shrouded valve
3A	Inlet Valve with 6 Vanes
4A	Reduced Valve Lift Inlet Valve with 4 Vanes
2B	Inlet Valve with 8 Vanes
3B	Intake fitted with Delta Wings

TABLE (5-4) continued

4 Local Turbulence Promoter at the Spark Plug Location

Cylinder Designation	Engine Speed	Throttle Setting
3A	1000	Fully Opened

5.1.2 Details of the Experimental Test Programme Carried out on the Ford Engine .

The limited power of the available motoring set has represented a major difficulty in investigating the performance of the Rolls-Royce engine at higher speeds. However, the power was quite sufficient to motor the Ford engine over a wide range of speeds between 1000 r.p.m. and 3500 r.p.m.

The motoring tests on the Ford engine were carried out to simulate two typical loading conditions on this engine namely a 90 p.s.i. BMEP and a 60 p.s.i. BMEP. The throttle setting was adjusted, therefore, to give the same intake vacuum at these loading conditions. Table (5-5) lists the values of engine speeds used in this investigation and their corresponding intake vacuum and the percentage of throttle opening relative to the fully opened condition.

The first set of tests in this programme were carried out with the engine fitted with its original plain valves, while the second set of tests have included the investigation of two modified inlet valves which have shown significant changes in tests on the Rolls-Royce engine and cause minimum restrictions to the inlet flow. The latter effects were studied in blowing rig tests Fig. (5-15) and will be discussed later. The modified valves shown in Fig. (5-16) were as follows:

a) An inlet valve fitted with six guide vanes inserted on the valve seat at an angle of 60 degrees to inlet flow direction. The slant height of these vanes was 9.4 mm.

b) An inlet valve fitted with four long vanes inclined at an angle of 20 degrees to the axis of inlet valve stem.
The slant height of these vanes was 30.86 mm and the outer edges of their bases were nearly on the outer diameter of the valve.

The effect of a local turbulence promoter at the spark plug was also investigated for the two loading conditions. The dimensions of the turbulence promoter were similar to those described for tests on the Rolls-Royce engine.

Table (5-5) lists the test conditions for the experimental test programme carried out on the Ford engine. Measurements were carried out at two traverses inside the combustion chamber, namely, a position where the wires were nearly at the cylinder head surface (denoted by Z = 0.0) and at a location 3.8 mm downwards from cylinder head surfaces. In the latter position the wires were inside the bowl with piston at TDC.

The hot wires for these tests were set at an angular position which have produced the maximum signal. This direction is marked as X-X in Fig. (4-10).

TABLE (5-5) LOADING CONDITIONS AND THEIR CORRESPONDING INTAKE VACUUM SETTINGS FOR THE FORD ENGINE

Loading Condition	60	BMEP	90	BMEP
Engine Speed r.p.m.	Intake Vacuum (mm Hg)	Throttle Setting (as % of W.O.T.)	Intake Vacuum (mm Hg)	Throttle Setting (as % of W.O.T.)
1000	282	9.23%	101.6	21.538%
1500	308.5	16.923%	165.0	26.13%
2000	320	21.538%	183.0	35.38%
2500	321	27.69%	183.0	40.0%
3000	318	30.769%	180.4	44.6%
3500	310	32.3%	167.6	50.7%

TABLE (5-6) TEST CONDITIONS FOR EXPERIMENTS ON THE FORD ENGINE

a) Original Engine Design

Probe Position (measured from the flat surface of cylinder head) mm	Engine Speed (r.p.m.)	Throttle Setting
0.0) 3.8)	) 1000) 2000) 3000))	At the corresponding values given in Table (5-5) for the two loading conditions

TABLE (5-6) Continued

b) Modified Intake System and Turbulence Promoter

Probe Position	Engine Speed (r.p.m)	Throttle Setting
3.8 For modified valves and 0.0 for the turbulence promoter	1000 2000 3500	At the corresponding values given in Table (5-5) for the two loading conditions

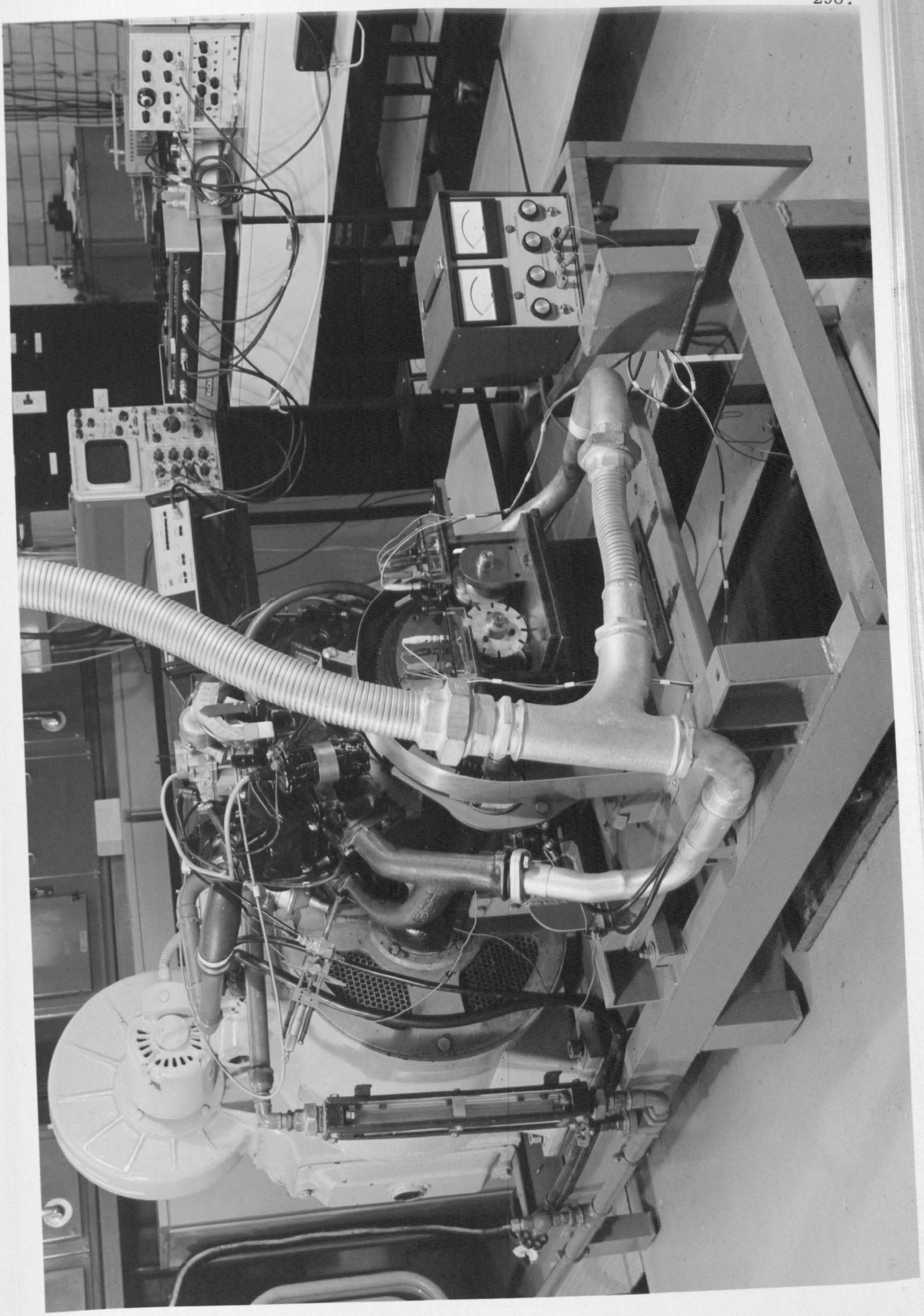

Fig. (5-1) Motored Configuration of the FORD V4 Engine

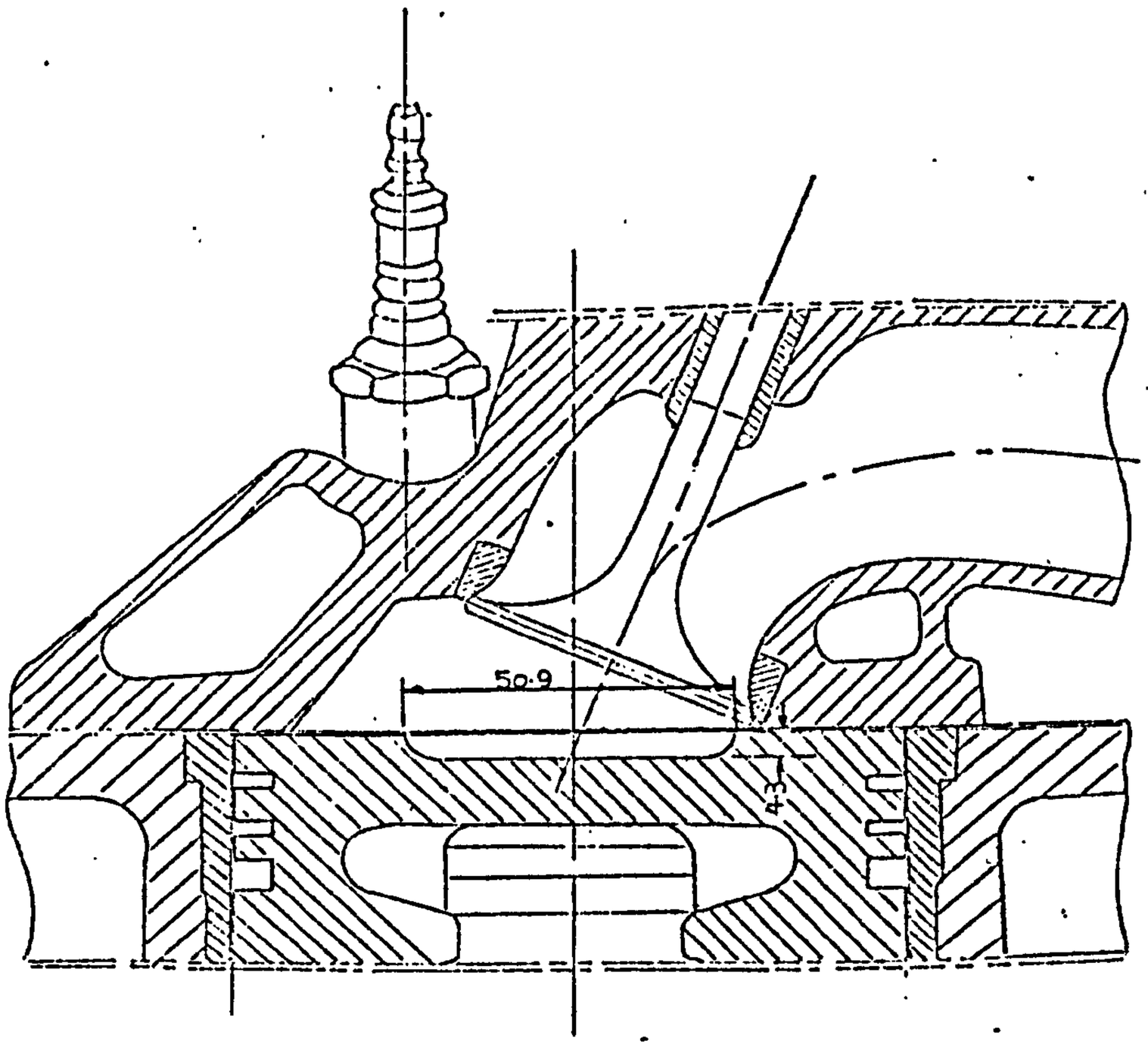

Fig (5-2) Cross section of a cylinder of the Rolls-Royce engine showing the wedge combustion chamber.

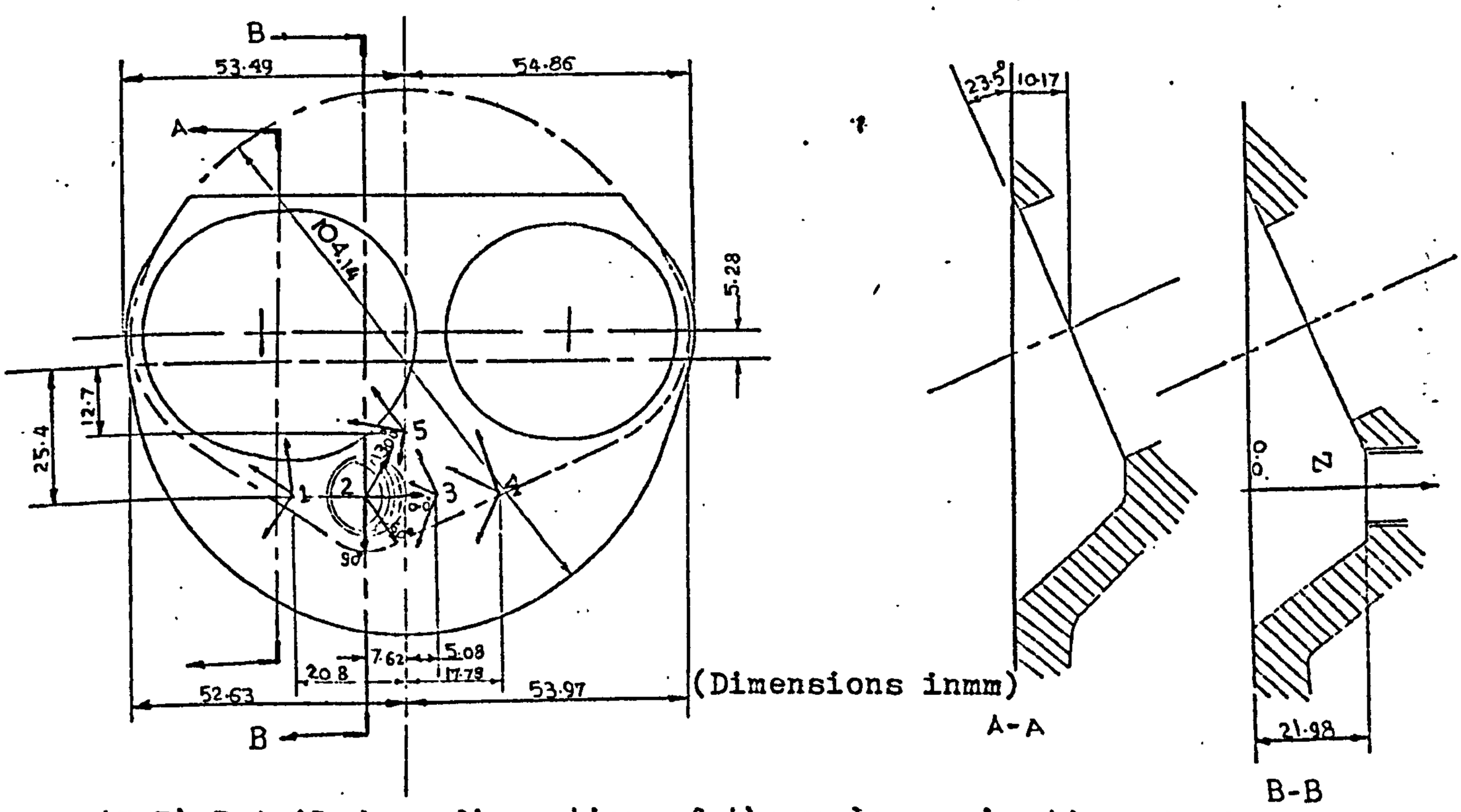

Fig (5-3) Detailed configuration of the wedge combustion chamber showing the different locations of velocity measurements and the directions of reference axes of hot wires at each loction.

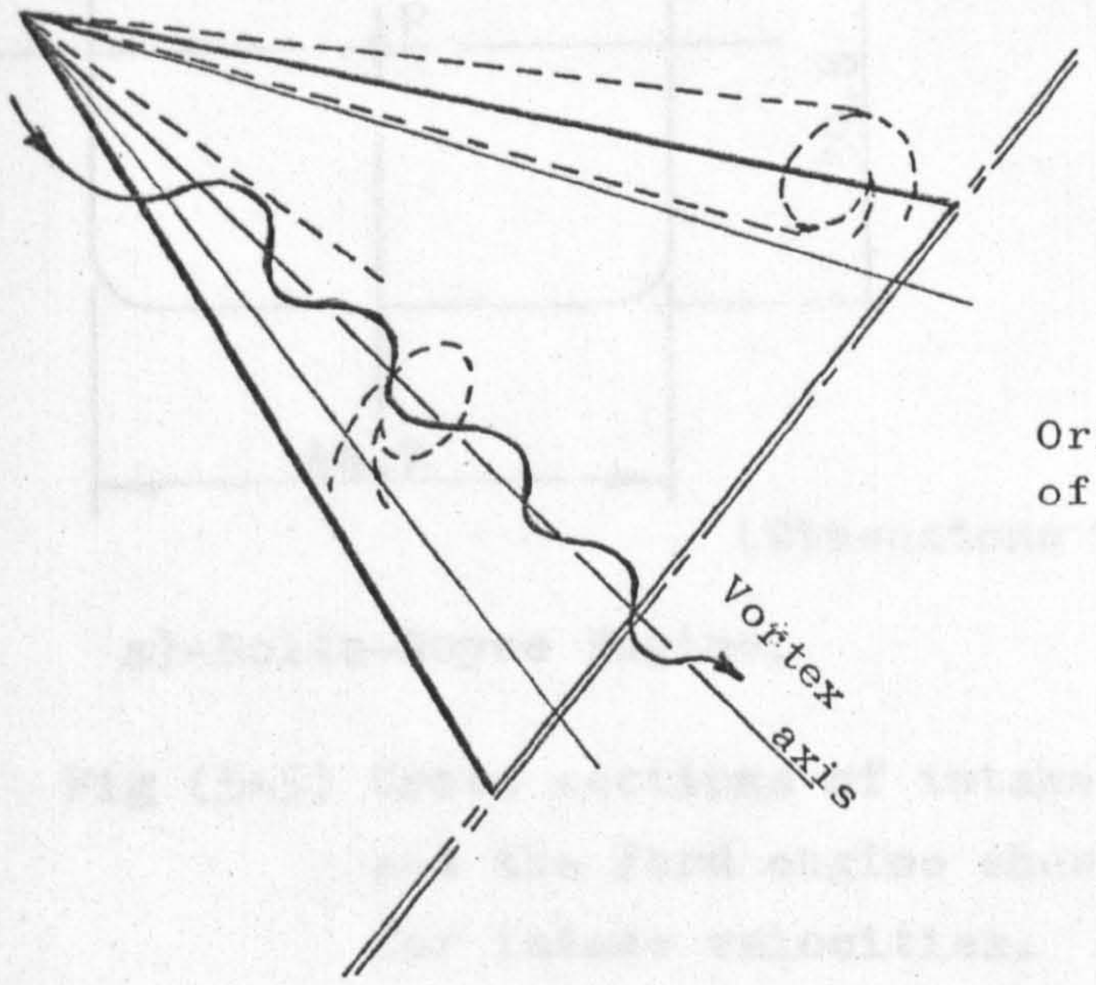

Fig (5-4a) Formation of Laminar Vortices for Sharp-Edged Delta Plate

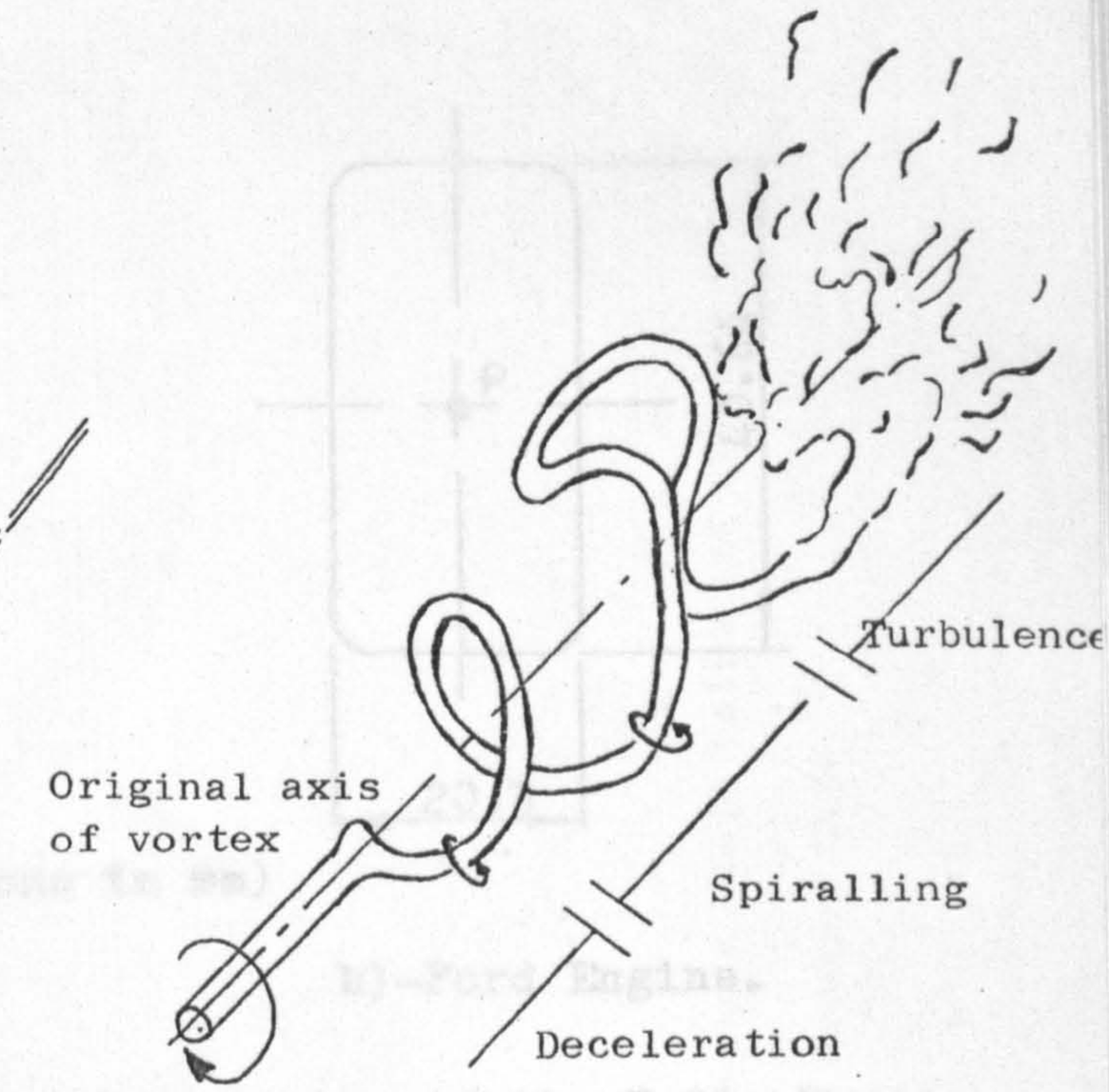

Fig (5-4b) Stages in Behaviour of Axial Filament, (152)

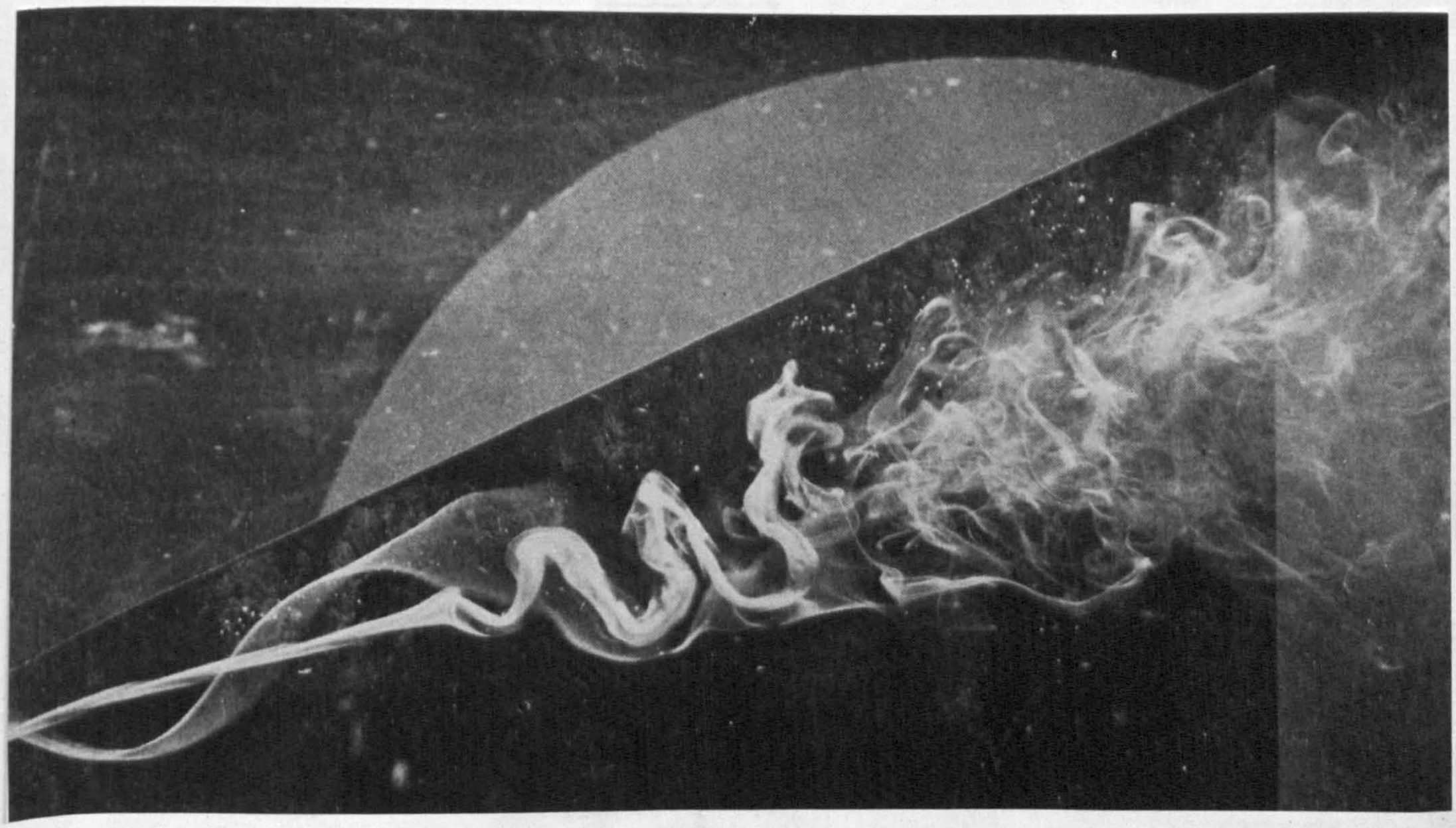

Fig. (5-4c) Details of the Bursting Process in a Water Tunnel Test (152)

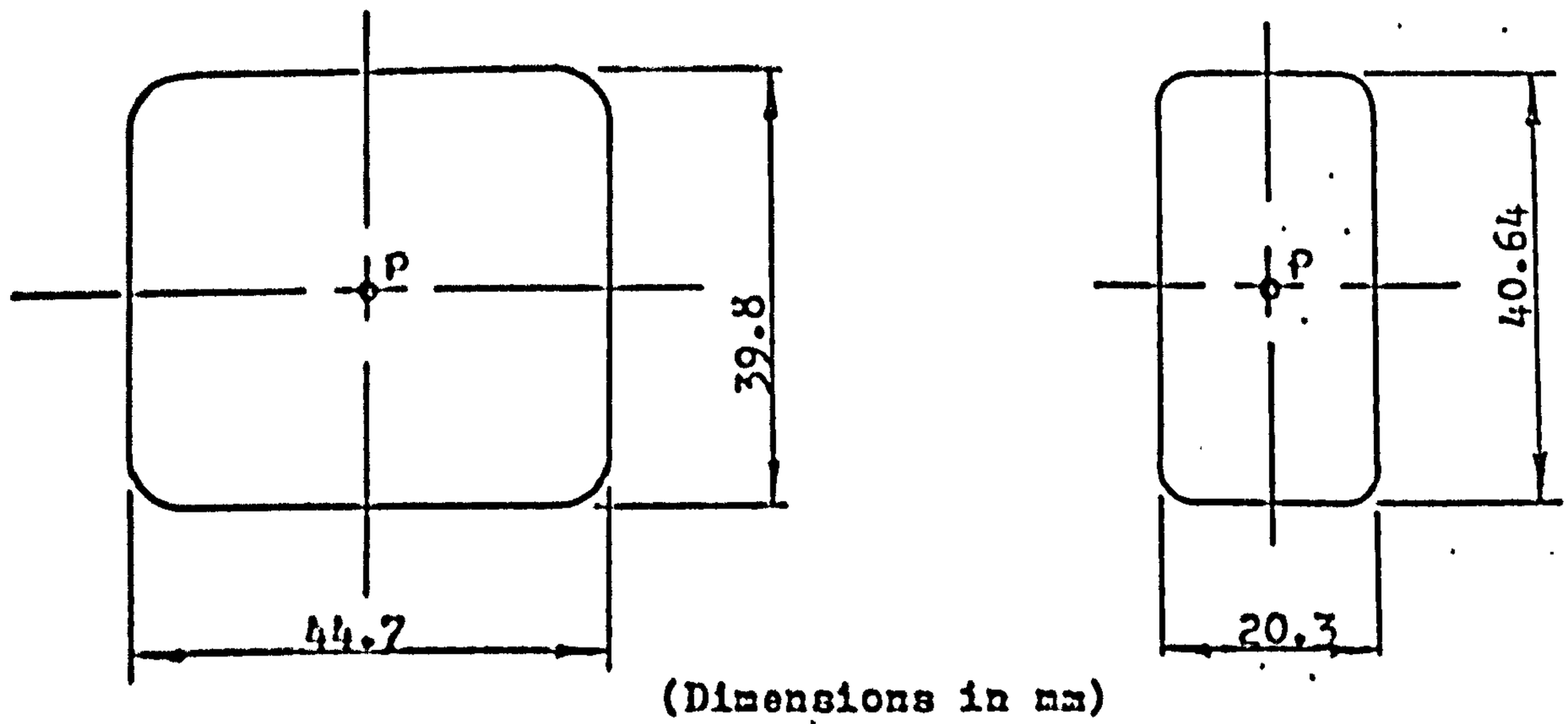

(Dimensions in mm)

a)-Rolls-Royce Engine. b)-Ford Engine.

Fig (5-5) Cross sections of intake manifolds of the Rolls-Royce and the Ford engine showing the locations (P) of measurements for intake velocities.

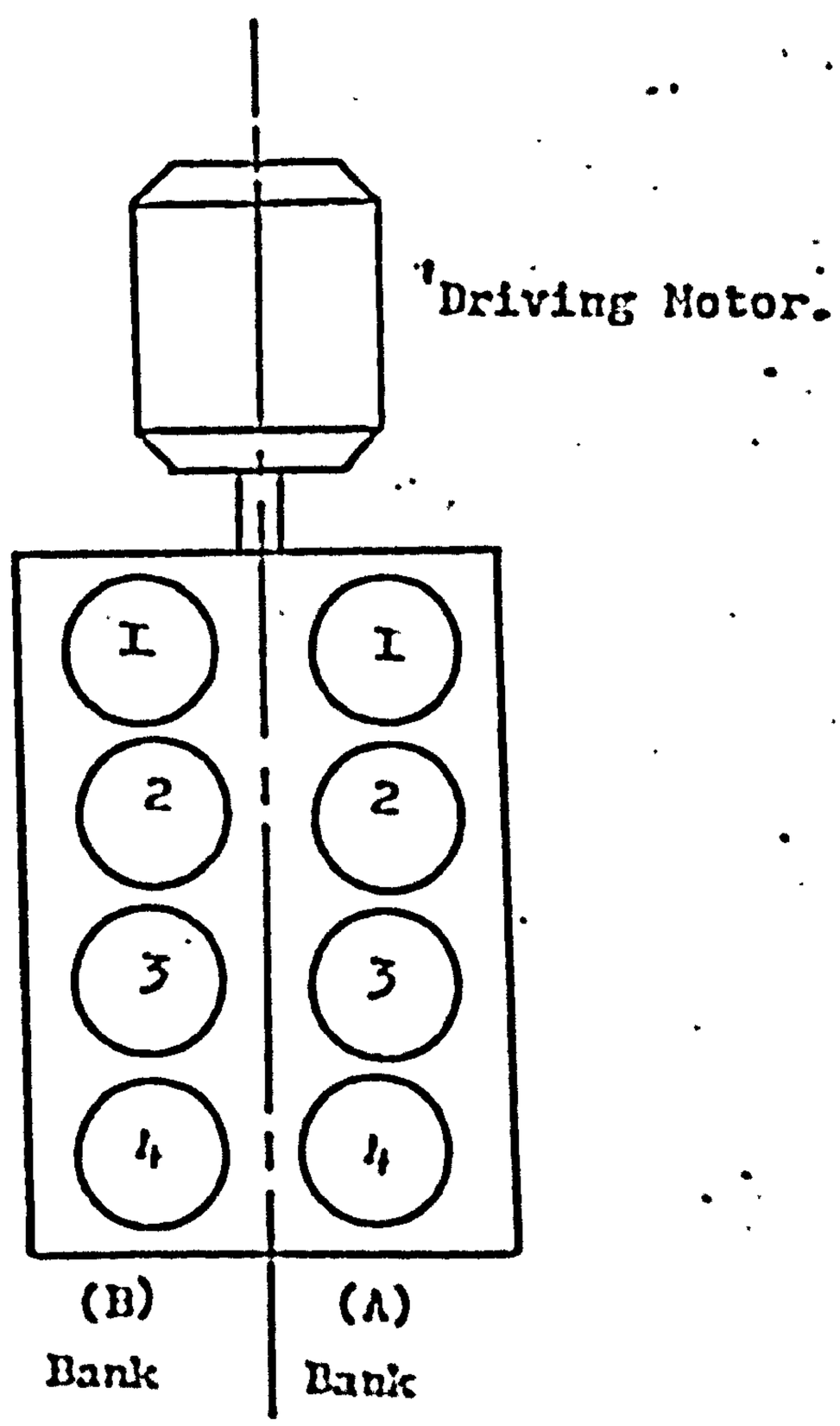

Fig (5-14) Schematic diagram showing the denignation used for different cylinders of the Rolls-Royce V8 engine.

Fig. (5-6) A Masked Inlet Valve

Fig. (5-7) Comparison between a Plain Valve and a Valve for Reduced Lift

Fig. (5-8) An Inlet Valve fitted with eight vanes

Fig. (5-9) An Inlet Valve fitted with six vanes

Fig. (5-10) An Inlet Valve fitted with four vanes.

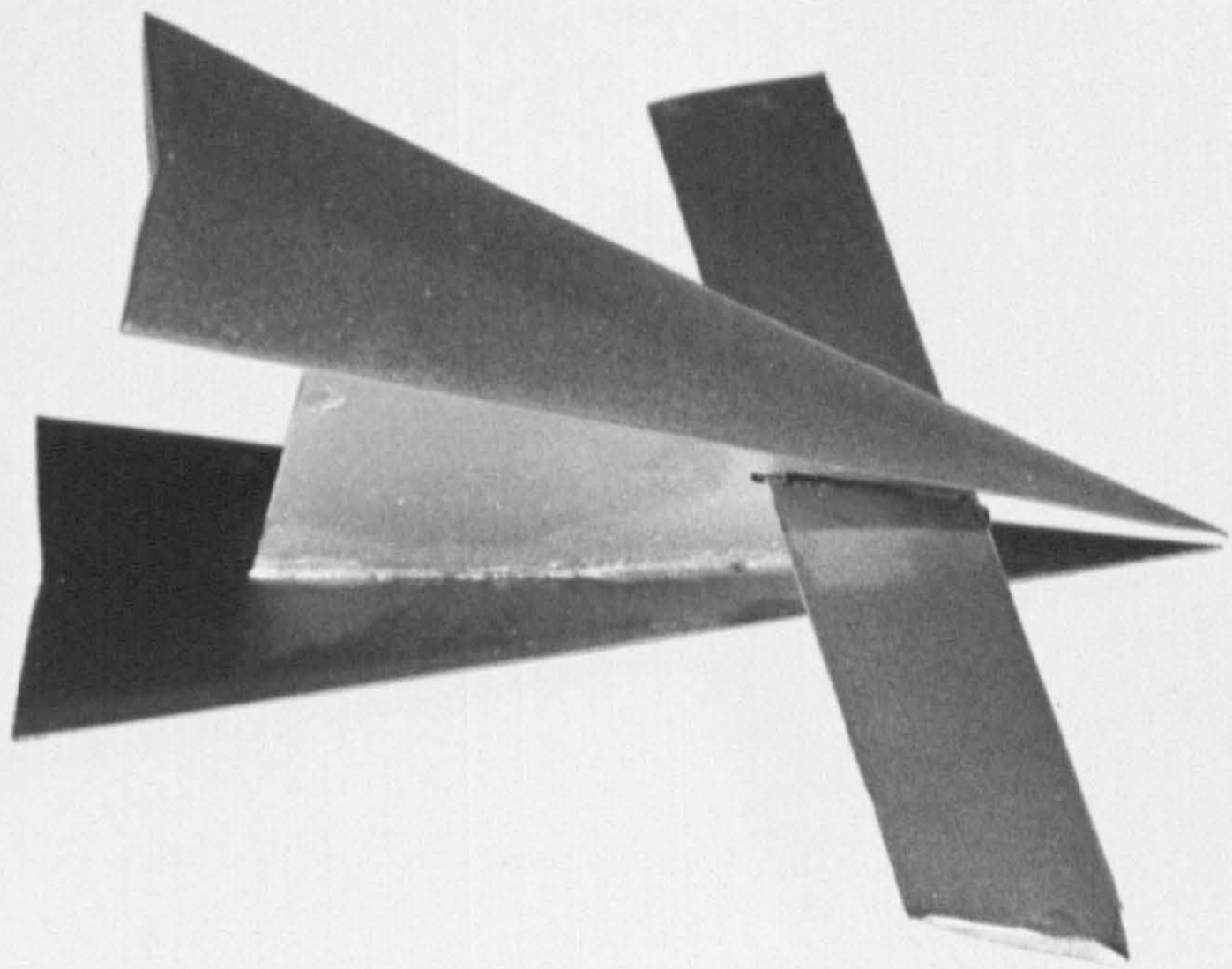

Fig. (5-11) A set of two delta wings

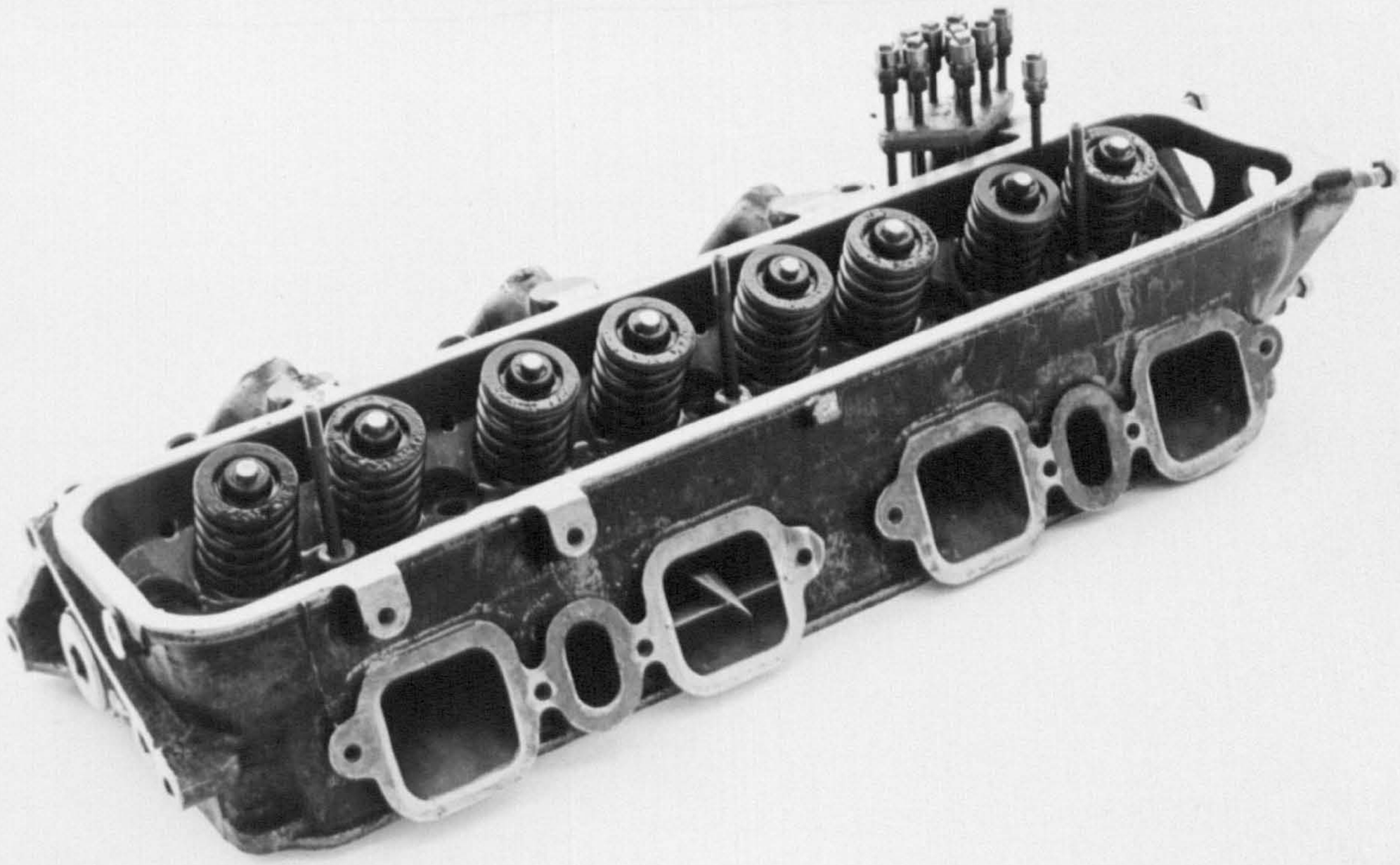

Fig. (5-12) A view of a ROLLS-ROYCE cylinder head showing the location of delta wings inside the intake manifold

Fig. (5-16) A view of the modified valves used on the FORD V4 engine.

Fig. (5-13) A local turbulence promoter

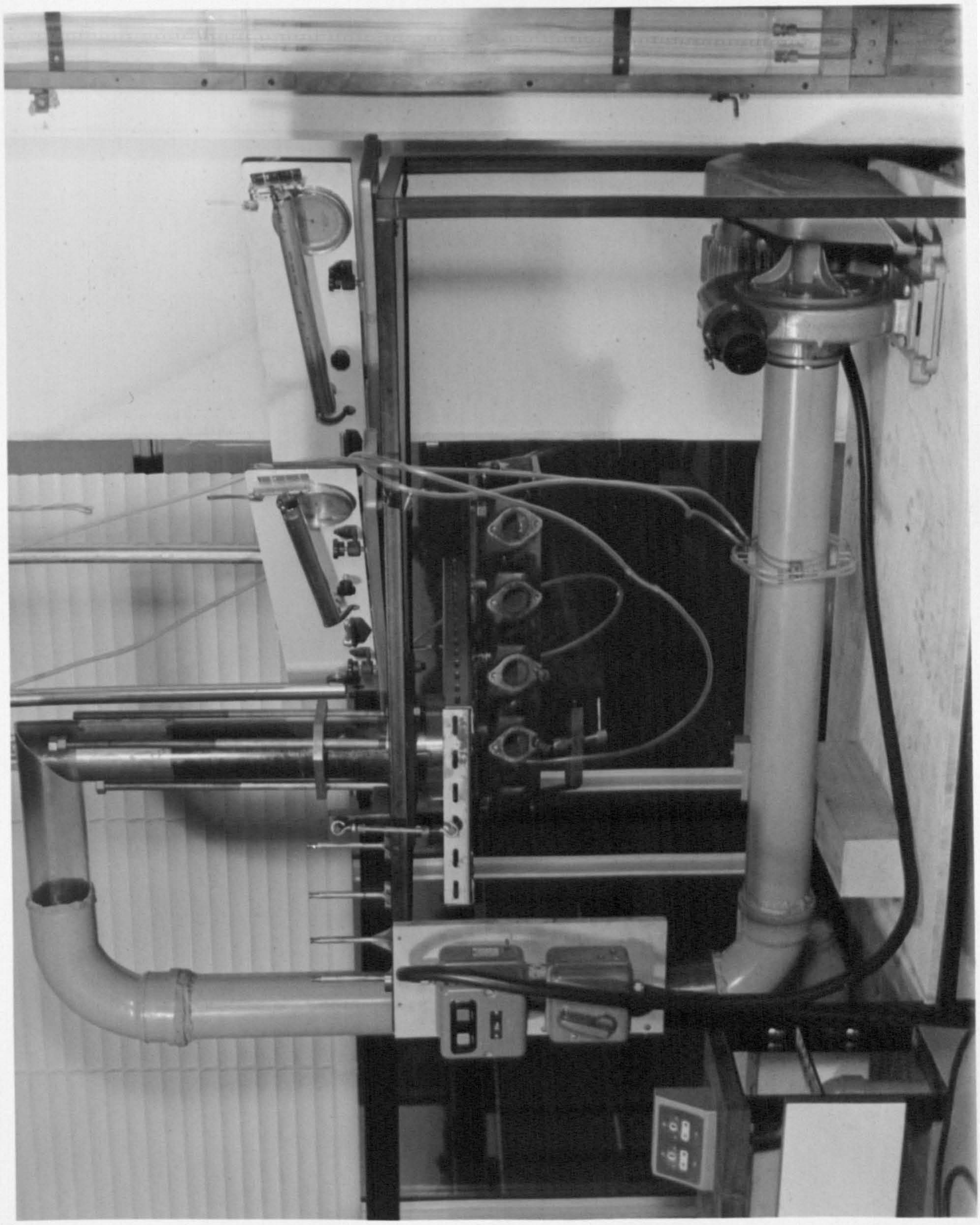

Fig. (5-15) A view showing the mounting of a ROLLS-ROYCE cylinder head on a blowing rig for the determination of the istropic port area for different intake system modifications

6. DISCUSSION OF RESULTS

6.1 General Characteristics of Gas Velocities Inside the Combustion Chambers of Spark Ignition Engines

Measurements of gas velocities inside the combustion chambers of a Rolls-Royce V8 engine and a Ford V4 engine have indicated some general characteristics during the engine cycle. These can be summarised, using Figures (6-1) and (6-2), as follows:

i) Different strokes of the cycle can be clearly identified on each trace, irrespective of the severe cyclic variation. Gas velocities start to increase on the induction period, reach a maximum at about 100° ATDC and then decay until inlet valve closure. Gas velocities remain at this minimum level for about one third of the compression stroke, increase slightly to a maximum at about 40 degrees BTDC and decay smoothly to a minimum at TDC. A sharp increase in gas velocities occur at about 30-40 degrees ATDC on the expansion stroke. A third peak occurs on the exhaust stroke due to the exhaust valve opening.

ii) Gas velocities vary considerably during the induction period at different locations inside the combustion chamber, as will be discussed later.

iii) Examination of Figures (6-1b) and (6-2b) for the maximum and minimum values of gas mean velocities over ten consecutive cycles reveals a large extent of cyclic variations. However, the general shapes of velocity traces appear very repeatable and the variations are mainly in the levels of gas velocities, as well as their time of occurrence. This reflects clearly the turbulent (random) nature of the flow field inside the combustion chamber.

iv) The standard deviations in gas velocities (S(U)) are proportional to gas velocities, e.g. regions of higher velocities (induction or expansion) are associated with large variations and vice versa. This results in standard deviation curves, Figures (6-1c) and (6-2c) which are very similar in their shapes to the gas mean velocity curves during the cycle. This suggests that the coefficient of variation ($S(U)/\bar{U}$) would be nearly constant, as reported by Matsuoka (15) and Winsor (23). However due to the time delays in the occurrence of these velocities, as mentioned earlier, very high values of the coefficient of variation are observed in the region just after TDC. Nevertheless a mean level of the coefficient of variation could be established at least during induction and compression period.

6.1.1 Effect of Hot Wire Direction on the Measured Gas Velocities

Measurements of flow velocity by hot wire anemometers are based on the assumption that the rate of heat transfer from the wire depends on the flow field through the normal component of velocity across the wire. This component is given by (U Cos θ), where U is the magnitude of velocity and θ is the angle between the normal to the wire and the flow direction. In spark ignition engine applications, it is impossible to set the wire perpendicular to the flow direction, which is continuously changing during the cycle. Measurements with a probe having three mutually perpendicular wires are suggested to overcome this difficulty, but at least five wire orientations must be investigated to resolve the ambiguities in velocity direction (140). Moreover, a large number of cycles should be analysed at each wire orientation because of the cyclic variation in gas velocities. This makes the data analysis a very laborious and time consuming process. However, measurements at three orientations of a single hot wire probe, as well as simultaneous measurements using two mutually perpendicular wires, were carried out in the present work. The notation 'vertical wire', as will be used later, refers to a wire direction parallel to the probe body axis, while a 'horizontal wire' refers to a wire in a plane perpendicular to that axis.

Figures (6-1), (6-3) and (6-4) give a comparison between the measured signals at three orientations of a horizontal wire in a Rolls-Royce engine at the spark plug gap location and fixed engine conditions of 1000 RPM and fully opened throttle. These results show similar statistical trends, this is shown by the fact that the values of the coefficient of variation $S(U)/\bar{U}$ are practically the same for the three cases during most of the cycle, (e.g. $S(U)/\bar{U}$ $\simeq$ 27% for induction and most of compression period). Consequently, a fixed wire direction corresponding to that of Figure (6-1) is used for comparisons between different experiments at variable operating conditions or for different modifications of intake system, as will be discussed later. These comparisons will be carried out, in the following sections, in terms of mean velocities and values of the coefficient of variation.

Figures (6-2) and (6-5) show a similar comparison between the measured signals from a vertical and a horizontal wire at fixed operating conditions. Examination of these results shows that the vertical wire measured higher velocity components than the horizontal wire, due to the flat surface of the Ford engine cylinder head. A detailed analyses of the measured signals by both wires at different engine speeds will be discussed in Section 6.1.4.

6.1.2 Variaton of Gas Velocities with Depth Inside the Combustion Chamber of a Rolls-Royce Engine

Investigation of the variations in gas velocities inside the combustion chamber of a Rolls-Royce engine with depth was carried out by traversing the spark plug probe along its axis starting from a level where the wire was at the piston surface at TDC (Z = 0.0 mm) to the highest level investigated, i.e. the spark plug gap location (Z = 17.78 mm (0.7")). The latter position was at about 3 mm from the cylinder head wall surface. Figures (6-6) and (6- 7) summarise the results of these measurements for different crank angles during induction and compression periods. Average values within six crank angle degrees are presented in these figures, though the original calculations were carried out at three degree sampling intervals. These are believed to be more representative because of the relatively small number of cycles analysed (10-15 cycles). The conclusions of this study can be summarised as follows:

a) Induction Period

i) The jet nature of the intake flow can be easily observed by comparing the magnitudes of gas velocities at any particular crank angle for different depths.

Early in the induction stroke, with very small opening of inlet valve, a directed jet is detected by the wire at the highest level,

(Z = 17.78 mm (0.7")), which expands inside the combustion chamber volume and consequently lower values are measured at other traverses. A reflection of this jet by the cylinder head walls may explain the increase in the detected velocity at Z = 0.0 mm after reaching a minimum value midway on the traverses.

ii) With wider openings of inlet valve, the location of the maximum velocity inside the combustion chamber moves as the jet axis changes its position. This is clearly identified by the movement of the peak in the velocity trace with increasing crank angle in the cycle (e.g. from 80 to 160 degrees).

iii) Immediately before inlet valve closure, the flow field seems to consist of an irregular homogeneous motion where very small velocity gradients could be detected at different measuring locations, (e.g. at 200 and 240 crank angle degrees).

iv) Examination of the extent of cyclic variation in gas velocities during induction period for different measuring locations indicates that such variations are purely random with the location and at most one can conclude that a mean value can be associated with each crank angle.

The above mentioned conclusions (i), (ii) and (iii) are in very good agreement with the results of Semenov (22) and Molchanov (62).

b) Compression Period

i) Examination of Figure (6-7a) indicates that the gas velocities are higher at the level of the spark plug than at any other level. The slight increase in gas velocities to a maximum at about 40 degrees BTDC (as discussed in 6.1) can be observed at the highest location, while for the two intermediate measuring locations, a practically constant value is maintained. The relatively higher value of gas velocity at TDC for the lowest measuring location (Z = 0.0 mm) could be attributed to the existence of a squish component originating at higher levels. This squish component reaches, theoretically,(137) its maximum value at about 5-7 degrees BTDC as shown in Figure (6-8) irrespective of the over-estimation of the predicted values by the theoretical model. For example, velocities of the order of 30 m/sec are predicted theoretically as compared with measured values of about 2 m/sec. Though Winsor (23) has reported a negligible variation in gas velocities with depth, plotting of his data at TDC, Figure (6-9) shows similar trends as the present results of Figure (6-7a). This may be explained by the existence of a certain

flow pattern inside the combustion chamber where some systemmatic circulation of eddies exists.

ii) Cyclic variations in gas velocities during the compression period show some systemmatic variation with depth where maximum variations occur roughly at the lowest depth investigated, (Z = 0.0 mm). It is also interesting to note the intersection of all curves for different crank angles at the central depth of the chamber. This may indicate the existence of some centre of vorticity inside the core of the combustion chamber where the average flow characteristics are constant during the compression period. Nevertheless minimum variations at different locations occur at a crank angle of 20 degrees BTDC.

6.1.3 Investigation of the Flow Pattern Inside a Wedge Combustion Chamber

Attempts to investigate the flow pattern inside the wedge combustion chamber of a Rolls-Royce engine were carried out by measuring gas velocities at different locations, Figure (5-3) using single wire probes which were traversed through a number of brass tubes fixed in the cylinder head parallel to the cylinder axis, Figures (4-11a) and (4-11b). The hot wire probes were rotated, about their axes, and set at three orientations having 45 degrees

angular difference. Theoretical analyses were derived for the determination of the magnitudes and directions of velocity vectors at each measuring point from the measurements at three wire orientations, as given in reference 157. Unfortunately the computer program used failed to resolve the ambiguities in the velocity directions, especially at crank angles where an almost equal magnitude of velocity components were detected at the three orientations of the hot wire. Moreover, since these velocity components were measured for different cycles, cyclic variation in gas velocities introduced another difficulty in the analysis. This required that analysis of a very large number of cycles at each measuring location and for the three wire orientations to be carried out for representative mean values. Consequently the measured mean values (over 10 consecutive cycles) of the velocity components at each measuring location will be presented in this Section, Figures (6-10a) - (6-10j). The direction of the velocity components in these figures are decided from pure intuition based on comparisons of velocity components at the different points and making use of the combustion chamber geometry. The flow pattern inside the combustion chamber can be described therefore as follows:

i) During the early part of the induction period, (Crank angles from 20 to 120 degrees, Figures (6-10a) - (6-10d), the jet is detected mainly at point No. 1, the nearest to inlet valve, at the highest level (Z = 20 mm), while probes at other points in the chamber and the same level did not

detect the directed jet. However, an increase in the level of the eddy velocities at the two lower levels (Z = 15, 0.0 mm) indicates that the issuing jet is directed towards the centre of the combustion chamber with a tendency to swirl in an anticlockwise direction following the inclination of the combustion chamber walls. This is understandable in relation to the inclination of inlet valve axis and the curvature of the upper surface of valve seat. The movement of the jet axis can also be observed by comparing gas velocities at different locations and levels.

ii) It is very interesting to note that the measurements at the middle plane show a very marked tendency of flow towards local isotropy, irrespective of the differences in velocity levels at different points on the same plane which could be attributed to the characteristics of velocity distributions in the field.

iii) A remarkable reduction in the magnitudes of gas velocities can be observed during the period of inlet valve closure (crank angles from 200 to 240 degrees, Figures (6-10e) and (6-10f)).

iv) It is also interesting to note the existence of the condition of local isotropy during the period from 200 to 280 crank angle degrees, which represents conditions of inlet valveclosure and earlier part of the compression stroke.

v) The appearance of squish components (secondary flow created by compression), can be easily observed on the velocity diagrams during the period from 300 to 340 crank angle degrees. This is very clear at the measuring location number (1) at the highest level (Z = 20 mm), Figures (6-10h) - (6-10j). However, a transfer of this kinetic energy into local eddies at different stages of decay could be observed at different locations.

It is also noted that the measured velocities during this period are higher at the top level of the combustion chamber than at the lower ones (near to piston surface). This shows that the squish component is directed along the wedge wall rather than at a direction perpendicular to cylinder axis as proposed by theoretical models, similar to the one elaborated by Lichty (137). The measured values are much smaller than the theoretical predictions, as mentioned before, because of the complex nature of the flow.

6.1.4 Variation of Gas Velocity Characteristics with Engine Speed

The effect of engine speed on the characteristics of gas velocities in spark ignition engines has been investigated mainly on the Ford V4 engine. The tests cover a wide range of engine speeds between 1000 and 3500 RPM. Unfortunately, the capacity

of the driving motor has limited the investigation of this variable on the Rolls-Royce V8 engine to a maximum speed of 1500 RPM. However, the results obtained from both engines are sufficient to provide enough knowledge about the effect of engine speed on the flow field characteristics. These results will be compared with all the published investigations in this field, though these were mainly carried out on single cylinder engines at a maximum engine speed of about 1800 RPM. Because of the variation in the directions of velocity vectors inside the combustion chamber during different strokes of the cycle, simultaneous signals from a double wire probe will be discussed for the induction and compression periods as follows:

a) Induction Period

i) The variation of gas velocities at different crank angles during the induction period are shown in Figures (6-11) and (6-14). These results indicate that gas velocities increase proportionally with engine speed, but the concave shapes of most of the graphs suggest that the relation is of a slightly higher order than unity as proposed by Semenov (22).

ii) The coefficients of variation ($S(U)/\bar{U}$) for the measured signals by both wires have practically a constant value between 35 to 40% over the whole induction period, Figures (6-15a) and (6-15b).

b) Compression Period

i) Figures (6-11b) and (6-12b) show the variations of gas velocities with engine speed during the compression period at the spark plug location and a depth of 3.8 mm from the cylinder head surface, while Figures (6-13b) and (6-14b) show similar results at a level of the cylinder head surface. Examination of these graphs indicate corresponding increases in gas velocities with engine speed. However, the trends of the measured velocity components seem to depend on the location of measurements and the wire direction. This discrepancy can be explained by the fact that each wire detects a velocity component normal to its axis which is mainly governed by the effect of the spatial location of measurements on the motion of eddies and the mechanism of breakdown of large eddies into smaller ones. It is, also, worth noting that the vertical wire detects higher velocity components than the horizontal wire. This can be explained by the fact that a vertical wire is highly sensitive to squish velocities, especially for the Heron shape combustion chamber, with its flat surface cylinder head.

In fact, discrepancies in the trends of gas velocities in spark ignition engines with increases in engine speed exist between almost all the published investigations. For example, Semenov (22) has reported an almost quadratic relation between gas velocities and RPM during compression as given by

$$\bar{U} \sim RPM^{2.1} \tag{6-1}$$

while James (24) and Winsor (23) have interpreted their measurements at TDC as linear relations. The former has suggested an equation of the form

$$\bar{U} = a \ RPM \tag{6-2}$$

where a is a function of the combustion chamber shape and the compression ratio, which increases from a value of 0.227 at a compression ratio of 3.9 to a value of 0.379 at a compression ratio of 8.88.

This is contrary to the data of Semenov, where $\bar{U}$ was found to decrease by about 20% with an increase in compression ratio from 4 to 9.5. Unfortunately, the two engines used in the present work have nearly equal compression ratios (9:1 and 8.9:1 for the Rolls-Royce and the Ford engine respectively).

This did not permit resolving the discrepancy between Semenov's and James' data. In fact, one may attribute part of the difference in magnitudes of gas velocities in engines to differences in intake systems, engine capacities and combustion chamber shapes in each case. Nevertheless, plotting of the available data of all the published investigations, Figure (6-17) shows similar trends of gas velocities with engine speeds as those of the present work.

ii) The measured velocity components by the horizontal wire at different crank angles during compression period have shown that the coefficient of variation ($S(U)/\bar{U}$) has an almost constant value of about 40%, Figure (6-16b), while an increase by about 12.5% at TDC for a variation in engine speed between 1000 and 3000 RPM could be observed.

On the contrary, the vertical wire signal has shown a minimum variation at an engine speed of 2000 RPM as compared with the corresponding values at 1000 and 3000 RPM, Figure (6-16a). For the period between 20 to 40 degrees BTDC, a sharp increase in the coefficient of variation can be observed at engine speeds above 2000 RPM.

The order of magnitudes of the coefficient of variation in gas velocities, in the present work, are in agreement with the reported data of Winsor (23) and Barton (10). For the former case, values between

33 to 47% were reported for measurements at TDC over a speed range between 500 and 1500 RPM, while for the latter values between 42.3 to 52.8% were reported at crank angles corresponding to ignition timing (36 to 52 degrees BTDC), over a speed range between 600 and 1800 RPM.

6.1.5 Investigation of Gas Velocity Characteristics Inside the Intake Manifolds

Measurements inside cross sections of the intake manifolds of the Rolls-Royce and the Ford engines were carried out in the present work. Figures (6-18) and (6-19) show examples of these measurements for the Ford engine at an engine speed of 3500 RPM and two loading conditions. These loading conditions correspond to 90 BMEP and 60 BMEP and will be designated hereafter as full load and part load conditions respectively. The corresponding values of intake vacuum and throttle settings were given in Table (5-5). Figure (6-20) shows similar results at 2000 RPM and full load condition. A summary of the statistical analysis of maximum intake velocity at different enginespeeds and loading conditions is shown in Figure (6-21). Similar results for the Rolls-Royce engine at different engine speeds between 700 and 1500 RPM and fully opened throttle are shown in Figures (6-22) - (6-24). The main conclusions of this study can be summarised as follows:

i) The flow conditions inside the inlet manifolds represent a fully developed turbulent flow as revealed from velocity traces during the induction period.

ii) Intake gas velocities increase linearly with engine speed and throttle opening.

iii) Cyclic variations in gas velocities inside the combustion chambers of spark ignition engines start earlier in the flow path inside the inlet manifolds. However, the magnitudes of these variations inside the intake manifolds are less than the corresponding values inside the combustion chambers.

The coefficient of variation is nearly constant within a limited range of engine speeds, but seems to drop for large increases in engine speed. It drops also with increases in the throttle opening.

iv) Examination of the curves for the occurrence of maximum and minimum velocities during inlet valve opening reveals that the shapes of the velocity traces are very repeatable and that variations are mainly in the absolute magnitudes of these velocities, as well as their time of occurrence. This suggests that cyclic variations in gas velocities are caused partly by non-repeatable mechanical processes and partly by the random nature of the turbulent field.

6.2 Variation of Flow Field Characteristics with Different Modifications of Intake System

Investigation of the characteristics of the flow field produced by modifications of the intake system were carried out by statistically analysing the gas mean velocities at the spark plug location of the Rolls-Royce engine. All tests were carried out at a constant engine speed of 1000 RPM and fully opened throttle. Figures (6-25) to (6-30) show the gas mean velocity ($\bar{U}$), the range of variation in gas velocities (U_{max} and U_{min}) and the standard deviations of these velocities S(U) at different crank angles during the cycle for the following modifications:-

1. A masked inlet valve (180 degrees mask).
2. Inlet manifold fitted with delta wings.
3. Inlet valve for reduced lift.
4. Inlet valve fitted with four guide vanes.
5. Inlet valve fitted with six guide vanes.
6. Inlet valve fitted with eight guide vanes.

Detailed description of the geometries of different modifications were given in Chapter 5.

Comparisons of these statistical analyses for maximum intake velocity and velocities during the latter period of the compression stroke (60 degrees BTDC) are also given in Figures (6-31) and (6-32). Examination of these results reveals the following observations:

i) The masked valve has increased the intake velocity by a factor of three compared with the plain valve. This high level of swirl velocity was not very critically damped as in the case of other valves, but continued for a considerable period during compression.

ii) The coefficient of variation ($S(U)/\bar{U}$) for the masked valve at maximum intake velocity has shown the lowest level between all intake modifications. However, the values of the coefficient of variation for the masked valve during the compression period was very nearly of the same level as the minimums of other types of valves, especially during the period between 60 to 20 degrees BTDC. Its value near TDC is of the same level as other valves.

It is worth noting that the comparisons on a relative basis ($S(U)/\bar{U}$) eliminates the effect of absolute values of variations and consequently the factor of cylinder-to-cylinder variation, which will be discussed later in Section (6.4).

Similar observations about the effect of swirl motion on reducing cyclic variation was reported by Lange, (150).

iii) Fitting of delta wings inside the intake manifold produced the minimum levels of coefficients of variation during the compression period, as compared with other intake system modifications. The corresponding value of $S(U)/\bar{U}$) at maximum intake velocity was approximately the same as the minimum level observed when a masked valve was used.

iv) It is interesting to note that the intake manifold fitted with delta wings has produced higher compression velocities which continued to increase during the latter period of the compression stroke, though the maximum intake velocities were not as high as other valves. This may be explained by the effect of the delta wings in assisting the process of turbulence breakdown into smaller eddies. Therefore, increases in the fluctuating components during the induction period can be expected (as will be seen in Section (6.3.5) at the expense of some reductions in the directional mean velocity. On the other hand, one can regard the measured mean velocities during the compression period as a measure of the levels of kinetic energy of the very low frequency eddies which has also been energised by the flow field produced by the delta wings.

v) The valve with six vanes gave results which are in between the four vanes and eight vanes valves, though the geometries of vanes in the latter two cases are completely different. Gas velocities of the six vanes valve are nearly constant during most of the compression period.

vi) The valve with four vanes has shown the highest levels of the coefficient of variation for all the modifications, though its value during induction was below those of other valves with the exception of the masked valve.

vii) The use of reduced valve lift increased the gas velocities during compression and reduced their coefficients of variation. However, these improvements in performance are still below the levels achieved by using an intake fitted with delta wings or a masked valve.

The above mentioned observations could be attributed to the particular flow patterns produced by different modifications, which may be explained as follows:

1. The insertion of delta wings in the intake manifold has accelerated the process of turbulence breakdown and resulted in a homogeneous flow field which show low levels of variation, while for the normal design of plain valve and free manifold passage, the resulting flow field inside the combustion

chamber will consist of zones of different velocity levels moving inside the chamber in a random manner, and what is really detected as cyclic variation at a fixed point of measurement is an indication of the non-homogeneity in the turbulent field. This mechanism was proposed also by Molchanov (62) and Barton (10).

2. The function of a masked valve is to assist the existing swirl in the inlet flow. This effect was highly intensified in the present case since the masked valve had a 180 degree mask and was rotated to the angular position that produced the highest possible swirl. The existence of a strong directed motion inside the combustion chamber after inlet valve closure resulted in a continuous process of generating small eddies and hindered to some extent the damping of the flow field, as will be the case with a plain valve and its associated shear motion after inlet valve closure.

3. The geometry of the valve used for reduced lift has resulted in the creation of a strong jet during the latter period of inlet valve closure which energised the motion of eddies inside the combustion chamber during this critical period.

However, due to the absence of any additional swirl, the flow decays in nearly the same manner as other types of valves. This effect is clearly observed on the turbulence graphs as will be shown in Section (6.3.5).

6.3 Investigation of Turbulence Characteristics Inside the Combustion Chambers of Spark Ignition Engines

As mentioned in Chapter 4, the analysis of turbulence signals were carried out, in the present work, on 'ensèmble records' sampled from a large number of engine cycles. The number of the cycles analysed varied with engine speed and are given in Table (4-4), for different test conditions, while the width of the 'cycle samples' was fixed at 10 crank angle degrees for all tests. These analyses yield the average characteristics of the turbulent field in engines. However, a study of the cyclic variations in these characteristic parameters was carried out also on individual data records for consecutive cycles. The analysis was carried out on the measurements at the spark plug gap location for the Rolls-Royce engine and for two different locations for the Ford engine. In the latter case, the locations of measurements are at the spark plug gap which is flush with the cylinder head surface (Z =0.0 mm), and at a point 3.8 mm from the cylinder head surface inside the piston bowl at TDC. These studies can be divided as follows:

i) A study of the structure of the turbulent field inside the combustion chambers of spark ignition engines.

ii) A study of the variation of the turbulence characteristics for two shapes of combustion chambers namely: the wedge shape and the heron shape.

iii) A study of the effect of engine speed on the flow field characteristics in engines.

iv) A study of the effect of the throttle setting on flow field characteristics in engines.

v) A study of the effect of different modifications in intake systems and a local turbulence promoter at the spark plug on the structure of the turbulence field in engines.

6.3.1 General Characteristics of Turbulence Field in Engines

Figure (6-33) shows the variation of the turbulence characteristics for the Rolls-Royce engine at 1000 RPM and fully opened throttle as measured at three different orientations of the hot wire. Examination of these results reveals the following characteristics of turbulence in engines as follows:

i) The turbulent field is definitely anisotropic during the induction period where the flow field is generated by a turbulent jet with a moving axis, as discussed in Section (6.1.2). However just before inlet valve closure a shear motion seems to exist inside the combustion chamber and the turbulent streams are reduced to local vortices

and one can consider the field, at this time, as a statistically steady one where isotropy prevails and continues during its decay period on the compression stroke.

ii) The fluctuating velocity component follows exactly similar trends to the mean velocity. It decreases sharply to a minimum value just before inlet valve closure, remains practically constant for one third of the compression period, increases to a maximum at 20 - 40 degrees BTDC and drops smoothly again at TDC. A very large increase in the fluctuating velocity component occurs at about 30 to 40 degrees ATDC, due to the motion of the piston on the expansion stroke. These latter data are not shown on the graphs, but could be easily seen by examining the mean velocity graphs given in Section 6.1.

iii) The time micro-scale of turbulence (λ_t) increases from its low value during the induction period to a maximum level just before inlet valve closure, remains at this level for about two thirds of the compression stroke and then decays to a minimum at about 20 - 40 degrees BTDC. It increases once again at TDC. This variation of λ_t describes clearly the variation of turbulent field characteristics during different periods of the cycle. Initially, during the induction period of higher turbulence

intensities, dissipation of turbulent energy is caused by eddies rotating at very high frequencies. When the turbulence decays, considerably during the early part of the compression stroke, dissipation is caused by slower eddies rotating at low frequencies (longer times). When the flow field is partly energised by the creation of secondary flows (squish velocities), the frequencies of eddies correspondingly increase as shown by the minimum of λ_t at 20 - 40 degrees BTDC. While at TDC with the piston at rest and where any secondary flows no longer exist a slowing down process of the eddies causing dissipation could be observed. The increased surface to volume ratio is also contributing towards higher damping rates during the compression period. Obviously the turbulent energy during the compression period is continuously dissipated into heat by the chain process of breakdown of larger eddies into smaller ones which dissipate their energy as heat.

The above discussion could be, alternatively, observed on the power spectrum function curves for different crank angles during the cycles, Figures (6-34a) - (6-34h). Initially, during the induction period the flow field consists of eddies at very high frequencies. However a slowing down process follows the inlet valve closing and a

minimum level of eddy rotation is reached just before inlet valve closure and continues for the early part of the compression period. In the latter part of the compression period, the flow gains some of its energy and eddies are accelerated to a maximum level at about 20 - 40 degrees BTDC. Figure (6-35) shows the variation of frequencies corresponding to eddies containing 10%, 50% and 90% of the total energy of the turbulent field.

More recently, 1973-1974, Tsuge and Kido (153,154) introduced the notion of dividing the process of turbulence decay in a closed vessel into two stages. The first one was termed the 'pre-relaxation' stage where the influence of the method of generating the turbulence lasts, while the second stage was termed the 'relaxation' stage where the turbulence is nearly homogeneous and the decay process is little influenced by the way of generation. These definitions can be applied in the engine investigations where the induction period corresponds to the pre-relaxation stage and is mainly influenced by the characteristics of the specific intake system used, while the compression period corresponds to the relaxed stage, especially for the cases when secondary turbulence generated by compression is small.

Comparing the results of Tsuge and Kido (153), Figures (6-36a) and (6-36b) with the data of Figures (6-34a) - (6-34h) shows very good agreement between the two investigations, where the induction period (pre-relaxation stage) shows regions of irregular and higher frequencies while the compression period (relaxed stage) shows that the turbulence is homogeneous and contains smooth and lower frequency fluctuations.

v) The variation of the spatial micro-scale of turbulence (λ_y) during the cycle, Figure (6-33d) shows that its value is relatively larger during the induction period than during the early part of the compression stroke. However, it increases during the period between 20 - 40 degrees BTDC and then smoothly decays at TDC. The graphs are very similar to the mean velocity curves which represent the dominating factor in equations (3-77) and (3-72).

$$\lambda_x = U \cdot \lambda_t \qquad (3\text{-}77)$$

$$\lambda_x = \sqrt{2}\, \lambda_y \qquad (3\text{-}72)$$

The average size of these eddies is about 0.5 - 0.7 mm during the induction and the period between 20 - 40 degrees BTDC on compression stroke, while a value of about 0.3 mm could be observed for the latter part of the induction and the earlier part of compression.

6.3.2 Variation of Turbulence Characteristics with Engine Speed

The discussions of the preceding Section (6.3.1) have shown that turbulence characteristics during different periods of the cycle are, mainly, functions of the nature and levels of gas mean velocities during these periods. On the other hand, gas mean velocities were shown in Section (6.1.4) to increase proportionally with engine speed. Summing up these two observations, one can deduce the effect of engine speed on turbulence characteristics during the cycle (for fixed geometries of the intake system and combustion chamber), as increases in fluctuating velocity components and frequencies of eddy rotation (lower time micro-scales) at higher engine speeds. These deductions could be compared with actual measurements and turbulence analyses at different engine speeds. The later tests were carried out on the Rolls-Royce engine at fully opened throttle over the speed range of 1000, 1200 and 1500 RPM as shown in Figures (6-37a) - (6-37e). Similar tests were carried out on the Ford engine at full load conditions over a wide range of engine speeds between 1000 and 3500 RPM as shown in Figures (6-38a) - (6-38f). The conclusions of these studies can be summarised as follows:

i) The fluctuating velocity components (u') increase with increases in engine speed in a non linear manner as increases in gas mean velocities, as discussed in Section (6.1.4).

ii) The time micro-scale of turbulence (λ_t) decrease with increases in engine speed at any particular crank angle. This indicates that shortening of the time intervals of different strokes in the cycle results in a corresponding increase in the frequencies of eddy rotation.

Comparing the variations of the time micro-scale (λ_t) at different gas velocities during induction and compression periods, Figures (6-39a) and (6-39b) shows very good agreement with the reported data of Tsuge and Kido (153), Figure (6-39c) for turbulence decay in a closed vessel during the 'pre-relaxation stage' and the 'relaxed stage' (as defined earlier).

iii) Comparing the power spectrum curves at different engine speeds shows a corresponding increase in the higher frequency content of the turbulence field at higher engine speeds. Similar conclusions can be obtained by examining Figure (6-40) for the frequencies of eddies containing 10%, 50% and 90% of the turbulent energy at engine speeds of 1000 and 3500 RPM.

This means that the spectral characteristics of the flow field (frequency composition) inside the combustion chamber of spark ignition engines are mainly functions of: mean velocity levels, combustion chamber shape, as well as the residence

times of the charge inside the combustion chamber which vary with engine speed. This explains the observed constancy of combustion period in the cycle (in terms of crank angle degrees) at different engine speeds (36), (41), Figures (2-76) and (2-77b). This is usually reported as reductions in burning times at higher engine speeds.

iv) The spatial micro-scale of turbulence (λ_y) at any particular crank angle increases almost linearly with engine speed, since the mean velocity term is a dominating factor as discussed earlier in Section (6.3.1).

Figure (6-41) shows the variation of micro-scale (λ_y) with mean velocity for the Ford engine at different engine speeds as well as a typical example for the Rolls-Royce engine at 1000 RPM. It indicates that the micro-scale increases linearly with mean gas velocity but the rate of increase decreases with engine speed. It shows also some dependence on combustion chamber configuration. The highly turbulent (wedge) combustion chamber of the Rolls-Royce engine shows smaller rates of increase than the heron shape of the Ford engine.

v) It is also interesting to note that the turbulence intensities ($u'/\bar{U}$) do not increase indefinitely with engine speed. For example Figure (6-38b) shows that the intensities of turbulence during the induction period remain almost constant above 2000 RPM. The increases in the fluctuating velocity components during this period at higher engine speeds are mainly due to the increased levels of gas mean velocities. The rate of increase in turbulence intensities during the compression period seems also to decrease with increases in engine speed. However, the fluctuating velocity components during compression continue to increase at higher engine speeds for the same reasons mentioned for the induction period.

Summing up the above conclusions, one can attribute the increases in flame speed with engine speed to the mutual effect of higher fluctuating velocity components and faster eddy rotation. The data of Lefebvre et al (49) for turbulent combustion of confined flames in combustion chambers tend to support the above findings, where turbulent flame speed measurements were interpreted as functions of both the fluctuating velocity component and gas mean velocity, Figure (6-42) as given by:

$$\frac{S_t}{S_\ell} = 1 + 0.43\, u' + 0.04\, \bar{U} \qquad (6\text{-}3)$$

The gas mean velocity term in equation (6-3) can be interpreted to represent the effect of gas mean velocities in increasing the frequency of eddy rotation (lower time micro-scales) as observed in the present work.

The increase in the size of small scale eddies with engine speed may suggest that cyclic variation in the growth of the flame kernel will increase at higher engine speeds, but the faster burning rates (due to increases in the fluctuating velocity u' and consequently $\mathcal{E}$ and S_t, equation (2-19) tend to decrease the initial burn time (as defined in page 86) and its variations. The total flame arrival time also decreases and consequently a reduction in cyclic variation can be expected, Figs. (2-17) and (2-18). This conclusion is in agreement with tests of Barton (10) and Winsor (23). However, the effect of improved mixing due to higher intake velocities, at higher engine speeds, will also improve the situation.

On the other hand, the problem of cyclic combustion variation will be very critical for weak mixtures around the idling condition of about 800 - 900 RPM due to the reduced levels of turbulence intensities and consequently the reduced flame speeds.

6.3.3 Variation of Turbulent Field Characteristics with Throttling

The effect of throttling on the characteristics of the turbulent field inside the combustion chamber was investigated on the Ford engine at full and part load conditions, as stated

in Table (5-5). Comparisons of the performance of different intake systems at the two loading conditions during the latter part of the compression stroke, will be discussed in the next section. Two typical examples of these comparisons during the induction and compression strokes at two engine speeds of 1000 RPM and 3500 RPM are shown in Figures (6-43a) - (6-43e). Examination of these results indicate the following differences:

i) Gas mean velocities decrease with reducing throttle opening and consequently the fluctuating velocity components. Similar conclusions were reported by Semenov (22).

ii) The time micro-scale of turbulence are practically constant for the two loading conditions and seem to be a function of engine speed only. However, some reduction in the time micro-scale could be observed at part load condition for the latter part of induction and the earlier part of compression which indicates the existence of higher frequency eddies during this period.

iii) The size of the small-scale eddies is reduced by throttling due to the dominant effect of reductions in gas mean velocities.

The above mentioned observations indicate that although gas mean velocities and their fluctuating components are reduced by throttling the frequencies of eddy rotation

remain almost constant. Moreover the process of eddy breakdown into smaller ones is accelerated. Therefore, in spite of the reduced intensities at partly opened throttle, the effect of small scale eddies on the growth of the initial flame kernel is advanced and comes into effect earlier at smaller kernel sizes than for fully opened throttle. One may expect, therefore, that in the absence of other factors affecting cyclic combustion variation, such as the amount of exhaust residuals in the engine and the mixing of these residuals with fresh charge which are mainly affected by gas mean motion, reduction in cyclic variations at partly opened throttle could be achieved. In this respect, Broeze (134) has reported that "it has been found by accident, when running near the lean limit, that the partial closure of a throttle valve, immediately before the inlet valve, brought about an improvement in the running of the engine". This latter experiment was carried out using a dry, homogeneous mixture, obtained by its being heated to the right temperature in a mixing vessel, installed between the carburettor and engine, which had a capacity 40 times the stroke volume. It would appear that Broeze's findings support the earlier explanation of the effect of throttling on turbulent characteristics and its expected effect on cyclic combustion variation.

6.3.4 Investigation of the Extent of Cyclic Variations in Turbulence Characteristics

The analysis of 'ensemble' data records of turbulence signals, as presented in the preceding section, yield the average values of turbulence characteristic parameters. However, a study of the extent of cyclic variations in these parameters could be investigated by statistical analysis of turbulence signals sampled from individual consecutive engine cycles.

This analysis was carried out, in the present work, for the Rolls-Royce and the Ford engines over sixty consecutive cycles. For the former engine comparisons were made at 1000 RPM and fully opened throttle conditions for a plain valve and an inlet valve fitted with eight guide vanes as shown in Figure (6-44), while the analysis of the Ford engine was carried out for a plain valve, an inlet valve with four vanes and a turbulence promoter at the spark plug. In this latter case, turbulence signals were analysed at 10 degrees BTDC for full load and part load conditions as shown in Figure (6-45). Examination of these data yields the following conclusions:

i) For the Rolls-Royce engine, a valve with eight vanes has reduced the cyclic variations in turbulence intensities, while the micro-scale variations has increased as compared with plain inlet valve data. This result may be explained by the highly random flow produced by a valve with vanes which contributes to the homogenity in the levels of turbulence inside the combustion

chamber and consequently results in a faster process of turbulence eddy generation. The resultant effect could be expected as improvement in the mixing of fuel and air and probably lower combustion variation.

ii) For the Ford engine at full load condition, a valve with four vanes has shown slightly higher variation in turbulence intensities than a plain valve, while a turbulence promoter did not affect this variation.

The effect of the valve with vanes on reducing variations in turbulence intensities at part load condition can be easily observed. The turbulence promoter has improved the situation to some extent.

The variations in the micro-scale are observed once again to increase with modifications in intake system and insertion of turbulence promoter. The levels of these variations are nearly the same for the valve with four vanes and the turbulence promoter at part load and are about 9% higher than the plain valve data.

Figures (6-46a) - (6-46c) show typical examples of cyclic variations in turbulence characteristic parameters over 60 consecutive cycles for a test on the Rolls-Royce engine.

6.3.5 Effect of Different Intake System Modifications and Local Turbulence Promoter at Spark Plug on the Characteristics of the Turbulent Field

The structure of the turbulent fields produced by different intake system modifications and turbulence promoters at spark plug locations was investigated on both the Rolls-Royce and the Ford engines at an engine speed of 1000 RPM. The analysis covered the whole induction and compression periods for the Rolls-Royce engine while the latter part of the compression stroke (60° BTDC to 10° BTDC) was investigated for the Ford engine. Figures (6-47 and (6-48) show the results of this extensive test program. Examination of these data yields the following conclusions:

a) The Masked Valve

The performance of the masked valve is shown in Figure (6-37) where data for a plain valve used in the same cylinder at different engine speeds are presented for comparisons. The use of a 180 degrees mask has resulted in a tremendous increase in gas mean velocities during the induction period which is about eight times the corresponding values for a plain valve at the same engine speed. These very high levels of gas velocities continued during the compression period at lower rates (between 1.5 to 3 times the case of a plain valve).

It is interesting to note that the turbulence intensities ($u'/\bar{U}$) have decreased for the masked valve by about 0.4 - 0.7 times the case of a plain valve during the induction period and were slightly higher than the plain valve data during compression. It is also interesting to note that the turbulence intensities for the masked valve are approximately constant over the whole cycle and are of the order of 15%. Consequently the fluctuating velocity components follow the same trends of gas mean velocities. This means that the mechanism of generating turbulence has reached its maximum limit (equilibrium condition between generation and dissipation of turbulence) for this particular flow field conditions. Similar observations are reported for turbulence measurements at the centre line of pipes (111, 112, 119) where turbulence intensities are constant for different values of inlet mean velocities. This observation could be compared with a similar observation mentioned in Section (6.3.2)about the constancy of turbulence intensities at very high engine speeds (above 2000 RPM) during the induction period.

The time micro-scales of turbulence for the masked valve are much lower than those for a plain valve during the induction period which indicates the

existence of high frequency eddies during this period. An improvement in mixing of fuel and air could be expected, therefore, as well as the mixing of fresh charge with exhaust residuals. Both effects result in lower cyclic variations. The time micro-scale reaches approximately the same values of a plain valve during the compression period. This observation supports the suitability of the definitions introduced in Tsuge and Kido for the decay process in a closed vessel.

The spatial micro-scale of turbulence (λ_y) increases with the masked valve, which indicates that the growth of the flame kernel from its initial value after the spark discharge to the stable flame front will occur under practically the same conditions as those of a plain valve. However the increased fluctuating velocity components will result in much faster flame speeds and consequently higher burning rates which mean that the percentage of cyclic variations relative to the mean value will be decreased. This explains the observations of Patterson (2) with masked valves, where cyclic variations in the rates of pressure rise remained essentially constant but the percentage $(S(\dot{P}_{max})/\bar{\dot{P}}_{max})$ were much lower than the case of a plain valve, Figures (2-63a) and (2-63b).

b) Valve for Reduced Lift

The main objective of this valve design was to produce flow field characteristics similar to the conditions of Stivender (19) with sonic intake valve throttling where improvement in the engine performance during lean mixture operation was reported. Figures (6-47a) - (6-47e) shows the performance of this valve at full and quarter throttle opening at 1000 RPM. These show the following observations:

The gas mean velocities at the spark plug were not greatly affected during the induction period and slightly decreased during the compression period as compared with plain valve results. However, the turbulence intensities increase sharply just before inlet valve closure, indicating the creation of a strong directed jet during this period of very small valve opening. This results in a violent agitating motion inside the combustion chamber which remains at a higher level for considerable periods during the compression stroke. The time micro-scale of turbulence were not greatly affected while the size of micro-scale eddies are increased during the early part of the compression stroke but decay to values similar

to the plain valve results later in the stroke. The flow mechanism developed by this valve could be described, therefore, as an increase in the fluctuating velocity component and the reduction of their rate of decay with the consequent result of faster flame speeds. The performance of this valve could be imagined to be the same as introducing a squish velocity component during the period of higher damping rates of the flow velocities. The improvement in engine performance in Stivender's experiment (19) where extremely small valve lifts were required at light loads (0.01 - 0.05 inch) to produce a significant effect, may be attributed, therefore, to increases in turbulence intensities and better mixing of fuel, air and residuals rather than enhancing the small scale turbulence.

c) Turbulence Promoter at Spark Plug

Since the effect of this modification will be confined locally, measurements were carried out at the levels of the serrations at the spark plug location. Figures (6-47a) - (6-47e) show the results for the Rolls-Royce engine at full throttle conditions, while Figures (6-48a) - (6-48f) show similar results for the Ford engine at full and part load conditions.

The flow mechanism produced by this modification could be described as follows:

i) Gas mean velocities during the induction period remain constant while a rapid decrease in their values occur during the compression period.

ii) The turbulence intensities decrease during the cycle as compared with the normal engine case, which results in a rapid decrease in the fluctuating velocity components.

iii) The time micro-scale of turbulence is nearly the same as the unmodified case while the size of small scale eddies is greatly reduced.

The above mentioned conclusions indicate that using this modification will result in a region of low velocities where the flame kernel will develop at a more repeatable value than the normal case and could propagate as a flame front at the same rate of normal operation, since all effects of this modification are confined to a local region. It may result in an extension of the lean limit operation since more favourable conditions for flame kernel growth exist (see for example the results of Bolt (3) for the variation of lean ignition limit as a function of mixture velocity, Figure (2-29)).

d) Valves with Guide Vanes

Figures (6-47f) - (6-47j) show comparisons between the turbulence characteristics produced by different modified valves fitted with four, six and eight vanes, as well as the case of a plain valve of the Rolls-Royce engine, while Figures (6.48a) - (6-48f) show similar results for valves with four and six vanes and a plain valve, for two measuring locations inside the combustion chamber of the Ford engine. The Rolls-Royce data covers the induction and compression strokes while the Ford data corresponds only to the compression period. Discussions of the two sets of data are given below:

a) Rolls-Royce Engine (Wedge Shape Combustion Chamber)

i) The use of valves with guide vanes resulted in increases in gas velocities during the induction and early part of the compression period.

ii) The turbulence intensities are higher for valves with vanes than a plain valve and consequently the fluctuating velocity components are higher for most parts of the cycle. This indicates conditions of greater homogenity as compared with a plain valve.

iii) The time micro-scales of turbulence for valves with vanes are higher than the corresponding values for a plain valve during most of the compression period. However, the size of small-scale eddies for valves with vanes during the period from 40 degrees BTDC to TDC are nearly half the corresponding values for a plain valve.

iv) A valve fitted with four long vanes inclined at 20 degrees to the flow direction produced higher intake velocities than the two valves fitted with short vanes inclined at 60 degrees to flow direction.

b) Ford Engine (Heron Shape Combustion Chamber)

i) The valve with four vanes has shown higher gas velocities at full load conditions than a plain valve or a valve with six vanes, Figure (6-48a). However both plain valve and the valve with four vanes gave similar results at part load conditions, Figure (6-48b). The fluctuating velocity components follow similar trends, Figures (6-48c) and (6-48d).

ii) The micro-scale of turbulence (λ_y) is slightly higher for a valve with four vanes than a plain valve while the valve with six vanes has shown much lower values, Figure (6-48c). The valve with four vanes has also shown some reduction in the micro-scale at part load conditions, Figure (6-48f).

iii) The data for measurements with plain valves at the cylinder head surface are also shown on the graphs, (6-48a) - (6-48f) which indicate a reduction in both mean velocities, and micro-scale of turbulence, while the values of fluctuating velocity components (u') at full load conditions remain practically constant at the two locations of measurements. The values of u' decrease at part load conditions.

The improved engine performance and extension of lean limit operation reported by Tanuma et al (20) when valves fitted with vanes were used, could be attributed (in view of the earlier results) to a combination of the following effects:

1. Improved homogeneity of fuel/air mixture due to higher intake velocities without much sacrifices in engine volumetric

efficiency as would be the case of a masked valve. Figure (6-49) shows a comparison between the isotropic port area for the different valves investigated as obtained from blowing rig tests. These areas are calculated from the conventional equation of orifices with compressible flow (154) as given by:

$$\frac{\dot{m}}{A^*} = \left(\frac{P_c}{P_o}\right)^{\frac{1}{\gamma}} \sqrt{\frac{2\gamma}{\gamma-1} P_o \rho_o \left[1 - \left(\frac{P_c}{P_o}\right)^{\left(\frac{\gamma-1}{\gamma}\right)}\right]} \quad (6\text{-}4$$

where $\dot{m}$ is the rate of mass flow

A^* is the effective port area

P pressure

ρ density

and the subscripts (o), (c) refer to conditions in inlet manifold and combustion chamber respectively.

2. The existence of bladed surfaces in the flow path resulted in improved fuel atomisation and evaporation at the vanes edges.

3. The increased levels of turbulence intensity and fluctuating velocity components during most of the compression period resulted in faster flame speeds and

consequently lower cyclic variations. Moreover, the almost constant levels of turbulence intensities during compression, certainly contribute towards better repeatability of flame front propagation between different cycles.

d) Intake Fitted with Delta Wings

It is interesting to note that this modification has produced the highest levels of intake velocities and shows also higher velocities during compression. However, the fluctuating velocity components remain the same as other types of valves, which are higher than the plain valve data for most of the compression period. The time micro-scale of turbulence is significantly lower (for this modification) than for other valves during the compression period. However, they are still higher than the plain valve data during the latter part of the compression period. The spatial micro-scales of turbulence are of the same levels as other valves with vanes and smaller than the plain inlet valve data during the latter part of the compression period. All the earlier discussions of the characteristics of valves with vanes are applicable also for this case.

6.4 Investigation of Cylinder-to-Cylinder Variation in the Flow Field Characteristics

The discussions of the preceding sections were mainly concerned with investigating the cyclic variations in the flow field characteristics for a particular engine cylinder which are believed to be the main causes of cyclic combustion variations. However, a good cylinder-to-cylinder air distribution is of equal importance for good fuel distribution and lower emissions from a multi-cylinder engine. The importance of this factor on combustion variation was first reported by Patterson (2) as discussed earlier in the literature survey.

A study of the cylinder-to-cylinder variations in flow characteristics was carried out in the present work on the Rolls-Royce engine at 1000 RPM and fully opened throttle conditions. Measurements of gas velocities and turbulence characteristics were carried out at the spark plug location for different cylinders and statistically analysed. Figures (6-50a) - (6-50e) show the results of this study which could be summarised as follows:

i) Cylinder-to-cylinder variation in flow field characteristic parameters may be as large as 30% of their mean values.

ii) Average values of cylinder-to-cylinder coefficients of variation during the induction period are 27% for gas mean velocities ($\bar{U}$) and the spatial micro-scales (λ_y) while for the compression period the coefficients

of variations are 29.3% and 30.6% for $\bar{U}$ and λ_y respectively. The average value of cylinder-to-cylinder variations in the intensity of turbulence are 12.7% and 14.1% of the mean values during induction and compression stroke respectively.

iii) It is interesting to note that the cylinder-to-cylinder variations in the time micro-scales of turbulence are relatively small. For example, the mean values of the deviations are 2% and 10.4% of the mean values during the induction and compression periods respectively. This may be explained by the fact that this time characteristic parameter represents the rate of turbulence dissipation which is a function of combustion chamber shape and time events in the cycle (e.g. induction and compression strokes). The latter processes are more or less repeatable from cycle-to-cycle and cylinder-to-cylinder. Once again this observation is in agreement with Tsuge and Kido (153) where the pre-relaxation period, corresponds to induction in our case, shows regions of irregular composition while the relaxed stage, corresponds to compression period in our case, consists of nearly homogeneous conditions.

6.5 Effect of Combustion Chamber Configuration on Turbulence Characteristics

The discussions of the previous sections have shown that the flow field characteristics vary considerably with combustion chamber configuration. The main differences between the wedge shape of the Rolls-Royce engine and the heron shape of the Ford engine can be summarised as follows:

i) Because of the difference in induction capacities of the Rolls-Royce and Ford engines, higher intake velocities were observed for the former engine which continue during the compression period. However, a comparison of the turbulence intensities ($u'/\bar{U}$) in both engines eliminates this factor in the comparisons between the performance of the two shapes of combustion chambers. The wedge shape chamber has shown much higher turbulence intensities during the induction period and correspondingly higher levels of fluctuating velocity components, Figures (6-33b), (6-48c) and (6-48d). Consequently the mixing characteristics of the wedge shape chamber is better than the heron shape.

ii) The time micro-scale of turbulence for the heron shape are much higher than those of the wedge shape, especially during the induction period. This indicates that eddies of higher frequencies are generated in the wedge chamber than those produced by

the heron. Consequently one may expect poorer mixing characteristics of the heron shape.

It is also interesting to note that an almost constant value of the time micro-scales are observed for the heron shape chamber during most of the cycle while clear variations could be observed for the wedge shape during different strokes of the cycle.

iii) The spatial micro-scale of turbulence are much smaller for the heron shape than the wedge. Consequently, one may expect a better performance of the heron shape with lean mixtures where the small-scale eddies will accelerate the initial growth of the flame kernel and consequently results in lower cyclic combustion variations. The lower fluctuating velocities observed for this chamber will provide also favourable conditions for the growth of the flame kernel due to lower heat losses to the surrounding flow.

These conclusions are in agreement with the experimental data of Tanuma et al (20) where the wedge chamber shows the worst lean mixture performance, while the heron shape was the best of all chambers investigated. The disc and pancake chambers were in between these limits. In fact, the analysis of Semenov's data for disc combustion chamber supports this conclusions where higher values of micro-scales (λ_y) than those of the heron

chamber were obtained, but smaller than the Rolls-Royce wedge.

The studies of Dodd (156) on the effect of combustion chamber shape on exhaust emissions are also in agreement with the above mentioned conclusions. In this latter work, single cylinder engines were tested with fully vapourised mixture, which eliminates the effect of induction period turbulence on the mixing process. The heron shape chamber showed lower levels of emissions than a wedge shape chamber, Figure (6-51). In this case, the flat disc chamber showed lower levels of emissions than both the wedge and heron shape, however its specific fuel consumptions were higher in some experiments.

Table (6-1) shows a comparison between the values of micro-scales of turbulence for different types of combustion chambers.

Blizard and Keck (133) have developed a turbulent burning model for internal combustion engines, where experimental data were used to develop a correlation between the 'average' radius of eddies and engine geometry as given by the following relationship:

$$\text{Eddy Radius} = 0.17 \frac{\text{(Maximum valve lift)}}{\text{(Compression Ratio)}} \qquad (6\text{-}5)$$

Substituting the corresponding data of the Rolls-Royce and the Ford engines into equation (6-5) gives values of eddy size of the order of 0.40 and 0.34 mm respectively, which agrees with the order of magnitudes of the measured values in the present work.

TABLE (6-1) A Summary of the Values of the Micro-Scale of Turbulence for Different Types of Combustion Chambers

Combustion Chamber Configuration	Compression Ratio	Engine Speed (r.p.m)	Crank Angle	Micro-Scale λ_y (mm)
1. Wedge	9:1	))1000)	40° BTDC 20° BTDC TDC	0.6178 0.7125 0.459
2. Heron	8.9:1	))1000)	40° BTDC 20° BTDC 10° BTDC	0.19937 0.09755 0.07527
		))2000)	40° BTDC 20° BTDC 10° BTDC	0.28689 0.17661 0.099519
		))3500)	40° BTDC 20° BTDC 10° BTDC	0.35472 0.23521 0.14169
3. Disc (New Analysis of Semenov's data (22))	4.0:1 6.0:1 8.0:1 9.5:1	)))) 900	TDC	0.479 0.368 0.313 0.264
4. Squish Chamber used by James (24) Fig.(2-74)	3.9:1 5.29:1 8.88:1	950 950 900	TDC	0.248 0.2428 0.4665

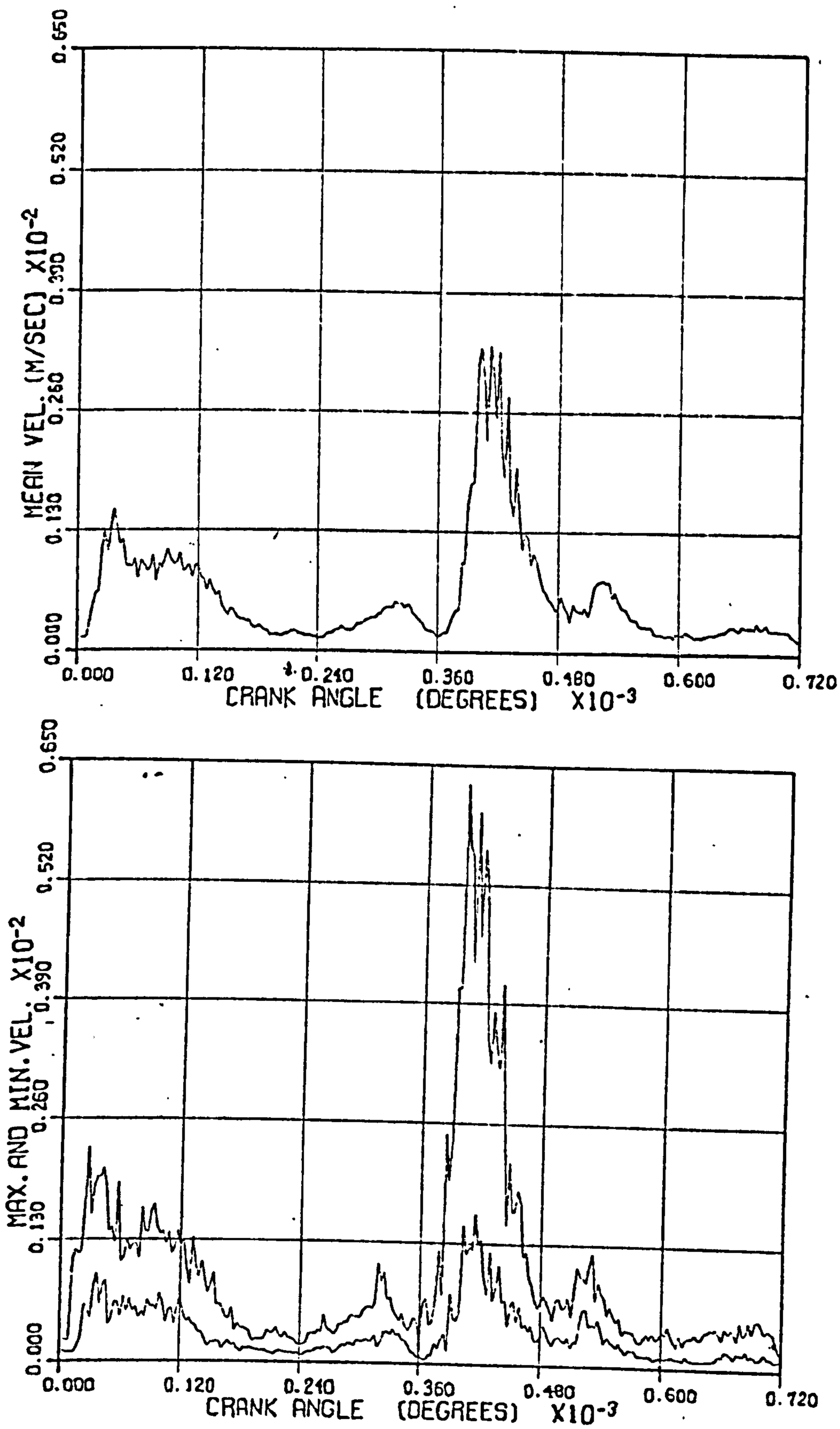

Fig. (6-1) Statistical Analysis of Gas Mean Velocities at Different Crank Angles During the Cycle. Analysis for 10 Consecutive Cycles, Rolls-Royce V8 Engine, Plain Inlet Valve, 1000 RPM and Fully Opened Throttle. Probe at Spark Plug Location (Z=17.78 mm), Wire Direction = 300°, (See Fig. (5-3) for definitions).

(a) Mean Values ($\bar{U}$). (b) Occurrence of Max. & Min. Gas Velocities.

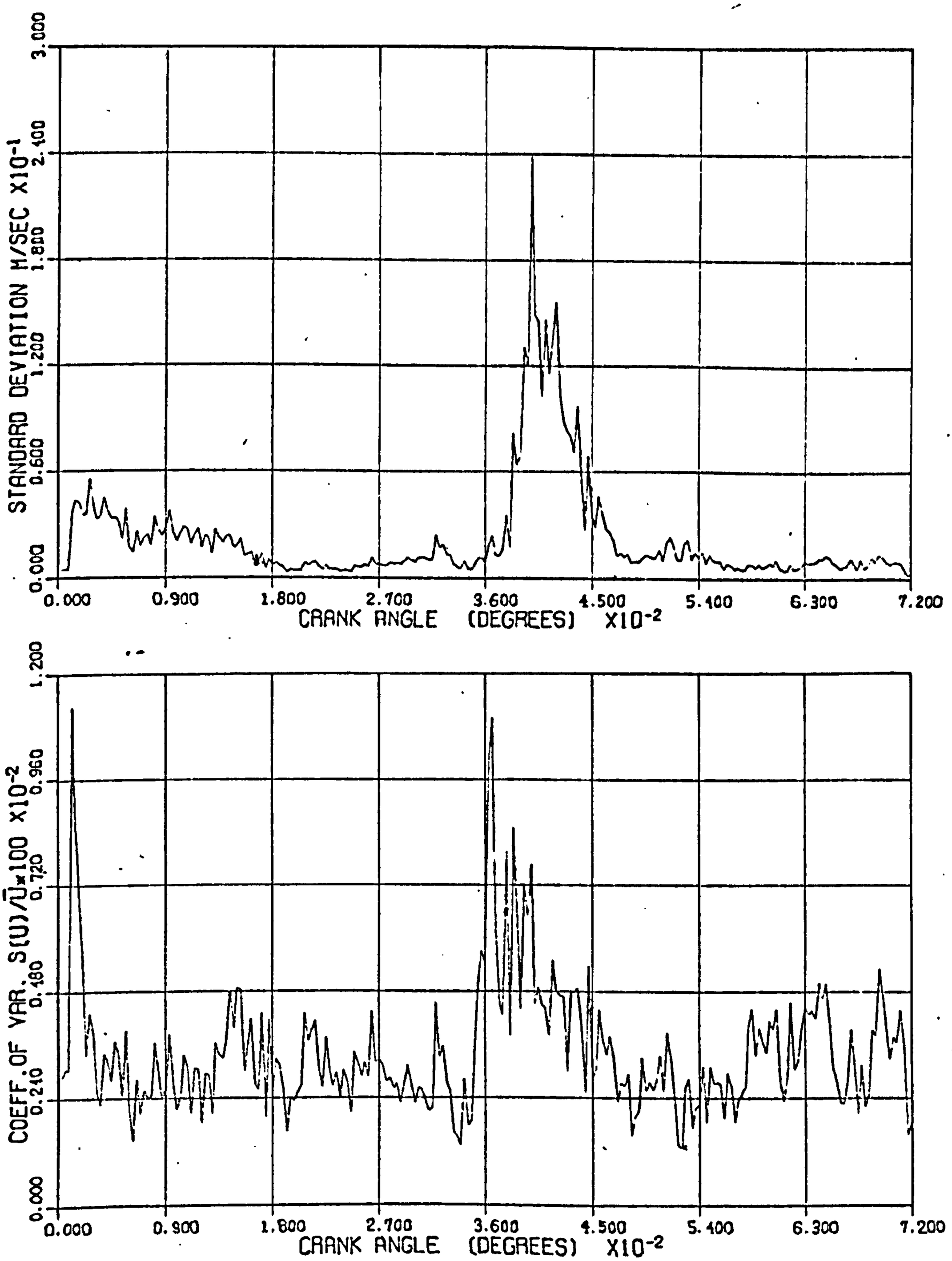

Fig. (6-1) Statistical Analysis of Gas Mean Velocities at Different Crank Angles During the Cycle. Analysis for 10 Consecutive Cycles, Rolls-Royce V8 Engine, Plain Inlet Valve, 1000 RPM and Fully Opened Throttle. Probe at Spark Plug Location (Z = 17.78 mm), Wire Direction = 300°, (See Fig. (5-3) for definitions).

(c) Standard Deviations, S(U). (d) Coefficient of Variation $(S(U)/\bar{U}).100$.

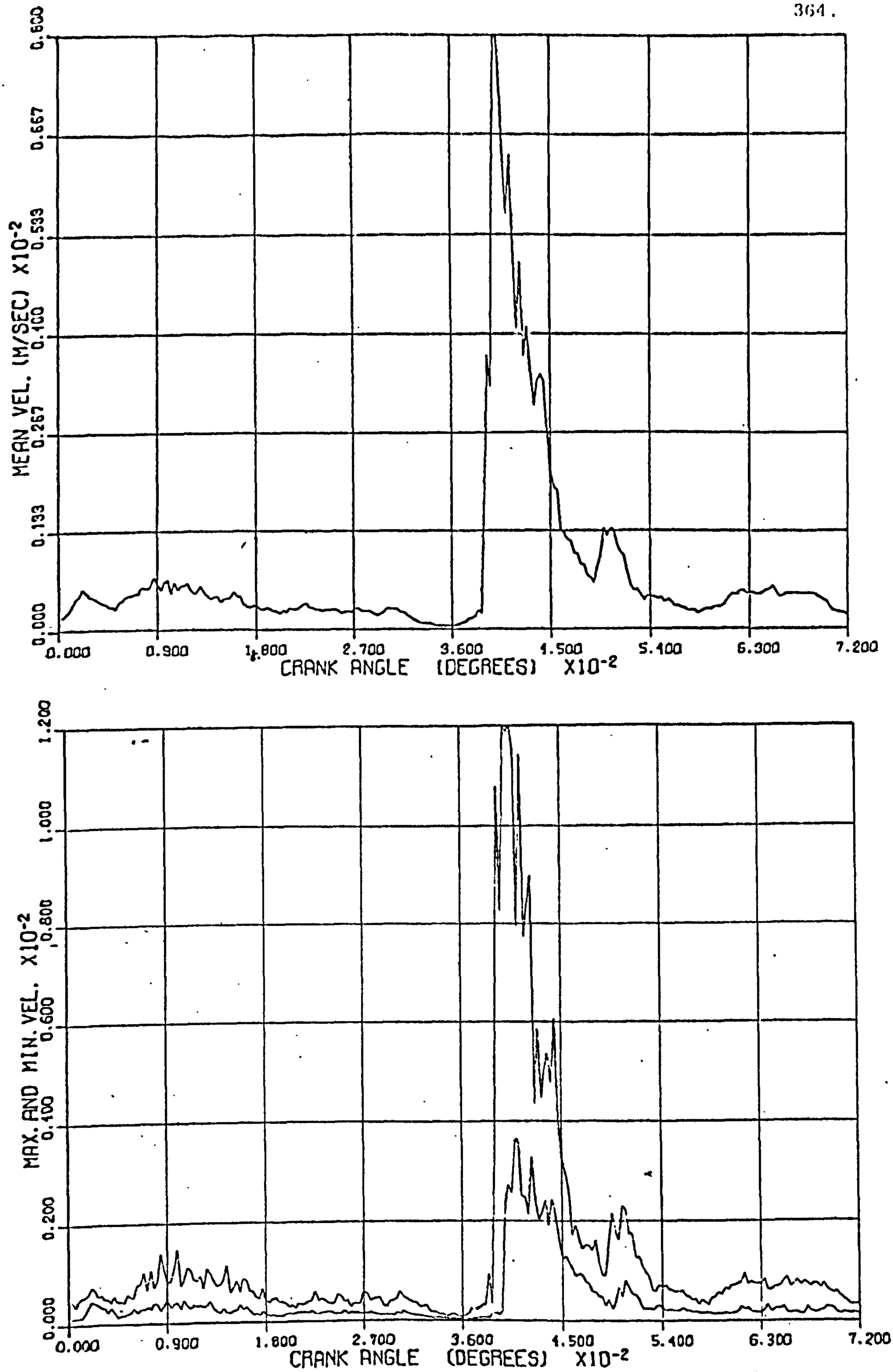

Fig. (6-2) Statistical Analysis of Gas Mean Velocities at Different Crank Angles During the Cycle. Analysis for 10 Consecutive Cycles, Ford V4 Engine. Plain Inlet Valve, 1000 RPM and 102 mm Intake Vacuum. Probe at Spark Plug Location, Horizontal Hot Wire at 3.8 mm from Cylinder Head Surface.

(a) Mean Values ($\bar{U}$). (b) Occurrence of Max. & Min. Gas Velocities.

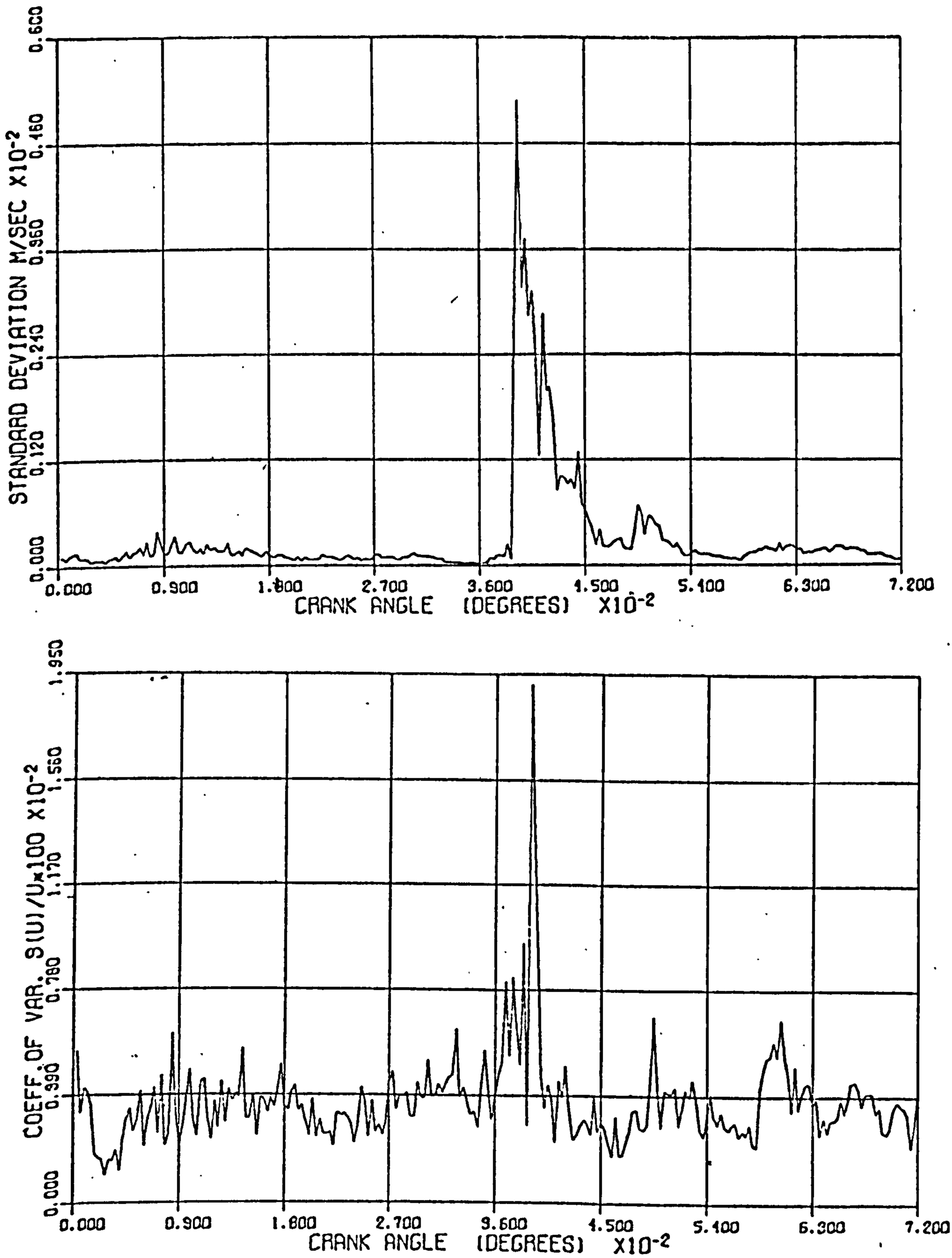

Fig. (6-2) Statistical Analysis of Gas Mean Velocities at Different Crank Angles During the Cycle. Analysis for 10 Consecutive Cycles, Ford V4 Engine. Plain Inlet Valve, 1000 RPM and 102 mm Intake Vacuum. Probe at Spark Plug Location, Horizontal Hot Wire at 3.8 mm from Cylinder Head surface.

(c) Standard Deviations, S(U). (d) Coefficients of Variation $(S(U)/\bar{U}).100$.

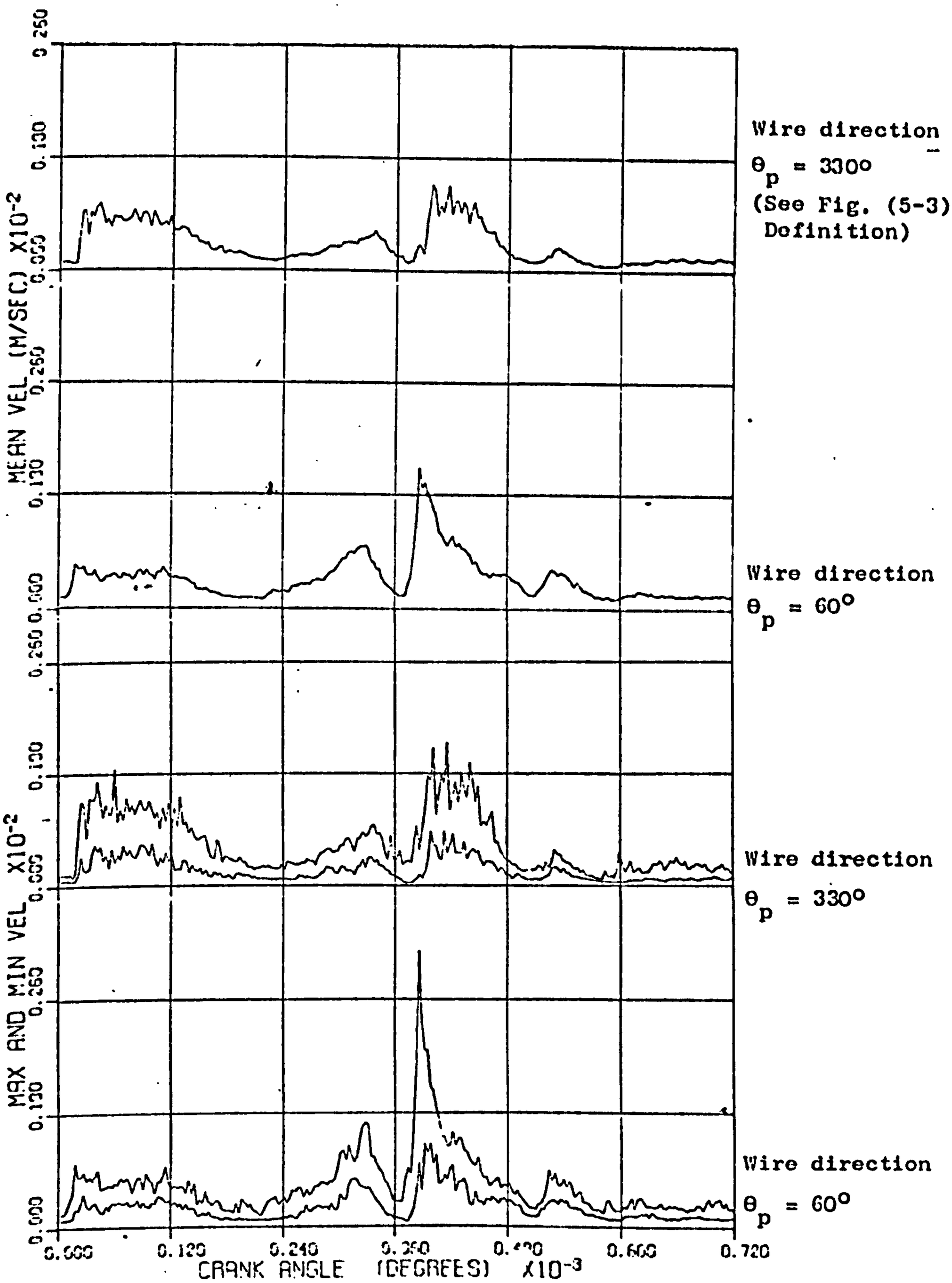

Fig. (6-3) Comparison Between the Measured Components of Gas Velocities and the Occurrence of Maximum and Minimum Values for two Different Orientations of the Hot Wire. Other Test Conditions are the Same as those of Fig. (6-1).

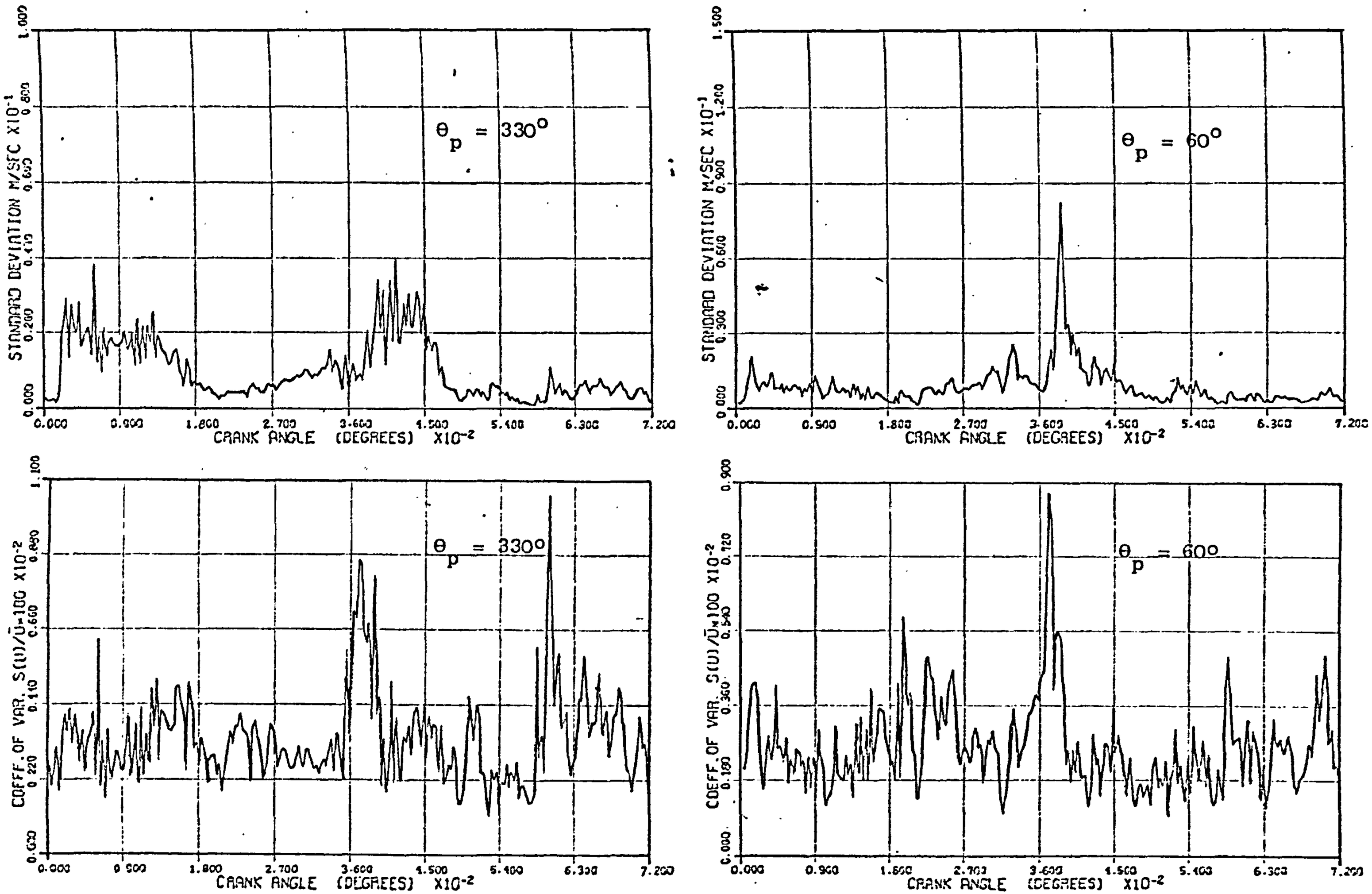

Fig. (6-4) Comparison Between the Values of Standard Deviation and Coefficient of Variation in Gas Mean Velocity for Two Different Oreintations of the Hot Wire. Same Test Conditions as Fig. (6-3).

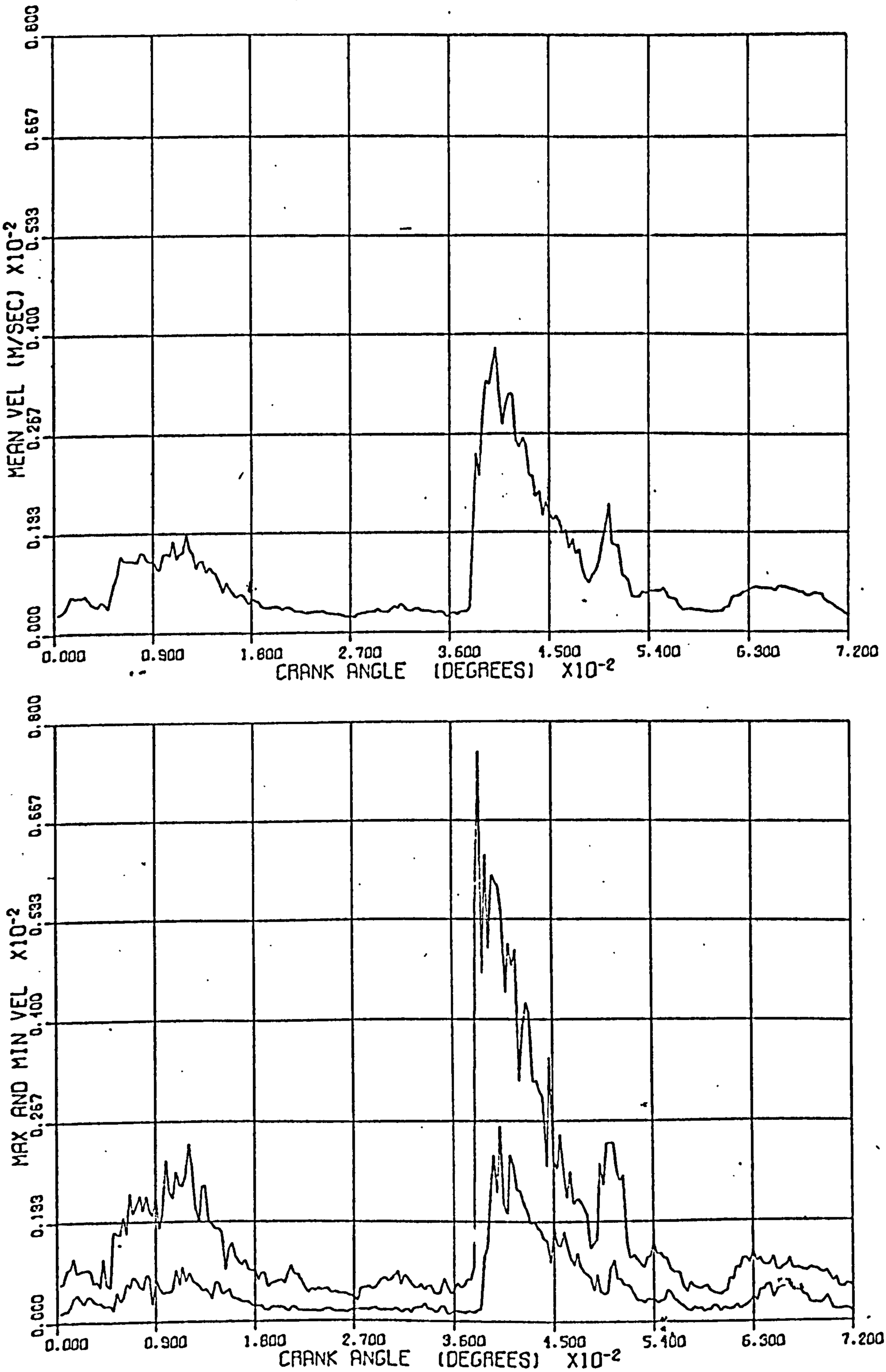

Fig. (6-5) Statistical Analysis of Gas Mean Velocities at Different Crank Angles during the Cycle Analysis for 10 Consecutive Cycles, Ford V4 Engine, 102 mm Intake Vacuum, Probe at Spark Plug Location, Vertical Hot Wire at 3.8 mm from Cylinder Head Surface.
(a) Mean Values ($\bar{U}$). (b) Occurrence of Max. & Min. Gas Velocities

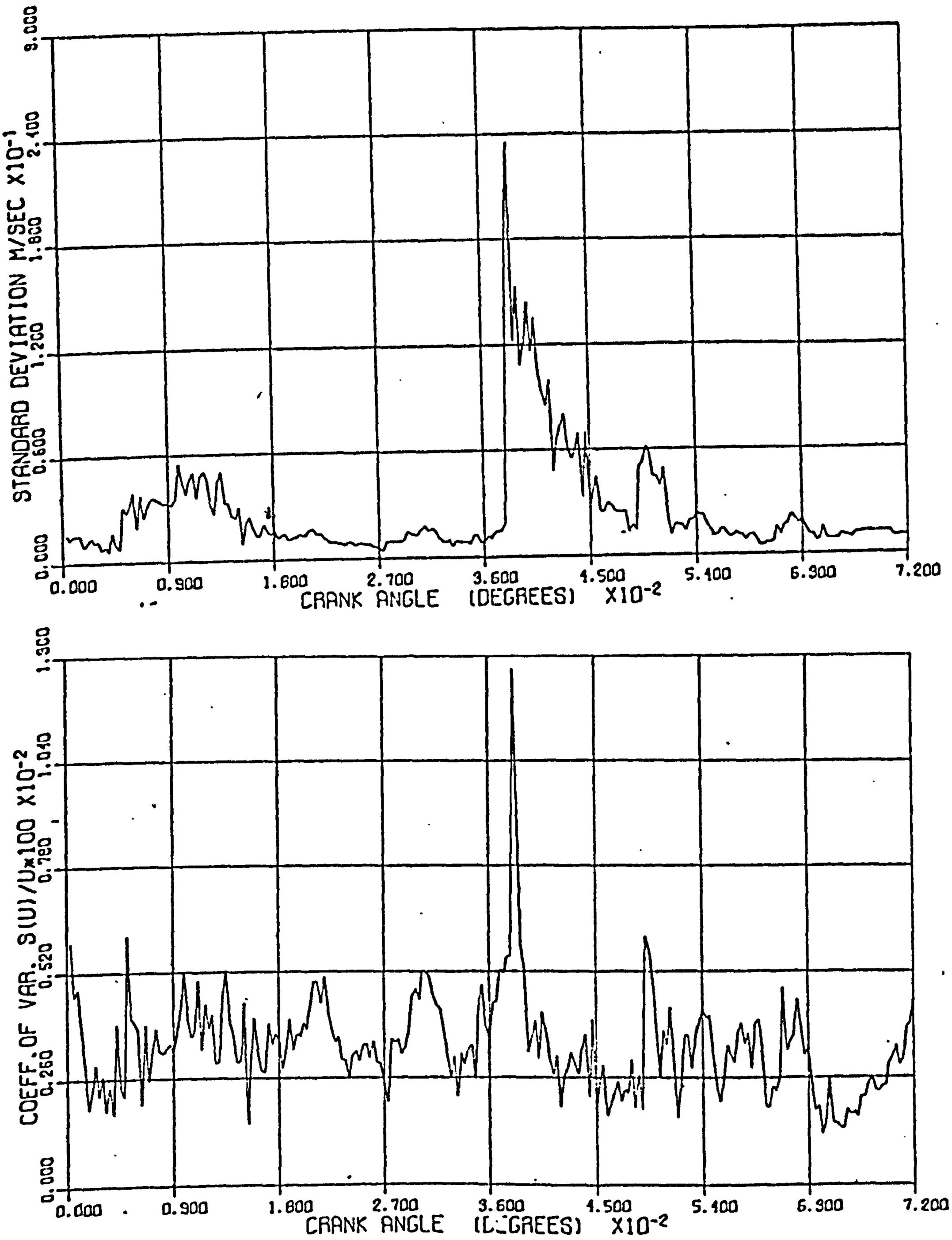

Fig. (6-5). Statistical Analysis of Gas Mean Velocities at Different Crank Angles during the Cycle Analysis for 10 Consecutive Cycles, Ford V4 Engine, 102 mm Intake Vacuum, Probe at Spark Plug Location, Vertical Hot Wire at 3.8 mm from Cylinder Head Surface.

(c) Standard Deviations S(U). (d) Coefficients of Variation $(S(U)/\bar{U}).100$.

Figs(6-6) and (6-7) Variation of Gas Mean Velocity Characteristics with Depth Inside a Wedge Combustion Chamber. (Rolls-Royce Engine, 9:1 Compression Ratio ,1000 RPM and Fully Opened Throttle Conditions).

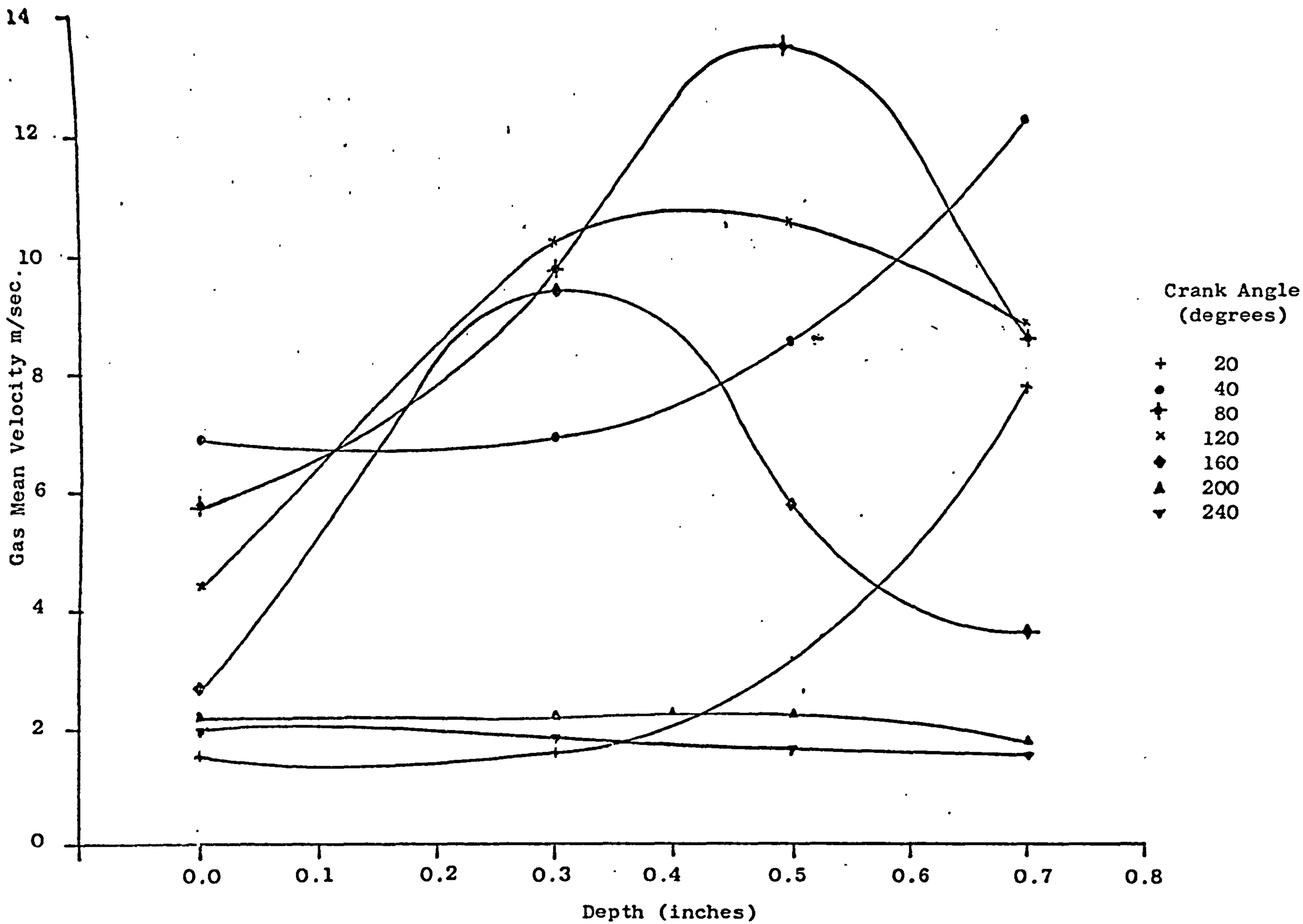

Fig. (6-6a) Variation of gas Mean Velocities with Depth Inside a Wedge Combustion Chamber During the Induction Period. (Rolls-Royce V8 Engine, 9:1 Compression Ratio, 1000 RPM and Fully Opened Throttle). Probe traverses along the spark plug axis.

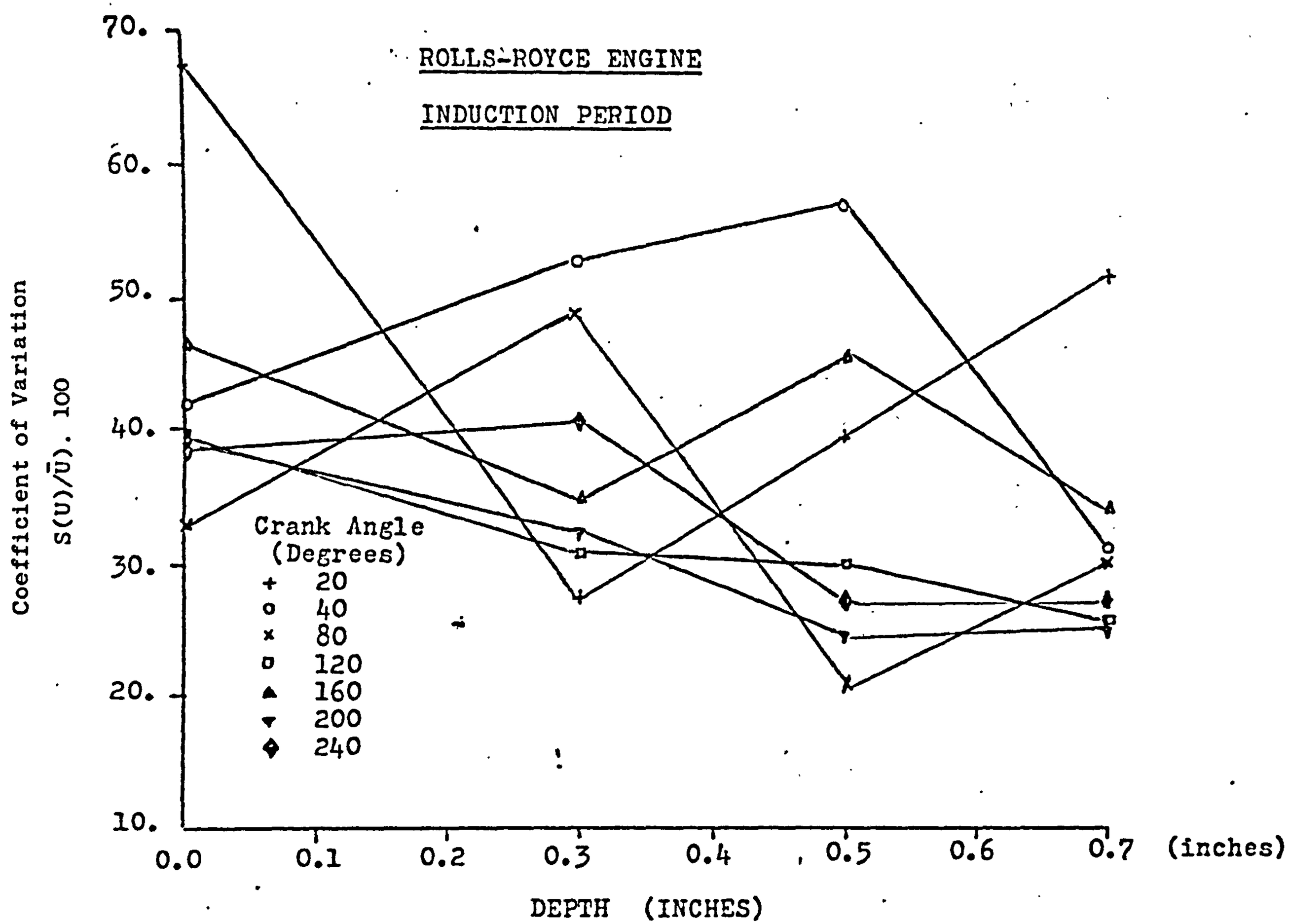

Fig. (6-6b) Variation of the Coefficient of Variation($S(U)/\bar{U}$).100 with Depth Inside A Wedge Combustion Chamber During the Induction Period. (Data corresponds to test conditions of Fig. (6-6a)).

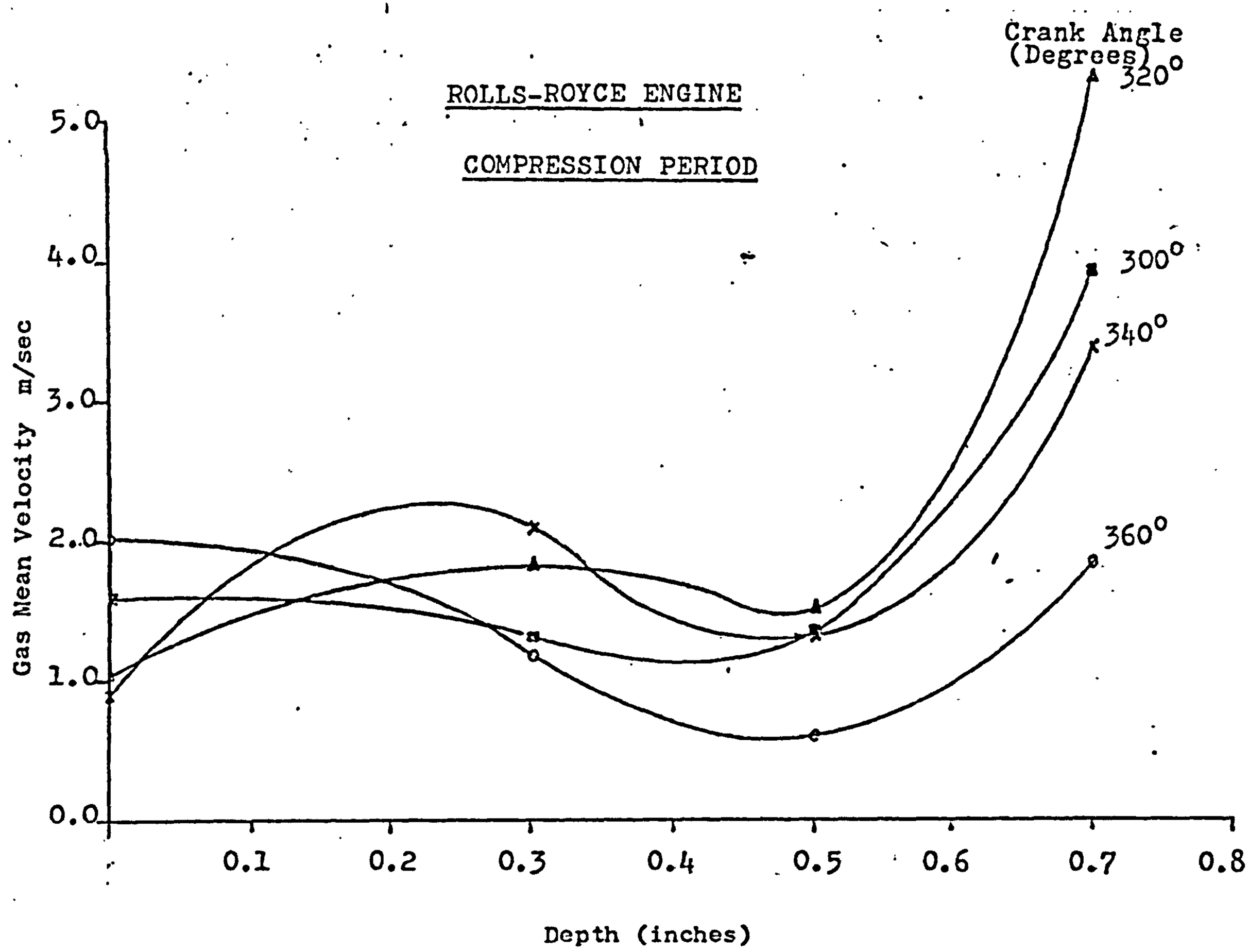

Fig. (6-7a) Variation of Gas Mean Velocities with Depth Inside a Wedge Combustion Chamber During the Compression Period. (Data corresponds to test conditions of Fig. (6-6a).

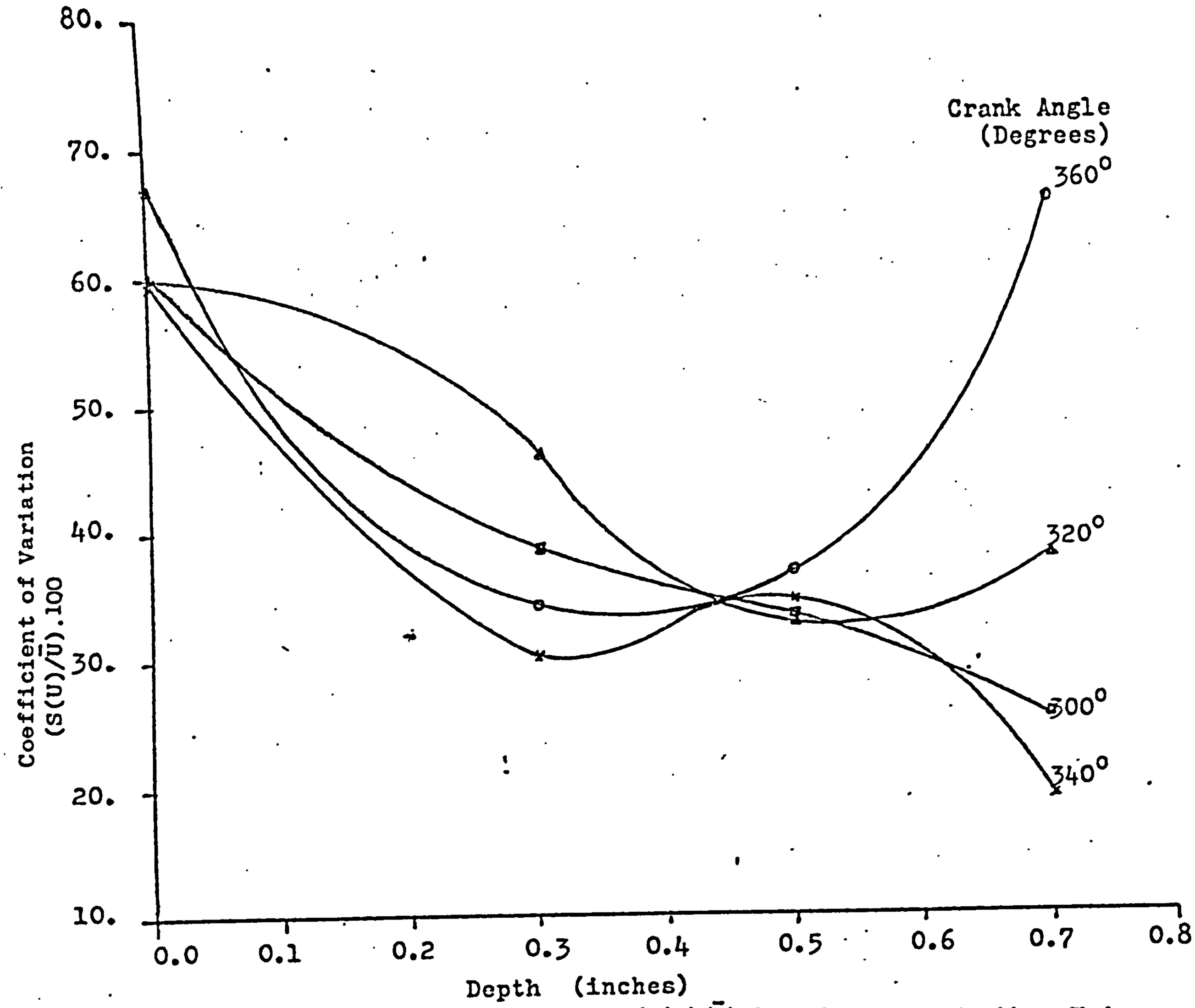

Fig. (6-7b) Variation of the Coefficient of Variation(S(U)/Ū).100 with Depth Inside a Wedge Combustion Chamber During the Compression Period. (Data corresponds to test conditions of Fig. (6-6a)).

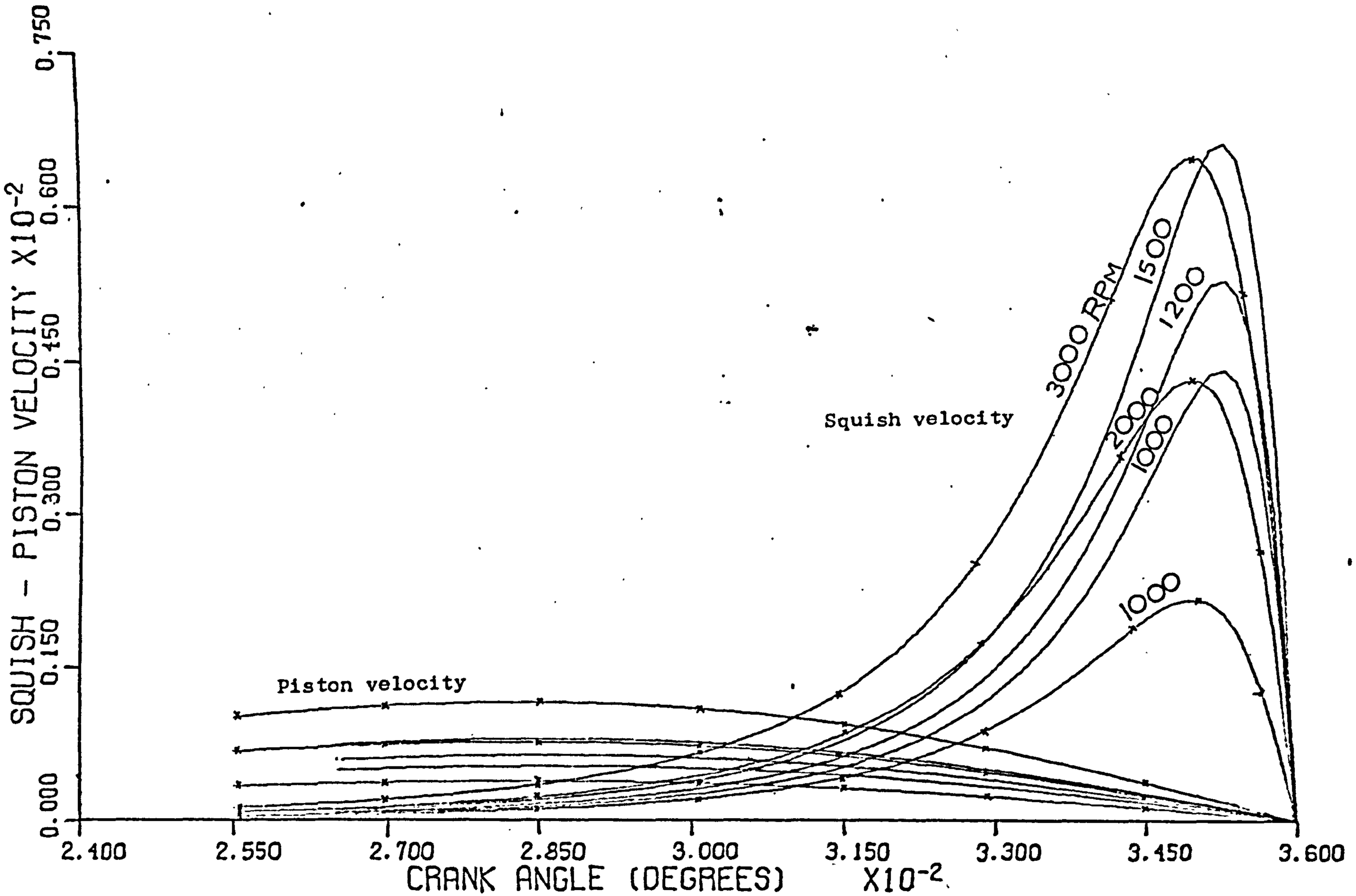

Fig. (6-8) Variation of Piston Speed and Theoretical Predictions of Squish Velocities During the Compression Period.

—— Rolls-Royce V8 Engine. *—* Ford V4 Engine.

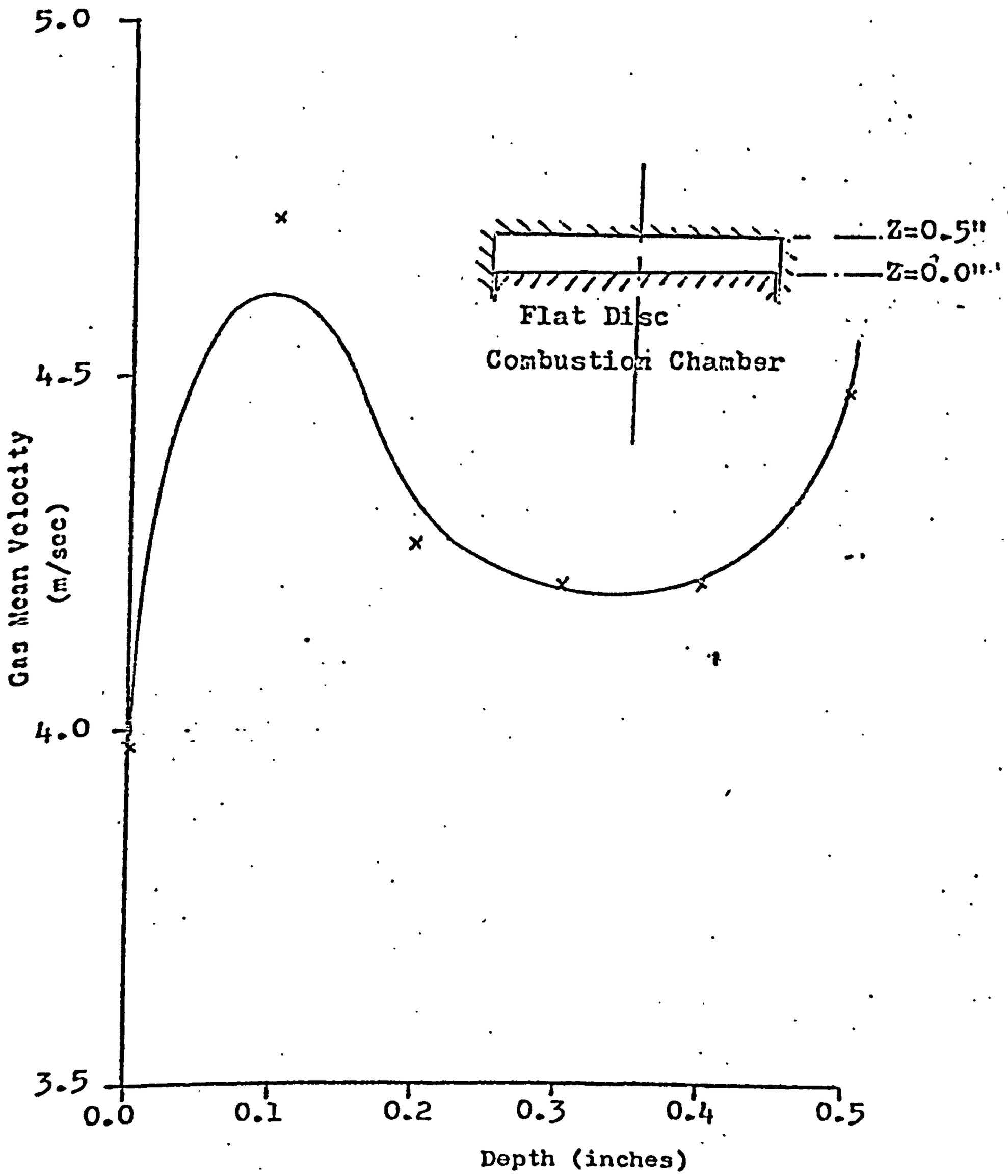

Fig. (6-9) Variation of Gas Mean Velocity at TDC with Depth Inside a Flat Disc Combustion Chamber. Data from Winsor's Investigation (23).

Fig. (6-10) Investigation of the Flow Pattern Inside a Wedge Combustion Chamber.
(Rolls-Royce V8 Engine, Compression Ratio 9:1, 700 RPM and Fully Opened Throttle).
Probe Traverses Parallel to Cylinder Axis.
(See Figs. (5-2) and (5-3)).

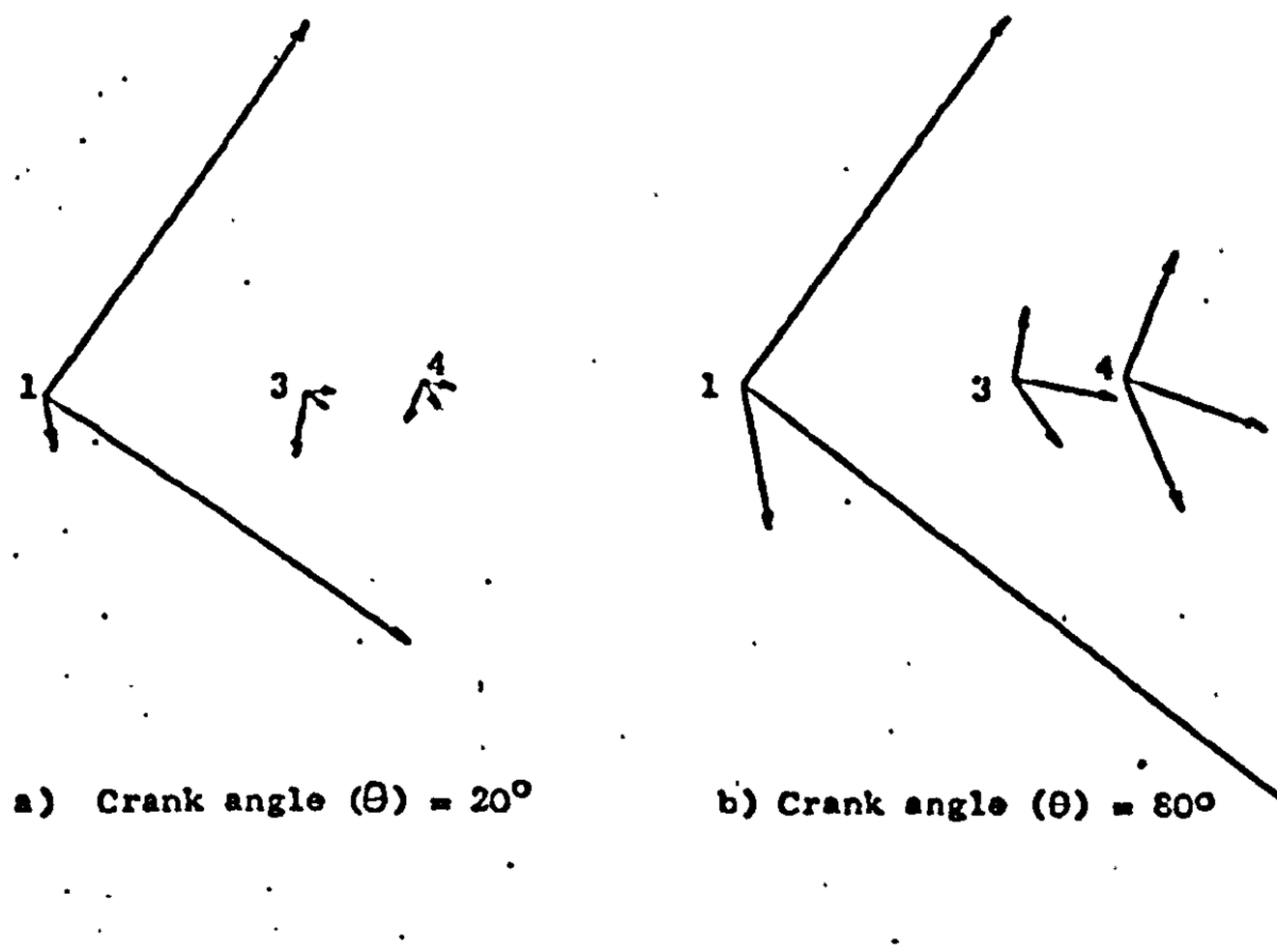

a) Crank angle (θ) = 20° b) Crank angle (θ) = 80°

LEVEL: Z = 20 mm

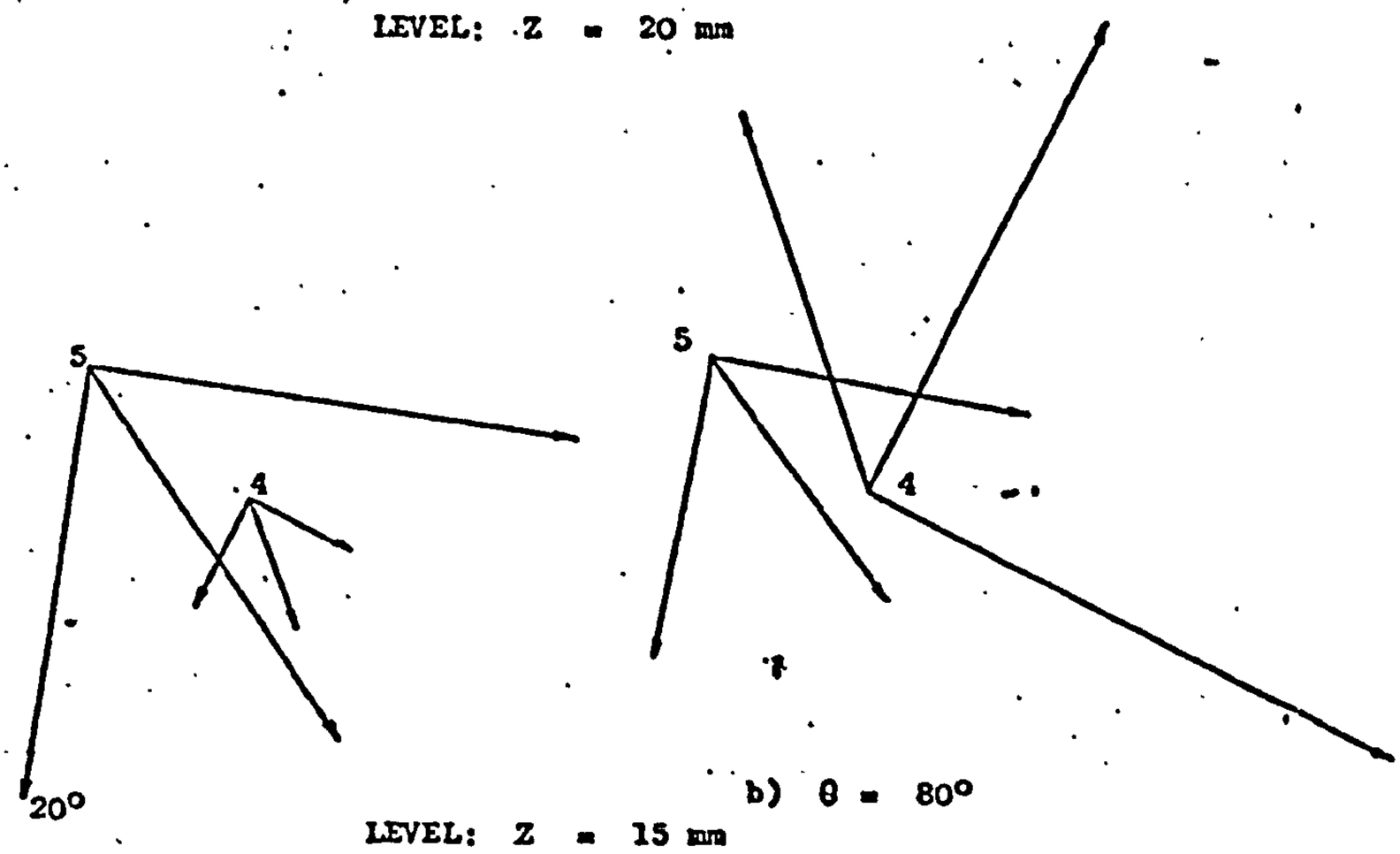

a) θ = 20° b) θ = 80°

LEVEL: Z = 15 mm

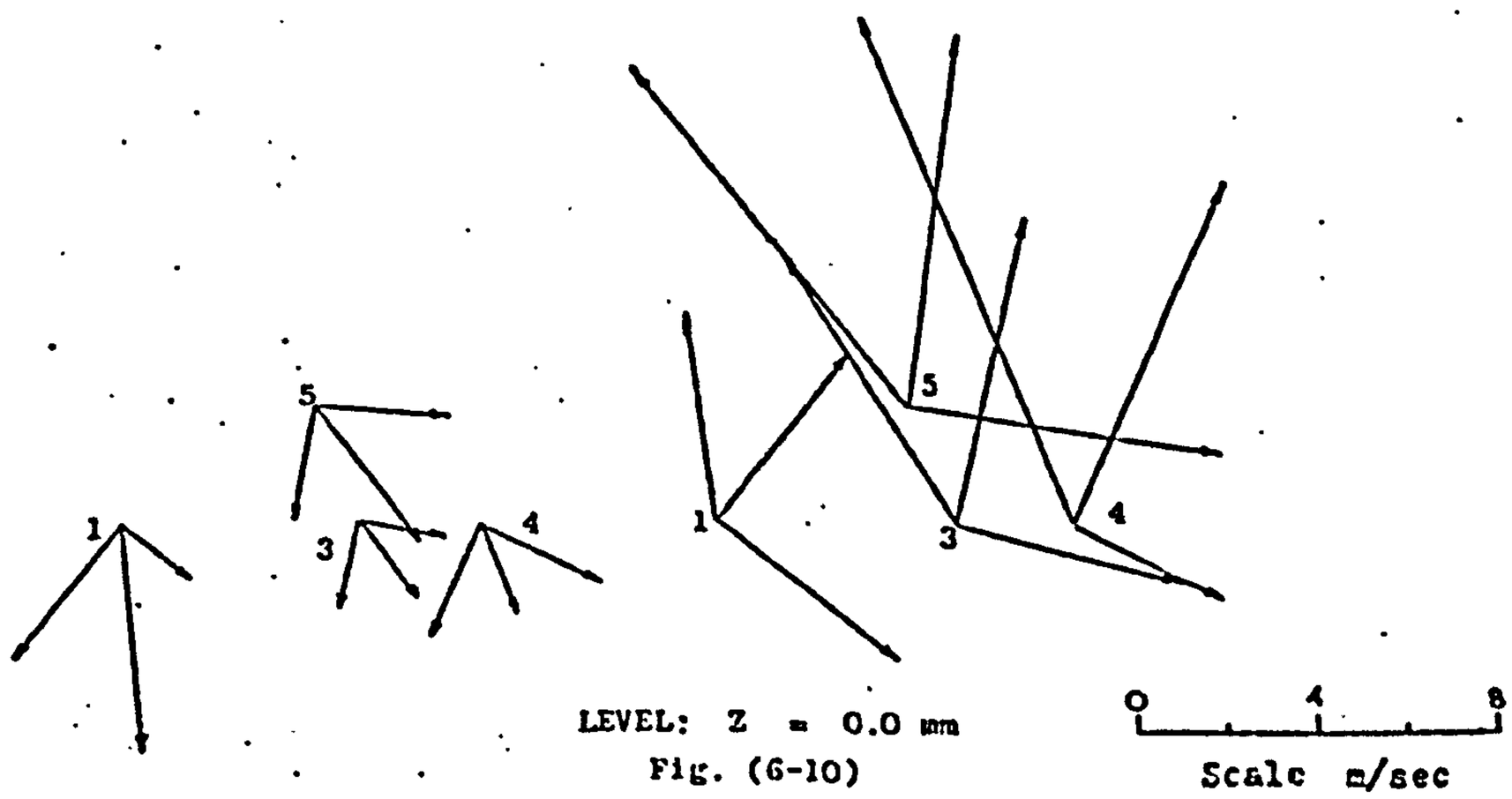

LEVEL: Z = 0.0 mm

Fig. (6-10)

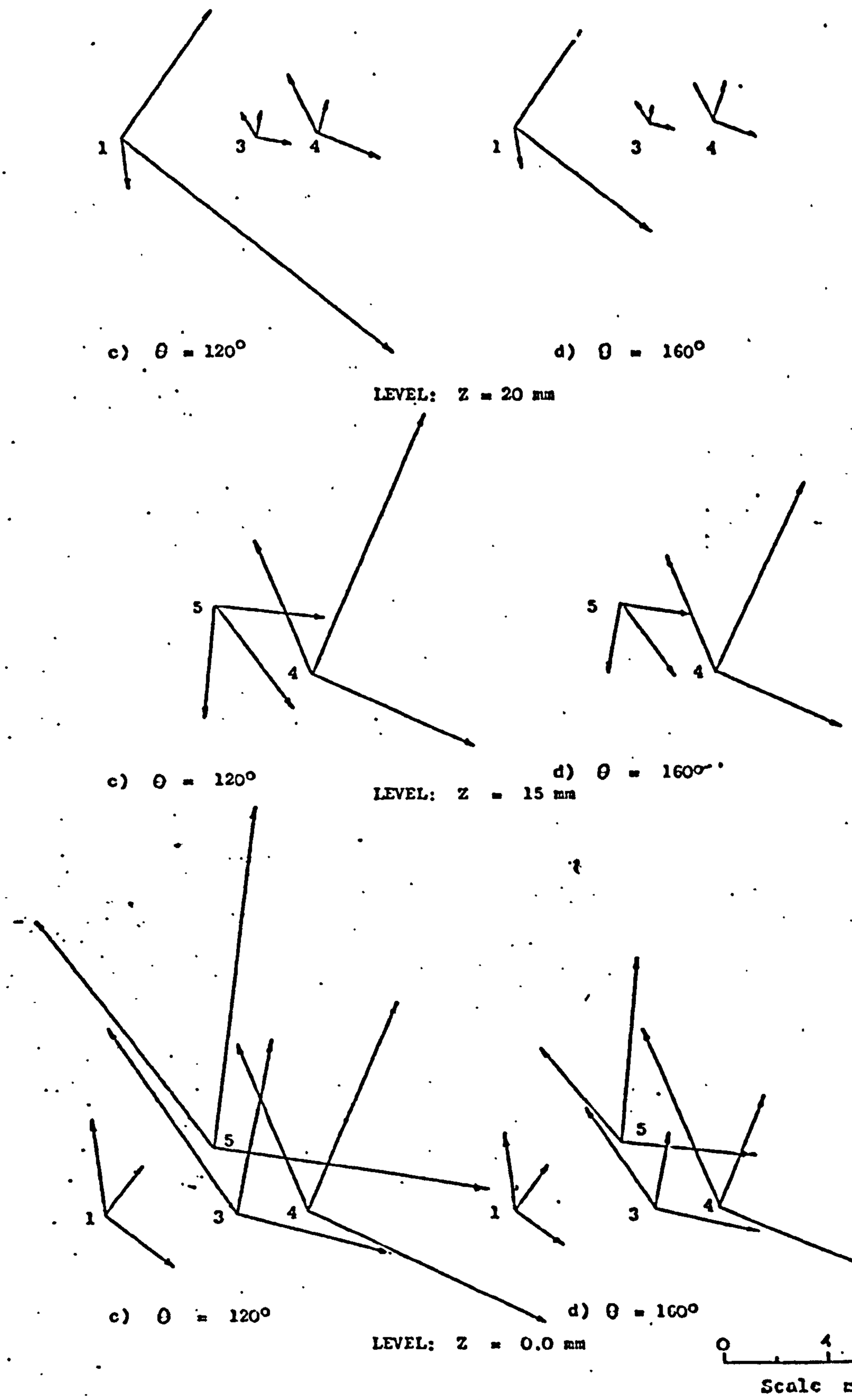
1
3
4
c) θ = 120°
d) θ = 160°
LEVEL: Z = 20 mm
5
4
c) θ = 120°
d) θ = 160°
LEVEL: Z = 15 mm
5
1
3
4
c) θ = 120°
d) θ = 160°
LEVEL: Z = 0.0 mm
0
4
8
Scale m/sec

Fig. (6-10)

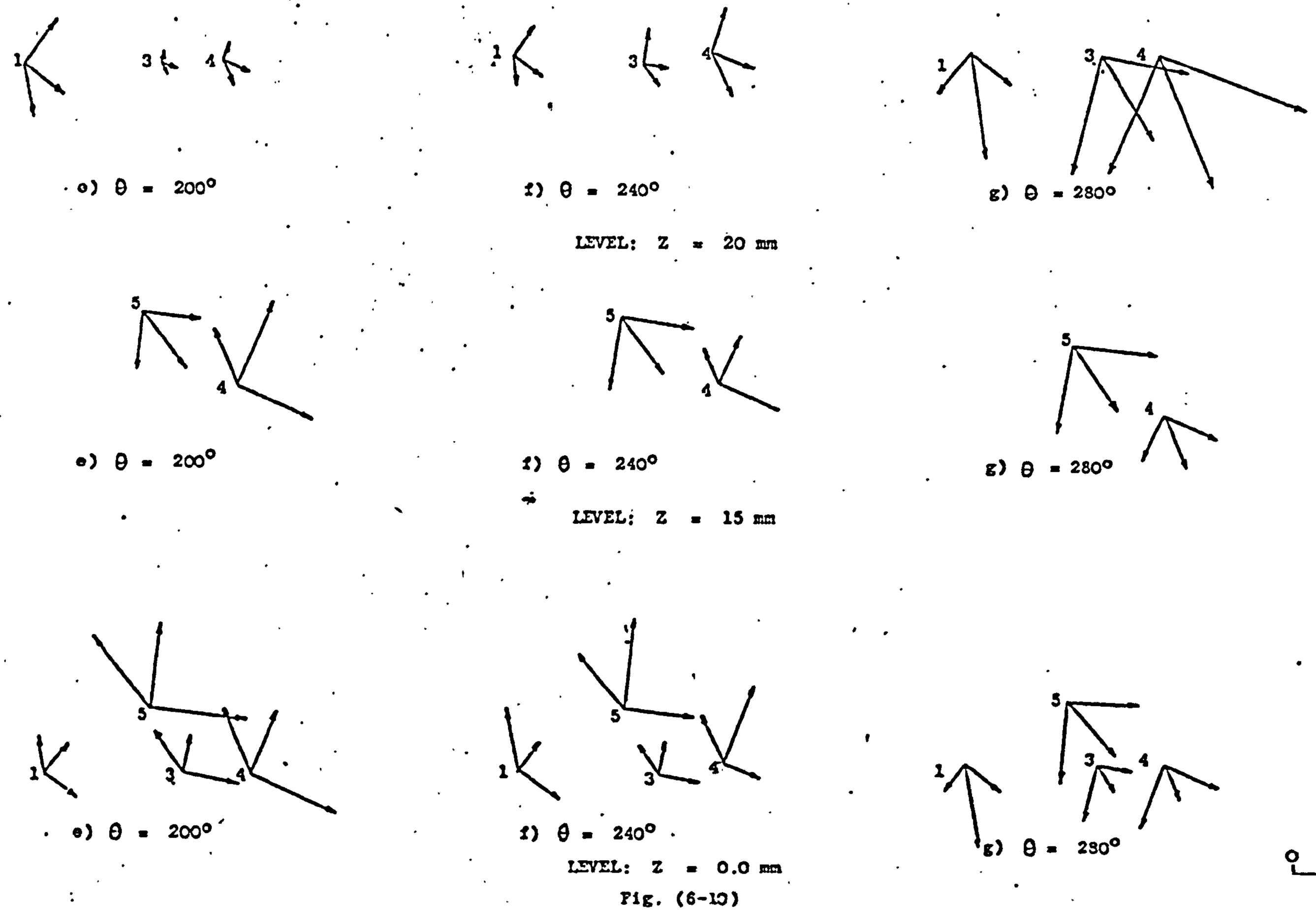
1
3
4
e) θ = 200°
1
3
4
f) θ = 240°
1
3
4
g) θ = 280°
LEVEL: Z = 20 mm
5
4
e) θ = 200°
5
4
f) θ = 240°
5
4
g) θ = 280°
LEVEL: Z = 15 mm
5
1
3
4
e) θ = 200°
5
1
3
4
f) θ = 240°
5
1
3
4
g) θ = 280°
LEVEL: Z = 0.0 mm
0
4
8
Scale m/sec

Fig. (6-10)

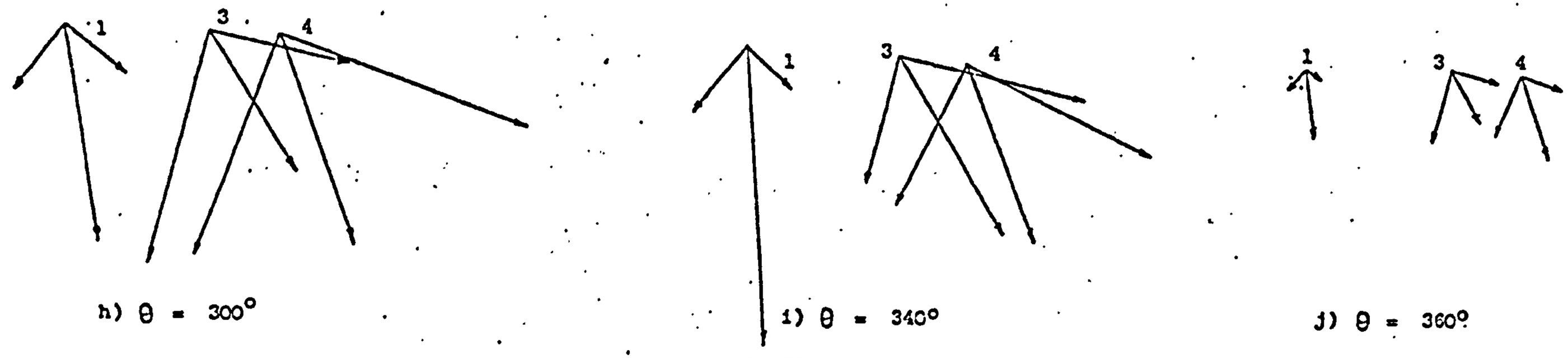

h) θ = 300° i) θ = 340° j) θ = 360°

LEVEL: Z = 20 mm

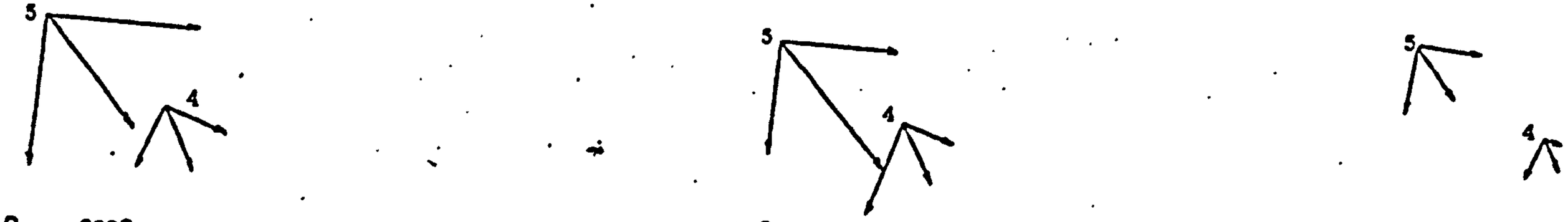

h) θ = 300° i) θ = 340° j) θ = 360°

LEVEL: Z = 15 mm

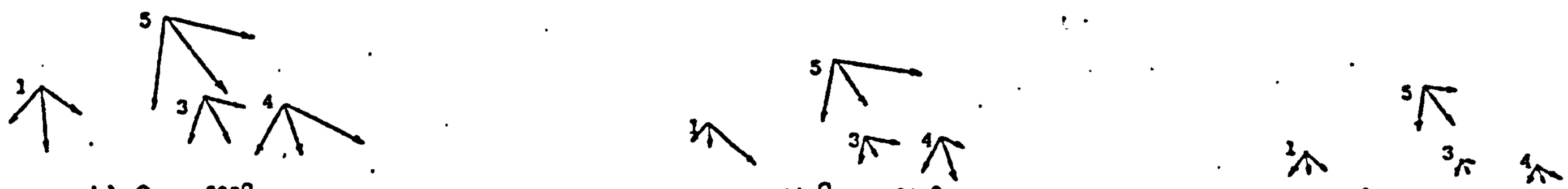

h) θ = 300° i) θ = 340° j) θ = 360°

LEVEL: Z = 0.0 mm

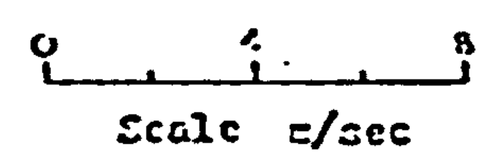

Fig. (6-10)

Figs. (6-11) - (6-14)

Variation of Gas Mean Velocity with Engine Speed. Ford V4 Engine. Analysis of Ten Consecutive Cycles with Probes at the Spark Plug Location.

Z = 3.8 mm: A Hot Wire Positioned at 3.8 mm from the Cylinder Head Surface

Z = 0.0 mm: A Hot Wire Positioned at the Level of the Cylinder Head Surface (Spark Plug Gap Location for this type of engine)

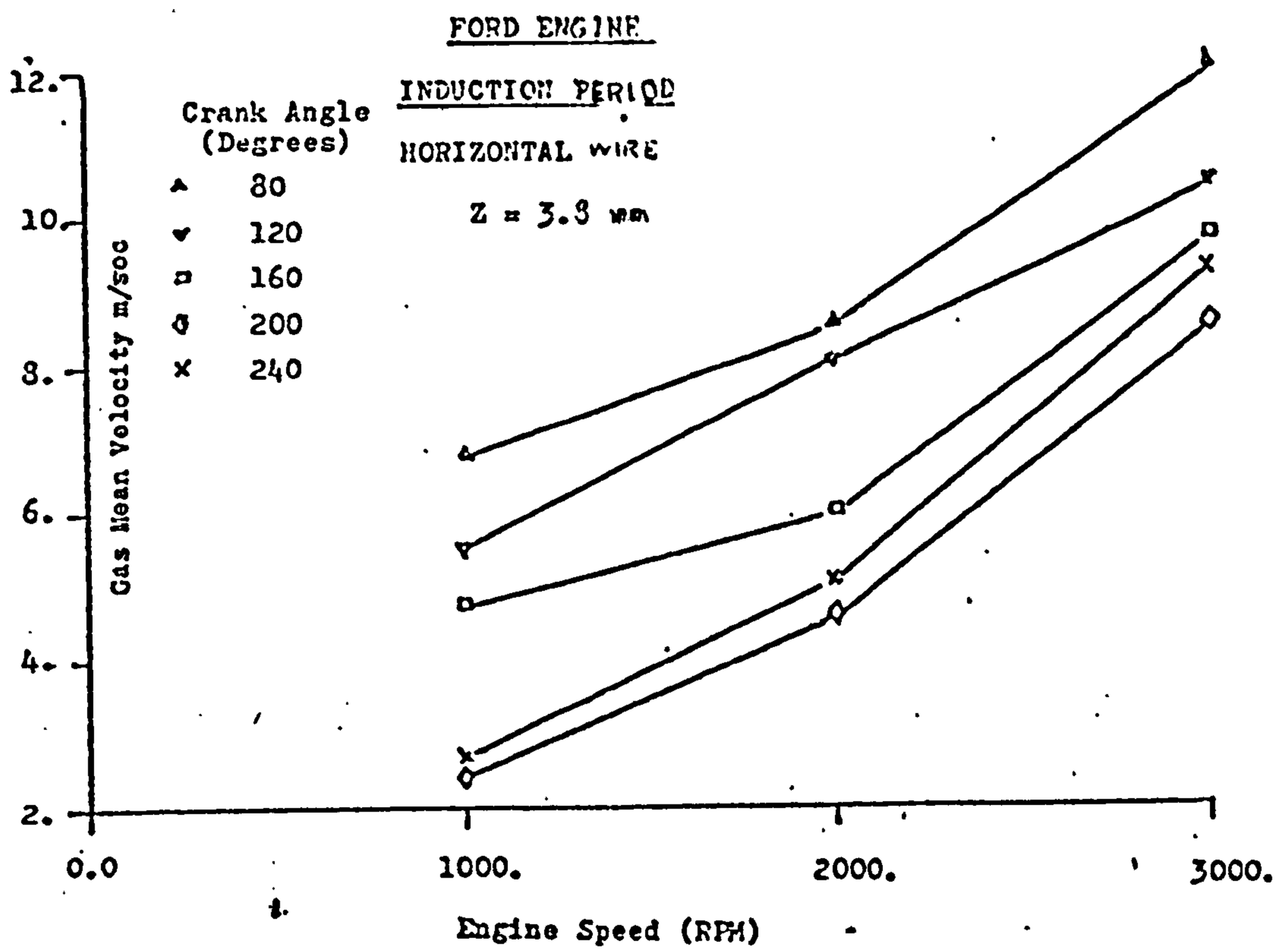

Fig (6-11a)

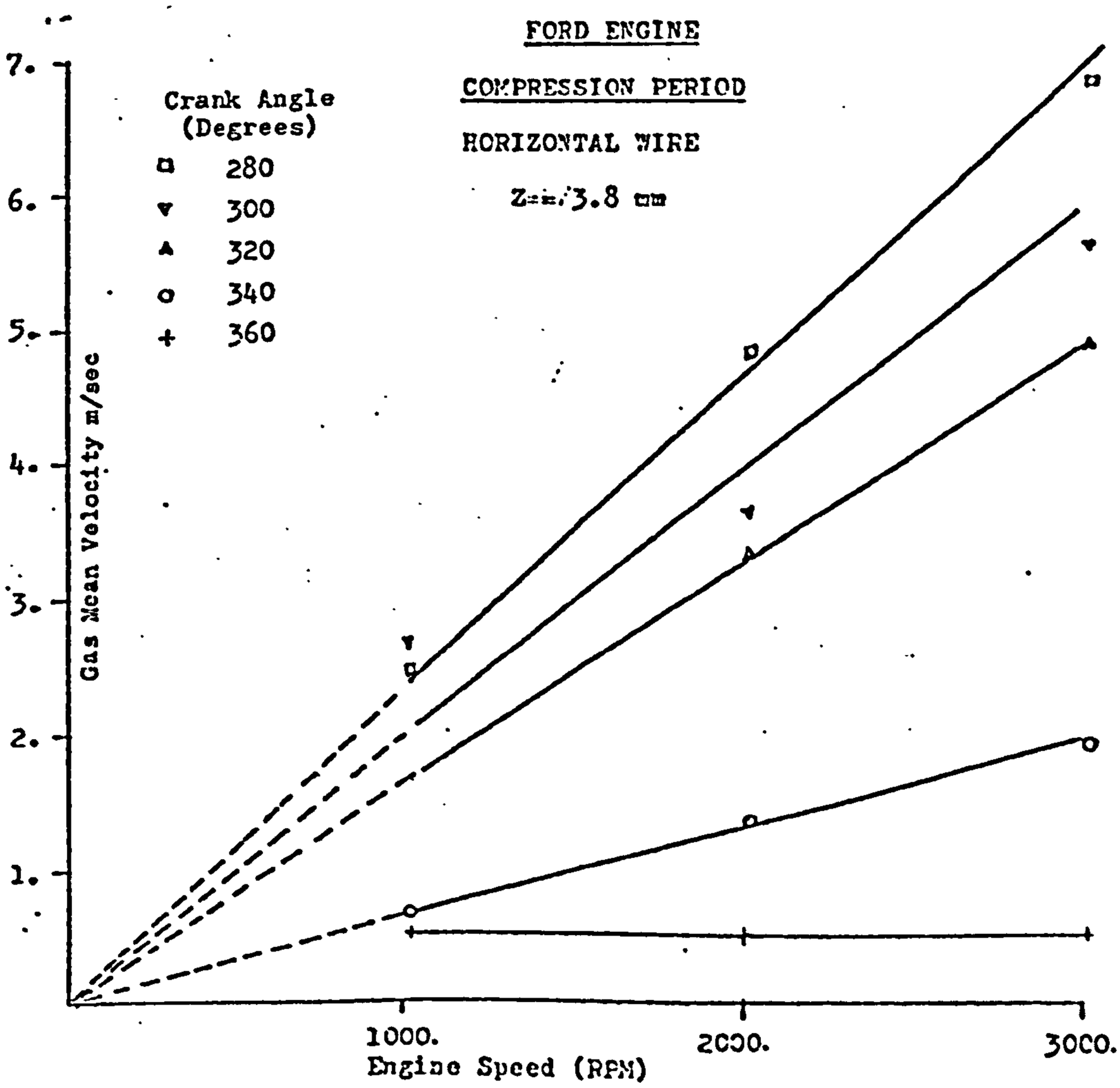

Fig. (6-11b)

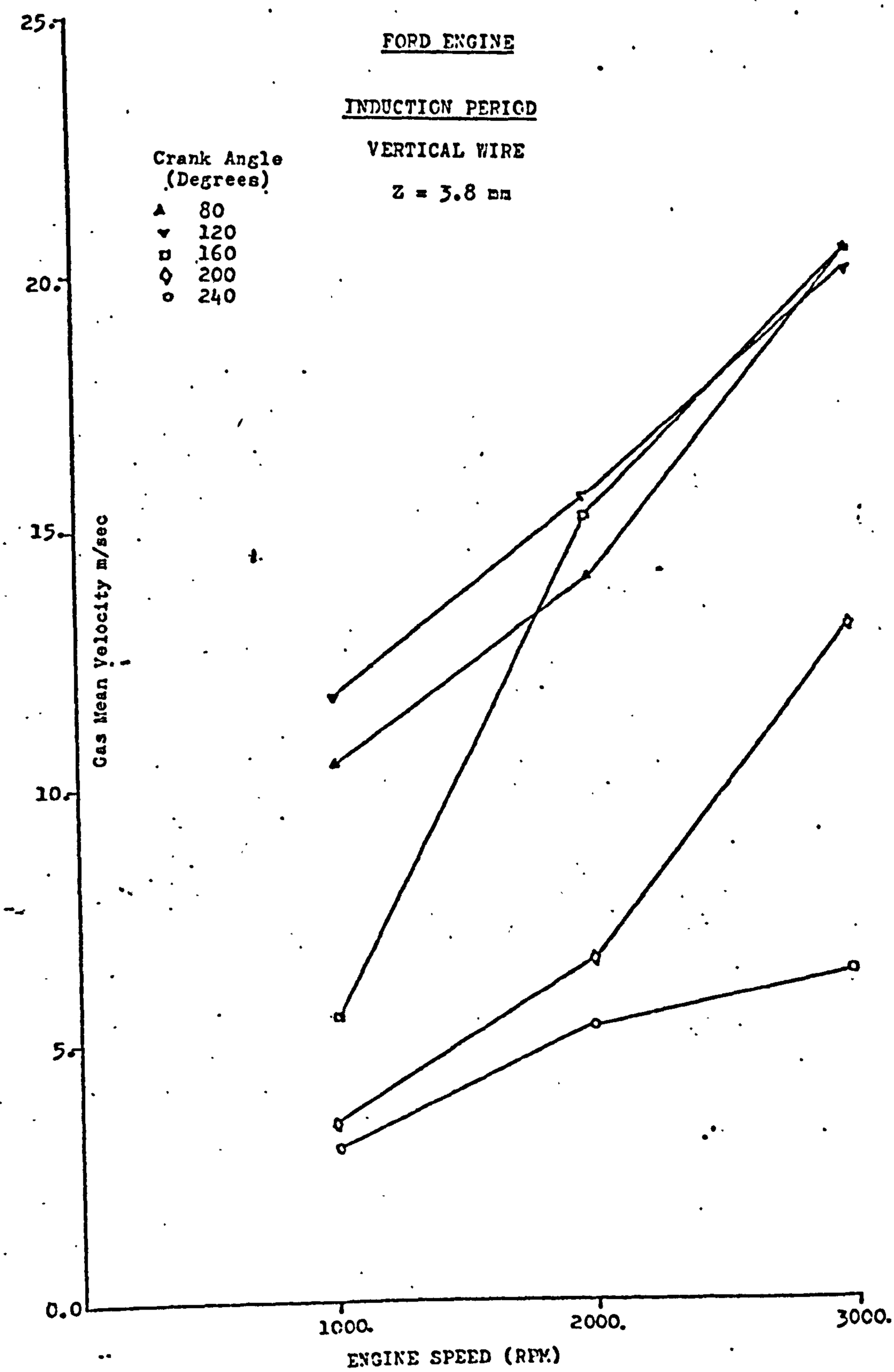
FORD ENGINE
INDUCTION PERIOD
VERTICAL WIRE
Z = 3.8 mm
Crank Angle (Degrees)
80
120
160
200
240
Gas Mean Velocity m/sec
25.
20.
15.
10.
5.
0.0
1000.
2000.
3000.
ENGINE SPEED (RPM)

Fig. (6-12a)

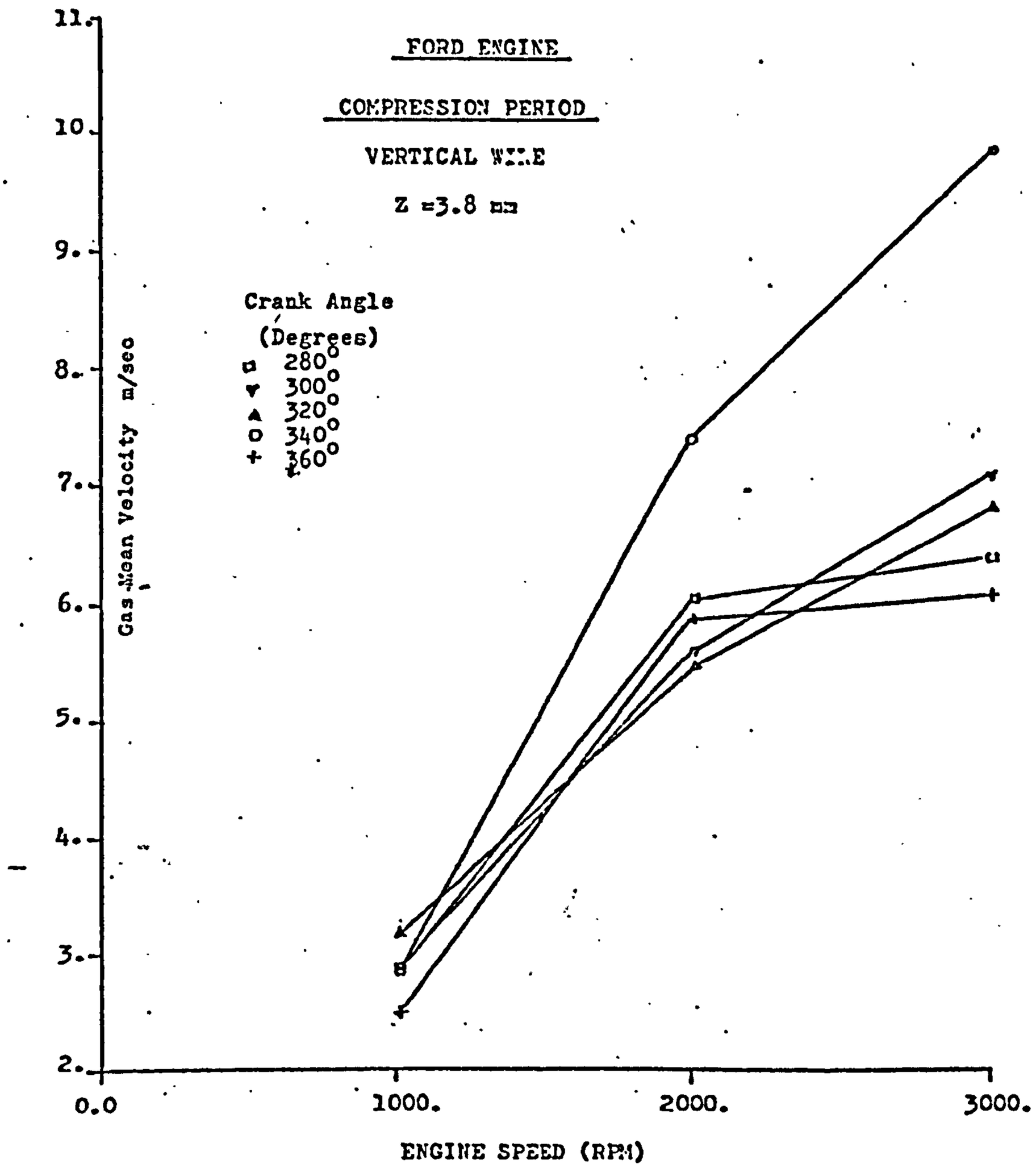
FORD ENGINE
COMPRESSION PERIOD
VERTICAL WIRE
Z =3.8 mm
Crank Angle
(Degrees)
280°
300°
320°
340°
360°
Gas Mean Velocity m/sec
11.
10.
9.
8.
7.
6.
5.
4.
3.
2.
0.0
1000.
2000.
3000.
ENGINE SPEED (RPM)

Fig. (6-12b)

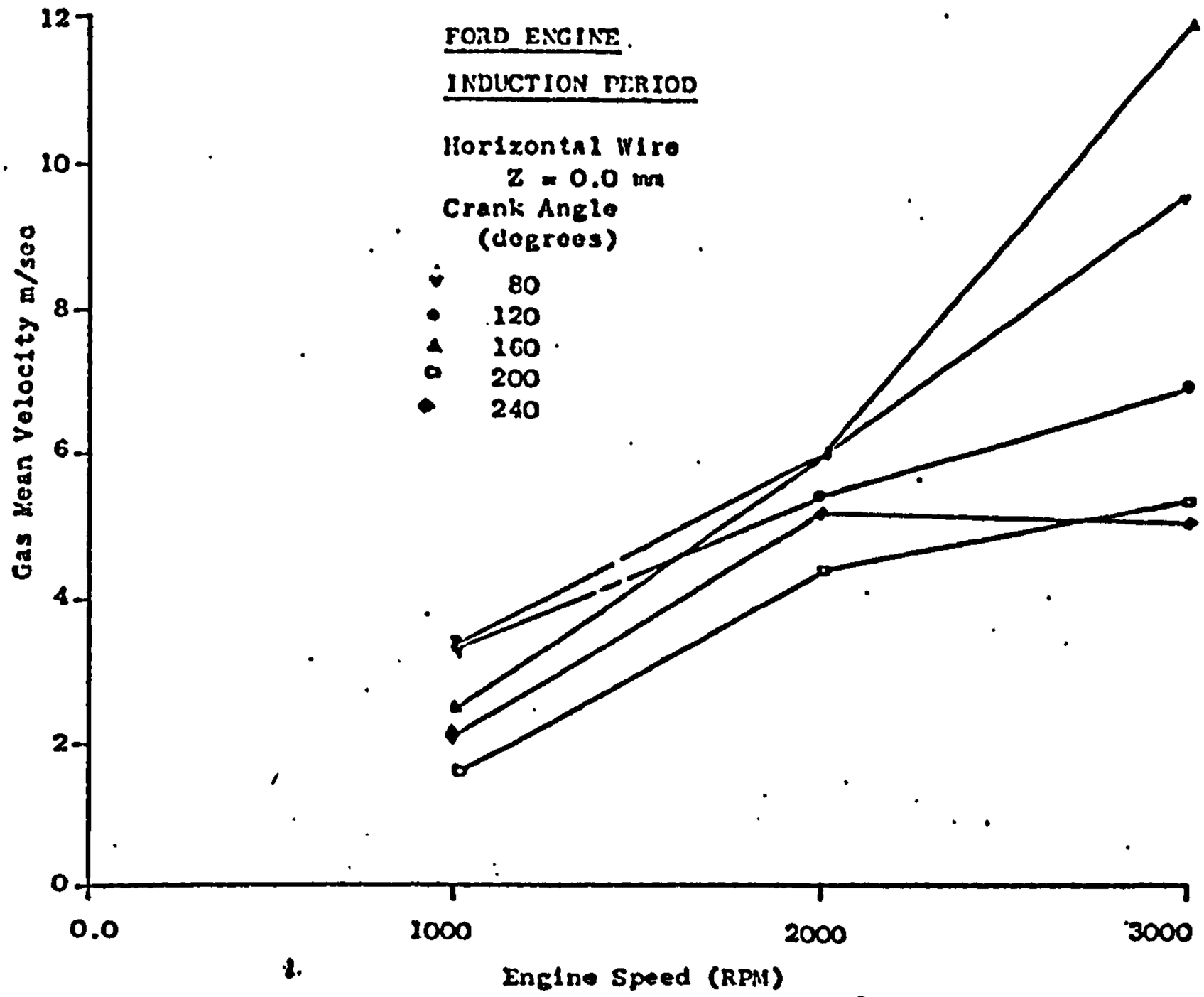

Fig. (6-13a)

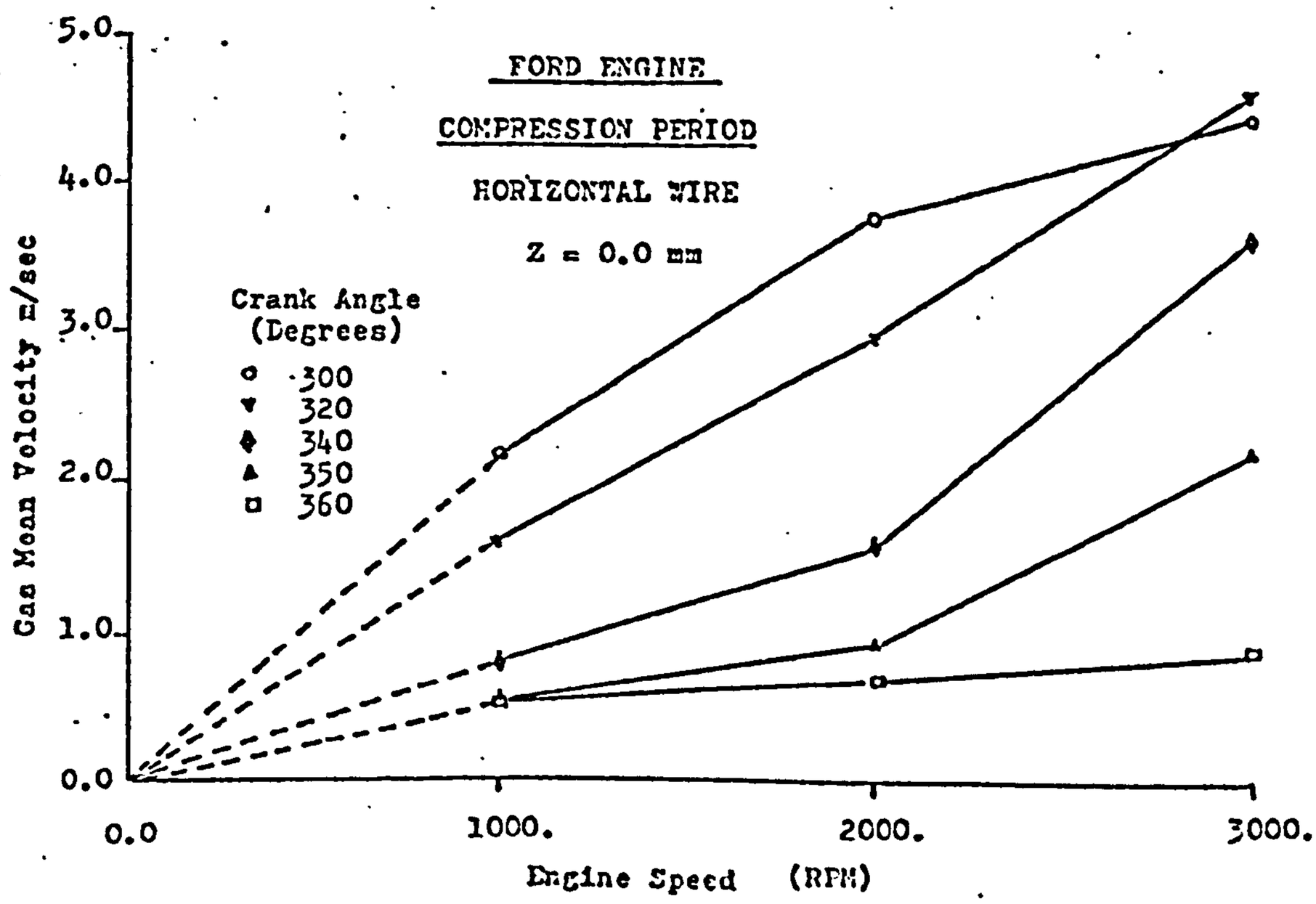

Fig. (6-13b)

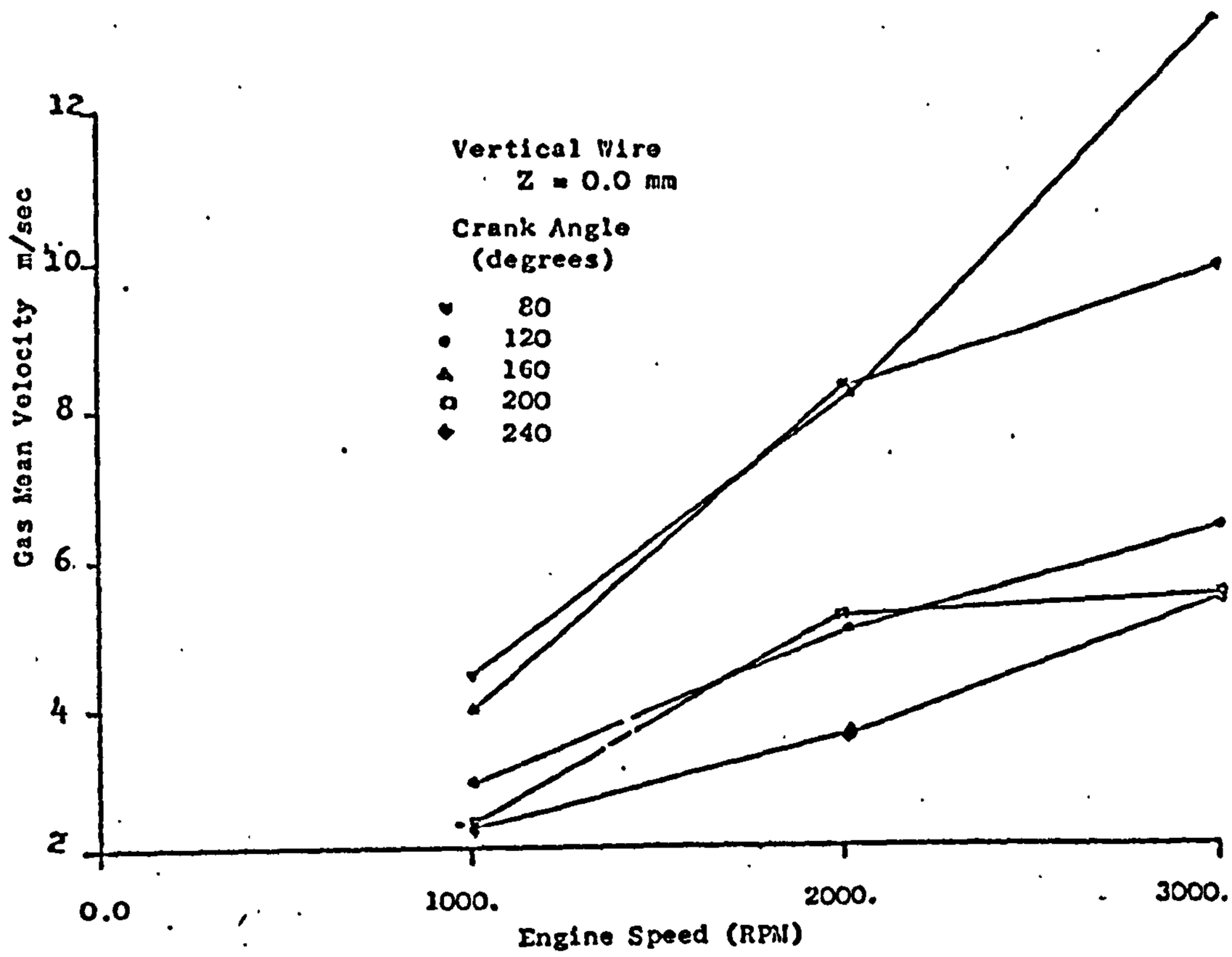

Fig. (6-14a)

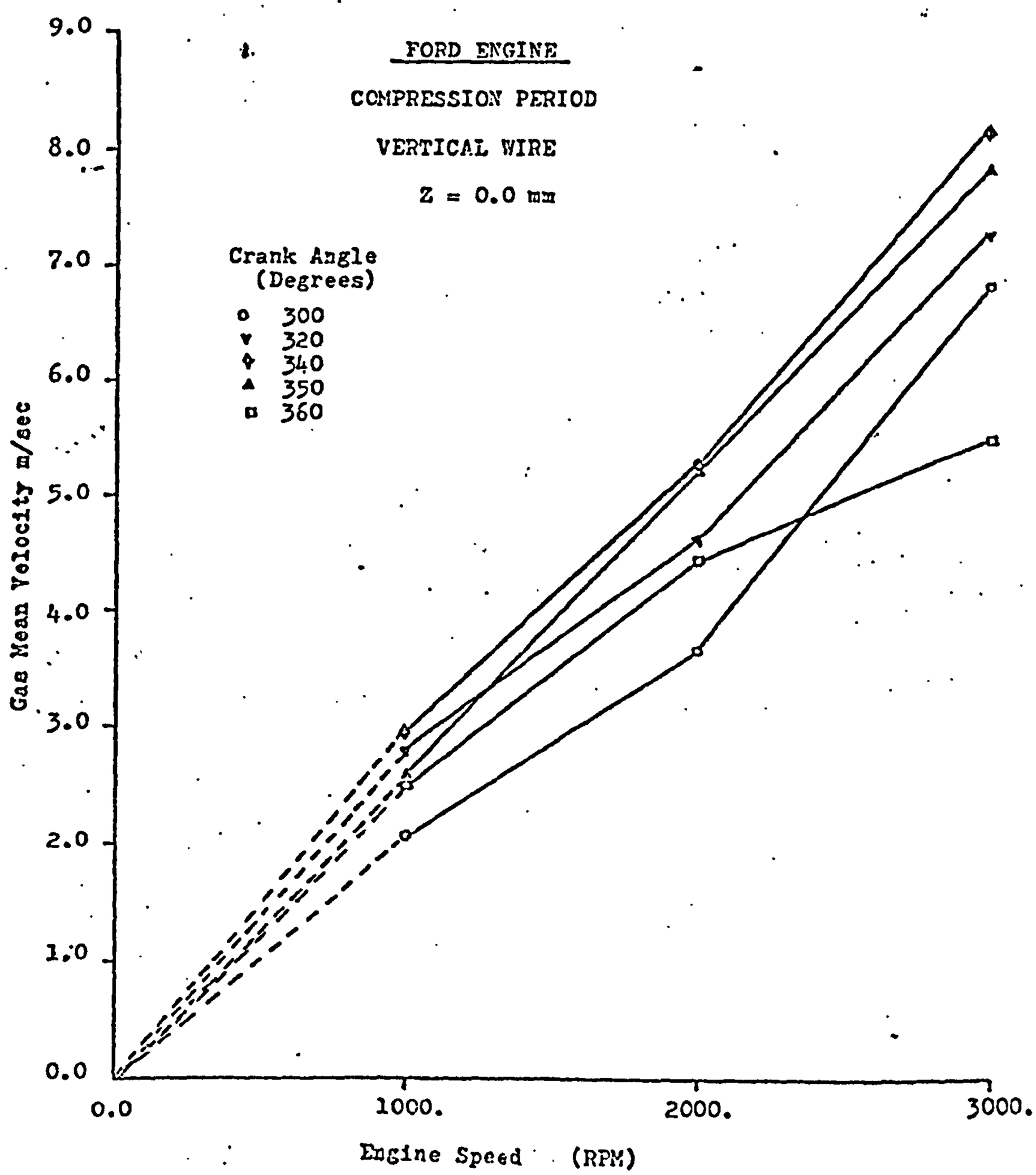

Fig. (6-14b)

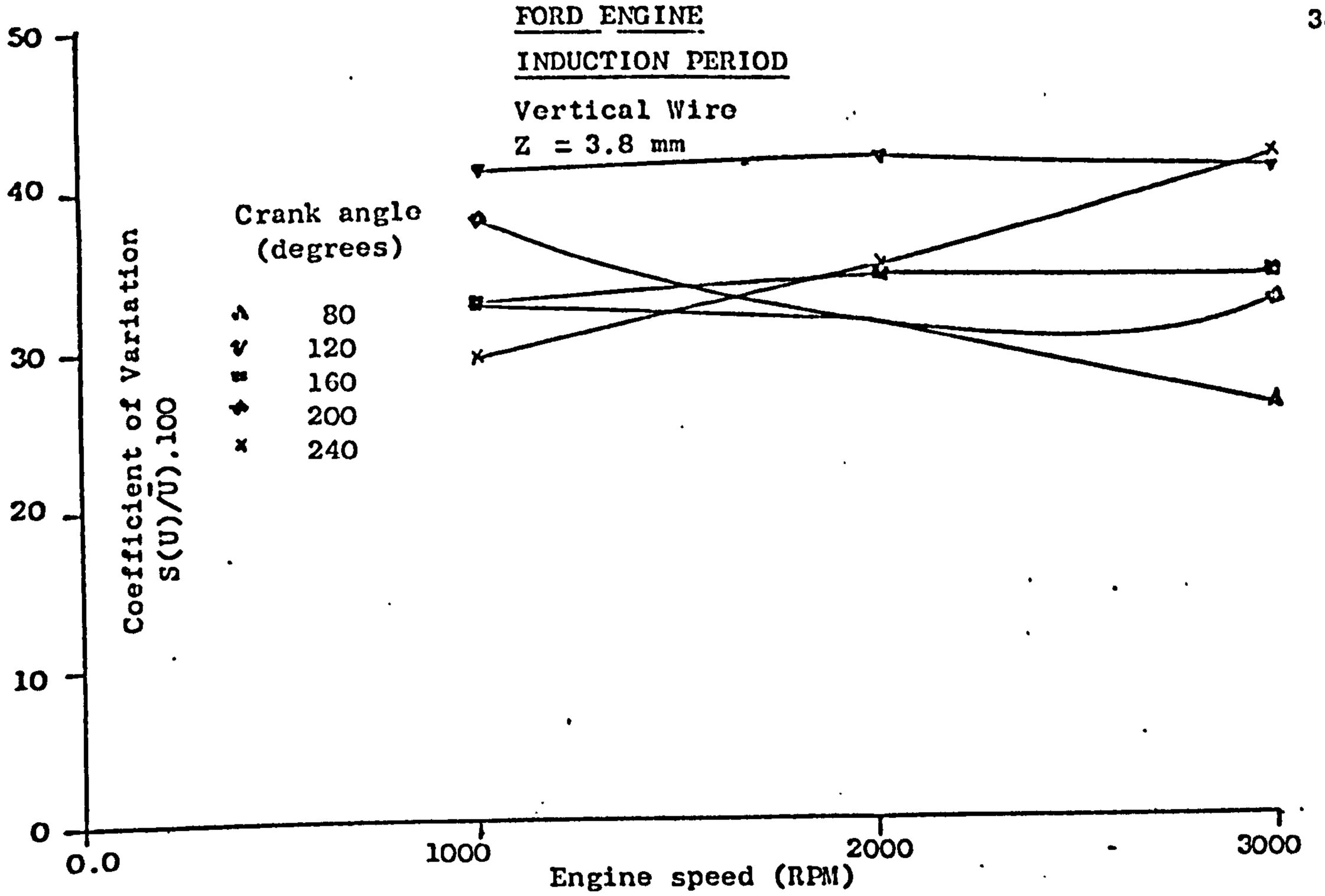

Fig. (6-15a)

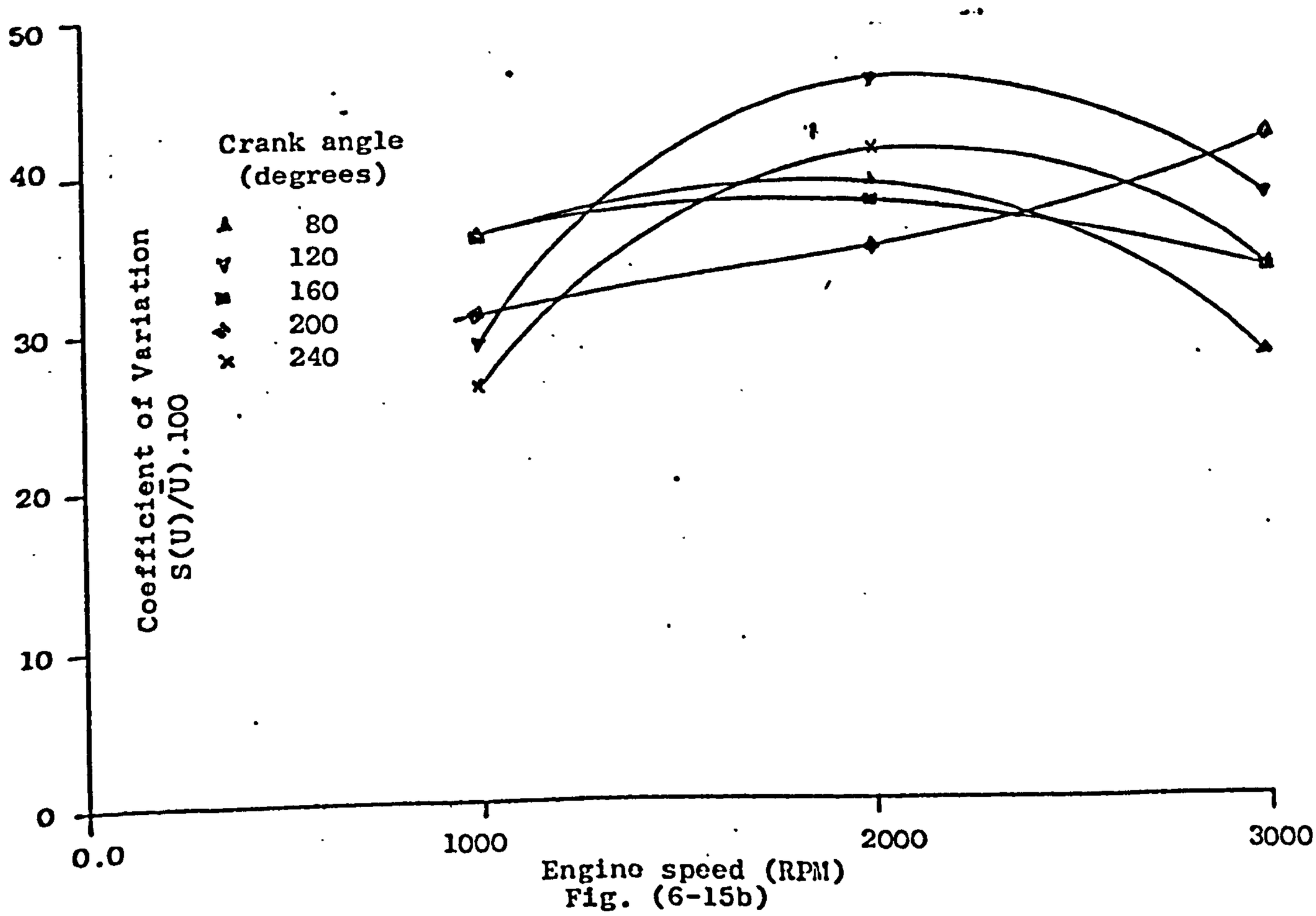

Fig. (6-15b)

Fig. (6-15) Variation of the Coefficient of Variation in Gas Mean Velocity with Engine Speed During the Induction Period.
Ford Engine, Probe at the Spark Plug Location. Hot Wires at 3.8 mm from Cylinder Head Surface.

FORD ENGINE

COMPRESSION PERIOD

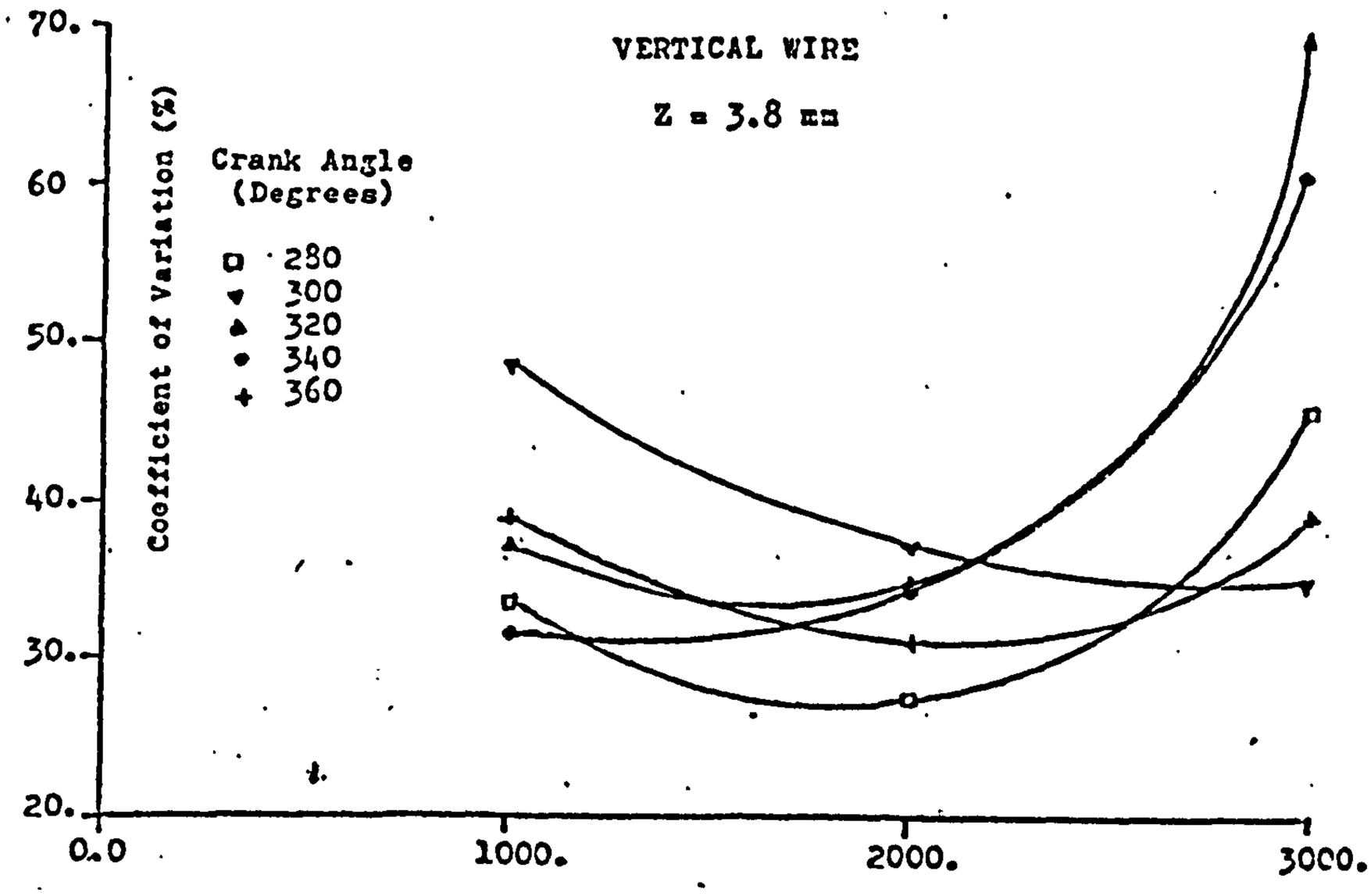

Fig (6-16a)

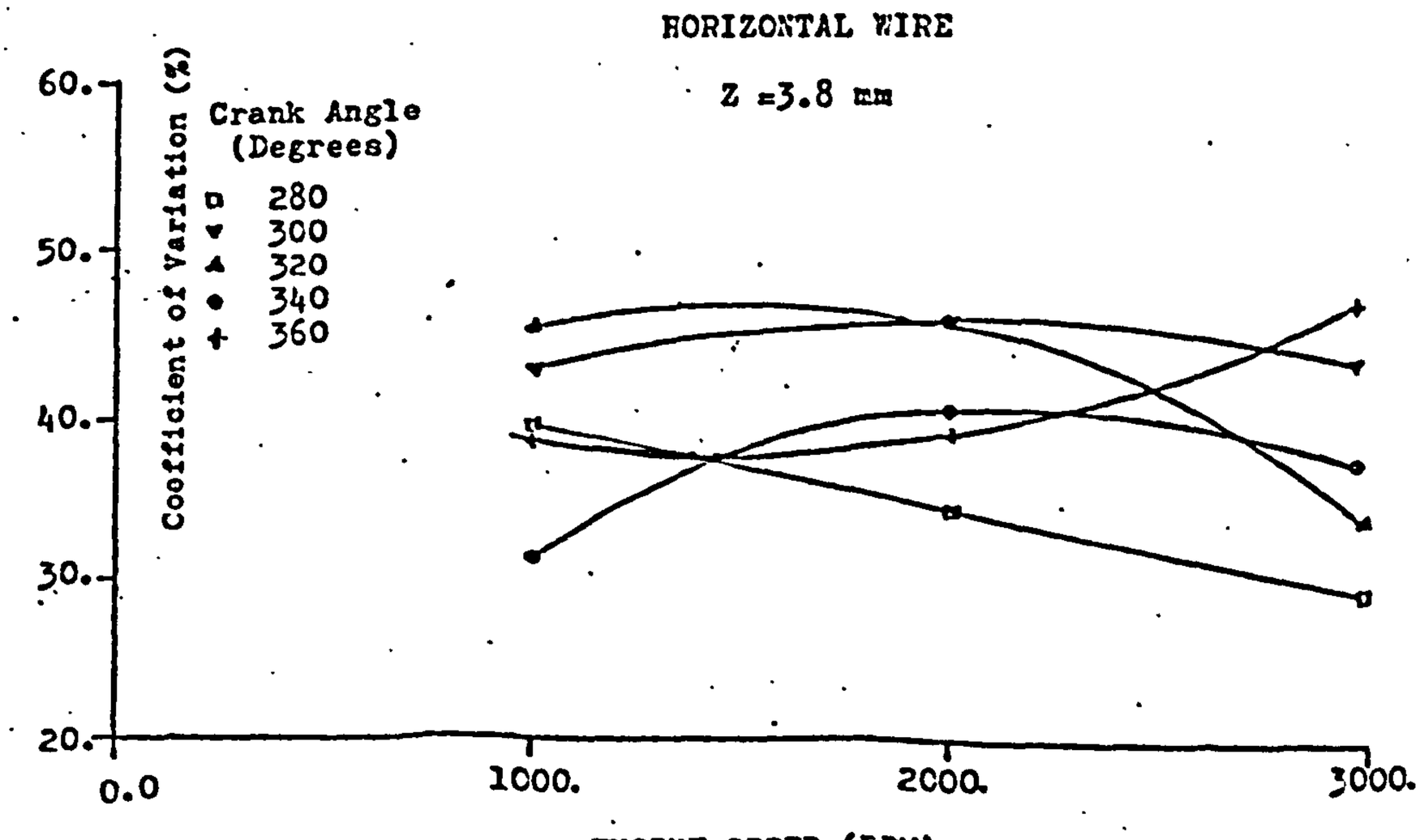

Fig (6-16b)

Fig. (6-16) Variation of the Coefficient of Variation $(S(U)/\bar{U}).100$ with Engine Speed. (Data corresponds to test conditions of Figures (6-11b) and (6-12b).

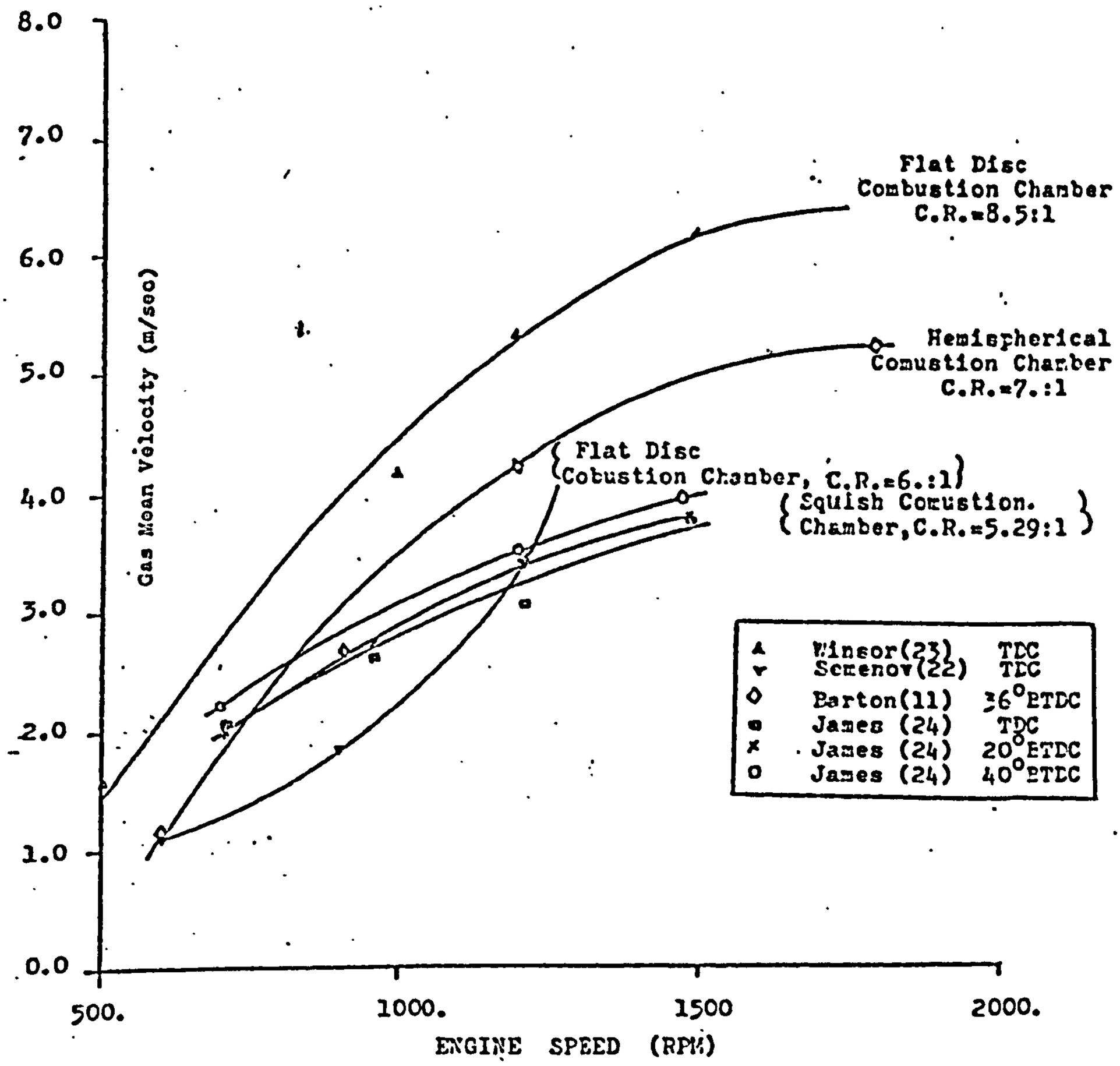

Fig. (6-17) Variation of Gas Mean Velocity with Engine Speed for Different Types of Combustion Chambers (Data from Published Investigations).

Figs. (6-18) - (6-24)

Investigation of Gas Velocity Characteristics
Inside the Intake Manifolds of S.I. Engines.

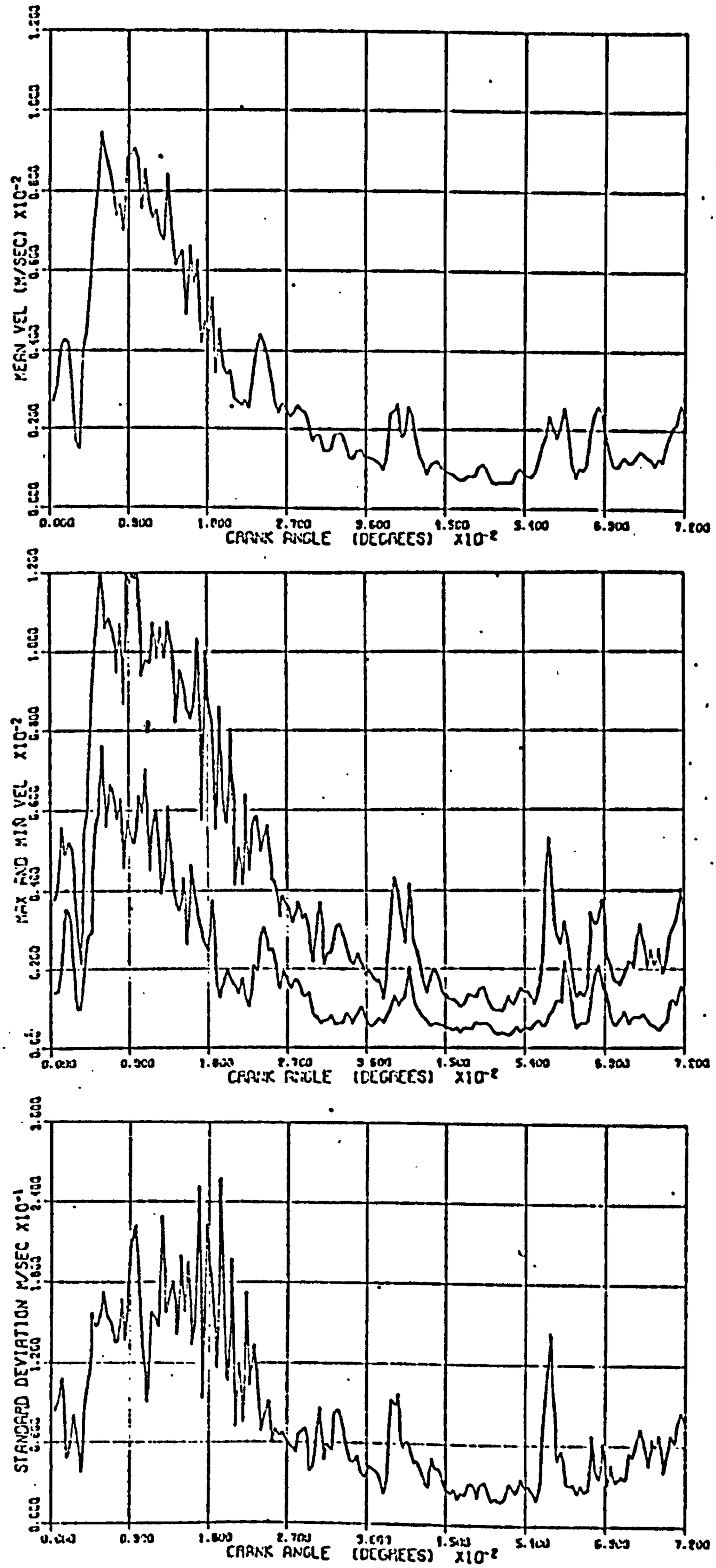

Fig. (6-18) A Statistical Analysis of Gas Mean Velocities Inside an Intake Manifold of a Ford V4 Engine at 3500 RPM and 168 mm Intake Vacuum (see Fig. (5-5) for the dimensions of cross section).

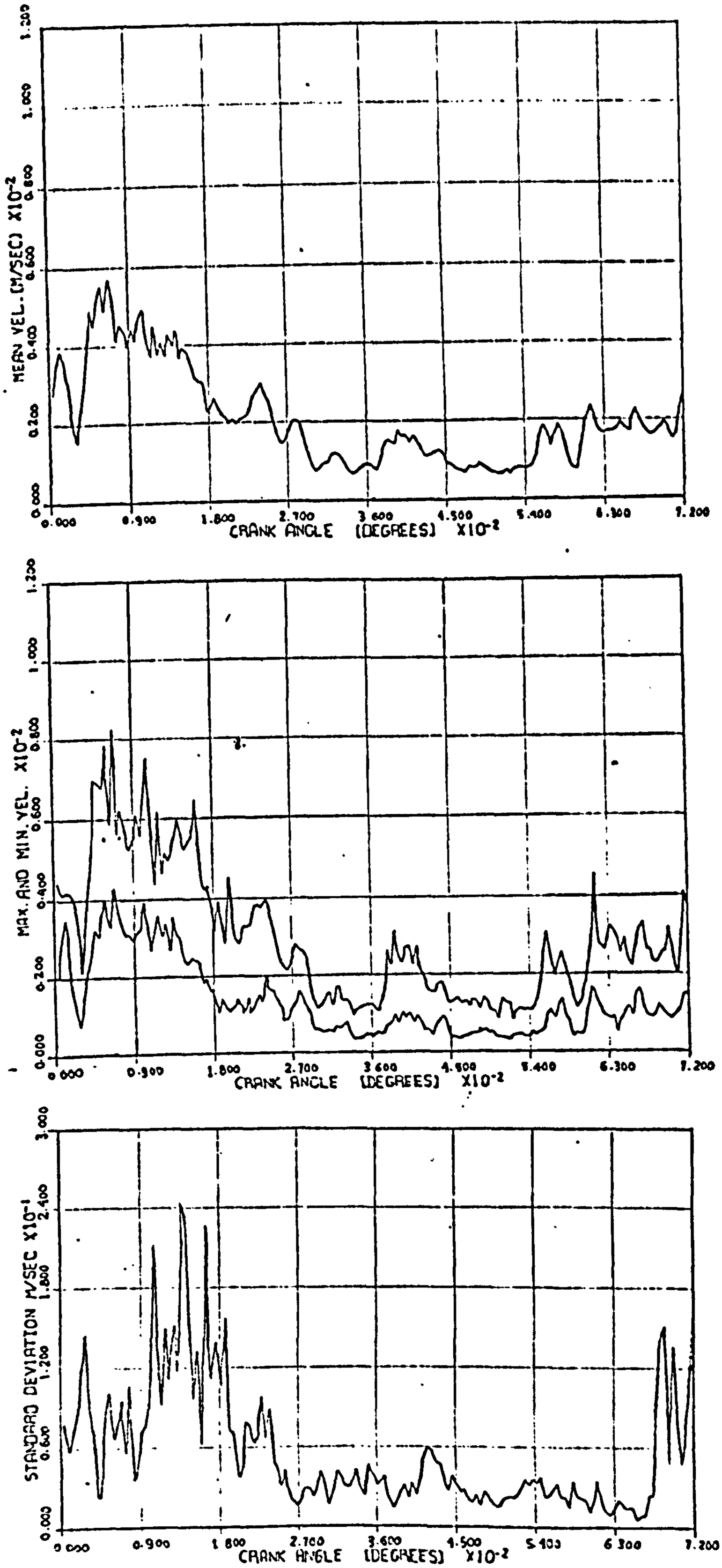

Fig. (6-19) A Statistical Analysis of Gas Mean Velocities Inside an Intake Manifold of a Ford V4 Engine at 3500 RPM and 310 mm Intake Vacuum.

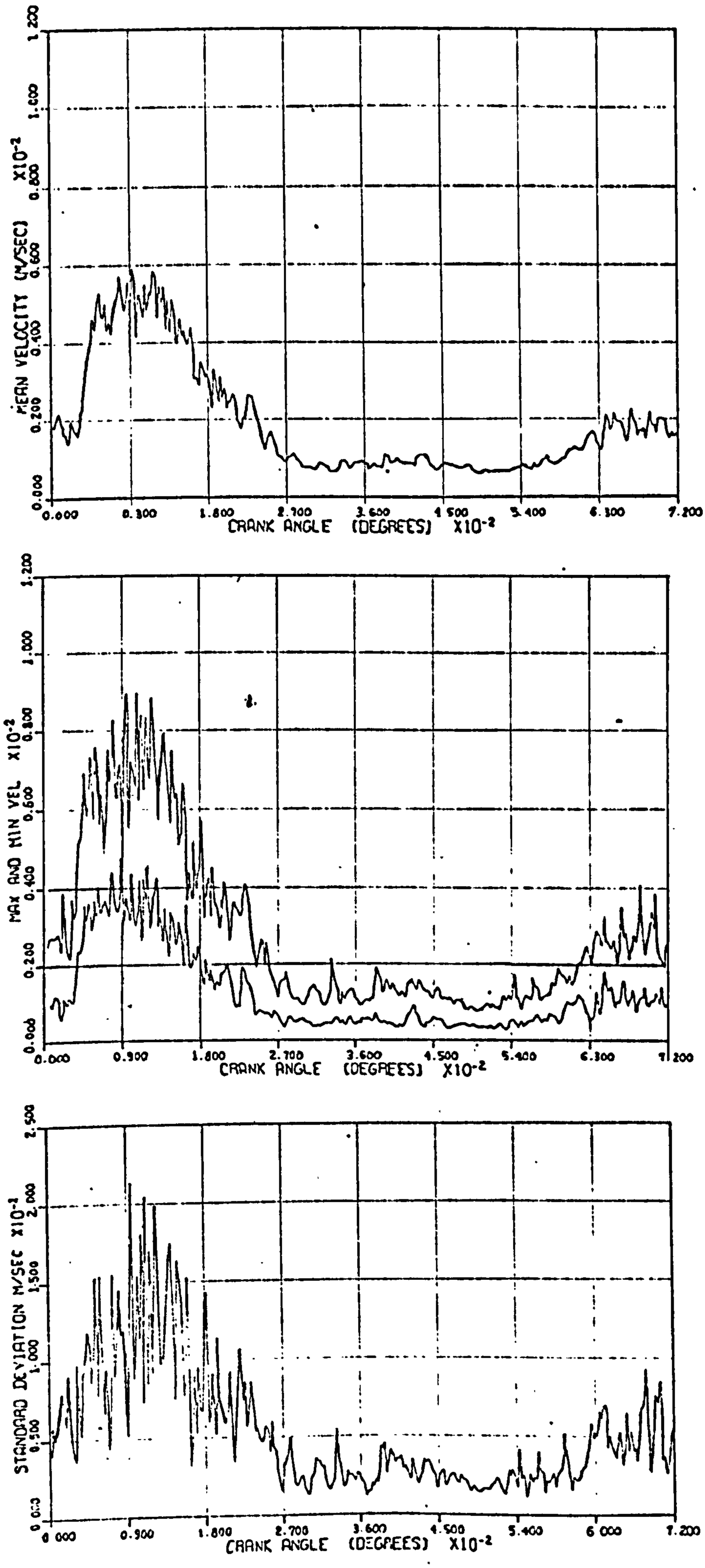

Fig. (6-20) A Statistical Analysis of Gas Mean Velocities Inside an Intake Manifold of a Ford V4 Engine at 2000 RPM and 183 mm Intake Vacuum.

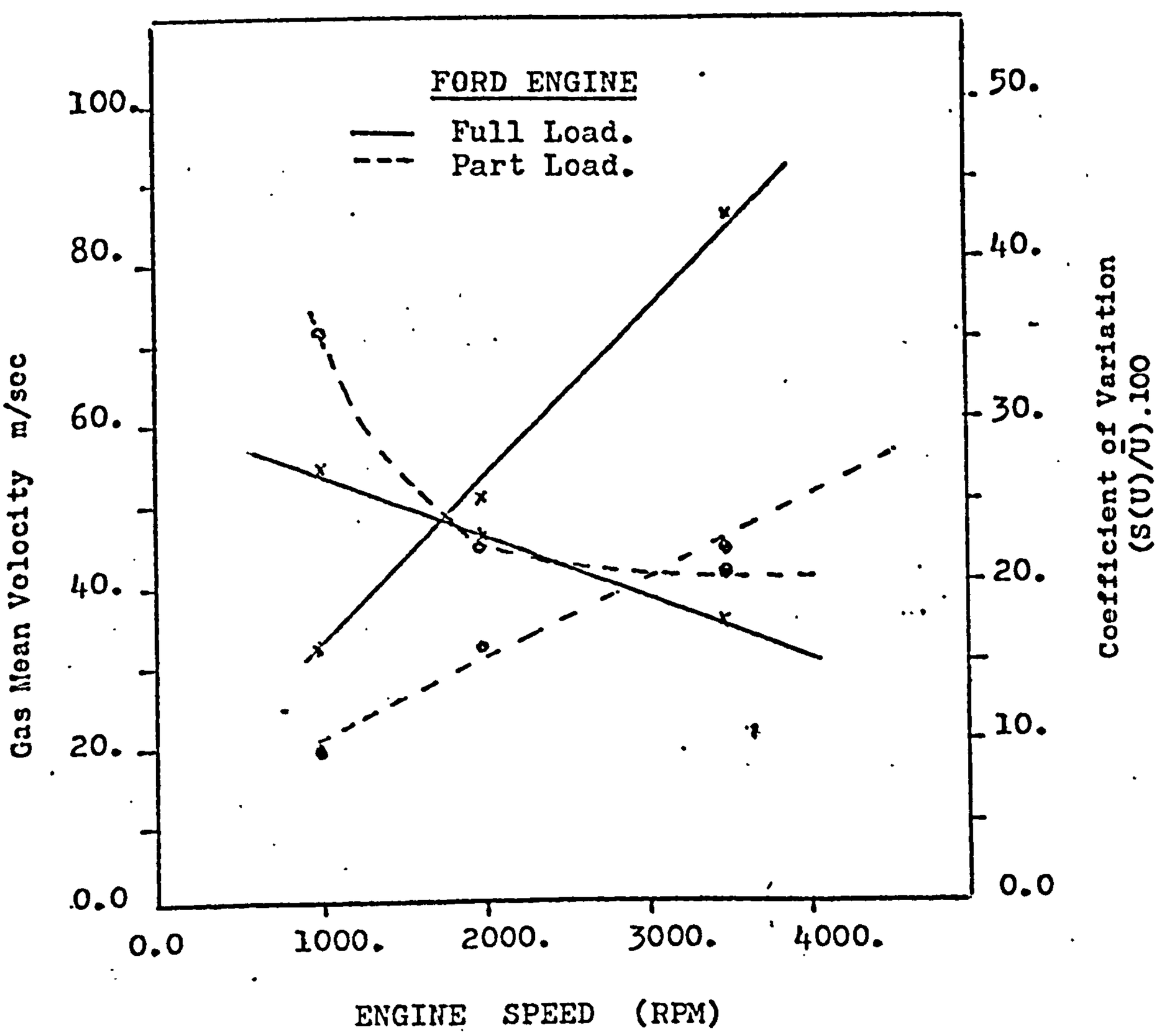

Fig. (6-21) A Summary of the Statistical Analyses of Maximum Induction Velocities Inside an Intake Manifold of a Ford V4 Engine at Different Engine Speeds and Loading Conditions.

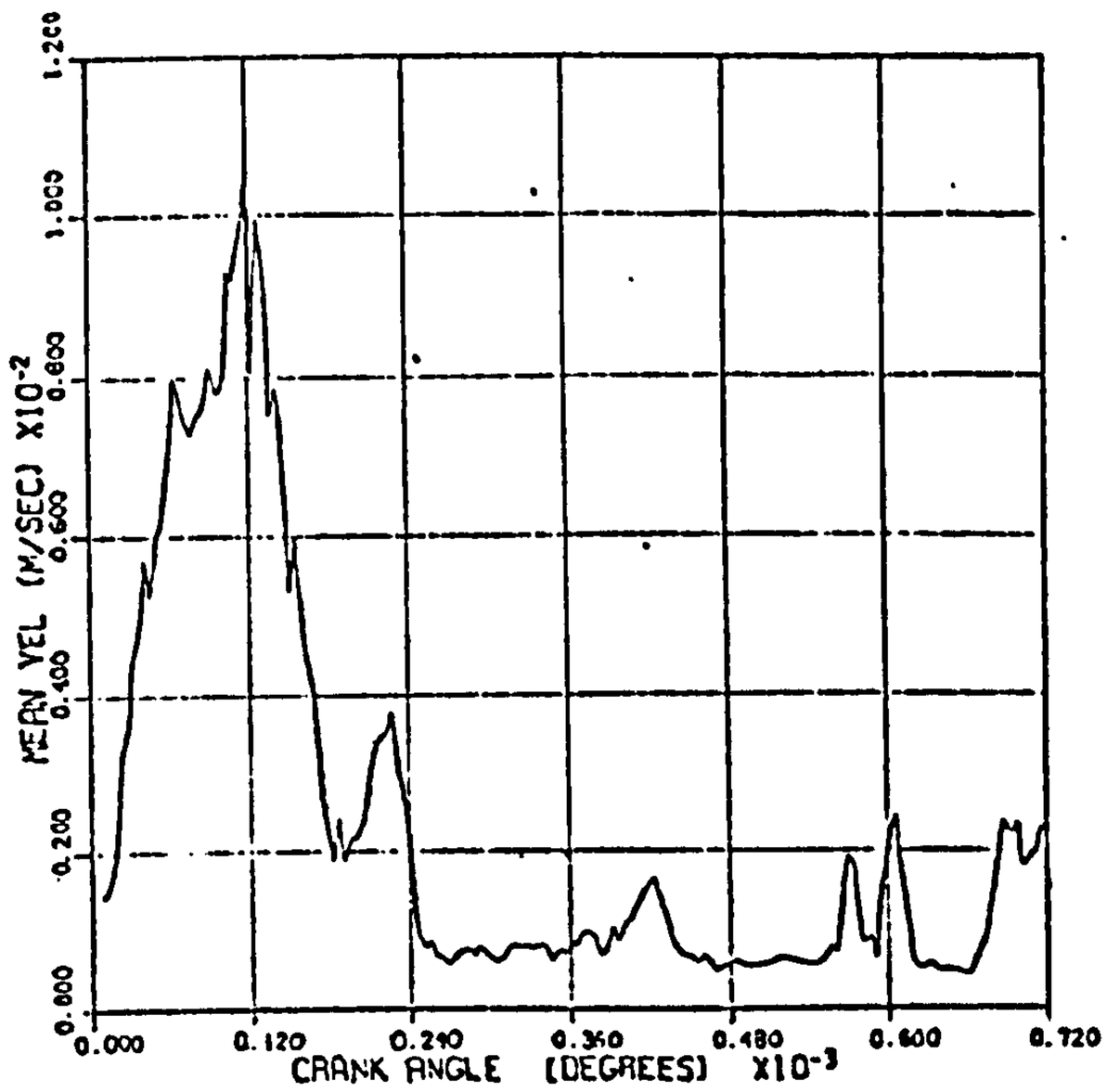

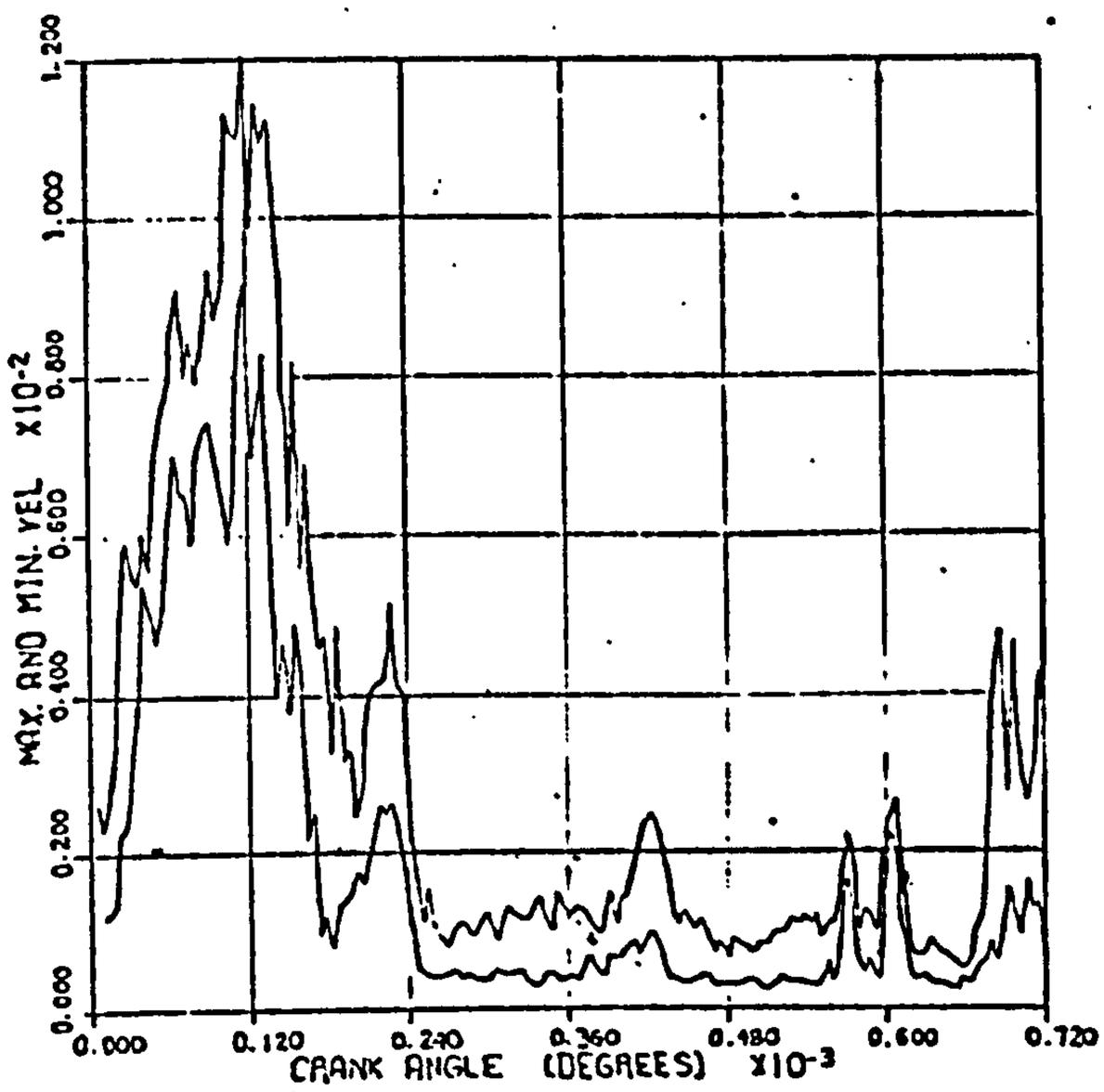

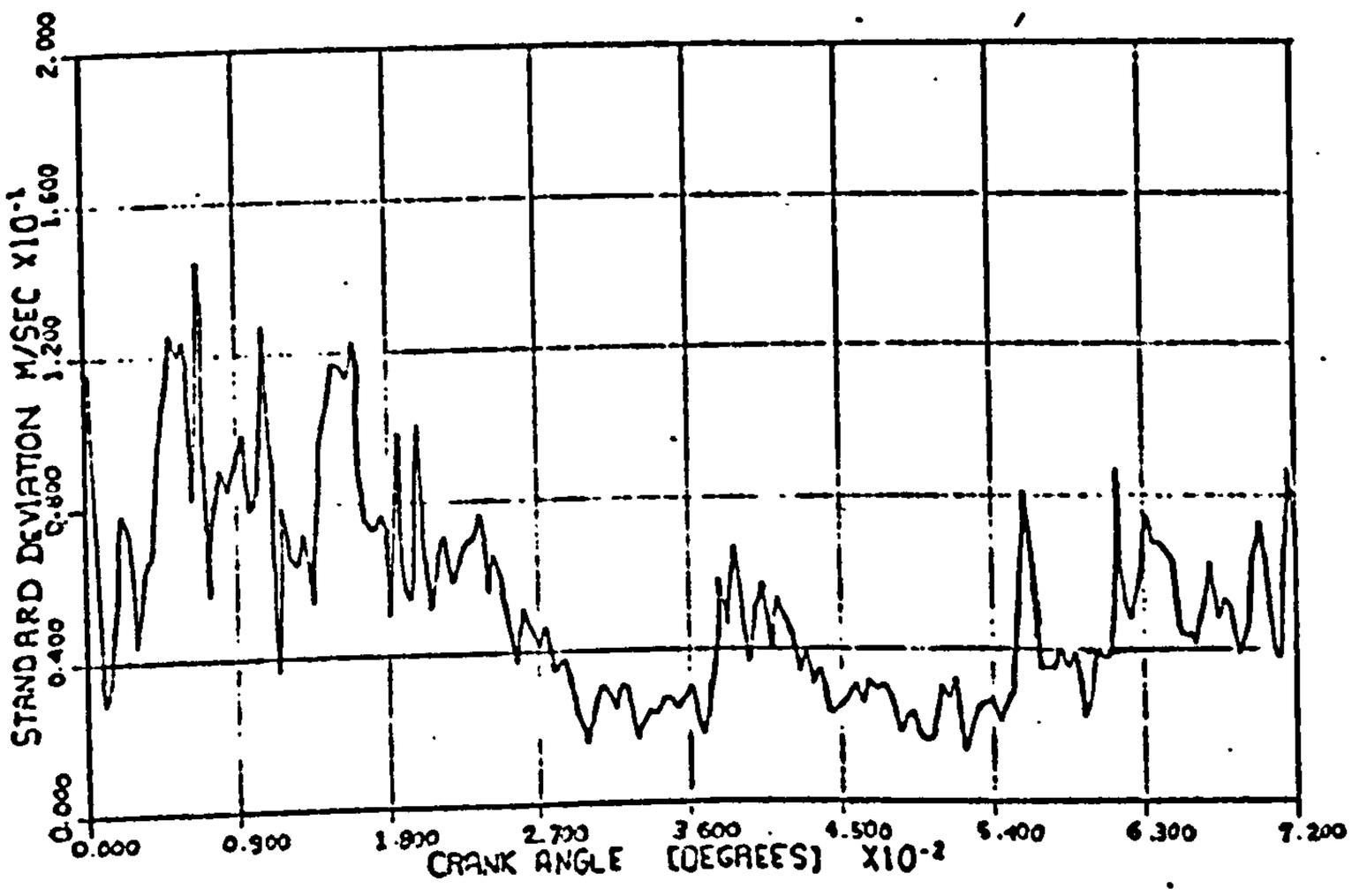

Fig. (6-22) A Statistical Analysis of Gas Mean Velocities Inside an Intake Manifold of a Rolls-Royce V8 Engine at 1500 RPM and Fully Opened Throttle. (See Fig. (5-5) for the Dimensions pf Cross Section).

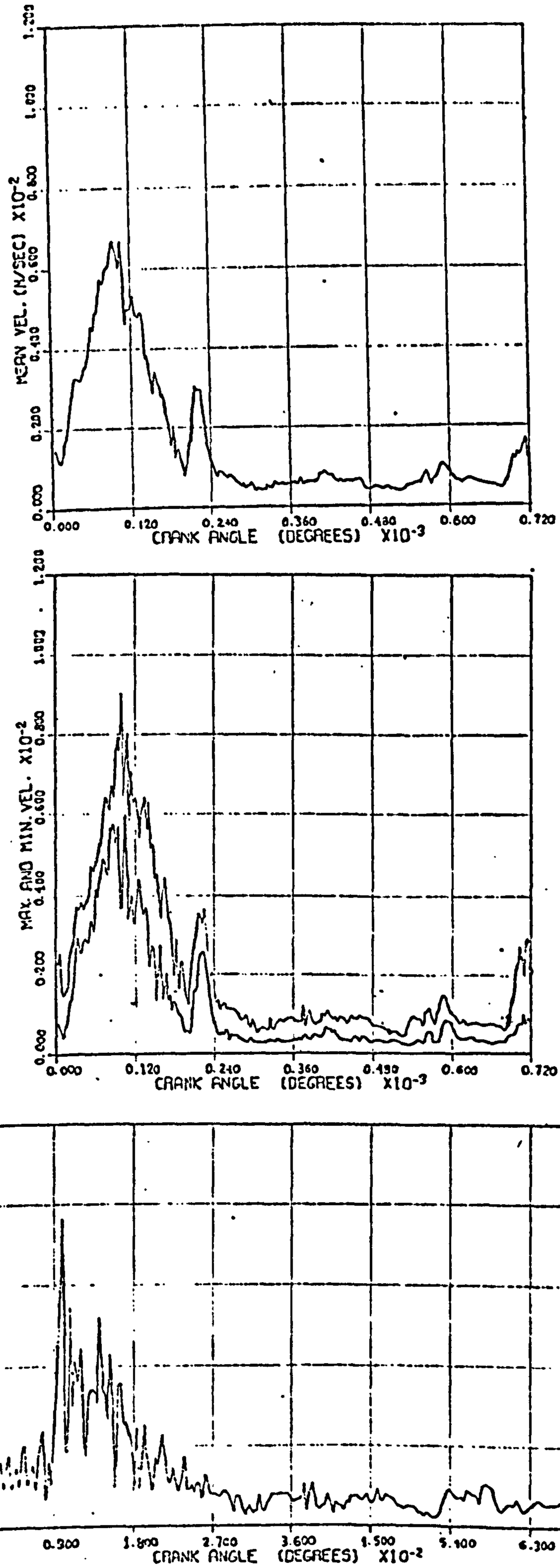

Fig. (6-23) A Statistical Analysis of Gas Mean Velocities Inside an Intake Manifold of a Rolls-Royce Engine at 1000 RPM and Fully Opened Throttle.

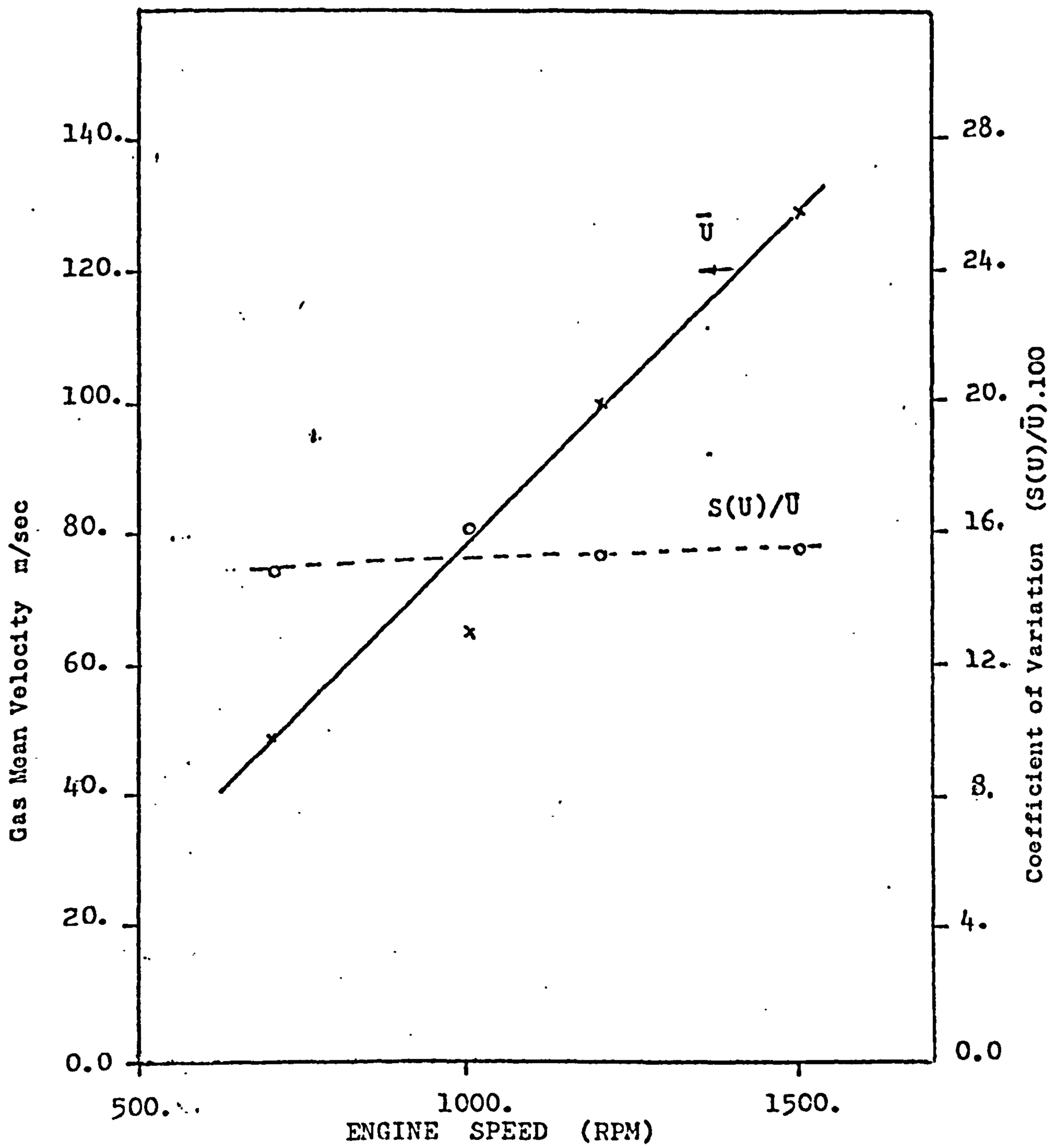

Fig. (6-24) A Summary of the Statistical Analyses of Maximum Induction Velocities inside an Intake Manifold of a Rolls-Royce V8 Engine at Fully Opened Throttle Condition and Different Engine Speeds

Figs. (6-25) - (6-30)

Statistical Analyses of Gas Mean Velocities Inside a Wedge Combustion Chamber of a Rolls-Royce V8 Engine at 1000 RPM and Fully Opened Throttle. Measurements at the Spark Plug Location (Z = 17.78 mm) and Hot Wire Direction of 300 Degrees.

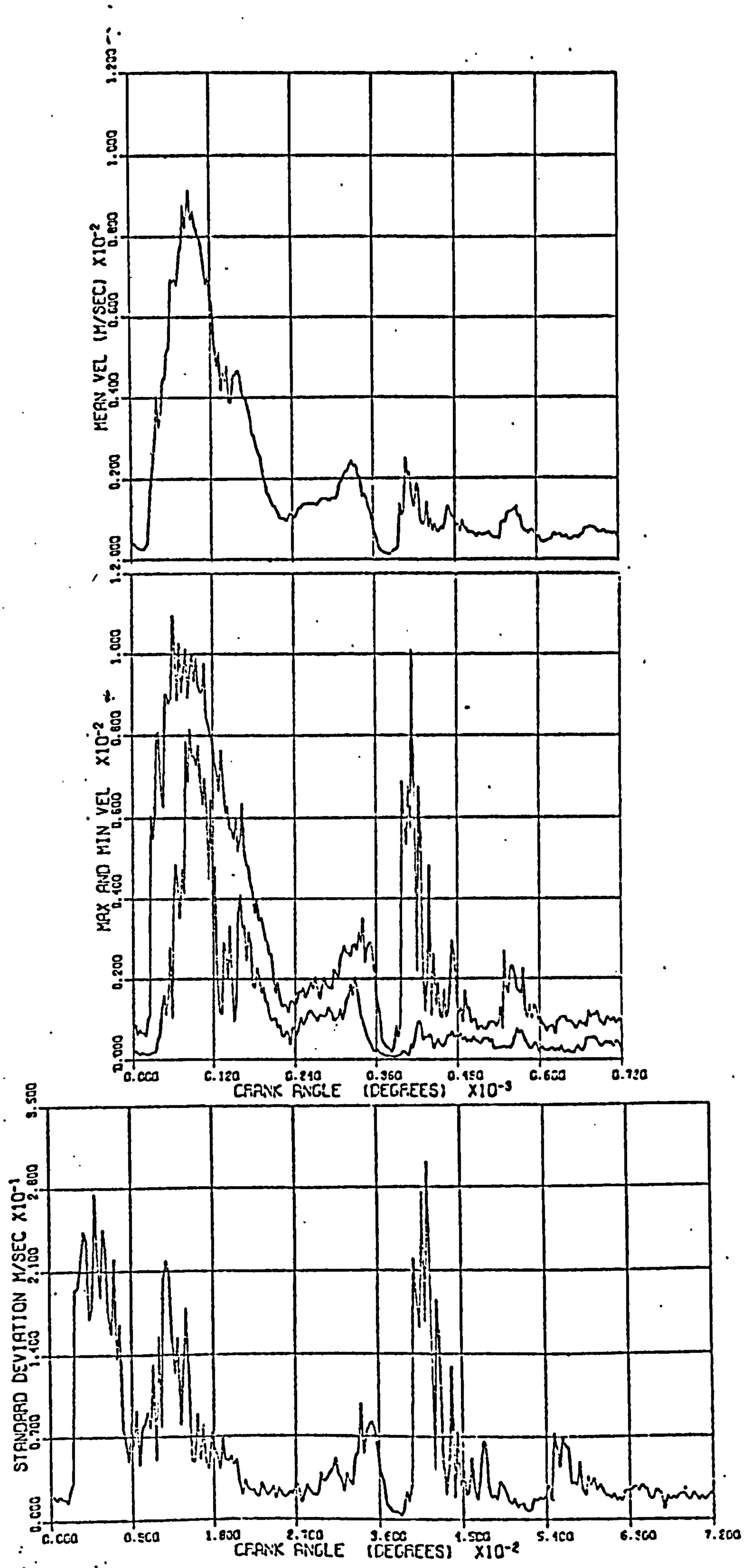

Fig. (6-25) A Statistical Analysis of Gas Mean Velocities for a Test with a Masked Inlet Valve.

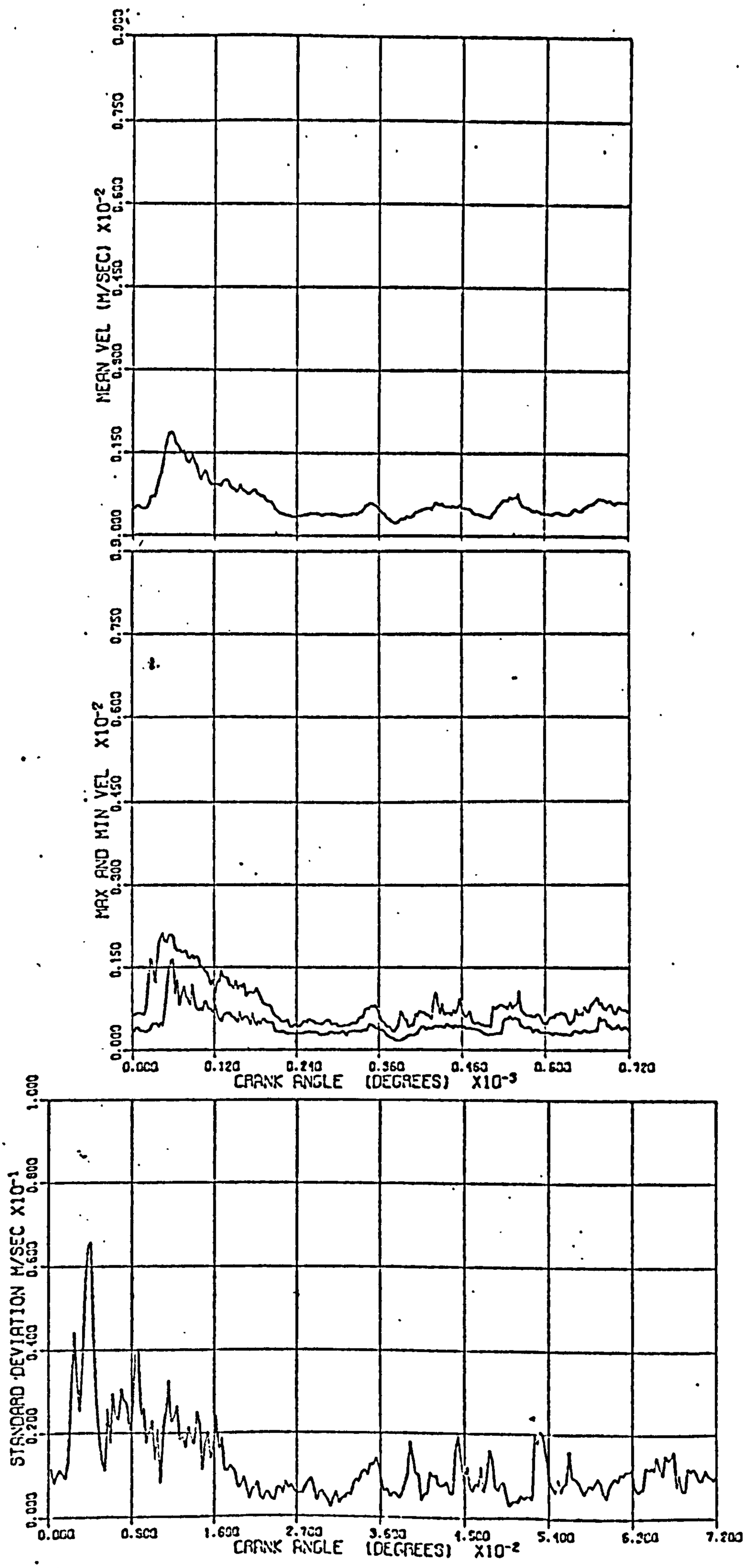

Fig. (6-26) A Statistical Analysis of Gas Mean Velocities for a Test with an Intake Manifold Fitted with Delta Wings.

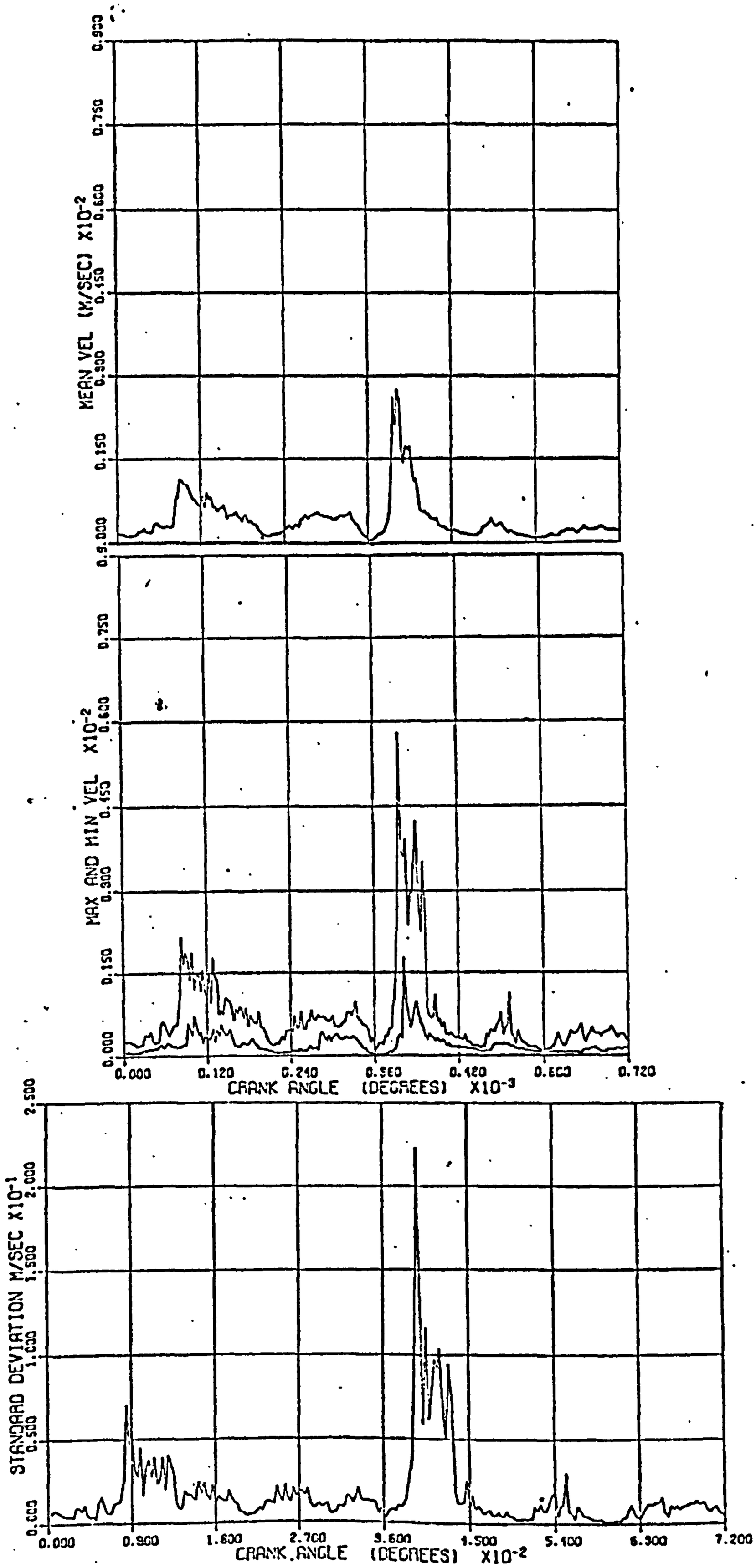

Fig. (6-27) A Statistical Analysis of Gas Mean Velocities for a Test with an Inlet Valve Designed for Reduced Lift.

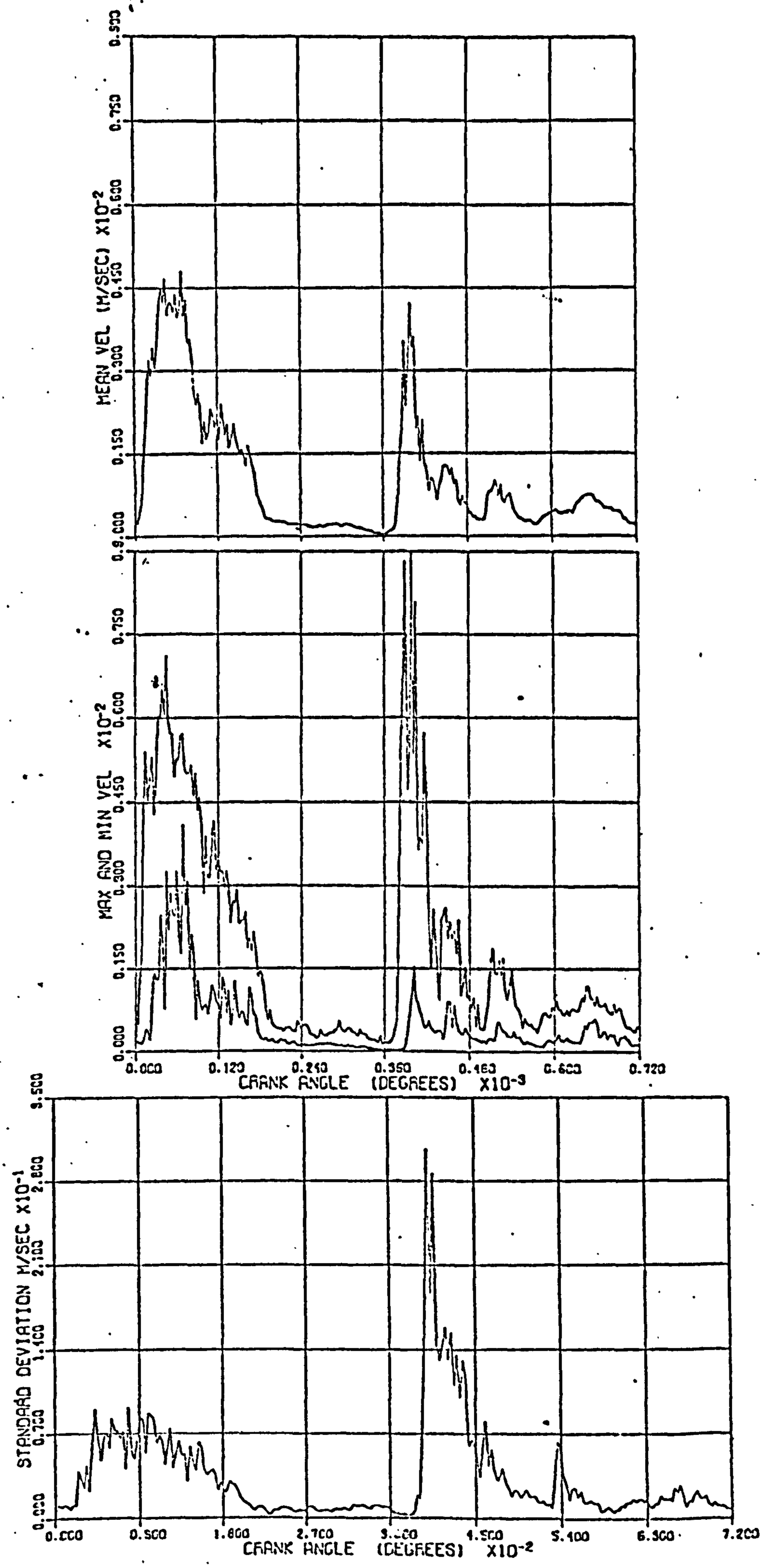

Fig. (6-28) A Statistical Analysis of Gas Mean Velocities for a Test with an Inlet Valve Fitted with Four Vanes.

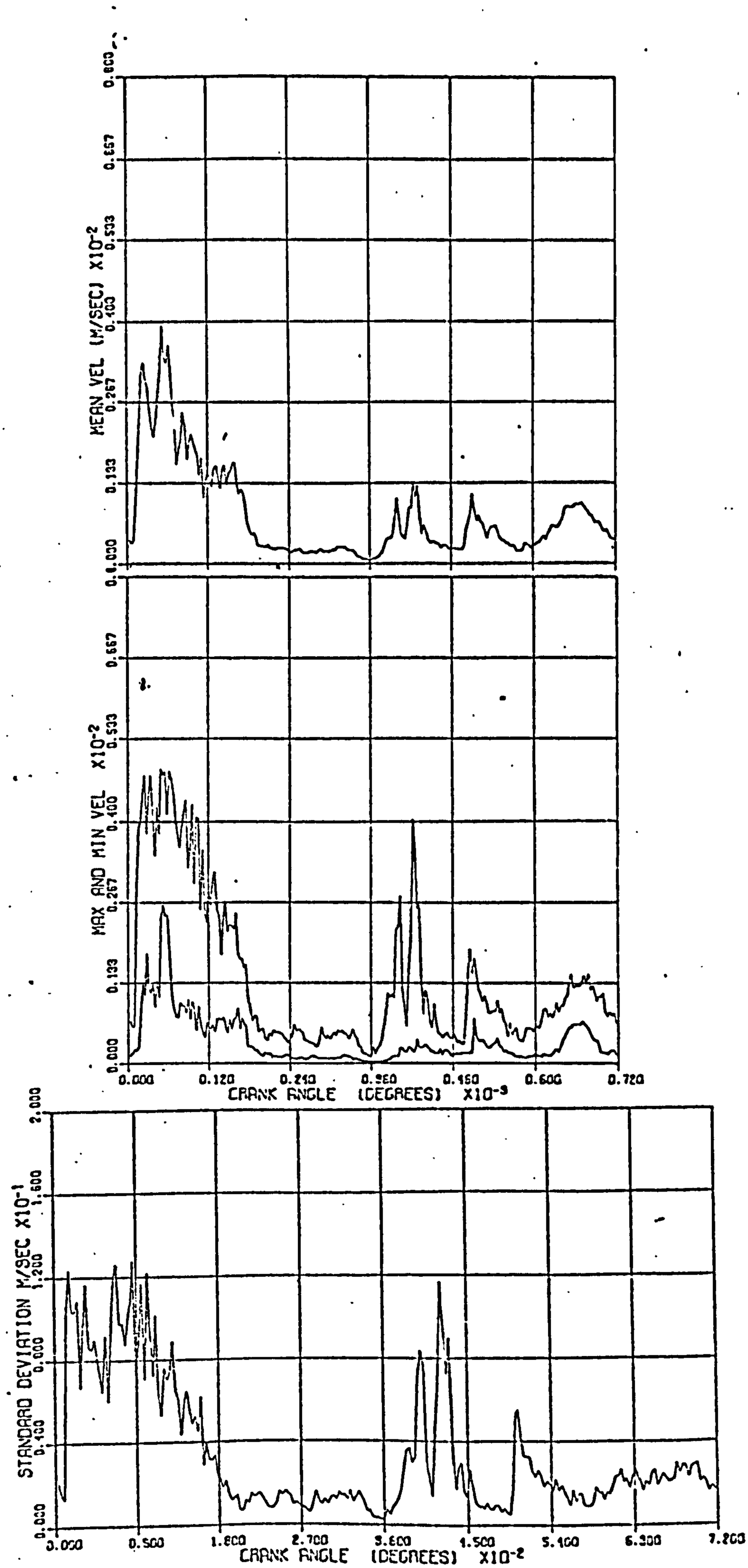

Fig. (6-29) A Statistical Analysis of Gas Mean Velocities for a Test with an Inlet Valve Fitted with 8 Vanes.

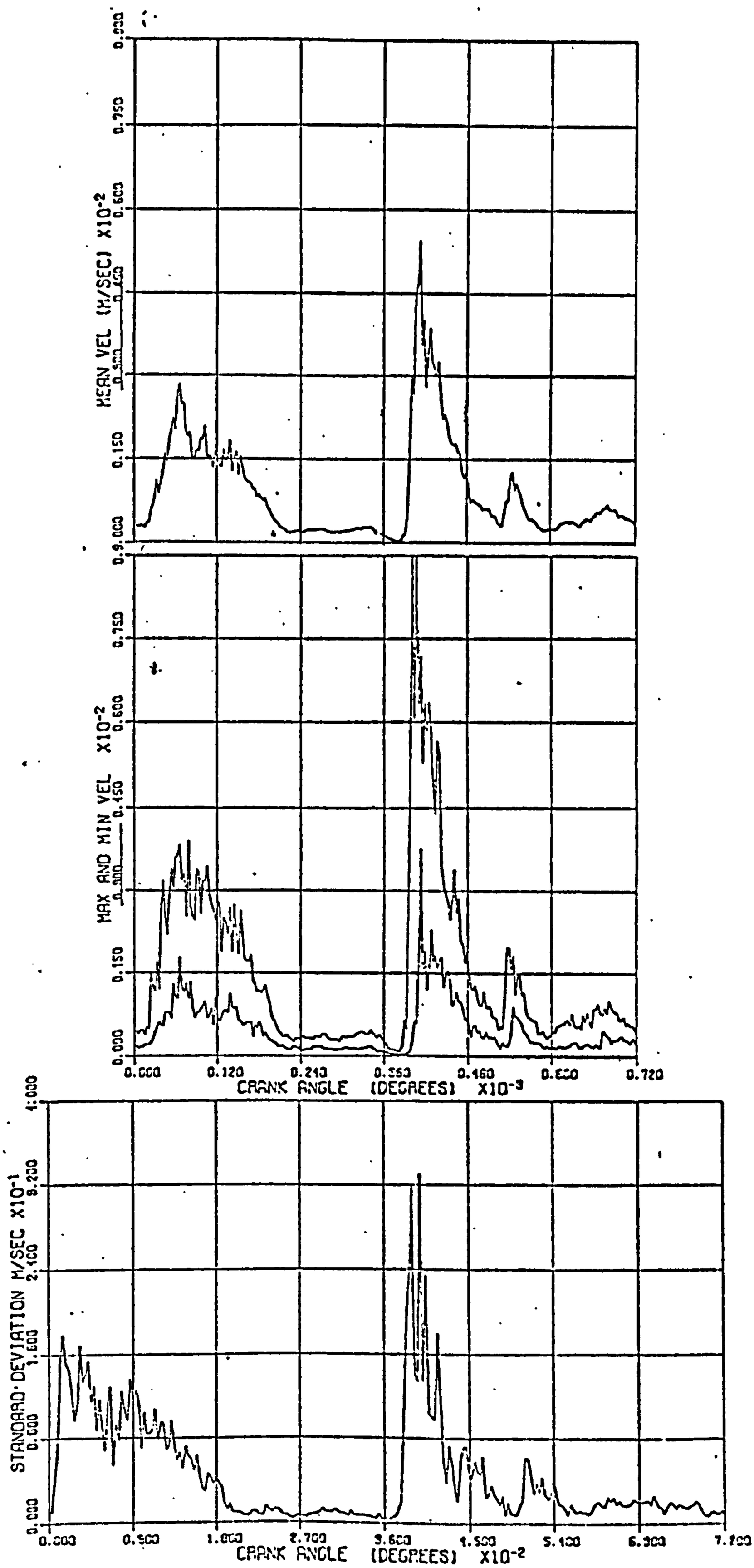

Fig. (6-30) A Statistical Analysis of Gas Mean Velocities for a Test with an Inlet Valve Fitted with Six Vanes.

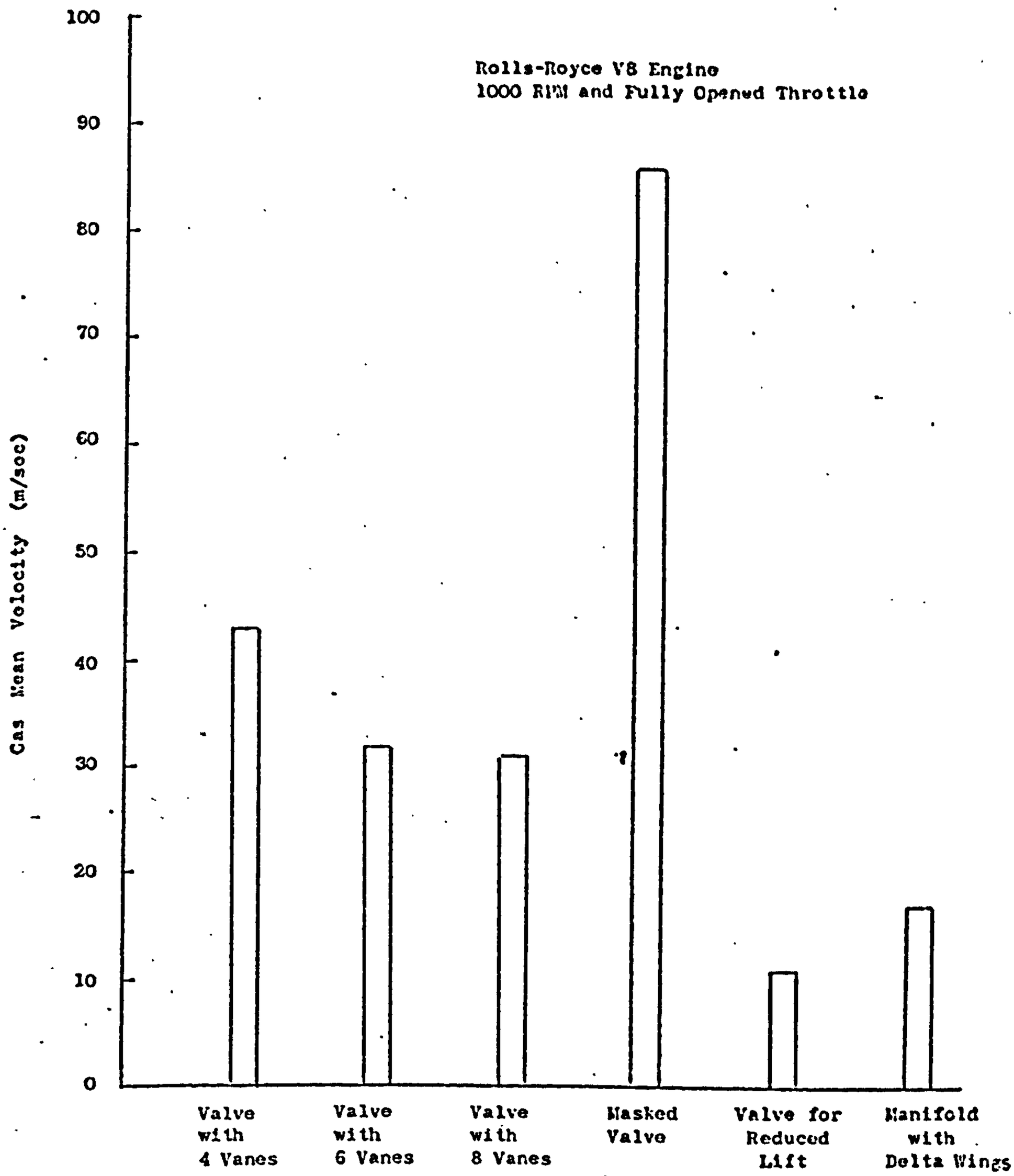

Fig. (6-31a) Comparison Between Maximum Induction Velocity for Different Modifications of Intake System

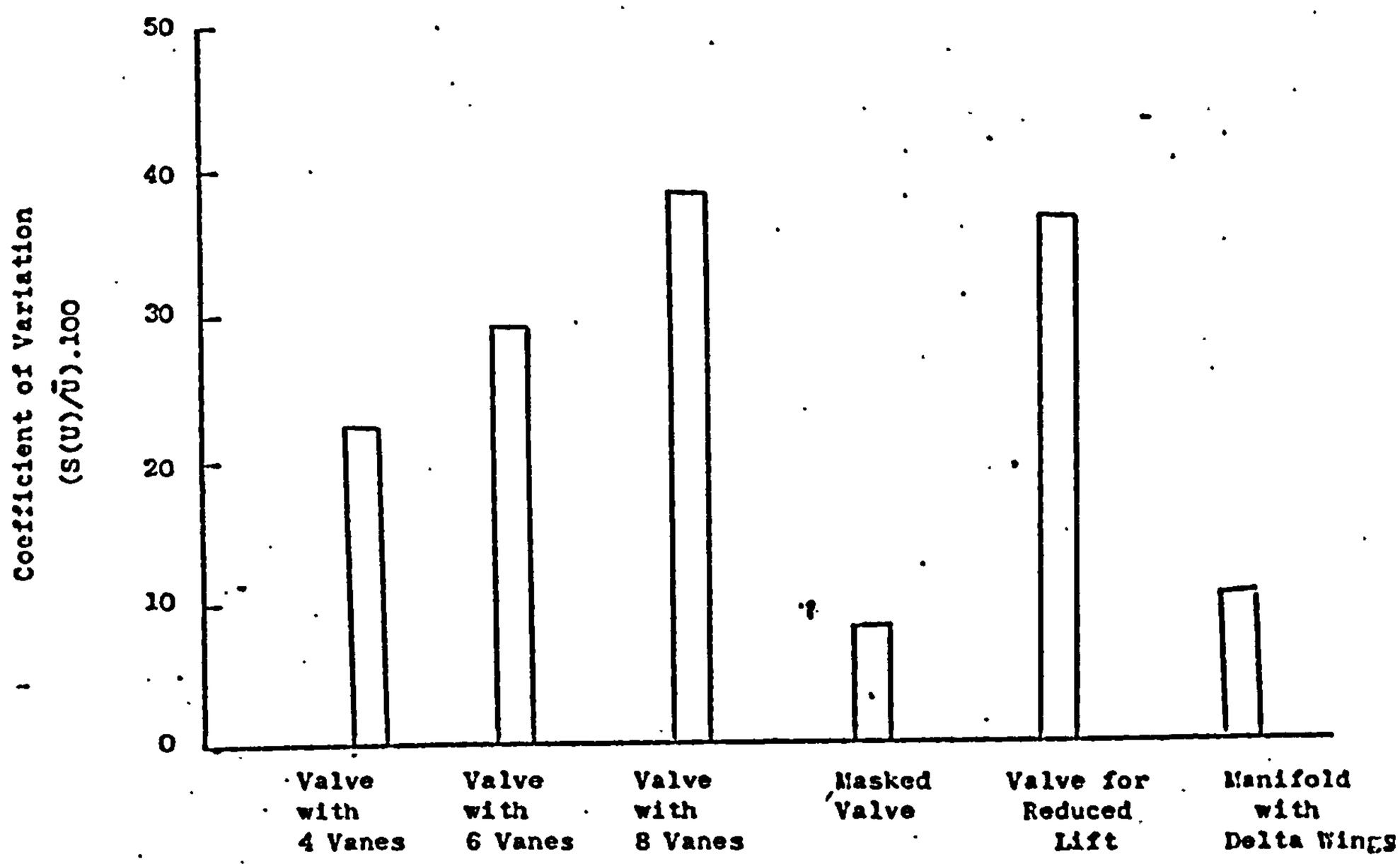

Fig. (6-31b) Comparison Between the Values of Coefficients of Variation of Maximum Induction Velocity for Different Modifications of Intake System

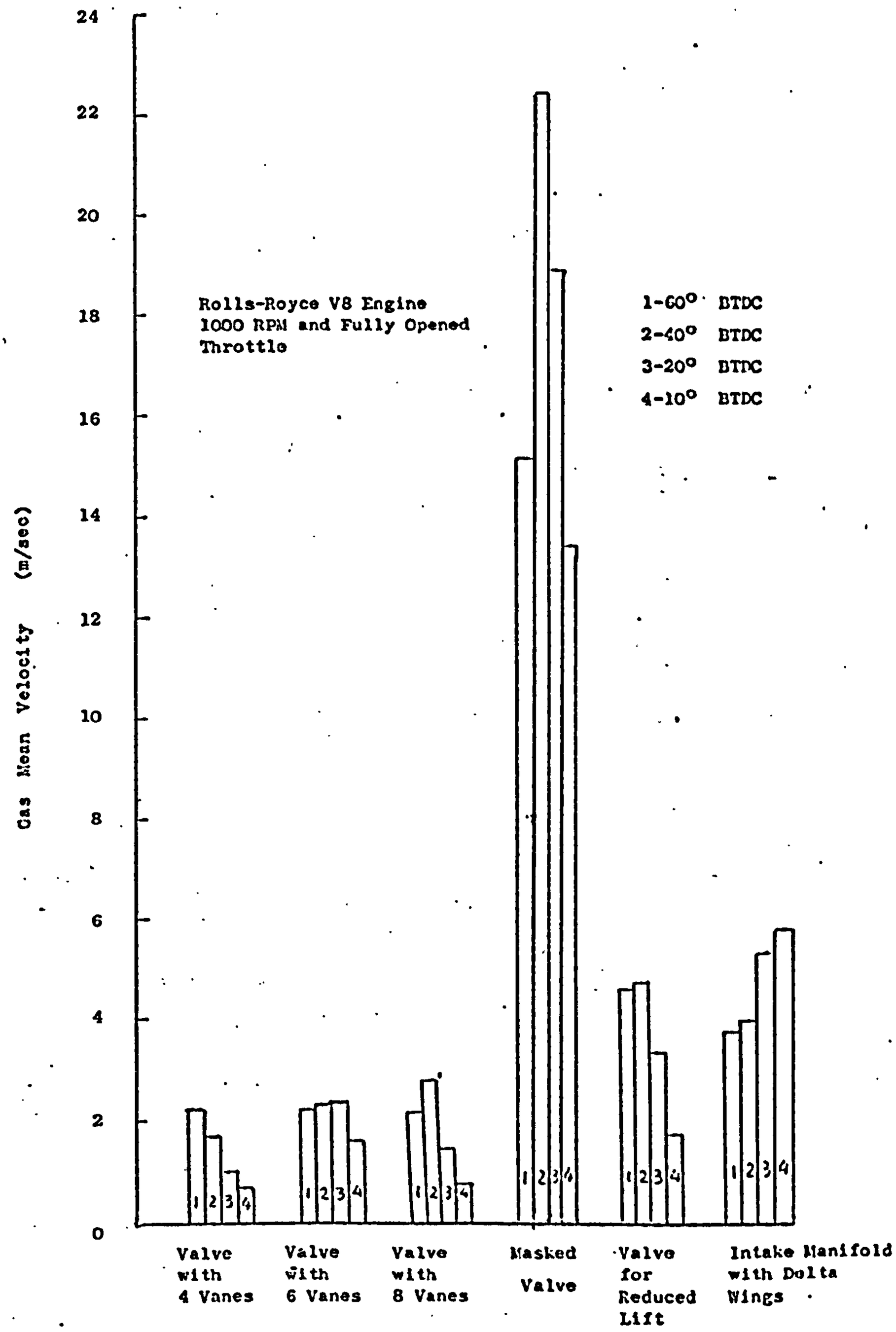

Fig. (6-32a) Comparison Between Gas Mean Velocities During Compression Period for Different Modifications of Intake System

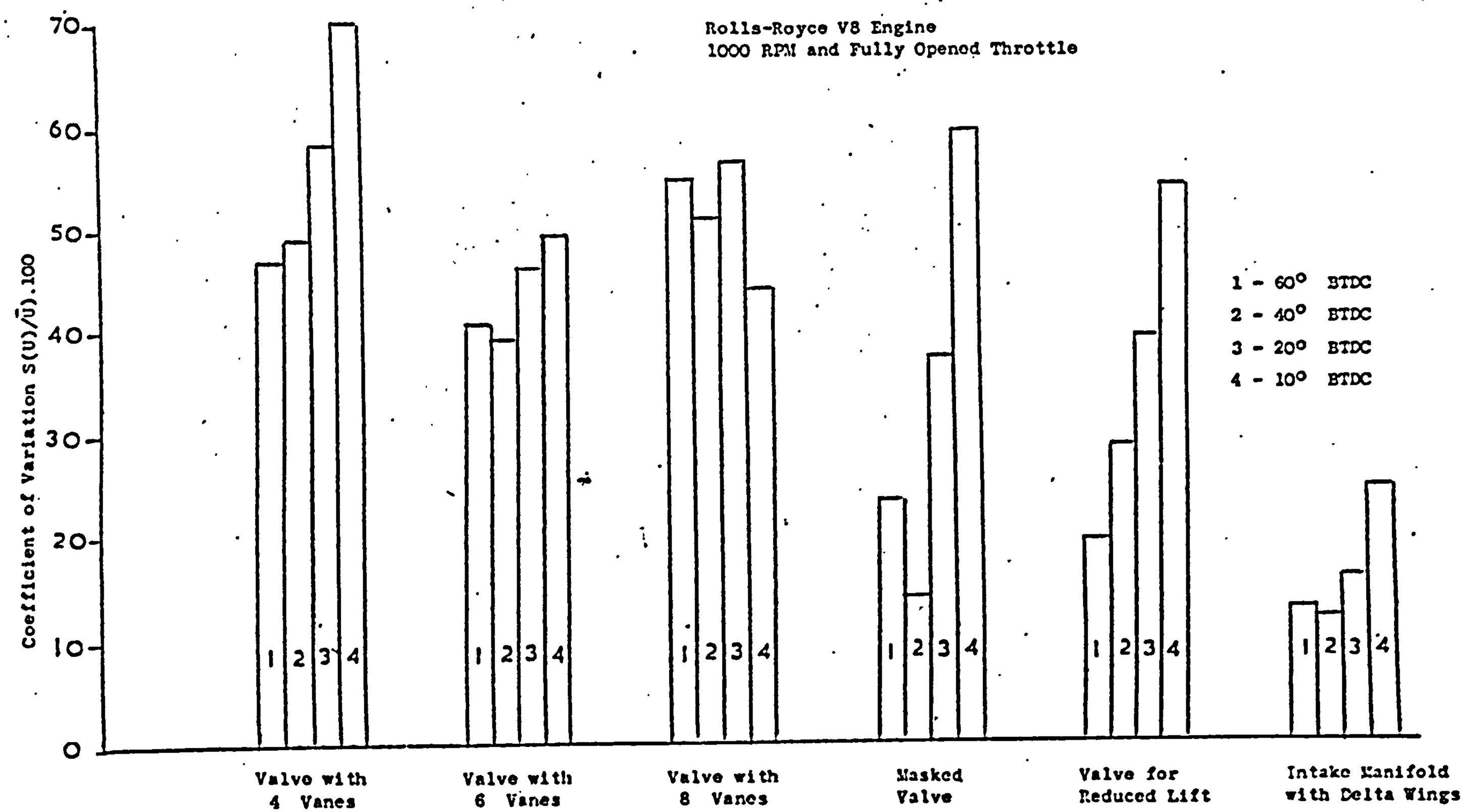

Fig. (G-32b) Comparions Between the Values of the Coefficient of Variation in Gas Velocities During Compression Period for Different Modifications of Intake System.

Fig. (6-33) Analyses of Turbulence Signals During the Cycle for Three Different Orientations of the Hot Wire Anemometer , (See Fig (5-3) for Difinitions of Reference Axes). Measurements at the Spark Plug Location (Z = 17.78 mm),Rolls-Royce V8 Engine, 1000 RPM and Fully Opened Throttle.

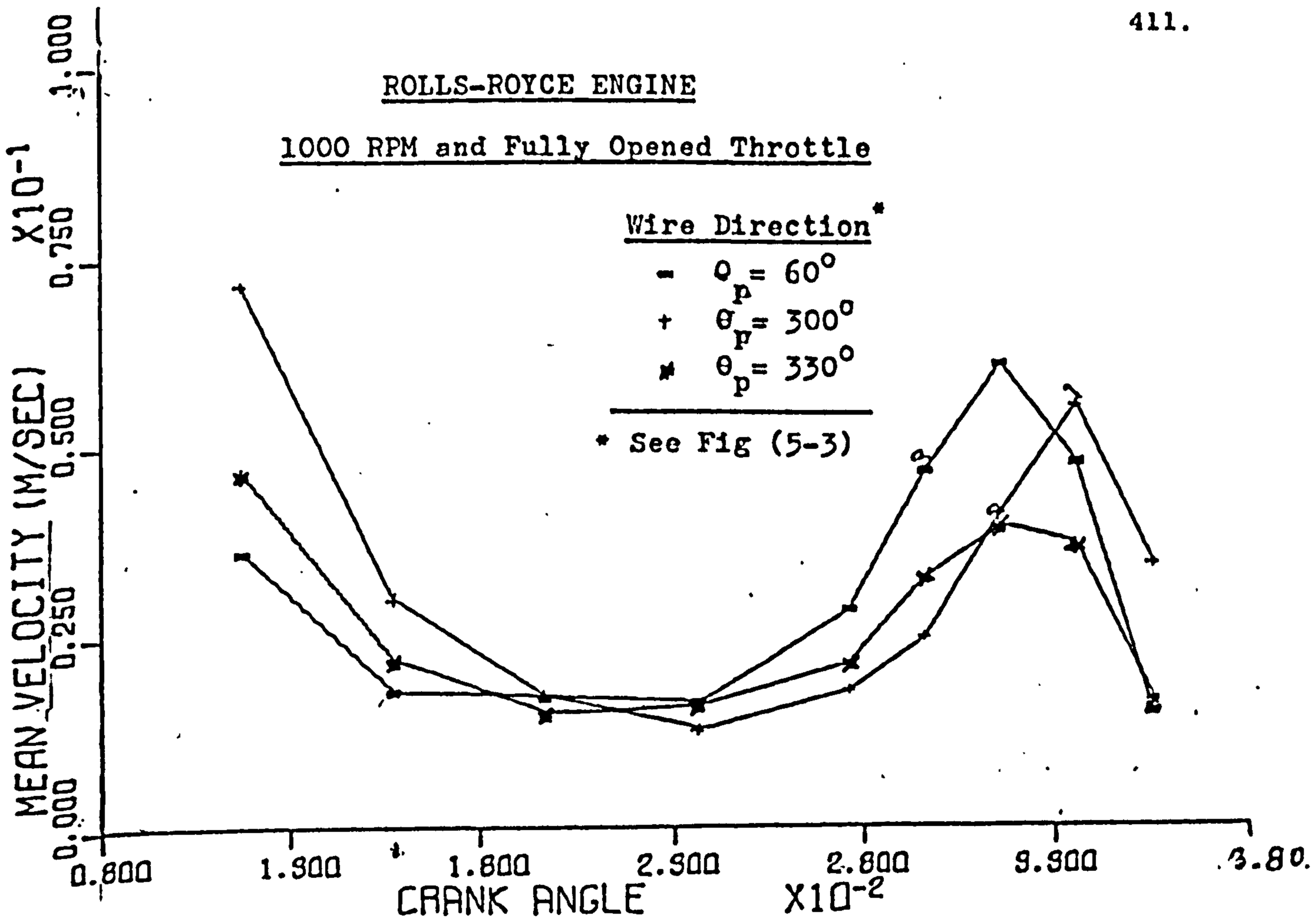

Fig (6-33a)

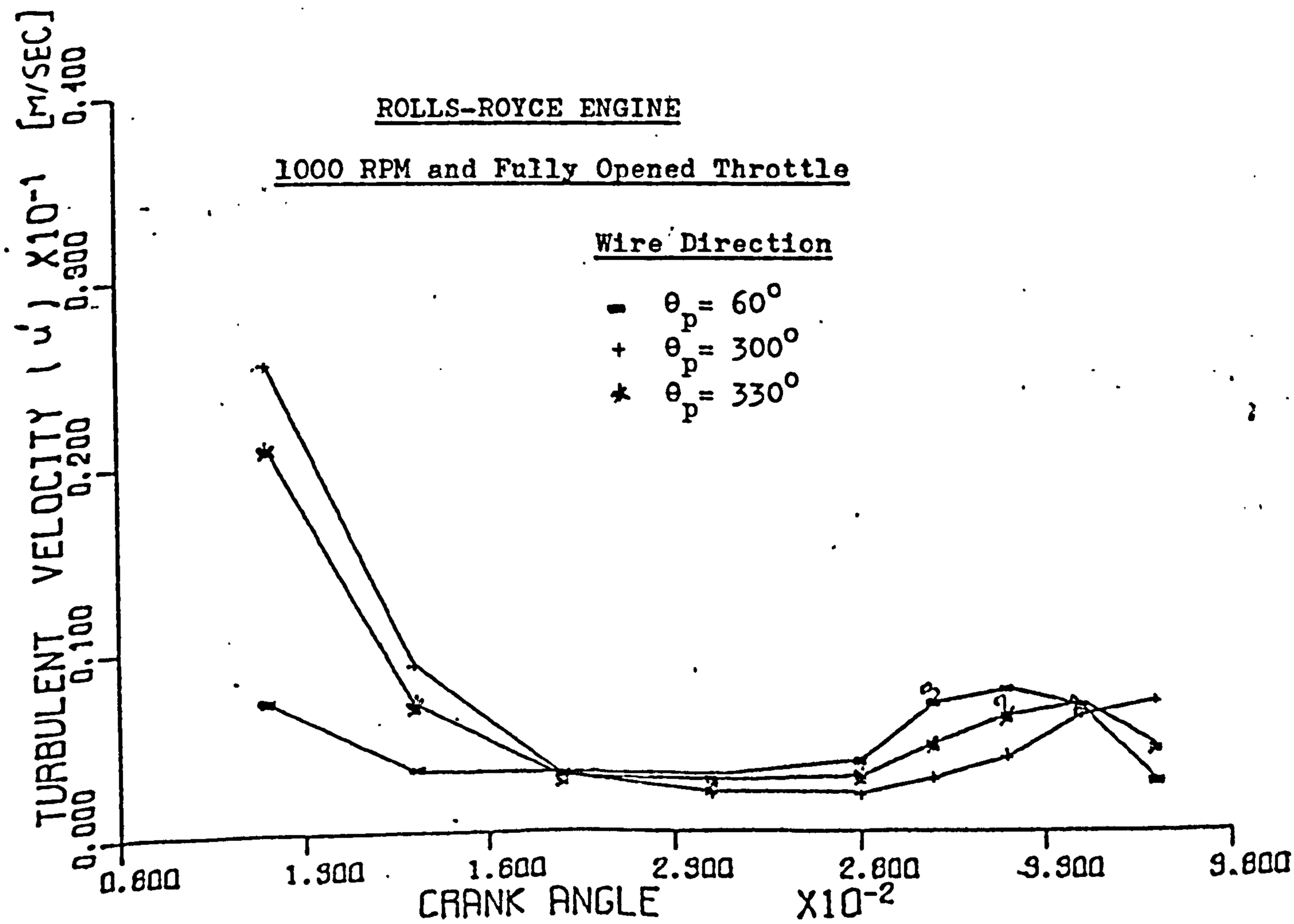

Fig (6-33b)

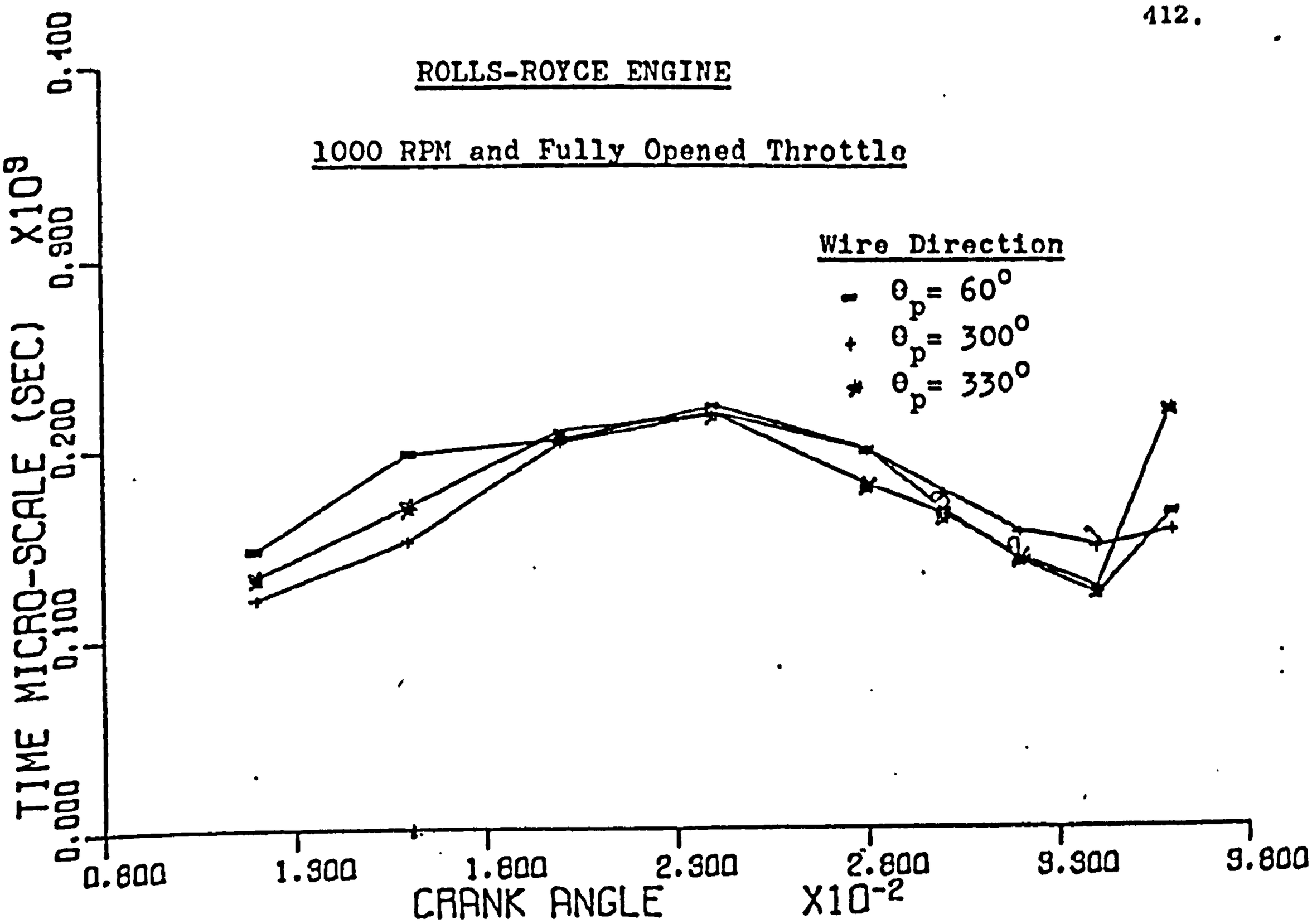

Fig (6-33c)

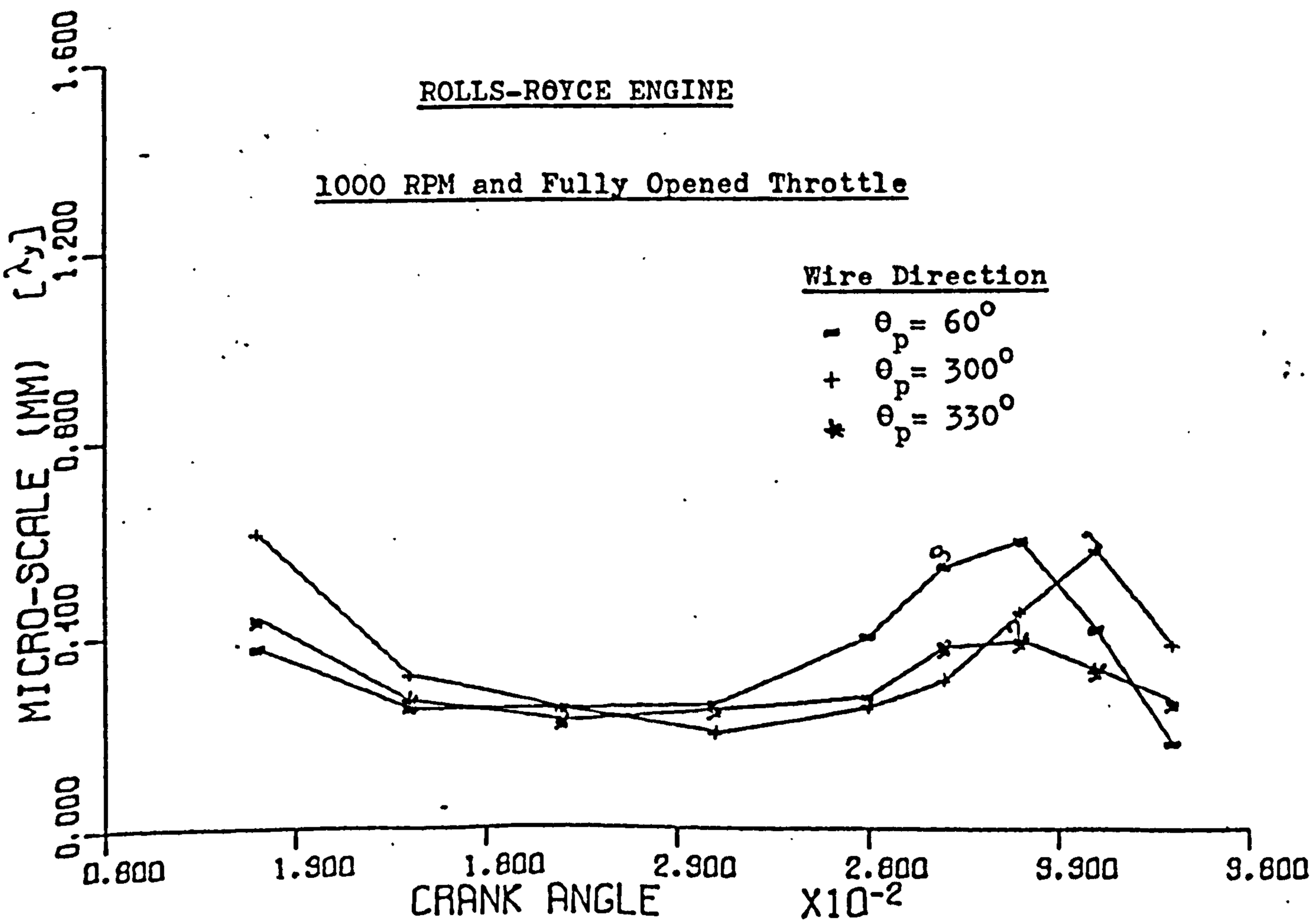

Fig (6-33d)

ROLLS-ROYCE ENGINE

1000 RPM and Fully Opened Throttle

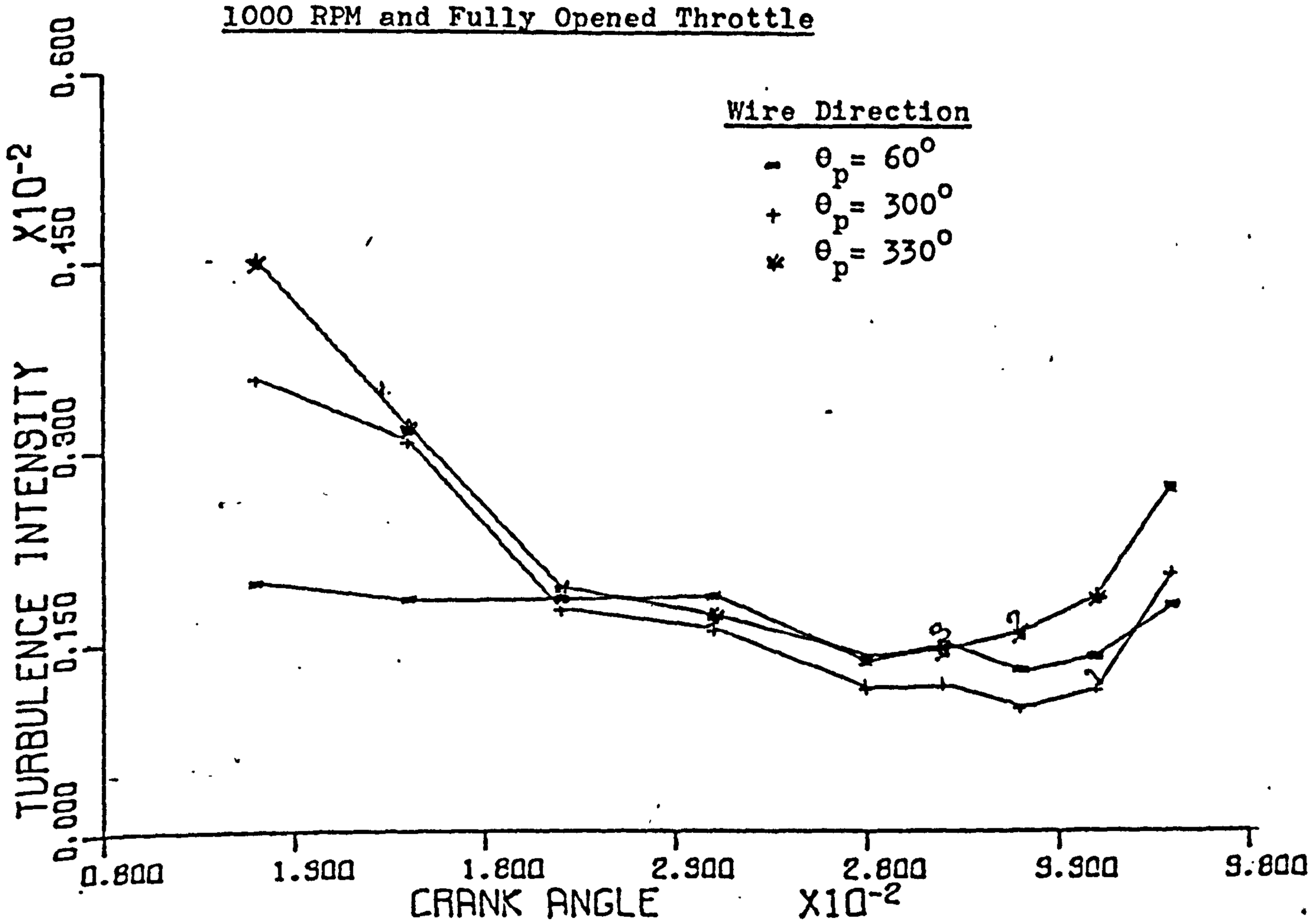

Fig (6-33e)

Fig. (6-34) Power Spectrum Functions for Different Crank Angles During the Cycle.
(Rolls-Royce V8 Engine, Compression Ratio = 9:1, 1000 RPM and Fully Opened Throttle. Measurements at the Spark Plug Location (Z= 17.78 mm) and a Wire Direction of 300 Degrees).

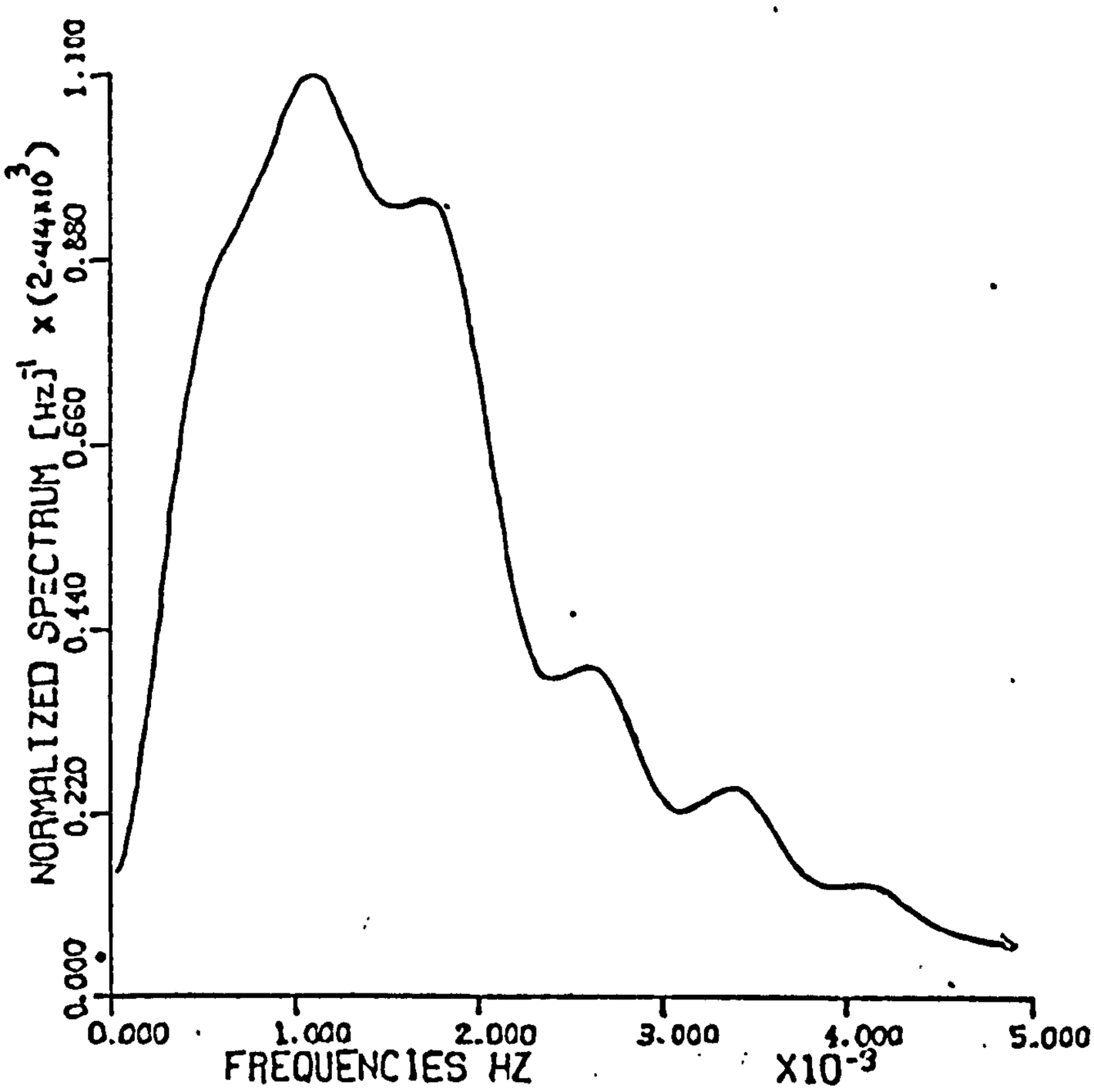

Fig. (6-34a) Power Spectrum Function at a Crank Angle of 80 degrees.

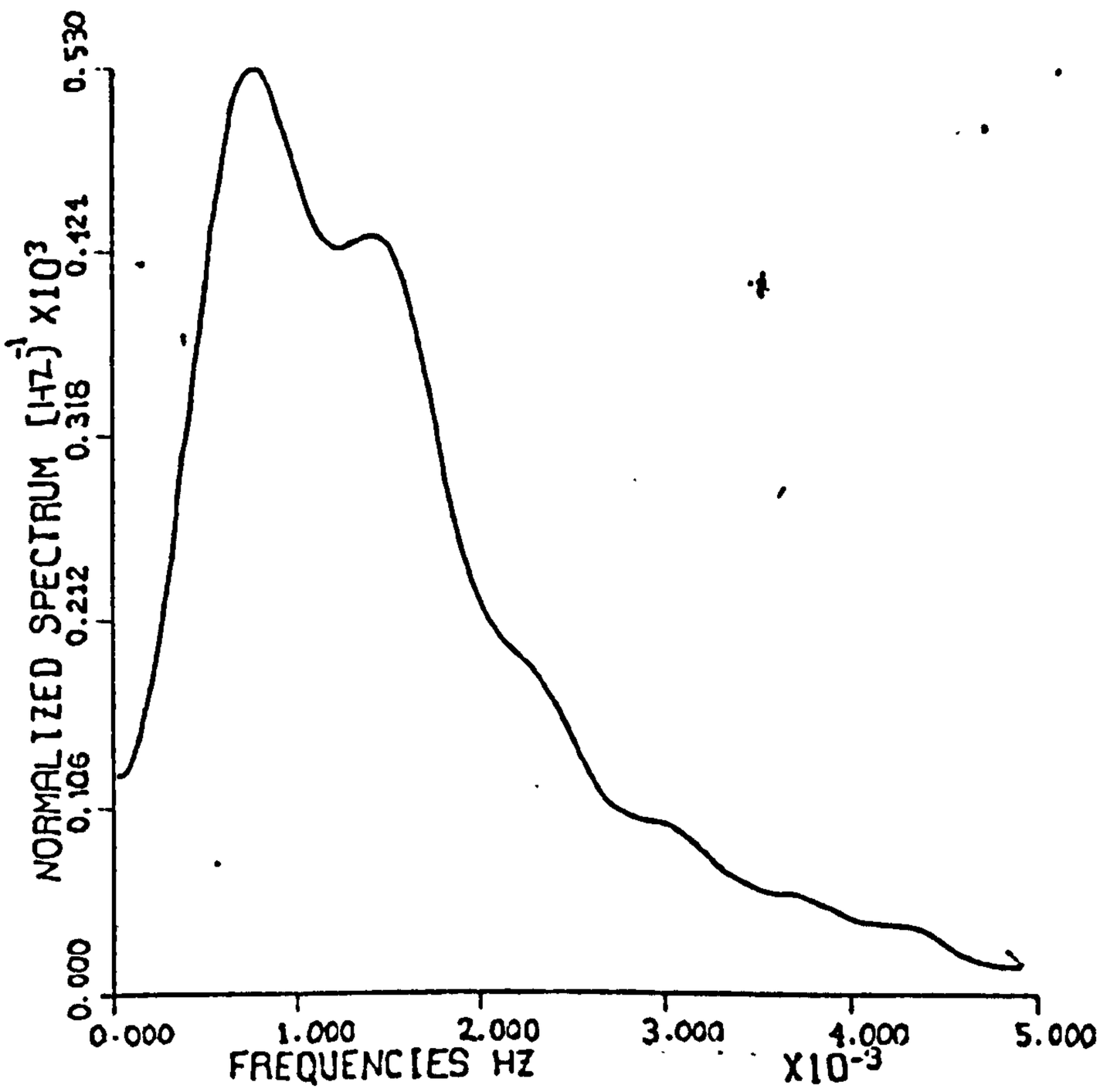

Fig. (6-34b) Power Spectrum Function at a Crank Angle of 120 degrees.

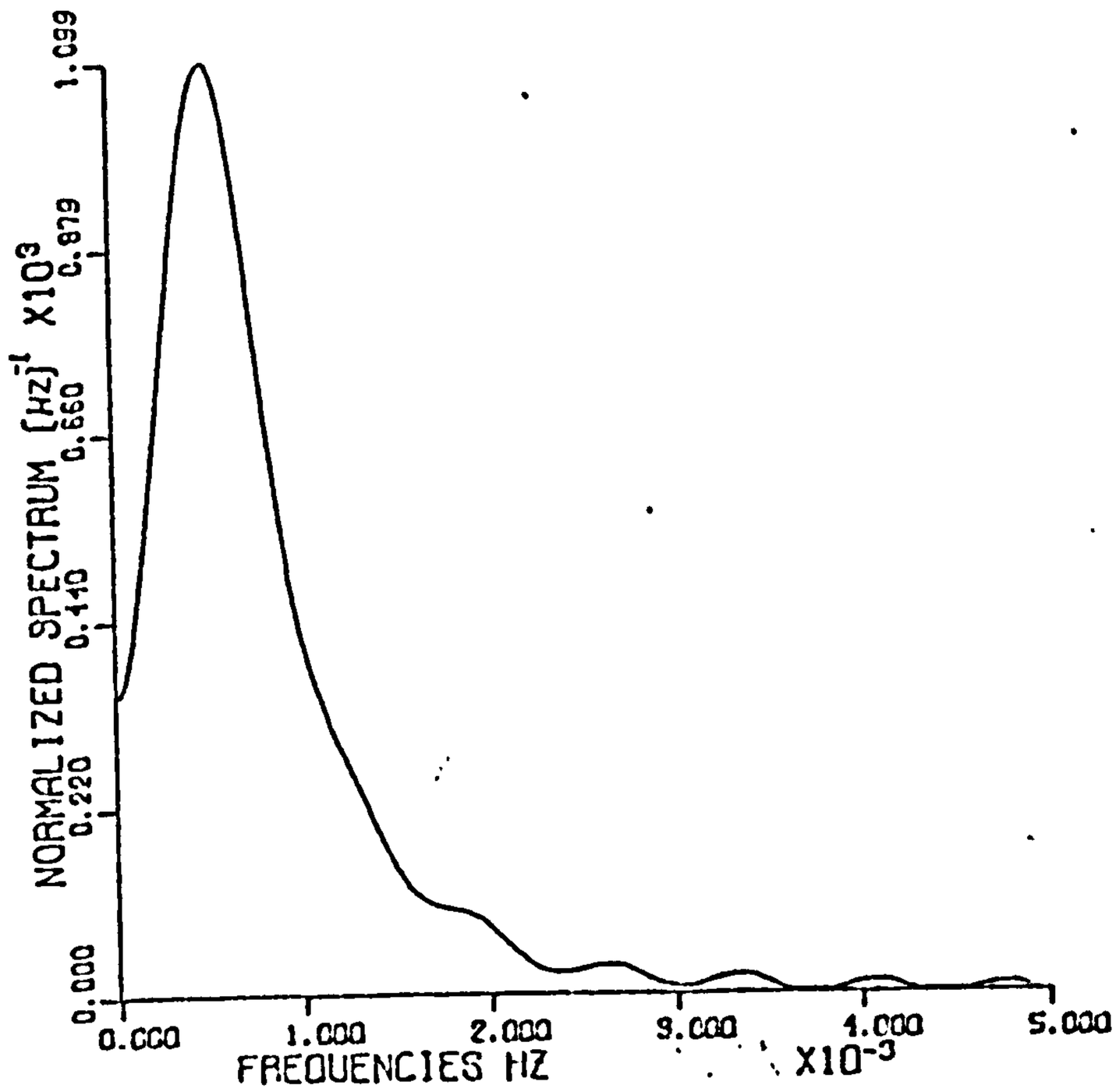

Fig. (6-34c) Power Spectrum Function at a Crank Angle of 200 degrees.

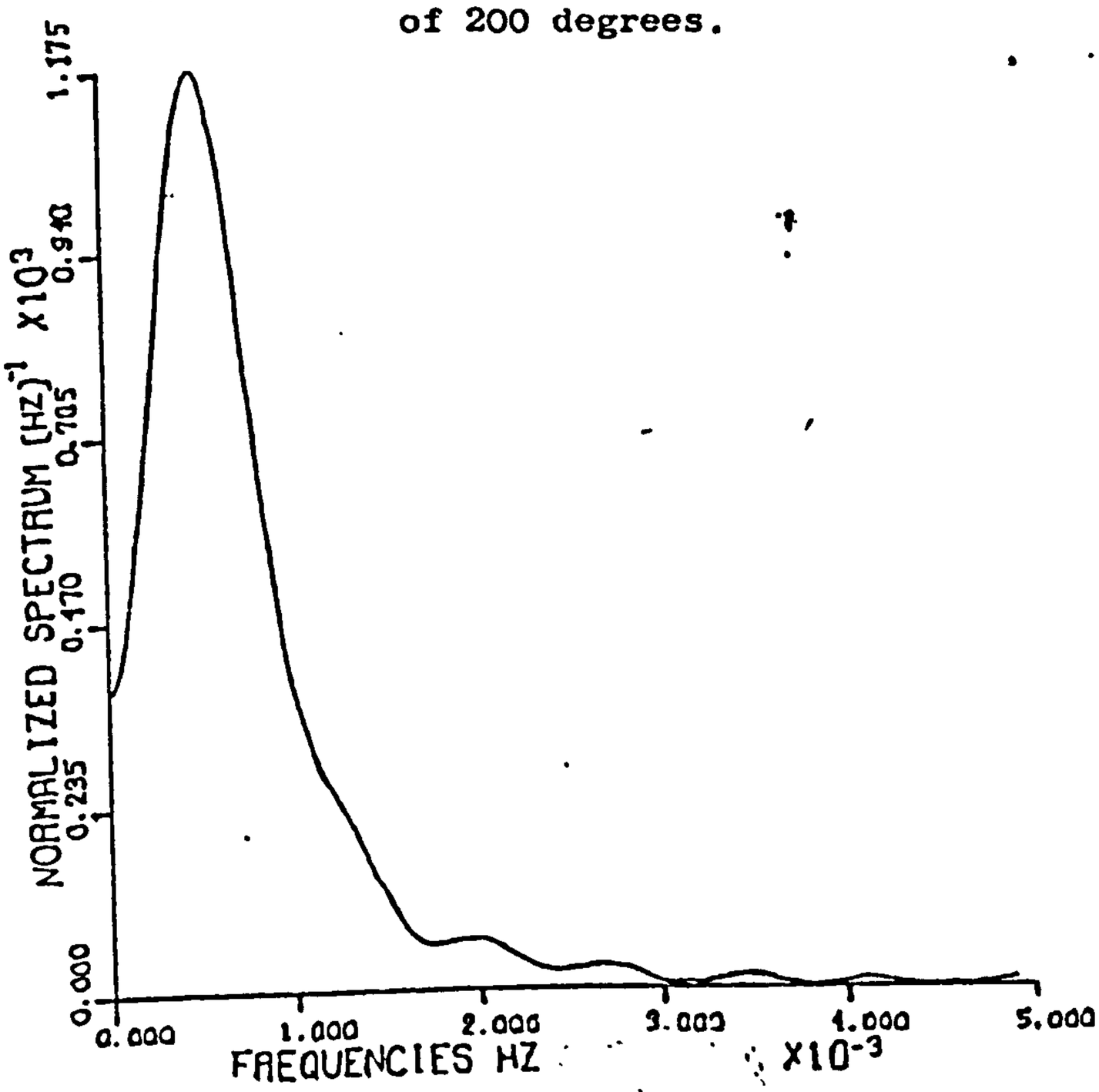

Fig. (6-34d) Power Spectrum Function at a Crank Angle of 240 degrees.

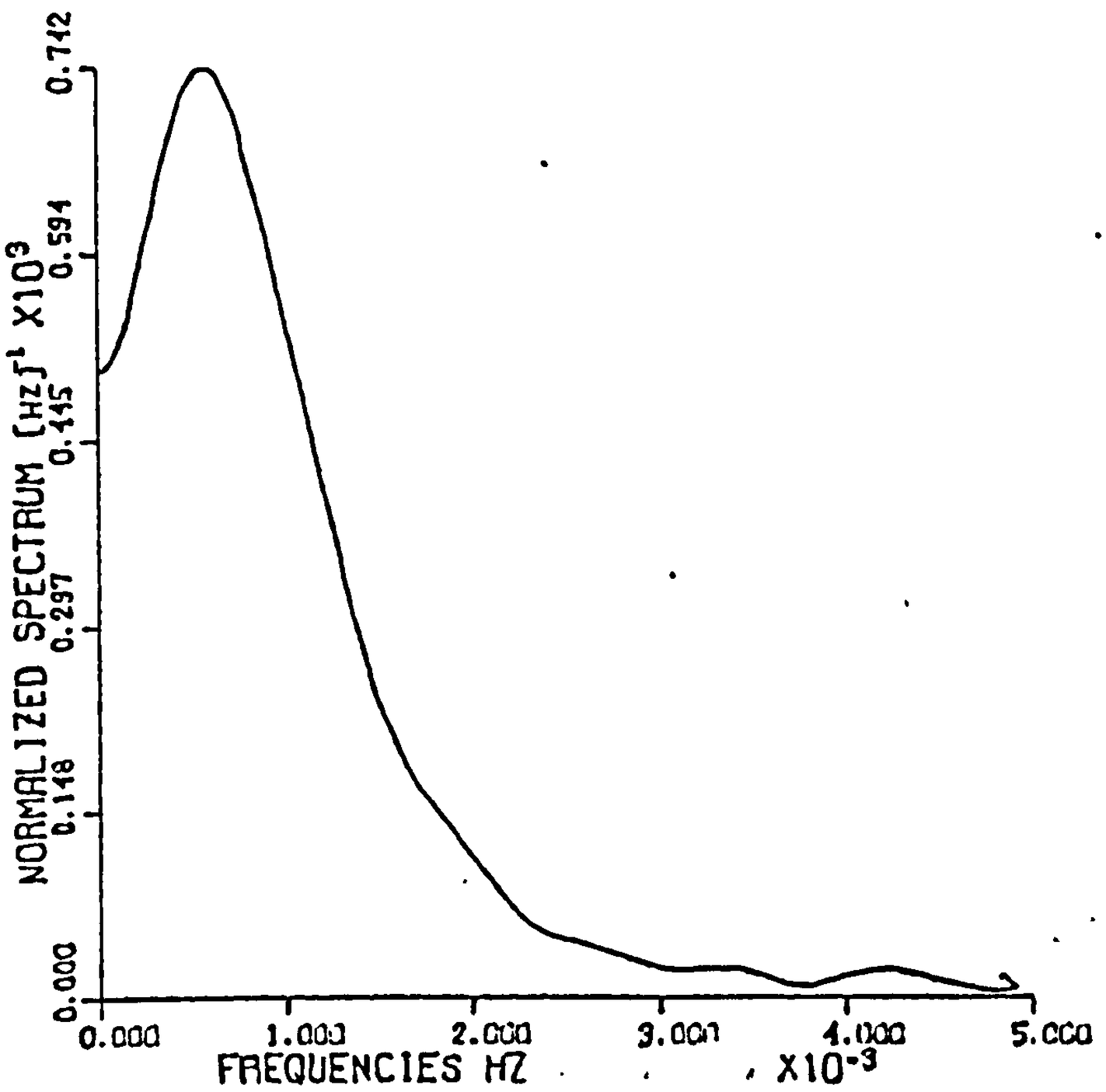

Fig. (6-34e) Power Spectrum Function at a Crank Angle of 300 Degrees

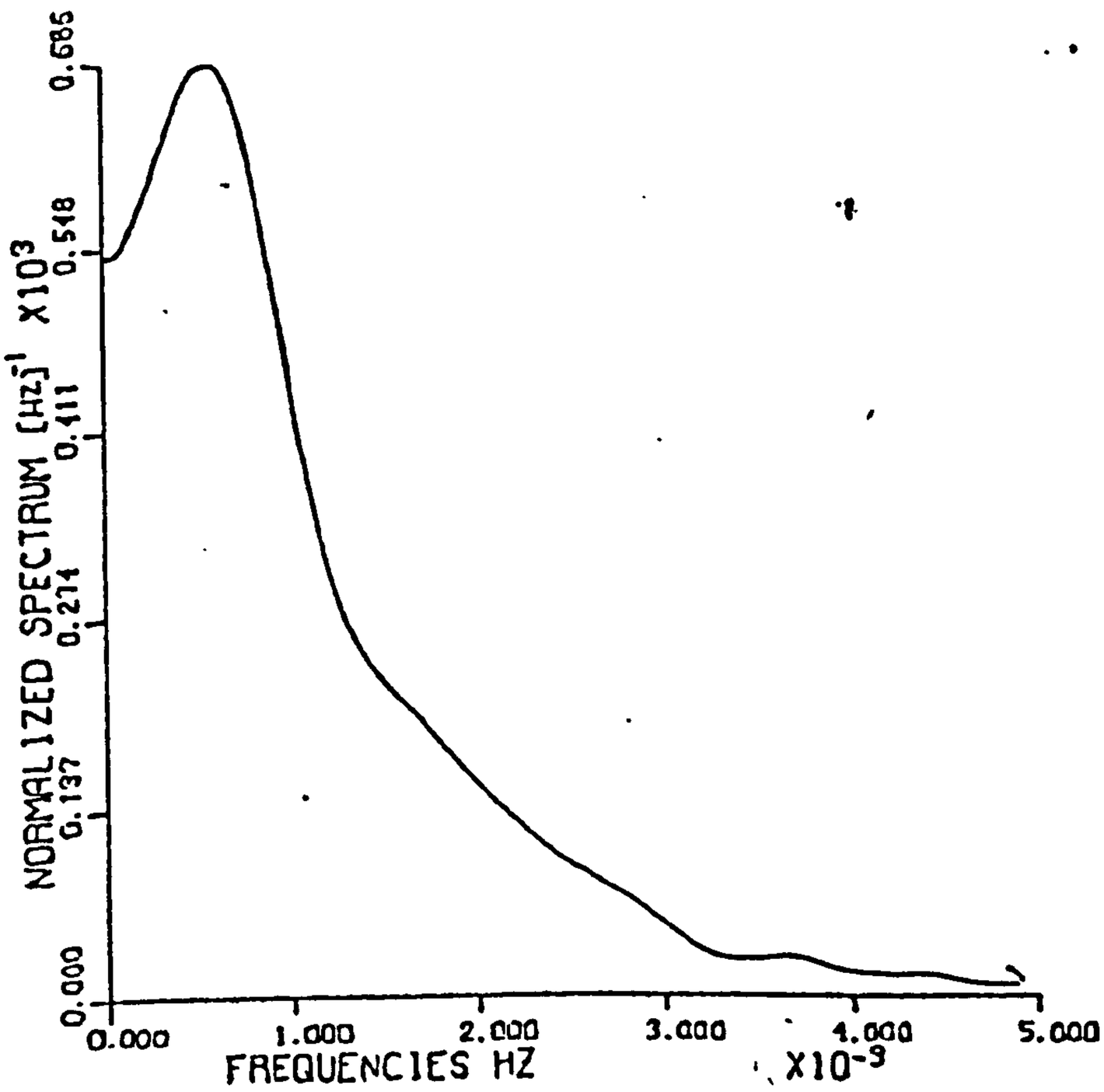

Fig. (6-34f) Power Spectrum Function at a Crank Angle of 320 Degrees.

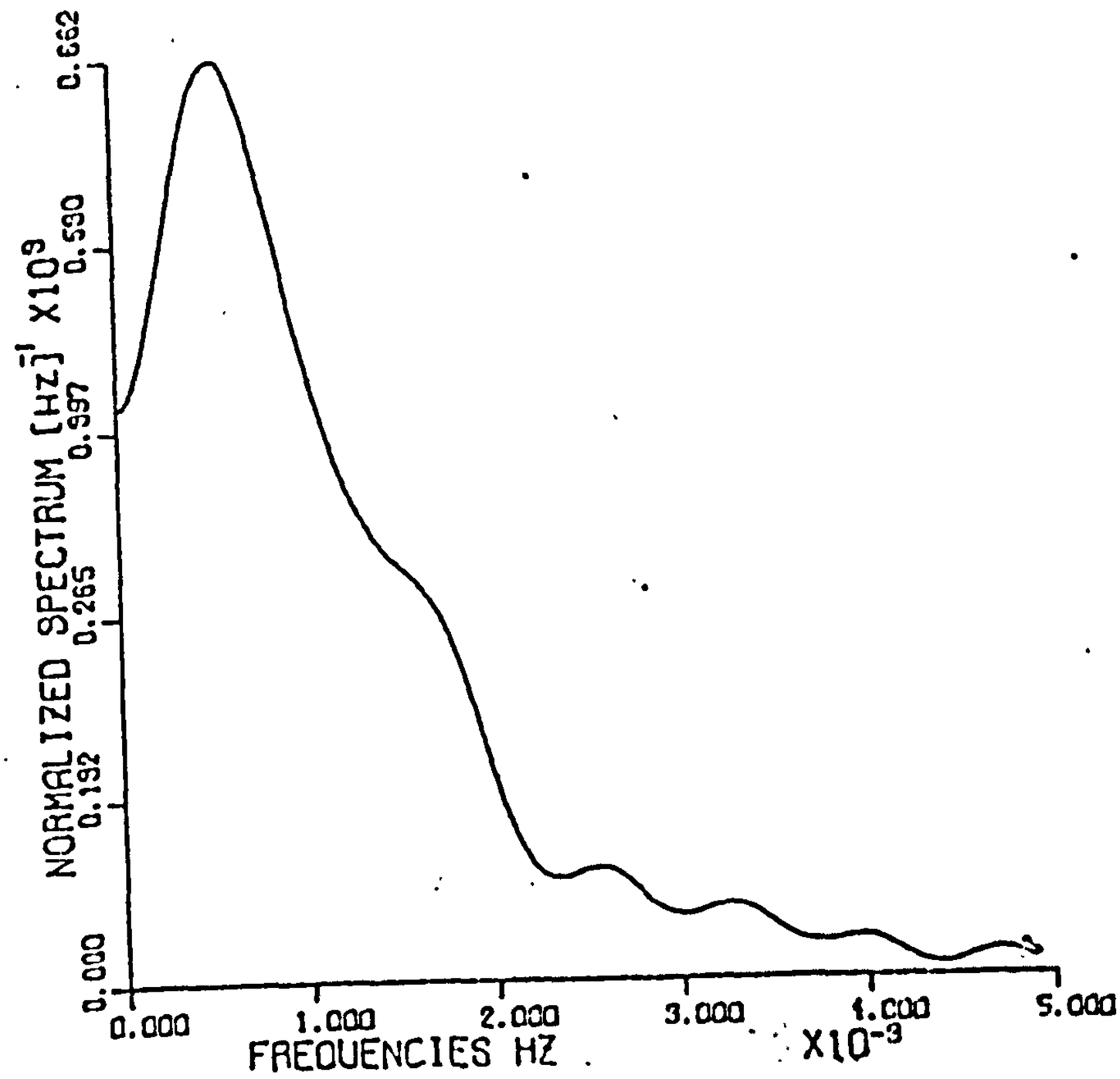

Fig. (6-34g) Power Spectrum Function at a Crank Angle of 340 degrees.

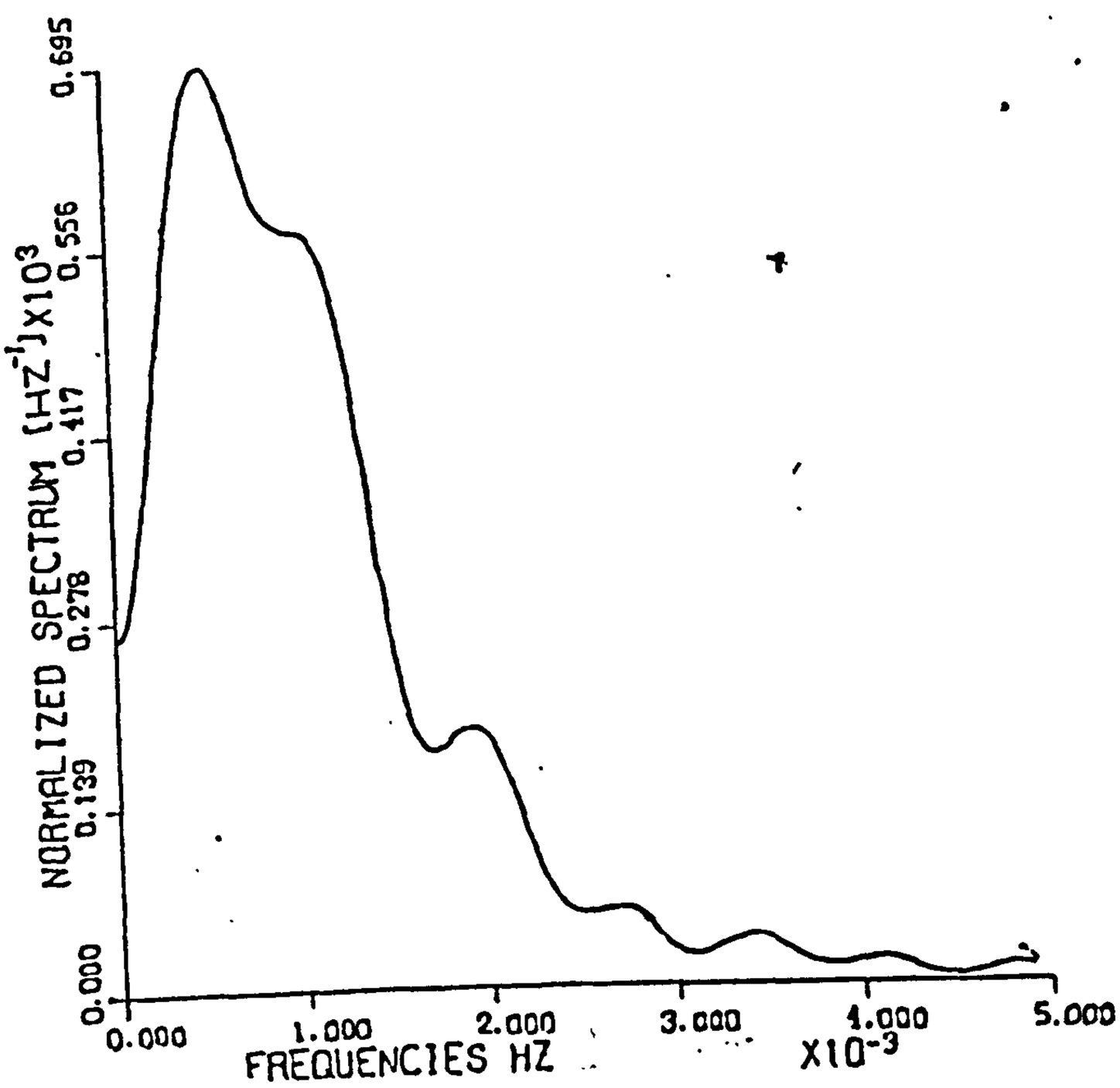

Fig. (6-34h) Power Spectrum Function at TDC.

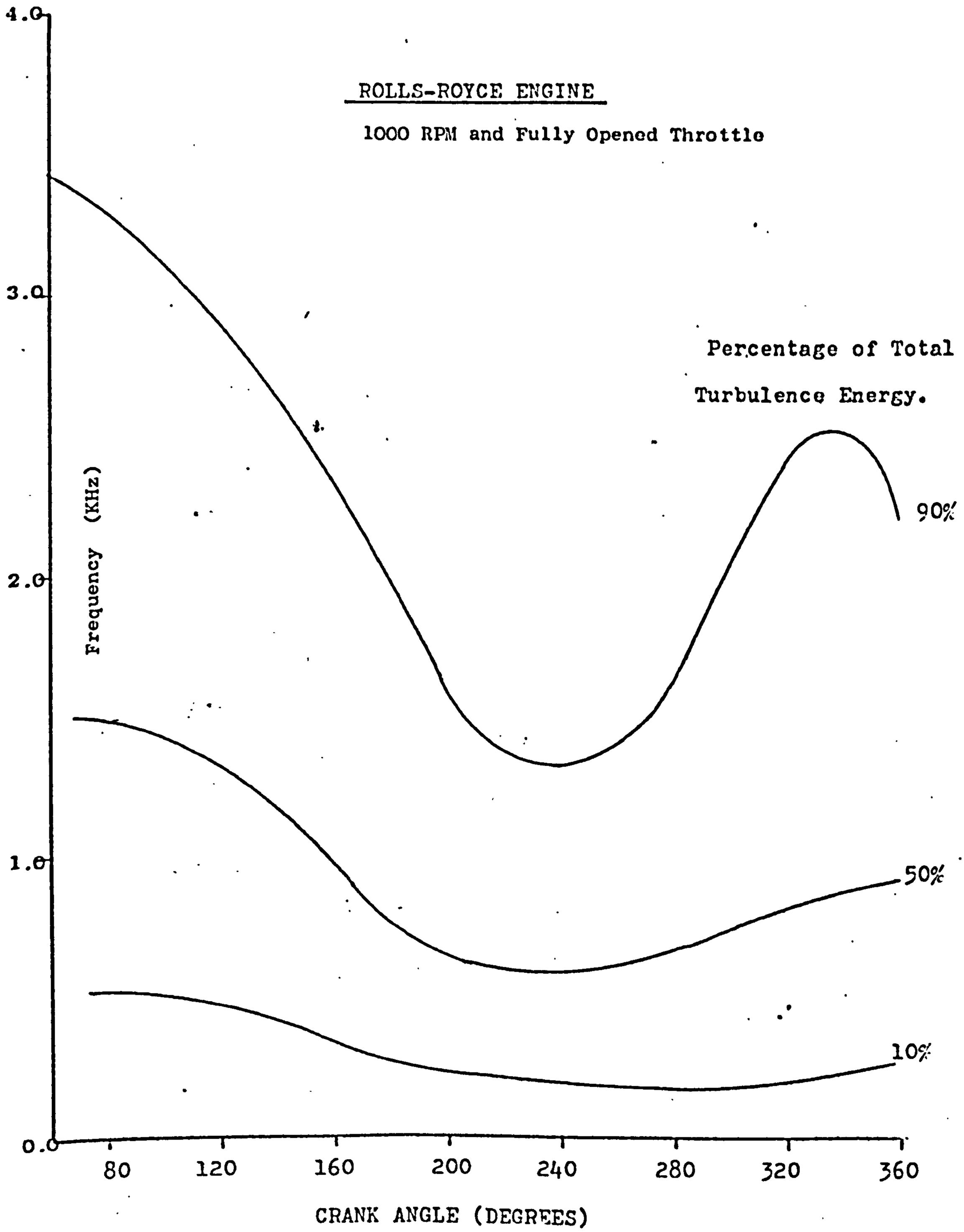

Fig. (6-35) Maximum Frequencies for Eddies Containing 10%, 50% and 90% of the Turbulent Energy. (Data from Fig. (6-34))

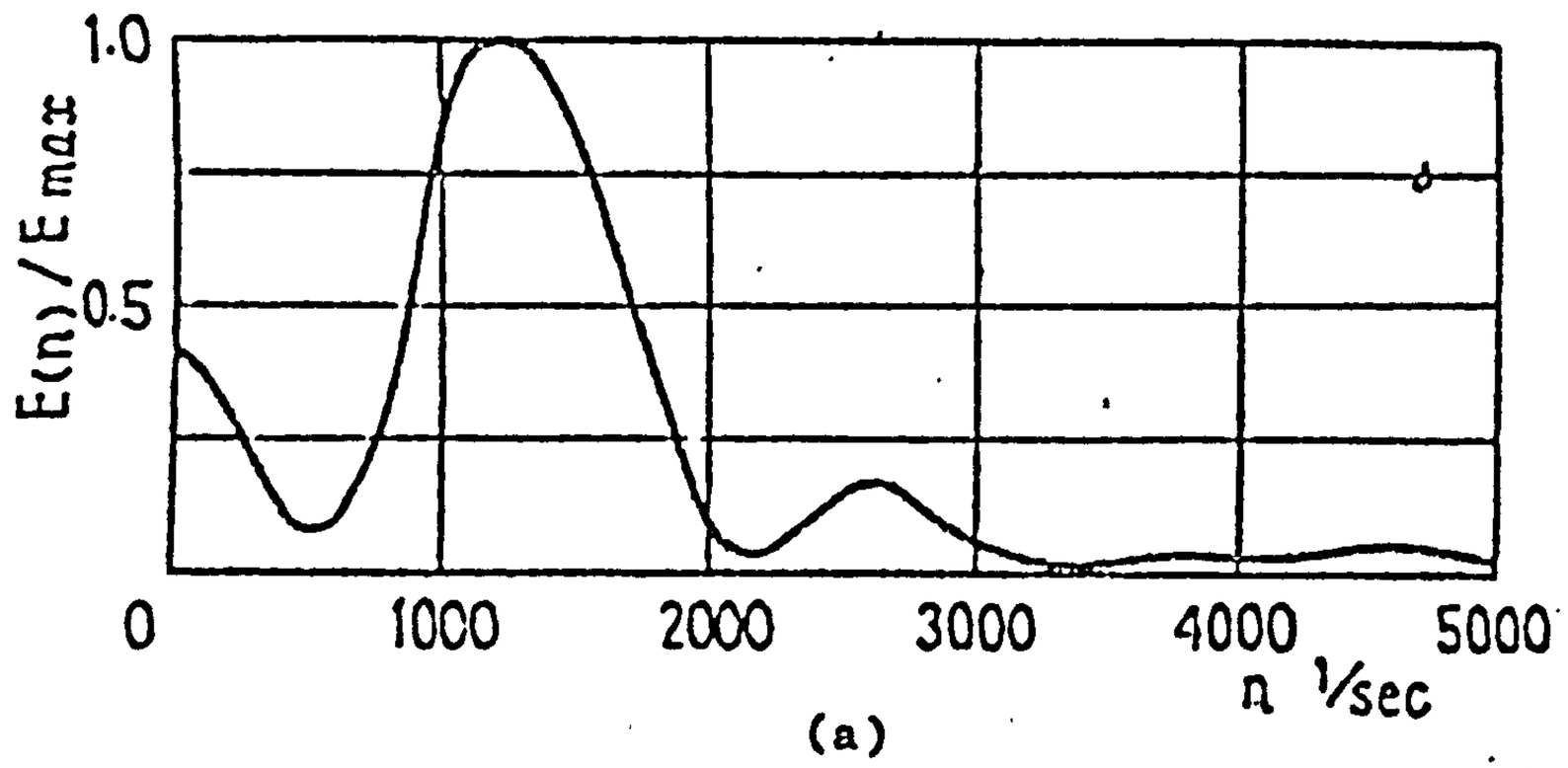

Typical example of energy spectrum function in pre-relaxation stage

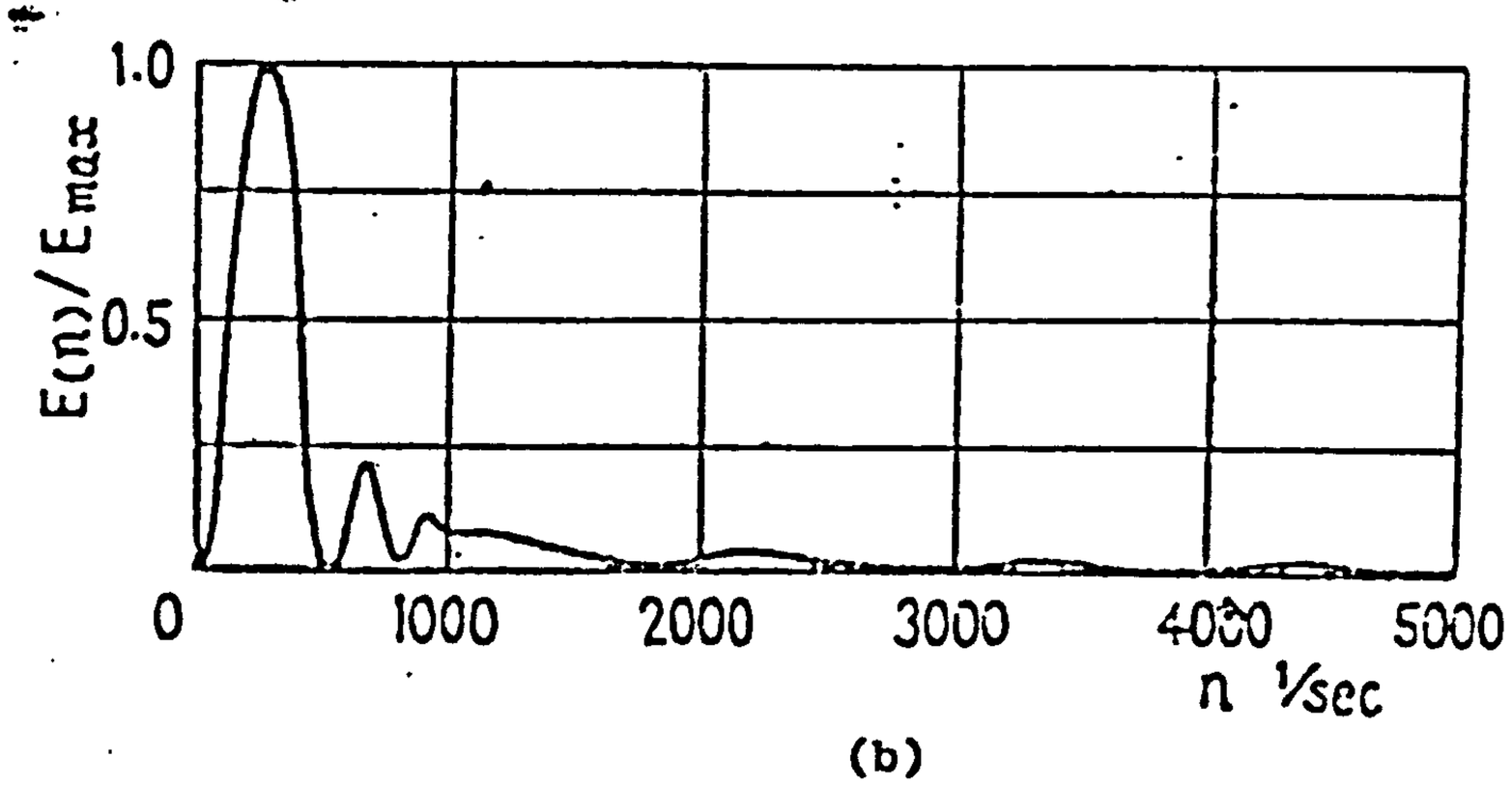

Typical example of energy spectrum function in relaxed stage

Fig. (6-36) Power Spectrum Functions for Turbulent Flow Inside A Closed Vessel (according to Tsuge and Kido (154))

Fig. (6-37) Effect of Engine Speed and the Use of a Masked Inlet Valve on the Turbulence Characteristics Inside a Wedge Combustion Chamber.
(Rolls-Royce V8 Engine, Compression Ratio = 9:1, 1000 RPM and Fully Opened Throttle. Measurements at the Spark Plug Location (Z= 17.78 mm) and a Wire Direction of 300 Degrees).

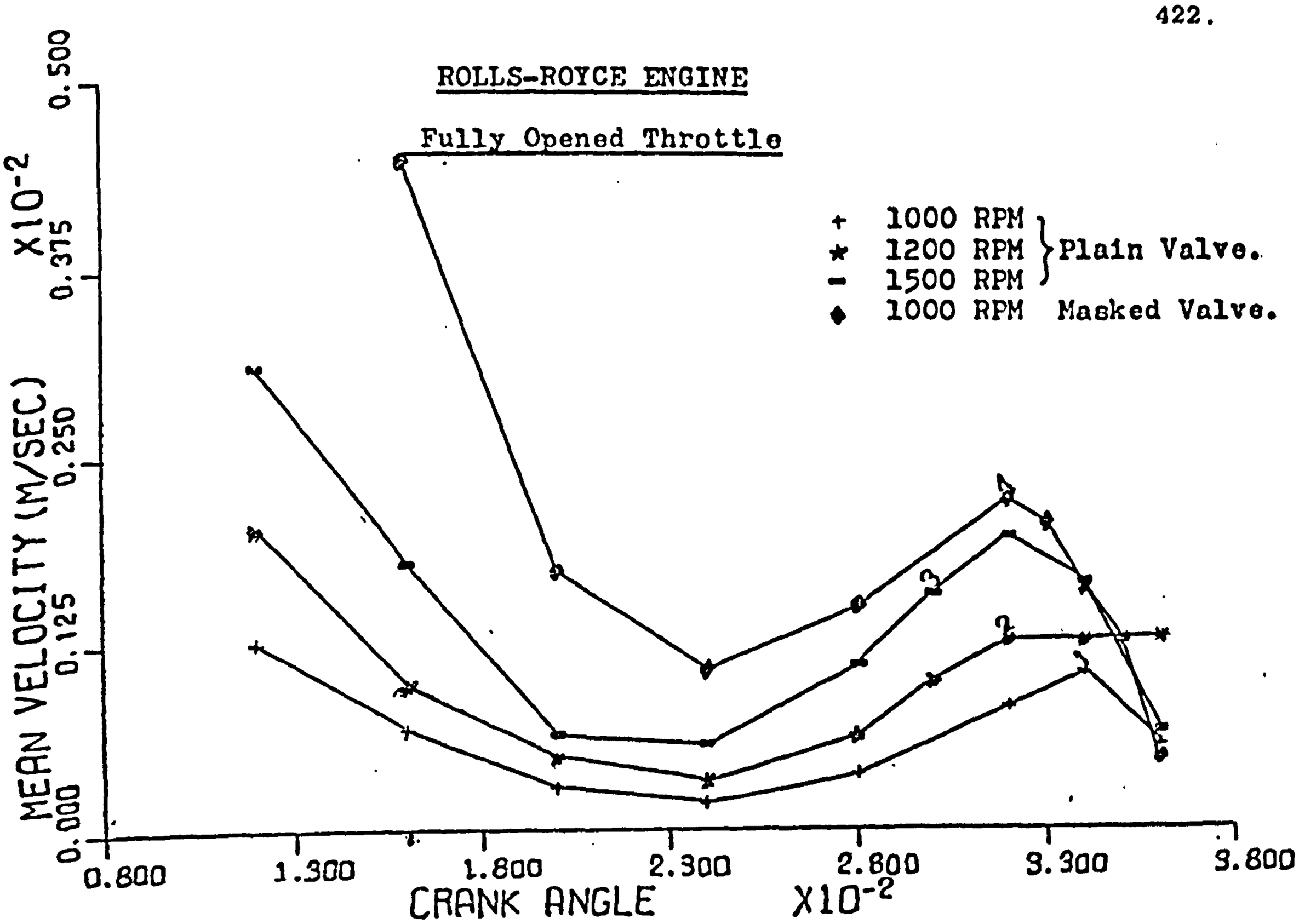

Fig (6-37a)

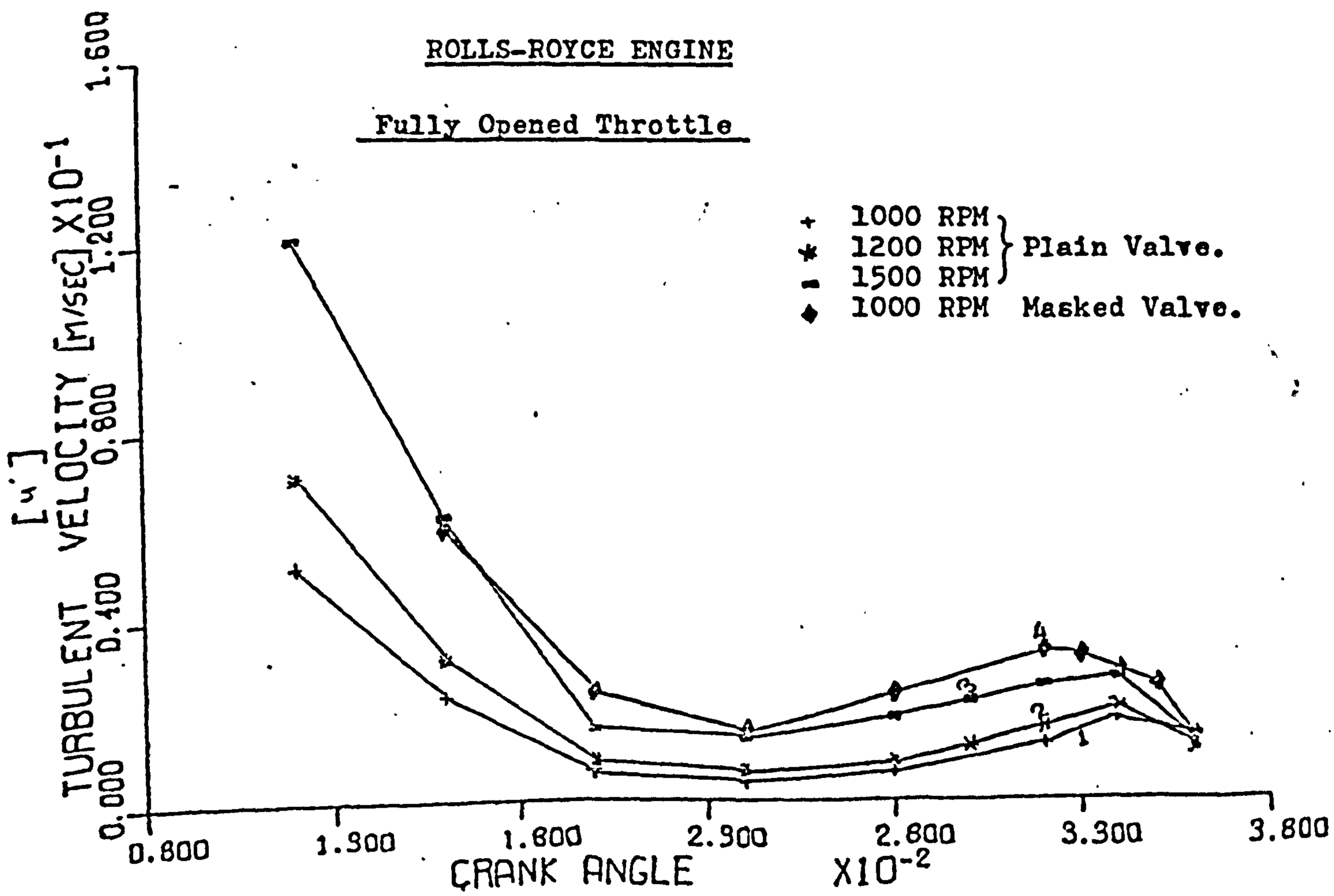

Fig (6-37b)

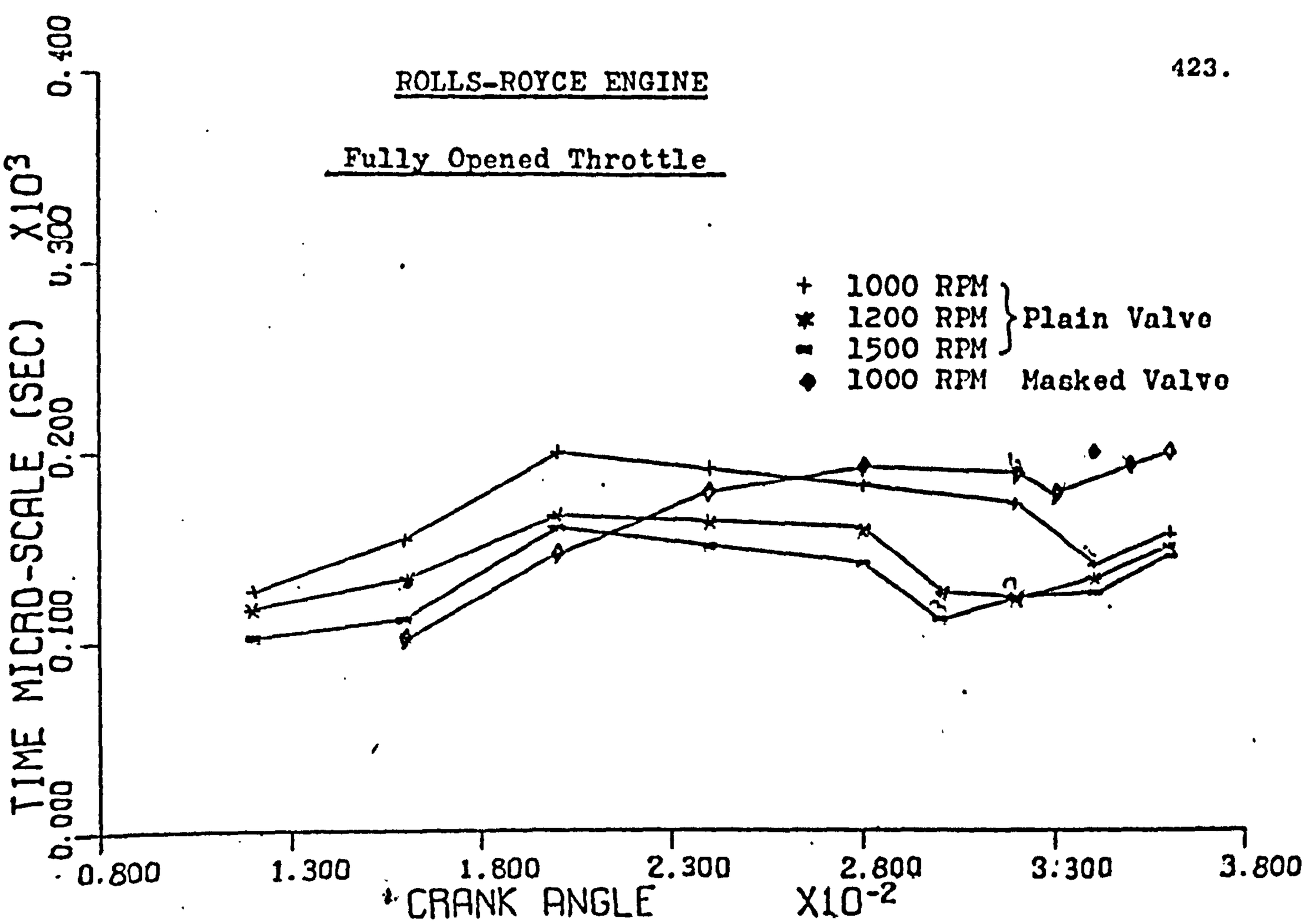

Fig (6-37c)

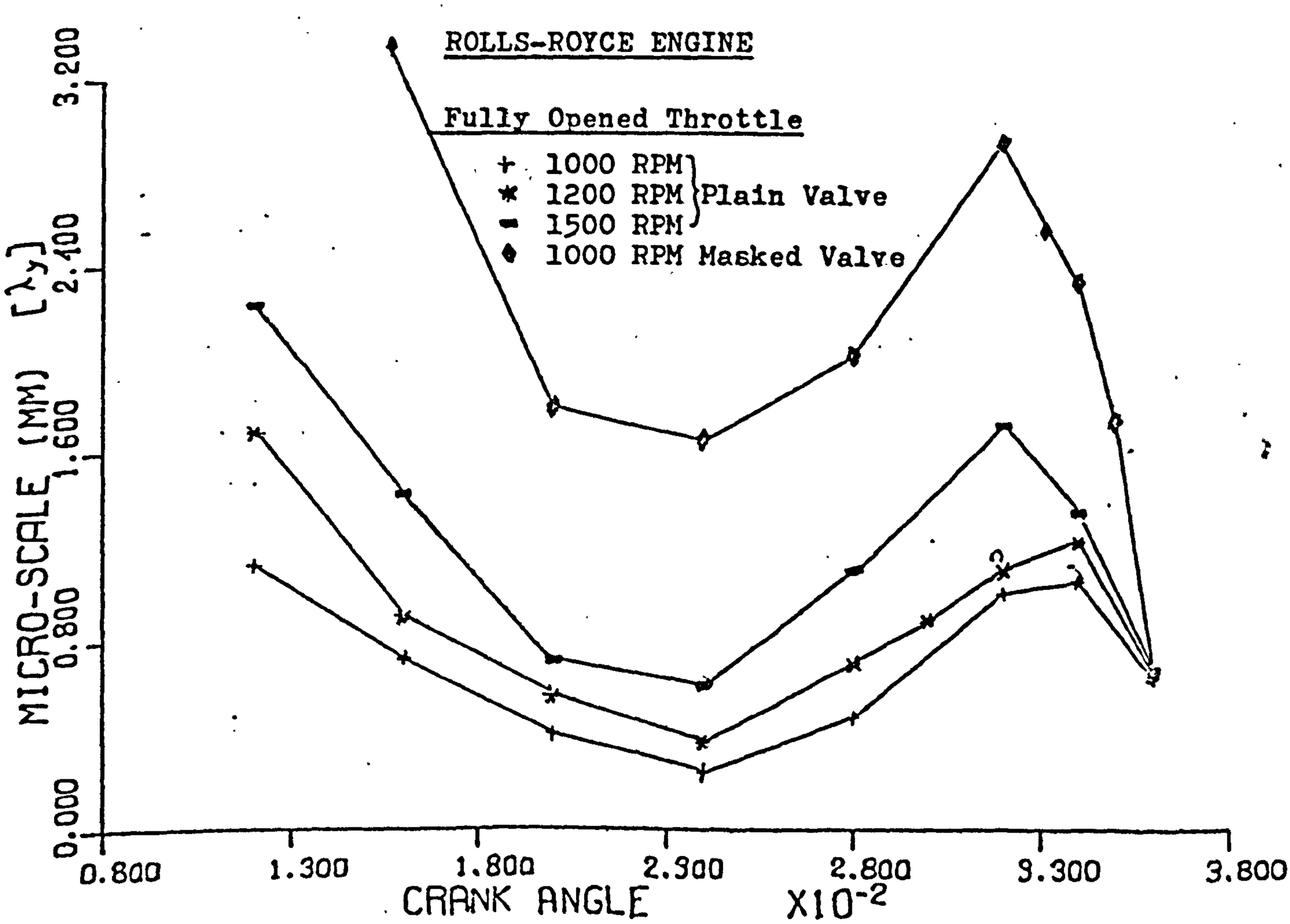

Fig (6-37d)

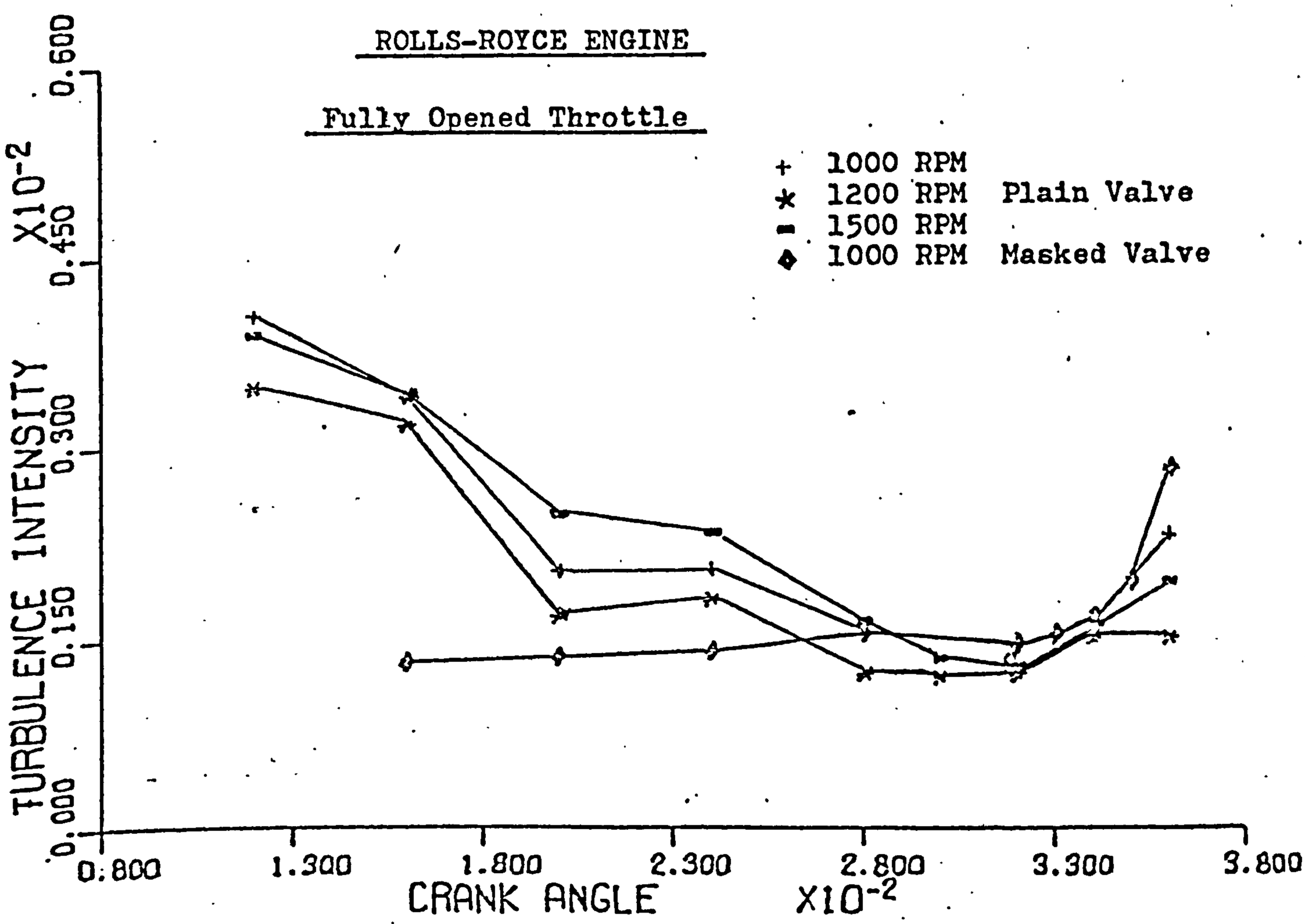
ROLLS-ROYCE ENGINE
Fully Opened Throttle
+ 1000 RPM
* 1200 RPM Plain Valve
■ 1500 RPM
◆ 1000 RPM Masked Valve
TURBULENCE INTENSITY X10-2
0.000
0.150
0.300
0.450
0.600
0.800
1.300
1.800
2.300
2.800
3.300
3.800
CRANK ANGLE X10-2

Fig (6-37e)

Fig. (6-38) Effect of Engine Speed and Throttling, at a Constant Loading Condition of 90 BMEP, on the Turbulence Characteristics inside a Heron Combustion Chamber.
(Ford V4 Engine, Inlet Valve Fitted with Six Vanes. Measurements at the Spark Plug Location, Horizontal Hot Wire at 3.8 mm from Cylinder Head Surface).

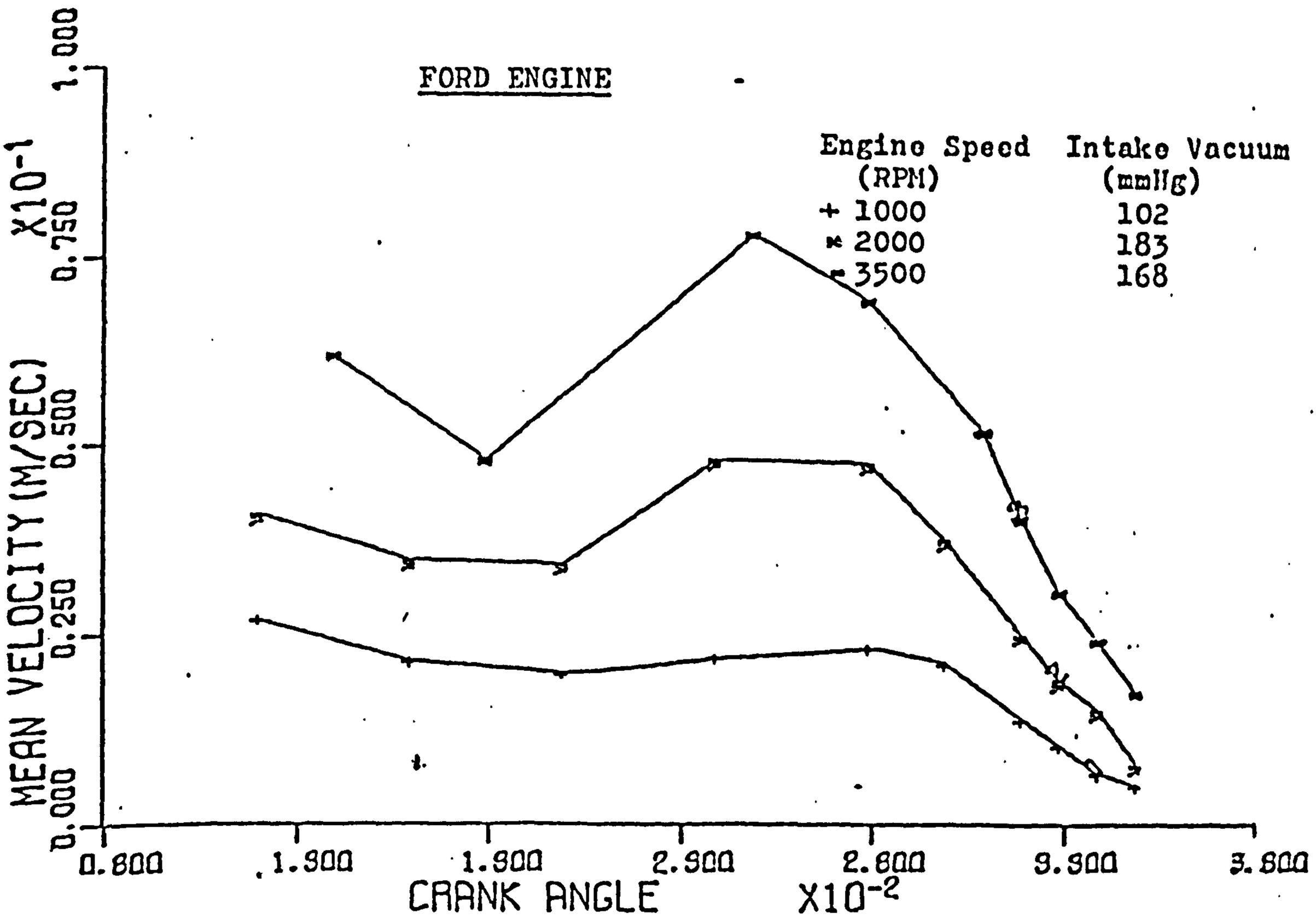

Fig (6-38a)

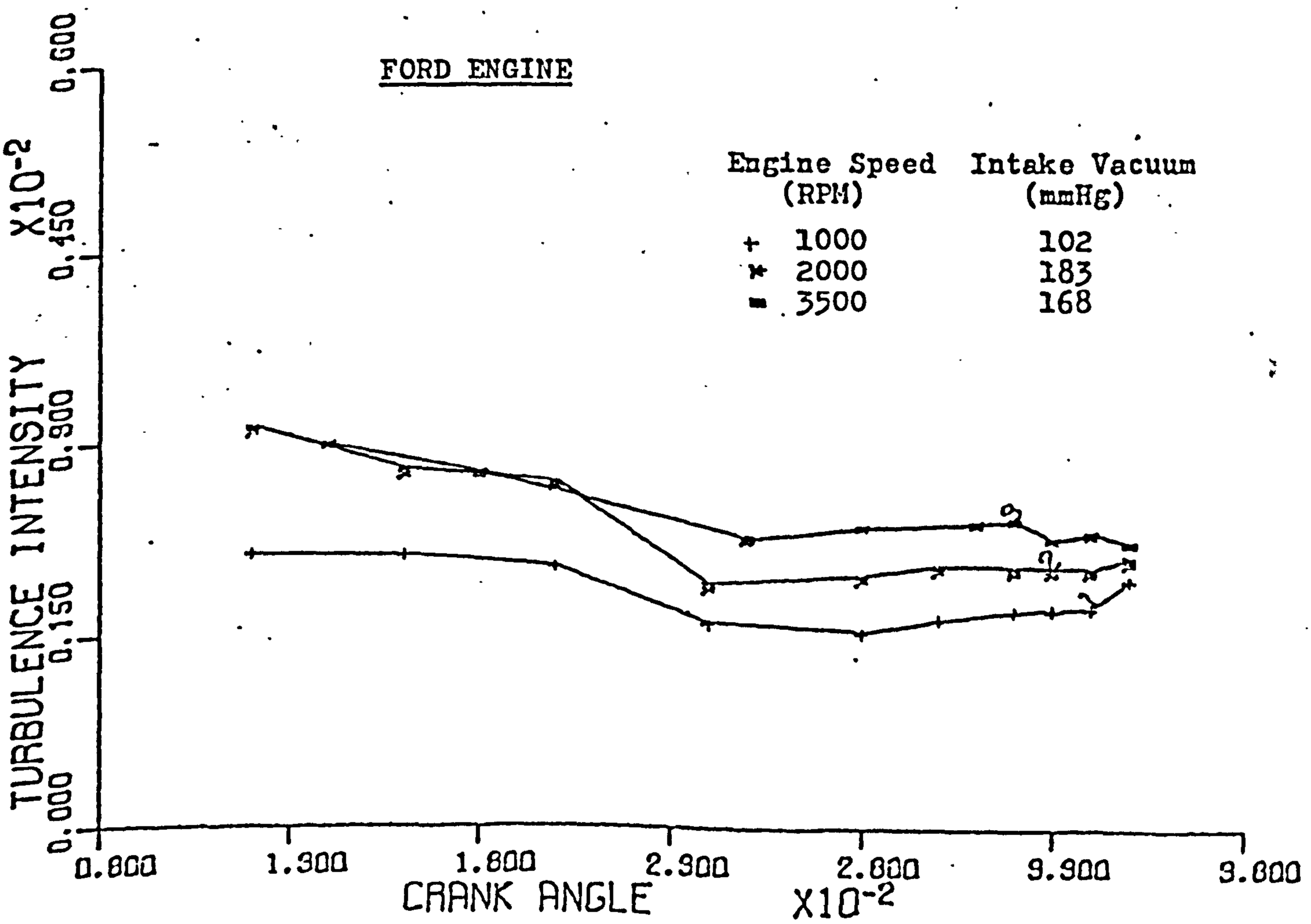

Fig (6-38b)

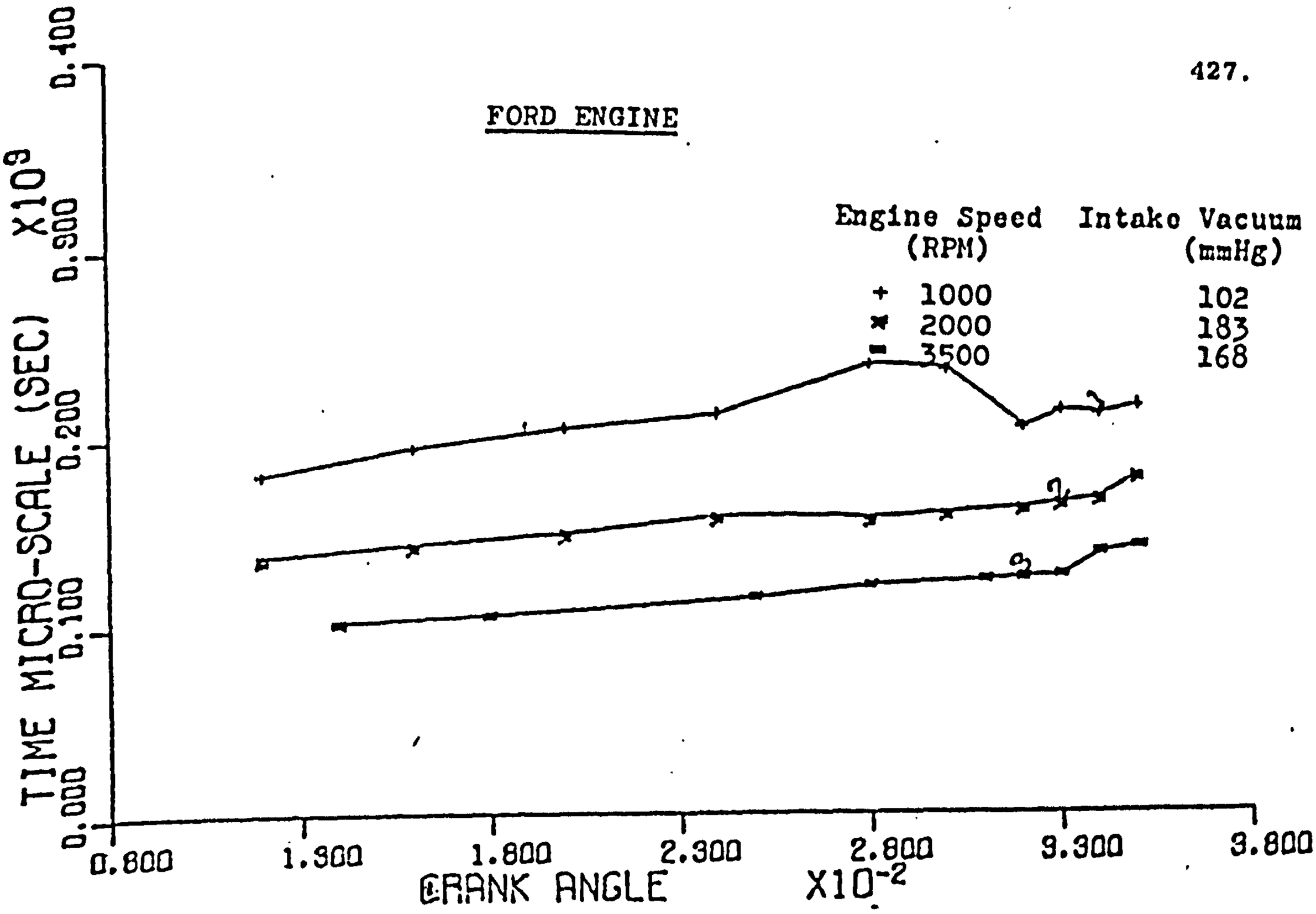

Fig (6-38c)

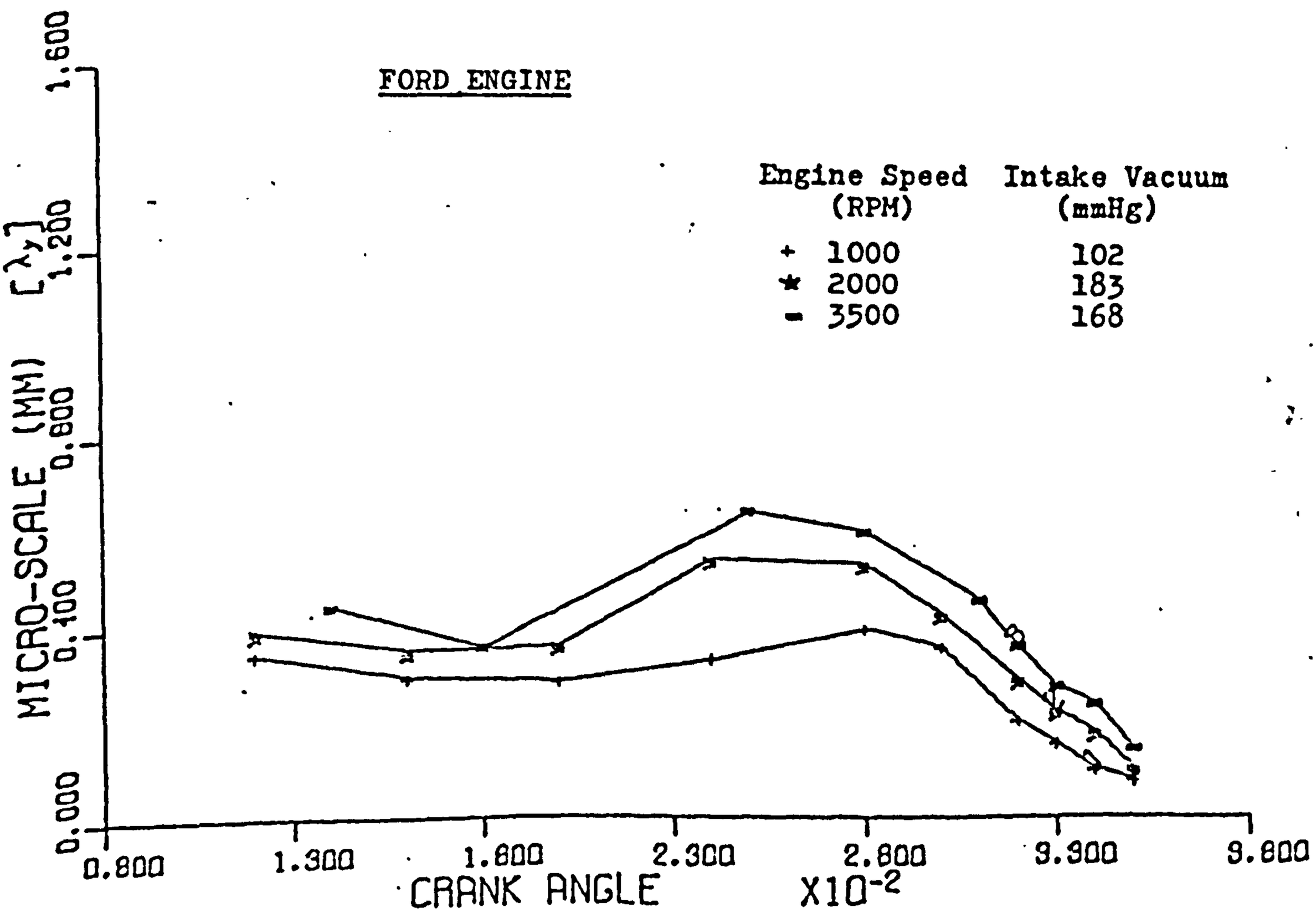

Fig (6-38d)

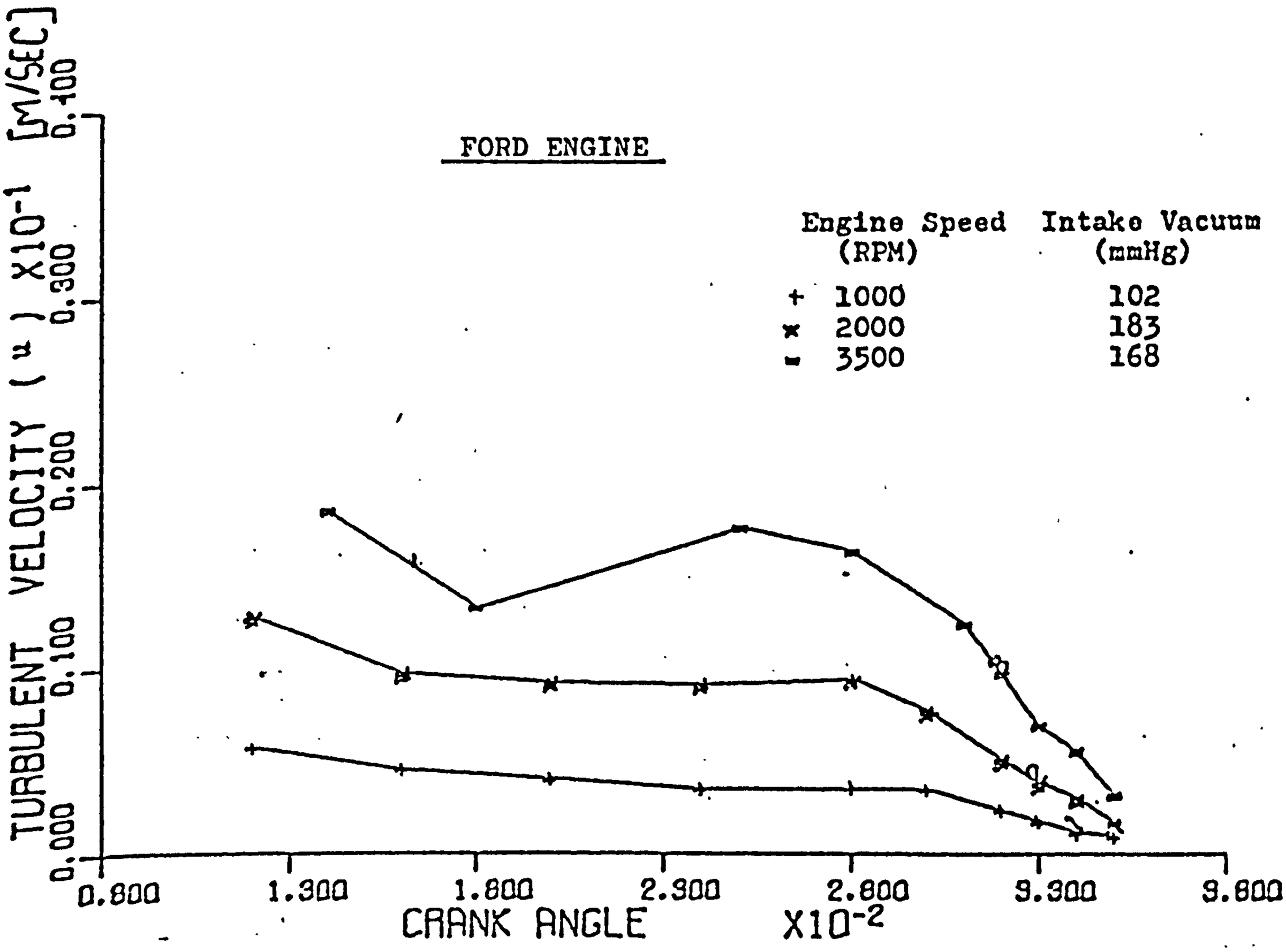
FORD ENGINE
Engine Speed (RPM)
Intake Vacuum (mmHg)
+ 1000 102
× 2000 183
▪ 3500 168
TURBULENT VELOCITY (u) X10-1 [M/SEC]
0.000
0.100
0.200
0.300
0.400
0.800
1.300
1.800
2.300
2.800
3.300
3.800
CRANK ANGLE X10-2

Fig (6-38e)

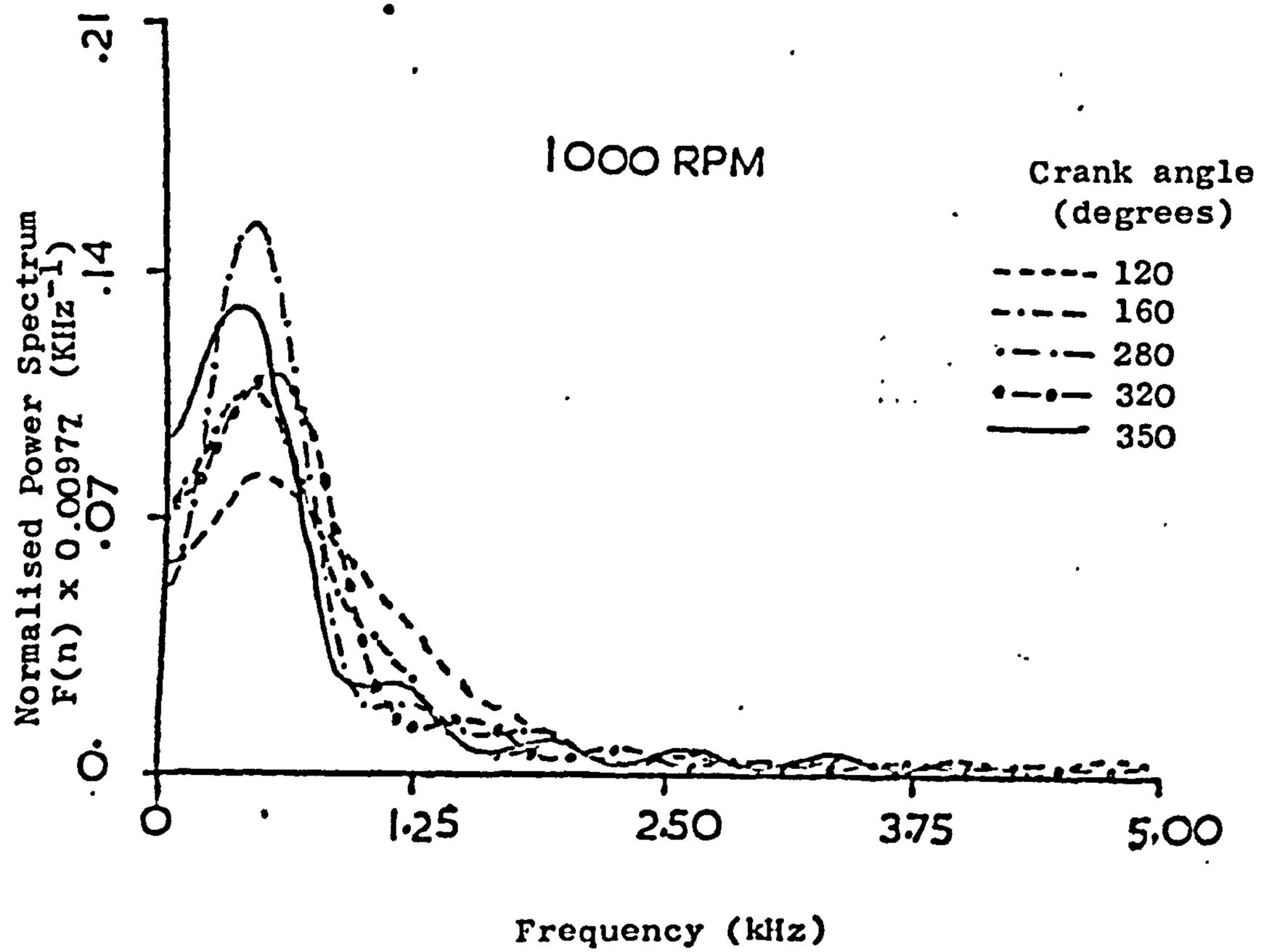

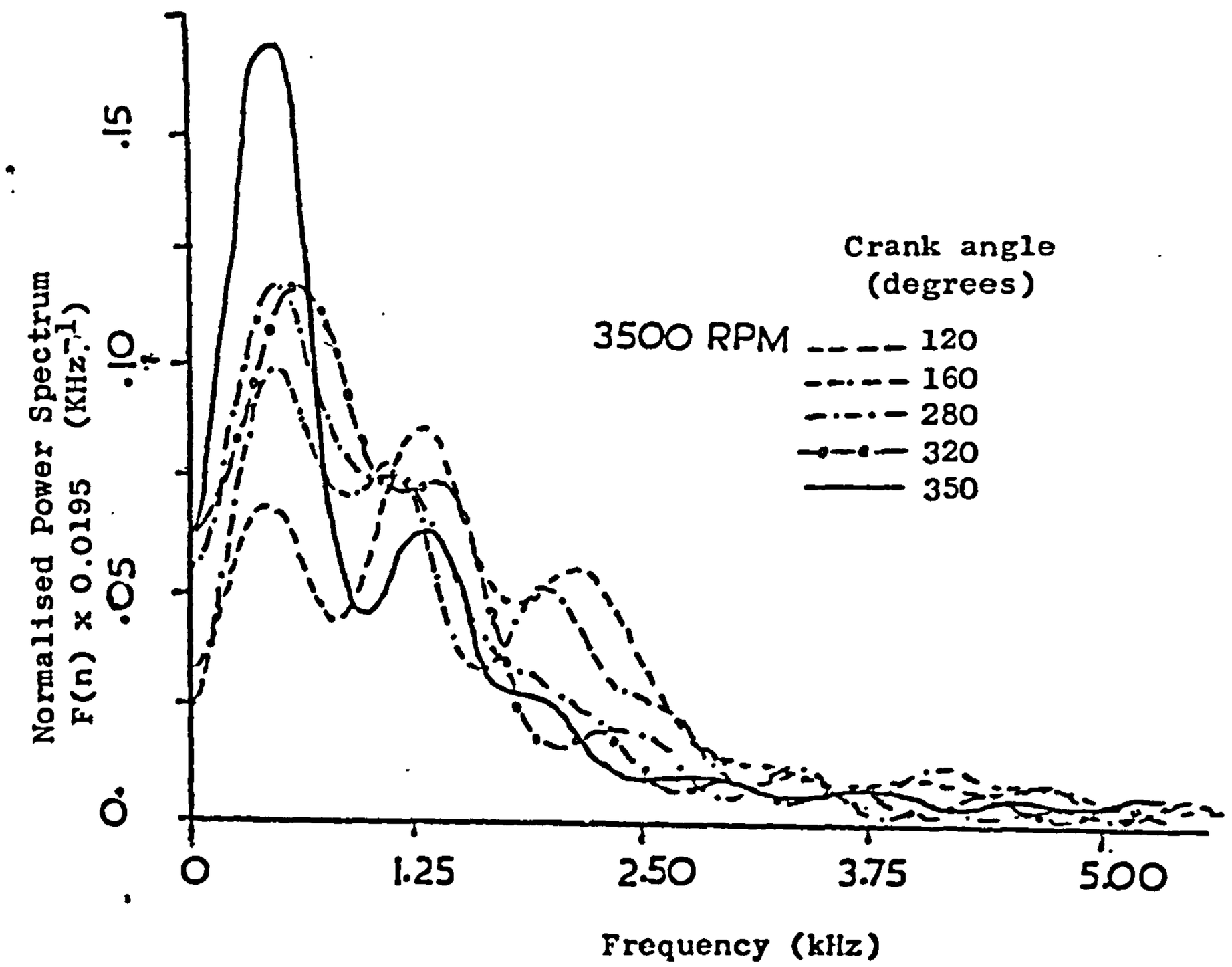

Fig. (6-38f) Effect of Engine Speed on the Frequency Composition of the Turbulence Field Inside a Heron Combustion Chamber Showing the Increase in the High Frequency Content of Turbulence Eddies at the Higher Speed. (Ford V4 Engine, Intake Vacuum = 102 mm Hg at 1000 RPM).
Intake Vacuum = 168 mm Hg at 3500 RPM).

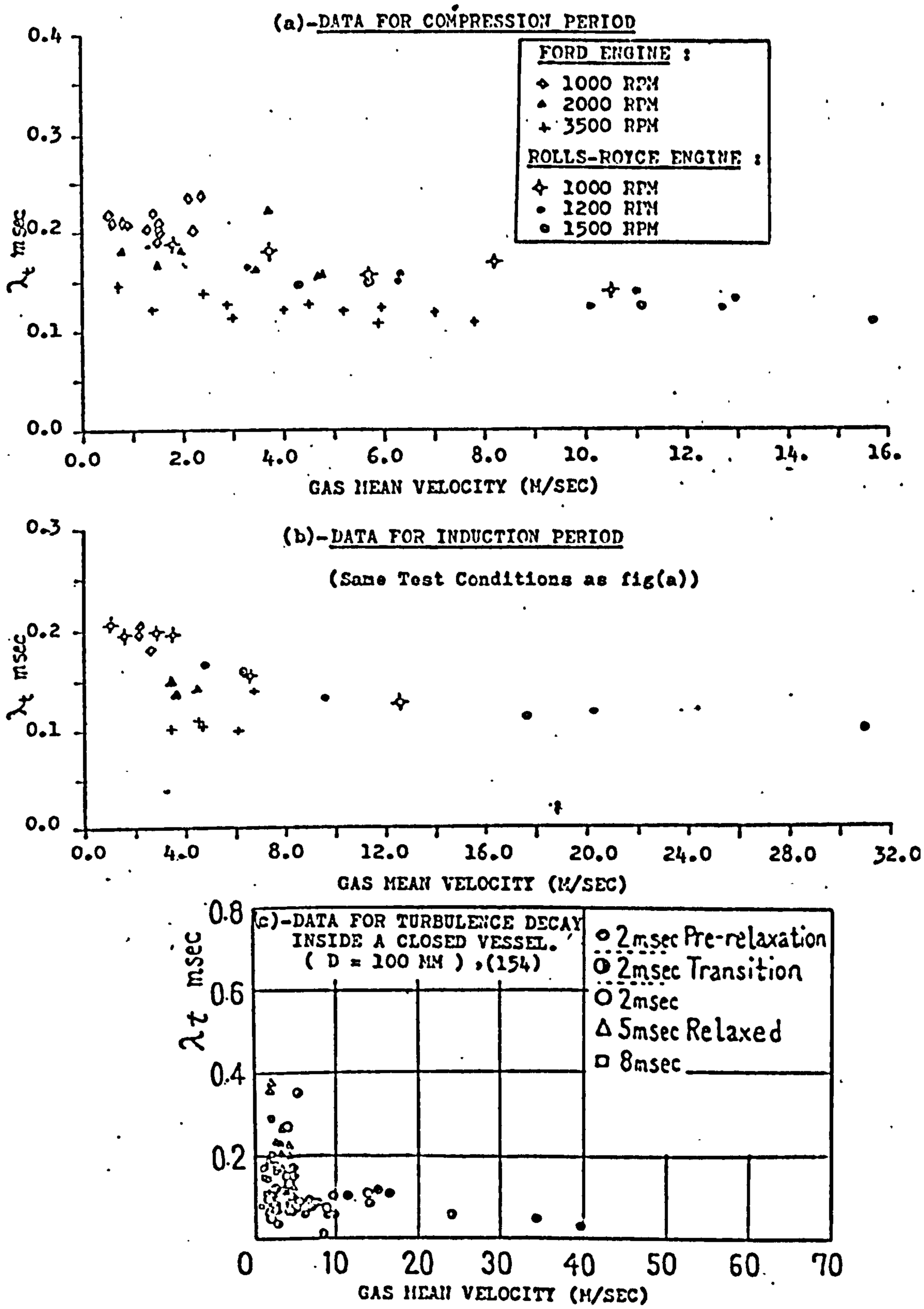

Fig (6-39) Variation of Time Micro-Scale with Gas Mean Velocity.

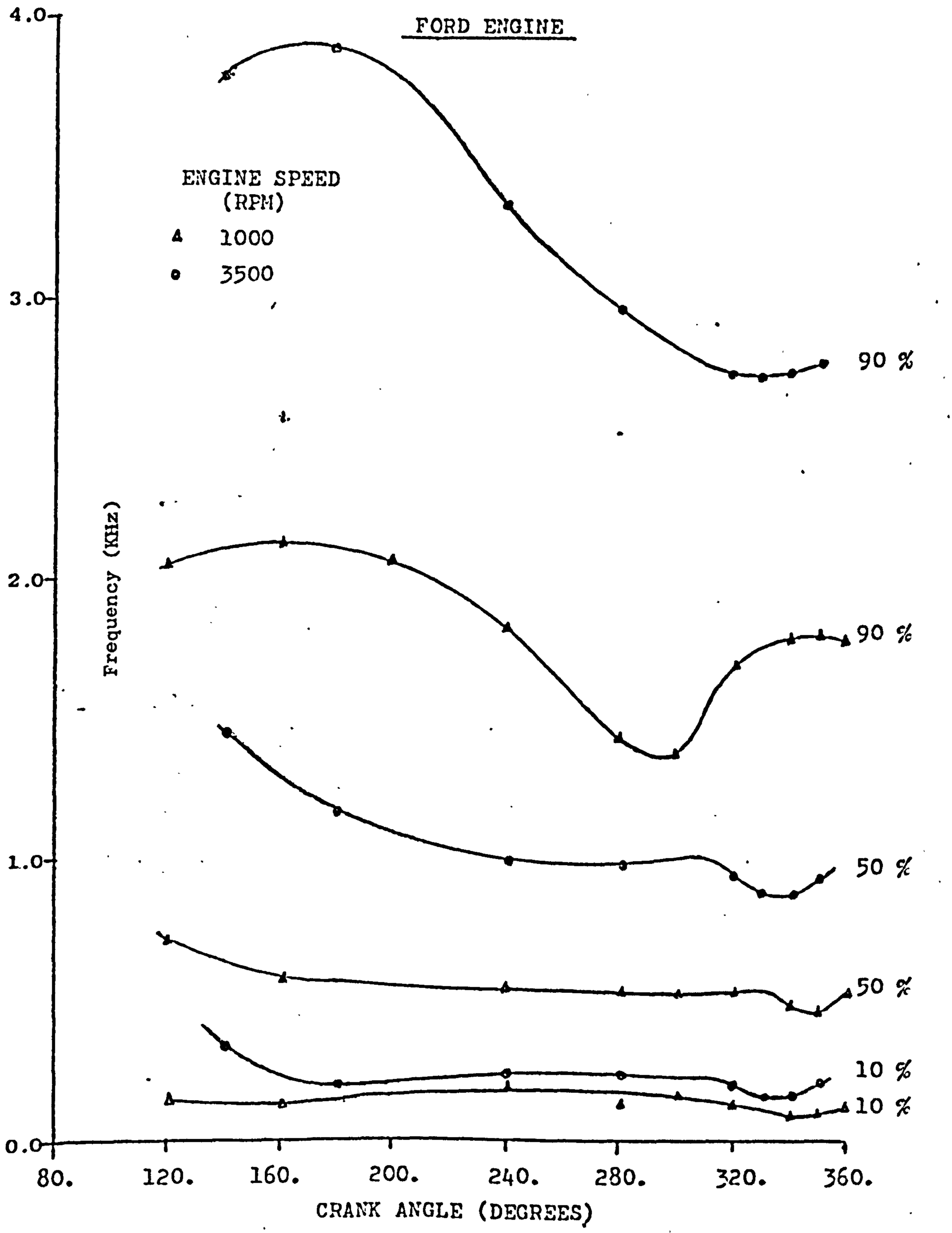

Fig. (6-40). Maximum Frequencies for Eddies Containing 10%, 50% and 90% of the Turbulence Energy at Two Different Engine Speeds. Test on a Heron Combustion Chamber. (Data from Fig. (6-38f).

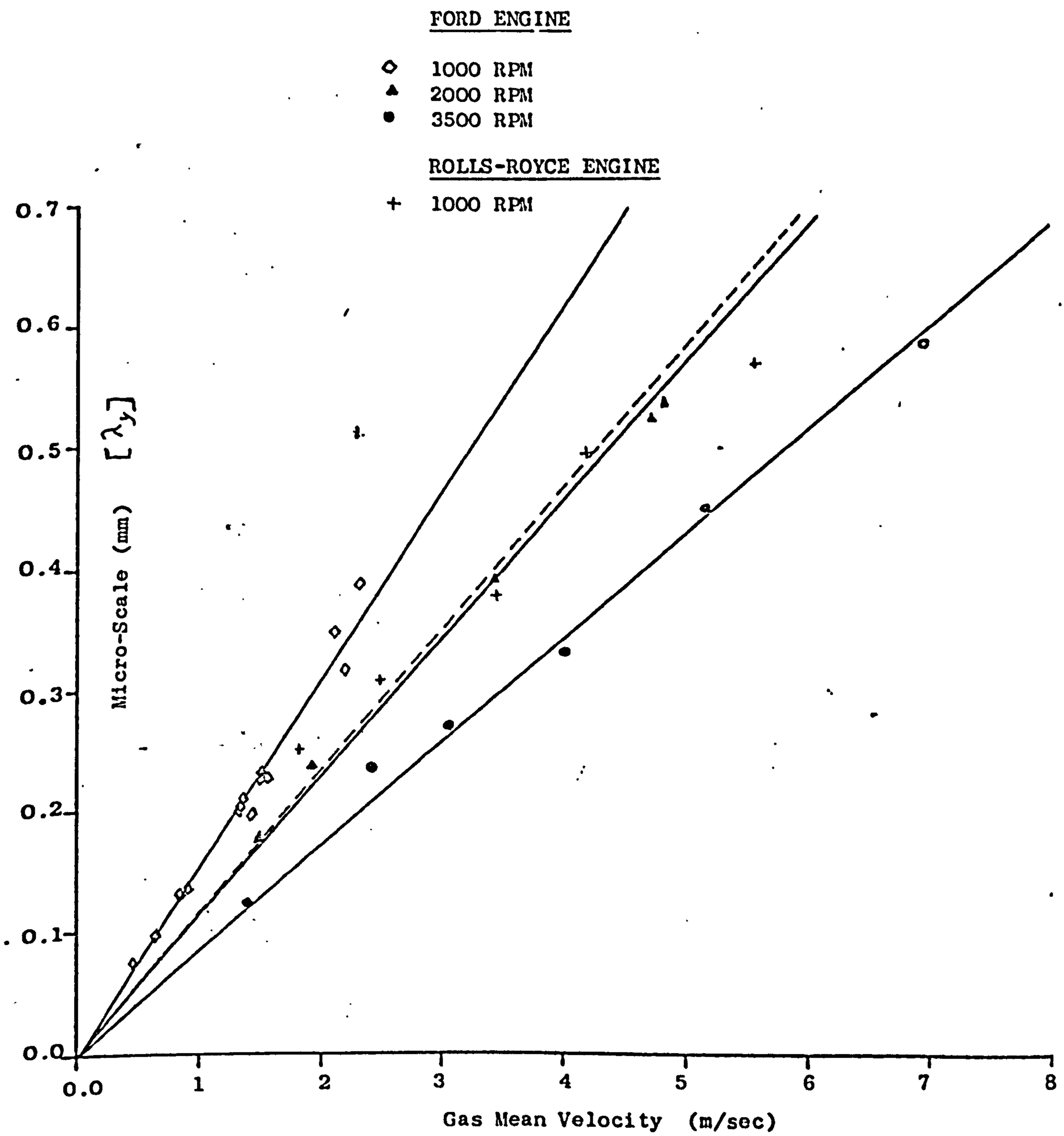

Fig. (6-41) Variation of the Micro-Scale of Turbulence with Gas Mean Velocity at Different Engine Speeds.

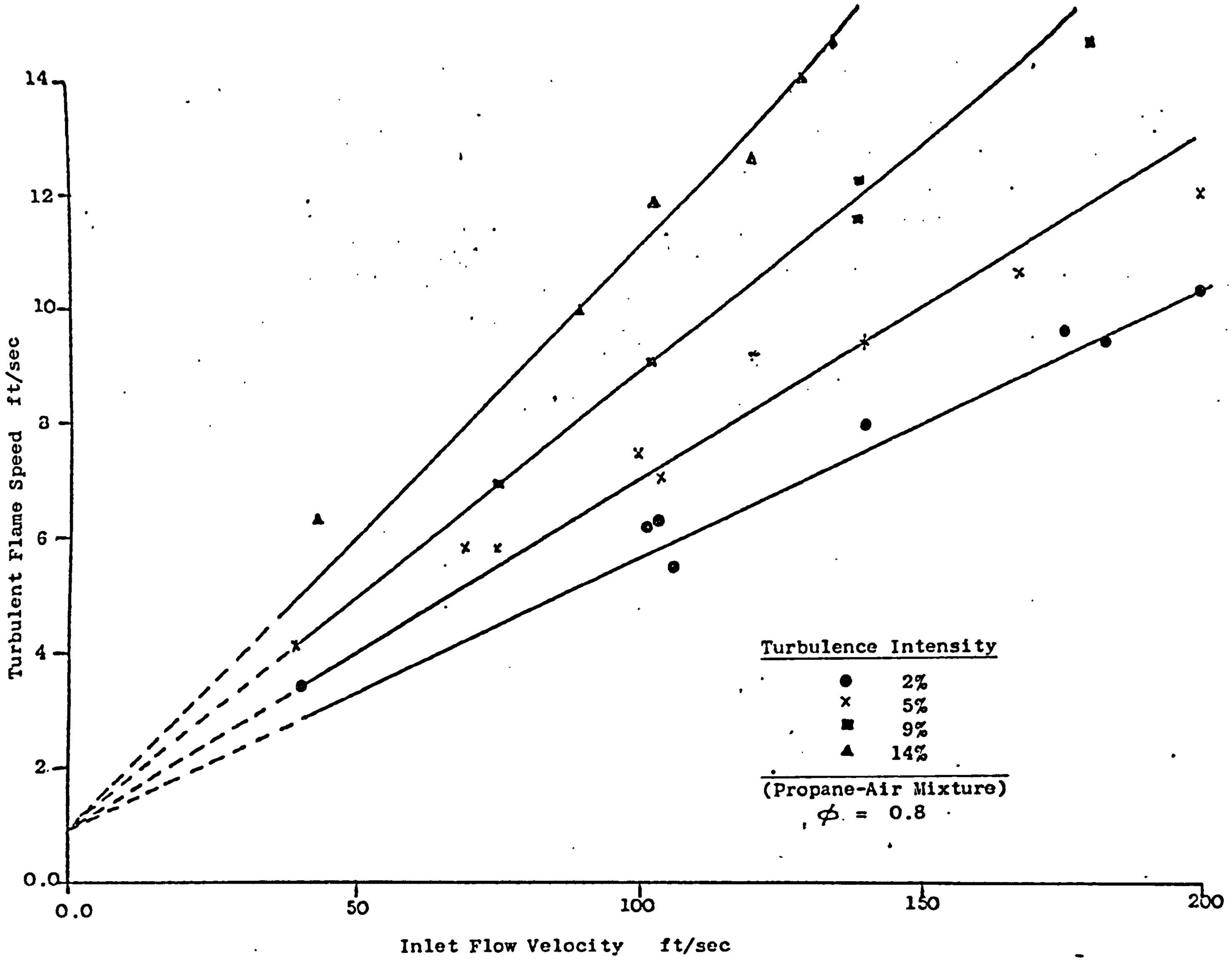

Fig. (6-42). Influence of turbulence fluctuations and mean velocity on turbulent flame speed at constant fuel/air ratio, (49)

Fig. (6-43) Effect of Throttling on the Turbulence Characteristics Inside a Heron Combustion Chamber of a Ford V4 Engine.

a) Engine Speed = 3500 RPM, Horizontal Hot Wire at 3.8 mm from Cylinder Head Surface, Inlet Valve with Six Vanes.

a1 - Intake Vacuum = 168 mm Hg

a2 - Intake Vacuum = 310 mm Hg

b) Engine Speed = 1000 RPM, Horizontal Hot Wire at the Level of Cylinder Head Surface, Plain Inlet Valve.

b1 - Intake Vacuum = 102 mm Hg

b2 - Intake Vacuum = 282 mm Hg

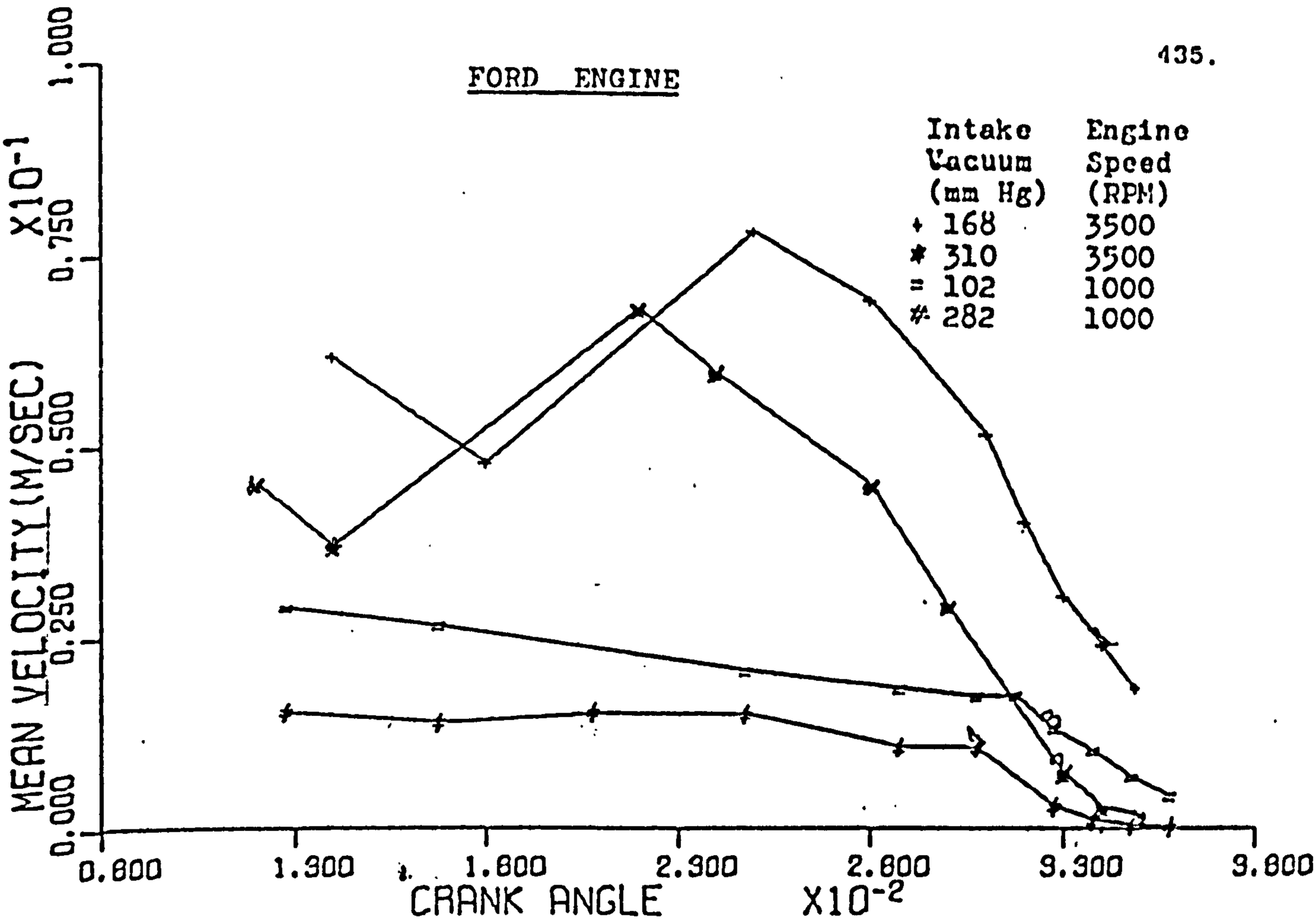

Fig (6-43a)

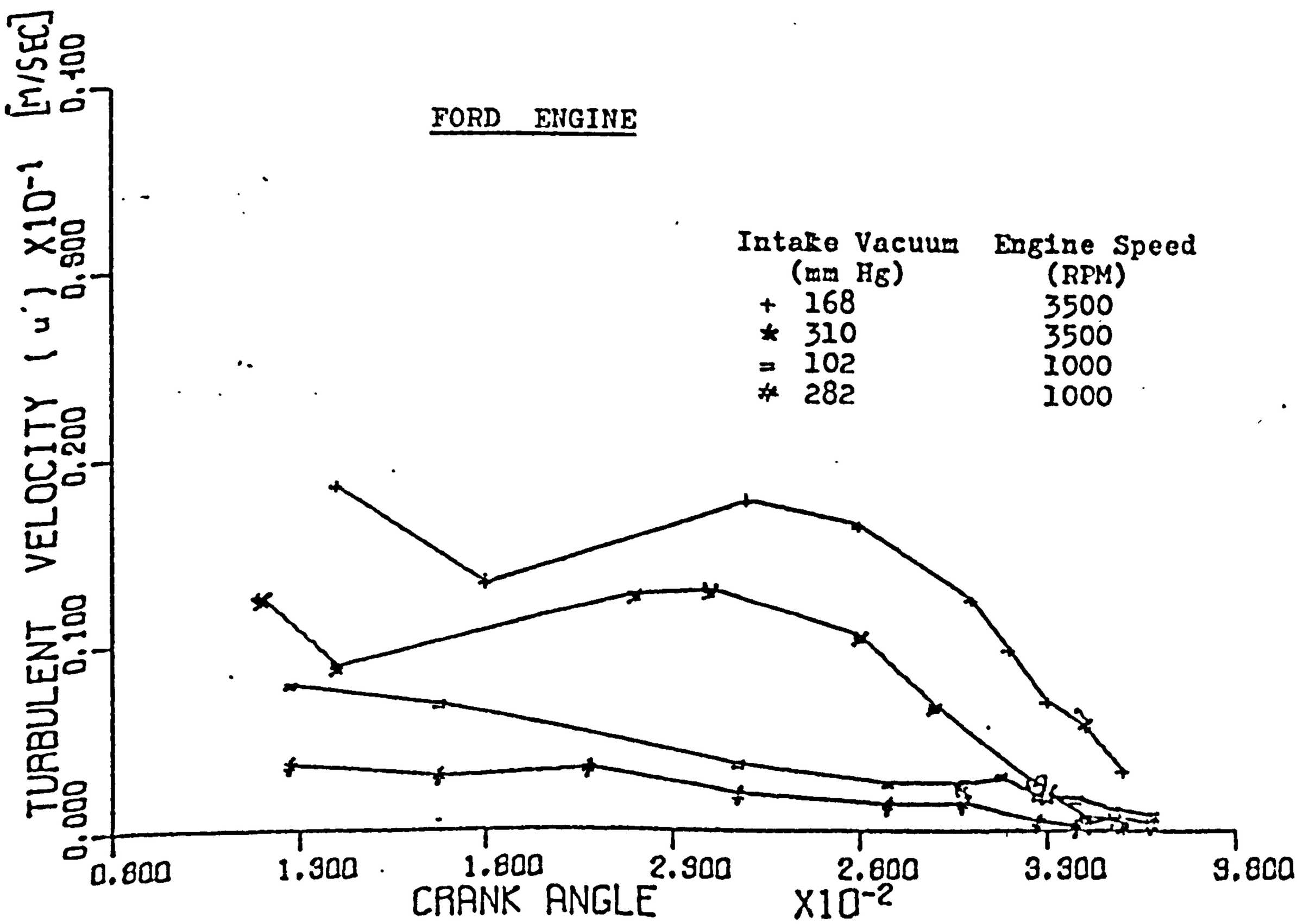

Fig (6-43b)

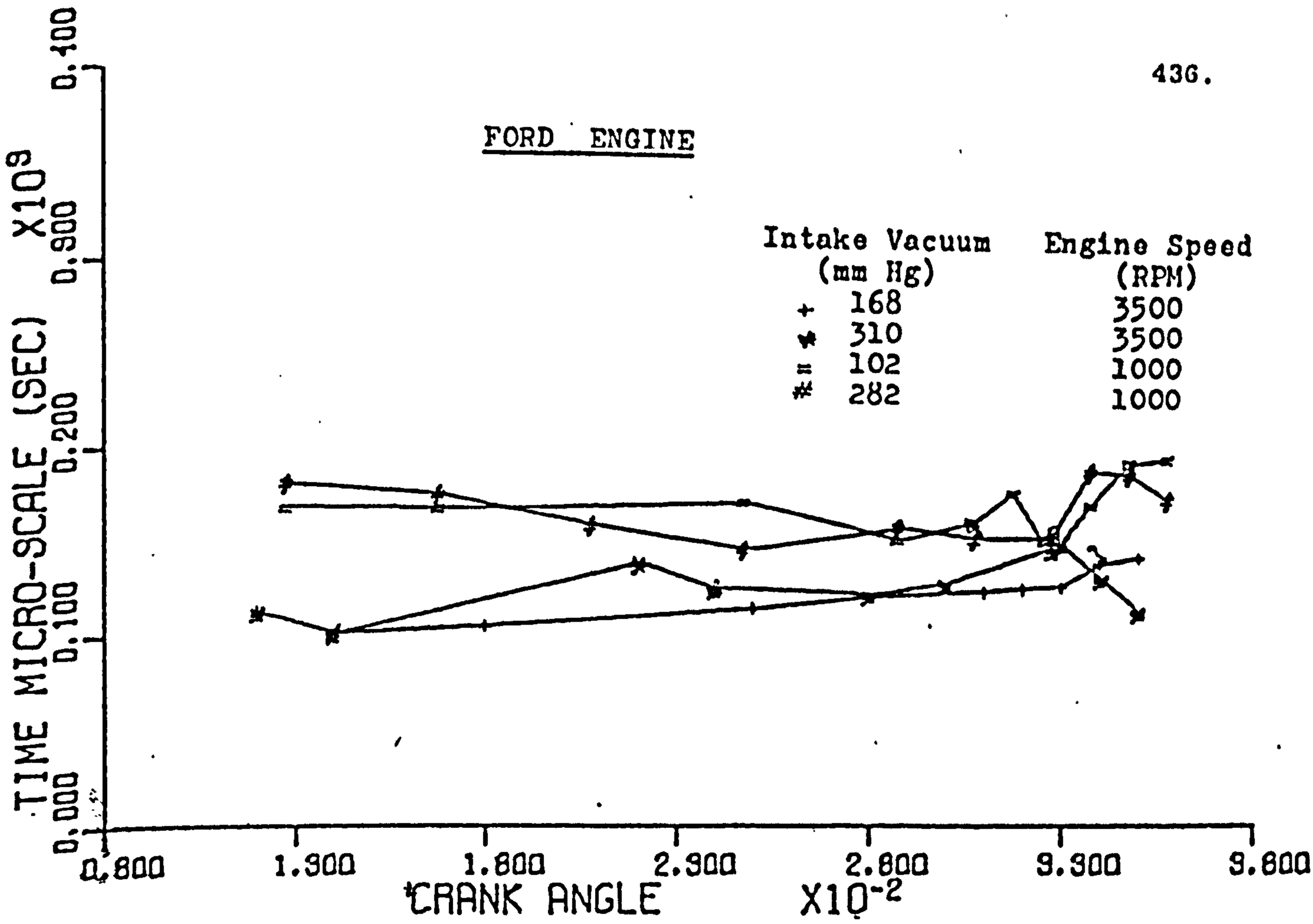

Fig (6-43c)

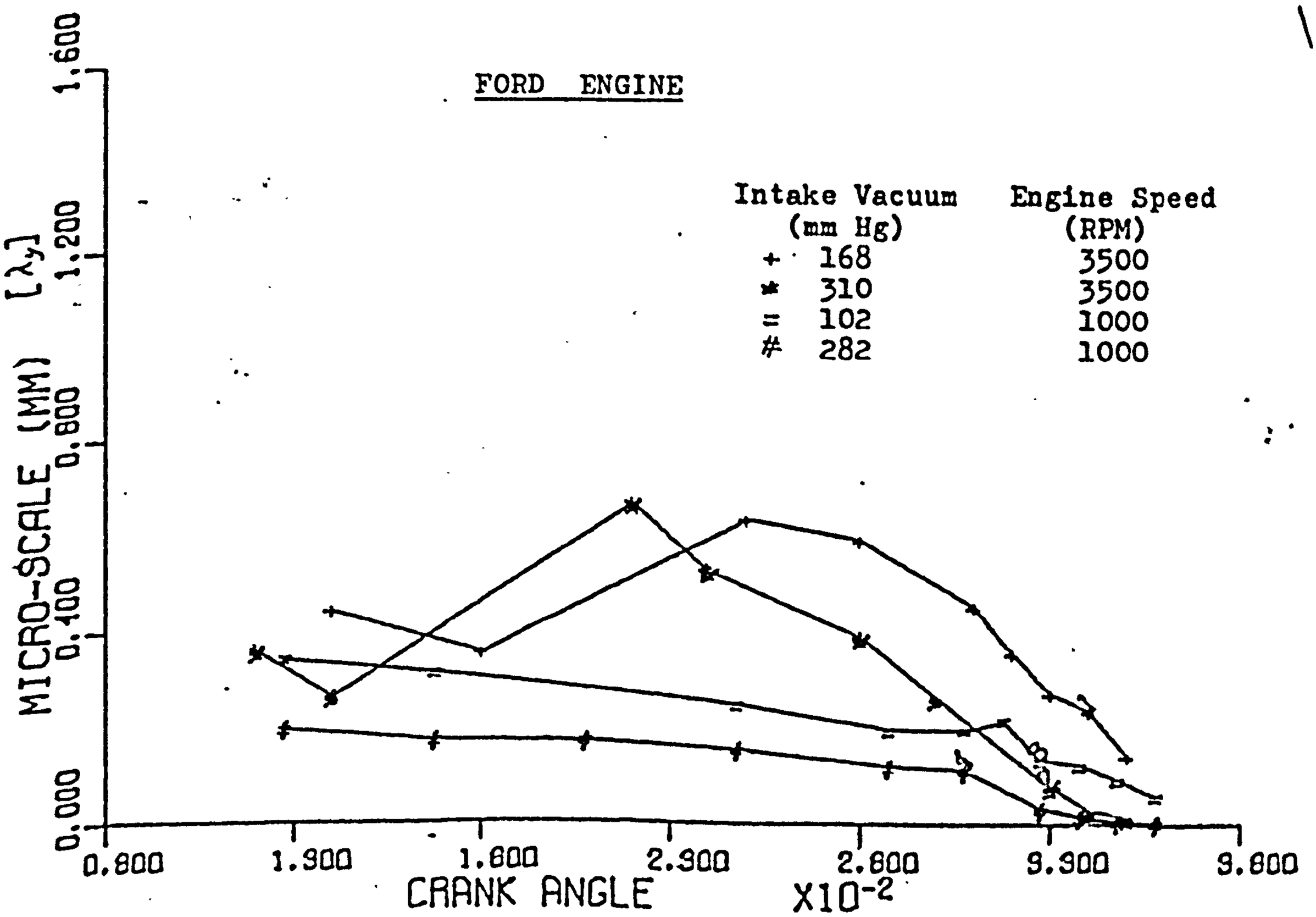

Fig (6-43d)

FORD ENGINE

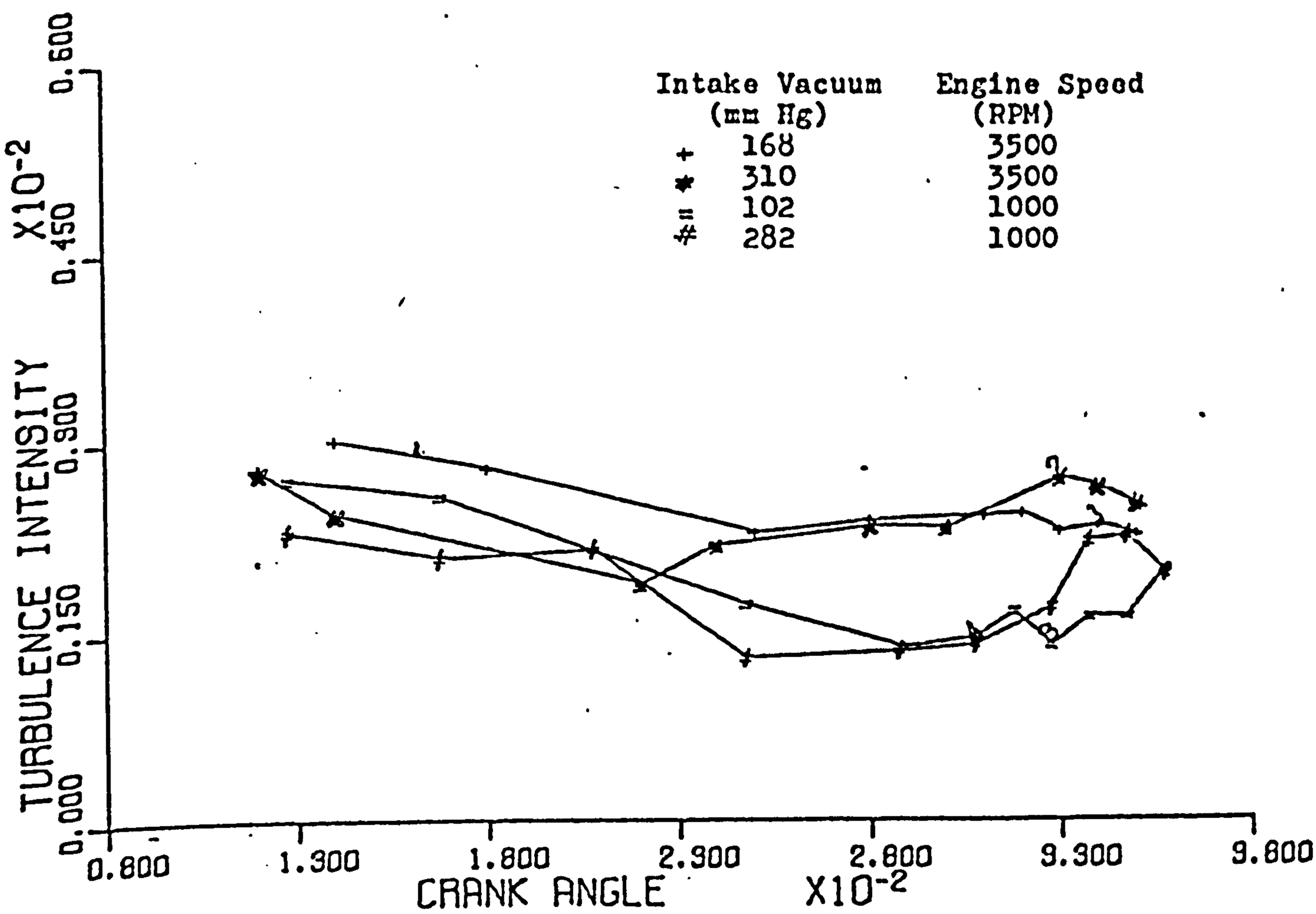

Fig (6-43e)

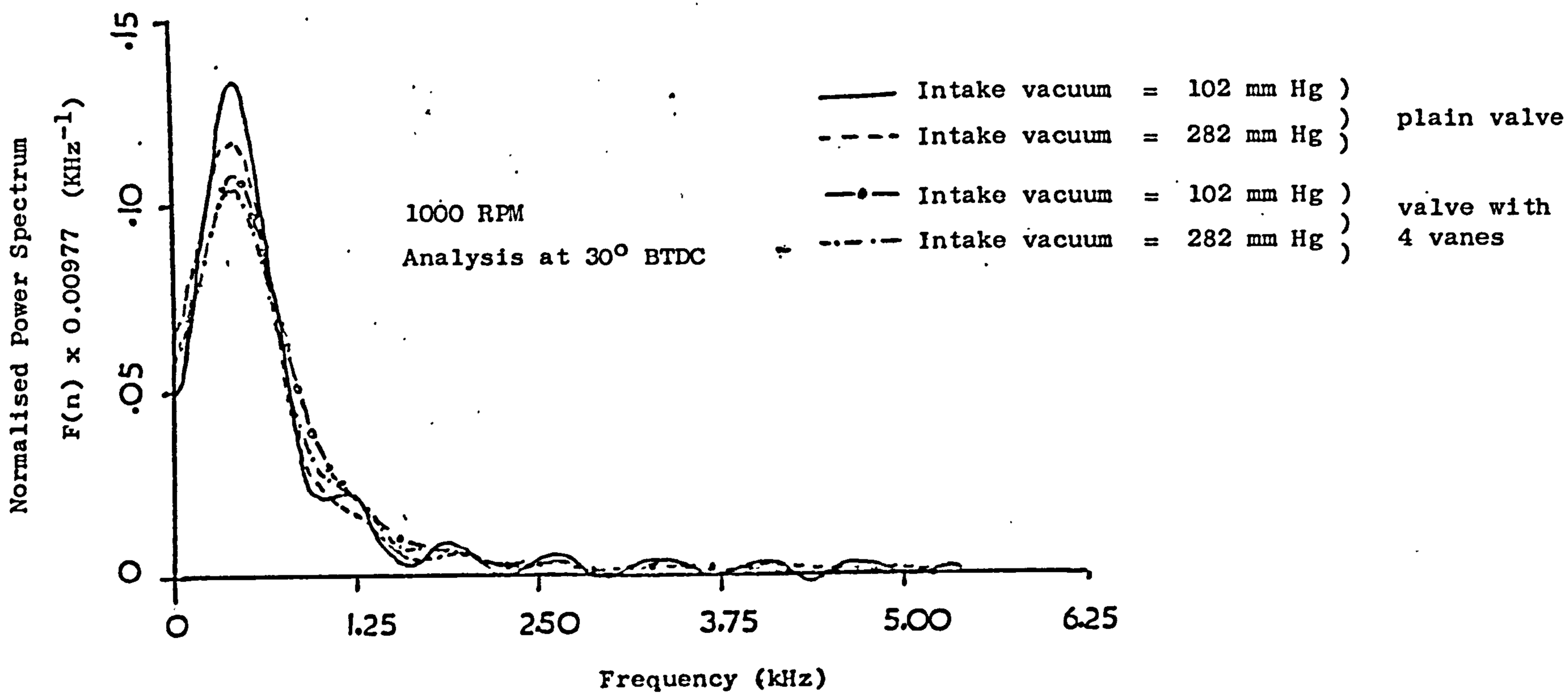

Fig. (6-43f) Variation of Power Spectrum Function with Throttling During Compression. (Ford V4 Engine, Probe at the Spark Plug Location, Horizontal Wire at 3.8 mm from the Cylinder Head Surface).

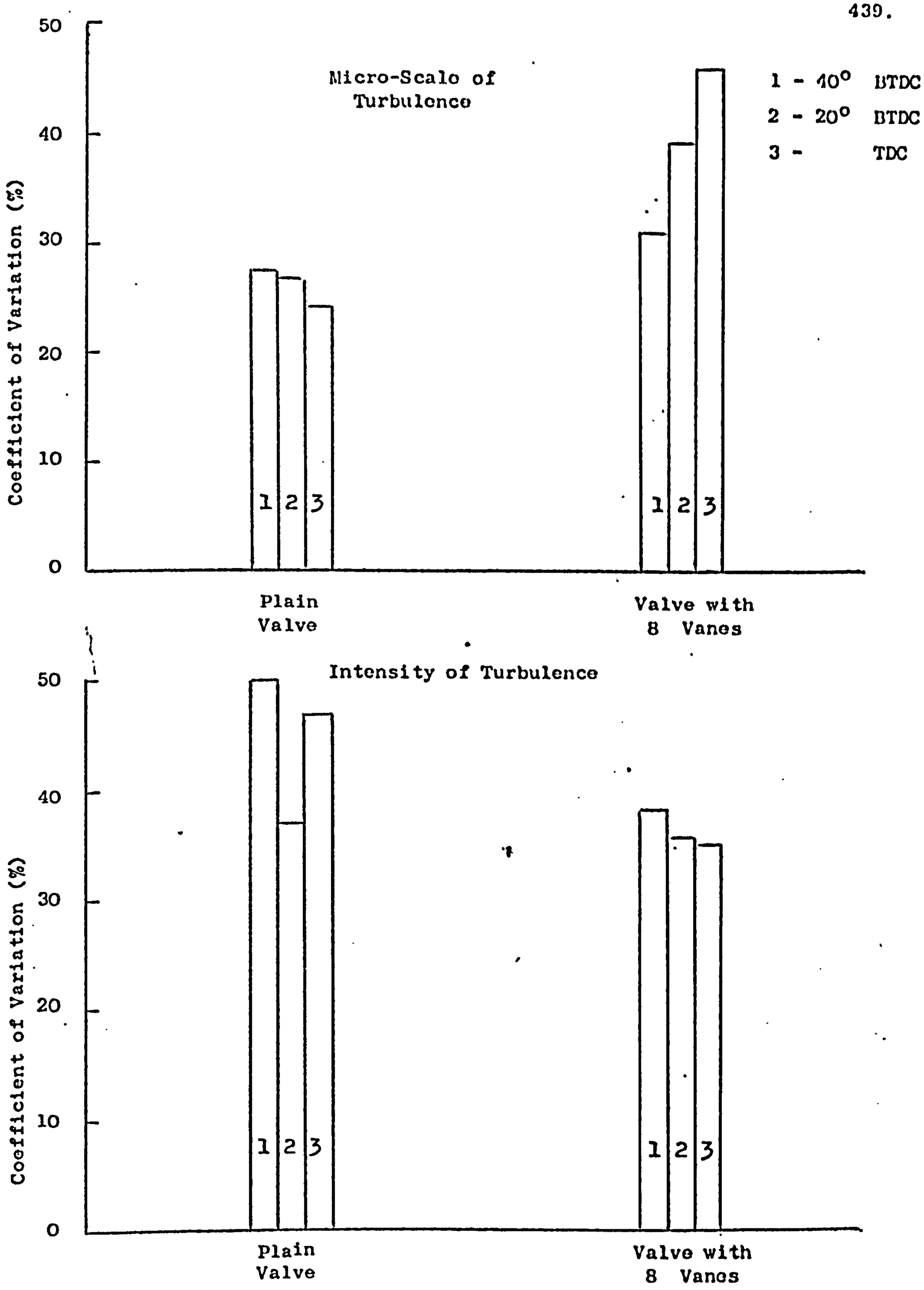

Fig. (6-44) Statistical Analysis of Cyclic Variation in Turbulence Characteristic Parameters. Rolls-Royce Engine, 1000 RPM and Fully Opened Throttle.

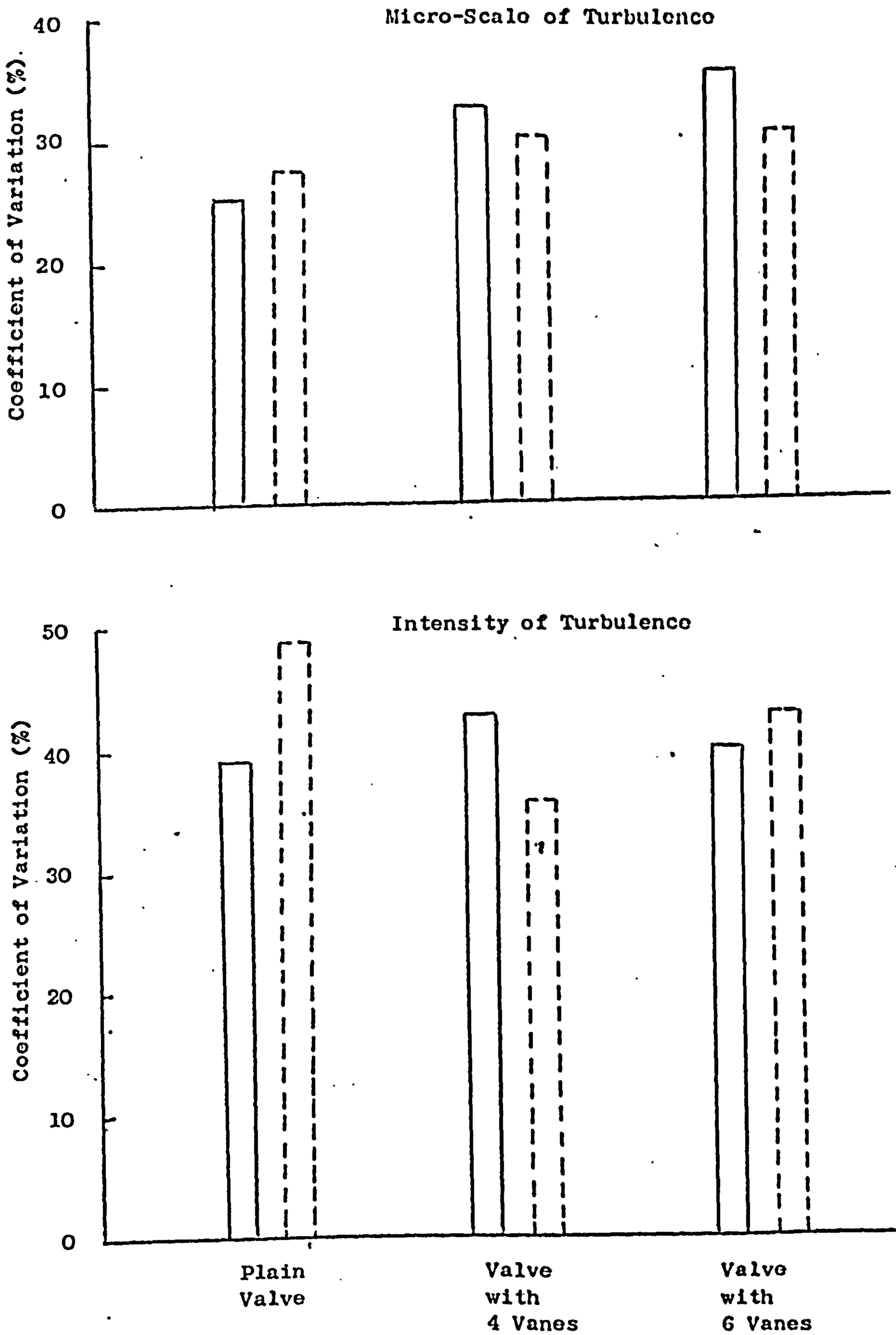

Fig. (6-45) Statistical Analysis of Cyclic Variation in Turbulence Characteristic Parameters (Ford Engine at 1000 RPM) and 10° BTDC.

---- Intake Vacuum = 282 mm Hg

—— Intake Vacuum = 102 mm Hg

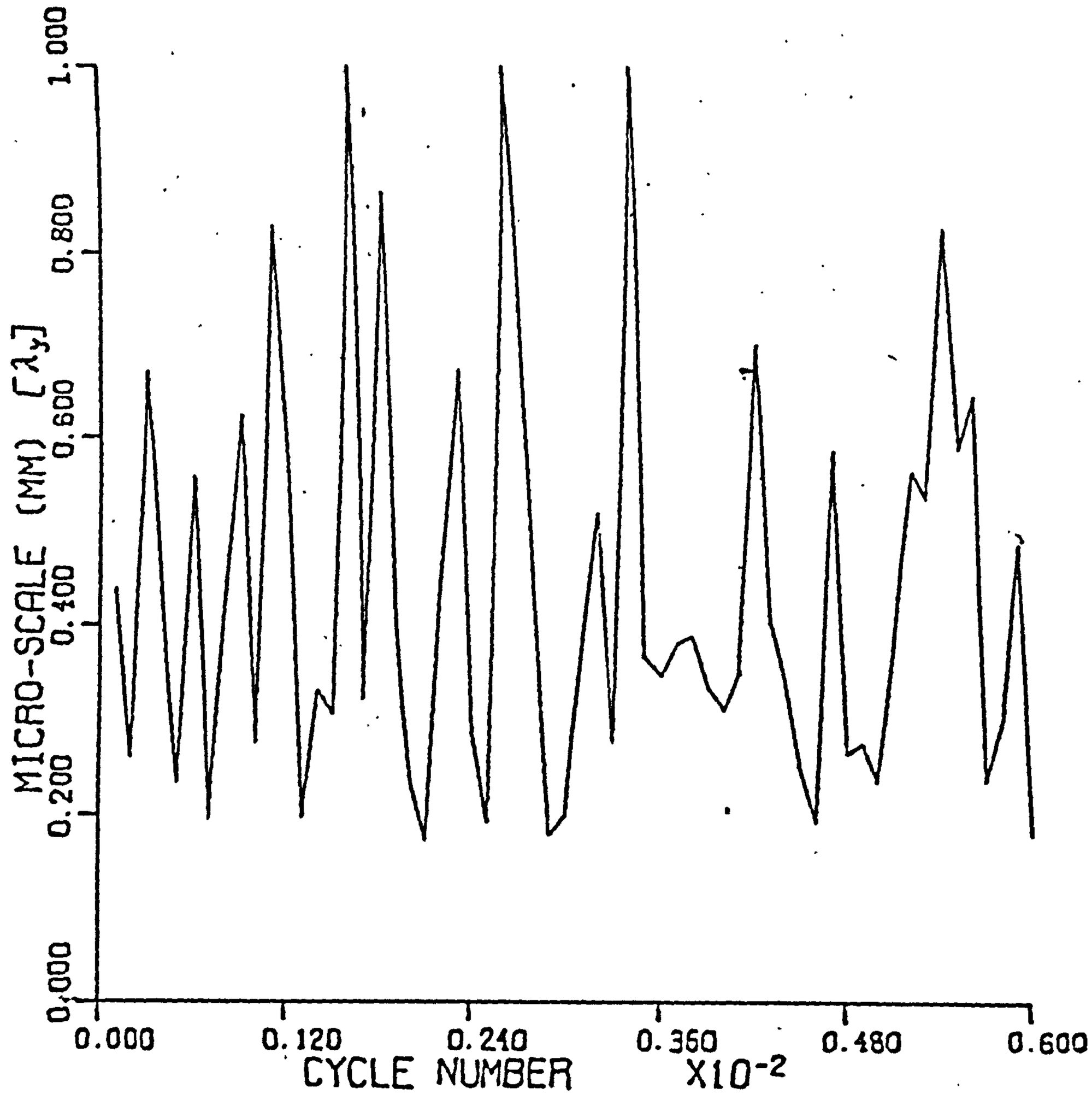

Fig. (6-46a) An Example of the Cyclic Variation in Micro-Scale of Turbulence Inside a Wedge Combustion Chamber at 40 degrees BTDC. Analysis for 60 consecutive cycles, Rolls-Royce Engine, Inlet Valve with 8 Vanes, 1000 RPM and Fully Opened Throttle.

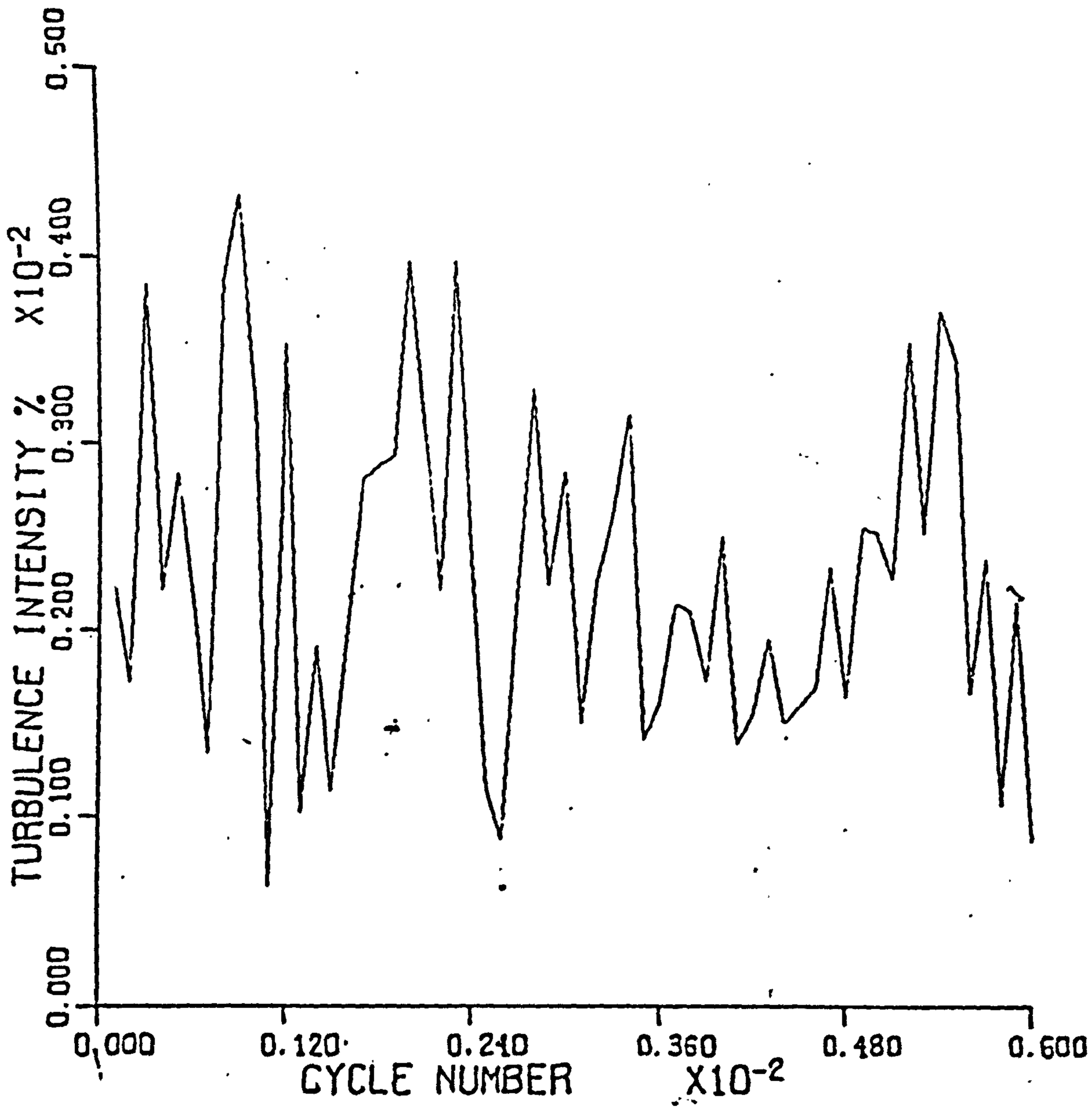

Fig. (6-46b) An Example of the Cyclic Variation in the Turbulence Intensity Inside a Wedge Combustion Chamber at 40 degrees BTDC. (Same test conditions as Fig. 6-46a).

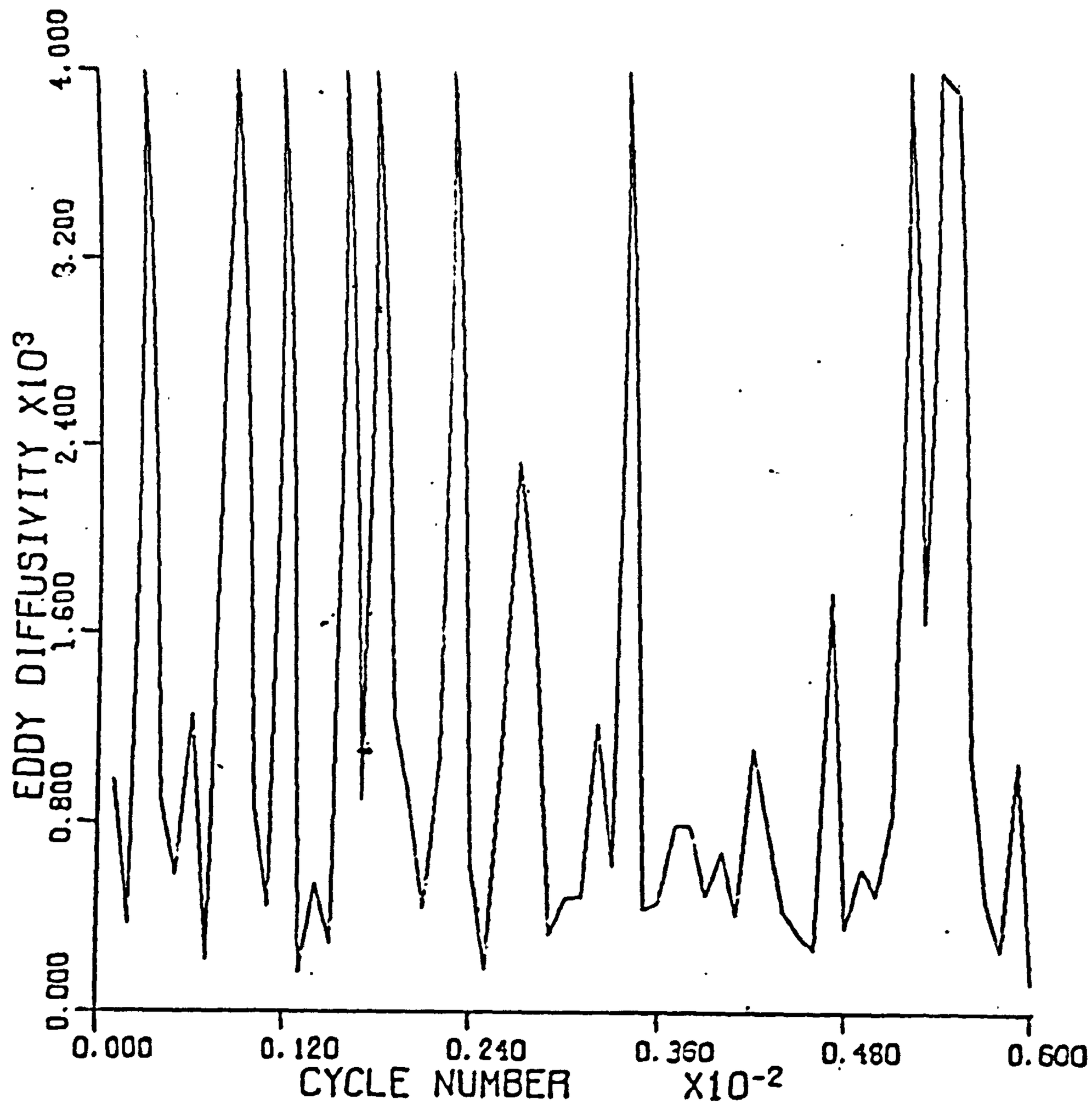

Fig. (6-46c) An Example of the Cyclic Variation in Eddy Diffusivity Inside a Wedge Combustion Chamber at 40 degrees BTDC. (Same test conditions as Fig. 6-46a).

Fig. (6-47) Effect of Intake System Modifications and the Use of a Local Turbulence Promoter at the Spark Plug on the Turbulence Characteristics in a Wedge Combustion Chamber.
Analysis of 124 Cycles, Rolls-Royce V8 Engine, Compression Ratio = 9:1, 1000 RPM and Fully Opened Throttle.

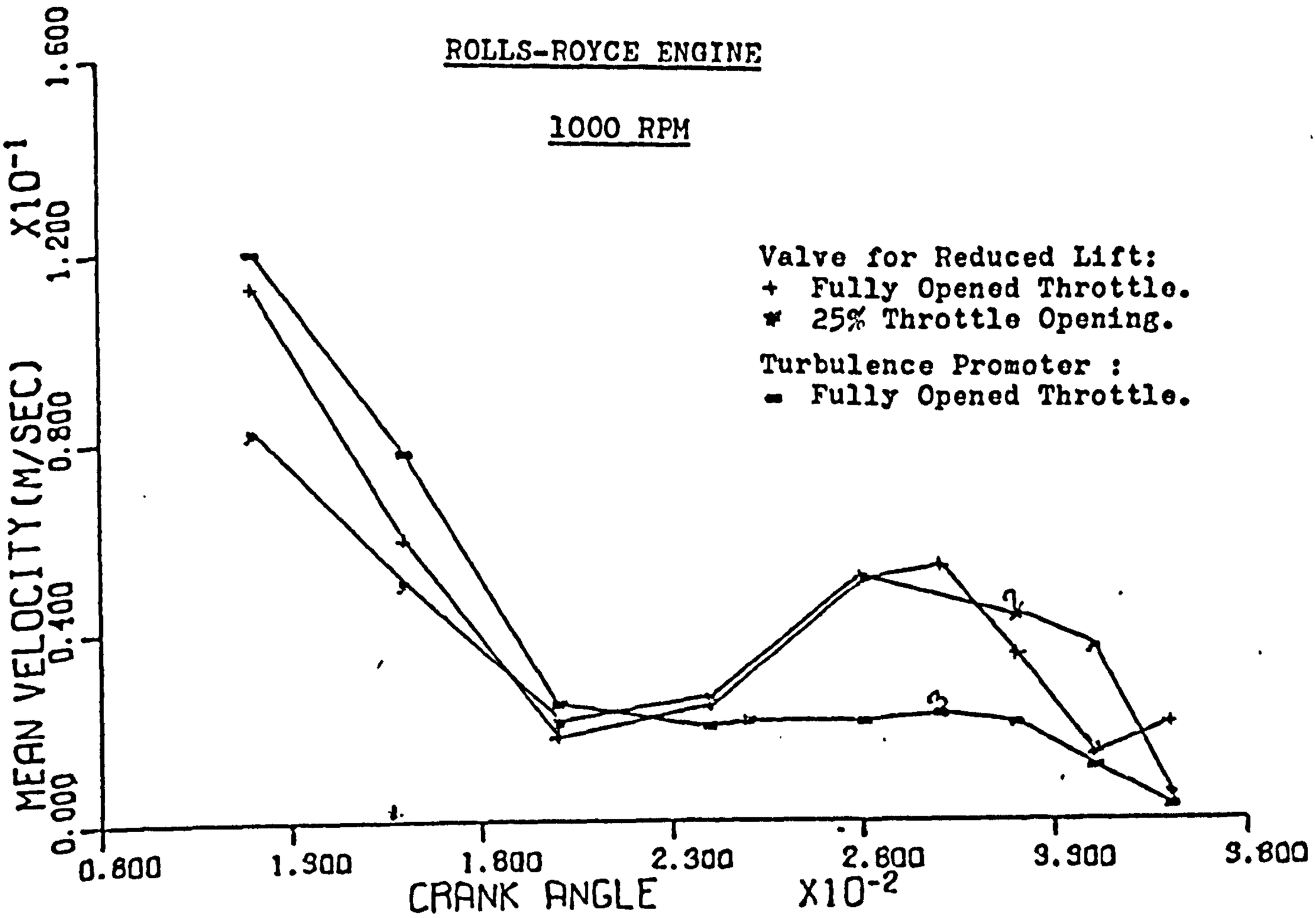

Fig (6-47a)

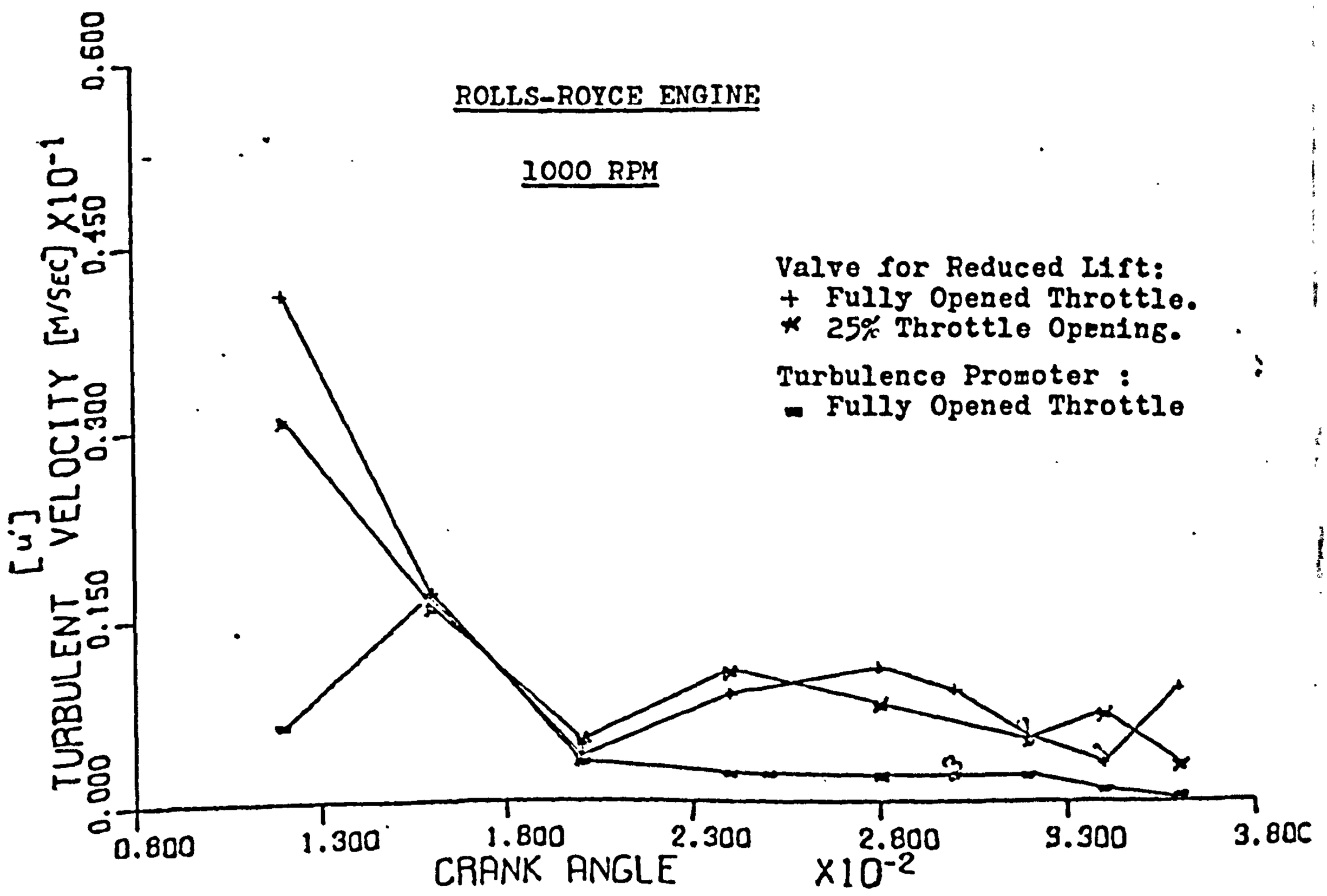

Fig (6-47b)

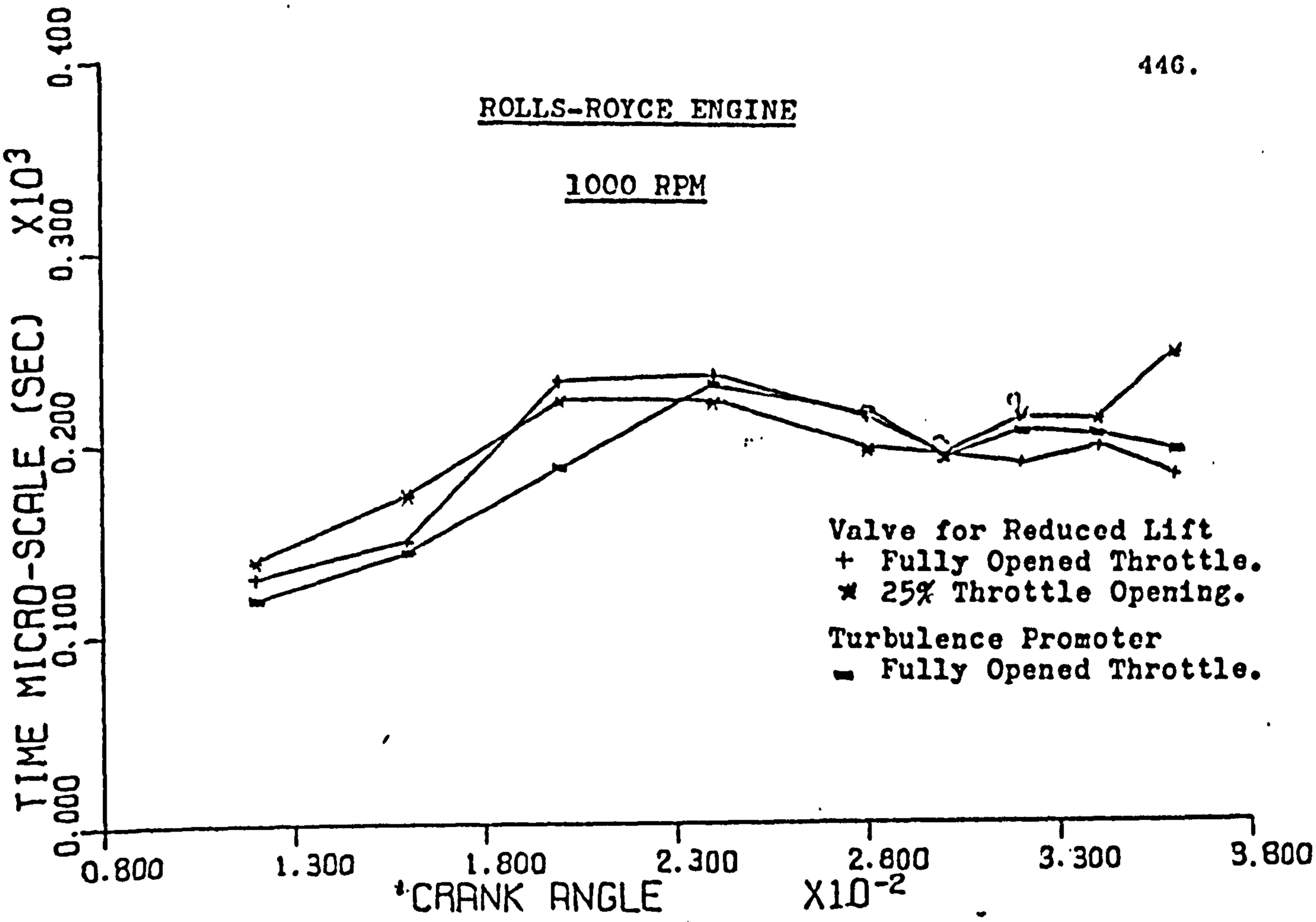

Fig (6-47c)

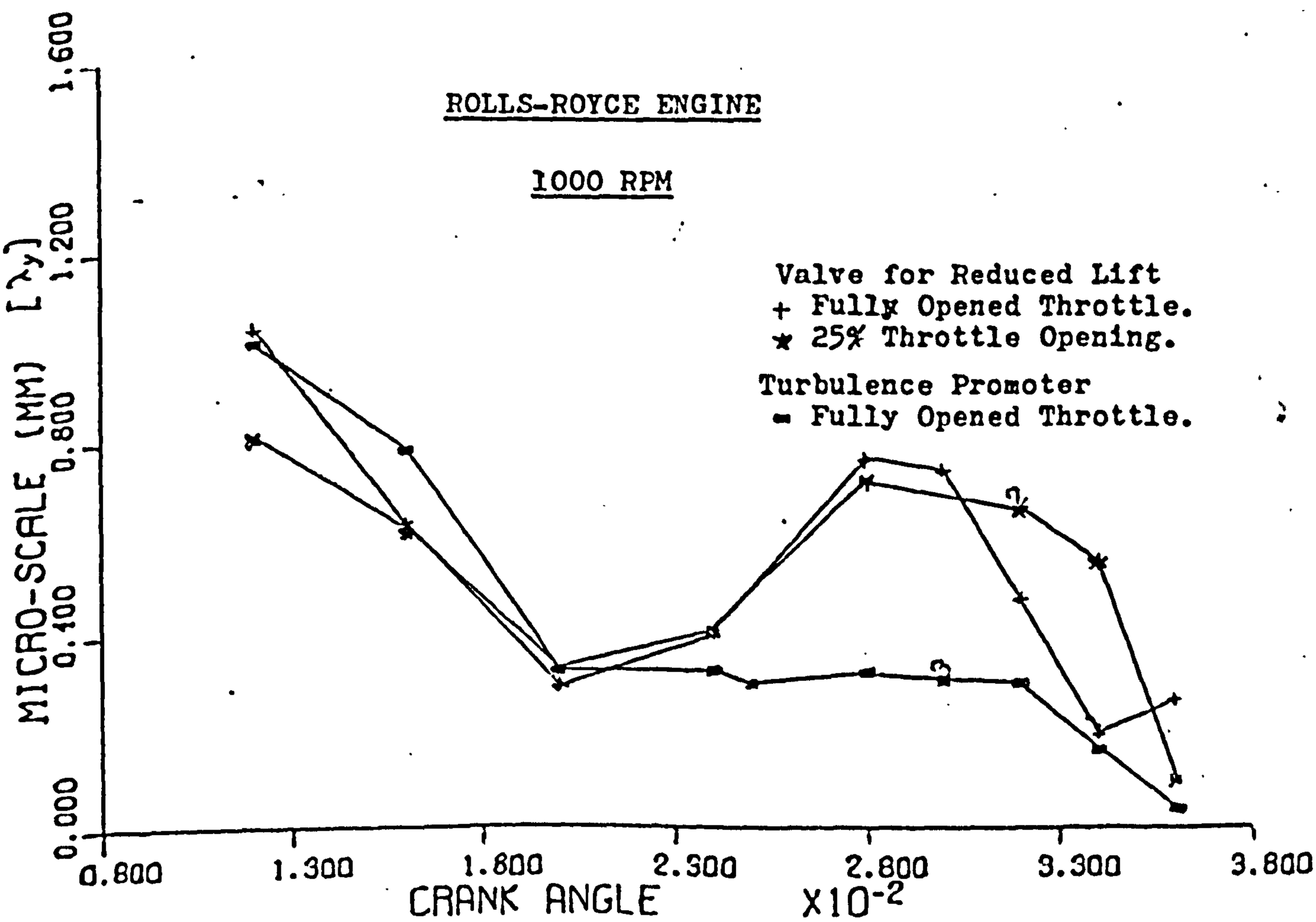

Fig (6-47d)

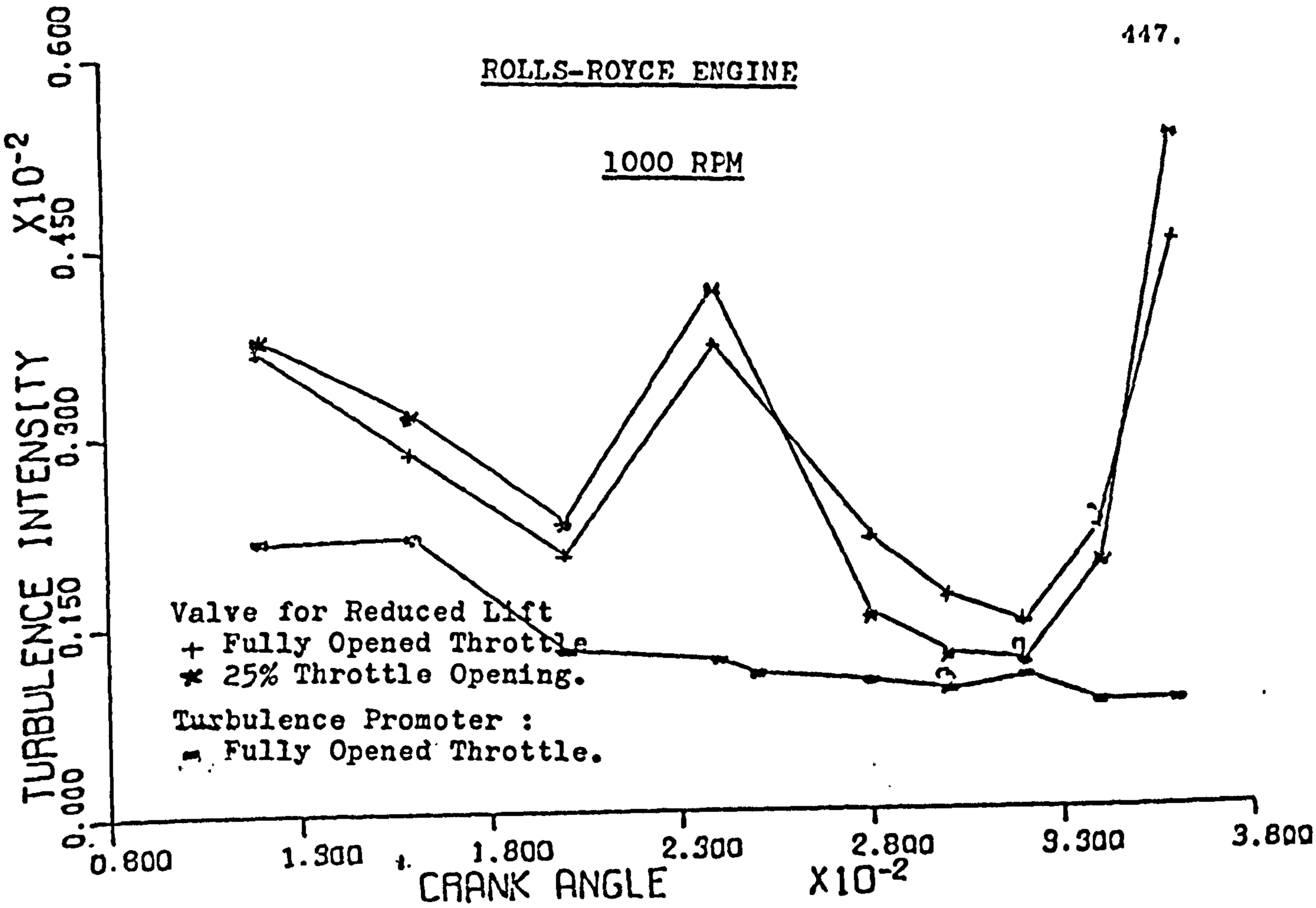

Fig (6-47e)

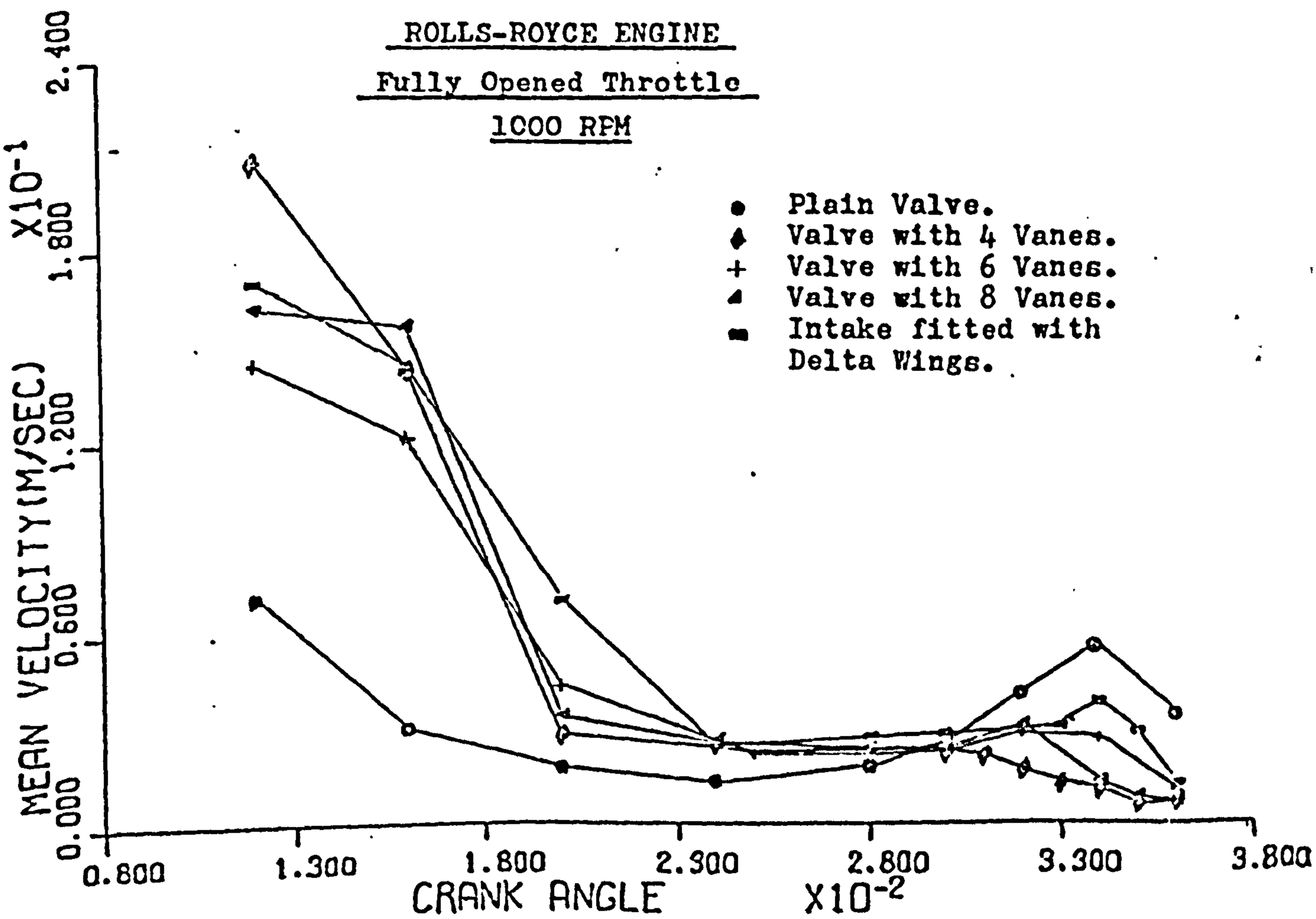

Fig (6-47f)

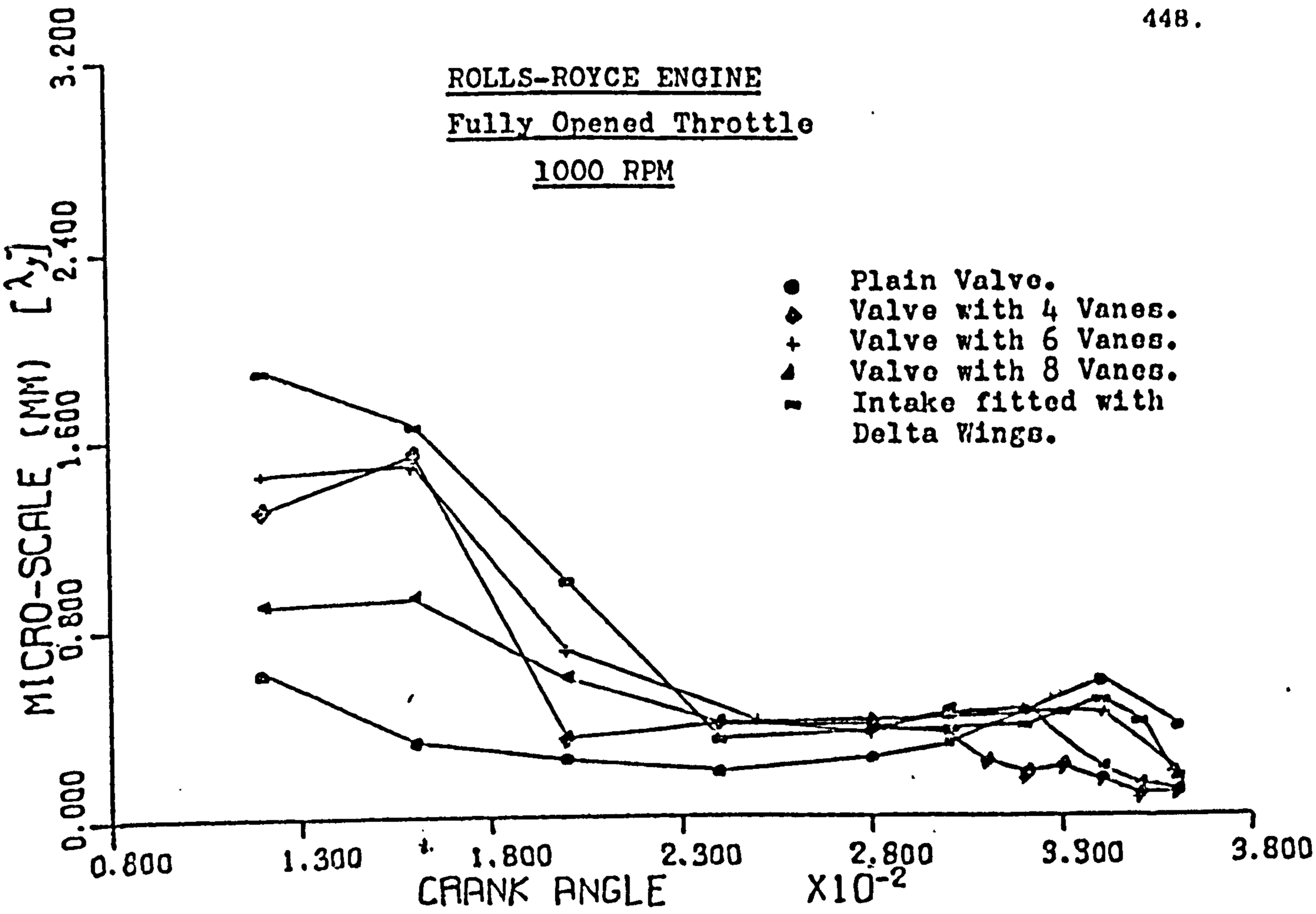
ROLLS-ROYCE ENGINE
Fully Opened Throttle
1000 RPM
Plain Valve.
Valve with 4 Vanes.
Valve with 6 Vanes.
Valve with 8 Vanes.
Intake fitted with Delta Wings.
MICRO-SCALE (MM) [λy]
0.000
0.800
1.600
2.400
3.200
0.800
1.300
1.800
2.300
2.800
3.300
3.800
CRANK ANGLE X10-2

Fig (6-47g)

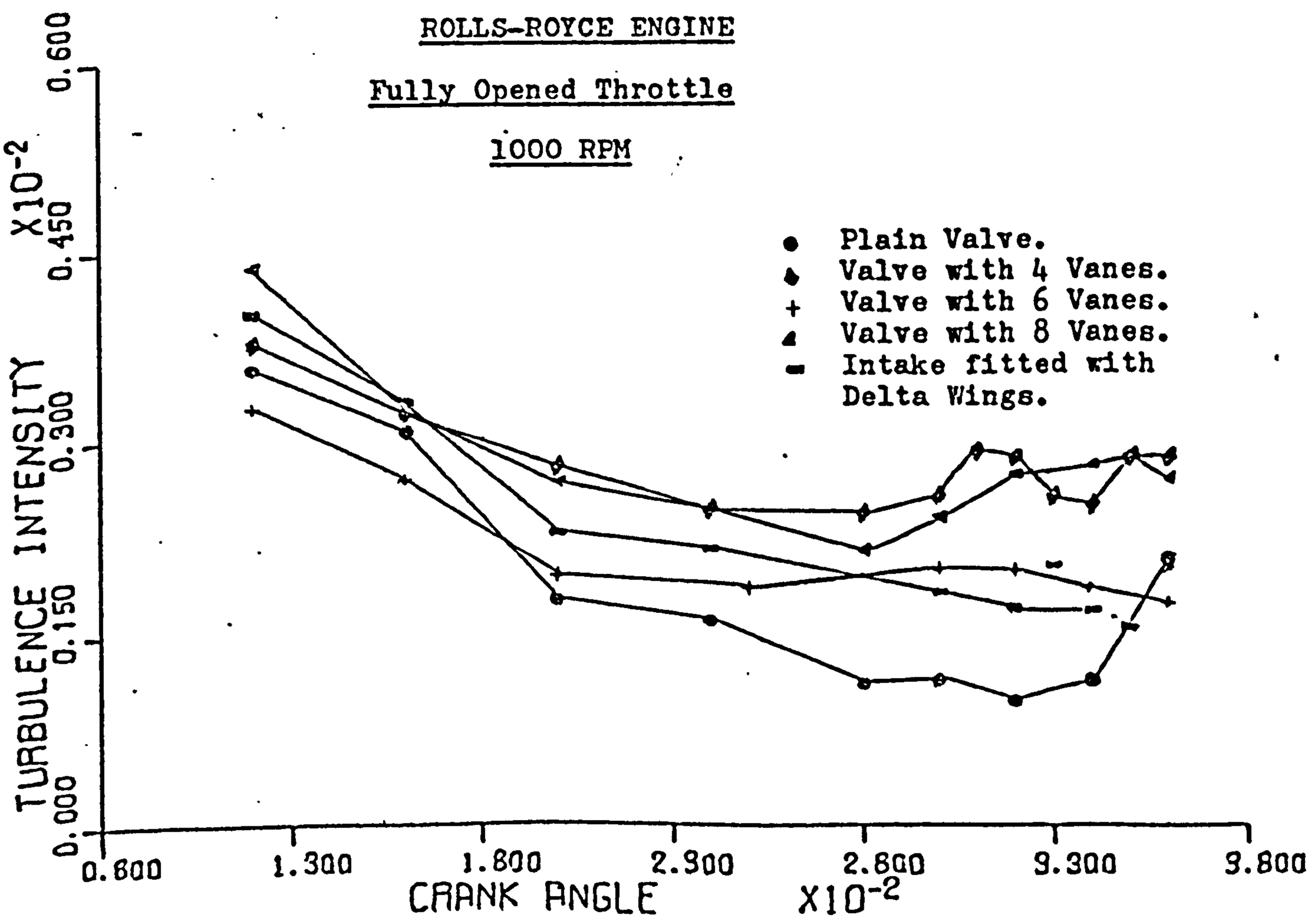
ROLLS-ROYCE ENGINE
Fully Opened Throttle
1000 RPM
Plain Valve.
Valve with 4 Vanes.
Valve with 6 Vanes.
Valve with 8 Vanes.
Intake fitted with Delta Wings.
TURBULENCE INTENSITY X10-2
0.000
0.150
0.300
0.450
0.600
0.800
1.300
1.800
2.300
2.800
3.300
3.800
CRANK ANGLE X10-2

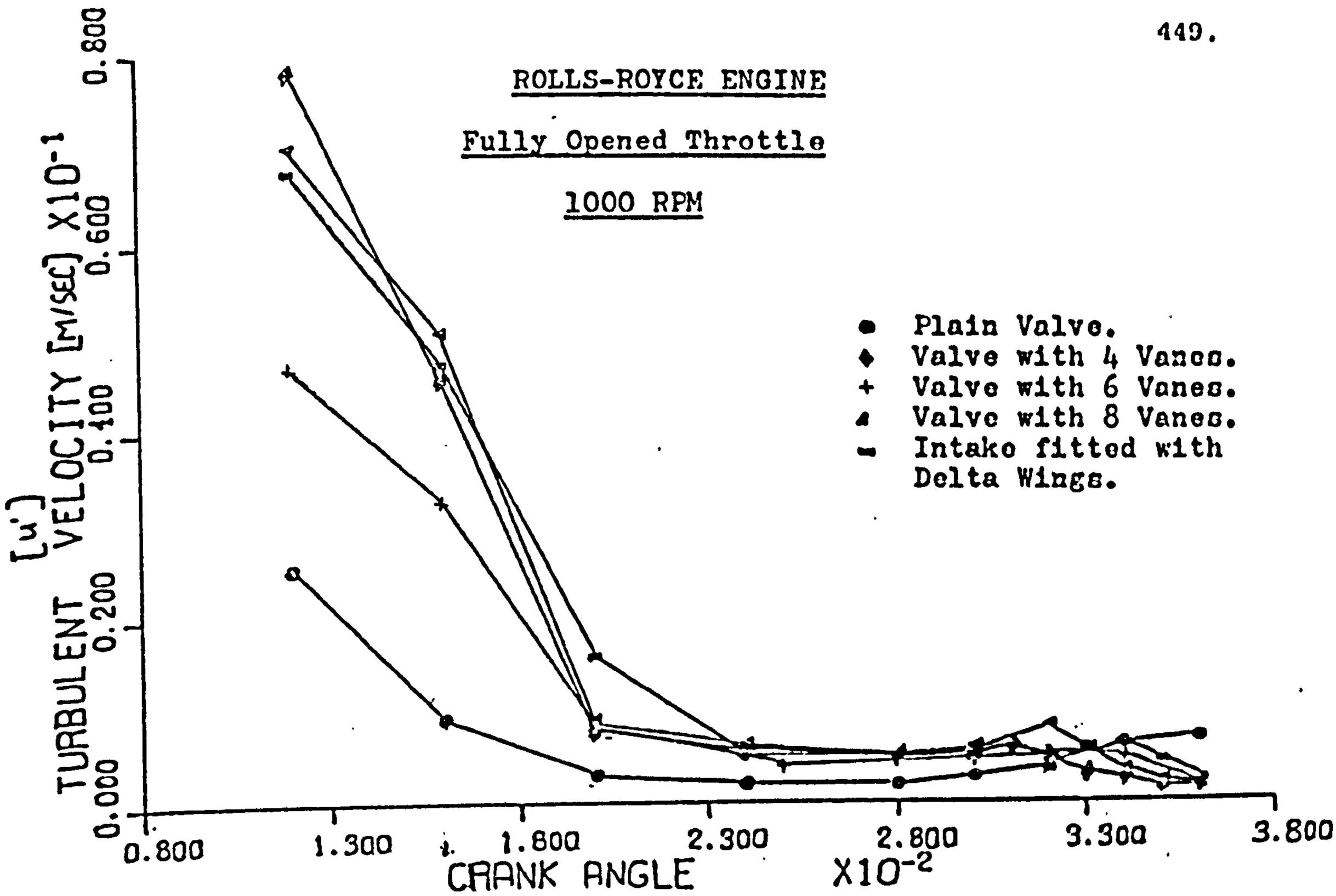

Fig (6-471)

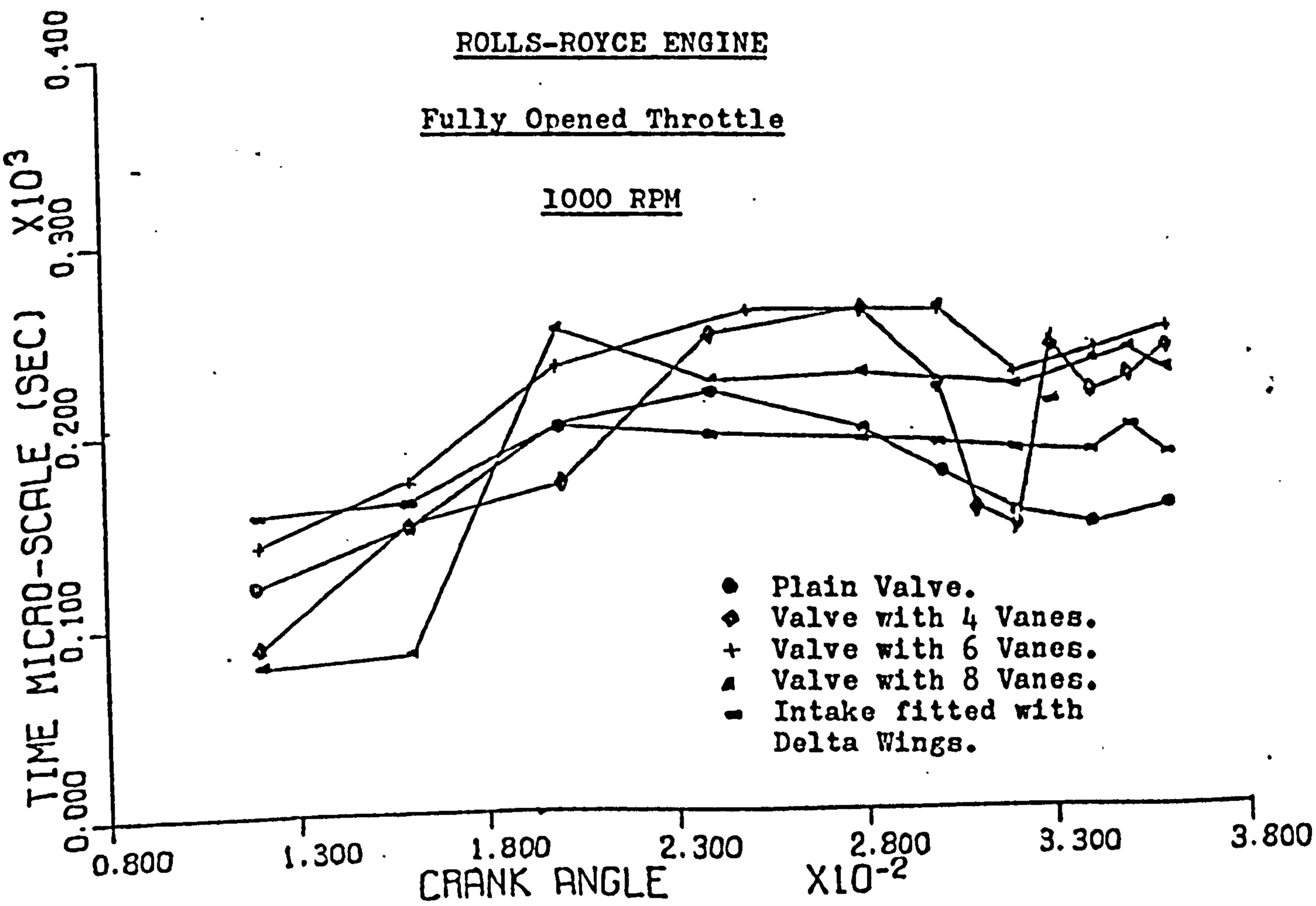

Fig (6-47j)

Fig. (6-48) Effect of Intake System Modifications and a Local Turbulence Promoter on the Turbulence Charactoristics Inside a Heron Combustion Chamber.
Analysis of 124 Cycles, Ford V4 Engine, Compression Ratio = 8.9:1, 1000 RPM. Measurements at the Spark Plug Location, using a Horizontal Wire.

a) Full Load Condition: Intake Vacuum of 102 mm Hg.

b) Part Load Condition: Intake Vacuum of 282 mm Hg.

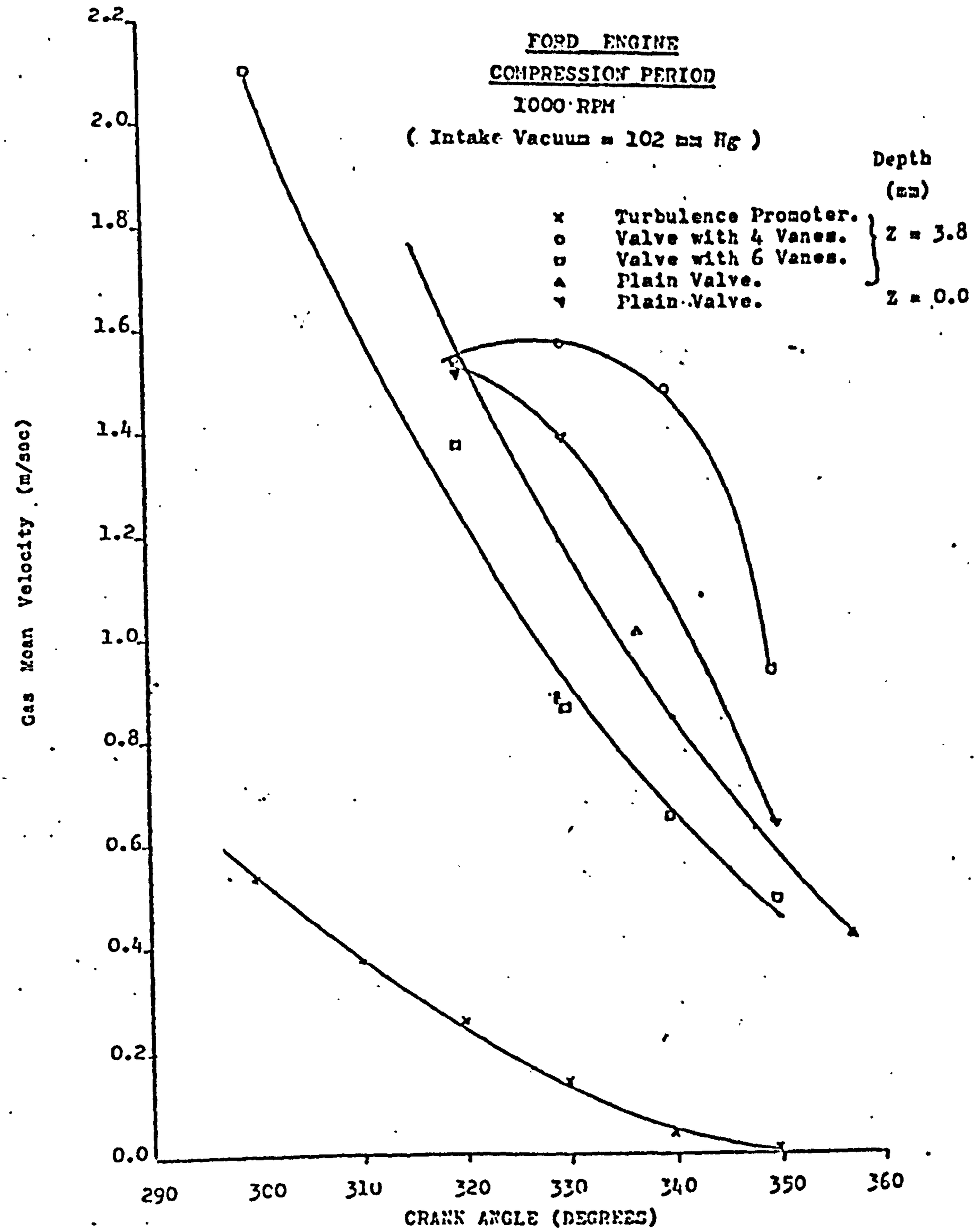
FORD ENGINE
COMPRESSION PERIOD
1000 RPM
(Intake Vacuum = 102 mm Hg)
Depth (mm)
x Turbulence Promoter.
o Valve with 4 Vanes.
□ Valve with 6 Vanes.
▲ Plain Valve.
▼ Plain Valve.
Z = 3.8
Z = 0.0
Gas Mean Velocity (m/sec)
2.2
2.0
1.8
1.6
1.4
1.2
1.0
0.8
0.6
0.4
0.2
0.0
290
300
310
320
330
340
350
360
CRANK ANGLE (DEGREES)

Fig. (6-48a)

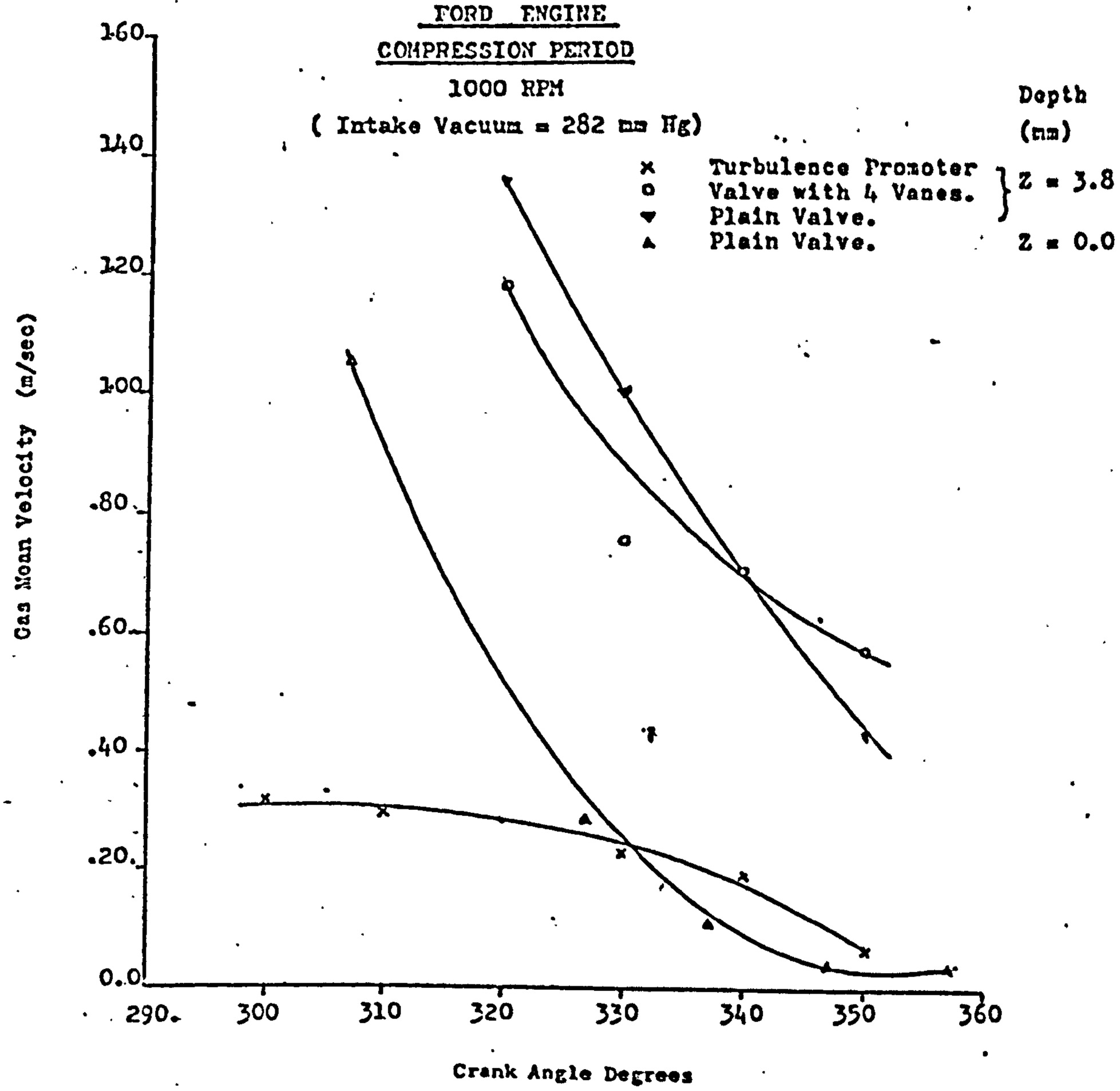
FORD ENGINE
COMPRESSION PERIOD
1000 RPM
(Intake Vacuum = 282 mm Hg)
Depth (mm)
× Turbulence Promoter
o Valve with 4 Vanes.
▼ Plain Valve.
▲ Plain Valve.
Z = 3.8
Z = 0.0
Gas Mean Velocity (m/sec)
1.60
1.40
1.20
1.00
.80
.60
.40
.20
0.0
290
300
310
320
330
340
350
360
Crank Angle Degrees

Fig. (6-48b)

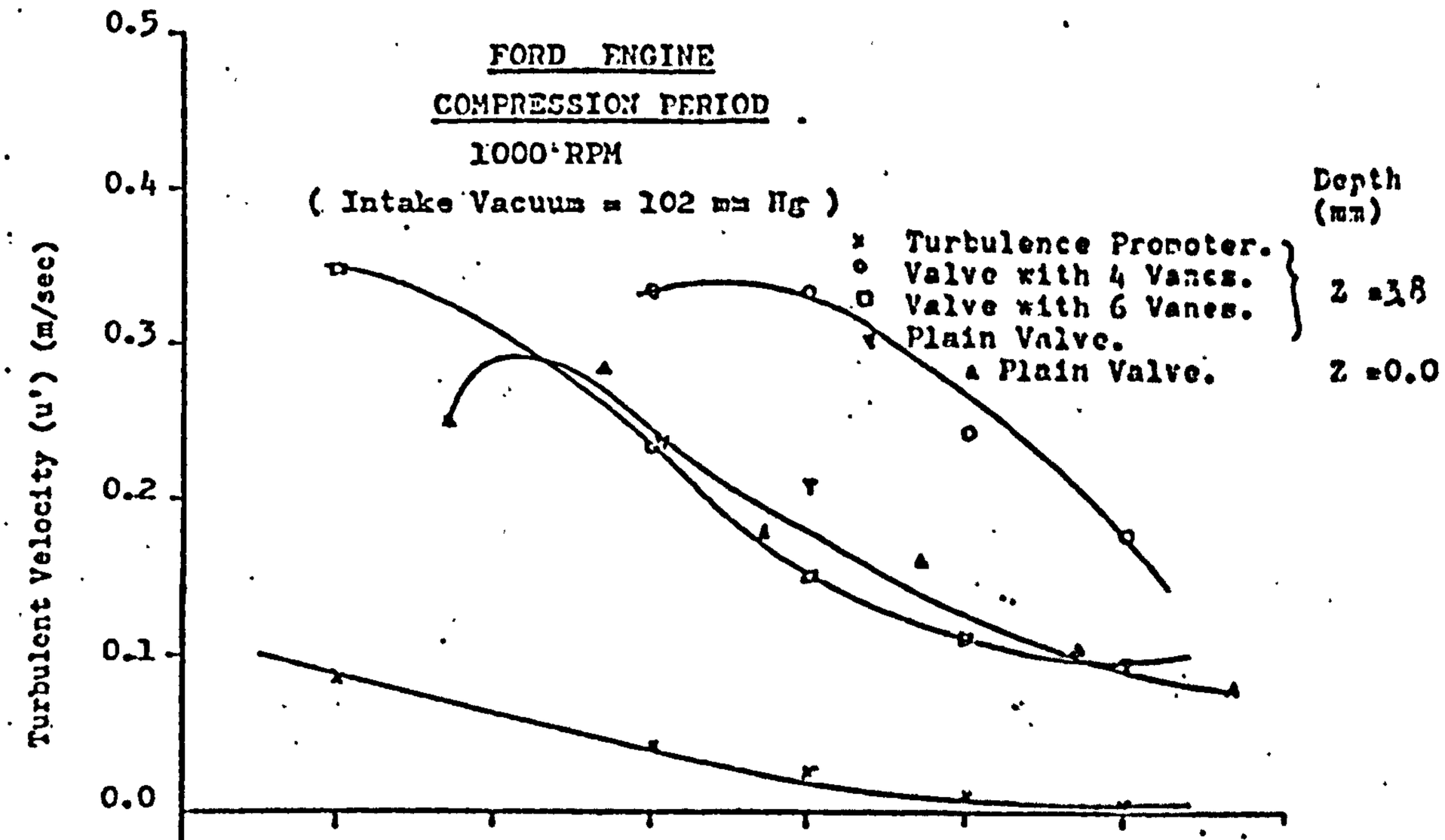

Fig. (6-48c)

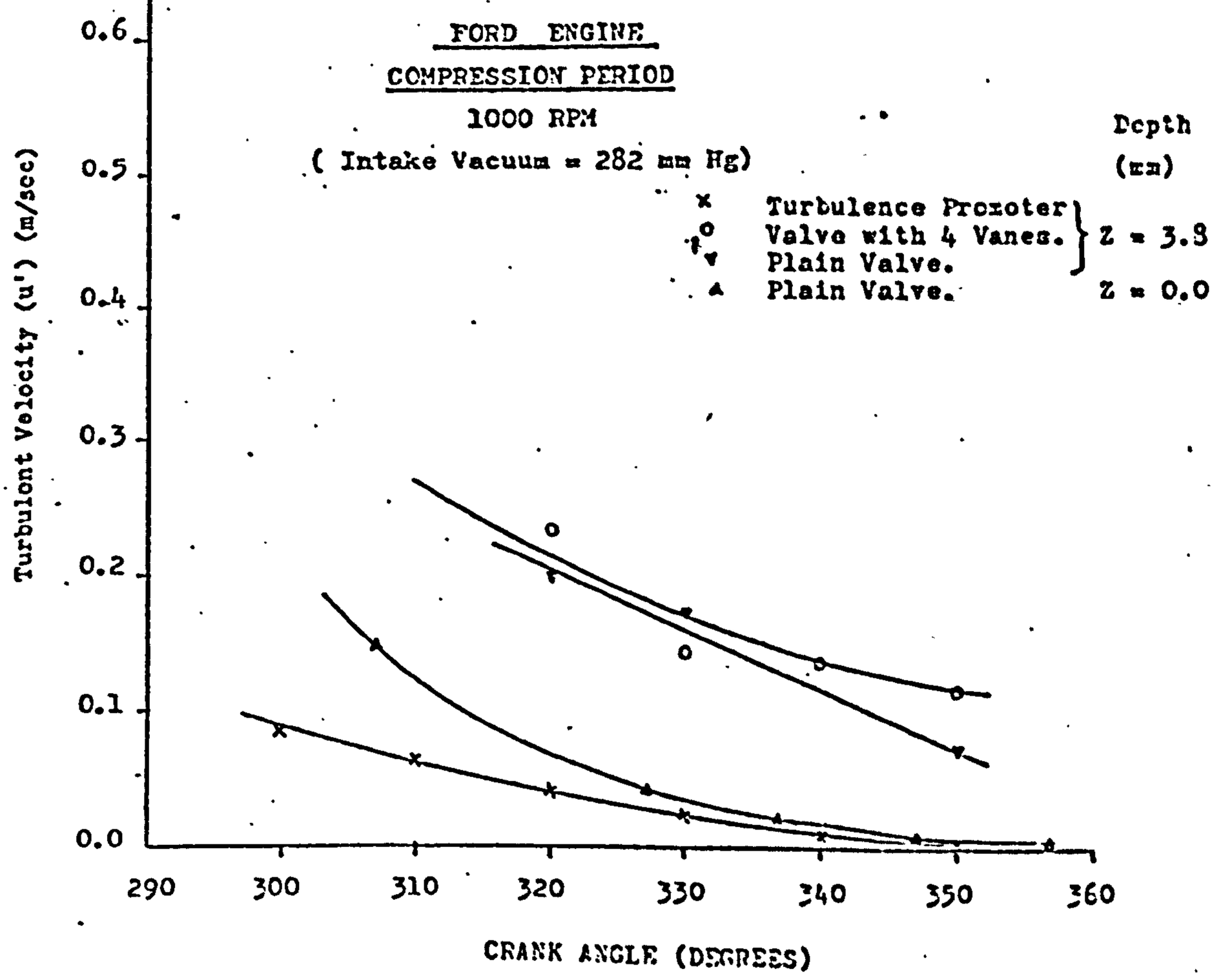

Fig. (6-48d)

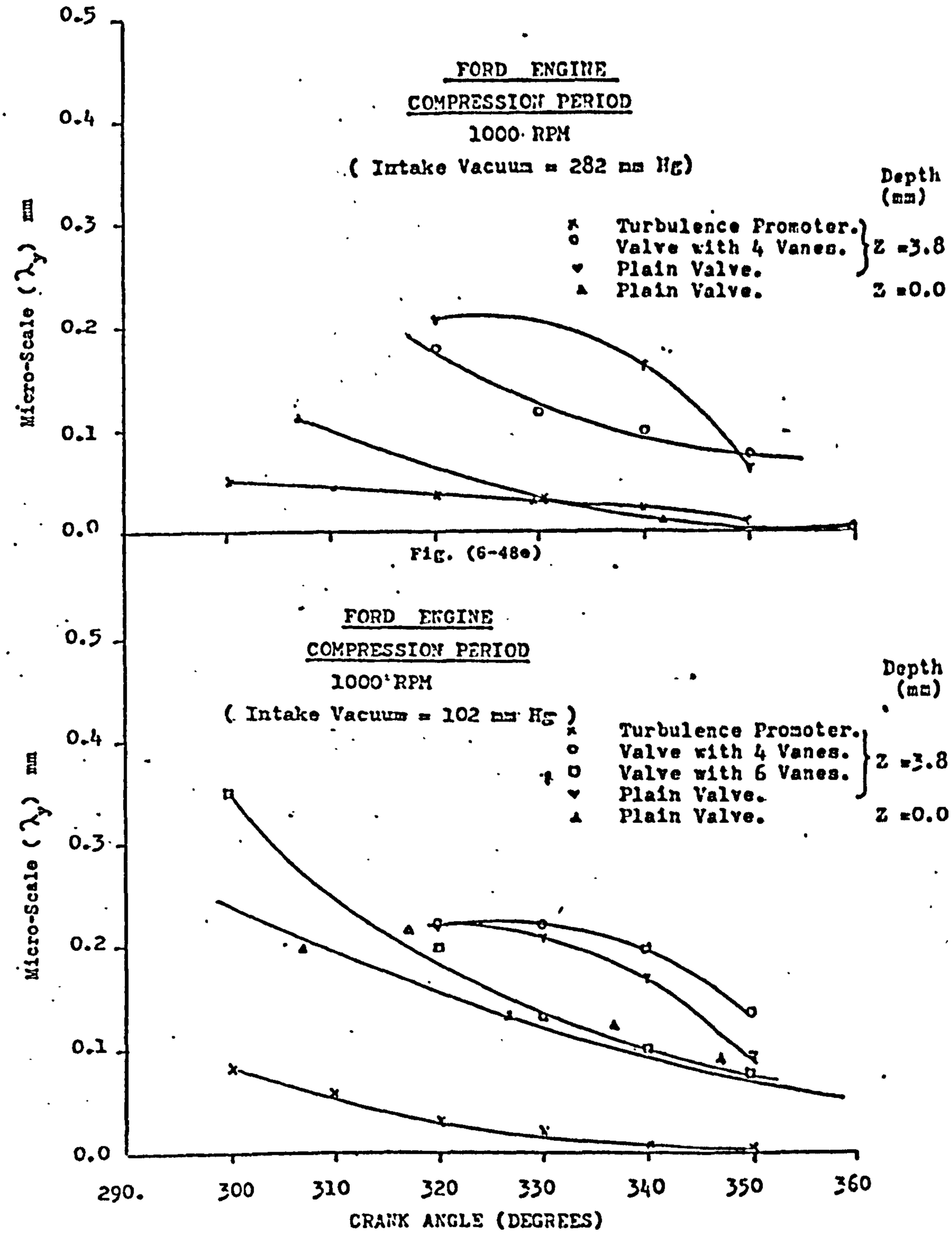
FORD ENGINE
COMPRESSION PERIOD
1000 RPM
(Intake Vacuum = 282 mm Hg)
Depth (mm)
Turbulence Promoter.
Valve with 4 Vanes.
Z =3.8
Plain Valve.
Plain Valve.
Z =0.0
Micro-Scale (λ_y) mm
0.5
0.4
0.3
0.2
0.1
0.0
Fig. (6-48e)
FORD ENGINE
COMPRESSION PERIOD
1000 RPM
(Intake Vacuum = 102 mm Hg)
Depth (mm)
Turbulence Promoter.
Valve with 4 Vanes.
Valve with 6 Vanes.
Z =3.8
Plain Valve.
Plain Valve.
Z =0.0
Micro-Scale (λ_y) mm
0.5
0.4
0.3
0.2
0.1
0.0
290.
300
310
320
330
340
350
360
CRANK ANGLE (DEGREES)

Fig. (6-48f)

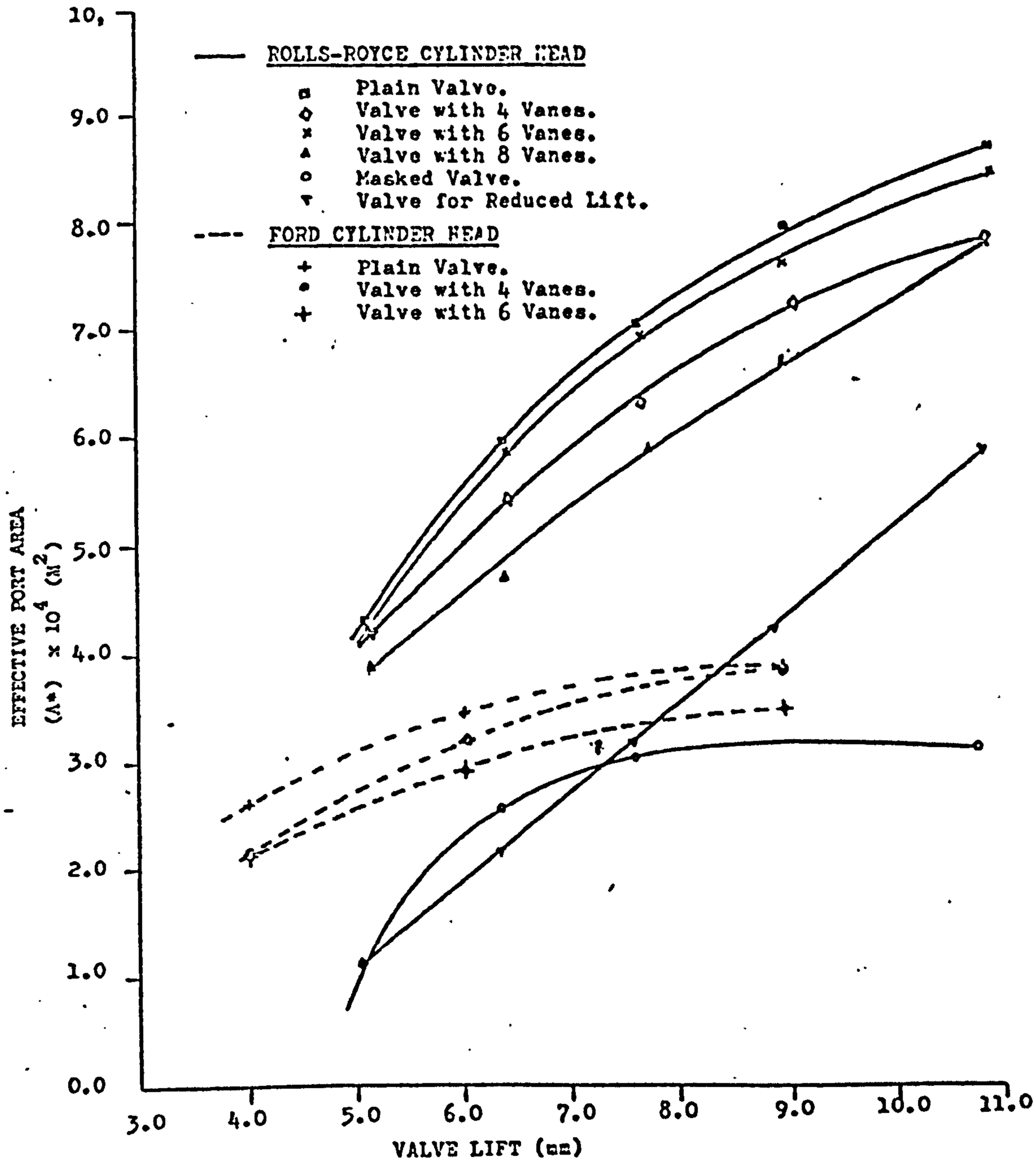

Fig. (6-49) A Comparison Between the Port Area (A*) for the Different Types of Inlet Valves Used in the Investigation.

Fig. (6-50) A Study of the Cylinder-to-Cylinder Variation in the Turbulence Characteristics Inside a Wedge Combustion Chamber.
Rolls-Royce V8 Engine, Compression Ratio = 9:1, 1000 RPM and Fully Opened Throttle.
Probe at the Spark Plug Location (Z = 17.78 mm) and a Wire Direction of 300 Degrees..

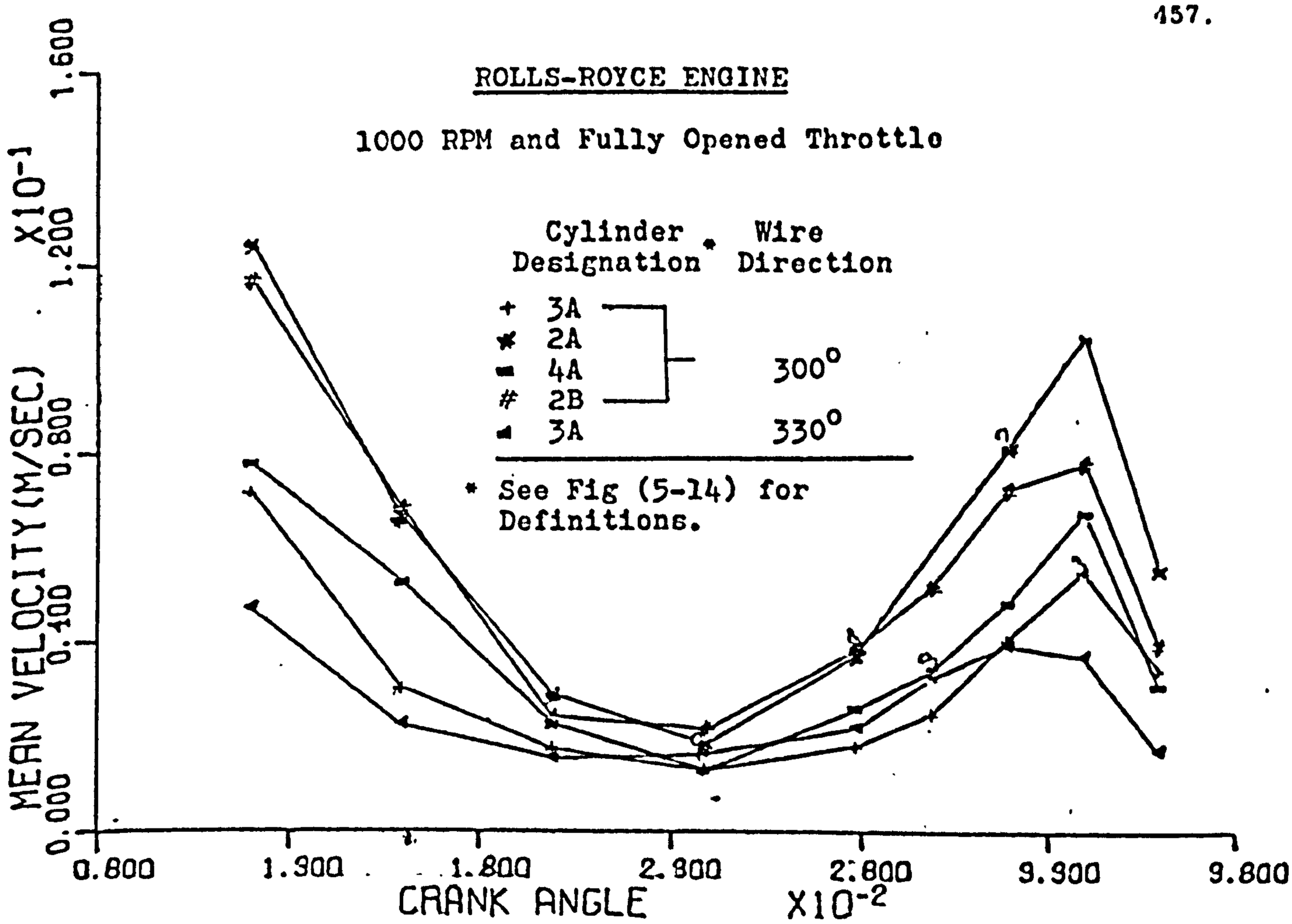

Fig (6-50a)

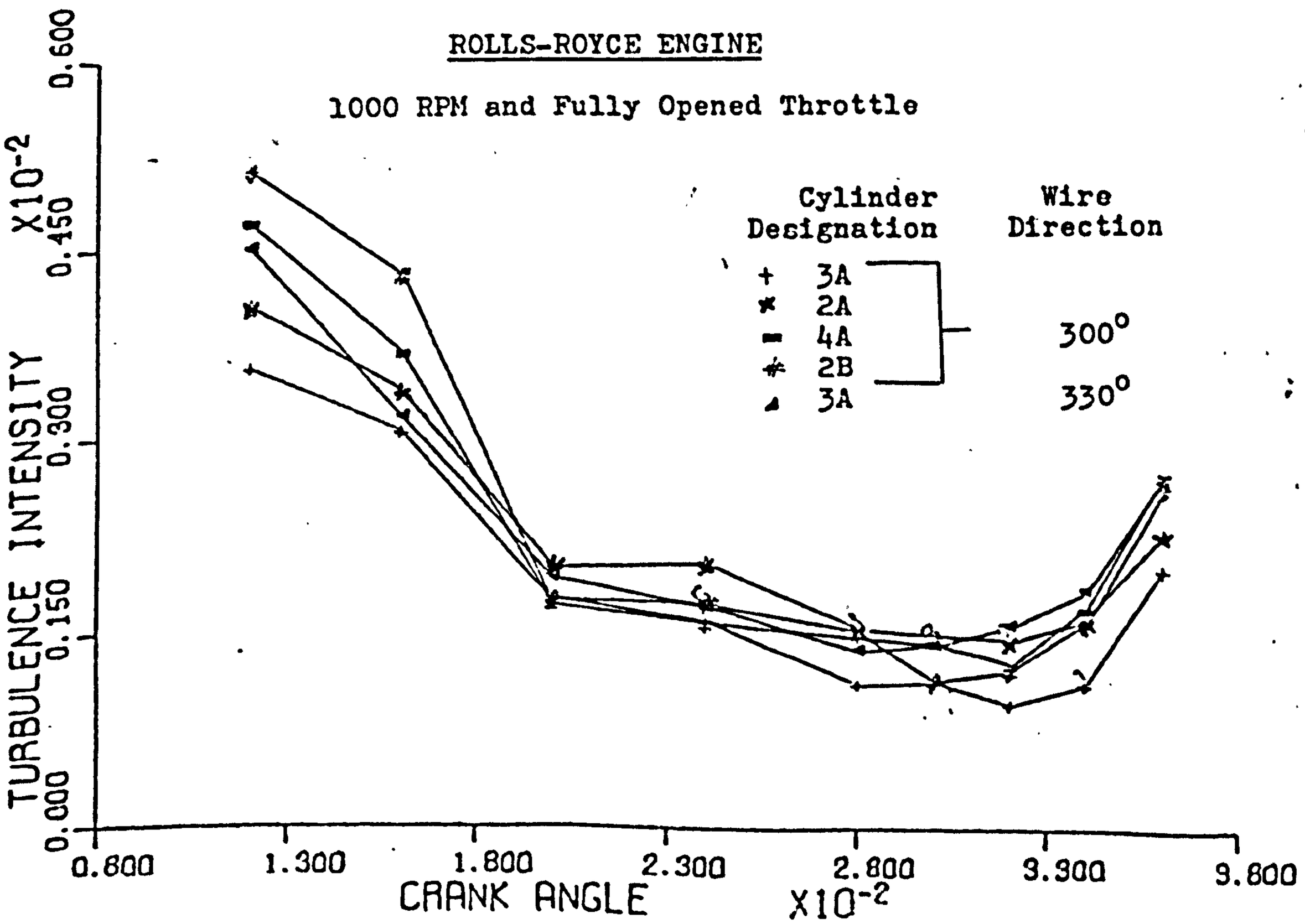

Fig (6-50b)

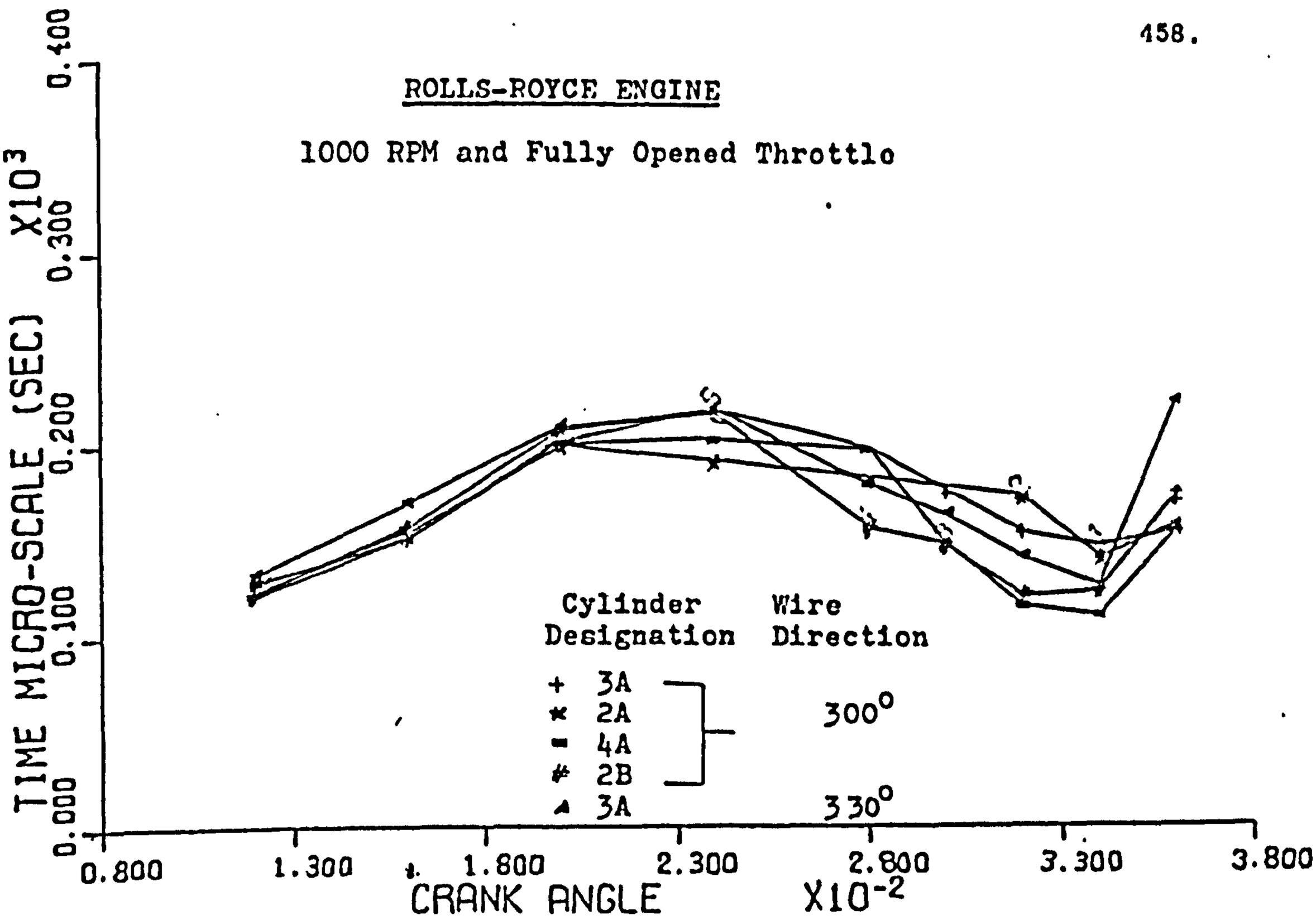

Fig (6-50c)

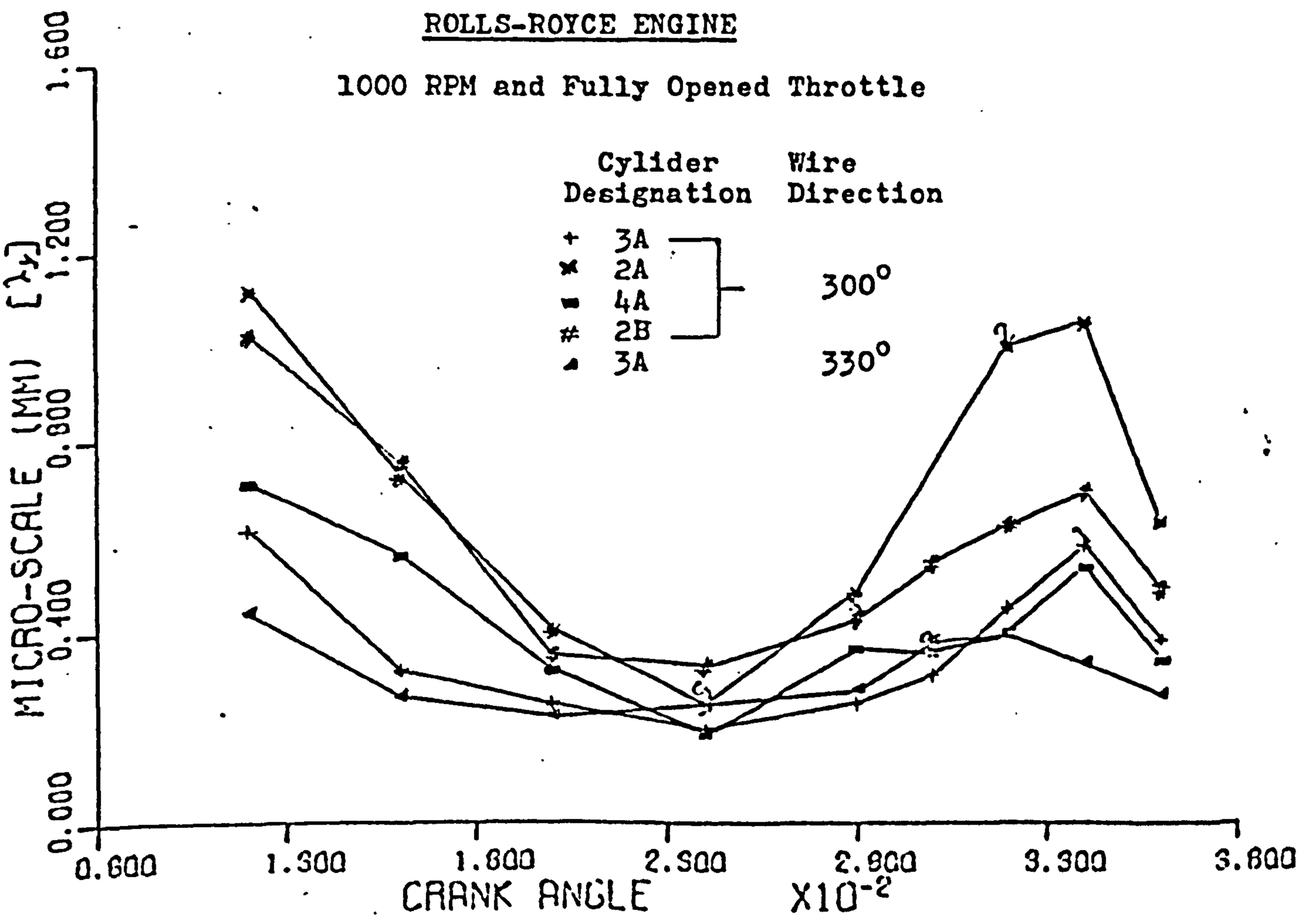

Fig (6-50d)

ROLLS-ROYCE ENGINE

1000 RPM and Fully Opened Throttle

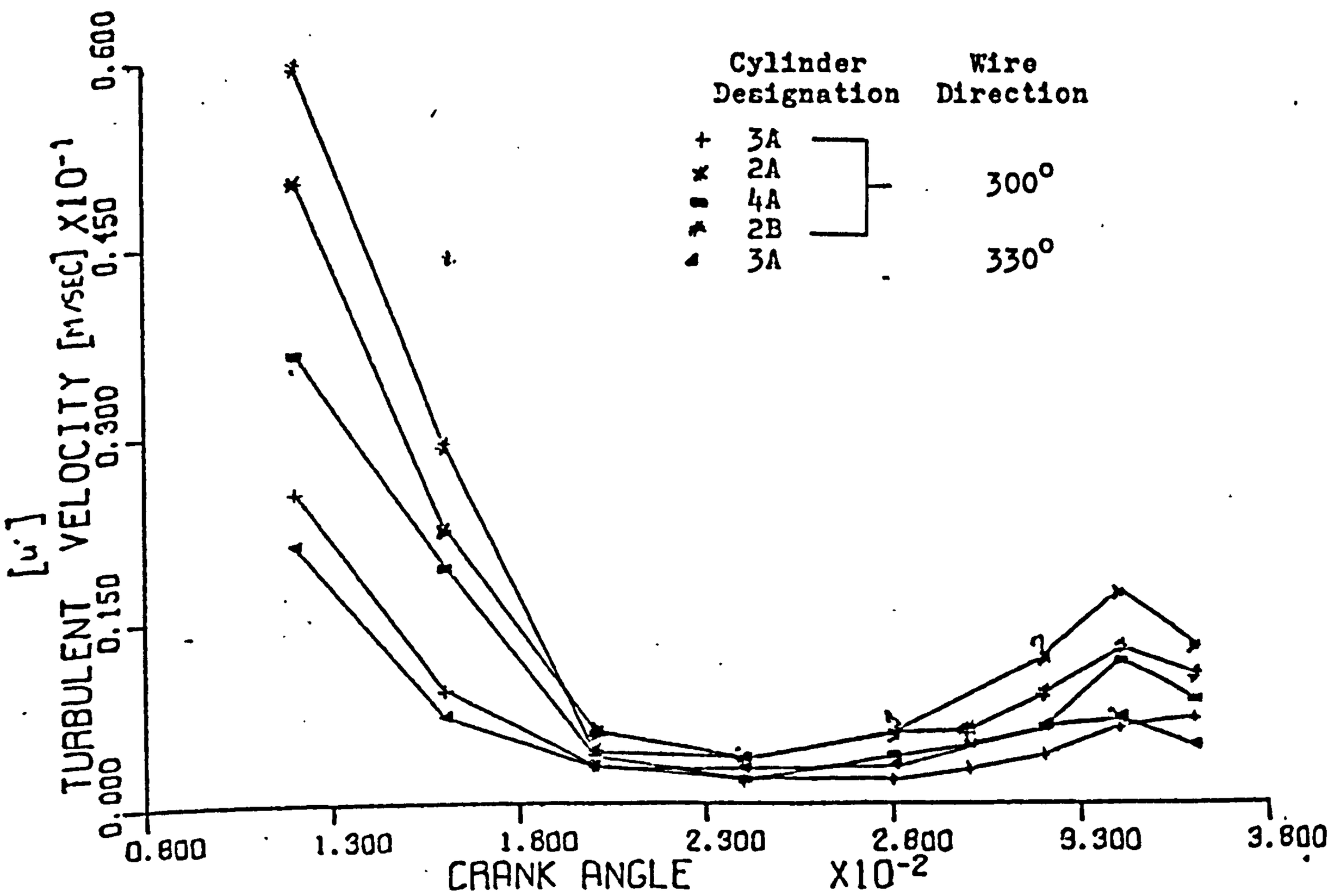

Fig (6-50e)

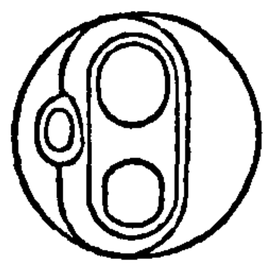

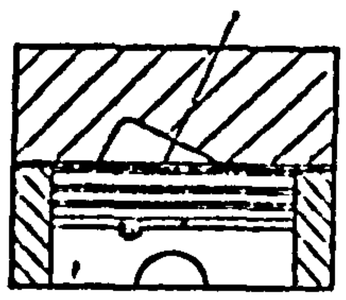

(A) Wedge

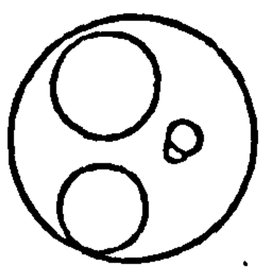

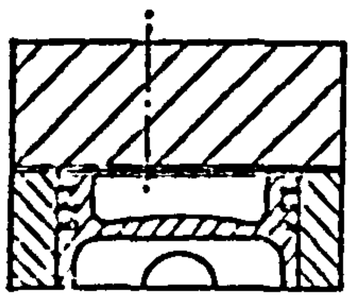

(B) Heron

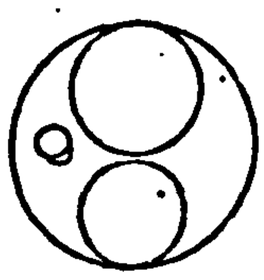

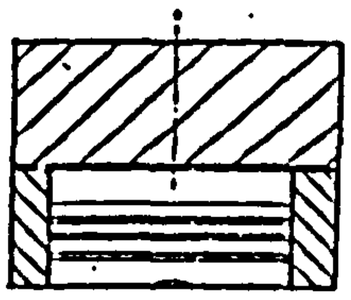

(C) Disc

Combustion Chamber Configurations.

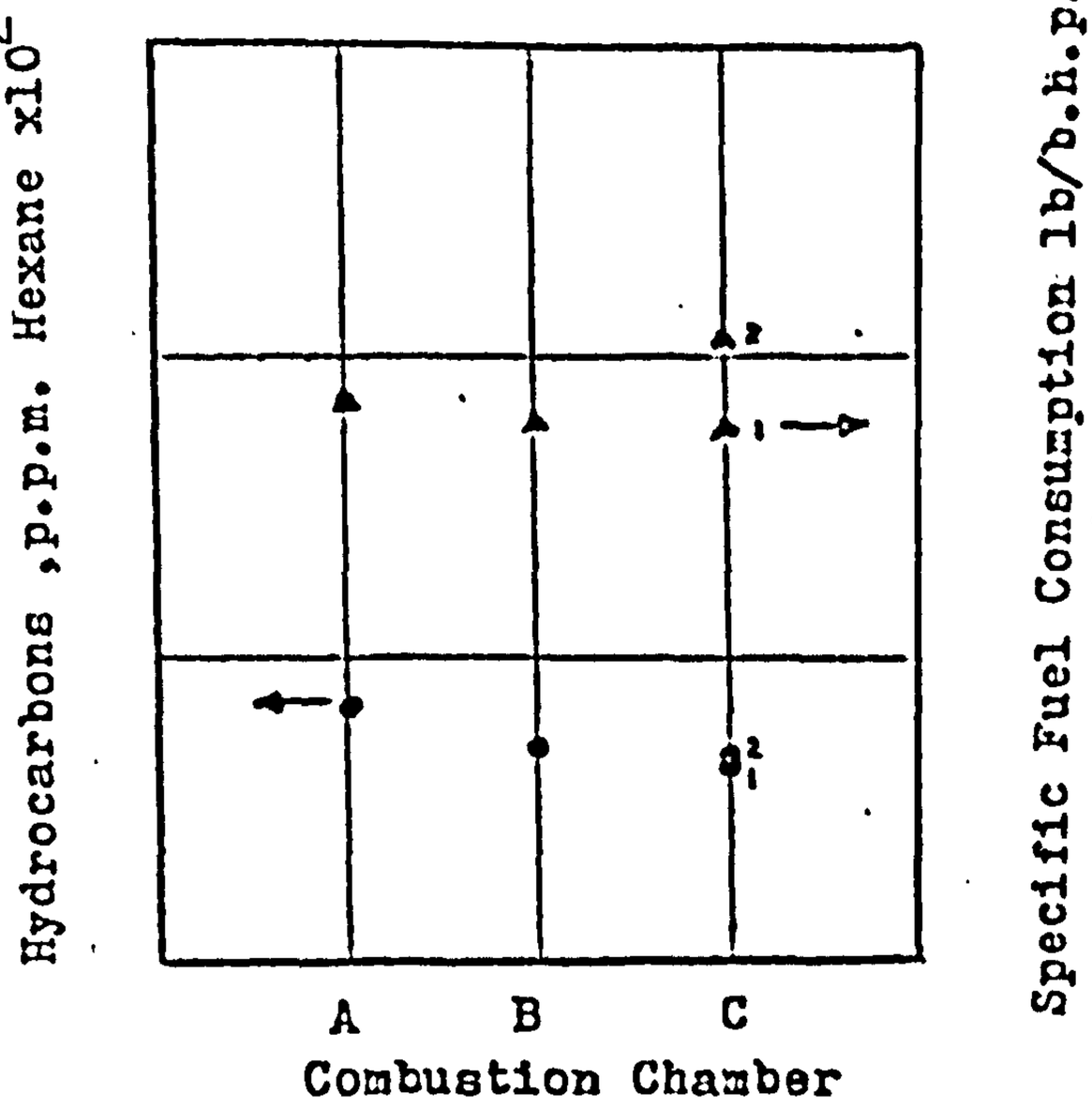

(a)- Merit order of combustion chambers based on mean minimum hydrocarbon emissions together with corresponding mean specific fuel consumptions.

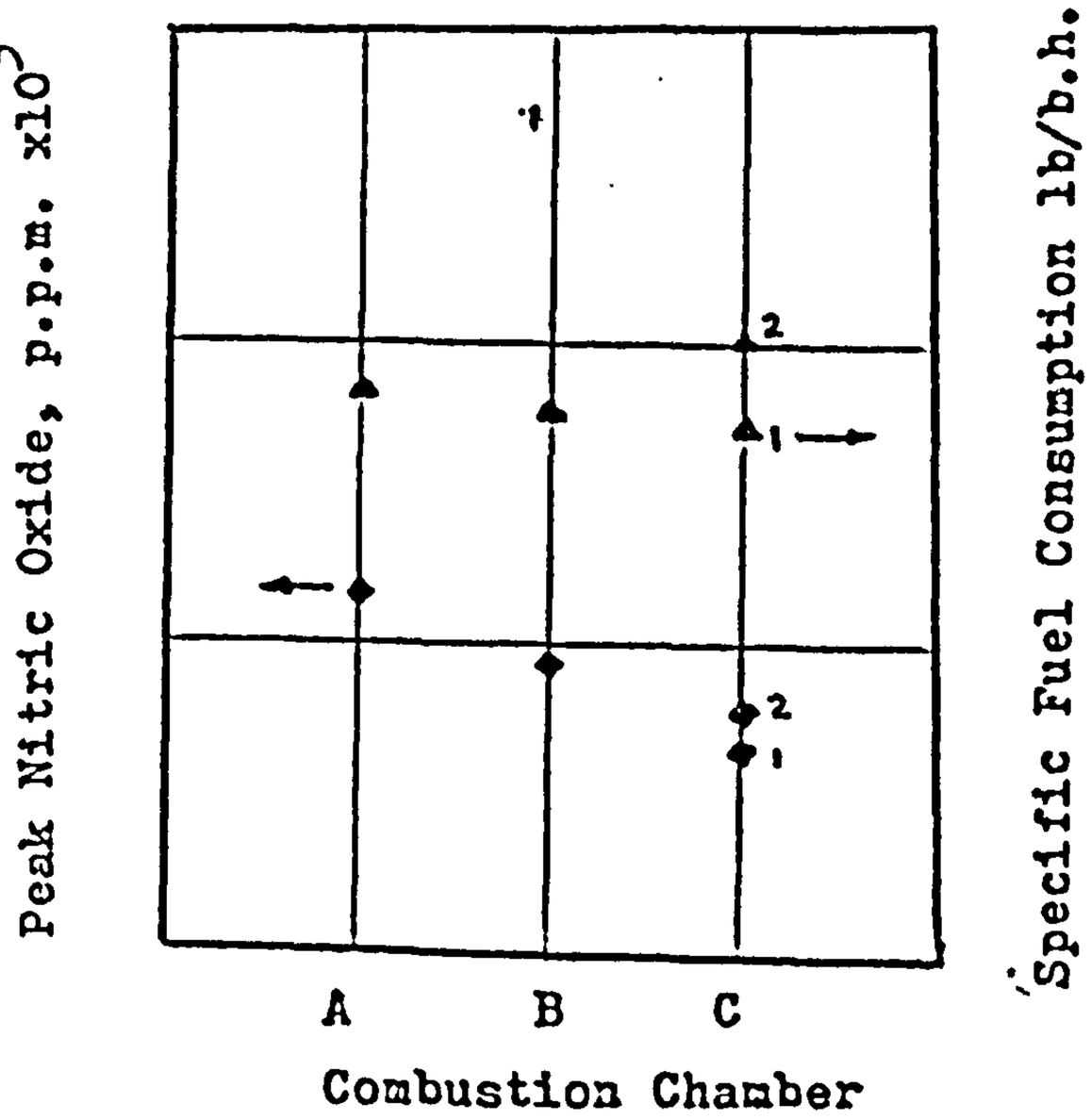

(b)- Merit order of combustion chambers based on mean of peak nitric oxide together with mean specific fuel consumptions.

Fig (6-51) Effect of Combustion Chamber Configuration on Exhaust Emissions (156).

7. CORRELATION BETWEEN THE CHARACTERISTICS OF TURBULENT FIELD INSIDE THE COMBUSTION CHAMBERS OF SPARK IGNITION ENGINES AND OTHER FLOW FIELDS

Because of the complexity of the turbulent flow field, no rational theory which could enable the determination of its characteristics by calculations has been established. Semi-empirical theories, however, have been developed into more or less complete theories. These theories are mainly concerned with mean velocity distribution. On the other hand, the notions introduced by the statistical theory of turbulence enables measurements of some characteristic parameters of the turbulent field.

This suggests that an attempt should be made to establish some correlations between the turbulence characteristics inside the combustion chambers of spark ignition engines as measured in the present investigation and the predictions of the conventional semi-empirical theories and the available experimental data for flow over a flat plate or inside constant cross-sectional pipes.

Difficulties arise in such situations because of the main differences in the physical process of generating turbulence in either field. Inside the combustion chamber of an engine a highly turbulent condition exists with very small directional velocities (if any exist). Also, the flow conditions are time dependent during the engine cycle, while all the available information about turbulent fields have been obtained for fully developed steady state flow conditions.

There is also a need for assuming some charactoristic length for the engine flow field, if comparisons have to be made in terms of Reynolds number or any other non-dimensional variables. Nevertheless, it is conventional in the field of heat transfer, to use some dimension of the experimental apparatus as a characteristic length. This suggests that the cylinder diameter could be employed in this situation, which avoids assuming any developing length based on conjectures about the flow pattern associated with the special geometries of the combustion chambers used in the investigation. Such a length has been proposed by Spalding in a definition for Reynolds number in engines where engine speeds are used to give some characteristic gas velocity. Similar expressions were proposed by Siringnano (132) in his development of a combustion model using piston speed as a characteristic velocity. A Reynolds number for engine investigation is defined, in the present work, as follows:

$$Re_D(\theta) = \frac{U(\theta).D}{\nu(\theta)} \qquad (7\text{-}1)$$

where $U(\theta)$ and $\nu(\theta)$ are the gas mean velocity and kinematic viscosity at the crank angle θ, respectively, and D the cylinder diameter.

Boussinesq (123) was the first to introduce the notion of a mixing coefficient (eddy viscosity) E_M in the expression of the turbulent shear stress

$$\tau_t = -\rho\overline{u\,v} = E_M \frac{d\,\bar{U}}{d\,y} \qquad (7\text{-}2)$$

The eddy viscosity is analogous to the molecular viscosity μ, since the product of eddy viscosity and velocity gradient gives the turbulent shear stress. The total shear stress on the walls could be expressed therefore by:

$$\tau = \tau_l + \tau_t = (\mu + E_M) \frac{d\,\bar{U}}{d\,y} \qquad (7\text{-}3)$$

It is also convenient to define an eddy diffusivity ε_m (kinematic viscosity for turbulent flow) similar to the kinematic viscosity ν as:

$$\varepsilon_m = \frac{E_M}{\rho} \qquad (7\text{-}4)$$

Therefore:

$$\frac{\tau}{\rho} = (\nu + \varepsilon_m) \frac{d\,\bar{U}}{d\,y} \qquad (7\text{-}5)$$

Different hypotheses have been assumed for the definitions of this eddy diffusivity, among them are the well known Prandtl mixing length hypothesis (124) and the Von Karman similarity hypothesis (80).

Prandtl tried to connect the eddy diffusivity with the characteristics of turbulence. According to the kinetic theory of gases, the kinematic viscosity is equal to the product of the root mean square velocity of the molecules and the mean free path; analogously, Prandtl assumed that the coefficient of eddy diffusivity is equal to the product of a mixing length and some suitable velocity. This condition could be expressed as follows:

$$\varepsilon_m = -\overline{v' L_m} \qquad (7\text{-}6)$$

Assuming that the longitudinal fluctuating velocity component u' of a lump of particles is determined by the difference in mean velocity $\bar{U}$ between the plane considered and the plane from which the lump originates, thus

$$u' \propto L_m \cdot \frac{d\bar{U}}{dy} \qquad (7\text{-}7)$$

and consequently

$$v' \simeq u' \propto -L_m \cdot \left| \frac{d\bar{U}}{dy} \right| \qquad (7\text{-}8)$$

Since the sign of v' is determined by that of L_m, hence

$$\varepsilon_m = -\overline{v' L_m} = \text{const.} \cdot \overline{L_m^2} \left| \frac{d\bar{U}}{dy} \right| \qquad (7\text{-}9)$$

The constant of proportionality may be included conveniently in a new length $\ell_m^2 = \text{const.} \overline{L_m^2}$. The expression for the eddy diffusivity then reads:

$$\varepsilon_m = \ell_m^2 \cdot \left| \frac{d\bar{U}}{dy} \right| \qquad (7\text{-}10)$$

Further assumptions about the mixing length being proportional to the distance from the wall ($\ell_m = K\ y$) led to the conventional logarithmic velocity distribution law which fits the experimental data very well.

Von Karman (80) assumed that the turbulent transport processes are determined by local flow conditions. For dimensional reasons ε_m may be written as before as the product of a velocity and a length, for the velocity Von Karman used v'. This gives

$$\varepsilon_m = v' \cdot \ell^* \qquad (7\text{-}11)$$

This length ℓ^* is not identical with Prandtl mixing length. According to Von Karman, the value of ℓ^* must be determined by quantities that have a local character, such as the micro-scale of turbulence λ_y, and the local Reynolds number or Reynolds number of turbulence Re_λ . Thus

$$\ell^* = \lambda_y \cdot f\ (Re_\lambda) = \lambda_y . f\ \left(\frac{u'\lambda_y}{\nu}\right) \qquad (7\text{-}12)$$

The simplest form is

$$\ell^* = \text{const.}\ \lambda_y\ Re_\lambda$$

or

$$\ell^* = \text{const.}\ u' \cdot \lambda^2_y/\nu \qquad (7\text{-}13)$$

Various investigators have suggested expressions for the eddy diffusivity based on interpretations of experimental data. A summary of these expressions could be found in reference (126). However, two or three separate algebraic equations were usually proposed in each case for different regions in the turbulent field.

A single equation for the eddy diffusivity ε_m has been proposed by Spalding (125) which provides continuity throughout the whole turbulent region and is given by:

$$\frac{\varepsilon_m}{\nu} = \frac{K}{E}\left[e^{KU^+} - 1 - KU^+ - \left(\frac{KU^+}{2!}\right)^2 - \left(\frac{KU^+}{3!}\right)^3 \right] \quad (7\text{-}14)$$

where $K = 0.407, \quad E = 10$

$$U^+ = U/u^* \quad (7\text{-}15)$$

u^* is called the friction velocity and is a measure of the intensity of turbulent eddying and the transfer of momentum due to these fluctuations

$$u^* = \sqrt{\frac{\tau_w}{\rho}} \quad (7\text{-}16)$$

τ_w is the shear stress at the walls

The turbulent shear stress is usually expressed as the product of a friction factor and the dynamic head of the fluid.

$$\tau_w = \frac{1}{2} f \cdot \rho \cdot U_x^2 \quad (7\text{-}17)$$

where U_x is the undisturbed velocity for flow over a flat plate and the bulk mean velocity for the case of pipe flow.

Different expressions are proposed for the friction factor as a function of a characteristic Reynolds number of the flow. A summary of these expressions for external flow over a flat plate and flow inside smooth pipes are given below:

a) Flat Plate

$$f = 0.0585\ (Re_x)^{-0.2} \qquad \text{Von Karman (127)} \qquad (7\text{-}18)$$

$$f = 0.37/(\log Re_x)^{-2.584} \qquad \text{Schultz-Grunow (127)} \qquad (7\text{-}19)$$

$$f = (2 \log Re_x - 0.65)^{-2.3} \qquad \text{Prandtl -Schlichting(128)} \qquad (7\text{-}20)$$

$$f = 0.0262\ (Re_x)^{-1/7} \qquad \text{Falkner (129)} \qquad (7\text{-}21)$$

$$f = 0.02296\ (Re_x)^{-0.139} \qquad \text{Nikuradso (130)} \qquad (7\text{-}22)$$

where $Re_x = \frac{U.x}{\nu}$ (7-23)

The last two expressions (7-21) and (7-22) are especially recommended for flow at very high turbulent conditions (large values of Re_x)

b) Pipe Flow

$$f = 0.046\ Re_D^{-0.2} \qquad (126,127) \qquad (7\text{-}24)$$

$$f = 0.0014 + 0.125\ Re_D^{-0.32} \qquad \text{Drew et al (127)} \qquad (7\text{-}25)$$

$$\frac{1}{\sqrt{f}} = 4.06 \log(Re_D \sqrt{f}) - 0.6 \qquad \text{Von Karman (127)} \qquad (7\text{-}26)$$

$$\frac{1}{\sqrt{f}} = 4.0 \log(Re_D \sqrt{f}) - 0.4 \qquad \text{Nikuradse (127)} \qquad (7\text{-}27)$$

where $Re_D = \frac{U.D}{\nu}$ (7-28)

The expressions proposed by Falkner and Nikuradso for flat platesagree reasonably well with those for pipo flow at very high values of Reynolds number Figure (7-1). The expression for pipe flow (7-24) was, therefore, employed to give an estimate of friction factor and correspondingly the friction velocity. The latter quantity was substituted in equation (7-14) for the eddy

diffusivity. Figures (7-2) - (7-4) show a comparison between the values of eddy diffusivity using different expressions for the friction factor at typical values of Reynolds number in an engine during the compression period.

The second problem which arises in attempts to establish correlations between the flow inside the engine cylinder and that over a flat plate or inside the cross-sections of pipes is the influence of temperature variations on the calculated fluid properties. All the flow friction laws (7-18) - (7-28) and the experimental data were obtained under constant fluid properties throughout the flow field, while in an engine both temperature and pressure are continuously varying during the engine cycle and their variations are very pronounced. The general effect of the variation of the transport properties with temperature is to change the velocity and temperature profiles, yielding different friction coefficients than would be obtained if properties were constant.

For engineering applications it has been found convenient to employ the constant property analytic solutions, or the experimental data obtained with small temperature difference and then to apply some kind of correction to account for property variation. Most of the variable property results indicate that fairly simple corrections will generally suffice over a moderate range of temperature.

Two schemes for corrections of constant property results are in common use. The first one assumes a 'reference temperature' which is a combination of the wall temperature and the free stream temperature and is used for evaluating all the fluid properties

appearing in (Re, Pr, etc). The second scheme is the 'property ratio' method, where all properties are evaluated at the free stream temperature, or the mixed mean temperature and then all of the variable property effects are lumped into a function of a ratio of some pertinent property evaluated at the surface temperature to that property evaluated at the free stream or mixed mean temperature.

Kays (126) discussed the use of both schemes and showed that the first method leads to ambiguities for internal flow applications but could be employed for external flow over flat plates. The second scheme could be employed for both types of flow fields and the temperature dependent property effects can usually be adequately correlated by the following equations:

$$\frac{Nu}{Nu_{cp}} = \frac{S_t}{S_{t_{cp}}} = \left(\frac{T_o}{T_m}\right)^n \tag{7-29}$$

and

$$\frac{f}{f_{c_p}} = \left(\frac{T_o}{T_m}\right)^m \tag{7-30}$$

where Nu, S_t are Nusselt and Stanton numbers, respectively, f is the friction factor and T is the absolute temperature. The subscripts o and m refer to the wall and the mixed mean conditions and C_p refers to the constant property solution. Kays discussed the work of other investigators and suggested that for turbulent flow in tubes the values of the exponents n and m for air between 100 to 3000°F could be given by

$$\frac{T_o}{T_m} < 1 \qquad m = -0.1 \qquad n = 0 \tag{7-31}$$

Application of the proposed corrections (7-31) for engine conditions over the range of compression ratios between 4:1 to 20:1 results in a variation of the friction factor by 3.6 to 8% of the constant property values. These correction values are within the range of experimental errors and could be, therefore, neglected in calculations of eddy diffusivity using equation (7-14).

On the other hand, the Taylor's theory of diffusion by continuous movements (86) provides another definition of the eddy diffusivity, as the product of the fluctuating velocity component v' and the Lagrangian integral scale $\mathcal{L}_L$ as defined in Section (3-7).

$$\varepsilon_m = v' \cdot \mathcal{L}_L \tag{3-150}$$

$$\mathcal{L}_L = v' \int_o^\infty R_L'(\tau)\, d\tau \tag{3-151a}$$

where $R_L'(\tau)$ is the Lagrangian correlation coefficient.

Comparisons between equations (7-6), (7-11) and (3-150) show that the Eulerian (Prandtl, or Von Karman) mixing length equals the Lagrangian integral scale of turbulence, i.e.

$$\mathcal{L}_L = L_m = \ell^* \tag{7-32}$$

Our main concern was concentrated, therefore, in investigating the existence of a relation between the predictions of the empirical expression of eddy diffusivity as proposed by

Spalding's equation (7-14) for pipe flow and the results of the present anemometer measurements in engines using equation (3-150). Such a relation, if it should exist, would provide a simplified technique for predicting the turbulence characteristics in engines from measurements of mean gas velocities only. This would reduce, to a great extent, the amount of experimental work involved and the need for very sophisticated instruments and complicated data processing systems as discussed in Chapter 4.

The main problem in such an attempt lies in the fact that the Lagrangian correlation coefficients cannot be measured directly by existing instruments. However, the measurements of the Eulerian correlation coefficients could serve for such a purpose if some relation exists between both types of correlations.

Experimental evidence has shown that, at least at large Reynolds numbers, the overall shapes of the Lagrangian correlation coefficients $R'_L(\tau)$ and the longitudinal spatial (Eulerian) correlation coefficient $R'_x(x)$ can be approximated by the following exponential functions.

$$R'_L(\tau) = e^{-\tau/\mathcal{L}_L} \tag{7-33}$$

$$R'_x(x) = e^{-x/L_x} \tag{7-34}$$

Thus these correlation coefficients have the same functional form and one can assume, therefore, that the Lagrangian and Eulerian integral scales must be proportional. Such an assumption has been made by Mickelson (110) which could be written as follows:

$$\tau = \frac{x\mathcal{L}_t}{L_x} = \frac{x\mathcal{L}_L}{u'L_x} = \frac{x}{\beta u'} \tag{7-35}$$

where $\beta = L_x/\mathcal{L}_L$ (7-36)

Mickelson has experimented with almost homogeneous isotropic turbulence in the central core of a turbulent air flow through a pipe 20 cm in diameter. The Reynolds number Re_D was varied between roughly 2×10^5 and 6×10^5. Mickelson measured separately the longitudinal correlation coefficient R'_x and the Lagrangian correlation coefficient from the diffusion of helium downstream of a fixed injection point. He found that within experimental accuracy for equal values of $R'_x(x)$ and $R'_L(\tau)$, x was proportional to τ with a constant value of β. This proportionality constant increased with increases in the fluctuating velocity component u'. Its average value, in the range of u' considered was 0.6, Figure (7-5). Hinze (79) discussed the unreliability of the determination of Lagrangian correlations for fluid particles from diffusion of a tracer gas due to the unknown effect of molecular diffusion and concluded that "at the most, we may conclude from Mickelson's experiments that the rough shapes of the Lagrangian and Eulerian correlation coefficients is the same".

Uberoi and Corrsin (112) have also investigated the relation between the Lagrangian and Eulerian scales of turbulence. The former scales were measured from the thermal diffusion behind a heated wire stretched perpendicular to (grid produced) isotropic flow in a wind tunnel. While the latter ones were deduced from similar measurements on grids having the same geometry. Though there was considerable scatter in the values of $\beta = L_x/\mathcal{L}_L$ as shown in Figure (7-6), its value increases roughly from 0.5 at

values of $Re_L \simeq 10$ to about 0.8 at values of $Ro_L \simeq 100$. Also, a regular decrease of $\mathcal{L}_L$ was observed with decreases in turbulence intensity ($u'/\bar{U}$).

Baldwin et al (111) have investigated the turbulent diffusion in pipe flow downstream of a line source of heat. The authors used a similar method to Mickelson's work with the exception that the factor of proportionality β was calculated at different separation distances of the correlation curve, Figure (7-7). The Eulerian scale L_x was found to increase with mean flow velocity, while the Lagrangian scale was apparently constant for all flow rates studied. The nett result is that the ratio of Eulerian to Lagrangian integral scales increases from 3.5 to 6.5 as the mean velocity $\bar{U}$ varies from 72.6 to 160 ft/sec. Baldwin et al have concluded that the hypothesis of similarity between the shapes of $R'_x(x)$ and $R'_L(\tau)$ is reasonable. However, the two fold variation of the empirical factor(β) with mean velocity over the small range of their experiments certainly limits its utility. Also, such similarity fails completely at large separation distances where $R'_x(x)$ becomes negative which suggests that nothing fundamental should be implied from this empirical comparison.

Hay and Pasquil (114) have carried out similar studies in atmospheric diffusion which indicated a rapid variation of the Eulerian auto-correlation while the Lagrangian correlation showed some persistence for longer time intervals. The proportionality factor (β) was suggested, therefore, to be not less than about 10.

In spite of the scattered and even contradictory results in the published investigation for the relationship between the Lagrangian and Eulerian scale of turbulence, there is strong evidence that their ratio ($\mathcal{L}_L/L_x$) is a function of the turbulence Reynolds numbers $Re_L = u' L_x/\nu$. This confirms the earlier assumption of Von Karman (80) for the expression of the mixing length as a function of the turbulence Reynolds number $Re_{\lambda'} = u' \lambda_y/\nu$. The relationship between both Reynolds numbers has been discussed earlier in Section (3.4.3).

It is believed, therefore, that there is no point in applying any specific relation, deduced from other investigations, to check the existence of a correlation between the measured eddy diffusivities in the engine and the predictions from pipe flow empirical relations (as equation 7-14). Hence an attempt was made to establish a functional relationship between ($\mathcal{L}_L/L_x$) and Re_L from the measured data in the present investigation which provides the minimum scatter in the data and to evaluate the coefficient of correlation between the measured values of eddy diffusivities and the predictions of equation (7-14).

The simplest form of the relationship between the Lagrangian and Eulerian scales was proposed as

$$\frac{\mathcal{L}_L}{L_x} = a + b \; Re_L^n \qquad (7\text{-}37)$$

The value of the exponent n, has to satisfy the condition of providing the least square errors between the predicted and measured eddy diffusivities in the engine, where the latter was calculated by the following relation

$$\mathcal{E}_{meas} = (u' \; L_x)_{meas} \; (\frac{\mathcal{L}_L}{L_x}) \qquad (7\text{-}38)$$

or

$$\mathcal{E}_{meas} = (u' \cdot L_x)_{meas} \cdot (a + b \, Re_L^n) \qquad (7\text{-}39)$$

It is believed, also, that obtaining the values of a, b and n from the measured data eliminates the need for applying any temperature correction on the values of friction factor, used in equation (7-14). Such correction will be included in the coefficient b as well as the value of the exponent n of R_{e_L} as governed by the variation of kinematic viscosity ν with gas temperature.

A computer program (appendix B8) was employed to search for the best value of n, as well as the determination of the values of a and b by a least square errors regression line between $(\mathcal{L}_L/L_x)$ and (Re_L^n). Figure (7-8) shows the variations of the root mean square value of the errors and the coefficient of correlation with the exponent (n). Also, Figure (7-9) shows a plot of the experimental values versus $(Re_L^{-0.8})$ which gave the best correlation of 0.9722. Figure (7-10) shows a plot of equation (7-37) for the ratio of $(\mathcal{L}_L/L_x)$ versus Re_L using the values of a, b, n of the best correlation. Figure (7-11) too shows a comparison between the values of eddy diffusivities calculated from equation (7-39) and the predictions of pipe flow relation (7-14). These experimental data include tests on the Rolls-Royce and Ford engines for plain valves and modified intake systems, as well as a new analysis of Semenov's work.

Comparison between the measured values of the macro-scale of turbulence using equation (3-68) and the predictions of pipe flow data under isotropic conditions has also shown very good correlation, Figure (7-12). The latter values were obtained from the relationship between the ratio of the scales λ_y/L_x and the turbulence Reynolds number Re as reported by Robertson et al (102) and Sato et al (103), Figure (3-101).

Robertson (102) has suggested that the fluctuating velocity component (u') is proportional to some characteristic fluid velocity such as the friction velocity (u*). Therefore, in spite of the scatter in the data, which is a characteristic feature of all turbulence experimental investigations, some universal constant values could be established for the ratio $(\frac{u'}{u*})$ for different types of flow. For example, a value of 1.7 is reported by Robertson for turbulent flow at 10% of boundary layer thickness or the pipe radius, Figure (7-13), where the pressure gradients in both types of flow are very small. While for strong pressure gradients, such as turbulent flow in a diffuser boundary layer, this ratio is quite high (144), Figure (7-14). A similar attempt was carried out for turbulent flow in engines during the compression stroke where turbulence intensities are much higher than those of pipe flow or external boundary layers. A summary of the average values during compression periods for various types of combustion chambers is given in Table (7-1) which indicates that an average value of 5.89 could be established for such a flow field at the spark plug location.

Table (7-1) A Summary of the Average Ratio Between Fluctuating Velocity Component and Friction Velocity for Different Types of Combustion Chambers During Compression Period

Engine Type	Combustion Chamber Shape	Test Conditions	u'/u*
ROLLS-ROYCE V8	WEDGE SHAPE (9:1 COMPRESSION RATIO)	1. Cylinder 3A, plain valve. (1000 r.p.m. and fully opened throttle).	
		Wire direction: θ = 60°	4.239
		θ = 300°	4.565
		θ = 330°	3.885
		2. Intake System Modifications	
		a) (1000 r.p.m. and fully opened throttle).	
		i) Inlet valve fitted with 4 vanes	7.710
		ii) Inlet valve fitted with 6 vanes 1st Test	6.0392
		2nd Test	6.5014
		iii) Inlet valve fitted with 8 vanes	6.736
		iv) Masked inlet valve	4.16
		v) Intake manifold fitted with delta wings	4.55
		b) (1000 r.p.m. and quarter throttle)	
		Inlet valve fitted with 6 vanes	4.731
FORD V4	HERON SHAPE (8.9:1 COMPRESSION RATIO)	3. Plain valve at 1000 r.p.m.	
		a) Full load conditions	5.86
		b) Part load conditions	6.664
		4. Intake System Modifications	
		a) Inlet valve fitted with 6 vanes, and full load conditions	
		i) Engine speed = 1000 rpm	6.5215
		ii) Engine speed = 2000 "	6.364
		iii) Engine speed = 3500 "	7.10325
		b) Inlet valve fitted with 4 vanes at 1000 r.p.m.	
		i) Full load conditions	7.046
		ii) Part load conditions	8.152

Table (7-1) Continued.

Engine Type	Combustion Chamber Shape	Test Conditions	u'/u^*
CFR	Disc Surface Combustion Chamber	Semenov's Data at TDC (900 r.p.m. and 71% volumetric efficiency)	
		Compression Ratio: 4:1	5.843
		6:1	6.748
		8:1	7.645
		9.5:1	9.68

7.1 Approximate Design Procedure for Predicting Turbulence Characteristics in Spark Ignition Engines

It has been shown, in the preceding discussion, that the characteristics of the turbulent flow field in engines could be predicted using the pipe flow experimental data and a knowledge of the mean gas velocity at the crank angles of interest.

Figure (7-13) shows a proposed procedure for obtaining the turbulence characteristics during the compression stroke which could be summarised as follows:

a) Obtain the mean gas velocities at the crank angle of interest (θ), as well as the gas properties, $T(\theta)$, $P(\theta)$.

b) Calculate a characteristic Reynolds number $Re(\theta)$ as given by equation (7-1).

c) Calculate the friction factor f in the friction velocity u^* and the non-dimensional velocity u^+, equations (7-24), (7-17), (7-16) and (7-15).

d) Calculate the fluctuating velocity component by multiplying the friction velocity by the universal constant ratio of (u'/u^*), obtained from Table (7-1).

e) Calculate the coefficient of eddy diffusivity by equation (7-14).

f) Obtain the Lagrangian scale of turbulence using equation (3-150).

g) Obtain the Eulerian scale of turbulence (L_x) using equation (7-37) by an itoration procedure.

h) Obtain the microscale of turbulence (λ_y) using the relationship between the macro and microscales of turbulence for isotropic conditions, e.g., equation (3-101) or Figure (3-14).

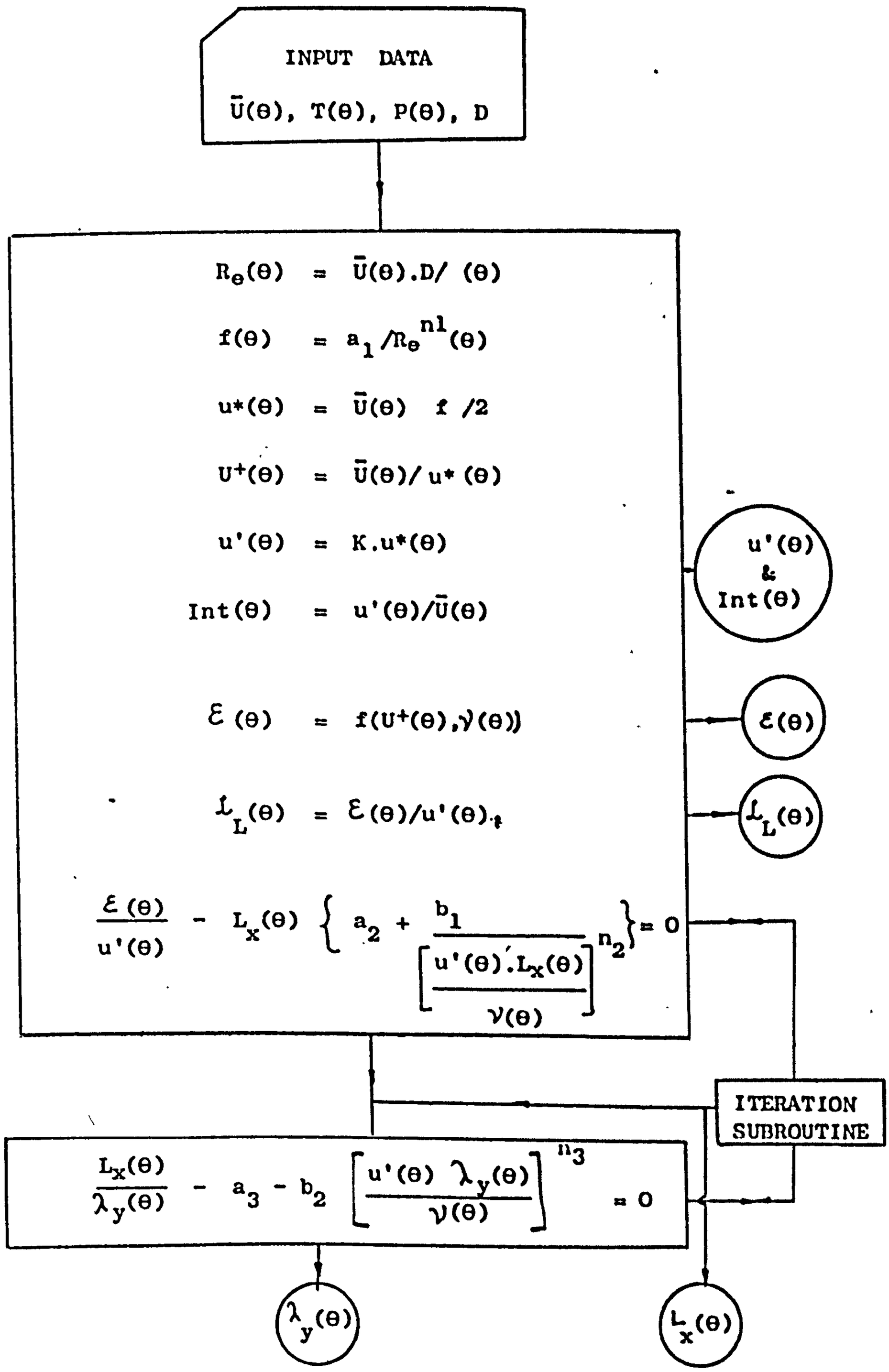

Fig. (7-14) Flow Chart Showing the Analytical Procedure for Predicting Turbulence Characteristics in S.I. Engines

Table 7-2 Values of Constants and Exponents Used for the Prediction Procedure

$a_1 = 0.046$	$b_1 = 28.582$	$n_1 = -0.2$
$a_2 = 0.121386$	$b_2 = 0.0228$	$n_2 = -0.8$
$a_3 = 0.53$	$K = 5.8935$	$n_3 = 1.23$

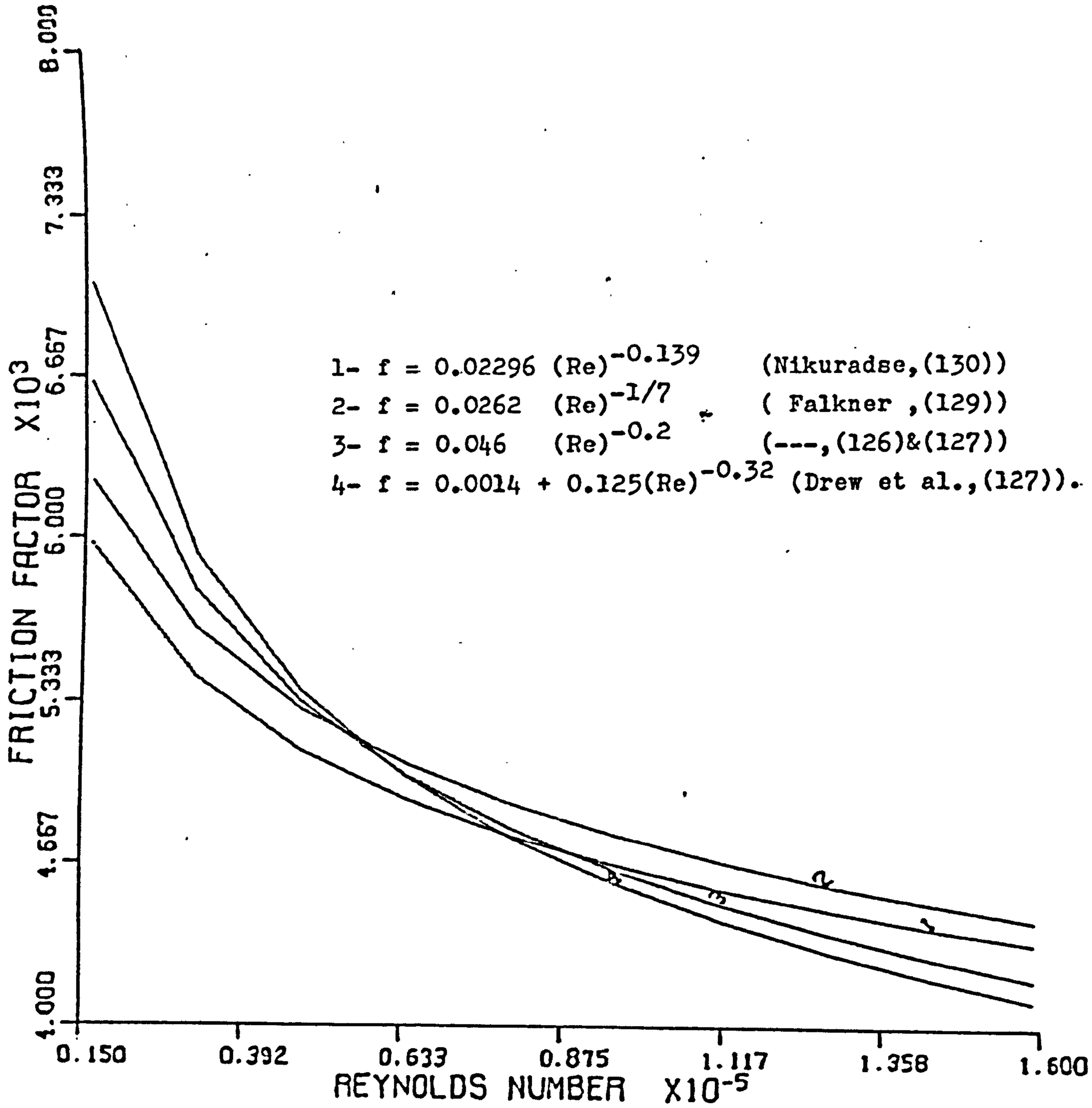

Fig (7-1) Comparison between different expressions of the friction factor

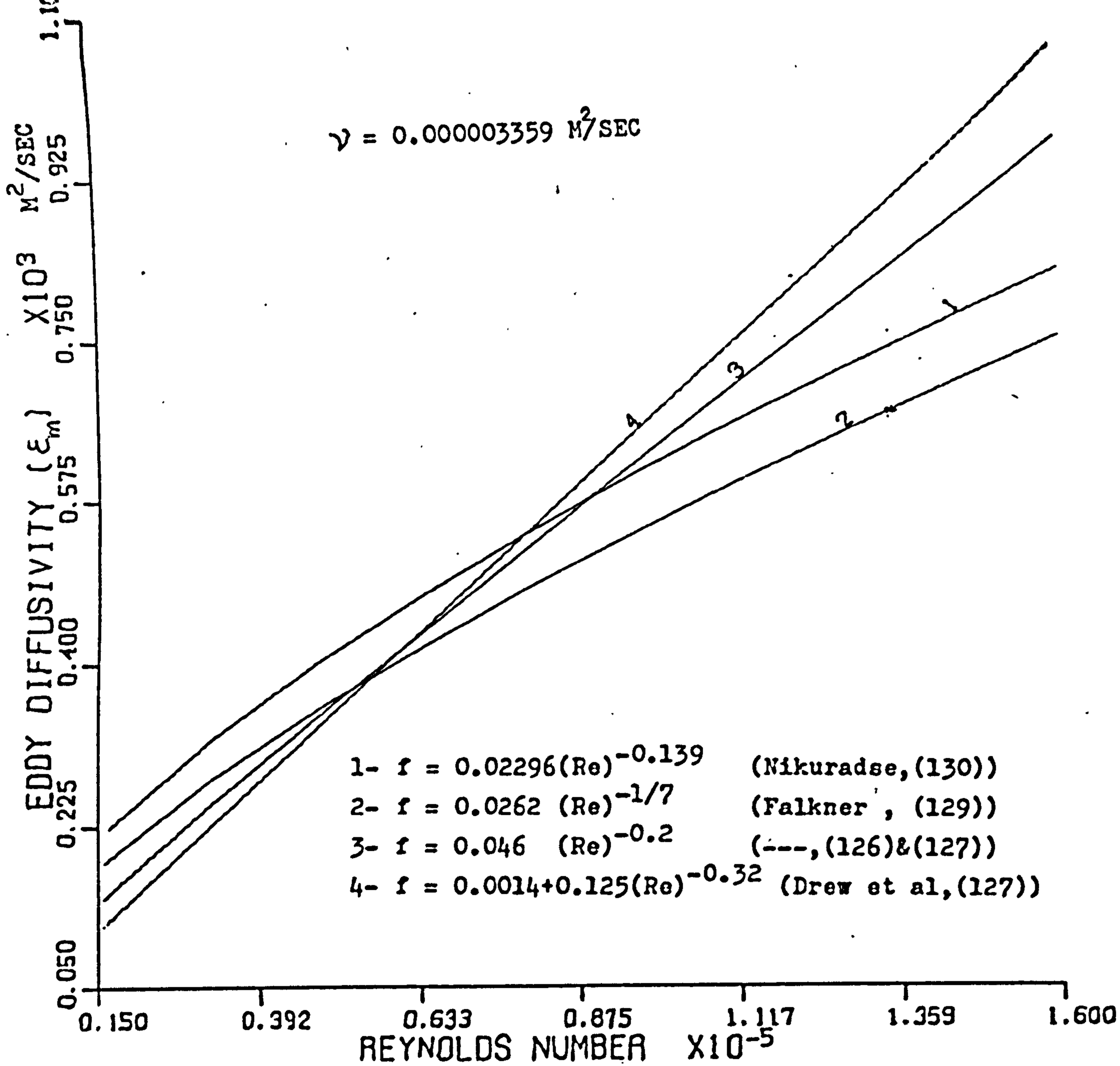

Fig (7-2) Comparison between the values of eddy diffusivity for different expressions of the friction factor at typical values of Reynolds number in an engine.

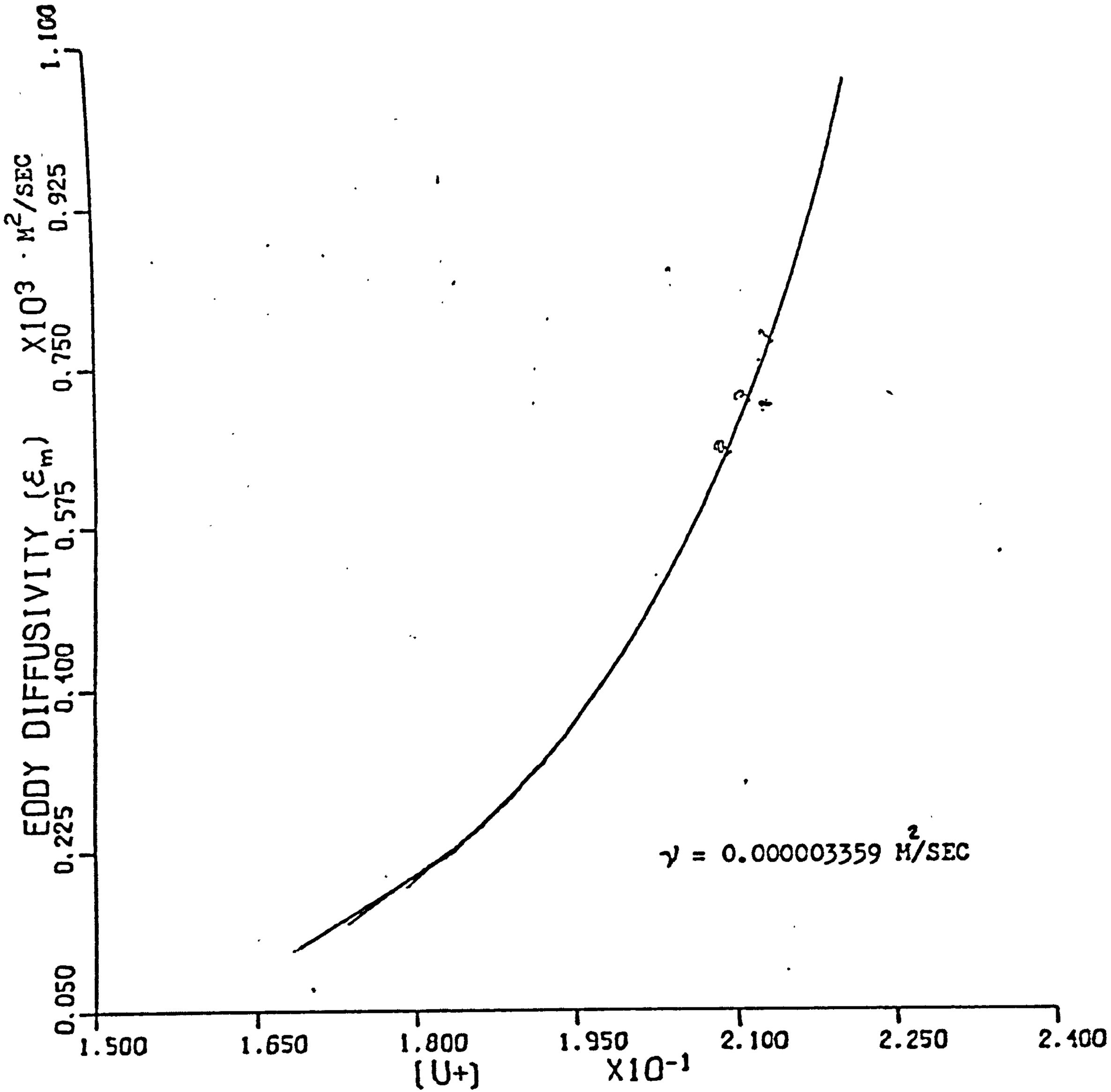

Fig (7-3) Variation of eddy diffusivity with the non-dimensional velocity U^+, using equation (7-14).

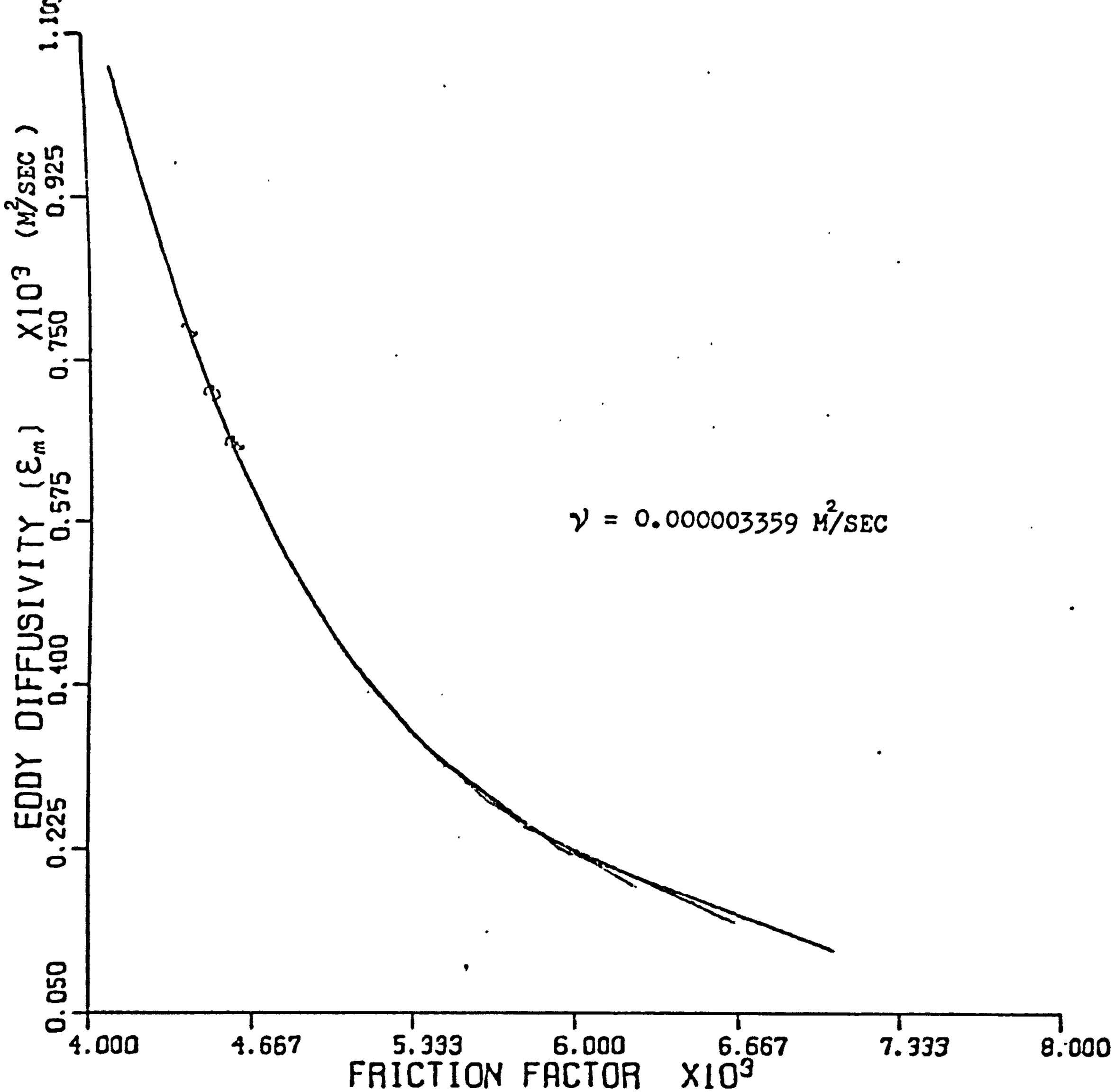

Fig (7-4) Variation of eddy diffusivity with the friction factor at typical values of Reynolds number in an engine.

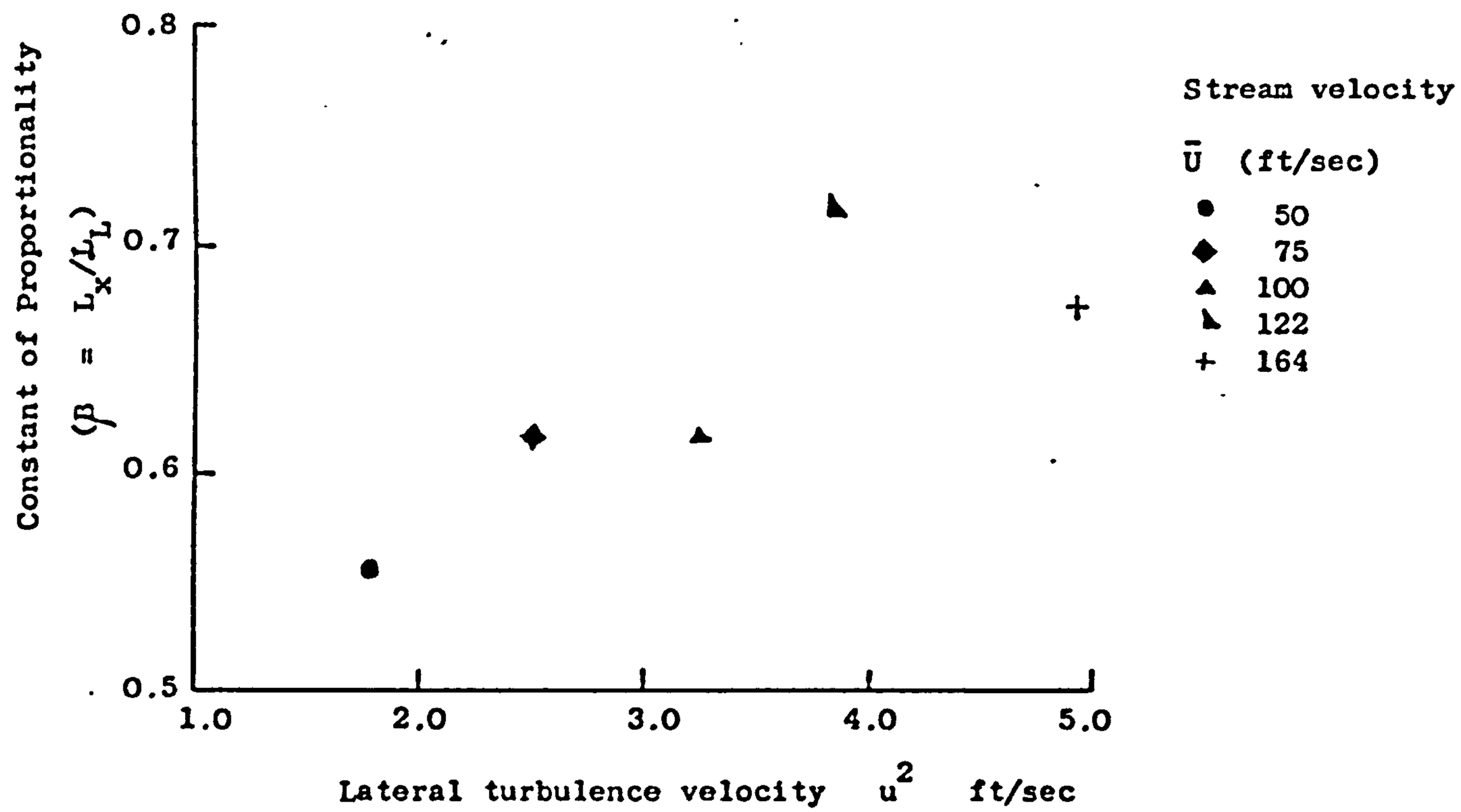

Fig. (7-5). Values of the constant of proportionality (β) between the shapes of Lagrangian and Eulerian correlation coefficients, (110).

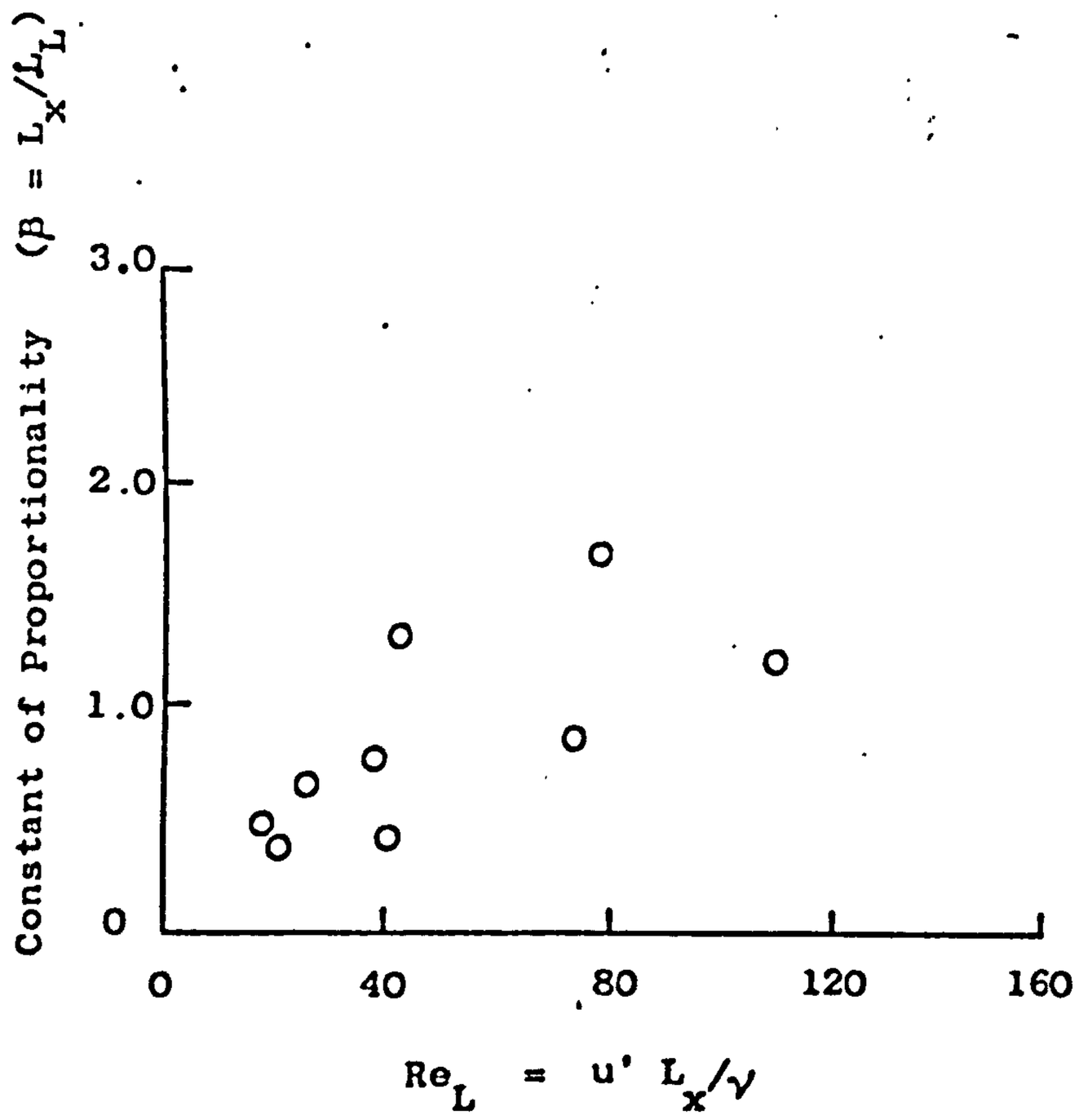

Fig. (7-6) Variation of the constant of proportionality (β) with Re_L, (112)

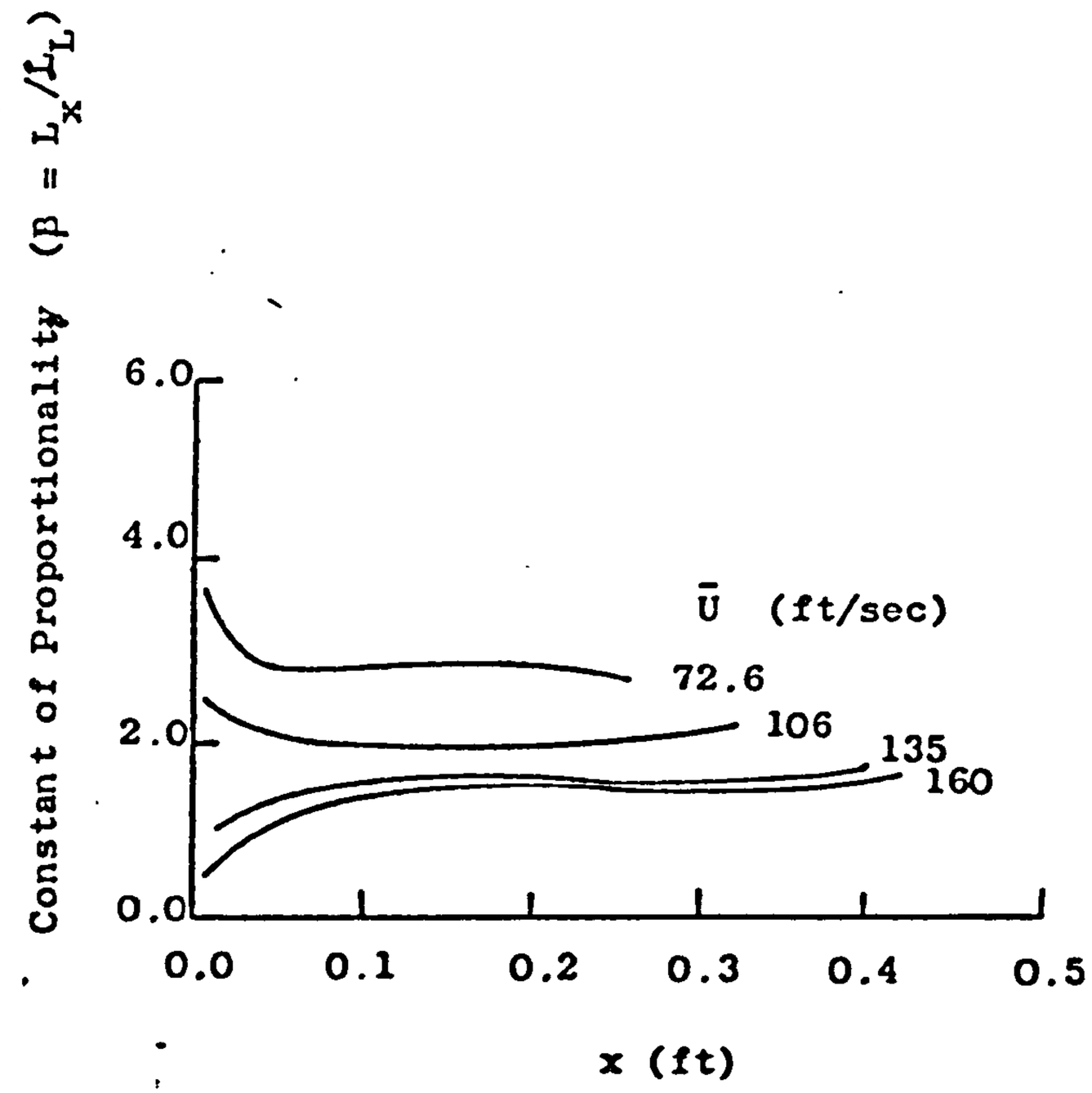

Fig. (7-7). Variation of the constant of proportionality (β) with the Separation Distance x and Mean Velocity (111).

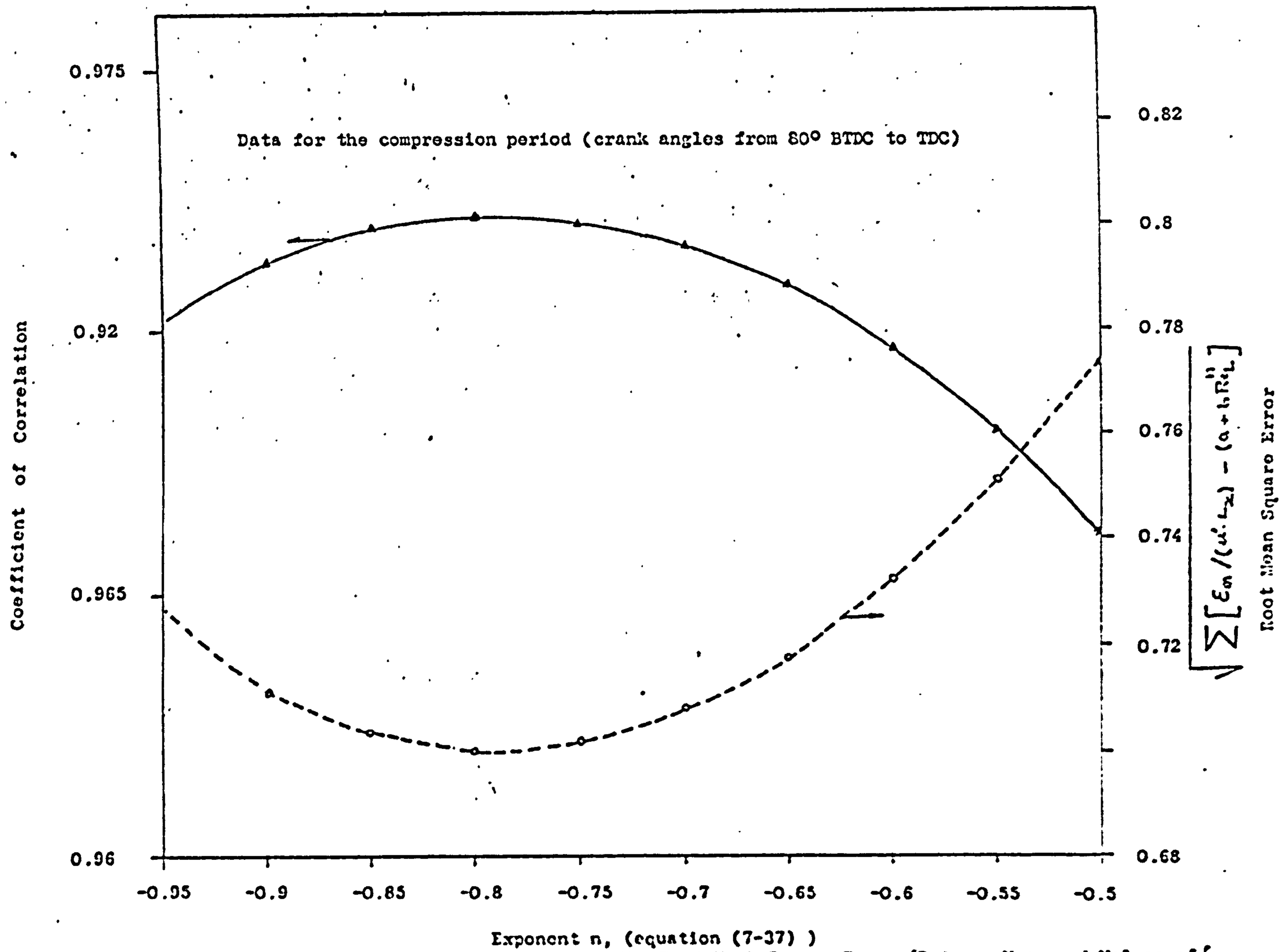

Fig. (7-8) Variation of the Coefficient of Variation and the Root Mean Square Error (Between Measured Values of ℓ_L/L_x and Predictions of Equation (7-37)) versus Re^n.

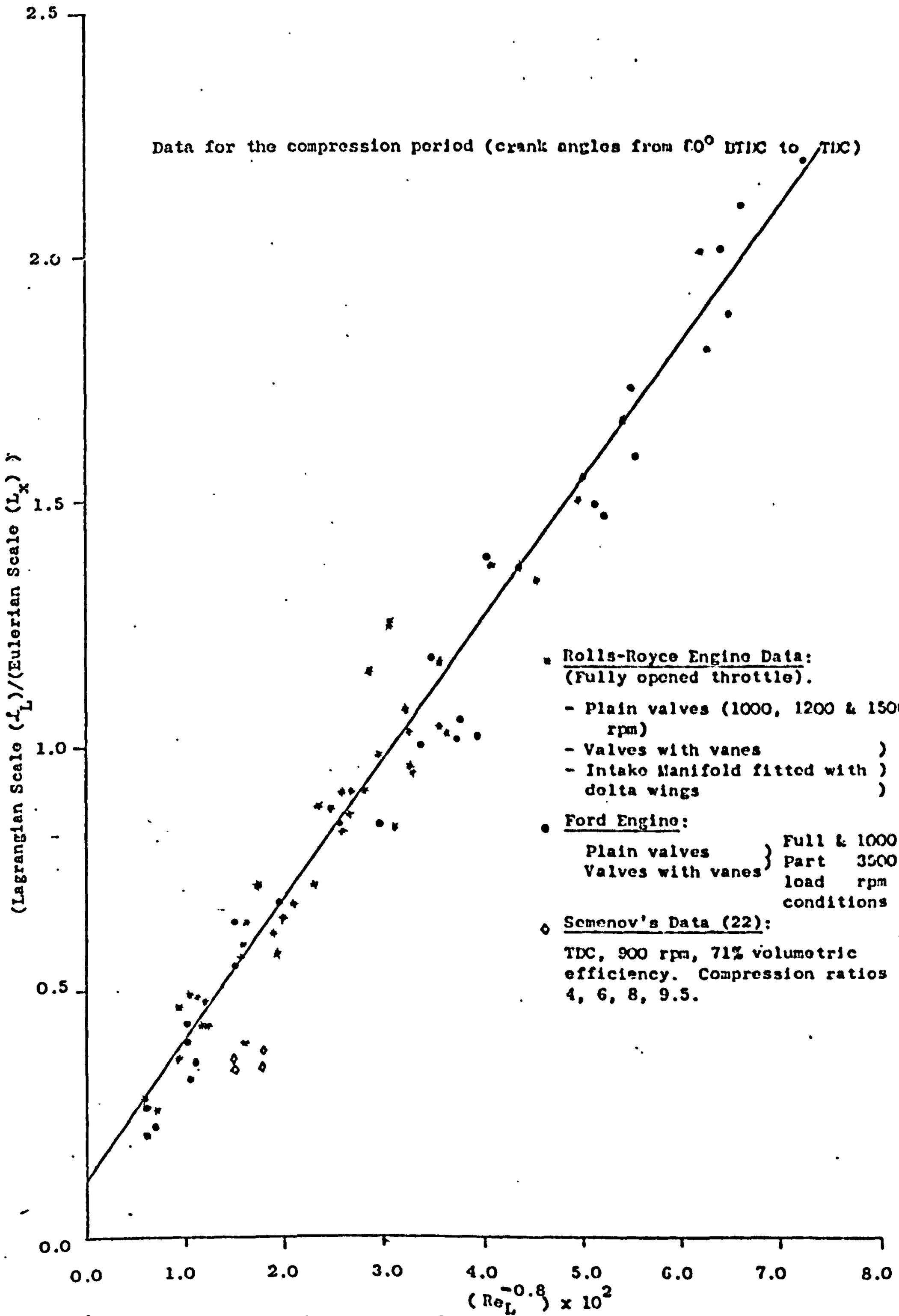

Fig. (7-9) Variation of the Ratio ($\mathcal{L}_L/L_x$) with Turbulence Reynolds Number.

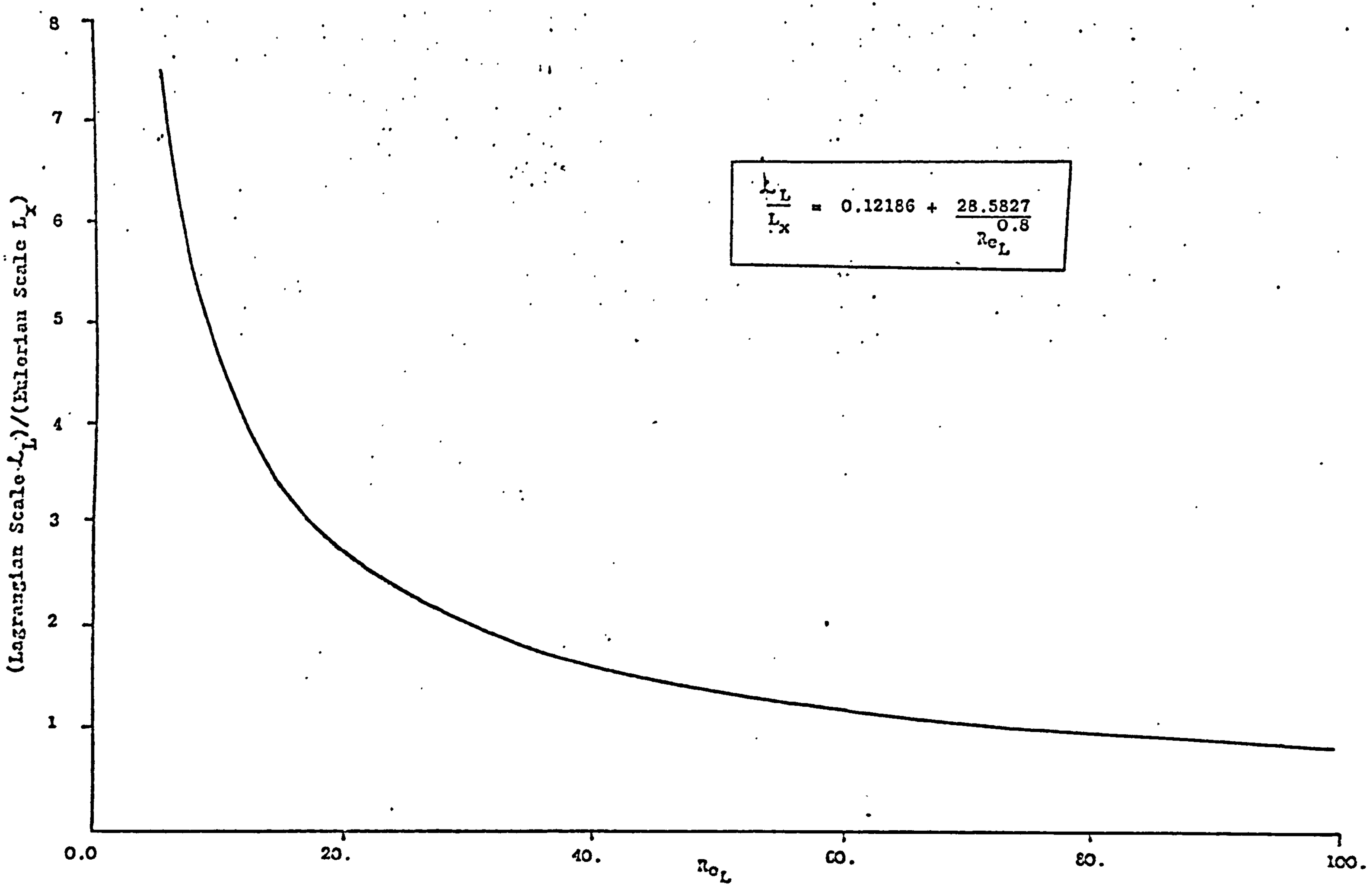

Fig. (7-10). Variation of the Ratio Between Lagrangian and Eulerian Scales at Different Values of Reynolds Number

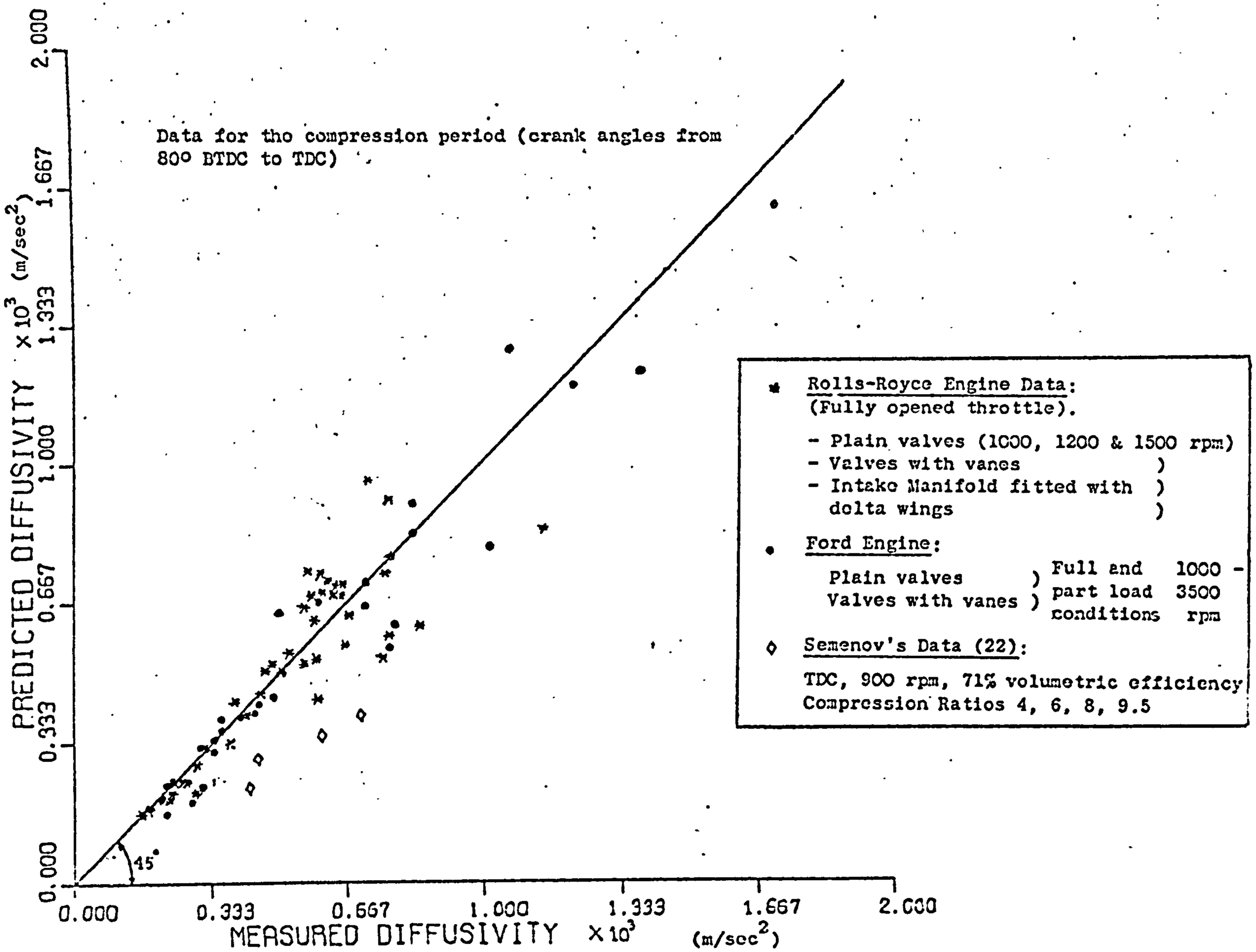

Fig. (7-11) Comparison Between Measured and Predicted Values of Eddy Diffusivity.

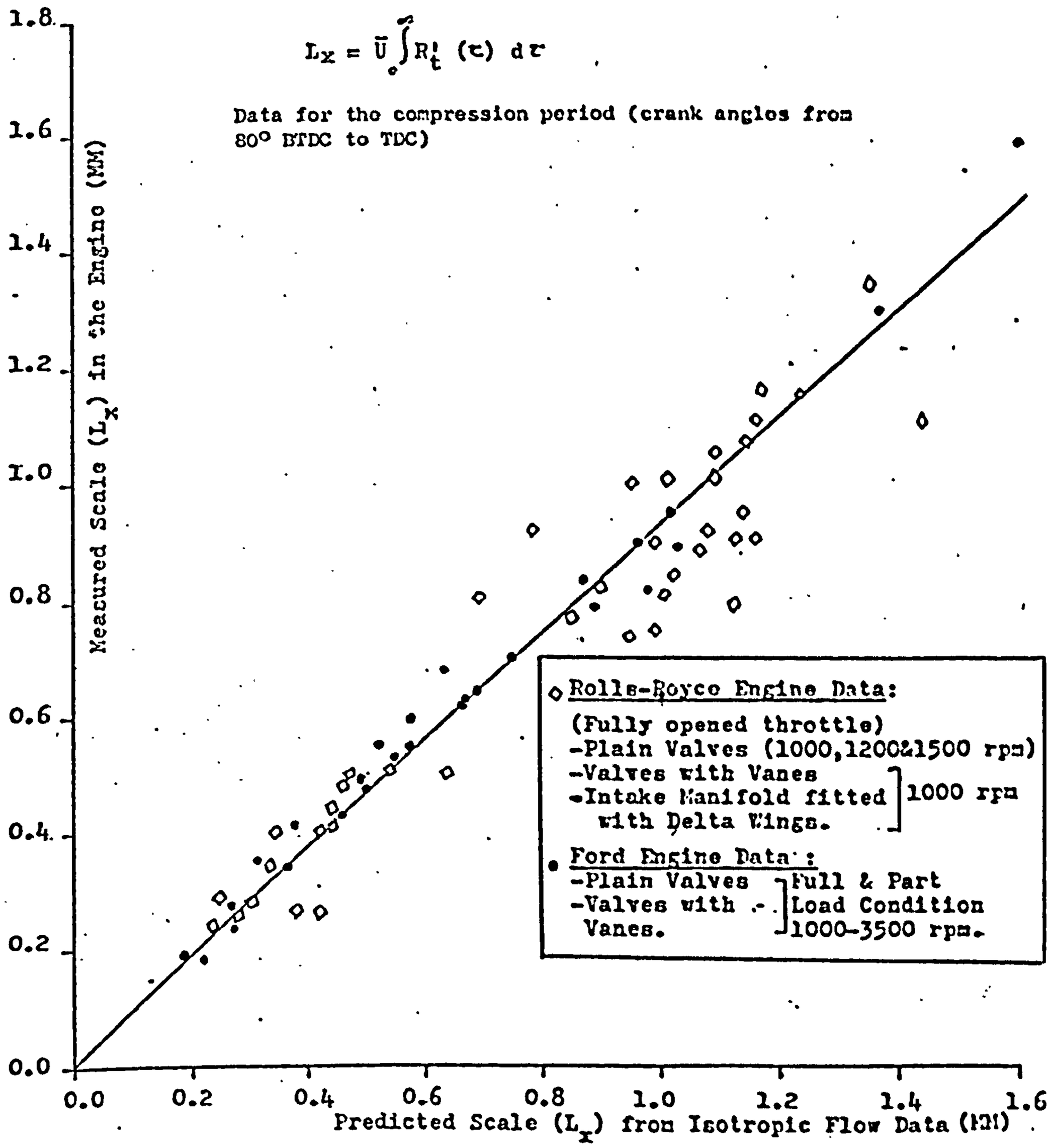

Fig (7-12) Comparison between the measured values of the macro-scale of turbulence in engines and the predictions from the experimental data of isotropic flow fields.

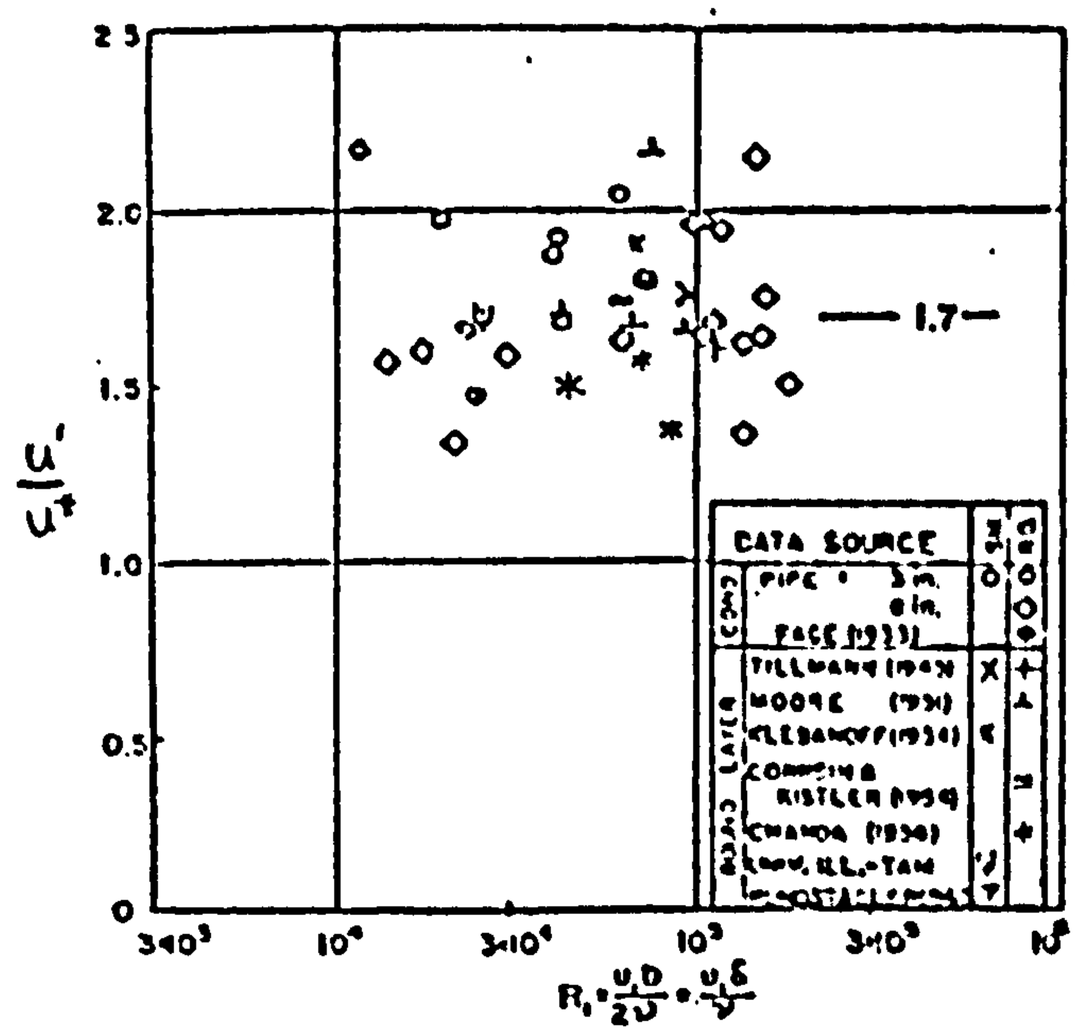

FIG. (7-13). Ratio Between Fluctuating Velocity Component and Friction Velocity for Rough and Smooth Surfaces at 10% Wall Distance, (102).

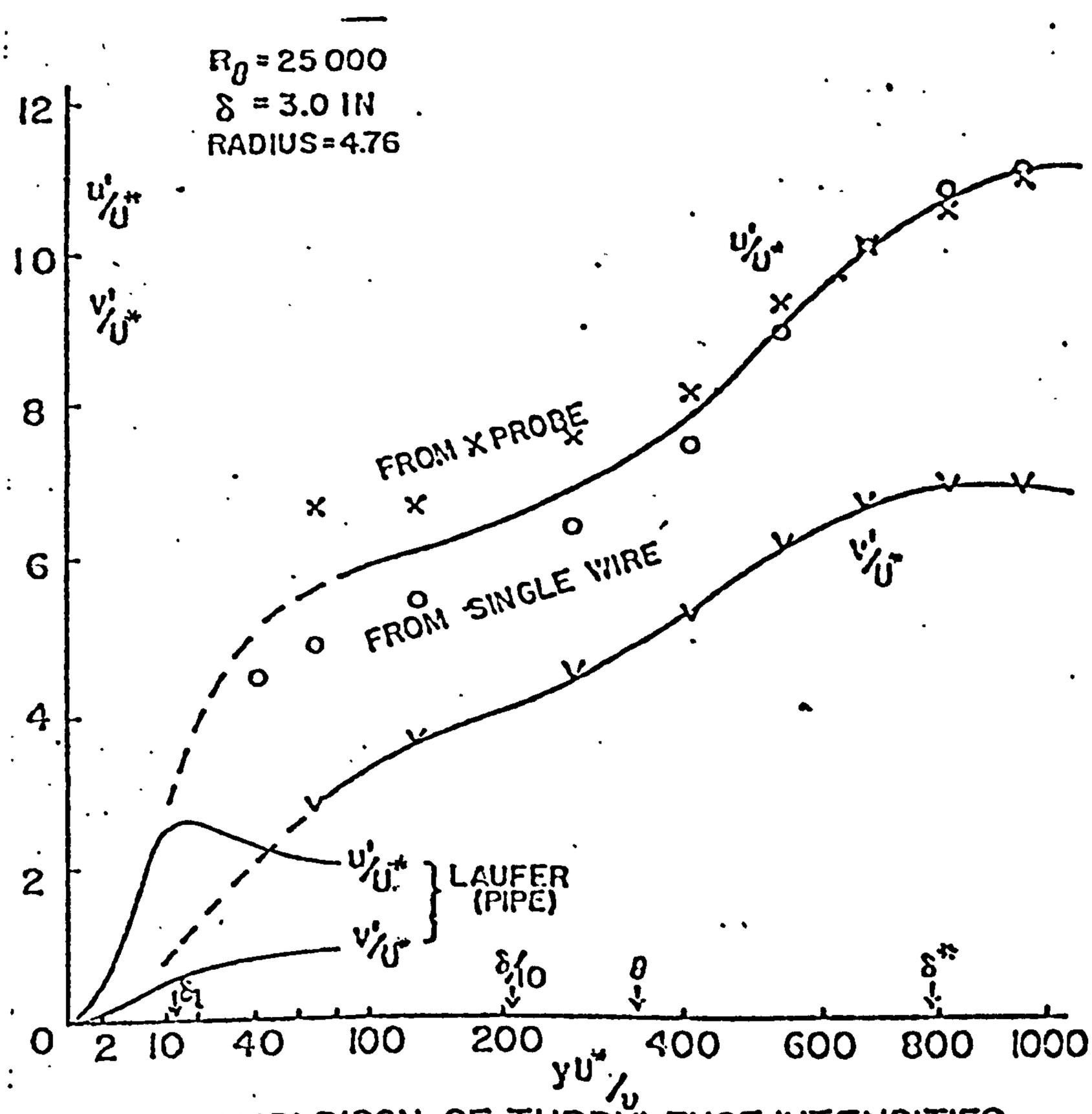

FIG. (7-14) COMPARISON OF TURBULENCE INTENSITIES WITH PIPE RESULTS (144)

8. MODEL OF CYCLIC COMBUSTION VARIATION

It has been concluded from the literature survey that most of the cyclic variation originates during the early development of the flame kernel (10, 13, 23). It has also been stated explicitly by Barton et al (10) and Miller et al (38) that after a certain percentage of the charge is burnt, little difference exists in the rate of burning for different engine cycles. Such percentage was estimated to be of the order of 2 - 5% in the former investigation and 10% in the latter.

Models of cyclic variation were constructed, therefore, to relate the observed variations in the cylinder pressure development or the flame speed to the corresponding variations in the time required to burn such a quantity of the mixture. Such variations are believed to be caused by velocity fluctuations at the spark plug gap at the time of ignition which consequently affects the flame speed and the burning time.

Barton et al (10) attempted to establish from their experimental data, a form of a velocity dependent function which could represent the effect of gas velocity on the flame speed and satisfies, at the same time, the assumptions of the proposed model. Their model could be expressed, therefore, as follows:

$$\frac{dV_b}{dt} = A_b . E . S_t \qquad (2\text{-}10)$$

or

$$\frac{dr_b}{dt} = E . S_t \qquad (2\text{-}11)$$

and

$$S_t = S_\ell \cdot f(U) \qquad (8\text{-}1)$$

where V_b, r_b are the volume of burnt gas and the corresponding radius of the flame front

E is the expansion ratio $= T_b M_u / T_u M_b$

T is the mixture temperature

M is the molecular weight of the mixture

S_ℓ is the laminar flame speed

and $f(U)$ is some unknown function of gas velocity which has to be established from experimental data

The subscripts b, u refer to burnt and unburnt conditions. Assuming that a constant ratio of the charge is burned during the initial period and that velocity variations and the initial burn time are correlated, the following expression could be obtained.

$$F(O.V.) \qquad \frac{S(t_b)}{S(U_i)} = C.g\,(\bar{U}_i) \qquad (2\text{-}13)$$

where $S(t_b)$, $S(U_i)$ are the standard variation in the initial burn time and gas velocity, respectively.

and $F(O.V.)$ is a function of the operating variables $= \Psi\,(A/F,\ T_i,\ P_i)$

The subscripts i refers to mixture conditions at the time of ignition.

The form of the function $g(U_i)$ which satisfies the assumptions of the model was obtained, therefore, by least square fit of $\log \left[F(O.V.) \frac{S(t_b)}{S(U_i)} \right]$ and $\log (U_i)$ and is given by

$$g(\bar{U}_i) = \left[\frac{1}{\bar{U}_i} \right]^{1.3} \tag{2-14}$$

Winsor (23) has proposed a similar model, which assumes that the average flame speed is sensitive to local turbulent velocity, only when the flame radius lies in a certain incremental range (dc) which is located at a finite but unknown distance from the spark electrodes. The author attempted, in this case, to find the value of such a critical radius, again by relating variations in flame speed (burn time) and gas velocity variations. Such a model could be described by the following relationship:

$$d_c = S_t . t_c \tag{8-2}$$

and

$$S_t = K.U \tag{2-15}$$

where t_c is a critical time period during which combustion variations occur.

Again, assuming constant value for such a radius and that variations in the burn time (defined as the time from ignition until combustion cessation) and the initial burn time are related to velocity variations, the following relations were obtained:

$$S(t_b) = S(t_c) = \frac{dt_c}{dU} \quad S(U)$$

or

$$S(t_b) = -\frac{d_c}{S_t} \cdot \frac{S(U)/\bar{U}}{1 + S(U)/\bar{U}} \quad 2 \qquad (2\text{-}17)$$

where the subscripts b, c, t refer to total burn time, critical period (initial burn time) and turbulent conditions. Substituting numerical values, from the experimental data, the value of the critical radius was obtained as 0.4 inch.

Examination of both models reveals that their basic concepts are similar. Both have assumed a critical radius of the flame kernel which has a constant value or a constant ratio of the total charge volume. Also, the effect of turbulence on flame speed was considered as a function of the gas mean velocity. Such a function was of unknown form in the first case and was assumed linear in the second one. Their basic hypothesis could be summarized, therefore, in the following:

1. Cyclic combustion variations are, mainly, due to gas velocity variations and the effect of turbulence on the development of the initial flame kernel which is required to produce a steady state flame propagation.

2. After a certain critical radius is reached, the flame front propagates at a constant speed and the corresponding rates of burning the charge will be repeatable from one cycle to another.

In fact, these conclusions explain that the effect of turbulence is very critical during the early development of the flame kernel, when its size is smaller than the size of the turbulence eddies. When the flame front thickness exceeds the size of the eddies, their effect will be confined to local disturbances on the flame front and the flame will propagate at a more or less constant speed. The effect of turbulence on this second stage will be averaged across the whole front and consequently such a stage will be statistically repeatable from one cycle to another.

A model of cyclic variation can be developed based on the assumption that small scale turbulence eddies are governing the propagation of the flame kernel until the size of such a kernel reaches some critical value comparable to the large scale eddies. Such a critical value can be assumed either equal to the large scale eddies or of some multiple value of the small scale eddies. The case of a universal constant value can be also considered, based on the assumption of similar turbulence fields in the engine during the later part of the compression period when the turbulence is decaying.

The effect of small scale turbulence on the propagation speed is usually known to intensify the transport process by

virtue of altering the fluid diffusivity from its molecular value to the turbulent one. Such a process can be described by the following expression of Shchelkin (47)

$$\frac{S_t}{S_\ell} = \sqrt{\frac{\varepsilon_{micro} + \nu}{\nu}} \qquad (2\text{-}10a)$$

where ν is the kinematic viscosity

ε_{micro} is the eddy diffusivity of micro-scale turbulence $= v'_{micro} \cdot \mathcal{L}_{L(micro)}$. (2-44)

v'_{micro} is the contribution of micro-scale eddies to the fluctuating velocity component

$\mathcal{L}_L$ is the Lagrangian scale of turbulence

Assuming that the spectrum curve (F(n) versus n) can be divided into two regions of small scale and large scale turbulence at a certain partitioning frequency n_o as follows

$$\int_o^{no} F(n)\ dn \qquad \text{and} \qquad \int_{no}^{\infty} F(n)\ dn$$

where n_o corresponds to the condition of transition as formulated by Kovasznay (57) as follows

$$\Gamma = \frac{\text{typical velocity gradient in approaching cold flow}}{\text{typical velocity gradient in laminar flame}}$$

or

$$\Gamma = \frac{v'}{\lambda_x} \cdot \frac{S_\ell}{\delta_\ell} \qquad (2\text{-}42a)$$

where $\Gamma > 1$ for disintegrated flame front by the action of small scale eddies

δ_ℓ is the thickness of laminar flame

and λ_x is the micro-scale of turbulence

we can write the following relations

$$v'_{micro} = v'_{total} \cdot \sqrt{\int_{no}^{\infty} F(n)\, dn} \qquad (2\text{-}45a)$$

and consequently

$$\varepsilon_{micro} = \varepsilon_{total} \frac{\mathcal{L}_{L\ micro}}{\mathcal{L}_{L\ total}} \sqrt{\int_{no}^{\infty} F(n)\ dn} \qquad (2\text{-}47)$$

where ε_{total} is the mean value of eddy diffusivity of the all turbulent eddies in the flow

$$= \mathcal{L}_{L\ total} \quad v'_{total} \qquad (2\text{-}46)$$

$\mathcal{L}_L$ is the Lagrangian scale of turbulence which could be expressed in terms of the Eulerian scales L_x and λ_x as follows:

$$\mathcal{L}_{L(micro)} = K_1 \ \lambda_x \qquad (8\text{-}3a)$$

$$\mathcal{L}_{L(total)} = K_1 \ L_x \qquad (8\text{-}3b)$$

K_1 is the ratio between the Lagrangian and Eulerian correlation functions.

Moreover the range of very high frequencies in the power spectrum curve of turbulent flow could be considered as statistically steady in its mean values and independent of external conditions (universal range in Kolmogoroff hypothesis (89)). Therefore, we can use a mean value for the expression under the radical ($\sqrt{\int_{no}^{\infty} F(n)\, dn} \simeq$ constant) for any particular engine speed, and equation (2-47) reduces to

$$\varepsilon_{micro} = K_2 \quad \varepsilon_{total} \quad \frac{\lambda_x}{L_x} \qquad (8\text{-}4)$$

It is also concluded by the present investigation that the total value of eddy diffusivity could be predicted from the proposed expressions for pipe flow under appropriate conditions. A general expression for such eddy diffusivity which applies throughout the whole turbulent regions (laminar sublayer, buffer layer and the turbulent core), is proposed by Spalding (128) as follows:

$$\varepsilon_{total} = \varepsilon_m = \frac{\nu.K}{E} \left[e^{KU^+} - 1 - KU^+ - \frac{(KU^+)^2}{2!} - \frac{(KU^+)^3}{3!} \right] \qquad (7\text{-}14)$$

where $U^+ = u/u^*$

u^* is the friction velocity

U is the local gas velocity

and the constants K and E have the following values K = 0.407 and E = 10.

The ratio between the micro-scale and macro-scales of turbulence in equation (8-4) could be obtained from the isotropic flow theory as discussed in Chapter 3 and is given by the following relation

$$\frac{L_x}{\lambda_x} = K_3 \sqrt{\frac{u' \; L_x}{\nu}}$$

or

$$\frac{L_x}{\lambda_x} = K_4 \cdot \sqrt{\frac{\varepsilon_{total}}{\nu}} \qquad (8\text{-}5)$$

Substituting for $\frac{L_x}{\lambda_x}$ from equation (8-5) into equation (8-4) gives

$$\varepsilon_{micro} = \frac{K_2}{K_4} \; \varepsilon_{total} \sqrt{\frac{\nu}{\varepsilon_{total}}} = K_5 \sqrt{\varepsilon_{total} \cdot \nu} \qquad (8\text{-}6)$$

Knowing that the coefficient of eddy diffusivity is of the order of 200 times the kinematic viscosity during compression period in the engine cycle (as shown in Chapter 7) equation (2-19a) could be written as

$$\frac{S_t}{S_\ell} = \sqrt{\frac{\varepsilon_{micro}}{\nu}} \qquad (2\text{-}19)$$

Substituting for ε_{micro} from equation (8-6) into equation (2-19) gives

$$\frac{S_t}{S_\ell} = K_6 \left(\frac{\varepsilon_{total}}{\nu} \right)^{0.25}$$

$$\equiv K_6 \left(\frac{\varepsilon_m}{\nu} \right)^{0.25} \qquad (8\text{-}7)$$

The rate of change of the burned volume could be expressed by a relation similar to that used for a constant volume bomb (135), equation (2-10)

$$\frac{d\,V_b}{dt} = A_b.\ S_t.\ E \qquad (2\text{-}10)$$

which could be reduced for the case of hemispherical shell flame front to

$$\frac{d\,r_b}{dt} = E.\ S_t \qquad (2\text{-}11)$$

Integrating equation (2-11) and assuming that both S_t and E are constant during the short time interval of flame kernel growth for any particular cycle, gives

$$r_b = S_t.\ E.\ t_b \qquad (8\text{-}8)$$

where r_b is some critical radius of the flame kernel which is required to produce a stable and steady flame propagation thereafter.

Two assumptions could be made about the value of such a radius, either a constant value as assumed in the models of Barton et al and Winsor or some multiple value of the (mean) micro-scale of turbulence. The latter one seems more significant because it introduces the physical process of transition from a flame kernel of a size smaller than the eddies existing in the field to a flame front which could average many eddies.

The definition of such a value is much more difficult because of the artificial distinction of the turbulence field into small and large scale turbulence while a wide spectrum of eddies of different sizes actually exists. Moreover, the reference length of comparison can only be the flame thickness and the more intense the turbulence the thicker this is.

The hypotheses used in the present model are the same as discussed earlier, where all combustion variations are attributed to the fluctuations in the rate of growth of the initial flame kernel due to the nature of the fluctuations in eddy diffusivities which controls such a combustion process. We can write, therefore, the following relation

$$S(t_b) = \left(\frac{dt_b}{dS_t} \right) S(S_t) \qquad (8\text{-}9)$$

where t_b is the initial burn time

S_t is the turbulent flame speed

$S(t_b)$ and $S(S_t)$ are the standard deviations in t_b and S_t respectively

and $\left(\frac{dt_b}{dS_t} \right)$ is a mean value of the derivative of burning time with respect to turbulent flame speed during the initial period of flame kernel growth.

Similiar expressions can be written for the relationship between the fluctuations in flame speed and the corresponding fluctuations in eddy diffusivities as follows:

$$S(S_t) = \left(\frac{dS_t}{d\varepsilon_m}\right) S(\varepsilon_m) \tag{8-10}$$

which can be reduced with the aid of equation (8-7) to

$$S(S_t) = \frac{K_6}{4} \frac{S_\ell \quad S(\varepsilon_m)}{\varepsilon_m^{0.75} \quad \nu^{0.25}} \tag{8-11}$$

Substituting equation (8-11) into equation (8-9) gives

$$S(t_b) = \frac{K_6}{4} \overline{\left(\frac{dt_b}{dS_t}\right)} \frac{S_\ell \cdot S(\varepsilon_m)}{\varepsilon_m^{.75} \quad \nu^{.25}} \tag{8-12}$$

If we assume that a minimum value of the critical radius is nearly constant, we may write the following relation

then $\quad r_b = \text{constant} \qquad (8\text{-}13)$

$$dr_b = 0 = \frac{\partial r_b}{\partial t_b} dt_b + \frac{\partial r_b}{\partial S_t} d S_t$$

or

$$\overline{\left(\frac{dt_b}{dS_t}\right)} = - \frac{\left(\frac{\partial r_b}{\partial S_t}\right)}{\left(\frac{\partial r_b}{\partial t_b}\right)} \tag{8-14}$$

Using equation (8-8) we get

$$\overline{\left(\frac{dt_b}{dS_t}\right)} = - \left(\frac{\bar{t}_b}{\bar{S}_t}\right) = - \left(\frac{\bar{r}_b}{\bar{S}_t^{\,2} E}\right) \tag{8-15}$$

Substituting equation (8-15) into equation (8-12) we got

$$S(t_b) = \frac{-K_6}{4} \frac{\bar{r}_b}{S_t^2 E} \frac{S_\ell}{\nu^{0.25} \varepsilon_m^{0.75}} S(\varepsilon_m)$$

or

$$S(t_b) = \frac{K_7 \cdot \nu^{0.25}}{S_\ell \cdot E \cdot \bar{\varepsilon}_m^{1.25}} S(\varepsilon_m) \qquad (8\text{-}16)$$

Now let us consider the case of a minimum radius which is of some multiple ratio of the small scale eddies. This condition could be written as follows.

$$r_b = K_8 \cdot \lambda_x \qquad (8\text{-}17)$$

Equation (8-8) can be written in the form

$$t_b = \frac{r_b}{S_t E} \qquad (8\text{-}8a)$$

Differentiating equation (8-8a) with respect to turbulent flame speed gives

$$\frac{dt_b}{dS_t} = \frac{S_t \left(\frac{dr_b}{dS_t} \right) - r_b}{S_t^2 E} \qquad (8\text{-}19)$$

The variation of the critical radius with flame speed can be obtained by differentiating equation (8-7) with respect to the critical radius as follows

$$\frac{dS_t}{dr_b} = \frac{K_6}{4} \cdot \frac{S_\ell \cdot (d\,\varepsilon_m/dU)}{\nu^{0.25}\ \bar{\varepsilon}_m^{0.75}} \cdot (dU/dr_b) \qquad (8\text{-}20)$$

Since the eddy diffusivity is a function of gas velocity and kinematic viscosity, the problem is reduced to establishing a relationship describing the variation of the critical radius with gas velocity in the engine. In this respect we can make use of the experimental data obtained in the present work and the available knowledge about variation of turbulent characteristics with operating variables.

The micro-scale of turbulence was found to have a linear relationship with gas velocity. Therefore we can write

$$\lambda_x = a.\ U \qquad (8\text{-}21)$$

where a is a constant value which decreases with engine speed.

Making use of equations (8-17) and (8-21) equation (8-20) can be simplified to the following form

$$\frac{dS_t}{dr_b} = K_9 \frac{S_\ell}{\nu^{0.25}} \cdot \frac{(d\,\varepsilon_m/dU)}{\varepsilon_m^{0.75}} \qquad (8\text{-}22)$$

where $K_9 = \left(\frac{K_6}{4a\ K_8}\right)$ a constant value for any particular engine speed.

Substituting equation (8-22) into equation (8-19) and making use of equation (8-7) we got

$$\frac{dt_b}{dS_t} = \frac{(a\ K_8)\ (4\ \varepsilon_m/(d\ \varepsilon_m/dU) - U}{E\ S_\ell^{\ 2}\ (\varepsilon_m/\nu)^{\ 0.5}} \qquad (8\text{-}23)$$

Substituting equation (8-23) into equation (8-12) yields the final model equation as follows

$$S(t_b) = \frac{K_{10} \cdot \left[4\ \varepsilon_m/(d\ \varepsilon_m/dU) - U\right] . \nu^{\ 0.25}}{S_\ell\ \ \varepsilon_m^{\ 1.25} .\ E}\ S(\varepsilon_m) \qquad (8\text{-}24)$$

where $K_{10} = (a\ K_8)/(4\ K_6)$

The variations in eddy diffusivity could be related to the corresponding variations in gas mean velocities as follows:

$$S(\varepsilon_m) = \frac{d\varepsilon_m}{dU^+} .\quad S(U^+) \qquad (8\text{-}25)$$

But

$$\frac{d\varepsilon_m}{dU^+} = \frac{\nu K^2}{E}\left[\ e^{KU^+} - 1 - U^+ - \frac{U^{+2}}{2}\ \right] \qquad (8\text{-}26)$$

Therefore

$$S(\varepsilon_m) = \frac{\nu K^2}{E}\left[\ e^{KU^+} - 1 - U - \frac{U^{+2}}{2}\right] S(U^+) \qquad (8\text{-}27)$$

Similarly

$$S(U^+) = \left(\frac{dU^+}{d\ U}\right) .\quad S(U) \qquad (8\text{-}28)$$

Consequently, equation (8-25) could be written in the following form

$$S(\mathcal{E}_m) = f(U,\nu). \quad S(U) \qquad (8\text{-}29)$$

Comparing the model equation (8-16) and (8-24) shows that the difference between the two expressions is the introduction of the term $\frac{K_{10}}{K_7}$ $(4\mathcal{E}_m/(d\,\mathcal{E}_m/dU) - U)$ for the latter case. This term will have an almost constant value for any particular engine speed within a close range of ignition timing.

8.1 Experimental Verification of Cyclic Combustion Variations Model

The proposed model of equations (8-16) and (8-24) suggests that cyclic combustion variations are caused, mainly, by variations in the early propagation of the flame kernel. The model relates these variations to the random variation in the eddy diffusivity of the flow which are responsible for the transport process during this period. Therefore, if the resultant combustion variation (as reflected in variations of flame speed, cylinder peak pressure and peak rates of pressure changes) has originated during the propagation of the flame kernel into a stable flame front of nearly constant speed, a high correlation must exist between measured values of standard deviations of flame speed and gas mean velocity as governed by the velocity functions of equations (8-16) and (8-24).

The model could be tested, therefore, using the experimental data of other investigators such as those of Barton et al (10) or Winsor (23).

Although Barton et al did not measure the flame speed directly, the angle of occurrence of either the peak cylinder pressure or the peak rate of pressure change can be used to represent the flame travel times. We can therefore write

$$S(t_b) = \frac{S(\theta_{p_{max}})}{720} \quad \frac{120}{rpm} \quad .$$

or

$$S(t_b) = \frac{S(\theta_{p_{max}})}{6 \text{ rpm}} \quad \text{(seconds)} \qquad (8\text{-}30)$$

Similarly

$$S(t_b) = \frac{S(\theta_{\dot{p}_{max}})}{6 \text{ rpm}} \qquad (8\text{-}31)$$

Substituting the numerical values for the different variables in equations (8-16) and (8-24) at different engine operating conditions should give consistent values of the ratio between the expressions on both sides of the equations, if the assumptions of the model are satisfied.

The second set of experimental data which could be used for testing the hypotheses of the model is that of Winsor's work where a certain characteristic time was measured from the time of ignition until the combustion cessation. The reported

measurements of gas velocities, in this work, corresponds only to the TDC position with the exception of a run at 1000 r.p.m. where gas velocities versus crank angles were shown. However, estimation of the velocity traces at this engine speed suggests that approximate estimation of gas velocities at the other two speeds (1200 and 1500 r.p.m.) could be obtained using the reported values at TDC and assuming the same rate of decay as that for the 1000 r.p.m. Also, the values of the coefficient of variation ($\frac{S(U)}{\bar{U}}$) at TDC could be assumed valid also at the time of ignition to give an estimation of the standard deviations in gas velocities at ignition. These two approximations are justified because of the close range of speeds under consideration and the absence of any secondary flow created during compression for the flat disc combustion chamber used in that work.

Once again we can relate the variations in the critical burning time to the corresponding variations in the total burn time as defined earlier. Thus

$$S(t_b) = S(t_c) \tag{8-32}$$

The above mentioned approximations could be formulated as follows

$$U_i \simeq b \; U_{TDC} \tag{8-33}$$

and

$$\frac{S(U_i)}{U_i} \simeq \frac{S(U_{TDC})}{U_{TDC}}$$

or

$$S(U_i) = b\, S(U_{TDC}) \qquad (8\text{-}34)$$

The model equations could be applied therefore on velocities and their standard deviations at TDC.

Application of the model equation (8-16) to the experimental data of Barton et al (10) and Winsor (23) have shown good agreement between the predictions of the model and the experimental results as shown in Figures (8-1) and (8-2). The deviations in the ratio between predicted and measured variations in flame speed were found to be 18% for Barton's data and 16.7% for Winsor's data.

Unfortunately, turbulence measurements were not carried out in either Barton's or Winsor's work to enable checking the validity of the second assumption about a critical radius which is of multiple ratio of micro-scale eddies. Moreover, the application of the approximate method presented in Section (7-1) for predicting turbulence characteristics from mean velocity, fluid properties and engine dimensions . will not be helpful in this situation. This is mainly because only few experiments were carried out in these investigations at each engine speed (one in most cases) which makes the process of estimating the variation of micro-scales with gas velocity unreliable. Nevertheless application of the model to a reasonable sample of Barton's data at a fixed engine speed of 900 r.p.m. where the slope of U-versus λ_x could be included in the constants has shown an excellent result where the scatter of the ratio between the predicted and measured

variations in the burning time were found to be about 10% only, which is of the same order of magnitudes of experimental errors. However, the application of the model equation for a constant critical radius on the same set of data gives results of the same order of magnitude. This could be explained by the fact that in this model the variation of flame speed with the critical radius are mainly a function of gas velocities at a fixed engine speed which are nearly constant within the range of ignition timing used in Barton's investigation. Figure (8-3) shows a plot of the variation of the factor $(4\xi_m/(d\xi_m/dU) - U)$ versus U which indicates an almost constant value for the particular engine speed considered.

In fact exact comparisons of predictions of the model and experimental data should be carried out using variation in flame speeds (travel times between ionization gaps) rather than variations in the angle of occurrence of maximum pressure (or rate of pressure change) as used in Barton's work or the burn time defined by Winsor.

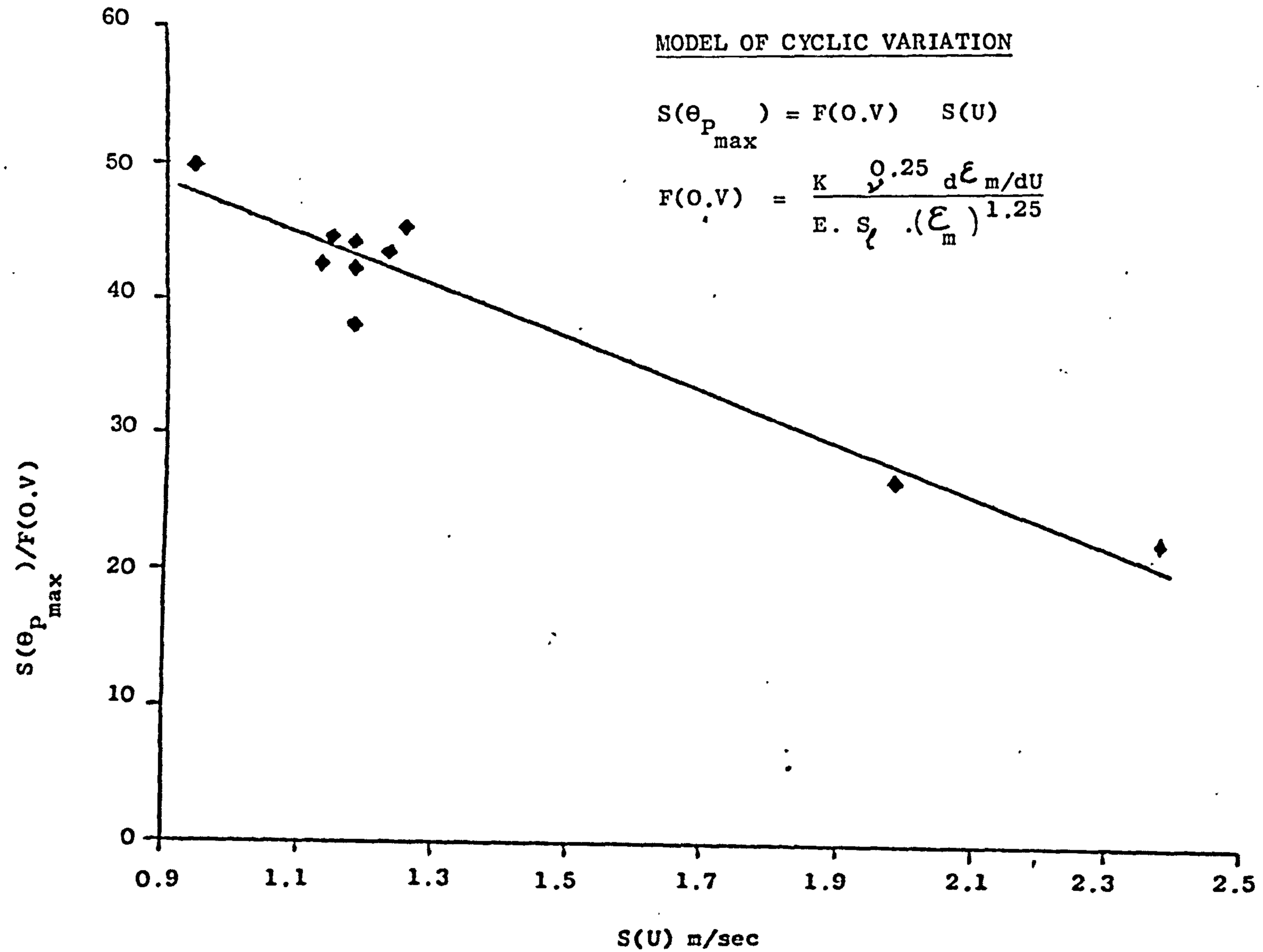

Fig. (8-1) Verification of the theoretical model of cyclic variation, equation (8-16) using the experimental data of Barton (10).

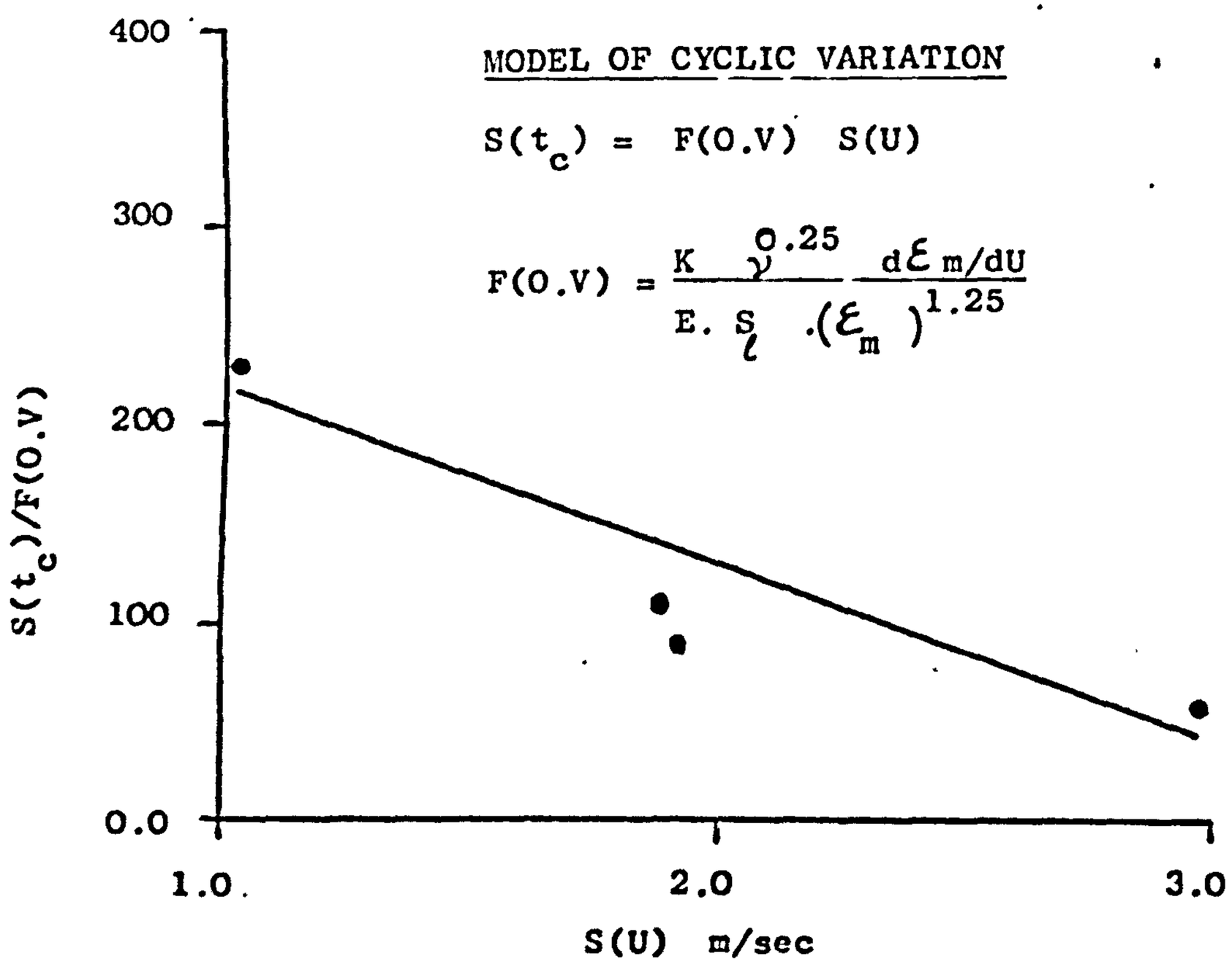

Fig. (8-2) Verification of the theoretical model of cyclic variation, equation (8-16) using the data of Winsor (23).

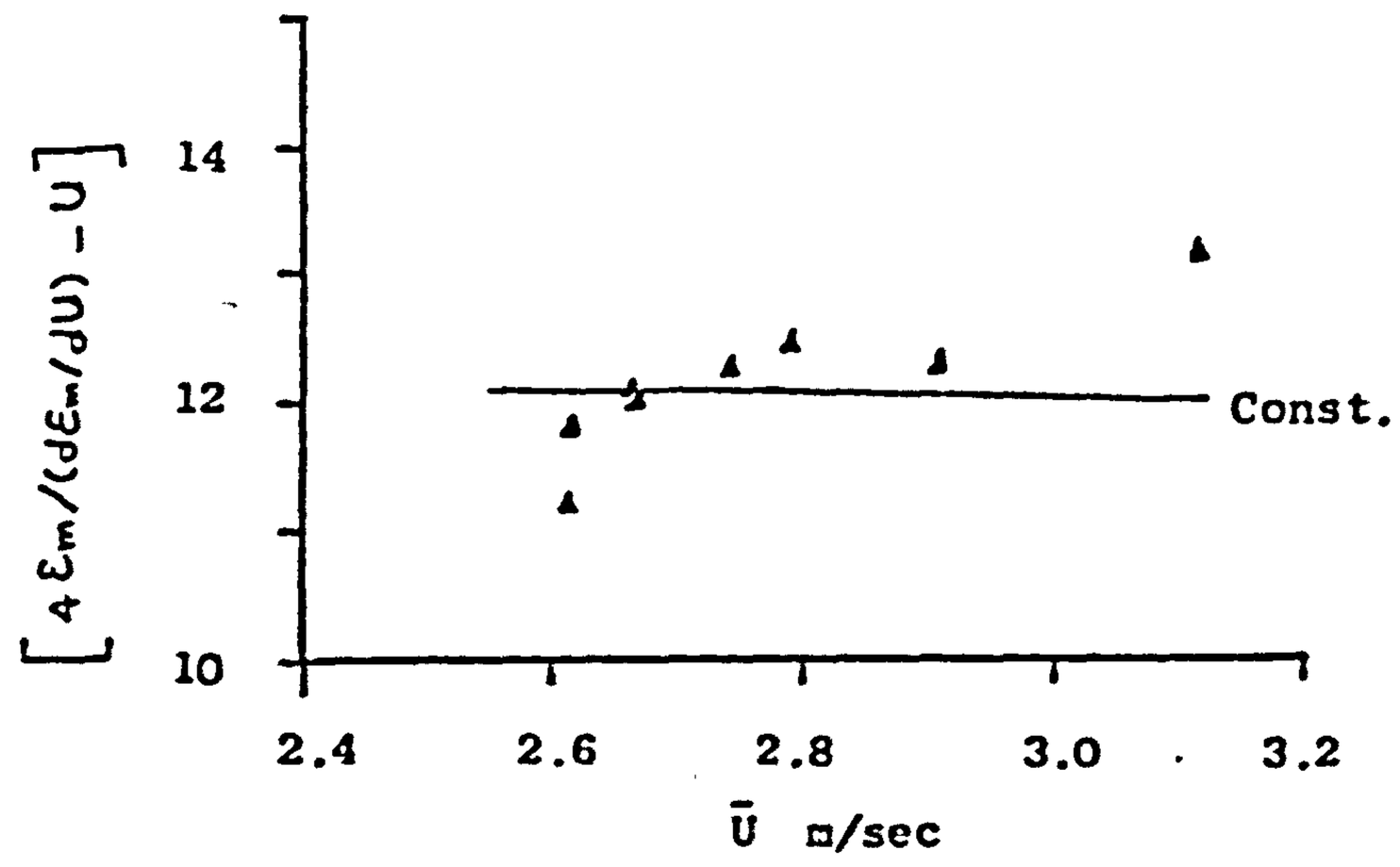

Fig. (8-3) Justification of the assumption of constant critical radius of the flame kernel.

9. CONCLUSIONS AND RECOMMENDATIONS FOR FURTHER WORK

9.1 Conclusions

The present work was carried out on two types of combustion chambers found in commercial spark ignition engines, namely: a wedge shape and a heron shape. Measurements of gas velocities and turbulence characteristics were carried out over a wider range of operating conditions than any published investigation in this field.

The results obtained have shown that the general characteristics in gas velocities are similar for most shapes of combustion chambers used for spark ignition engines. However, the turbulence characteristics and the levels of gas mean velocities during different strokes of the cycle are mainly functions of the combustion chamber and intake system configurations. Measured gas velocities at various locations inside the combustion chamber show a considerable cyclic variation in both their levels and time of occurrence in the cycle, though the general shapes are very similar for different cycles. These variations could be as high as 40 - 50% of the mean values.

The turbulence characteristics in engines are mainly affected by gas mean velocities during different strokes of the cycle. The fluctuating velocity components and the size of small-scale eddies follow similar trends to gas mean velocities. In particular, the size of small-scale eddies were found to increase linearly with gas mean velocity according to

a relation of the form:

$$\lambda_y = a\,\bar{U} \tag{8-21}$$

where a is a constant value which decreases with engine speed and depends also on combustion chamber and intake system configuration. The time micro-scale of turbulence was found to decrease with engine speed, indicating an increase in the high frequency content of turbulence eddies in the combustion chamber.

Increases in gas mean velocities with engine speed were found, therefore, to cause increases in both the fluctuating velocity components and the frequencies of eddy rotation. Consequently increases in flame speed with engine speed could be attributed to the mutual effect of the two factors mentioned above. This finding is in close agreement with the experimental data of Lefbevre et al (49) for the effect of turbulence on confined flames as given by the following relationship:

$$\frac{S_t}{S_\ell} = 1 + 0.43\,u' + 0.04\,\bar{U} \tag{6-3}$$

where the mean velocity term in equation (6-3) could be interpreted to represent the effect of higher mean velocity on increasing the frequencies of eddies in the field.

The wedge shape chamber shows that high frequency eddies are generated during the induction period, but decay later on during the compression stroke to slower eddies, while the heron

shape chamber shows a similar level of low frequency eddies during most of the cycle especially at low engine speeds. However the size of small-scale eddies in the wedge chamber are larger than the corresponding values for the heron shape at comparable conditions. This means that the heron shape may result in better performance with lean mixtures than the wedge shape providing that similar mixture homogeneities were used. The use of inlet valves fitted with guide vanes seems to provide a mutual effect of higher intake velocities at much higher rates of mixing that eventually result in smaller sizes of the small-scale eddies during compression.

The performance of the masked valve clearly indicates that the directional velocities created during intake period continue for a considerable time during compression. However, the frequencies of eddies during compression are not greatly affected and the reported improvements in the combustion process for engines fitted with masked inlet valves (Marvin and Best (1), Patterson (2), Caris et al (8), and Matsuoka et al (15)) can only be explained by higher flame speeds resulting from the associated higher fluctuating velocity components and improved mixture homogeneity.

The creation of a strong jet inside the combustion chamber during the periods of inlet valve closure as the case of a valve used for reduced lift,is very helpful in energising the flow field during this period of very high damping rates. The improved engine performance at part load conditions in Stivender's tests (19)

with a throttled intake valve may be attributed to a similar flow condition rather than enhancing the small scale turbulence. Also, the measured values of the large scale eddies inside the combustion chamber are very much smaller than the cylinder diameter as postulated by Stivender.

An intake manifold fitted with delta wings has produced a significant reduction of cyclic variation in gas velocities, and contributed towards better homogeneity of the mixture.

A study of the variation of flow field characteristics with depth inside the combustion chamber has revealed the following points:

i) A zone inside the middle of the combustion chamber seems to exist where flow properties are statistically steady and cyclic variation in gas velocities are nearly constant during the whole compression period.

ii) The minimum cyclic variation in gas velocities at any location occurs during the period of secondary flow created by compression (squish velocities).

iii) The squish components were observed to develop along the wedge wall parallel to the cylinder head surface (Rolls-Royce engine) rather than a simple transfer of mass normal to cylinder axis as thought to be the case. The measured values of those components are very much smaller than the predictions of theoretical models. One may explain this by the fact that the

squish velocities created during the compression period are transferred into circulating eddies inside the combustion chamber rather than any hypothesised directional stream velocities.

Summing up the previously mentioned findings about the flow field characteristics inside the combustion chambers and the effect of different intake modifications on these characteristics, one can outline some possible sources of potential gains in engine performance by modification of the combustion chamber and intake system configurations as follows:

i) Proper directing of intake manifolds can produce strong swirl velocities which persist during the compression period. These swirl velocities were shown, in the present work, to produce higher levels of fluctuating velocity components and contributed towards better mixture homogeneity. Consequently faster flame speeds and minimum levels of combustion variation could be achieved. Such swirl velocities will also reduce the amount of unburnt hydrocarbons and the formation of deposits on the walls of the combustion chamber (28).

ii) The insertion of swirl generators inside the intake manifolds or on valve seats are also very helpful in reducing the combustion variation, for the above mentioned reasons in item (i) without sacrifices in engine breathing at higher engine speeds.

iii) Placing the spark plug gap inside the centre of the charge during the compression period (by using long reach plugs) locates the flame kernel in a region of more uniform flow properties which reduces the cyclic variation in its rate of growth and consequently reduces combustion variation and extends the 'lean limit' of engine operation. Other advantages are obtainable when applying this modification such as: creating more favourable temperature conditions for the growth of the flame kernel by reducing its quenching by central electrodes and cylinder head surface (20), (27) and reducing flame travel distances which shorten the combustion period and reduced the octane requirement of the fuel (8).

iv) Proper shaping of the cylinder head walls (in relation to squish area) to direct the squish velocities towards the spark plug location is highly desirable for making use of this source of turbulent energy before its dissipation into decaying eddies inside the volume of the combustion chamber. This will result in accelerating the growth of the flame kernel with all the consequent improvements in engine performance as mentioned earlier. This will also reduce the octane requirement of the fuel and make it possible to increase engine efficiency by increasing the compression ratio while still using available fuels (8), Figure (9-1).

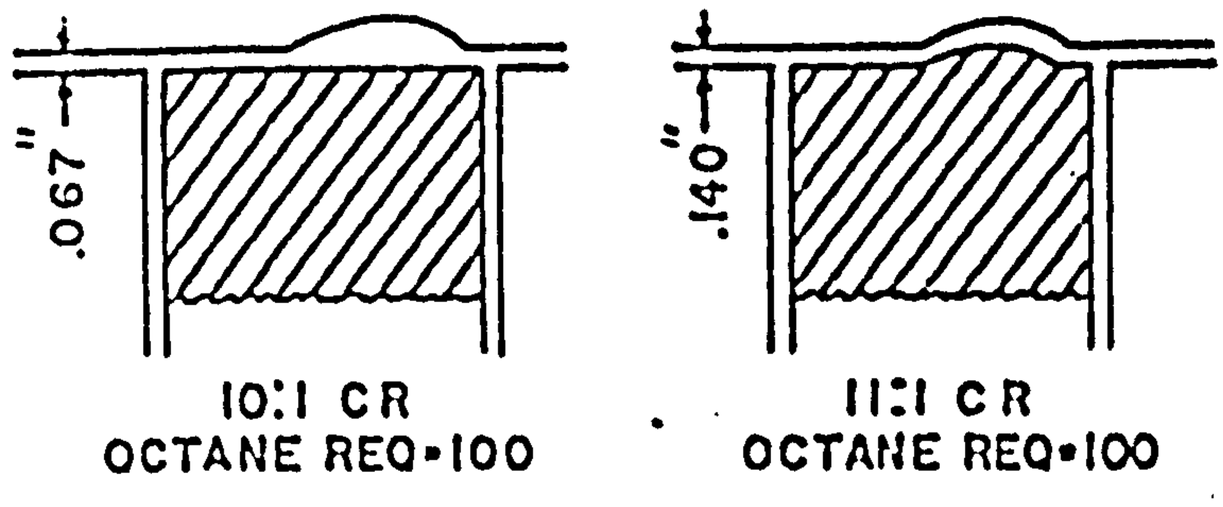

Fig. (9-1) Effect of better utilisation of squish velocities on mechanical octanes in a multi-cylinder engine (according to Diggs (8)).

v) Igniting the mixture during the period of maximum squish velocities can also reduce combustion variation and improve engine performance.

The present turbulence measurements in combustion chambers of spark ignition engines have made it possible to check two proposed models for turbulent combustion in engines, namely the laminar model (43-50) and the three dimensional model (63,64). Using some mean value of the fluctuating velocity component during the ignition period of the order of 0.5 m/sec, a mean value for the micro-scale of turbulence of 0.6 mm, a flame front thickness of 0.22 mm (42) and a laminar flame speed of 1.3 m/sec (42) and applying Kovasznay's Criterion (57), equation (2-42), shows that the wrinkled flame mechanism prevails for combustion in engines:

$$r = \frac{\delta}{S_l} \quad \frac{u'}{\lambda_x} < 1 \quad \text{(for wrinkled flame)} \qquad (2\text{-}42)$$

Comparing the magnitudes of eddy diffusivities during the compression period with the corresponding values of kinematic viscosities gives ratios of the order of 200. Consequently, the three dimensional model of combustion proposed by Summerfield (63), equation (2-39) can be rejected for combustion in spark ignition engines:

$$\frac{S_t}{S_\ell} = \frac{\varepsilon}{\nu} \frac{\delta_\ell}{\delta_t} \qquad (2\text{-}39)$$

The ratio between turbulent and laminar flame speed in engines is usually reported of the order of 3 as stated by Harrow and Orman (30) and Phillips and Orman (42). The former investigation proposed a relationship of the following form:

$$\frac{S_t}{S_\ell} = 1 + 0.002\ (RPM) \qquad (9\text{-}1)$$

The same conclusion about the adequacy of wrinkled flame model for turbulent combustion in engines was also reported by De Soete(26).

The extensive test programme undertaken, in the present work, has enabled the establishment of direct correlation between the flow field inside the combustion chambers of spark ignition engines and pipe flow fields. This resulted in developing an approximate procedure for predicting turbulence characteristics in engines from a knowledge of the gas mean velocities, which requires simple equipment.

The comprehensive literature survey undertaken has shown that the propagation of flames in spark ignition engines is greatly influenced by the rate of growth of the initial flame kernel. This process is mainly governed by the small-scale eddies which exist in the combustion chamber during the time of ignition. Variation in the rate of growth of such a kernel due to variation in eddy diffusivities of the small-scale eddies between different cycles are believed to be the main cause of cyclic combustion variation. A theoretical model for cyclic combustion variation is developed based on the previously mentioned assumptions and making use of the established correlation between the flow fields in engines and pipe flow fields. The experimental data of Barton (10) and Winsor (23) were used to check the model and showed very good agreement between the measured and predicted values of the variations.

9.2 Recommendation for Further Work

It is obvious from the discussions of the present investigation, that an extension of the work is required to study the variation of turbulence characteristics inside the combustion chambers of S.I. engines with compression ratio. This problem represents a point of contradiction between the results of Molchanov (62), Semenov (22) and James (24), which have not been resolved yet. Some preliminary work on this problem has already started in the Department of Mechanical Engineering of Loughborough University. A Ricardo E6 engine has been used in this investigation.

Use of the Data Acquisition and Processing System, which has been developed in the present work for wider studies of the turbulence characteristics produced by other shapes of combustion chambers than the ones considered here is also desirable. Future studies should be concentrated on some configurations that have shown improved engine performance with regard to the levels of exhaust emissions and smoothness of lean mixture operation. In this respect, the author would like to draw the attention to the studies of Dodd (156) where low emissions were obtained with an annular chamber formed between a flat cylinder head and a bump on the piston. The work of Tanuma et al (20) can also be consulted for these studies (see Chapter 6).

On the other hand, modifications of the intake system by; proper shaping of inlet passage (16), insertion of swirl generators inside the intake manifold (60) or fitting guide vanes on valve seats, can be used to increase the charge turbulence and consequently reduce cyclic combustion variation. Some fired tests

are required for assisting the findings of the present anemometer measurements on the effect of those modifications in reducing the size of small scale turbulence eddies.

A detailed study of the flow mechanism of creating squish velocity components inside the combustion chambers of engines is also required. This source of creating secondary flow during the compression period represents one of the most fruitful areas for potential gains in engine performance, if carefully understood and utilised to hinder the decay process of the turbulence field during the combustion period. The use of dynamic models for simulating combustion chambers configurations represents some possible experimental set up.

An extension of the studies of Tsuge and Kido (153, 154) on the mechanism of turbulence decay in closed vessels, is also required for better understanding of the characteristics of this particular flow field. Employing different methods of creating turbulence inside the vessels and investigating simulated combustion chamber shapes represents new areas for exploitation. These studies may extend the applications of the proposed design procedure (section 7.1) for predicting turbulence characteristics inside engine cylinders.

A study of the combustion process inside the cylinders of spark ignition engines under carefully measured turbulence field characteristic parameters (intensities, scales and spectrum) can result in the development of turbulent combustion models for this type of problem. The work of Sirignano (131, 132) and Blizard and Keck (133) can be consulted in this respect. This possibility is already under consideration by Dent and his co-workers

for possible establishment of some correlations between combustion parameters, turbulence charactoristics and mixturo conditions. This may lead to resolving some of the present contradictions in the known combustion models discussed in Section 2.5. For example, the phenomena of 'flame generated turbulence' which is still a matter of dispute between different investigators. The use of the concepts introduced by the spectral theory of turbulent combustion represents a more appropriate line of approach for these studies.

R E F E R E N C E S

1. MARVIN, Charles F., Jnr., and BEST, Robert D.
Flame Momentum and Pressure Development in an Engine Cylinder.
T.R. No. 399, N.A.C.A. (1931).

2. PATTERSON, Donald, J.
Cylinder Pressure Variations, a Fundamental Combustion Problem.
S.A.E. Trans. 670467, Vol. 76, Sec. 3 (1967).

3. BOLT, Jay A., and HARRINGTON, David L.
The Effect of Mixture Motion upon the Lean Limit and Combustion of Spark Ignited Mixtures.
S.A.E. 700488.

4. SOLTAU, J.P.
Cylinder Pressure Variations in Petrol Engines.
Inst. Mech. Eng. Auto. Div. (1960-1961) p.99.

5. CLARKE, J.S.
Initiation and Some Controlling Parameters of Combustion in Piston Engines.
Journal of the Inst. of Mech. Eng. Auto. Div. (1960-1961).

6. VICHNIEVESKY, R.
Combustion in Petrol Engines.
Proceedings of the Joint I.M.E. and A.S.M.E. Conference on Combustion, June and October 1955, p.288.

7. ANDON, Jerar, and MARKS, Craig.
Engine Roughness - the Key to Lower Octane Requirements.
S.A.E. Trans. Vol. 72 (1964), p.638.

8. CARIS, D.F., MICHELL, B.J., McDUFFIE, A.D. and AWYCZLALEK, F.
Mechanical Octanes for Higher Efficiency.
S.A.E. Trans. (1956), Vol. 64, p.70.

9. ANNAND, W.J. and SUMMERS, I.G.S.
Observation on the Variability of Spark Ignition Combustion Using a Single-Cycle Simulator.
S.A.E. 70048.

10. BARTON, R.K.
Correlation Between Cycle-by-Cycle Cylinder Gas Motion and Combustion Variation of a S.I. Engine.
Ph.D. Thesis, Pennsylvania State University, 1970.

11. BARTON, R.K., LESTZ, S.S. and MEYER, W.E.
An Empirical Model for Correlating Cyclo-by-Cyclo Gas Motion and Combustion Variations of Spark Ignition Engines.
S.A.E. 710163.

12. COLE, David E.
The Effect of Directed Motion on the Flame Kernel Development in a Constant Volume Bomb.
Ph.D. Thesis, University of Michigan, May 1966.

13. HANSEL, James G.,
Lean Automotive Engine Operation, Hydrocarbon Exhaust Emissions and Combustion Characteristics.
S.A.E. Paper No. 71064.

14. POVINELLI, L.A. and FUHS, A.E.
The Spectral Theory of Turbulent Flame Propagation.
8th Symposium (International) on Combustion, 1962, p.554.

15. MATSUOKA, Shin, YAMAGUCHI, Tehehsia, and UMEMURA, Yutio.
Factors Influencing the Cyclic Variation of Combustion of Spark Ignition Engines.
S.A.E. No. 710586.

16. ROTHROCK, A.M. and SPENCER, R.C.
The Influence of Directed Air Flow on Combustion in a Spark Ignition Engine.
N.A.C.A. Report No. 657, 1939.

17. SALE, B, and VICHNIEVSKY, R.
Etude de la Combustion sur la Monocylindre I.F.R. Renault C.W.R.S.
T. Soc. In. Auto. Vol. 31, 1950, p.53.

18. LEE, Dana W.
A Study of Air Flow in an Engine Cylinder.
N.A.C.A. Report No. 653, 1939.

19. STIVENDER, Donald L.
Intake Valve Throttling (IVT), A Sonic Throttling Intake Valve Engine.
S.A.E. Trans. Vol. 77, 1968, (Paper No. 680399).

20. TANUMA, Takeshi, SOSAKI, Kenichi, KANEKO, Touro and KAWASAKI, Hajimu,
Ignition, Combustion and Exhaust Emissions of Lean Mixtures in Automotive Spark Ignition Engines.
S.A.E. Paper No. 71059, 1971.

21. WENGER, H.
Measurement of Flow Velocity in the Cylinder of a Motored Engine.
Luftfahrforschung, Vol. 16, 1939, p.62.

22. SEMENOV, E.S.
Studies of Turbulent Gas Flow in Piston Engines.
N.A.S.A. Technical Translation, F.97, 1963.

23. WINSOR, R.E.
Relationship of Cyclic Combustion Variations and Mixture Motion in a Spark Ignition Engine.
Ph.D. Thesis, University of Michigan, 1972.

24. JAMES, E.H.
Investigations of Turbulent Flow in the Combustion Chamber of a Spark Ignition Engine.
Ph.D. Thesis, University of Technology, Loughborough, 1972.

25. TINDAL, M.J., ARNOLD, M.J. and WILLIAMS, T.J.
Measurement of Induction Gas Velocities in a Reciprocating Engine Cylinder.
S.A.E. 720115.

26. DE SOETE, G.
A Survey of the Effect of Turbulence on Engine Combustion.
Advances in Automobile Engineering IV - 1966.
Cranfield International Symposium Series, p.35.
(Pergamon Press).

27. BURGETT, Richard R., LEPTICH, Joseph M., and SAMGWAN, Karmar S.
Measuring the Effects of Spark Plug and Ignition System Design on Engine Performance.
S.A.E. Paper 720007.

28. PANDURANGA, Venkatasubbaiah
Correct Turbulence, A Way to Reduce the Concentrations of Unburnt Hydrocarbons from Automotive Engines.
Combustion and Flame, Vol. 18, (1972), pp.461-467.

29. HARROW, G.A., ORMAN, P.L. and TOFT, G.B.
The Effect of Engine Operating Variables on the Time of Flame Propagation in a Spark Ignition Engine.
Journal of the Inst. of Petroleum, Vol. 49, 1963.

30. HARROW, G.A. and ORMAN, P.L.
A Study of Flame Propagation and Cyclic Dispersion in a Spark Ignition Engine.
Proceedings of a Symposium held at the Advanced School of Automobile Engineering, Cranfield, July 1965.

31. ELLISON, R.J., HARROW, G.R. and HAYWOOD, B.M.
The Effect of Tetraethyl-lead on Flame Propagation and Cyclic Dispersion in Spark Ignition Engines.
Journal of the Institute of Petroleum, Vol. 54, 1968, pp.243-250.

32. KARIM, G.A.
Random Cyclic Pressure Variations in a Spark Ignition Engine.
Journal of the Institute of Petroleum, Vol. 53, 1967.

33. PETERS, Bruce D., and BORMAN, Gray L.
Cyclic Variation and Average Burning Rates in a S.I. Engine.
S.A.E. 700064.

34. MORI, Toshiatsu, and YAMAZAKI, Kiroku.
Variation of the Flame Propagation Time in a Spark Ignition Engine.
Bulletin of J.S.M.E., Vol. 13, 1970, pp.600-606.

35. HIRAO, Osamu, and KIM, Yongkil.
Studies on Combustion Variations (Cycle-to-Cycle Variations of Flame Travels).
JARI Tech. Mem. No. 1, 1970, pp.119-131.

36. IINUMA, Kazuo,
A Study of Flame Propagation in Spark Ignition Engines.
JARI Tech. Mem. No. 1, 1970, pp.133.

37. CURRY, Shelly
A Three-Dimensional Study of Flame Propagation in a Spark Ignition Engine.
S.A.E. Trans. Vol. 71, 1963, pp.628-650.

38. MILLER, G.H., UYEHARA, O.A. and MAYERS, P.S.
Practical Application of Engine Flame Temperature Measurements.
S.A.E. Trans. Vol. 62, 1954.

39. RICARDO, H.R.
The High Speed Internal Combustion Engine.
Blackie and Son Limited, 1952.

40. TROUTMAN, C.L. and LESTZ, S.S.
Exhaust Emissions and Cycle-to-Cycle Irregularities.
Report No. 35, Automobile Satefy Research Programme.
The Pennsylvania State University, June 1969.

41. BOUCHARD, C.L., TAYLOR, C.F. and TAYLOR, E.S.
Variables Affecting Flame Speed in the Otto Cycle Engine.
S.A.E. Journal, Vol. 41, No. 5, November 1937, pp.514-520.

42. PHILLIPPS, R.A. and ORMAN, P.L.
Simulation of Combustion in a Gasoline Engine Using a Digital Computer.
Proceedings of the Symposium Held at the Advanced School of Automobile Engineering, Cranfield, July 1965.

43. DÄMKÖHLER, G.
The Effect of Turbulence on Flame Velocity in Gas Mixtures
N.A.C.A. TM 1112, 1947.

44. KARLOVITZ, B, DENNISTON, D.W., KNAPSCHAEFER, D.H. and WELLS, F.
Studies of Turbulent Flames. A.Flame Propagation Across Velocity Gradients. B. Turbulence Measurements in Flames.
Fourth Symposium (International) on Combustion.
Williams and Wilkins Co., Baltimore, 1953, p.613.

45. KARLOVITZ, B., DENNISTON, D. and WELLS, F.
Investigation of Turbulent Flames.
J.Chem. Phys. Vol. 19, No. 5, May 1951.

46. SCURLOCK, A.C. and GROVER, J.H.
Propagation of Turbulent Flames.
Fourth Symposium (International) on Combustion, p. 645.
The Williams and Wilkins Co., Baltimore, 1953.

47. SHCHELKIN, K.I.
Combustion in Turbulent Flow.
Soviet Phys. Tech. Phys., 13, p.520, 1943.

48. SOKOLIK, A.S.
Combustion in Turbulent Flow.
(L.N. Khitrin Ed). Israel Programme of Scientific Translations, 1963, p.52.

49. LEFEBVRE, A.H. and REID, R.
The Influence of Turbulence on the Structure and Propagation of Enclosed Flames.
Combustion and Flame 10, p.355, 1966.

50. MIZUTANI, Yukio.
Amplification of Turbulence Level by a Flame and Turbulent Flame Velocity.
Combustion and Flame, 19, pp.203-212, 1972.

51. VINCKIER, J. and TIGGELEN, A.V.
Structure and Burning Velocity of Turbulent Premixed Flames.
Combustion and Flame, Vol. 12, pp.561-568, 1968.

52. SHCHELKIN, K.I.
Combustion in a Turbulent Flow.
Zhurnal Eksperimental' noi. 1, Teoreticheskoi Fiziki, 13, pp.9-10, 1943.

53. ZEL'DOVICH, Ya.B., and FRANK-KAMENETSKII, D.A.
Kursteorii goreiya, Detonatsii Vzryva (A Course in the Theory of Combustion, Detonation and Explosion).

54. KHITRIN, L.N. and GOL'DENBERG, S.A.
The Propagation of a Turbulent Flame Front in the Presence of High Flow Velocities.
Gasdynamics and Physics of Combustion - A Collection of Articles by A.S. Predevoditelev, Israel Programme of Scientific Translations, Jerusalem, 1962.

55. SHCHELKIN, K.I. and TORSHIN, Ya, Ka.
Gas Dynamics of Combustion.
Translated by Boris W. Kavshinoff and Lester Holschlag, Applied Physics Laboratory, The John Hopkins University, Maryland, U.S.A., 1965.

56. WARREN, J.A. and HINKAMP, J.B.
New Instrumentation for Combustion Studies.
S.A.E. Trans., Vol. 64, p.665, 1956.

57. KOVASZNAY, L.S.G.
A Comment on Turbulent Combustion.
Jet Propulsion, Vol. 26, p.485, 1956.

58. VAN TIGGLEN, and DE SOETE, G.
Oxydations et Combustions, Vol. II, Chapter VII "La Deflagration en Regime Turbulent".
Editions Technip. Paris, 1968.

59. WINKLER, G.L., LESTZ, S.S. and MEYER, W.L.
Exhaust Gas Sampling Techniques for Relating Emissions and Cycle Characteristics.
S.A.E. Paper 680770.

60. EBERAN-EBERHORST, Von R.
Combustion Process and Exhaust Composition in Internal Combustion Engines Regarded as a Statistical Problem.
11 Internationaler, Autombiltechnischer Kongreb, 12-16 June, 1966 in München.

61. HIROYUKI, Hiroyasu and MORIO, Ohki
Correlation Between Exhaust Emission and Mixture Motion in a Combustion Chamber.
JARI, Tech. Mem. No. 1, p.139, 1970.

62. MOLCHANOV, L.K.
On the Problem of Gas Motion and Combustion in a Light Fuel Engine.
Trudy Makovwkogo Auombil'no-Dorozhnogo Instituta, Autatransizdat, Moscow, 1955, No. 17.

63. SUMMERFIELD, M.
The Structure and Propagation Mechanism of Turbulent Flames in High Speed Flow.
Jet Propulsion, Vol. 25, No. 8, August 1955, pp.377-384.

64. LONGWELL, J.P.
Flame Stabilization by Bluff Bodies and Turbulent Flames in Ducts.
Fourth International Symposium on Combustion.
Williams and Wilkins Co., Baltimore, 1953, p.90.

65. SEMENOV, E.S.
Device for Measuring the Turbulence in Piston Engines.
Institute of Chem. Phys. of the Academy of Science, USSR.
14 December 1956.

66. CHEBYSHEV, P.V.
VEI Reports NK 2-26-178, 1952, ND 26-223, 1947, 48
GI 26-109, 1952.

67. DUGGER, G.L.
Effect of Initial Mixture Temperature on Flame Speed of Methane-Air, Propane-Air, and Ethylene-Air Mixtures.
N.A.C.A. Tech. Note No. 2374, May 1951.

68. GARNER, O.B.E., LONG, R. and ASHFORTH, G.K.
Effect of Pressure on Burning Velocities of Benzene-Air, n-Heptane-Air and 2, 2, 4 Trimethylpentane-Air Mixtures.
Fuel Vol. 30, pp.17-19, 1950.

69. DUGGER, G.L.
Flame Speeds of Methane-Air, Propane-Air and Ethylene-Air Mixtures at Low Initial Temperatures.
N.A.C.A. Tech. Note, No. 2624, 1952.

70. WALKER, P.L. and WRIGHT, C.C.
Hydrocarbon Burning Velocities Predicred by Thermal Versus Diffusional Mechanisms.
J.Am. Chem. Soc. August 1952, p.3769.

71. DUGGER, G.L. and GRAAH, D.D.
Flame Speeds of 2, 2, 4 Trimethylpentane-Oxygen - Nitrogen Mixtures.
N.A.C.A. Tech. Note. No. 2680.

72. ULSAMER, J.
Die Warmeabgabe eines Drahtes Oder Rohres an einen Senkrecht zur Achse Stromenden Gasoder Flussigkeitsstrom
Forsch. Geb. Ing. 3, 94. 1932.

73. McADAMS, W.H.
Heat Transmission, Third Edition, p.260.
McGraw Hill, New York, 1954.

74. ANDREWS, G.E., BRADLEY, D. and HUNDY, G.F.
Hot Wire Anemometer Calibration for Measurement of Small Gas Velocities.
Int. J. Heat Mass Transfer, Vol. 15, pp.1765-1786.
Pergamon Press, U.K., 1972

75. HILPERT, R.
Warmeabgabe Von Geheizten Drahten und Rohren in Luftstrom,
Forsch, Geb. Ing. 4, pp.215-224, 1933.

76. COLLIS, D.C. and WILLIAMS, M.J.
Two Dimensional Convection from Heated Wires at Low Reynolds Number.
J. Fluid Mechanics, 6, pp.357-384, 1959.

77. DAVIES, P.O.A.C., and FISHER, M.J.
Heat Transfer from Electrically Heated Cylinders.
Proc. R. Soc., 280A, pp.486-527, 1964.

78. KING, L.V.
On the Convection of Heat from Small Cylinders in a Stream of Fluid. Determination of the Convection Constants of Small Platinum Wires with Applications to Hot Wire Anemometry.
Phil. Trans. Roy. Soc. A., Vol. 214, p.373, 1914.

79. HINZE, J.O.
Turbulence, An Introduction to its Mechanism and Theory.
McGraw Hill Co., New York, 1959.

80. VON KARMAN, T.H.
The Fundamentals of the Statistical Theory of Turbulence.
Journal of the Aero. Sc. Vol. 4, February 1937, No. 4, pp.131-138.

81. FRENKIEL, F.N.
Effect of Wire Length in Turbulence. Investigation with a Hot Wire Anemometer.
Aero. Quart. Vol, V, May 1954, pp.1-24.

82. DRYDEN, H.L., SCHUBAUER, G.B., MOCK, W.C., Jnr., and SKRAMSTAD, H.K.
Measurements of Intensity and Scale of Wind Tunnel Turbulence and Their Relation to the Critical Reynolds Number of Spheres.
N.A.C.A. Report No. 581, 1937.

83. PAI, SHIH-I,
Viscous Flow Theory - II Turbulent Flow.
D. Van Nostrand Co., Princetown, New Jersey, 1957.

84. TAYLOR, G.I.
Statistical Theory of Turbulence, Parts I-IV.
Proc. of the Roy. Soc. A 151, pp.421-478, 1935.

85. TAYLOR, G.I.
The Spectrum of Turbulence.
Proc. of the Roy. Soc. A 164-476-490, 1938.

86. TAYLOR, G.I.
Diffusion by Continuous Movements.
Proc. of the London Mathematical Society, Ser. 2, 20, pp.196-211, 1921.

87. DRYDEN, H.L.
A Review of the Statistical Theory of Turbulence.
Quarterly of Applied Mathematics 1, pp.7-42, 1943.

88. FRIEDLANDER, S.K. and TOPPER, Leonar
Turbulence Classic Papers on Statistical Theory.
Interscience Publishers, Inc. New York, 1961.

89. KOLMOGOROFF, A.N.
The Local Structure of Turbulence in Incompressible Viscous Fluid for Very Large Reynolds Numbers.
From Comptes Medus (Doklady) de l'Academi des Sciences de l'U.R.S.S., 31, pp.538-540, 1941.

90. VON KARMAN, T.H. and LIN, C.C.
On the Concept of Similarity in the Theory of Isotropic Turbulence.
Reviews of Modern Physics 21, pp.516-519, 1949.

91. CORRSIN, S.
Investigation of Flow in an Axially Symmetrical Heated Jet of Air.
N.A.C.A. Wartime Report, December 1943. (3L23).

92. HASSAN, H.
Unsteady Heat Transfer in a Motored Internal Combustion Engine.
Ph.D. Thesis, Loughborough University of Technology, 1968.

93. DENT, J.C. and DERHAM, J.A.
A Method for Checking the Consistency of Velocity Computations from Hot Wire Anemometer Measurements in Variable Density Flows.
Journal of Physics E: Scientific Instruments, 1972, Vol. 5.

94. MORRIS, C.J.
Calibration of Hot Wire Anemometer, Internal Report.
Department of Mechanical Engineering, Loughborough University of Technology, 1972.

95. ROGERS, G.F.C. and MAYHEW, Y.R.
Thermodynamic Properties of Fluids and Other Data.
Oxford, Basil Blackwell, 1964.

96. VARGAFTIK, N.B.
Teplofizicheskiye Svoystra Veshchestr.
(Thermophysical Properties of Substances).
Reference book, Gaseneragaizdat, 1956.

97. BROMLEY, L.A. and WILKE, C.R.
Viscosity Behaviour of Gases.
Ind. Eng. Chem., 43, 1641, 1951.

98. REID, C.R. and SHERWOOD, K.T.
The Properties of Gases and Liquids, Their Estimation and Correlation.
McGraw-Hill Co., 1958.

99. KUTATELADZE and BORISHANSKII
A Concise Encyclopaedia of Heat Transfer.
Pergamon Press 1966.

100. TSEDERBERG, N.V.
Thermal Conductivities of Gases and Liquids,
Chapter 3. Ed. Robert D. Cess, Arnold, 1965.

101. VON KARMAN, T.H. and HOWARTH, L.
On the Statistical Theory of Isotropic Turbulence.
Proc. Roy. Soc. (London), A 164, 1938, pp.92-215.

102. ROBERTSON, J.M. and MARTIN, J.D.
Turbulence Structure Near Rough Surfaces.
A.I.A.A. Journal, Vol. 4, No. 12, December 1966.

103. SATO, Yukinari and YAMATO, Kazuo.
The Local Structure of Isotropic Turbulence Relative Velocity Distribution in Isotropic Turbulence.
Journal of Chem. Eng. of Japan, Vol. 6, No. 6, 1973, pp.495-502.

104. TOWNES, H.W., GOW, J.L., POWE, R.E. and WEBER, N.
Turbulent Flow in Smooth and Rough Pipes.
Trans. of ASME Journal of Basic Engineering, June 1972, pp.353-362.

105. ROBERTSON, J.M., MARTIN, J.D. and BURKHART, T.H.
Turbulent Flow in Rough Pipes.
Industrial and Engineering Chemistry Fundamentals, Vol. 1, No. 2, May 1968, pp.253-265.

106. POWE, R.E. and TOWNES, H.W.
Turbulent Structure for Fully Developed Flow in Rough Pipes.
Trans. of ASME Journal of Fluid Engineering, June 1973, pp.255-262.

107. LAUFER, J.
Investigation of Turbulent Flow in a Two-Dimensional Channel.
N.A.C.A., Tech. Note, No. 2123.

108. LAUFER, J.
The Structure of Turbulence in Fully Developed Pipe Flow.
N.A.C.A. Report No. 1174, 1954.

109. LIN, C.C.
On Taylor's Hypothesis and the Acceleration Terms in the Navier-Stokes Equations.
Quart. Appl. Math., 10, p.295, 1953.

110. MICKELSON, W.R.
An Experimental Comparison of the Lagrangian and Eulerian Correlation Coefficients in Homogeneous Isotropic Turbulence.
N.A.C.A. Tech. Note No. 3570, 1955.

111. BALDWIN, L.V. and WALSH, T.J.
Turbulent Diffusion in the Core of Fully Developed Pipe Flow.
Am. Soc. Chem. Engs. J., 7, pp.53-61, 1961.

112. UBEROI, M.S. and CORRSIN, S.
Diffusion of Heat From a Line Source in Isotropic Turbulence.
N.A.C.A. Report No. 1142.

113. FLINT, D.L., KADA, H. and HANRATTY, T.J.
Point Source Turbulent Diffusion in a Pipe.
A.I. Ch.E. Journal, Vol. 6, No. 2, June 1960, pp.325-331.

114. HAY, J.S. and PASQUIL, F.
Diffusion from a Fixed Source at a Height of a Few Hundred Feet in the Atmosphere.
J. Fluid Mech. 2, p.299, 1957.

115. ANDERSON, O.K.
Time Resolution Power in Correlation Measurements with DISA Type 55 A01 Hot Wire and Hot Film Anemometers.
DISA Information No. 4, December 1966.

116. ACKROYD, M.H. and LOWSON, M.V.
Digital Processing and Analysis of Signals.
Short Course Notes, Loughborough University of Technology, November, 1972.

117. ENOCHSEN, D., LOREON and OTNES, K. Robert.
Programming and Analysis for Digital Time Series Data.
The Shock and Vibration Center, United States Department of Defence, 1972.

118. BENDAT, S. Julius and PIERSOL, G. Alan
Random Data: Analysis and Measurement Procedure.
Wiley-Interscience Co., 1971.

119. SANGAMO,
Magnetic Tape Instrumentation Portable Recorder/Reproducer Technical Manual, Model 3562.
Sangamo Electric Co., Springfield, Illinois, U.S.A.

120. RACAL Store-4,
Technical Handbook.
Racal-Thermionic Limited, Hytho, Southampton, England.

121. DISA
Instrumentation Manuals for 55M System and Type 55D26 Signal Conditioner.
DISA Elektronik, Denmark.

122. BATCHELOR, G.K.
The Theory of Homogeneous Turbulence.
Cambridge University, Press, 1953.

123. BOUSSINESQ, T.V.
Mem. Pres. Par. Div. Sav., XXIII, Paris, 1877.
Theorie de l'ecoulement Tourbillant 1897.

124. PRANDTL, L.
The Mechanics of Viscous Fluids.
Aerodynamic Theory, Vol. III, Div. G., 1935, Ed. by W.F. Durano.

125. SPALDING, D.B.
Heat Transfer to a Turbulent Stream from a Surface with a Stepwise Discontinuity in Wall Temperature.
Conf. Intern. Development in Heat Transfer.
ASME, Boulder, Colo., Part II, pp.439-446, 1961.

126. KAYS, W.M.
Convective Heat and Mass Transfer.
McGraw Hill Book Co., 1966.

127. KNUDSEN, J.G. and KATZ, D.L.
Fluid Dynamics and Heat Transfer.
McGraw Hill Book Co., New York, 1958.

128. SCHILICHTING, H.
Boundary Layer Theory.
Pergamon Press, New York, 1955.

129. FALKNER, V.M.
A New Law for Calculating Drag. The Resistance of a Smooth Flat Plate with Turbulent Boundary Layer.
Aircraft Engineering, 15:65, 1943.

130. NIKURADSE, J.
Turbulente Reibungsschiten an der Platte,
Ed. by Zentr. Wiss. Ber-Wesen. Pub. by R. Oldenbourg, Munich and Berlin, 1942.

131. SIRIGNANO, W.A.
One Dimensional Analysis of Combustion in a Spark Ignition Engine.
S.A.E. Paper No. 719010, pp.52-62.

132. ROSENTWEIG, Bellan Josotto and SIRIGNANO, W.A.
A Theory of Turbulent Flame Development and Nitric Oxide Formation in Stratified Charge Internal Combustion Engines.
Combustion Science and Technology, 1973, Vol. 8, pp.51-68.

133. BLIZARD, N.C. and KECK, J.C.
Experimental and Theorotical Investigation of Turbulent Burning Model for Internal Combustion Engines.
S.A.E. Paper No. 740190. Automotive Engineering Congress, Detroit, Michigan, February 25 - March 1, 1974.

134. BROEZE, Ir. J.J.
Combustion in Piston Engines.
De Technische Uitgenerig 17, Stam. N.V.
Haarlem-Antwerpen, Kenlen, 1963, pp.75-77.

135. ESCHENBACH, R.C. and AGNEW, J.T.
Use of Constant Volume Bomb Technique for Measurement Burning Velocity.
Combustion and Flame, Vol. 2, 1958, pp.273-285.

136. BROEZE, J.J.
Combustion in Internal Combustion Engines.
The Spark Ignition Engine.
Engineering, Vol. 169, No. 4396, April 28, 1950, pp.464-465.

137. LICHTY, L.C.
Internal Combustion Engines.
McGraw Hill Co., London, 1951.

138. BRANDSTETTER, W.R. and CARR, M.J.
Measurement of Air Distribution in a Multi-Cylinder Engine by Means of Mass Flow Probe.
S.A.E. Paper No. 730494, Auto. Eng. Meeting, Detroit, Michigan, May 14-18, 1973.

139. PINKEL, Benjamin
A Summary of NACA Research on Heat Transfer and Friction for Air Flowing Through Tubes with Large Temperature Difference.
ASME Paper No. 53, SA-34, February 1954.

140. LOBO, P.C.
The Determination of Velocity Patterns in Engine Cylinders by Means of the Hot Wire Anemometer.
Ph.D. Thesis, London University, 1966.

141. SPIEGEL, R.M.
Theory and Problems of Statistics.
Schaum Publishing Co., New York, 1961.

142. HEWLETT PACKARD FOURIER ANALYSER Model 5451A
User Manual, Hewlett Packard Co., California, U.S.A.

143. SPIERS, H.M.
Technical Data on Fuel
B.N.C. World Power Conference, 1961.

144. ROBERTSON, J.M. and CALEHUFF, G.H.
Turbulence in a Diffuser Boundary Layer.
Journal of the Hydraulics Division, Proc. of the Am. Soc. of Civil Eng.,
Paper No. 1393, October 1957.

145. ANTONIA, R.A.
Some Small Scale Properties of Boundary Layer Turbulence.
The Physics of Fluids, Vol. 16, No. 8, August 1973.

146. SHUNICHI, Ohigashi and YOSHISUKE, Hamamoto
Study on Ignition Lag and Flame Propagation in Spark Ignition Engines.
Bulletin of the J.S.M.E. Vol. 13, No. 64, 1970.

147. MANTEY, Harvey H.L.
The Effect of Combustion Chamber Shape on Smoothness of Power.
Engineering Know-how in Engine Design, Part 3.
Society of Automotive Engineers, Sp-137.

148. GIBSON, C.H. and SCHWARS, W.H.
The Universal Equilibrium Spectra of Turbulent Velocity and Scalar Fields.
Journal of Fluid Mechanics, Vol. 16, 1963.

149. GIBSON, M.M.
Spectra of Turbulence in a Round Jet.
Journal of Fluid Mechanics, Vol. 15, 1963.

150. LANGE, K.
Control of Exhaust Emissions from Internal Combustion Engines by Means of Engine Modification.
MTZ, Vol. 34, No. 7, pp.221-225, July 1973.
MIRA Translation No. 4/74, January 1974.

151. ELLE, B.J.
An Investigation at Low Speed of the Flow Near the Apex of Thin Delta Wings with Sharp Leading Edges.
A.R.C.R. & M. 3176, January 1958.

152. LAMBOURNE, N.C. and BRYER, D.W.
The Bursting of Leading Edge Vortices, Some Observations and Discussion of the Phenomenon.
Aero. Research Council R. & M. No. 3282, London, 1962.

153. TSUGE, Morio, KIDO, Hiroyuki, YANAGIHARA, Hiromichi.
Decay of Turbulence in a Closed Vessel.
1st Report, Decay of Turbulence Intensity.
Bulletin of the J.S.M.E. Vol. 16, No. 92, February 1973.

154. TSUGE, Morio and KIDO, Hiroyuki.
Decay of Turbulence in a Closed Vessel.
Bulletin of the J.S.M.E. Vol. 17, No. 107, May 1974.

155. TAYLOR, C.F. and TAYLOR, E.S.
The Internal Combustion Engine.
International Textbook Co., Scranton, Pennsylvania, 1962.

156. DODD, A.E.
Exhaust Emissions Studies using a Single Cylinder Engine.
Paper C131/41, Air Pollution Control in Transport Engines
Automobile Division and Combustion Engine Group,
Conference Volume, Inst. Mech. Eng. Symposium 1971.

157. SALAMA, N.
Three-Dimensional Analysis of Gas Velocity Vector Inside a Cylinder of a S.I. Engine.
Internal Report, Department of Mechanical Engineering, University of Technology, Loughborough, 1973.

APPENDIX A1

NEW ANALYSIS OF OTHER INVESTIGATIONS

The results of Semenov (22) and James (24) were analysed, using similar procedures to those presented in Chapter 4. However modifications of the general data processing procedures were necessary to suit the form of reported data in each investigation as follows:

A1-1 Semenov's Data

The power spectrum curves presented by Semenov were used to obtain the time micro-scale of turbulence as given by the following relationship:

$$1/\lambda_t^2 = 4\pi^2 \int_0^\infty F(n)\, n^2 \, dn \qquad (A1)$$

Different turbulence characteristic parameters were obtained using the measured values of gas mean velocities and fluctuating velocity components and making use of the relationship between micro-scales and macro-scales as discussed in Chapter 3. Corrections of the effect of finite wire length on turbulence measurements were also calculated assuming an exponential form of the correlation function as proposed by Semenov on his original data. However, the use of the predicted values of the scales of eddies rather than approximate values calculated from mean velocities and mean frequencies as given by equation (A2) results in much smaller values of the corrections as compared with Semenov's estimation.

$$L_x = \frac{\bar{U}}{2\pi n} \qquad (A2)$$

For example the calculated corrections using the predicted values of L_x vary between 1.36 at lower compression ratios (CR = 4:1) to 1.604 at 9.5 compression ratio while a value of 2.5 was used by Semenov. A summary of these analyses is given in Table (A1).

TABLE (A1) New Analysis of Semenov's Data at TDC Compression

Engine Speed = 900 r.p.m. and 0.71 volumetric efficiency

Compression Ratio	$\bar{U}$ m/sec	$u'_{measured}$	$u'_{corrected}$	Int. $\frac{u'_{meas}}{\bar{U}}$	λ_x (mm)	L_x (mm)	Eddy Diffusivity (m^2/sec)x10^3	Friction Velocity (U*) m/sec	$\frac{u'}{u^*}$
4.0	1.439	0.3489	0.4758	0.3306	0.6765	2.241	0.367	0.08143	5.843
6.0	1.31	0.336	0.4917	0.3753	0.52	1.737	0.3207	0.07287	6.748
8.0	1.181	0.3231	0.4917	0.4164	0.4475	1.529	0.2756	0.06433	7.645
9.5	1.084	0.3587	0.5754	0.5308	0.4156	1.305	0.2568	0.05944	9.68

A1-2 James' Data

Since the original data in this case were reported as variations of fluctuating velocity components with frequencies in six bandpass widths, representative values of total mean square values of the fluctuating velocity components were obtained by integrating power spectrum curves. These latter curves were calculated from the reported results using the following relations

$$F(n) = \lim_{t \to \infty} \frac{1}{T}\left[X(n) \quad X^*(n)\right] \tag{A3}$$

$$\overline{\hat{u}^2} = \int_0^\infty F(n) \quad dn \tag{A4}$$

where $X(n)$ and $X^*(n)$ are the Fourier transforms and its complex conjugate of the fluctuating velocity components.

An interpolation FORTRAN program was used to calculate the values of $u'(n)$ at specific frequencies corresponding to a fixed sampling rate on the Hewlett Packard Fourier Analyser. In this case a data block of 64 points were used with a maximum frequency of 5 KHz which resulted in a frequency resolution of 156 Hz/sample.

The time micro-scales of turbulence were obtained by two different methods:

1. From normalised power spectrum curves using equation (A1).
2. From the second derivatives of the auto-correlation coefficients. The latter values were obtained

2. continued.

from an inverse Fourier transform of the normalised power spectrum curves.

Figs. (A1) and (A2) show typical curves of these analyses while the complete analysis is given in Table (2-6).

The main concern about these analyses are the limited number of cycles used to evaluate average values of u' in the original work (12 cycles) especially with using instantaneous values at the particular crank angles of interest rather than a reasonable sample width of the signals. Also the large cyclic variations in gas mean velocities were superimposed on the actual fluctuations in the lower range frequencies.

A modification of the data processing procedure used by James will be discussed in the following section which uses a combination of a fast ADC and a digital computer.

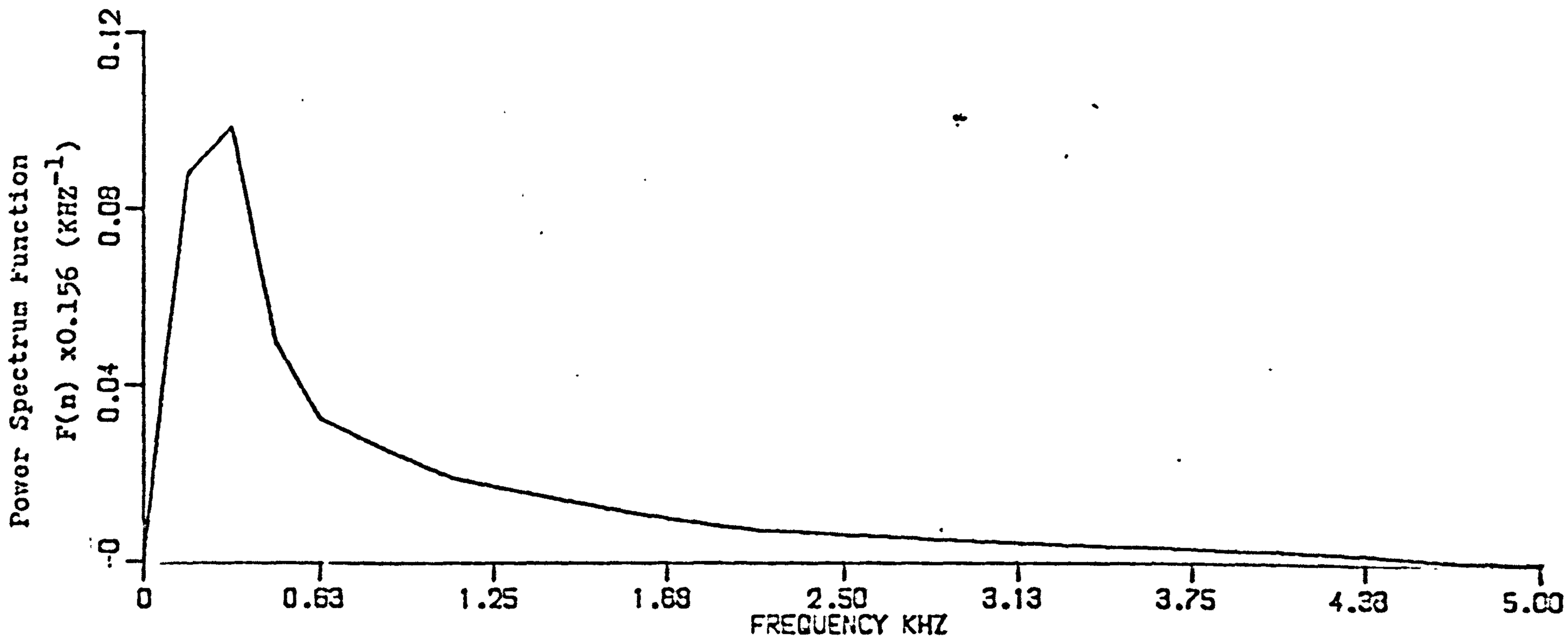

Fig (A1) A Typical Example of the Power Spectrum Functions obtained in a new Analysis of James' Data (22). (Squish Combustion Chamber, 5.29:1 Compression Ratio, 900 RPM & TDC Data)

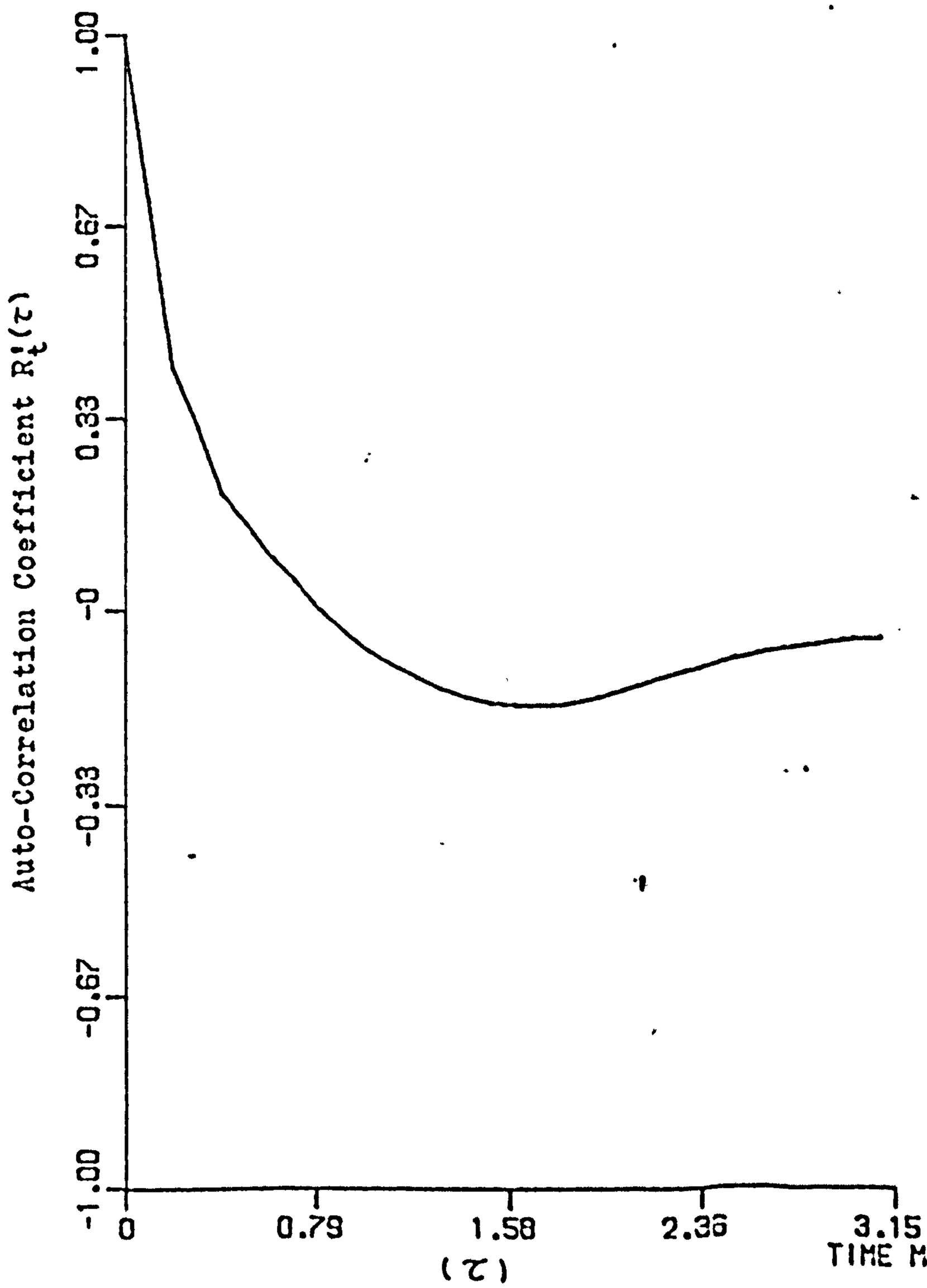

Fig (A2) A typical example of the auto-correlation coefficient curves obtained in a new analysis of James' data (22). (Squish combustion chamber, 5.29:1 compression ratio, 900 RPM and TDC data.)

A1-3 Proposed Data Processing System for Evaluating Turbulence Characteristic Parameters from Mean Velocities

i) Digitize instantaneous (original) hot wire signals at a fast sampling rate (Δt), e.g. 50 μ sec/sample.

ii) Isolate a cycle sample of a fixed width ($\Delta\theta$) from each engine cycle at the particular crank angle of interest θ.

iii) Calculate instantaneous values of gas velocities for different samples in the cycle sample.

iv) Resolve the gas velocity signals for the cycle sample into a mean value $\bar{U}_i$ and fluctuating velocity components u_i where the subscript (i) refers to the engine cycle under consideration.

v) Obtain the root mean square value of the fluctuating velocity component for the cycle number (i).

vi) Repeat steps from (i) to (v) for a large number of cycles.

vii) Calculate the mean values of the fluctuating velocity components and gas mean velocities for the test under consideration by averaging values of individual cycles. Consequently calculate the turbulence intensity from

$$\mathrm{Int}(\theta) = \frac{u'(\theta)}{\bar{U}(\theta)} \tag{A5}$$

$$u'(\theta) = \frac{\sum_{i=1}^{NC} u_i'(\theta)}{NC} \tag{A6}$$

$$\bar{U}(\theta) = \frac{\sum_{i=1}^{NC} \bar{U}_i(\theta)}{NC} \qquad (A7)$$

where

$$\bar{U}_i(\theta) = \frac{\sum_{i=1}^{N} U_i(\theta)}{N} \qquad (A8)$$

$$N = \frac{\Delta\theta}{\Delta t} \qquad (A9)$$

U_i is the instantaneous values of gas - velocities for different samples in the cycle sample (i).

and

$$u_i'(\theta) = \sqrt{\left[U_i(\theta) - \bar{U}_i(\theta)\right]^2} / N \qquad (A10)$$

viii) Obtain an average power spectrum curve by averaging individual power spectrum curves of each cycle.

ix) Obtain the micro-scale of turbulence using equation (A1).

x) Cyclic variations in gas mean velocities and turbulence characteristics can be obtained by statistical analysis of the values for different cycles.

APPENDIX A2

STATISTICAL DEFINITIONS

This appendix is concerned with defining the various statistical terms used in the present investigation.

1. The arithmetic mean.

The arithmetic mean or the mean of a set of N numbers $x_1, x_2 \ldots\ldots x_N$ is denoted by $\bar{X}$ and is defined as

$$\bar{X} = \frac{\sum_{i=1}^{N} x_i}{N} \qquad \text{(A11)}$$

2. The root mean square value

The root mean square of a set of numbers $x_1, x_2 \ldots x_N$ is defined by

$$\text{R.M.S.} = \sqrt{\bar{X}^2} = \sqrt{\frac{\sum_{i=1}^{N} x_i^2}{N}} = \sqrt{\frac{X^2}{N}} \qquad \text{(A12)}$$

3. The range of variation

The range of a set of numbers is the difference between the largest and smallest numbers in the set.

$$\text{Range of Variation} = X_{max} - X_{min} \qquad \text{(A13)}$$

The relative range of variation is defined as

$$\text{R.R.V.} = (X_{max} - X_{min})/\bar{X} \qquad \text{(A13a)}$$

4. Sample Variance

The variance of a set of data x_1, x_2 ..... x_N is defined as the square of the deviation of the data from their mean values as given by

$$S^2 = \frac{\sum_{i=1}^{N} (x_i - \bar{X})^2}{N} \qquad (A14)$$

5. The standard deviation

The standard deviation is defined as the root mean square of the deviations from the mean. Therefore

$$S = \sqrt{\frac{\sum_{i=1}^{N} (x_i - \bar{X})^2}{N}}$$

which could be simplified to the following relation

$$S = \sqrt{\frac{X^2}{N} - (\bar{X})^2} = \sqrt{\overline{X^2} - (\bar{X})^2} \qquad (A15)$$

6. Coefficient of variation

This is defined as a relative variation as given by

$$V = \frac{S}{\bar{X}} \qquad (A16)$$

7. Skewness

Skewness is the degree of symmetry or departure from symmetry of a distribution. If the frequency curve of a distribution has a longer 'tail' to the right of the central maximum than to the left, the distribution is said to be "skewed" to the right or to have positive skewness. If the reverse is true

7. Skewness (continued)

it is said to be skewed to the left or to have 'negative skewness'. This is defined by

$$CS(X) = \frac{\sum_{i=1}^{N} (x_i - \bar{x})^3}{N - 2} / S^3(X) \qquad (A17)$$

For a normal distribution, the coefficient of skewness equals zero.

8. Kurtosis

Kurtosis is the degree of peakedness of a distribution, usually taken relative to a normal distribution. A distribution having a relatively high peak is called 'leptokurtic' while a flat topped distribution is called 'platykurtic'. The normal distribution which is not very peaked or very flat-topped is called 'mesokurtic'.

The coefficient of kurtosis is defined as

$$CK(X) = \frac{\sum_{i=1}^{N} (x - \bar{x})^4 / S^4(K)}{N - 3} \qquad (A18)$$

For a normal distribution the coefficient of kurtosis equals 3.

9. Best fitting curve

This is a curve which approximates a given set of data points with the minimum square deviations

$$D_1^2 + D_2^2 + \ldots\ldots D_N^2 \quad \text{is a minimum Y}$$

9. Best fitting curve (continued)

The least square line approximating the set of points (X_1, Y_1) ..... (X_N, Y_N) is given by

$$Y = a_0 + a_1 X \tag{A19}$$

where

$$a_0 = \frac{(\Sigma Y)(\Sigma X^2) - (\Sigma X)(\Sigma XY)}{N \Sigma X^2 - (\Sigma X)^2} \tag{A20}$$

$$a_1 = \frac{N \Sigma XY - (\Sigma X)(\Sigma Y)}{N \Sigma X^2 - (\Sigma X)^2} \tag{A21}$$

10. Tests of hypothesis and significance (141)

If on the supposition that a particular hypothesis is true we find that results observed in a random sample differ markedly from those expected under the hypothesis on the basis of pure chance using sampling theory, we would say that the observed differences are 'SIGNIFICANT' and we would be inclined to reject the hypothesis.

If we reject a hypothesis when it should be accepted, we say that a type I error has been made. If, on the other hand, we accept the hypothesis when it should be rejected, we say a type II error has been made.

11. Level of significance

In testing a given hypothesis, the maximum probability with which we would be willing to risk a type I error is called the 'Level of significance'. This probability is often denoted by α .

In practice a level of significance of 0.05 or(0.01) is customary, which means that there are about 5(or 1) chances in 100 that we would reject the hypothesis when it should be accepted, i.e. we are about 95% confident that we have made the right decision.

APPENDIX A3

PHYSICAL PROPERTIES OF AIR

Examination of the thermal equilibrium equation for the hot wire, shows that accurate knowledge of gas properties are essential. These properties are: the thermal conductivity (k), the dynamic viscosity (μ), the specific heat at constant volume (C_v), or the specific heat at constant pressure and the ratio between the specific heats at constant volume and constant pressure (γ). These fluid properties are evaluated at the wire temperature and surrounding fluid temperature.

Different expressions are proposed in the literature for the variations of fluid properties with temperature and pressure. However for our practical situation where the maximum fluid pressure is of the order of 15 atms, the effect of pressure on fluid properties is negligible and, therefore, a least square polynomial fit of the published data from different references was employed to express the variation of fluid properties with temperature as follows:

a) The specific heat at constant pressure

The published data of Rogers and Mayhew (95) was used and a least square polynomial fit of the 8th order yields the values of various coefficients as shown in Table (A2) where the equation is given by:

$$Cp_T = \sum_{i=1}^{9} a_i \; T^{i-1} \qquad (A22)$$

where a_i (i = 1, 2.....9) are the polynomial coefficients.

TABLE (A2) Coefficients of the polynomial in equation (A22)

a_0	=	0.10036831684	x 10^{4}
a_1	=	0.4109764355	x 10^{-1}
a_2	=	0.109530395987	x 10^{-3}
a_3	=	0.2115430395987	x 10^{-3}
a_4	=	-0.74071031836	x 10^{-8}
a_5	=	0.116895608829	x 10^{-10}
a_6	=	-0.102415350074	x 10^{-13}
a_7	=	0.483599303466	x 10^{-17}
a_8	=	-0.961797673461	x 10^{-21}

b) Thermal Conductivity

Vargaftik (96) shows that the variation of thermal conductivity of diatomic and polyatomic gases at atmospheric pressure could be represented by the following expression (which agrees with the published data of Rogers and Mayhew (95) and Kutateladze(99)):

$$K_T = K_o \frac{(T + 273)}{T_o + 273}^{p} \qquad \text{(A23)}$$

where K_T is the thermal conductivity of the gas at temperature T.

K_o is the thermal conductivity at a reference temperature = (0.02435 $W/m^2\ {}^oC$)

T is the gas temperature ^oC

T_o is the reference temperature = (20^oC)

p is the exponent of temperature dependance = 0.82

c) Dynamic Viscosity

The viscosity of gas increases with increase in temperature. The rate of increase $\frac{d\mu}{dT}$ may increase, remain almost constant, or decrease as the temperature increases. As a rough rule for compounds of the same type, the higher the molecular weight, the greater the rate of increase of viscosity. Spiers (156) stated that at pressures in the neighbourhood of atmospheric, the viscosity of a gas is independent of pressure.

Bromley and Wilke (97) showed that the viscosity of a gas at any temperature T is related to the viscosity at reference temperature T_o by the relationship

$$\mu = \mu_o \frac{f\left(\frac{\sigma T}{\varepsilon}\right)}{f\left(\frac{\sigma T_o}{\varepsilon}\right)} \qquad \text{(A24)}$$

where μ is the dynamic viscosity at temperature T

μ_o is the dynamic viscosity at a reference temperature T

T is the gas temperature (^oK)

T_o is the reference gas temperature (^oK)

σ Stefan Boltzman's constant

ε constant characteristics of the chemical species

f denotes the viscosity temperature function.

Due to the difficulty of obtaining $\frac{\sigma}{\varepsilon}$ for some gases, the ratio $\frac{\sigma T}{\varepsilon}$ may be estimated from

$$\frac{\sigma T}{\varepsilon} = 1.33 \; T_r \tag{A25}$$

where T_r is the reduced temperature of the gas. Values of the viscosity temperature function $f(\frac{\sigma T}{\varepsilon})$ are tabulated by Reid and Sherwood (98) and are given in Table (A3). A least square fit of such a function in a polynomial of the 8th order was carried out, equation (A26), and the values of different coefficients are given in Table (A4).

$$f\left(\frac{\sigma T}{\varepsilon}\right) = \sum_{i=1}^{9} a_i \; T^{i-1} \tag{A26}$$

where a_i is the polynomial coefficient and T is the gas temperature.

Reid and Sherwood indicated that the use of the relationship (A24) is remarkably reliable over the temperature range 100 to 1500°K. The reference value of the dynamic viscosity and temperature used are μ_o = 0.00001717 Kg/m sec at 20°C.

TABLE (A3) Values of the Viscosity Temperature Function (98)

$\sigma T/\varepsilon$	$f(\sigma T/\varepsilon)$	$\sigma T/\varepsilon$	$f(\sigma T/\varepsilon)$
0.3	0.1969	3.1	1.7154
0.4	0.2540	3.2	1.7573
0.5	0.3134	3.3	1.7983
0.6	0.3751	3.4	1.8388
0.7	0.4384	3.5	1.8789
0.8	0.5025	3.6	1.9186
0.9	0.5666	3.7	1.9576
1.0	0.6302	3.8	1.9962
1.1	0.6928	3.9	2.0343
1.2	0.7544	4.0	2.0719
1.3	0.8151	4.1	2.1090
1.4	0.8744	4.2	2.1457
1.5	0.9325	4.3	2.1820
1.6	0.9894	4.4	2.2180
1.7	1.0453	4.5	2.2536
1.8	1.0999	4.6	2.2888
1.9	1.1529	4.7	2.3237
2.0	1.2048	4.8	2.3583
2.1	1.2558	4.9	2.3926
2.2	1.3057	5.0	2.4264
2.3	1.3547	6.0	2.751
2.4	1.4028	7.0	3.053
2.5	1.4501	8.0	3.337
2.6	1.4962	9.0	3.607
2.7	1.5417	10.	3.866
2.8	1.5861	20.	6.063
2.9	1.6298	30.	7.880
3.0	1.6728	40.	9.488

TABLE (A4) Coefficients of Dynamic Viscosity Function

a_0	=	0.011247287149	
a_1	=	0.6728087682	
a_2	=	-0.0487113925692	
a_3	=	0.2735028893	$\times 10^{-2}$
a_4	=	-0.8884856941	$\times 10^{-4}$
a_5	=	0.168231637794	$\times 10^{-5}$
a_6	=	-0.18336035233	$\times 10^{-7}$
a_7	=	0.106525921085	$\times 10^{-9}$
a_8	=	-0.255293477119	$\times 10^{-12}$

APPENDIX A4

A GUIDE FOR THE SOURCES OF DIFFERENT EQUATIONS PRESENTED IN CHAPTER 3

This Appendix is meant to be a precise guide for the reader who wants to follow the derivations of different equations presented in Chapter 3.

Equation Number	Reference	Page
(3-3) - (3-7)	22	126 -
(3-8)	23	16 - 21
(3-9) - (3-14)	77	495, 501-502
(3-53) - (3-57)	79	40
(3-60) - (3-67)	79	35 - 36
(3-70) - (3-72)	79	150 - 153
(3-73)	81	10
(3-75)	109	302 - 303
(3-76) - (3-78)	79	41
(3-81) - (3-88)	79	56 - 59
(3-94) - (3-97)	84	28 - 36
(3-99) - (3-100)	79	185
(3-102)- (3-107)	91	31 - 32
(3-108)- (3-115)	79	97 - 100
(3-118)- (3-141)	81	12 - 13
(3-146)- (3-151)	79	47 - 48

Note: The classical papers on turbulence (e.g. 84 - 90) are compiled in reference (88).